
Doctoral

Science

2023

Novel Therapeutic Approaches to Treat Brain Cancer Combining 3D Cell Culture Models, Cold Atmospheric Plasma and Airborne Acoustic

Janith Wanigasekara

Technological University Dublin, janith.manoharawanigasekara@tudublin.ie

Follow this and additional works at: <https://arrow.tudublin.ie/sciendoc>



Part of the [Environmental Public Health Commons](#), [Oncology Commons](#), and the [Other Public Health Commons](#)

Recommended Citation

Wanigasekara, J. (2023). Novel Therapeutic Approaches to Treat Brain Cancer Combining 3D Cell Culture Models, Cold Atmospheric Plasma and Airborne Acoustic. Technological University Dublin. DOI: 10.21427/YMWP-ZV47

This Theses, Ph.D is brought to you for free and open access by the Science at ARROW@TU Dublin. It has been accepted for inclusion in Doctoral by an authorized administrator of ARROW@TU Dublin. For more information, please contact arrow.admin@tudublin.ie, aisling.coyne@tudublin.ie, gerard.connolly@tudublin.ie, vera.kilshaw@tudublin.ie.



This work is licensed under a [Creative Commons Attribution-NonCommercial-Share Alike 4.0 International License](#).
Funder: Science Foundation Ireland



**Novel Therapeutic Approaches to Treat
Brain Cancer Combining 3D Cell
Culture Models, Cold Atmospheric
Plasma and Airborne Acoustic**

Thesis submitted to the Technological University Dublin in fulfilment of the
requirements for PhD examination

Submitted

by

Wanigasekara Mudiyansele Janith Manohara Bandara

Wanigasekara, B.Sc., M.Sc

School of Food Science and Environmental Health (FSEH),

Environmental Sustainability & Health Institute (ESHI),

Technological University Dublin

Supervisors:

Prof. James F. Curtin, Prof. Brijesh K. Tiwari, Prof. Patrick J. Cullen

May 2023

ABSTRACT

Glioblastoma (GBM), an adult-type diffuse grade 4 glioma (IDH wild type), is the most prevalent, aggressive, fatal, highly vascularized, malignant primary brain tumour in adults with a poor prognosis. Despite existing therapies such as surgical resection, radiation therapy and chemotherapy such as temozolomide (TMZ), patient survival remains largely unchanged over the last three decades. There is an urgent need for novel and effective therapeutic strategies that can overcome drug resistance, cross the blood brain barrier, and minimise off-target side effects that can negatively impact a patient's quality of life. The high failure rate of clinical trials is due to inefficient treatment methods and imperfect pre-clinical models, which limit our ability to predict efficacy and toxicity in humans.

Thus, the aim of this project is to investigate the effectiveness of non-thermal therapies, such as cold atmospheric plasma (CAP), ultrasound (US), and plasma microbubble (PMB) (alone or in combination) for the treatment of GBM using *in vitro* three-dimensional (3D) tumour spheroid models to closely mimic the natural *in vivo* environment, shape, and cellular response.

In an effort to mitigate the issue of inaccurate pre-clinical therapeutic outcomes resulting from imperfect pre-clinical models, we have optimized and integrated the usage of 3D tumour spheroid models into our research using the low attachment plate, hanging drop plate, and scaffold-based approaches. During efforts to address the issue of inefficient treatment methods, we found out that the use of novel therapeutic methods such as CAP (alone), US (alone), and the combination of US and CAP / PMB treatments can effectively induce 3D GBM and epidermoid tumour spheroid cell death in a time-, dose-, treatment frequency-, and reactive oxygen species- dependent manner. Additionally, these single or synergistic treatments were also able to significantly reduce 3D GBM

spheroid regrowth cell proliferation, growth metabolic and while induce, cytotoxic effects, DNA double strand breaks, damage to the tumour sphere's cell membrane, spheroid shrinkage, and damage to the tumour microenvironment (TME). We also found out that CAP (alone), PMB (alone) and in combination of US treatments were able to induce cytotoxicity throughout the tumour sphere, likely via long-lived reactive oxygen and nitrogen species (RONS) (H_2O_2 , NO_2^- , and NO_3^-) and also other reactive species, with multiple treatments augmenting this cytotoxic effect. The combination of US and CAP has a synergistic effect that leads to higher cytotoxicity in 3D tumour sphere models compared to either CAP or US alone, and this effect is dependent RONS. Single treatments of CAP and US activate the JNK signaling pathway, while multiple treatments can trigger multiple cell demise pathways, including caspase-dependent, JNK-dependent, and calpain-mediated cell death. Our study on drug delivery demonstrated that combining US and TMZ enhances the cytotoxicity of GBM and epidermoid carcinoma in 3D tumour spheres compared to two-dimensional (2D) cells. We used doxorubicin as a reporter to show that US improves drug diffusion in 3D models and drug uptake into cells in tumour spheres, leading to enhanced cytotoxicity that is not observed in 2D culture models, where the cells are exposed to drug directly and the effects of sonoporation are minimal.

These findings set an important limitations on the likely approach needed when translating CAP / US / PMB into a clinical settings and also emphasize the importance of using 3D cell culture models in pre-clinical research, as relying solely on 2D cell culture models followed by animal testing and clinical trials has resulted in a 95% failure rate due to inadequate prediction of human efficacy and toxicity.


DECLARATION

I certify that this thesis which I now submit for examination for the award of Doctor of Philosophy, is entirely my own work and has not been taken from the work of others, save and to the extent that such work has been cited and acknowledged within the text of my work.

This thesis was prepared according to the regulations for graduate study by research of the Technological University Dublin and has not been submitted in whole or in part for another award in any other third level institution.

The work reported on in this thesis conforms to the principles and requirements of the TU Dublin's guidelines for ethics in research.

TU Dublin has permission to keep, lend or copy this thesis in whole or in part, on condition that any such use of the material of the thesis be duly acknowledged.

Signature  _____

Date 24/03/2023

Candidate

ACKNOWLEDGEMENTS

Throughout my PhD journey, I have received a great deal of support and assistance from countless individuals. Firstly, I would like to express my deep gratitude to my supervisor, Prof. James Curtin, for all the trust, support, and guidance I have received throughout my doctoral studies. I always appreciate him for giving me the opportunity to join his research group, and learn from him. His guidance was essential for the realisation of my research so far, he is a role model for me both as a researcher and personally. Your endless support, guidance, advice, and contribution to the project has been unequivocal. I am lucky to have James as my main supervisor that despite his busy schedule, has never failed to show his support and guidance. Words are not enough to thank him for giving me the opportunity to work with and learn from him. I also would like to thank my co-supervisor, Prof. Brijesh Tiwari, it has been an absolute pleasure to be part of the AFT group in Teagasc, Ashtown. His expertise and support are fundamental for the realisation of my project. A huge thanks to second co-supervisor, Prof. Patrick J Cullen, whose expertise was invaluable in the formulating of the work presented. I would like to thank them all for all the time they have dedicated to the project and me, which has allowed me to grow and learn so much. I've learned so much from all my supervisors, and I wouldn't be the researcher I am today if not because of you all.

I would like to show my gratitude to the Science Foundation Ireland and the Teagasc Walsh Scholar programme for the financial support for this research project.

A huge thank you to all my colleagues, friends of the cancer therapeutics lab, ESHI, staff in ESHI, FSEH, and Central Quad for all the help and support they have offered me during the past years. Thank you so much for all your help, the exchange of expertise, and the well-deserved coffee and lunch breaks. This journey has been much pleasure with you.

I would also like to thank all the lab technicians in ESHI and FSEH, especially Plunket, Tony, Tara, Claudio, and Ola, for the scientific support and the great times.

To my research friends who turned out to be friends for life : Julie, Andressa, Christeen, Gouri, Alessandro, Priya, Jack, Sam, Ekene, Hitika, Ajay, Dileshwar, Apurva, Shubham, Beatriz, Maame, Laurence, Sebnem, Shaba, Toby, thank you all for the valuable memories and support throughout my journey.

My heartfelt gratitude to my ever supportive family and teachers around the globe for believing in me from the very start. You are all my strength and motivation. I wish to extend a special thanks to my secondary school science teacher, Mrs. Sriyani, for igniting my passion and curiosity for science, and for playing a significant role in shaping the person I am today.

In special to my father, mother, mother-in-law, father-in-law, and siblings (Madushani, Thilini, Akila, and Dhanu) who always encouraged me to pursue my dream. Thank you so much for your patience and understanding, your endless love, and your support. You are always there for me, and it will be forever appreciated.

Last but not least, I could not have completed the work here presented without the support and unconditional love of my wife, Kalpani. Her understanding, patience, and cherishing of my success will always be valued.

ABBREVIATIONS

2D	Two dimensional
3D	Three dimensional
ABC	ATP-binding cassette
AgNps	Silver nanoparticles
ANOVA	Analysis of variance
ATP	Adenosine triphosphate
ATV	Atorvastatin
AuNps	Gold nanoparticles
BBB	Blood brain barrier
BBM	Bio-inspired brain matrix
BCNU	Carmustine
BM-DC	Bone marrow derived dendritic cells
BXR	Bexarotene
CAF	Cancer associated fibroblasts
CAP	Cold atmospheric plasma
CAR	Chimeric antigen receptor
CBTRUS	Central brain tumor registry of the United States
CCNU	Lomustine
CFSE	Carboxyfluorescein succinimidyl ester
CMF	Channel microfluidics
CNS	Central nervous system
COVID-19	Coronavirus
CRISPR	Clustered regularly interspaced short palindromic repeats

CSC	Cancer stem cells
DA	Dopamine
DAMP	Damage associated molecular patterns
DBD	Dielectric barrier discharge
DCF	2', 7'-dichlorofluorescein
DDP	Cisplatin
DMEM	Dulbecco's modified Eagle medium
DMF	Digital microfluidics
DMSO	Dimethyl sulfoxide
DNA	Deoxyribonucleic acid
DOX	Doxorubicin
DOX.H	Doxorubicin hydrochloride
ECM	Extracellular matrix
EDTA	Ethylenediaminetetraacetic acid
EGFR	Epidermal growth factor receptor
EMA	European medicines agency
EMT	Epithelial to mesenchymal transition
ER	Endoplasmic reticulum
ES	Electrospinning
FBS	Fetal bovine serum
FDA	Food and drug administration
FITC	Fluorescein isothiocyanate
FL-1	Fluorescence channel 1
GBM	Glioblastoma
GSC	Glioblastoma stem cells

H2DCFDA	2, 7-dichlorodihydrofluorescein diacetate
HCC	Hepatocellular carcinoma
HIF-1	Hypoxia inducible factor
HRP	Horse Radish Peroxidase
IDH	Isocitrate dehydrogenase
IL-10	Interleukin-10
IP3-RR	Inositol trisphosphate receptor
JNK	c-Jun N-terminal kinases
MAb	Monoclonal antibodies
MB	Microbubbles
MCS	Multicellular spheroids
MET	Mesenchymal epithelial transition factor receptor
MGMT	O6-Methylguanine-DNA Methyltransferase
miRNAs	MicroRNAs
MMP	Matrix metalloproteinases
MR	Magnetic resonance
mRNA	Messenger RNA
NAC	N-acetyl cysteine
NADPH	Nicotinamide adenine dinucleotide phosphate
NB	Nanobubbles
NCAD	N-cadherin
NEA	Nitroethanolamine
NGF	Nerve growth factor
NK	Natural killer
NP	Nanoparticles

OSF	Open Science Framework
PAM	Plasma activated media
PBS	Phosphate buffered saline
PDMS	Polydimethylsiloxane
PE-A	Phycoerythrin
PI	Propidium Iodide
PI3K	Phosphoinositol-3-kinase
PLA	poly-L-lactic acid
PMB	Plasma microbubble
Poly-HEMA	Poly-2-hydroxyethyl methacrylate
PtNPs	Platinum nanoparticles
RB	Retinoblastoma
REACH	Registration, evaluation, authorisation, and restriction of chemicals
REDOX	Oxidation-reduction
RNS	Reactive nitrogen species
RONS	Reactive oxygen and nitrogen species
ROS	Reactive oxygen species
RTK	Receptor tyrosine kinase
SCPL	Solvent-casting particulate leaching
SEM	Standard error of the mean
shRNA	Short hairpin RNA
TAM	Tumour-associated macrophages
TERT	Telomerase reverse transcriptase
TGF- β	Transforming growth factor beta

TME	Tumour microenvironment
TMZ	Temozolomide
TNF α	Tumor necrosis factor alpha
US	Ultrasound
US-WB	Ultrasound waterbath
UV	Ultraviolet
VEGF	Vascular endothelial growth factor
WHO	World health organization

Table of Contents

1	Introduction.....	16
1.1	Cancer.....	16
1.2	Glioblastoma	18
1.2.1	Epidemiology	19
1.2.2	Etiology	19
1.2.3	Gliomagenesis	20
1.2.4	Prognosis of GBM	20
1.3	Current treatment methods for GBM	21
1.3.1	Surgery	21
1.3.2	Radiotherapy	22
1.3.3	Chemotherapy	22
1.4	Novel treatment methods for GBM.....	24
1.4.1	Immunotherapy	25
1.4.2	Nano therapy	26
1.4.3	Novel chemotherapy	26
1.5	Plasma	27
1.5.1	Hot plasma	28
1.5.2	Cold atmospheric plasma (CAP).....	28
1.5.3	Biological activated components	29
1.5.4	Different CAP devices	30

1.5.5	Bioeffects of CAP on GBM	31
1.5.6	Molecular mechanism and selectivity of CAP.....	32
1.5.7	Pre-clinical application of CAP	34
1.5.8	Clinical application of CAP	35
1.6	Ultrasound (US)	36
1.6.1	Biological effects of US	37
1.6.2	Resisting cell death	40
1.6.3	Sustaining cell proliferation	41
1.6.4	Induced angiogenesis	42
1.6.5	Invasion and metastasis.....	43
1.6.6	Evading immune destruction	44
1.6.7	Deregulated metabolism.....	44
1.6.8	Clinical application of US.....	45
1.7	3D cell culture	48
1.8	Comparison of 2D and 3D cell culture.....	54
1.9	Comparison of 3D cell culture with animal <i>in vivo</i> models	59
1.10	Different types of 3D cell culture techniques and methods	62
1.10.1	Anchorage independent (scaffold free).....	63
1.10.2	Anchorage dependent (Scaffold Based).....	67
1.10.3	Anchorage dependent (Hydrogels)	70
1.10.4	Microfluidic devices.....	73

1.10.5	3D Bio printing	75
1.11	Advance TME models and applications.....	83
1.11.1	Cancer stem cells (CSC)	83
1.11.2	Blood–brain barrier (BBB)	84
1.11.3	Immune cells	84
1.11.4	Microbiome	85
1.11.5	GBM / normal tissue interactions	86
1.11.6	GBM organoids.....	87
1.12	Research question.....	88
1.13	Research aim and objectives	89
2	Materials and Methods.....	92
2.1	Chemicals	92
2.2	2D cell culture	92
2.3	3D cell culture	92
2.3.1	Low attachment plate method	92
2.3.2	Hanging drop plate method.....	93
2.3.3	Scaffold based method	94
2.4	Image J analysis.....	95
2.5	Growth analysis at different incubations.....	95
2.6	Growth analysis at different seeding densities	96
2.7	Spheroid cells health analysis.....	96

2.8	Pin to plate system.....	97
2.9	Ultrasound probe device.....	99
2.10	Plasma microbubble (PMB) device.....	100
2.11	Ultrasound water bath (US-WB) device.....	102
2.12	CAP and US treatments.....	103
2.12.1	CAP treatment.....	103
2.12.2	PMB treatment	104
2.12.3	US-WB treatment.....	104
2.12.4	US probe treatment	104
2.12.5	CAP and US combination	105
2.13	AlamarBlue cell viability assay.....	106
2.14	CellTiter-Glo® 3D cell viability assay.....	107
2.15	Live / Dead cell staining using Propidium Iodide (PI).....	107
2.16	PI staining and confocal imaging	108
2.17	3D rendering.....	108
2.18	Chemical analysis of reactive species in cell culture medium	108
2.19	Inhibitor studies	109
2.19.1	ROS scavenger assays – NAC	109
2.19.2	Sodium pyruvate	110
2.19.3	Hydrogen peroxide scavenger assay - Catalase	110
2.19.4	E-64.....	111

2.19.5	SP600125	111
2.19.6	zVAD-fmk.....	111
2.20	Detect ROS production using H2DCFDA Assay.....	112
2.21	Tumour sphere sonoporation assay	113
2.22	TMZ and DOX induced glioma cytotoxicity	114
2.23	DOX sonoporation analysis.....	114
2.24	Mitochondrial membrane potential measurement.....	115
2.25	CFSE Cell Proliferation Assay.....	116
2.26	Statistical analysis	117
2.27	Data availability	117
3	Optimization of three-dimensional (3D) <i>in vitro</i> cell culture models to enhance glioblastoma research.....	120
3.1	Rationale.....	120
3.2	Results and discussion.....	121
3.2.1	3D cell culture	121
3.2.2	Effects of different growth media	125
3.2.3	Optimization of low attachment plate method.....	127
3.2.4	Optimization of hanging drop plate method	133
3.2.5	Optimization of 3D scaffolds based method.....	139
3.2.6	Analysis of 3D cell viability	144
3.3	Conclusion.....	147
4	Plasma induced ROS dependent cytotoxicity in glioblastoma 3d tumour spheres	149

4.1	Rationale.....	149
4.2	Results and discussion.....	150
4.2.1	Pin-to-plate discharge presents cytotoxicity towards GBM cells in a time / dose-dependent manner	150
4.2.2	Effect of CAP treatment on tumour sphere cell membrane damage.....	156
4.2.3	CAP induced morphological changes	160
4.2.4	Quantification of nitrite and hydrogen peroxide on medium.....	163
4.2.5	ROS production in U-251 MG tumour spheres	165
4.2.6	Pin-to-plate presents RONS dependent cytotoxicity	166
4.2.7	Catalase as a hydrogen peroxide scavenger	169
4.3	Conclusion.....	172
5	Ultrasound mediated drug diffusion, uptake, and cytotoxicity in GBM 3D tumour sphere model and synergistic effects of US and CAP.....	174
5.1	Rationale.....	174
5.2	Results and discussion.....	175
5.2.1	US probe presents cytotoxicity towards GBM and epidermoid carcinoma cells in a time / dose-dependent manner.	175
5.2.2	Effect of US treatment on tumour sphere cell membrane damage	184
5.2.3	Tumour spheres morphological changes induced by US probe.....	185
5.2.4	Ultrasound presents RONS-dependent cytotoxicity	188
5.2.5	Effect of US on TMZ delivery in human GBM and epidermoid carcinoma cell models	192

5.2.6	Effect of US on DOX delivery in human GBM and epidermoid carcinoma cell models	195
5.2.7	Cold atmospheric plasma and ultrasound presents synergistic cytotoxicity towards GBM and epidermoid carcinoma	202
5.2.8	US and CAP promotes synergistic effect dependent of apoptosis, JNK, caspases and cysteines	207
5.2.9	Mitochondrial membrane depolarisation and cell proliferation assay	211
5.3	Conclusion.....	218
6	Synergistic cytotoxicity effect of ultrasound and plasma microbubble in glioblastoma 3D tumour sphere model.....	221
6.1	Rationale.....	221
6.2	Results and discussion.....	222
6.2.1	US-WB presents cytotoxicity towards GBM and epidermoid carcinoma 222	
6.2.2	PMB presents cytotoxicity towards GBM and epidermoid carcinoma...	226
6.2.3	PMB and US presents synergistic cytotoxicity towards GBM and epidermoid carcinoma.....	229
6.2.4	Effect of US and PMB treatment on tumour sphere cell membrane damage 232	
6.2.5	US and PMB induced morphological changes	235
6.2.6	ROS production in U-251 MG tumour spheres	239
6.2.7	PMB presents RONS - dependent cytotoxicity.....	242
6.2.8	Catalase as hydrogen peroxide scavenger.....	246

6.2.9	Mitochondrial membrane potential analysis	250
6.3	Conclusion.....	253
7	General Discussion	255
8	Conclusion and future work.....	270
8.1	Conclusion.....	270
8.2	Future work / new research questions	273
8.2.1	First new research question.....	273
8.2.2	Second new research question	275
8.2.3	Third new research question	275
8.2.4	Fourth new research question.....	276
9	Appendix.....	359
9.1	Appendix I All the Data and statistical outcomes	359
9.2	Appendix II First Pages of Peer-reviewed Publications.....	359
9.3	Appendix II Additional Publications and Outputs not Peer-reviewed	365
9.4	Appendix III Professional Development	386

LIST OF FIGURES

Figure 1. The hallmarks of cancer. Core hallmarks and recently proposed emerging hallmarks and enabling characteristics	17
Figure 2: Structures of different chemotherapeutic alkylating agents for GBM treatment	24
Figure 3: A summary of the current understanding of molecular mechanisms underlying the effectiveness of CAP treatment.	34
Figure 4: Ultrasound targets the hallmarks of cancer	39
Figure 5: Acoustically sensitive nano-platforms include nanobubbles, nanodroplets, micelles, nano-emulsions, liposomes, colloid NPs, viral vectors, and antibodies	39
Figure 6: Components of GBM TME, consists of cellular, non-cellular and extracellular materials.	49
Figure 7: Structure of multicellular 3D spheroid	52
Figure 8: Different anchorage dependent and independent methods to develop 3D multicellular tumour spheroids.	63
Figure 9: Anchorage independent methods available for multicellular tumour spheroids formation	64
Figure 10: Anchorage dependent methods and specialized 3D culture platforms available for multicellular tumour spheroids formation.....	70
Figure 11: Dielectric barrier discharge (pin) system	98
Figure 12: Ultrasound probe system	100
Figure 13: A schematic diagram of the plasma-bubble generator	101
Figure 14: A schematic diagram of the US-WB used, illustrating the treatment position of the 96-well plate as well as the positioning of the transducers and power generator.	102

Figure 15: Scheme of the combination of cold atmospheric plasma with ultrasound .	106
Figure 16: Development of U-251 MG human GBM 3D in vitro cell culture model .	122
Figure 17: Development of U-251 MG, U-87, A-172 and A431 3D in vitro cell culture models using low attachment plate, hanging drop plate and scaffold based method ...	123
Figure 18: Development of U-251 MG human GBM 3D in vitro cell culture model in different media compositions	126
Figure 19: Development of human GBM 3D in vitro cell culture models using low attachment plate method	130
Figure 20: Development of A431 human epidermoid carcinoma 3D in vitro cell culture models using low attachment plate method	131
Figure 21: Development of human GBM 3D in vitro cell culture model using hanging drop plate method.....	136
Figure 22: Development of human epidermoid carcinoma 3D in vitro cell culture model using hanging drop plate method.	137
Figure 23: Development of human GBM 3D in vitro cell culture model using cellusponge 3D scaffolds..	141
Figure 24: Development of human epidermoid carcinoma 3D in vitro cell culture model using cellusponge 3D scaffolds.....	142
Figure 25: TMZ induced cytotoxicity in U-251 MG, U-87 MG and A-172 tumour spheres with 6 days post treatment incubation.....	146
Figure 26: U-251 MG CAP treatment.....	155
Figure 27: U-251 MG CAP treatment with and without sodium pyruvate medium ...	156
Figure 28: PI uptake in pin-to-plate treated U-251 MG tumour spheres. PI uptake was measured by flow cytometry and used as an indicator of cell death.....	158
Figure 29: PI uptake in pin-to-plate treated U-251 MG tumour spheres	159

Figure 30: U-251 MG and A431 tumour spheres size (diameter) and cell count analysis followed by CAP treatment.....	162
Figure 31: Measurement of H ₂ O ₂ and NO ₂ ⁻ concentrations.....	164
Figure 32: ROS production in U-251 MG tumour spheres.....	165
Figure 33: U-251 MG single and multiple CAP treatment with and without NAC in with and without pyruvate media.....	168
Figure 34: Titration of NAC using 0.5 mM, to 8 mM of NAC.	169
Figure 35: PI uptake in CAP treated U-251 MG tumour spheres in the presence and absence of catalase.....	171
Figure 36: GBM cell line U-251 MG and epidermoid carcinoma cell line A431 US probe treatment.....	177
Figure 37: U-251 MG tumour sphere single and multiple US treatments with different incubations.	181
Figure 38: PI uptake in ultrasound probe treated U-251 MG tumour spheres.....	184
Figure 39: U-251 MG tumour sphere morphology and size (diameter) variation analysis followed by US treatment	187
Figure 40: U-251MG single, double and triple US treatment with and without NAC..	190
Figure 41: TMZ cytotoxicity analysis with and without US (3 min) combination using U-251 MG and A431 2D cells and 3D tumour spheroids.....	192
Figure 42: DOX cytotoxicity analysis with and without US (3 min) combination using U-251 MG and A431 2D cells and 3D tumour spheres.....	195
Figure 43: Ultrasound enhanced penetration of DOX.H fluorescence analysis using flow cytometry of U-251 MG and A431 tumour spheres.....	200

Figure 44: Synergistic effect of CAP and US (1, 3, 10 and 20 min) treatments on U-251MG GBM 3D tumour spheres with 96 h of post treatment incubation.....	204
Figure 45: Synergistic effect of CAP and US (1, 3, 10 and 20 min) treatments on A431 epidermoid tumour spheres with 96 h of post treatment incubation.....	206
Figure 46: Inhibitor studies of 320 s CAP and different US treated U-251 MG tumour spheres with 96 h of post treatment incubation.....	210
Figure 47: Mitochondrial membrane depolarisation in U-251 MG tumour spheres analysis by JC-1 dye and flow cytometry.	213
Figure 48: Histograms of CFSE proliferation of U-251 MG tumour spheres with CAP and US treatments.	217
Figure 49: <i>U-251 MG and A431 tumour sphere single and multiple US-WB treatments (US treatment time from 3 to 10 min and US frequency of 25 kHz and 45 KHz) with different incubations</i>	225
Figure 50: U-251 MG and A431 tumour sphere single and multiple PMB treatments with different incubations	228
Figure 51: High speed image of a discharge forming PMB and plasma chemistry in the bubble.....	229
Figure 52: Synergistic effect of US and PMB treatment on U-251 MG tumour sphere with different incubations	231
Figure 53: PI uptake in US and PMB treated U-251 MG tumour spheres. PI uptake was measured by flow cytometry and used as an indicator of cell death.....	234
Figure 54: U-251 MG tumour sphere morphology and size (diameter) variation analysis followed by US and PMB treatments.....	238
Figure 55: ROS production in U-251 MG tumour spheres.....	241

Figure 56: U-251 MG tumour sphere multiple US and PMB treatment with and without NAC and sodium pyruvate.....	245
Figure 57: PI uptake in PMB treated U-251 MG tumour spheres in the presence and absence of catalase.	249
Figure 58: Mitochondrial membrane depolarisation in U-251 MG tumour spheres analysis by JC-1 dye and flow cytometry.	252
<i>Figure 59:</i> A schematic of the proposed 3D microbiome model.	274
Figure 60: A schematic of the proposed standardize vascular monolayer model.....	277

LIST OF TABLES

Table 1: List of the most common ROS and RNS species found in normal cells	30
Table 2: Clinical trials combining ultrasound and microbubbles / nanomaterials.....	46
Table 3: The current 3D cell culture systems for cancer research applications: Key Strengths and Weaknesses	53
Table 4: Comparison of 2D and 3D cell culture methods.....	57
Table 5: Different types of 3D cell culture techniques and their applications, outcomes in glioma research	78
Table 6: Comparison of different 3D cell culture techniques and equipments, highlighting their respective merits and demerits for both 3D tumour model production and applications.	80
Table 7: IC ₅₀ Values and ranges of, U-251 MG single and multiple CAP treatment with, without NAC in with and without pyruvate media	167
Table 8: IC ₅₀ Values and ranges of, U-251 MG single and multiple US treatment with different incubations.....	180
Table 9: IC ₅₀ values and ranges of, U-251 MG single and multiple US treatment with different incubations with and without NAC:.....	190

CHAPTER 1 – INTRODUCTION

Part of this chapter has been published in Trends in Cancer journal. (See Appendix II – Peer-reviewed)

- **Wanigasekara, J.**, de Carvalho, A.M.A., Cullen, P.J., Tiwari, B., Curtin, J.F. Converging technologies: targeting the hallmarks of cancer using ultrasound and microbubbles. Trends Cancer. 2021, 7(10):886-890, PMID: 34426143, DOI: [10.1016/j.trecan.2021.07.004](https://doi.org/10.1016/j.trecan.2021.07.004)

Part of this chapter has been published in Drug Discovery Today journal. (See Appendix II – Peer-reviewed)

- **Wanigasekara, J.**, Cullen, P.J., Bourke, P., Tiwari, B., Curtin, J.F. Advances in 3D culture systems for therapeutic discovery and development in brain cancer. Drug Discov Today. Volume 28, Issue 2, 2023, 103426, ISSN 1359-6446, <https://doi.org/10.1016/j.drudis.2022.103426>.

Part of this chapter has been published in TRResearch magazine (See Appendix II - Non peer-reviewed)

- **Wanigasekara, J.**, Tiwari, B. and Curtin, J.F. 3D mammalian cell culture models in toxicology testing. TRESEARCH | spring 2020 | Volume 15: Number 1, 2020, DOI: [10.21427/6sx4-wq76](https://doi.org/10.21427/6sx4-wq76).

1 Introduction

1.1 Cancer

The World Health Organization (WHO) defines cancer, also known as neoplasm and malignant tumour, as a large group of diseases that can start in almost any organ or tissue of the body as an uncontrolled and abnormal cell proliferation that may be influenced by a variety of internal and external environmental factors [1]. In some instances, a cancer cell may turn malignant and extend beyond its usual boundaries to infiltrate adjoining parts of the body and / or other organs; this process is known as metastasis [2]. Widespread metastasis are the leading cause of cancer related mortality and a significant obstacle to improving global life expectancy [2]. Therefore, prevention, early detection, accurate diagnosis, and successful treatment are essential to increasing the life expectancy of individuals diagnosed with cancer [1]. According to GLOBOCAN cancer statistics survey in 2020, estimated 19.3 million new cancer diagnoses and about 10 million deaths ranking cancer the second leading cause of mortality worldwide [3, 4]. Breast, lung, and prostate cancers were the most frequently diagnosed, and lung, liver, and stomach cancers were the leading causes of cancer related mortality worldwide, while mesothelioma, pancreatic, and brain cancers had the lowest five-year survival estimates [3].

The hallmarks of cancer conceptualization is a heuristic approach that is used to condense the tremendous complexity of cancer phenotypes and genotypes into a tentative collection of underlying principles [5]. Hanahan and Weinberg (2000), have first proposed the involvement of six distinct fundamental hallmarks acquired by cancer cells. They include sustaining proliferative signaling, evading growth suppressors, resisting cell death, enabling replicative immortality, inducing angiogenesis, and activating invasion and

metastasis [6]. In 2011, it was suggested to include two emerging hallmarks, deregulating cellular energetics and evading immune destruction, and two enabling traits, genomic instability and tumour promoting inflammation [7]. Hanahan classified these enabling and emerging traits as core hallmarks (Figure 1) in 2022 [5] and advocated the inclusion of two additional emerging hallmarks: phenotypic plasticity unlocking and senescent cells, and two new enabling hallmarks: non-mutational epigenetic reprogramming and polymorphic microbiomes (Figure 1). These four hallmarks, together with the previously suggested ones, are crucial for understanding the transition of cells to the neoplastic stage, hence shedding light on cancer biology and treatment targets [5-7].

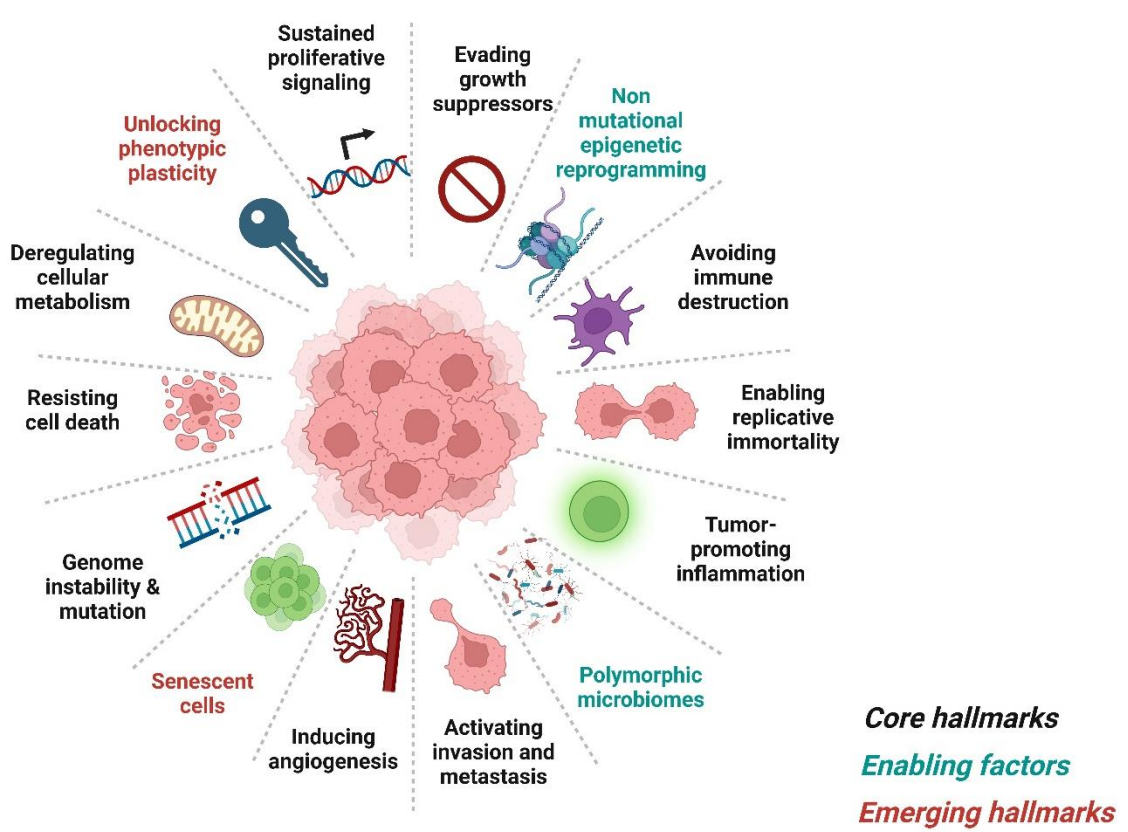


Figure 1. The hallmarks of cancer. Core hallmarks and recently proposed emerging hallmarks and enabling characteristics involving “unlocking phenotypic plasticity,” “non-mutational epigenetic reprogramming,” “polymorphic microbiomes,” and “senescent cells.” (Figure created with BioRender)

1.2 Glioblastoma

Brain cancers can be divided into two types, primary and secondary brain cancer. Primary brain cancer originates within brain cells, forms in the central nervous system (CNS), and usually does not metastasize to the outside of the CNS [8, 9]. Secondary brain cancers are originated and metastasize from external to the CNS, such as the lung, skin, breast, colon, and kidney. Secondary brain cancers are the most common, while primary brain cancers are more lethal [10, 11]. Primary brain cancers can be classified further as gliomas and nongliomas (meningiomas, medulloblastomas) [11, 12]. Gliomas are developed from glial cells, including astrocytes, oligodendrocytes, and ependymal cells or a mix of the above. Based on molecular diagnosis, histology, and immunohistochemistry, the fifth edition of the WHO classification divides gliomas into six groups: adult-type diffuse glioma; pediatric-type diffuse low-grade glioma; pediatric-type diffuse high-grade glioma; circumscribed astrocytic gliomas; glioneuronal and neuronal tumours; and ependymomas [13]. The majority of primary brain tumours are adult-type diffuse gliomas, which can be subdivided into astrocytoma, Isocitrate dehydrogenase (IDH) - mutant; oligodendroglioma, IDH-mutant and 1p/19q-codeleted; and glioblastoma, IDH-wild type; with the latter being the most common and malignant brain tumour [10, 13, 14]. Glioblastoma (GBM) is an adult-type diffuse grade 4 glioma, IDH wild type and is the most common, aggressive, fatal, highly vascularized, malignant primary brain tumour in adults [13]. GBM have at least one of the following characteristics: microvascular proliferation, necrosis, telomerase reverse transcriptase (TERT) promoter mutation, epidermal growth factor receptor (EGFR) gene amplification, or gain of entire chromosome 7 and loss of complete chromosome 10 [+7/10] [15].

1.2.1 Epidemiology

According to the most recent “central brain tumour registry of the United States (CBTRUS) statistical report”, the average annual age-adjusted incidence rate of all malignant and non-malignant brain and other CNS tumours was 24.25 per 100,000 between 2014 and 2018. The total rate was greater in females than in males (26.95 versus 21.35 per 100,000). The most often occurring malignant brain and other CNS tumour was GBM (14.3% of all tumours and 49.1% of malignant tumours), was more prevalent in males while the most common non-malignant tumour was meningioma (39.0% of all tumours and 54.5% of non-malignant tumours), was more common in females [16]. In comparison to other continents, Europe has the highest GBM incidence and mortality rates, accounting for around 65% of all primary brain tumours with a poor 10% five-year survival rate [17]. Treatment options for GBM remain very limited, and it has a low survival rate of less than 1 year for many patients and only about 6.8% survive beyond 5 years, which varies by age at diagnosis and by sex [10, 12, 18, 19].

1.2.2 Etiology

There is currently a lack of clarity on the risk factors related with GBM [20]. Prior radiation exposure, lower sensitivity to allergies or atopic disease (e.g., asthma, eczema, and psoriasis), immunological factors and immune genes, and certain nucleotide polymorphisms, detected by genome-wide association are all variables that have been linked to an increased chance of developing GBM [21, 22]. There is no significant evidence linking GBM with aspects of lifestyle, such as smoking, alcohol consumption, drug usage, or dietary exposure to nitrous compounds [21]. The resectability of the tumour, its location, size, and multifocality, as well as advanced age, comorbidities, and the patient's overall condition, are all prognostic variables that impact the survival rate of GBM patients [21, 22].

1.2.3 Gliomagenesis

Gliomagenesis is a multicomponent process that involves various genetic mutations that influence numerous molecular pathways. With the ongoing advancement of sequencing technology and high-throughput gene editing, it is now feasible to evaluate the genetic and epigenetic alterations in tumours [23]. In 2009, The Cancer Genome Atlas Network (TCGA) used gene sequencing to analyse the alterations in 601 different types of tumour-associated genes in more than 200 glioma samples [23, 24]. TCGA analysis of DNA methylation, DNA copy number and other genetic mutations in GBM revealed the core signalling pathways, and their commonly dysregulated regulatory functions – the activation of the receptor tyrosine kinase (RTK)/RAS/phosphoinositol-3-kinase (PI3K) pathway, inhibition of p53, and retinoblastoma (RB) signalling pathways [23, 25]. In glioma patients, at least one aberrant pathway among the RTK/PI3K/AKT, TP53 and RB1 signaling pathways was found in 80-90% of GBM, which resulting in uncontrolled cell proliferation, improved cell survival and escape of cell-cycle checkpoints, senescence and apoptosis, as well as cell invasion and angiogenesis [23, 25, 26]. GBM mutations may not impact a single pathway, but rather may be the result of alterations in many pathways [25, 26], which increases the difficulty of developing GBM therapeutics.

1.2.4 Prognosis of GBM

Patient prognosis remains poor and largely unchanged over the last 30 years due to the limitations of existing therapies such as surgical resection, followed by concurrent radiation therapy and chemotherapy such as temozolomide (TMZ) [19, 27].

The majority of therapies fail during clinical trials due to inefficient treatment methods and imperfect pre-clinical models that limit our ability to predict efficacy and toxicity in humans. This is particularly evident with GBM with no successful therapy that significantly improves survival since the introduction of TMZ 24 years ago [10, 12, 18].

GBM treatment is also hampered by barriers such as the blood brain barrier (BBB). The novel combinational treatments and active targeting techniques needed to overcome the tight junction, metabolic, and immunological barriers for effective drug delivery to the brain [28, 29]. Therefore, it is crucial to identify rational combinations between established treatments and novel technologies aiming, for example, at inhibition of cell proliferation, induction of cytotoxicity and apoptosis, or inhibition of several signal transduction pathways for efficient *in vivo* GBM diagnosis, prognosis, and treatment [21].

1.3 Current Treatment methods for GBM

GBM treatment often consists of maximal tumour resection, followed by radiation and chemotherapy (either alone or in combination) [30]. Currently, there is no standard of care for the treatment of recurrent GBM; instead, treatment is depending on new onset of recurrence, time of diagnosis, O-6-methylguanine-DNA methyltransferase (MGMT) methylation, location, the patient's performance condition and their age [31].

1.3.1 Surgery

Surgical excision is the mainstay of conventional therapy and the most effective strategy to improve GBM survival [20]. Surgery is recommended for the majority of patients because it reduces the bulk of the tumour, which in turn alleviates pressure that is produced by the brain tumour, and it also increases the likelihood of survival by around 15 months [32]. However, surgical resection may have some palliative effects, such as seizure control and reversal of neurological deficit [20]. GBMs that are newly diagnosed has better survival (7 months) by complete surgical resection in comparison to biopsy or subtotal resection depending on the region affected. However, the majority of tumours

reoccurs within 8 - 10 months of initial resection [20, 32, 33]. Even with breakthroughs in surgical resection, individuals with GBM have a poor prognosis, with a median survival of 14–15 months [34]. Consequently, resection surgery is paired with chemotherapy and/or radiotherapy [35].

1.3.2 Radiotherapy

Radiotherapy is often administered following surgery to eradicate any residual tumour cells, thereby increasing the life expectancy of GBM patients [20]. Doses of radiotherapy will be determined based on the tumour type and conditions of patients [36]. Radiotherapy, on the other hand, has risks and limitations due to the invasive nature of GBM, which includes radiation necrosis, radio-resistance in some tumours, and radiation-induced permanent neuronal damage [20, 36]. Both stereotactic radiosurgery and brachytherapy have been shown to be effective therapies for recurrent GBM; however, their roles in the treatment of newly diagnosed GBM remain unclear [20]. Gamma Knife radiosurgery, a type of stereotactic radiosurgery applied for recurrent GBM, does not require open resection while delivering a high dosage of radiation to deep tumours, hence reducing radiation-induced necrosis to surrounding brain tissue [32, 37].

1.3.3 Chemotherapy

The current GBM chemotherapy TMZ (Figure 2), an European medicines agency (EMA) and food and drug administration (FDA) approved DNA alkylating agent with great CNS penetration due to its diminutive size (194 Da), pH stability, and lipophilicity [20]. It was approved in 1999 and is often used in combination with radiation as a standard treatment for GBM patients [20].

TMZ significantly improved GBM patient survival and increased patient median survival rate from 12 to 14 months [38]. TMZ effects are time-dependent, with multiple doses of

TMZ being more effective than a single treatment [39, 40]. The daily dosage begins at 75 mg/m² along with 6 weeks of radiotherapy, followed by 6 adjuvant cycles of 150 – 200 mg/m² dose for 1-5 days [41]. However, there are limitations, as extended TMZ therapy leads to resistance and poor response to subsequent treatments, which is connected with the expression levels of DNA alkylating proteins, DNA repair enzymes, and a multiple molecular events [38, 39, 41, 42]. Higher dosages of TMZ are linked with an increase in toxicity, a decline in function and quality of life, and a number of adverse effects, including myelotoxicity, DNA damage, ulceration, nausea, vomiting, and fatigue [38, 42, 43]. Overexpression of MGMT, also known as O6-methylguanine-DNA methyl transferase, a DNA repair enzyme, causes TMZ treatment resistance [17, 44, 45]. Methylation of the MGMT promoter (seen in 30–50% of GBM) silences the MGMT gene, hence reducing the capacity of tumour cells to repair the damage caused by TMZ [10, 31].

Other than TMZ, many chemotherapeutic alkylating drugs, including carmustine (BCNU) (Figure 2) and lomustine (CCNU) (Figure 2), can induce cross-linking between DNA strands and causes damage in cells which then inhibits cell cycle progression leading to cell death [31]. These drugs demonstrated some benefit and have been clinically employed in the treatment of GBM [20]. However, BCNU and CCNU are very cytotoxic, and therapy with these drugs results in the early development of resistance, limiting their advantages and causing numerous side effects [20, 36, 46].

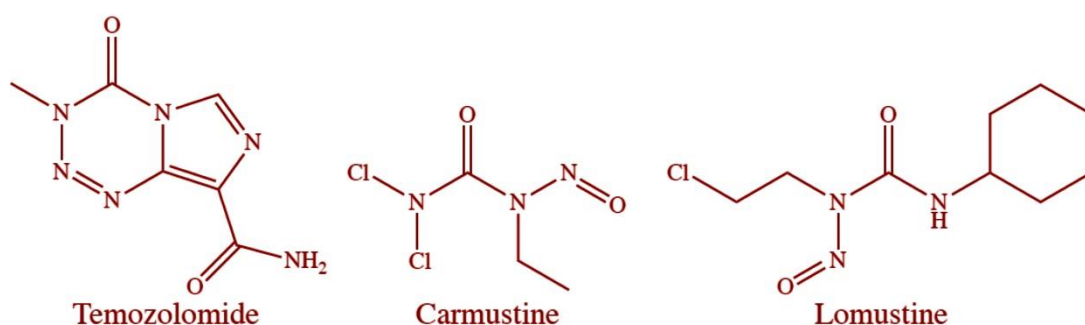


Figure 2: Structures of different chemotherapeutic alkylating agents for GBM treatment (Figure created with BioRender).

The combined therapy options are frequently shown to be ineffective since residual cells has the tendency to become radio and chemo resistant, with a 90% recurrence rate [20, 47]. Despite recent advances in advance three dimensional (3D) cell culture models, molecular biology and current combination strategies, GBM remains the most difficult to treat, with an extremely poor survival rate, due to the location of the disease, the existence of the BBB, GBM stem cells, multidrug resistance, its complex heterogeneity, and aggressive infiltrative growth [20, 48-50]. GBM stem cell (GSC) have been linked not only to infiltration and proliferation, but also to chemotherapy resistance, making them even another hurdle to conquer. This overall results in a poor prognosis, with therapy resistance and tumour relapses [32, 36, 51]. However, the limitations of conventional treatment in GMB therapy haven't been overcome and novel efficient therapeutic methods with low side effects are still urgently needed.

1.4 Novel treatment methods for GBM

Novel treatment strategies such as immune therapy [52], nano therapy [53], oncolytic viral therapy [32], hyperthermia [54], molecular targeted therapy (such as hypoxia-

inducible factor (HIF)-1 inhibitors)[55], tumour-treating fields [56], epigenetic therapy [57], hypoxia-selective drugs [58] and chemotherapeutic prodrugs [59] have also been investigated for GBM treatment. We are investigating the possibility of non-thermal techniques, such as cold atmospheric plasma (CAP) [60] and ultrasound (US) [28], for GBM therapy during this study.

1.4.1 Immunotherapy

Immunotherapy has ability to produce tumour specific immune response to selectively eliminate tumour cells [61]. This therapeutic strategy comprises passive treatments, such as monoclonal antibodies, adoptive cell transfer, chimeric antigen receptor (CAR) T-cell therapy, viral vector therapies, and cytokine-mediated therapies; active strategies, such as vaccines [41, 52, 61]. Immune checkpoint inhibitors are an additional class of drugs that boost anti-tumour immune responses [57]. Monoclonal antibodies (MAbs) can be used to induce cytotoxicity towards cells by their immune mediated mechanisms and their specific target effects [52]. Different types of MAbs have been investigated as potential GBM therapy, including conjugated/unconjugated; human/ murine/primate MAbs, either alone or in combination with chemotherapy or radiotherapy [41, 52]. However, effective immunotherapy implementation for GBM remains difficult. Phase III clinical trials, including those with checkpoint inhibitors [61, 62], the vaccine-based therapy rindopepimut [63], and the viral therapy Toca 511 [64], all proved unsuccessful. Nevertheless, several novel vaccine- and virus-based therapeutics, as well as CAR T cell-based therapy and combination methods using checkpoint inhibitors, are being research [61]. It is still feasible to implement immunotherapy for GBM treatment in the future, but various challenges need to be addressed. These challenges include antigen escape, tumour heterogeneity, tumour microenvironment (TME), drug delivery

strategies, patient selection based on tumour genetics, and the use of multimodality treatment approaches [61].

1.4.2 Nano therapy

Nano therapy provides benefits over conventional drug formulations. As a result, numerous nano-carriers have been employed in brain tumour targeted techniques [65, 66]. Nano-carriers such as liposomes, polymeric micelles, nano crystals, dendrimers, and nanoparticles (NP) [67-69] have been utilised in brain tumour targeted approaches because they protect drugs from degradation, increase drug solubility, enhance bioavailability, drug carrying capacity, and provide potential pathways to bypass drug resistance mechanisms [65, 68]. It is utilized to deliver drugs to specific areas of the brain while improving permeability [53]. Researchers have investigated gold nanoparticles (AuNps) due to its biocompatibility, high stability, and lower cytotoxicity [70, 71]. AuNps with a diameter of 20 nm have been reported to be optimal for crossing the BBB and are selective for cancer cell lines, turning them a promising therapy for GBM [70-72]. It has also been shown that silver nanoparticles (AgNps) influence metabolic activity, cell morphology and cell viability. They demonstrated selectivity for GBM and the ability to traverse the BBB [73, 74].

1.4.3 Novel chemotherapy

Prodrugs are a valuable source of anticancer drugs because of the potential for reduced toxicity and increased activity [75]. There are about 25% of plant-derived drugs that are clinically used [76]; while more than 60% of drugs with anti-cancer activity originated from plants [77]. These natural compounds have demonstrated efficacy as anti-inflammatory, anti-depressant, anti-microbial as well as anti-cancer agents [78]. Several research studies have been published over decades for the suitability and

effectiveness of a various bioactive compounds against cancer [79]. The various anticancer activities include anti-proliferative, pro-apoptotic, anti-metastatic, anti-angiogenic effects, as well as autophagy regulation, induced apoptosis, reverse multidrug resistance, immunity balance, and enhanced chemotherapy both *in vitro* and *in vivo* [80, 81].

1.5 Plasma

Plasma is one of the four fundamental states of matter that is often a form of ionized gas with electrons, ions, radicals, oxygen and nitrogen species, UV radiation, electromagnetic fields, and accounts for the majority of the known universe's matter [82, 83]. Plasma is classified in to thermal and non-thermal plasma and the temperature is determined by the thermal motions of electrons and heavy particles, including atoms and ions [84]. When the density of particles in a thermal plasma is high as a result of intense collisions between electrons and heavier particles, all particles approach thermal equilibrium. The temperature of such plasma exceeds 3000 °C [82, 84, 85]. Its early stage of biomedical applications is focus on the heat and high temperature of thermal plasma for tissue removal, sterilization, and cauterization [86].

Nevertheless, when the atmospheric pressure plasma discharge is rapid, the electrons and heavy particles are in thermal non-equilibrium, whilst the ions and neutral species maintain a low temperature, resulting in the so-called CAP [84, 85]. CAP operate at or near room temperature and so it can use for biological tissues without causing thermal damage [82, 85]. Due to its distinct properties, CAP has been exploited in a variety of biomedical applications, most notably as a promising anti-cancer modality, with studies demonstrating its cytotoxicity and selectivity potential [60, 82, 85, 87, 88].

1.5.1 Hot plasma

Hot plasmas, also known as high temperature / thermal plasmas, are frequently utilized in sterilizing, blood coagulation, tissue ablation, and tumour treatment, among other applications. Thermal plasma devices use high temperatures and kinetic energy to coagulate, cut, or ablate tissue surfaces [89, 90]. Since 2004, the PlasmaJet technology has been utilized in clinical surgery to successfully ablate and coagulate a tissue surface utilizing a small size, high-thermal and high-kinetic argon PlasmaJet [91]. The PlasmaJet induces slight thermal tissue damage by causing the production of a filmy coagulum [92]. It has proven to be safe and effective in plastic surgery, hepatic surgery, gastrointestinal, orthopaedics, and thoracic surgery [93]. PlasmaJet and other thermal plasma devices have been studied as safe and effective treatments for tumours that are untreatable by surgery [91, 94, 95].

1.5.2 Cold atmospheric plasma (CAP)

CAP is a partially ionized gas that contains charged particles, reactive oxygen and nitrogen species (RONS) (including hydroxyl, hydrogen peroxide, superoxide, hydroxyl radical, singlet oxygen, ozone, nitric oxide, nitrogen dioxide, dinitrogen tetroxide, nitrogen trioxide, nitrous oxide, and peroxyxynitrite), excited atoms, electrons, free radicals, UV photons and electromagnetic fields [96-98].

It is produced at atmospheric pressure by mixing UV light with oxygen, nitrogen, ozone, water and helium, under an electrical discharge [99]. CAP has been studied as a possible therapy strategy in a variety of fields. Cancer treatment [100], sterilization [101], wound healing [102], blood coagulation [103], and viral annihilation are among known biological uses of CAP [104]. CAP has also been researched as a unique approach to improve cell transfection and stimulate cell proliferation [103]. Research is on-going to

explore the combination of CAP with other cancer therapies, including nanotechnology based, radio and chemo therapy [59, 72, 85, 105, 106].

1.5.3 Biological activated components

CAP generates a distinct physical and chemical environment that activates both short- and long- lived reactive nitrogen species (RNS), such as peroxynitrite (ONOO^-), nitric oxide radicals (NO), excited N_2 , N_2^+) and reactive oxygen species (ROS), such as hydroxyl radicals (OH), oxygen atoms (O), oxygen negative ions (O_2^-), $^*\text{OH}$, $^*\text{O}_2^-$, O_3), photons as well as generation of heat, pressure gradients, charged particles, and electrostatic and electromagnetic fields [107, 108], many of which are known to induce biological effects. Between those species oxygen (O_2^* , O_2^- , and O_3 , $\text{OH}\cdot$, H_2O_2 , HO_2) and nitrogen species (N_2^+ , NO) plays a key role in CAP induced cytotoxicity and apoptotic effects [60, 85, 87]. Table 1 depicts a list of the most common ROS / RNS found in a cells. The modulation of the apoptotic machinery by nitric oxide (NO) serves as a critical mechanism in tumourgenesis, where NO acts as an intercellular messenger [109]. Peroxynitrite (ONOO^-) a powerful oxidant, which occurs naturally by the combine of superoxide (O_2^-) and NO [108], can trigger lipid peroxidation reactions and aid to defend against infection during inflammation [108] whereas ROS can cause DNA damage and promote apoptosis by activating tumour necrosis factor (TNF) / nerve growth factor (NGF) - family cell death receptors [110]. These high flux of ROS also have significant impact on the inactivating fungi, virus and bacteria [107, 111]. The production of ROS and RNS, as well as various hypohalous acids, specially hypochlorites, play an important role in oxidative bursts, which are used in the clearance of tumour cells by phagocytic immune cells such as neutrophils, macrophages, and monocytes [112]. The synergistic effect between NO_2^- , NO_3^- and H_2O_2 was already reported to induce cytotoxicity and apoptosis in cancer cells [60, 113].

Table 1: List of the most common ROS and RNS species found in normal cells

Reactive oxygen species (ROS - radicals)		Reactive oxygen species (ROS - non radicals)		Reactive nitrogen species (RNS)	
Hydroxyl	OH [•]	Hydrogen peroxide	H ₂ O ₂	Nitrous Oxide	N ₂ O
Superoxide	O ₂ ^{•-}	Ozone	O ₃	Nitrogen dioxide	NO ₂ [•]
Nitric Oxide	NO [•]	Singlet oxygen	¹ O ₂	Nitrous acid	HNO ₂
Peroxyl	RO ₂ [•]	Hypochloric acid	HOCl	Peroxynitrite	ONOO ⁻
Lipid peroxy	LOO [•]	Lipid peroxide	LOOH	Nitroxyl anion	NO ⁻

1.5.4 Different CAP devices

Devices that generate CAP can be divided into: direct-discharge (i.e. dielectric barrier discharge, pin to plate system), indirect-discharge (i.e. plasma jets, pens, torches) and hybrid discharge [97, 114]. With an indirect discharge, the active plasma species are carried by a gas flow originating from the primary discharge arc [84]. In a direct discharge, living tissue or cells are one of the electrodes and is an active part of the discharge [84]. CAP induced cancer cellular cytotoxicity has been demonstrated previously by using different direct and indirect discharge devices such as plasma jet [115-119], micro-sized devices [120], dielectric barrier discharge (DBD) [72, 121] and corona discharges [108, 122].

DBD plasma devices are the most commonly used CAP devices in cancer treatment [72, 88]. DBD plasma devices generate plasma by applying a high voltage to an electrode in a gas-filled chamber, which creates an electric field that ionizes the gas and produces plasma [84, 123]. DBD plasma devices have been shown to be effective in reducing tumour size, inducing apoptosis and improving survival rates in animal models [72, 84, 123].

PlasmaJet devices generate plasma by using a high voltage to ionize a gas stream, which produces a plasmaJet that can be directed at cancer cells [84, 123, 124]. PlasmaJet devices have been shown to be effective in inducing apoptosis in cancer cells, but their

effectiveness is limited by the distance between the device and the cells [84, 117, 124]. Surface plasma devices generate plasma on the surface of a material, which can then be applied to cancer cells [125]. Surface plasma devices have been shown to be effective in inducing apoptosis in cancer cells and have the advantage of being able to be used *in vivo* [123, 125]. Plasma-activated media (PAM) devices generate plasma in a liquid medium, which can then be applied to cancer cells [126, 127]. PAM devices have been shown to be effective in inducing apoptosis in cancer cells and have the advantage of being able to penetrate tissue more effectively than other types of CAP devices [126-128].

The physical and chemical characteristics of the CAP may be altered by using gases such as air, argon, helium, oxygen, and nitrogen [108]. Different plasma discharge modes, can result in different interaction between plasma and cells, a phenomena known as plasma self-adaptation [129]. These changes are influenced by variations in power supply, gas composition, and the distance between the plasma source and the cells [129]. Other factors that substantially impact CAP therapy include dose of CAP, cell type, cancer type, and culture conditions [83, 103, 130, 131].

1.5.5 Bioeffects of CAP on GBM

One of the major bioeffects of CAP is the induction of apoptosis, or programmed cell death, in GBM cells [60, 72]. This occurs through the generation of ROS and RNS, which trigger a cascade of events that ultimately leads to cell death [60, 113]. The mechanism behind CAP effects seems to be related to TP53, c-Jun N-terminal kinases (JNK) or caspases pathways [85, 132, 133]. In addition, CAP can also induce autophagy, a process by which cells recycle damaged or unwanted components, which can further contribute to the death of GBM cells [104, 134]. Another important bioeffects of CAP is its ability to modulate the expression of genes and proteins involved in tumour growth and metastasis [135]. For instance, CAP can downregulate the expression of matrix

metalloproteinases (MMPs), which are enzymes that degrade the extracellular matrix (ECM) and promote tumour invasion and metastasis [109, 136]. CAP can also upregulate the expression of tumour suppressor genes, such as p53, which can induce cell cycle arrest and prevent tumour growth [84, 133, 135]. CAP modulate the immune response to GBM, by activating immune cells such as dendritic cells and natural killer cells, which can recognize and eliminate cancer cells [137]. Additionally, CAP can increase the permeability of the BBB, which can enhance the delivery of chemotherapy drugs to the tumour site [72].

CAP has been found to induce several cancer hallmarks (Figure 1) and has the potential to be an effective therapeutic approach for GBM treatment [5, 60]. CAP induce apoptosis, ferroptosis which can inhibit the cellular growth and metastasis [82, 135, 138]. CAP also able to cause DNA damage, which can trigger cell death or senescence [60, 113]. Similarly, CAP has the ability to disrupt the normal cell cycle of cancer cells, leading to cell cycle arrest and inhibition of proliferation [133, 135]. Moreover CAP is also able to inhibit angiogenesis, which can ultimately reduce the cancer growth and metastasis [139, 140]. Additionally, CAP modulate the TME by affecting the immune response, reducing inflammation, and inducing immunogenic cell death [83, 137, 138]. Furthermore, CAP can modulate signaling pathways that are important for cancer cell survival and proliferation, such as the PI3K/AKT and MAPK pathways [138, 141].

1.5.6 Molecular mechanism and selectivity of CAP

CAP has become a potential cancer treatment method due to its ability to selectively target cancer cells compared to normal cells [83]. This selectivity is partially due to the fact that cancer cells are more sensitive to oxidative stress than normal cells [142]. One distinguishing factor between cancer cells and normal cells is the number of aquaporins in their cell membranes [83, 143]. Aquaporins are water channels [144] and they are

capable of transporting ROS, RNS, as well as other small molecules like carbon dioxide, nitrogen monoxide, ammoniac, urea, and glycerol [143]. Cancer cells typically have a higher number of aquaporins (Figure 3A), which can lead to an increase in intracellular ROS, RNS concentrations and oxidative stress, ultimately increasing their sensitivity to CAP treatment compared to normal cells [145, 146]. The amount of cholesterol in the membrane directly affects the diffusion of free radicals in addition to the expression of aquaporins [83]. Cholesterol is a most abundant lipid in cell membranes, and plays a vital role in maintaining membrane stability and fluidity [147]. When free radicals react with lipids, it can cause lipid peroxidation (Figure 3B), which may create pores in the membrane that allow the entry of ROS and RNS into the cell. Higher cholesterol content in healthy cells provide a barrier against the entry of reactive species [148]. However, tumour cells often have lower cholesterol content than healthy cells, making them more susceptible to oxidative stress [142, 148]. When intracellular oxidative stress exceeds the defence limit of the antioxidative system (consisting of Nicotinamide adenine dinucleotide phosphate (NADPH), glutathione, superoxide dismutase, catalases, and peroxidases), apoptosis is triggered through a signaling cascade [83, 142].

Elevated levels of RONS within cells disrupt calcium signaling, which can occur due to RONS interacting with the inositol trisphosphate receptor (IP3-RR) and ryanoid receptor, leading to an increase in calcium influx into the cytosol (Figure 3C) [83]. Additionally, RONS induced endoplasmic reticulum (ER) stress can also result in an increase in calcium influx into mitochondria, causing a decrease in membrane potential and initiating mitochondria dependent apoptosis (Figure 3D) [83]. CAP induces DNA double-strand breaks, which activates DNA damage responses including ATM, H2AX, p53, and p73. Yet, it is possible that these double-strand breaks are the result of CAP induced apoptosis and not from direct CAP exposure (Figure 3E) [83]. The high concentration of RONS

produced by CAP overloads the antioxidant system, reducing its ability to protect against oxidative stress (Figure 3F) [83]. Furthermore, decreased expression of integrins after CAP treatment may account for the reduction of cell adhesion, migration, and invasion (Figure 3G) [83]. Overall, CAP treatment leads to cell necrosis, apoptosis, and senescence (Figure 3H) [83].

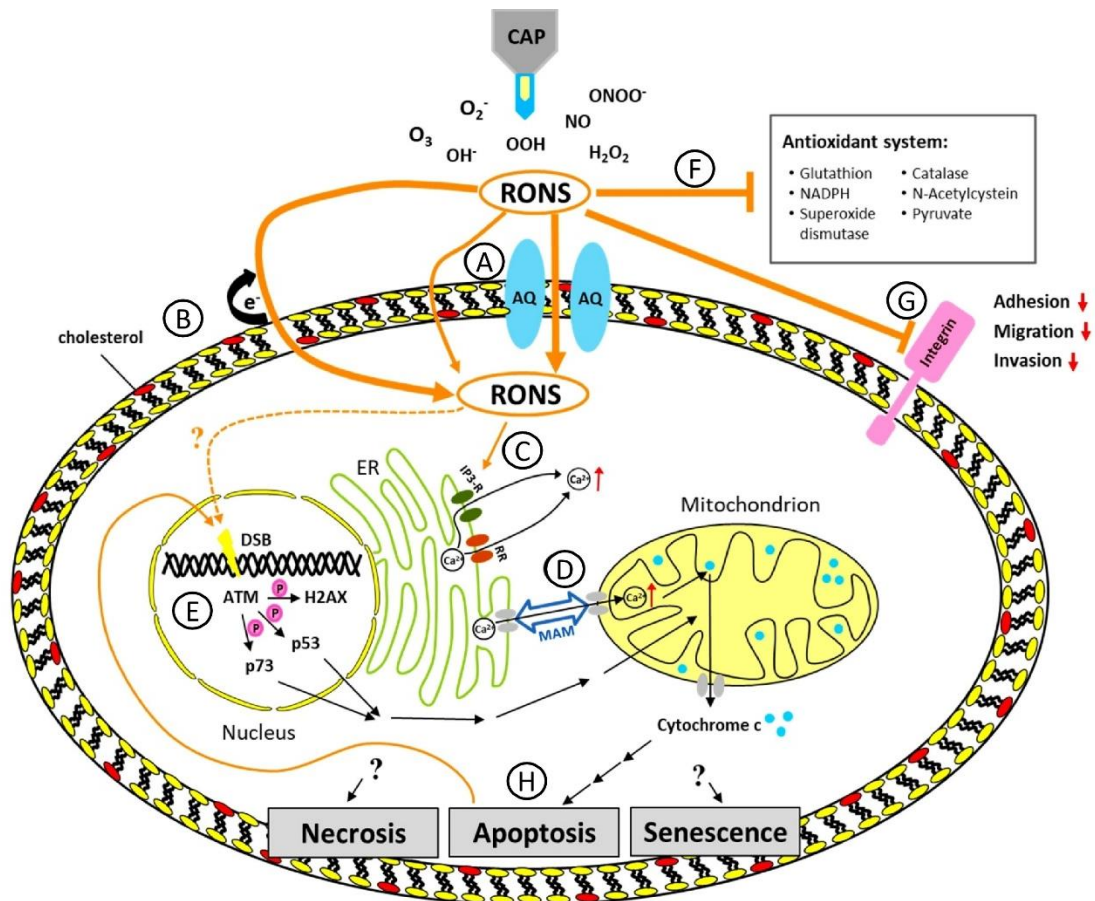


Figure 3: A summary of the current understanding of molecular mechanisms underlying the effectiveness of CAP treatment.

1.5.7 Pre-clinical application of CAP

CAP has been shown in several studies to be effective as a possible GBM treatment. Previous studies also have reported both direct and indirect CAP treatment efficacies in inducing anticancer effects (in numerous cancer types such as pancreatic [115], lung [116,

117], squamous cell carcinoma [118], brain [120] etc.) in *in vitro* [115, 116, 118] and antitumour effects *in vivo* [118-120]. *In vitro* studies are mostly conducted on 2D models [105], however 3D models have also been described [106, 149]. Pre-clinical research focuses on the selective potential, either *in vitro* or *in vivo* [135, 150, 151], to improve cancer chemo sensitivity and decrease of tumour size [85, 132, 150, 152]. The capacity to stimulate the immune system as well as trigger immunogenic cell death has also been investigated [150, 153-155]. CAP has been shown *in vivo* to have minimal effect on healthy brain tissues [120, 156]. It also inhibits cell proliferation and cell cycle arrest even in cells with unfavourable MGMT status [132]. Researchers also investigated synergic effect with various other treatment strategies such as chemotherapy, radiotherapy immuno therapy and nano therapy [150, 157, 158]. AuNPs, AgNPs, and platinum nanoparticles (PtNPs) have been studied in terms of nanomaterials combination. This combination has a synergistic anti-cancer impact by induction of membrane oxidation, stimulation of endocytosis, accumulation of lysosomes, promoting the uptake and accumulation of NP within the cells [72, 73, 88, 159]. Recently, gold quantum dots were evaluated in conjunction with CAP, and their cytotoxicity, as well as sphere formation and motility inhibition, were reported [153, 160]. Combination of CAP with chemotherapy such as TMZ and doxorubicin (DOX) were used to overcome the GBM resistance [85, 161]. Furthermore, the potential of CAP in combination with mesenchymal stem cell therapy and cancer stem cells (CSC) has been reported [155, 162]. In the pre-clinical applications of CAP in GBM treatment seem promising, its clinical applications are yet to be achieved.

1.5.8 Clinical application of CAP

The initial studies are from patients with locally advanced head and neck cancer, where the therapy resulted in palliative effects and at least nine months of partial remission in

two patients [163, 164]. CAP was also evaluated for cold plasma coagulation in patients with malignant pleural mesothelioma; the treatment was shown to be safe, and no disease recurrence occurred during the trial period [83, 165]. Friedman and colleagues (2017), also investigated the impact of CAP on actinic keratosis (NCT02759900), with some patients experiencing complete remission and no side effects identified [83, 166]. CAP for treatment of cervical intraepithelial neoplasia is currently on going (NCT03218436). Despite the promising pre-clinical findings, there are some limitations to the clinical application of CAP in cancer treatment. One of the main challenges is delivering CAP to tumours deep within the body. CAP has limited penetration depth, which makes it difficult to reach tumours that are located deep within the body [83]. Additionally, the safety of CAP in humans is not fully understood [167]. Further research is needed to assess the optimal parameters and utility of plasma in cancer treatment, particularly GBM [83].

1.6 Ultrasound (US)

US is defined as sound waves with frequency greater than 20 kHz [168]. It has the potential to penetrate deeply and supply targeted energy throughout the body [28]. There is a wide range of complex effects occur when US compressing waves pass through biological materials [169]. The main effects depending on US intensity can be divided in thermal and mechanical, being those resulting mainly from heat, radiation pressure and gas presence [170, 171]. The mechanical effects of US are classified as cavitation and non-cavitation [172]. The majority of these effects are caused by cavitation, which occurs when bubbles are formed during the acoustic pressure rarefaction cycle [170]. Cavitation is classified as either steady or inertial.

Stable cavitation occurs when bubbles in an ultrasonic field oscillated steadily over several cycles and develop in size, intercepting and radiating energy to adjacent tissue [173, 174]. The oscillation motion, micro-streaming, causes rapid movement of fluid near the cavitation bubbles, which can generate strong shear forces, expanding the gap between endothelial cells [174]. This is significant in US -assisted drug or gene delivery [175]. Ultimately US imparts focussed energy via ultrasonic compression waves directly to cells and tissues [169]. When used in combination with gas-filled microbubble (MB), the resultant MB oscillation, expansion and contraction, and bursting enhances the antitumour effects of US, broadly targeting several hallmarks of cancer [176]. Significant focus has been directed towards utilizing this technology in the treatment of cancer by taking advantage of its tumour ablation property and its anti-cancer bioeffects [28].

1.6.1 Biological effects of US

The hallmarks of cancer are a useful framework to distil and understand the underlying changes in this incredibly complex and diverse disease [176]. Six core and two emergent hallmarks underpin tumour development and metastasis [7]. Two enabling hallmarks provide “functional capabilities that allow cancer cells to survive, proliferate, and disseminate” (Figure 4). Drug development primarily focusses on singular receptors, whereas each hallmark is regulated by semi-redundant pathways allowing tumour adaptation and chemo-resistance via mutation [176]. Therapies that broadly target hallmarks of cancer are therefore advantageous to prevent tumour adaptation [177]. US imparts focussed energy via ultrasonic compression waves directly on cells and tissues [178]. When used combination with gas filled MB, resultant MB oscillation, expansion and contraction and bursting enhances the anti-tumour effects of US, broadly targeting several hallmarks of cancer [179, 180]. Nanomaterials also possess useful theranostic

properties including pharmacokinetic properties, bioavailability, drug carrying capacity, and *in vivo* stability, while minimizing solubility, degradation, plasma fluctuation, immunogenicity and toxic side effects [68, 69]. Acoustically sensitive nano-platforms can be used alongside US to augment nanomaterial effects (Figure 5) [28]. Among the core hallmarks (Figure 4), direct application of US can overcome resistance to cell death, inducing coagulative necrosis, apoptosis and reduction of tumour growth [181]. Mesenchymal epithelial transition (MET) activation is involved in epithelial to mesenchymal transformation, invasion and metastasis. US induces gas accumulation within cell membranes, altering cell membrane micro-morphology, thereby interrupting MET-induced cell motility [182]. Moreover, US inhibits tumour neovascularization, inducing thrombosis and preventing metastasis. Critically, US affects growth suppression [183]. Among enabling and emergent hallmarks (Figure 4), US promotes immune cell influx, releases tumour debris and damage-associated molecular patterns (DAMPs), although without inducing protective anti-tumour immunity [184]. Therapies combining tumour ablation with immune stimulation may therefore trigger robust anti-tumour immunity [181]. US enhances endocytosis and exocytosis thereby modifying nutrient, micronutrient and ion uptake [185] and potentially cancer cell metabolism. US induces cavitation, enhancing cell and tissue membrane permeability, and creates free radicals [180]. Direct biological effects, and bystander effects of cavitation and free radical production can be further enhanced using MB and sonosensitizers [186]. They can be controlled by adjusting duration, amplitude, intensity, frequency, shape, focus and type of transducer used [181, 183]. Therefore, US therapies can be codified within the hallmarks of cancer framework.

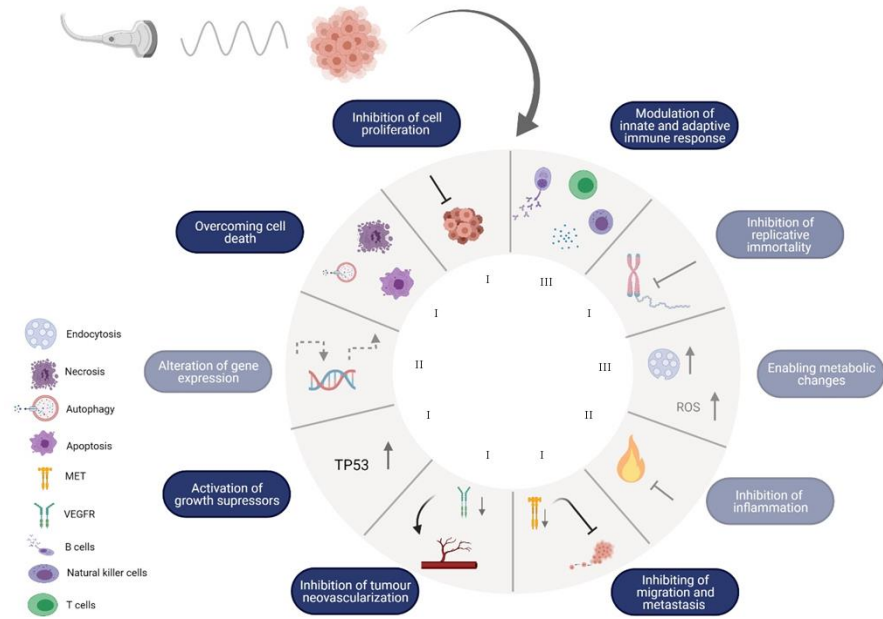


Figure 4: Ultrasound targets the hallmarks of cancer. Ultrasound directly modulates five core hallmarks and one emerging hallmark of cancer. Figure created with BioRender. Abbreviations: I, core hallmarks; II, enabling hallmarks; III, emerging hallmarks; ROS, reactive oxygen species; TP53, tumour protein P53.

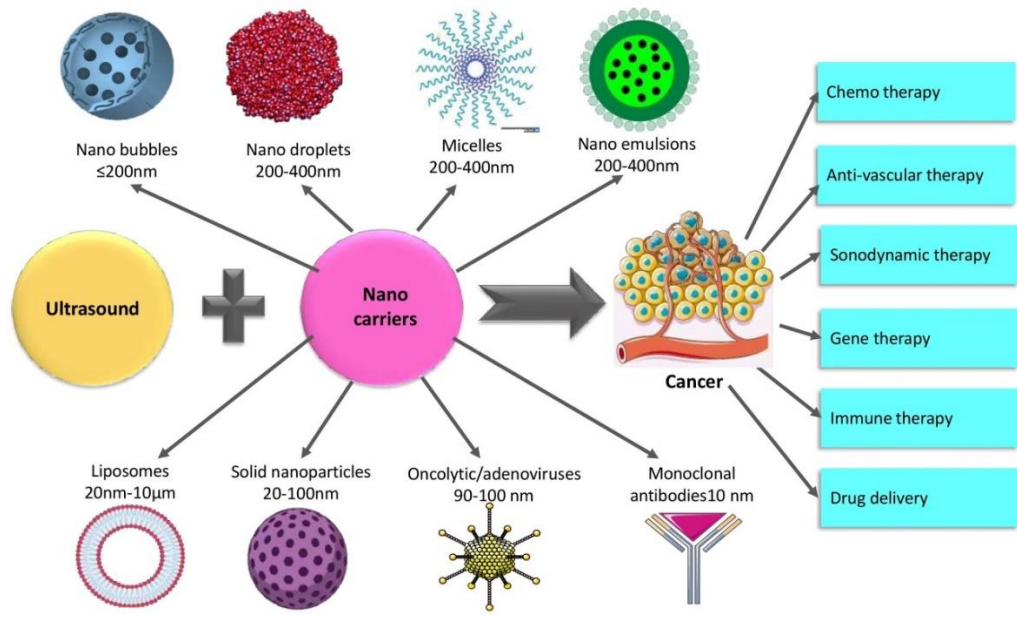


Figure 5: Acoustically sensitive nano-platforms include nanobubbles, nanodroplets, micelles, nano-emulsions, liposomes, colloid NPs, viral vectors, and antibodies.

Combined with ultrasound, these nanoplatfoms can promote sustained cavitation activity, while ultrasound can promote loading and releasing of active agents, enhance extravasation from tumour capillaries, and augment other therapeutics including gene therapy, sonodynamic therapy, biopharmaceuticals, drug delivery, contrast imaging and immune therapy

1.6.2 Resisting cell death

Many existing chemotherapies target receptors with the therapeutic intent to overcome or bypass inherent resistance of cancer cell to cell death [187]. Direct application of US can overcome resistance to cell death, inducing coagulative necrosis, apoptosis, and reduction of tumour growth [188]. In GBM and other brain tumours, the BBB prevents many chemotherapeutic agents from accumulating to effective concentrations in tumours [189, 190]. Two clinical trials used minimally invasive US to temporarily and repeatedly open BBB and enhance chemotherapeutic delivery without adverse effects [191, 192]. A phase I/II clinical trial (NCT02253212) enhanced carboplatin uptake without evident neurotoxicity using the implantable US device, sonocloud-1 combined with MB [191], and a second phase I trial (NCT02343991) effectively delivered DOX and TMZ loaded liposomes using low intensity magnetic resonance (MR)-guided focussed US [192]. These approaches demonstrate in human feasibility of micro/nano bubbles (NB) and US to enhance drug delivery, improve penetration and bioavailability in the brain parenchyma, increase local intracerebral drug concentrations, while reducing systemic toxicology [28, 193]. Development of a sonodynamic therapy complex incorporating chlorin e6 and hydroxychloroquite into a liposome illustrates this point. The complex selectively accumulated in the brain tumour during US –targeted MB destruction and hydroxychloroquine was released to glioma cells, inducing ROS production, mitochondrial dysfunction and MAPK/p38-PINK1-PRKN-dependent mitophagy [194].

Combining MB and gene loaded NPs with US also provides a safe, effective and targeted delivery system for genes. MB and a Lipid-polymer hybrid NP complex were used as an US-mediated gene delivery carrier of clustered regularly interspaced short palindromic repeats (CRISPR)-Cas9 plasmids, targeting MGMT, a DNA-repair gene protecting glioma cells from alkylating chemotherapeutics. US induced BBB opening allowing targeted delivery, gene protection from enzyme degradation, biocompatibility, prolonged survival, biosafety and augmented transfection efficiency while downregulating MGMT expression and thereby sensitising cells to TMZ [195].

MBs loaded with the halogenated xanthene contrast agent Rose Bengal conjugated via stable amine linkages to dihexadecylamine combined with US has been used as a novel sonosensitizer delivery system in a pre-clinical *in vivo* study. Loaded MBs were converted into NPs by US, resulting in enhanced drug accumulation in the tumour and ROS generation leading to tumour growth inhibition with minimal side effects [196]. Ultimately, MBs combined with US can overcome cell death resistance. Future progress will be dependent on further development of materials that increase tumour cell death while minimizing damage to surrounding cells. While not yet undergoing clinical trials, nanomaterials combined with US have the potential to selectively ablate tumour tissue deep within the body in the near future.

1.6.3 Sustaining cell proliferation

Cancer cells deregulate the normal signals that control entry and progression through the cell cycle, resulting in sustained cell proliferation [180, 197]. Antineoplastic agents have been developed such as gemcitabine to inhibit DNA synthesis in cancer cells [198]. Moreover, high expression of some micro-RNAs, such as miR-21 have been shown to downregulate tumour suppressors and modulate AKT phosphorylation, and others such

as miR-122 have tumour suppressor effects and are downregulated in various cancers, suggesting that targeting microRNA (miRNA)s could inhibit cancer cell proliferation [199, 200]. US –targeted MB destruction can enhance clathrin-mediated endocytosis of NPs and therefore enhance delivery of antineoplastic agents [201]. A pre-clinical pancreatic cell study using US -targeted MB disruption promoted uptake of dendrimer-entrapped AuNPs loaded with gemcitabine or a miR-21 antisense inhibitor, increasing cytotoxicity by more than 80 fold and 10 fold, respectively. This approach reduced tumour volume and increased blood perfusion *in vivo* [202]. Similar effects were seen in hepatocellular carcinoma (HCC) when sense miR-122 and antisense anti-miR-21 were encapsulated into poly (lactic-co-glycolic acid) NPs and delivered by US mediated MB disruption. This approach induced dose dependent decrease of anti-apoptotic proteins CD-320 and IGFR-1, and dose dependent increase of the pro-apoptotic protein programmed cell death protein 4, along with enhanced HCC death in DOX resistant and non-resistant human xenografts *in vivo* [203]. In a Phase 1 clinical trial (NCT01674556), US combined with MBs and gemcitabine was demonstrated to be clinically feasible and safe while enhance intratumoral drug delivery. This combination treatment also doubled median survival of patients with inoperable pancreatic cancer [204]. EGFR also promotes cell proliferation and is commonly overexpressed in cancers. Permeabilization of intact BBB using US in combination with MBs was applied before injecting ⁸⁹Zr-labeled anti-EGFR monoclonal antibody (cetuximab). This allowed prolonged exposure of the brain parenchyma to cetuximab with slow diffusion and clearance allowing for high and localised exposure to MAbs [205].

1.6.4 Induced angiogenesis

Angiogenesis is required to sustain tumour growth and much effort has been devoted to inhibiting blood vessel growth to reduce tumour burden [180]. US inhibits tumour

neovascularisation, inducing thrombosis and preventing metastasis [180, 206]. Moreover, heat caused by MB oscillation results in selective damage in tumour endothelial cell linings due to slower blood flow and a higher retention of MBs in the tumour neovasculature [180, 206]. This effect leads to inhibition of tumour neovascularization, and potentially necrosis, apoptosis, reduced tumour growth and improved survival [183]. It is expected to see a future a shift away from MBs towards NBs that damage tumour endothelial cell linings more effectively [28].

1.6.5 Invasion and metastasis

Invasion and metastasis is commonly associated with poor tumour prognosis. Tumour cells leave the primary tumour site and enter the vascular system before forming distal metastases [207]. MET activation is involved in epithelial to mesenchymal transformation, which is necessary for invasion and metastasis [208]. US induces gas accumulation within cell membranes, altering cell membrane micro-morphology, thereby interrupting MET-induced cell motility [182]. Therefore, efforts are underway to target tumour cells from entering the bloodstream or inhibiting blood vessel cells from allowing cells to pass through. Along with the above mentioned effects on plasma membranes affecting MET-induced migration [182], MBs can cause capillary damage, activating coagulation and inducing thrombosis, thereby limiting or preventing metastasis [183]. Moreover, as EGFR is also involved in cell migration, the combination of cetuximab with US with MBs increases permeability of cetuximab into the brain, thereby leading to reduced migration in a pre-clinical study [205]. While promising preclinical results have been demonstrated, clinical effects of US on invasion and metastasis remain unclear and further exploration will allow a more complete understanding of whether US can inhibit this hallmark [28].

1.6.6 Evading immune destruction

Evasion of the immune system and defective or suppressed immune responses against tumour antigen are common features of cancer [189, 209]. These immune responses can be (re)activated under certain conditions, making them an ideal target to fight cancer more effectively [209]. Recent efforts to counter tumour-induced immune suppression has led to the development of various immune-based therapies, including immune checkpoint inhibitors and adoptive cellular therapies [174, 210]. The feasibility of US -triggered transfection of bone marrow-derived dendritic cells (BM-DC) was demonstrated in preclinical models. Primary murine C57BL/6 BM-DC cultures were generated and US -triggered transfection of BM-DC cultures was achieved using MBs loaded with both antigen (OVA₂₅₇₋₂₆₄ SIINFEKL) mRNA as well as immunomodulating TriMix mRNA. This enabled potent OVA₂₅₇₋₂₆₄ antigen specific immune responses *in vivo* against MO4 melanoma cells and E.G7-OVA T lymphoma cells resulting in significant reduction of tumour growth, increased survival and long lasting antigen-specific protection against tumour recurrence [211]. By releasing DAMPs, increasing immune cell infiltration, decreasing immunosuppressive cytokine release from tumour cells and release cell debris including tumour antigen through above mentioned mechanisms [181] the potential for US to augment immune responses is not clear. Further studies should evaluate the combination of US with immune-based therapies [28].

1.6.7 Deregulated metabolism

Cancer cells adapt their metabolism to support biomass production, Adenosine triphosphate (ATP) generation, and maintain redox state [212]. Disrupting these processes can interfere with tumour growth and metastasis. US enhances endocytosis and exocytosis, thereby modifying nutrient, micronutrient, and ion uptake [213] and, potentially, cancer cell metabolism. US induces cavitation, enhancing cell and tissue

membrane permeability, and creates free radicals. Direct biological effects and bystander effects of cavitation and free radical production can be further enhanced using MBs and sonosensitisers and controlled by adjusting duration, amplitude, intensity, frequency, shape, focus, and type of US transducer used [180, 188].

1.6.8 Clinical application of US

US elicits a range of biological changes in a tumour with minimally invasive technology. Clinical trials demonstrate safe delivery of a range of therapeutic agents across the BBB and into cancer cells, along with in situ heat-dependent cytotoxicity to the tumour [183]. Advances in MB and NB technologies will further improve combinational therapy approaches [28, 214]. A wide array of clinical trials are planned or underway using chemotherapy, sonodynamic therapy, immunotherapy, and overcoming BBB, many incorporating MBs or nanomaterials [169]. Table 2 displays a list of clinical trials that have either been completed or are still ongoing, which involve the combination of US with MBs or nanomaterials. However, there are no reported clinical trials currently planned or underway using US and MBs to enhance gene delivery, despite successful preclinical studies including above mentioned CRISPR-Cas9 studies [195], miRNA studies [202, 203] and BM-DC transfection studies [211]. This demonstrate the potential of nucleic acid delivery by US and MBs and is a clinical research gap worth exploring.

Table 2: Clinical trials combining ultrasound and microbubbles / nanomaterials.

US device	Combination	Condition /disease	Phase	Hallmark	Status	Identifier (NCT)
Chemotherapy						
Focused US	Lyso-thermosensitive liposomal DOX	Liver tumour	1	I	Completed	NCT02181075 [215]
	FOLFIRINOX Regime, MBs	Pancreatic ductal adenocarcinoma	2	I	Recruiting	NCT04146441
	Panobinostat, MBs	Diffuse intrinsic pontine glioma	1	I	Recruiting	NCT04804709
	conventional chemotherapy, MBs containing sulfur hexafluoride stabilized by phospholipids	Colorectal neoplasms, breast neoplasms	1/2	I	Recruiting	NCT03477019
	Platinum, gemcitabine, MBs	Gastrointestinal neoplasms	1/2	I	Recruiting	NCT02233205
Contrast-enhanced US	Gemcitabine hydrochloride, Nab-paclitaxel, Fluorouracil, Irinotecan hydrochloride, Leucovorin calcium, Oxaliplatin, Perflubutane MB	Metastatic pancreatic ductal adenocarcinoma	1/2	I	Not yet recruiting	NCT04821284
	Perflutren protein-type A microspheres, MB	Hepatocellular carcinoma	2	I	Recruiting	NCT03199274
	Gaseous MBs, systemic chemotherapy, sonoporation	Colorectal cancer	2	I	Recruiting	NCT03458975
	Neoadjuvant chemotherapy, sulphur hexafluoride MBs	Breast cancer	N/A	I	Completed – (no results posted)	NCT00245869
	Gemcitabine, MBs	Pancreatic adenocarcinoma	1	I	Completed	NCT01674556 [216]
Magnetic resonance-guided high intensity focused US	Lyso-thermosensitive liposomal DOX, Cyclophosphamide	Metastatic breast cancer	1	I	Recruiting	NCT03749850
	Lyso-thermosensitive liposomal DOX	Refractory solid tumours	2	I	Not yet recruiting	NCT04791228
	Lyso-thermosensitive liposomal DOX	Pediatric cancer	1	I	Recruiting	NCT02536183
BBB disruption						
NaviFUS system	N/A	GBM	N/A	I	Completed – (no results posted)	NCT03626896
	Bevacizumab, MBs	GBM	N/A	I	Recruiting	NCT04446416
ExABlate system	Carboplatin	Recurrent GBM	1/2	I	Recruiting	NCT04440358

	MBs	Brain tumour	N/A	I	Active, not recruiting	NCT02343991 [192]
	Carboplatin	Recurrent GBM	1/2	I	Recruiting	NCT04417088
	N/A	Brain metastases	N/A	I	Recruiting	NCT03714243
	TMZ	GBM	N/A	I	Recruiting	NCT03712293
SonoCloud-9 system	albumin-bound paclitaxel, MBs	GBM	1/2	I	Recruiting	NCT04528680
	Carboplatin	GBM	1/2	I	Completed	NCT02253212 [191]
	Carboplatin	GBM	1/2	I	Active, not recruiting	NCT03744026 [217]
	Nivolumab Injection	Metastatic melanoma	1/2	I	Recruiting	NCT04021420
Focused US	N/A	GBM	N/A	I	Recruiting	NCT03616860
	N/A	GBM	N/A	I	Recruiting	NCT03551249
Immune therapy						
Focused US ablation (Echopulse)	PD-1 antibody blockade	Advanced solid tumours	1	III	Recruiting	NCT04116320
High intensity focused US	PD-1 antibody blockade (Pembrolizumab)	Metastatic breast cancer	1	III	Recruiting	NCT03237572
Low intensity pulsed US (SONOCLOUD)	PD-1 antibody blockade (nivolumab and pembrolizumab)	Metastatic melanoma	1/2	I	Recruiting	NCT04021420
Sonodynamic therapy						
Magnetic resonance-guided high intensity focused US	SONALA-001(5-Aminolevulinic Acid)	High grade glioma	1	I	Recruiting	NCT04559685
	5-Aminolevulinic Acid	GBM	N/A	II	Not yet recruiting	NCT04845919

1.7 3D cell culture

GBM is characterized by higher vascularization, significant cell heterogeneity, self-renewing CSCs and the interactions between tumour and microenvironment, all of which play an important role in tumour growth (Figure 6) [218]. Tumour development, metastasis, angiogenesis, cytotoxicity resistance, and immune cell modulation are all influenced by the TME [106, 219]. GBM also shows aggressive tumour growth due to multifaceted, recurrently hypoxic metabolic environment and Warburg effect. Therefore, it is critical to study GBM growth and treatment responses in an environments similar to *in vivo* [12]. There is a urgent need for accessible GBM pre-clinical models and 3D cell culture is able to fill this gap by providing more reliable models to study the correlation between TME, tumour reoccurrence and therapy resistance.

3D cell cultures describes a wide range of *in vitro* cell culture technique used to grow cells in three dimensions using an artificially created microenvironment. Cells in 3D cell culture have physiological cell-cell and cell–ECM component interactions which allow cells to grow *in vitro* in a TME that closely resembles GBM *in vivo* conditions [106, 220]. Tenascins, fibronectin, fibulin-3 and hyaluronic acid are the primary components of the GBM ECM [221]. These ECM components can be employed in 3D cell culture to mimic the composition and porosity of *in vivo* GBM ECM *in vitro* conditions to get better understanding of the therapeutic efficiency [222-224].

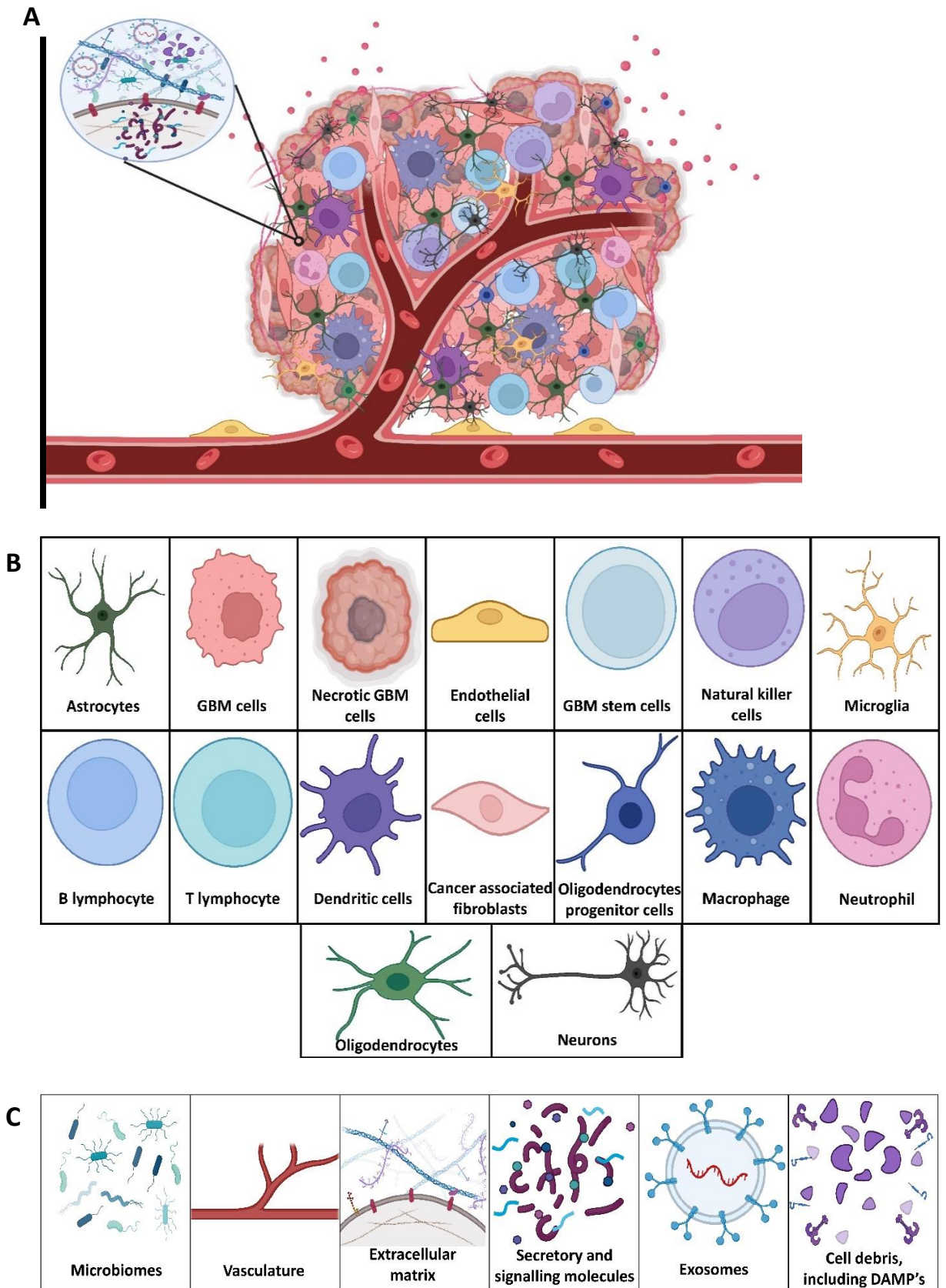


Figure 6: Components of GBM TME, consists of cellular, non-cellular and extracellular materials.

A) Components of GBM TME, consists of cellular and extracellular materials. B) Cells commonly found in the tumour microenvironment such as astrocytes, GBM cells, necrotic GBM cells, endothelial cells, GBM stem cells, natural killer cells, microglia, B and T lymphocytes, dendritic cells, cancer associated fibroblasts, macrophages, neutrophil and oligodendrocytes progenitor cells are shown here C) Non-cellular components such as vasculature, microbiomes, extracellular matrix, secretory and signalling molecules, exosomes and cell debris, including DAMP that are important features of a brain tumour (Figure created with BioRender).

In two dimensional (2D) culture, cells adhere primarily to coated surfaces of the tissue culture plate, whereas in 3D culture, adhesion is mostly with molecules of the ECM between cells along with directly interactions between adjacent cells. Matrix proteins, glycoproteins, glycosaminoglycans, proteoglycans, ECM sequestered growth factors, vascular endothelial growth factor, platelet derived growth factor, hepatocyte growth factor, and other secreted proteins are examples of secretory and signalling molecules [221]. These proteins and growth factors have critical roles in cell proliferation, tissue morphogenesis, migration, differentiation, adhesion, survival, immunosuppression, metastasis and homeostasis [221, 225-227]. Furthermore, the ECM can influence the cell's response to medications by altering the mechanism of action of the drug, increasing therapeutic effectiveness, or increasing the cell's inclination for drug resistance. A 3D culture model would have to imitate the microenvironment of tissue in which cells could proliferate, aggregate, and differentiate in order to predict the effectiveness of a treatment on a cell [222]. Further, integrins and receptor tyrosine kinases are examples of cell surface receptors that can interact with ECM components. Crosstalk between integrins and growth factor receptors regulates downstream cell signaling as well as growth factor induced biological activity, such as proliferation and invasion [106, 225].

Brain tumours are surrounded and infiltrated by many non-cancerous cells, including neurons, astrocytes, microglia, cancer associated fibroblasts, tumour associated macrophages, GSCs and endothelial cells, that provide both supporting and suppressive functions in the TME (Figure 6) [228-230]. Cancer progression and drug response are heavily influenced by cellular interactions in the TME [228, 231, 232]. 3D *in vitro* models can be utilized to simulate TME components and to evaluate novel therapies [226, 230]. Cells in a 3D spheroids have varying microenvironment conditions due to the non-homogeneous vascular supply [233]. For example, regions of a tumour further from vasculature have restricted oxygenation, nutrients and waste removal. 3D spheroid can possess a hypoxic (oxygen-deprived) core resembling these TMEs found in solid tumours, with cells at the centre of sphere with relatively low oxygen, glucose concentration and acidic extracellular pH due to accumulation of metabolic by-products (Figure 7) [234, 235]. The hypoxic cell population increase is proportional to the spheroid size also it is highly resistant to chemotherapy and radiotherapy. The outer layer of spheroid, which is highly exposed to medium and mainly composed of viable, proliferating cells. 3D spheroid has heterogeneous cellular subpopulation such as actively proliferating, quiescent, hypoxic and necrotic cells, which provides different cell proliferation zones, can be divided as proliferating zone, quiescent viable zone and necrotic core / hypoxic core (Figure 7) [220, 225, 236].

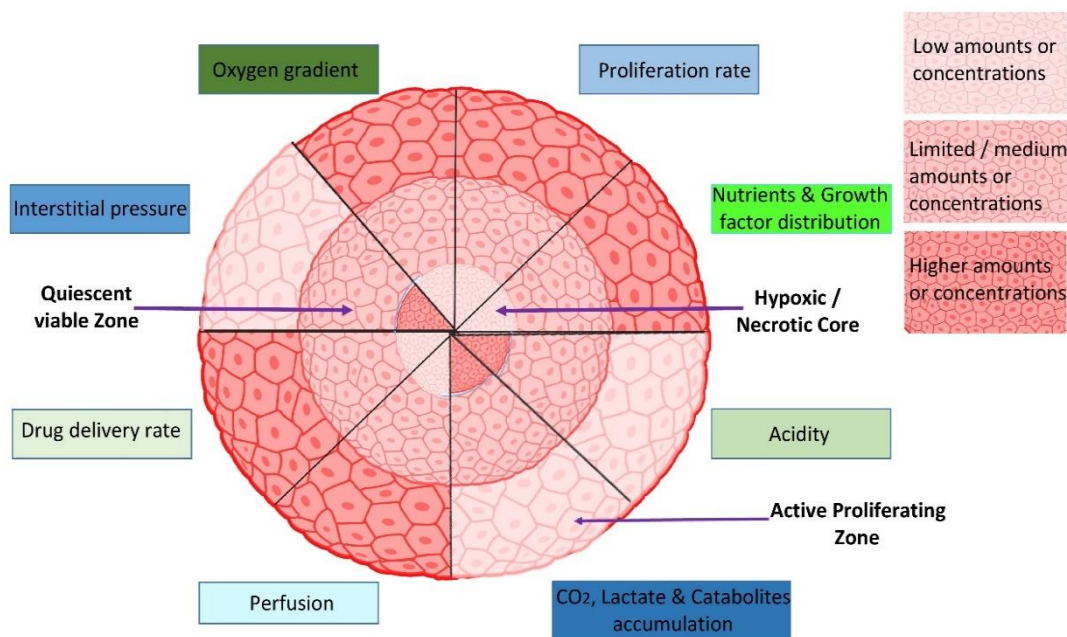


Figure 7: Structure of multicellular 3D spheroid. 3D spheroids have a spherical shape with an external proliferating zone and an internal quiescent viable zone that surrounds a necrotic core, resembling the cellular heterogeneity seen in solid tumours. Proliferation rate, drug delivery rate, interstitial pressure, perfusion, access to O_2 , nutrients and acidity in different zones are shown here (Figure created with BioRender).

The cellular organization, additional dimension, polarity, and geometry of 3D spheroids influence cellular functions such as proliferation, differentiation, survival, morphology, gene / protein expression, communication, and responses to external stimuli [222]. Ultimately this will provide a better understanding of complex biological / physiological behaviour, cell-to-cell interactions, tumour characteristics, drug discovery, metabolic profiling, and representation for toxicological testing improve drug screening accuracy, safety, increasing the chances of finding effective therapeutic methods or drug combinations to fight cancer [222].

The demerits of currently available 3D cell culture are that it is time consuming, expensive, lower reproducibility and limited intra-tumoural heterogeneity [237]. Further development needed in this field to assure reproducibility, high throughput analysis, compatible readout techniques and automation in order to establish validated 3D cell culture models [238]. The main strengths and weaknesses of 3D cell culture systems for cancer research applications are shown in Table 3.

Table 3: The current 3D cell culture systems for cancer research applications: Key Strengths and Weaknesses

Strengths	Weaknesses	Ref.
Matrices contain ECM components that promote cell–cell interaction, communication, and activation of signaling pathways.	Some models generate spheroids with a wide range of sizes, resulting in a number of variation inside the same well.	[239-241]
Heterogeneous cell populations resemble tumour cells at various stages of the cell cycle, such as proliferating, hypoxic, and necrotic cells	Vasculature, which is critical for tumour development, survival, and drug delivery, is still missing in 3D models.	[222, 225, 240]
Factors / proteins identified in a certain TME can be added to the culture setting.	Large-scale investigations and high-throughput tests are much more expensive and time consuming.	[236, 239, 240]
Cellular functioning, morphological differentiation, gene and protein expression levels, and hence cellular behaviours, are comparable to those seen <i>in vivo</i> .	Variability in biological matrices can lead to inconsistent experimental outcomes.	[237, 241, 242]
Ability to develop multicellular systems and bridges the gap between <i>in vitro</i> and <i>in vivo</i> cancer therapeutic outcomes.	Do not reassemble the complicated TME, and the technologies that can do so can only do so for a limited time	[237-239]

1.8 Comparison of 2D and 3D cell culture

In 2D cell culture, monolayer of cells adheres and grows on flat surfaces, while these cells are unable to grow in all directions. Due to this cells are flat and stretched hence it does not accurately reflect *in vivo* cellular morphology [234, 236]. The monolayer is mostly composed of proliferating cells, and any necrotic cells usually detach from the surface [243]. These attached proliferating cells receive homogeneous oxygen, nutrient and growth factors from the media and uniform exposure to drug candidates in efficacy and toxicity studies [244]. The morphological changes in 2D cells influences many cellular processes such as cell proliferation, cell–cell communication, tissue specific architecture, differentiation, migration, apoptosis and gene / protein expression, which leads to inaccurate organ-specific toxicity detection and have inadequate representation of cell migration, differentiation, signal transduction, metabolism, survival and growth [222, 233, 245].

3D cell culture can use to overcome these problems as cells are allowed to grow in any direction without interacting with the surface, while maintaining physiological cell-cell and cell-ECM interactions, more closely mimic the natural *in vivo* environment, shape, and cellular response [222, 245]. Cells in 3D cultures are not getting homogenous oxygen, nutrient and growth factors supply due to their larger size and diffusion gradient (Figure 7) leading to all major TMEs represented including proliferating, quiescent and necrotic stages found in an *in vivo* tumour (Figure 7) [236].

The proliferation rate of 2D and 3D cell culture are different and this is mostly depend on cell lines and matrix [246]. The proliferation rate of cells grown in 3D cell culture is a better represent the growth of *in vivo* tumour. When compare with 2D cell culture, additional dimension in 3D cell culture influence spatial organization of cell surface

receptors engaged in interaction with other cells and induce physical constraints to cells [246, 247]. Most drugs are designed either to targeting specific receptors accessible on the cell surface, or by crossing the plasma membrane and interacting with intracellular receptors to achieve therapeutic effectiveness. The availability of receptors in 2D and 3D cultures may be different due to differences in receptor expression, cell morphology, cytoskeletal and ECM arrangements, subcellular localization of receptors, modified endosomal trafficking, alterations to secretions, cell signalling and even differences in the spatial arrangement of receptors on the surface of cells [106, 222].

Overall the cellular responses varying between 2D and 3D cell culture is due to several factors such as differences in physical properties, physiological conditions, spatial organization of surface receptors, gene expression levels, microenvironment and cell stages are some of them. 2D cell culture doesn't reveal toxicological resistance, accurate cellular responses to drug treatment, architecture as *in vivo* tissues, accurate depiction of cell polarisation and gene expression [248]. It also provides unreliable predictions of *in vivo* drug efficiency and toxicity, which leads to low success rate in clinical trials [248]. 3D spheroids show increased drug resistance [249] (Figure 7) due to dynamic cellular interactions and restricted diffusion of nutrient, leading to activation of cell survival and drug sensitive genes [249]. Ultimately 3D cell culture can overcome the limitations of conventional 2D cell culture by providing an experimental models that more accurately represent the short- and long-term (time) effects of the drugs. The merits and demerits of 2D and 3D cell culture is compared in Table 4.

Han and colleges (2020), produced a scalable lung cancer spheroid model and carried out genome wide CRISPR screenings in 2D monolayers and 3D tumour spheroid cultures. CRISPR phenotypes in 3D more closely resemble those of *in vivo* tumours, and genes with differing sensitivities in 2D and 3D are highly enriched for important mutations in

malignancies. These analysis also revealed new drivers that are required for cancer development in 3D and *in vivo* but not in 2D [250]. A similar experiment utilizing GBM spheroid models will be beneficial in the future to understand which genes are essential for growth and survival in response to different environmental signals.

Table 4. Comparison of 2D and 3D cell culture methods.

Characteristics	2D cell culture	Animal models	3D cell culture	References
Morphology / Cell shape	<ul style="list-style-type: none"> Flat, stretched shape cells Cells grow into a monolayer Cells can only expand and proliferate in two dimensions 	<ul style="list-style-type: none"> Natural, shape of cells more representative of solid tumours Can differ from human cells in terms of type and quantity 	<ul style="list-style-type: none"> Natural, shape of cells more representative of solid tumours Cells grow into 3D spheroids Spheroids contain multiple layers of cells similar to <i>in vivo</i> 	[222, 236, 242, 247, 251, 252]
Cells interactions and microenvironment	<ul style="list-style-type: none"> Cell - cell contact only on edges and mostly contact with plastic Deprived cell extracellular environment interactions Lack of <i>in vivo</i> like microenvironment and “niches” 	<ul style="list-style-type: none"> Cell - cell and cell - ECM interaction Interactions with the microenvironment that vary from <i>in vivo</i> human interactions Inability to control composition of the microenvironment 	<ul style="list-style-type: none"> Physiologic cell - cell and cell - ECM interaction Cells communicate through exchange ions, small molecules, and electrical currents Micro environment and “niches” similar to <i>in vivo</i> Apical – basal polarization and lumen formation 	[220, 226, 227, 234, 236, 247]
Transport	<ul style="list-style-type: none"> No transport dynamics 	<ul style="list-style-type: none"> Complex transport dynamics 	<ul style="list-style-type: none"> Complex transport dynamics 	[236, 237]
Distribution of media / drug	<ul style="list-style-type: none"> Nutrients, growth factors and drug are equally exposed to all the cells 	<ul style="list-style-type: none"> Similar to human cells <i>in vivo</i> Vascularization feasible along with immune system activity 	<ul style="list-style-type: none"> Diffusion gradient of nutrients, growth factors, drugs and metabolic waste Core of the spheroid received lower amount of nutrients, growth factors and oxygen making hypoxic core (mimic <i>in vivo</i> tumour structure) 	[220, 253, 254]
Stage of cell cycle (cell differentiation)	<ul style="list-style-type: none"> Most of the cells in same stage of cell cycle Deprived cell differentiation 	<ul style="list-style-type: none"> Heterogeneous cell population with proliferating, quiescent, hypoxic and necrotic cells similar to human <i>in vivo</i> Rapid speed of reproduction 	<ul style="list-style-type: none"> Heterogeneous cell population with proliferating, quiescent, hypoxic and necrotic cells The cells have a higher level of differentiation. 	[220, 253, 255]
Phenotype and polarity	<ul style="list-style-type: none"> Forfeiture of diverse phenotype and polarity 	<ul style="list-style-type: none"> Similar to human cells <i>in vivo</i> 	<ul style="list-style-type: none"> Apical basolateral polarity is maintained Diverse phenotype and polarity similar to <i>in vivo</i> tumour 	[247, 251]
Gene / protein expression	<ul style="list-style-type: none"> Not provide accurate depiction Display differential gene and protein expression levels, mRNA splicing and cellular biochemistry compared to <i>in vivo</i> conditions 	<ul style="list-style-type: none"> Gene and protein expression cannot accurately reflect due to the species variations 	<ul style="list-style-type: none"> Provide more accurate depiction of gene and protein expression similar to those in <i>in vivo</i> tissues. Expressed genes, proteins, mRNA, and other cellular activities are effectively identified and quantified. 	[236, 242, 252]
Cell proliferation	<ul style="list-style-type: none"> Usually cellular proliferation is faster than <i>in vivo</i> cells 	<ul style="list-style-type: none"> Higher proliferation rates than human <i>in vivo</i> cells 	<ul style="list-style-type: none"> Mostly, proliferation rates are similar to the human <i>in vivo</i> cells 	[220, 247, 255]

Mutation	<ul style="list-style-type: none"> • Protracted genetic and phenotypic drifts, as well as cellular cross contamination, are common in cells 	<ul style="list-style-type: none"> • Complex and time consuming to identify genetic and phenotypic drifts 	<ul style="list-style-type: none"> • Improbable to genetic and phenotypic drifts 	[222]
Drug sensitivity	<ul style="list-style-type: none"> • Lower drug resistance • Poor drug metabolism • Misrepresentation of drug treatment efficiency 	<ul style="list-style-type: none"> • Ability to study side effects • Higher drug resistance to treatments similar to the <i>in vivo</i> cells 	<ul style="list-style-type: none"> • Higher drug resistance to treatments similar to the <i>in vivo</i> cells • Improved drug metabolism • Accurate representation of the treatment efficiency 	[247, 253]
Representation	<ul style="list-style-type: none"> • Inadequate representation 	<ul style="list-style-type: none"> • The representation is quite intricate 	<ul style="list-style-type: none"> • Improved models for cell migration, differentiation, survival and growth 	[235, 236, 253]
Metabolic profiling	<ul style="list-style-type: none"> • Augmented sensitivity to ATP synthase 	<ul style="list-style-type: none"> • Higher metabolic rates and ATP synthase sensitivity is distinct to <i>in vivo</i> human cells 	<ul style="list-style-type: none"> • Abridged sensitivity to ATP synthase 	[222, 255]
Quality and time of culture	<ul style="list-style-type: none"> • Higher performance and reproducibility • Easy to interpret • Culture handling is comparatively easy • Shorter time for culture (h) 	<ul style="list-style-type: none"> • Time consuming for the study (days) • Difficult to handle, maintain and interpret data • Lower performance and reproducibility • Long tumour latency 	<ul style="list-style-type: none"> • Lower performance and reproducibility • Difficult to interpret data • More difficult to handle and maintain • Time consuming for culture (days) 	[222, 236, 242, 253]
Cost of maintaining culture	<ul style="list-style-type: none"> • Low cost maintenance • Readily available test materials and media 	<ul style="list-style-type: none"> • Expensive when compared to both 2D and 3D cell culture 	<ul style="list-style-type: none"> • Expensive when compared to 2D cell culture • Limited commercially available products 	[220, 236, 247]
Apoptosis	<ul style="list-style-type: none"> • Lesser resistance to the drug - induced apoptosis 	<ul style="list-style-type: none"> • Apoptosis responses may vary 	<ul style="list-style-type: none"> • Greater resistance to the drug - induced apoptosis 	[242]
Response to stimuli	<ul style="list-style-type: none"> • The response of cells to mechanical stimuli is inaccurately portrayed • They are unable to respond to gravity 	<ul style="list-style-type: none"> • Different pathophysiology to humans 	<ul style="list-style-type: none"> • Accurate representation of response to mechanical stimuli of cells • They are continuously able to respond to gravity 	[242, 253]
Co-culturing cells	<ul style="list-style-type: none"> • Lower benefits and inadequate representation 	<ul style="list-style-type: none"> • Unable to control architecture of a tissue 	<ul style="list-style-type: none"> • Higher benefits and superior of co-culturing cells 	[222, 238]
Tumour heterogeneity	<ul style="list-style-type: none"> • Basic representation 	<ul style="list-style-type: none"> • Higher due to the species differences 	<ul style="list-style-type: none"> • Better approximation via the proliferation gradient, drug penetration and mobility variations 	[249, 254]
Multi cellular study	<ul style="list-style-type: none"> • When studying the immunological response, this is a better option 	<ul style="list-style-type: none"> • Most suitable for multi cellular studies 	<ul style="list-style-type: none"> • When there are more than two cell types in a co-culture, it becomes more challenging 	[236, 256]
Genetic engineering	<ul style="list-style-type: none"> • Not possible 	<ul style="list-style-type: none"> • Ease and precision of genetic manipulation 	<ul style="list-style-type: none"> • Possible only in advance 3D models 	[255]
Ethics	<ul style="list-style-type: none"> • No ethical concerns are required. 	<ul style="list-style-type: none"> • Many ethical considerations arise as a result of animal suffering, international and national regulations 	<ul style="list-style-type: none"> • A potential alternative that can eliminate animal experimentation. No ethical concerns are required but may raise due to the origins of primary and stem cells 	[252]

1.9 Comparison of 3D cell culture with animal *in vivo* models

3D cell culture plays a vital role in drug development, while it is also capable of replacing both 2D cell culture and animal trials. Initial testing stage of standard drug discovery begins with 2D cell culture, followed by animal tests and clinical trials, which resulted 95% of trial failures during clinical trials due to the insufficient prediction of the efficacy and toxicity in humans during pre-clinical studies [242, 248].

3D cell cultures represent a simplified reductionist model. It highly transparent, reproducible, easy to modelling the complex processes such as growth, invasiveness and toxicity, when compared to a whole animal [245]. 3D cancer cell models are able to provide better understanding of *in vivo* cancer therapeutic efficiency and also improve the efficacy of drug discovery, due to the clear understanding the relation between cells and the ECM in which they interact [222, 230]. This help to identify drugs/ therapeutic methods in early stages, which has better effects on cancer treatment and eliminating a lot of unnecessary testing.

The European registration, evaluation, authorisation and restriction of chemicals (REACH) regulation stated aim is “To ensure a high level of protection of human health and the environment from effects of hazardous chemicals. It strives for a balance: to increase our understanding of the possible hazards of chemicals, while at the same time avoiding unnecessary testing on animals” (European Chemicals Agency, 2020) [257]. 3D cell cultures supports 3Rs principles of animal research (Replacement, Reduction and Refinement) and REACH regulation while able to reduce the number of animal usage in testing, time, cost and ethical considerations [106, 252].

There are different animal models have been widely used to investigate GBM such as syngeneic implantation models (tumourigenesis is induced using carcinogens or genetic modification), genetically engineered animal models (delivery of cancer initiating genes using viral vectors to initiate tumour development), traditional xenograft models (transplanting human cancer cells into an immunocompromised rodent), patient derived xenograft and xenografts generated from patient derived cancer stem cells (direct implantation of freshly biopsied tumour tissue or cultured tumour spheres into immunodeficient animals) are some of them [258, 259]. These experimental animal models have several limitations since they do not always predict efficacy and / or toxicity, don't share the same clinical features, and do not have the same receptor responses as seen in human disease. Vital genetic, molecular, immunologic and cellular differences between humans and animal models prevent it from being an effective way of researching a cancer therapies [252, 260].

Animal testing is expensive and time consuming and they do not account for the whole intricacy of TME interactions [230]. Also, if animal is in pain or stress during the experiment, it might change the biochemical, physiological and metabolic reactions, which can inaccurately depict the effectiveness and side effects of drugs [106, 222, 245, 260]. Humans and animal models have distinct anatomical and physiological differences, the most apparent of which is size. The human brain is about 100 times greater in weight and more than 1,000 times larger in surface area and number of neurons, when compared with mice. Thus, in the study of GBM, well known for its infiltration of the brain parenchyma, important anatomical distinctions in the organ of origin impose potentially confounding factors in preclinical investigation [252, 255]. Preclinical modeling is complicated further by an increased proportion of neocortical astrocytes, pericyte

heterogeneity, and changes in vascular architecture between humans and animal models [255].

Some animal models such as mice have a short lifetime, they are less likely to development of certain types of cancers or highly penetrant cancers associated with loss of heterozygosity mutations. Animal models also have substantially greater metabolic rates than humans, which complicates pharmacodynamic and pharmacokinetic investigations [255]. Genetic modifications initiate tumours with homogenous genetic changes whereas human GBM cells are heterogeneous. Furthermore, the genetic background of animal models can influence tumour biology, gene function, and tumour susceptibility [258].

Many variables *in vivo* are uncontrollable, and their effects are often unknown due to the complexity of organisms, whereas 3D cell culture allows for better control of variables by using a series of carefully selected reductionist models [261]. The merits and demerits of 2D, 3D cell culture and animal models are compared in Table 4.

Current *in vitro* GBM treatment regimens fail to account for a large variety of factors such as brain's unique ECM, circulatory systems, existence of resident and non-resident brain cells inside the tumour, secreted factors and nutritional sources accessible for tumour metabolism [230]. The main benefits of using 3D cell culture models for *in vitro* GBM treatment rather than animal testing are include a wider selection of techniques, leading to better measurements of outcomes, better control of variables, scalable testing, comparatively lower cost, avoidance of ethical issues and reductionist approach to accurately model a specific feature of a disease, as opposed to animal models, which are complex and often differ from human disease. It is also capable of simulating *de novo* drug resistance [106]. Furthermore, juxtacrine signaling, in which molecules pass directly between cells via gap junctions or other structures without being released into the

extracellular environment, requires 3D tumour sphere cell–cell interactions. These receptor and juxtacrine signaling components alter a variety of intracellular signaling pathways, affecting how cancer cells react to their surroundings [106, 225]. The lack of vascular and immune system in 3D cell culture techniques is a drawback when compared to animal models, that may be solved in the future by constructing advanced 3D models utilizing specialized 3D techniques such as 3D printing [261]. Ultimately 3D brain cancer models can improve reproducibility and allow researching cellular and molecular pathways simpler to improve for personalized medicine.

1.10 Different types of 3D cell culture techniques and methods

Different elementary 3D culture techniques such as anchorage independent and anchorage dependent platforms can be used for 3D cell culture [220]. Anchorage dependent platforms can further classifies into scaffold and hydrogels based on their porosity, density and mechanical strengths [243]. These approaches are most commonly employed to create 3D spheroids, basic tumour models and multicellular tumour spheroids (Figure 8). Tumour spheroids are solid, 3D spherical formed by the proliferation of a single cancer stem / progenitor cell [262, 263]. Tables 5 and 6 list the applications and merits / demerits of different 3D culture techniques / methods for the development of 3D glioma spheroids, respectively.

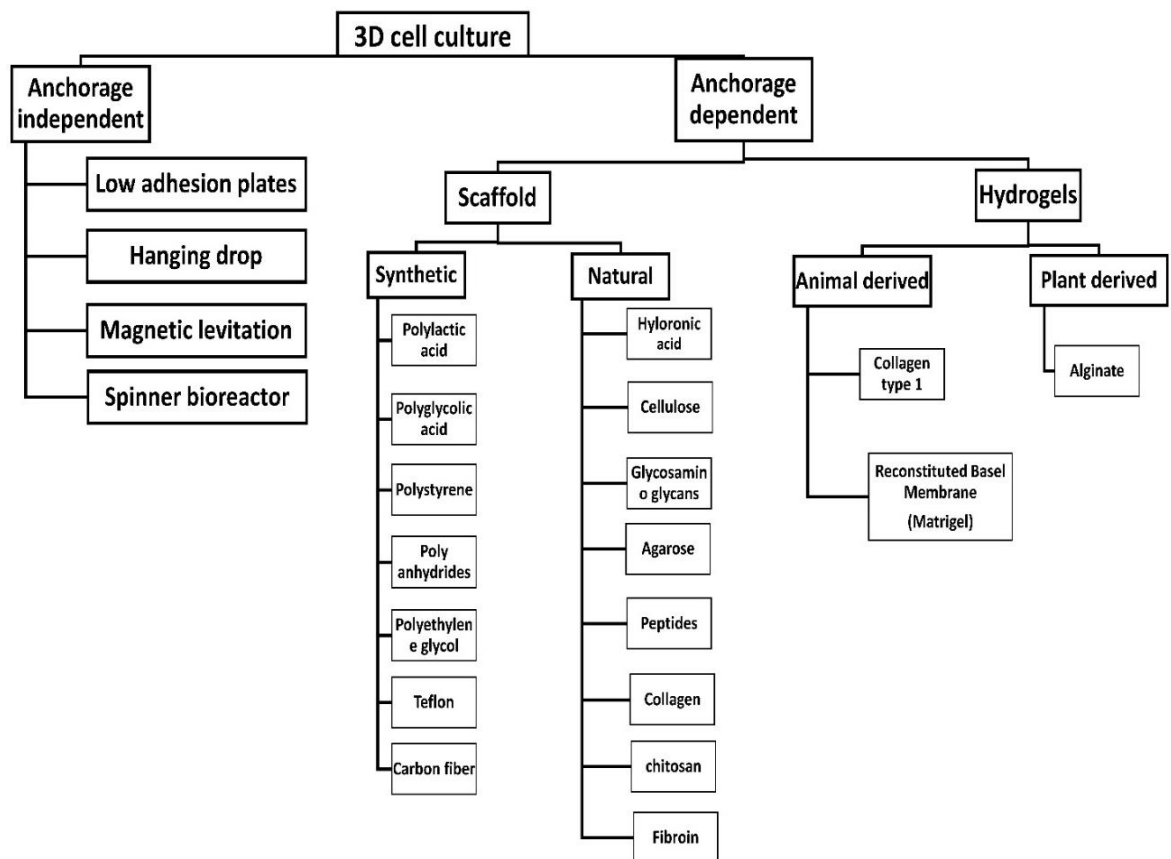


Figure 8: Different anchorage dependent and independent methods to develop 3D multicellular tumour spheroids.

1.10.1 Anchorage independent (scaffold free)

Anchorage independent/scaffold-free techniques rely on non-adherent cell to cell aggregation to form spheroids. Spheroids showing cell-cell interactions and secreting their own extracellular matrix. These spheroids are able to freely grow without a physical support resulting in consistency of shape and size, which provide better understanding about cellular cytotoxicity [222].

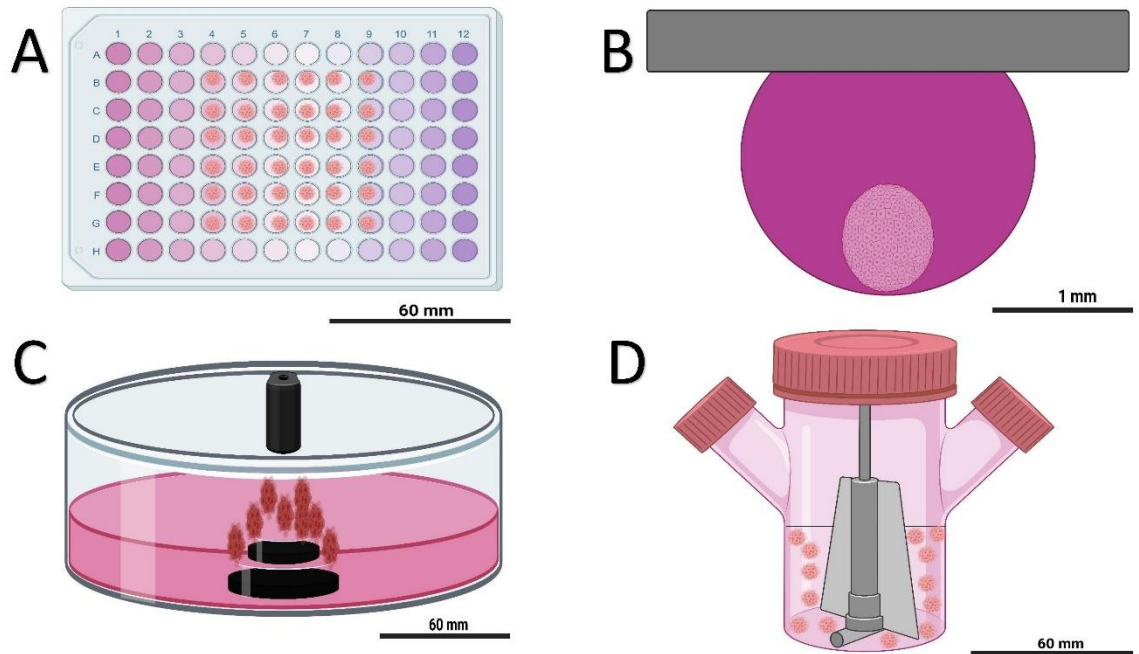


Figure 9: Anchorage independent methods available for multicellular tumour spheroids formation. These methods include, A) Low adhesion plate method; B) Hanging drop plate method; C) Magnetic levitation; D) Spinner bioreactor (Figure created with BioRender).

1.10.1.1 Low adhesion plates

Low adhesion plates (Figure 9A) are specialised culture plates with ultra-low attachment hydrophilic polymer coating Poly-2-hydroxyethyl methacrylate (Poly-HEMA), agarose, bovine serum albumin, or agar which promote cell aggregation to form spheroids [220, 264, 265]. Different culture plates are commercially available (e.g. Nunclon™ Sphera™, Costar®, PrimeSurface, Lipidure®-COAT) with modified surface shapes (flat and conical shaped bottom) [220, 264]. Usually ECM proteins such as collagen-I and fibronectin mediate cell attachment to the culture surface. Hydrophilic polymer coating prohibits protein adsorption to the culture ware surface, thereby minimizing monolayer cell adhesion to the culture vessel [266]. Ultimately low attachment plates promote

aggregation of cells by cell - cell and cell - ECM interactions, while blocking the ECM interaction to plastic surface [267]. Advantages of using low adhesion plates are simple, straight forward, efficient, spheroid production & handling is easy, higher reproducibility when compared to other anchorage independent methods, able to generate wide range of tumour cell types and co-culture can be incorporated [233, 236, 265, 268]. Disadvantage is time consuming and relatively labour intensive, continuous passage culture is difficult, only autocrine ECM is present, success rate in long term passage is low, cells in suspension has no migration movements [222, 235, 248, 265, 269]. The detailed protocol for developing 3D glioma spheroids published by [270, 271].

1.10.1.2 Hanging drop method

Hanging drop plates are open bottom-less wells that promote the formation of droplets of media (Figure 9B) that provide space to form spheroids via self-aggregation through the use of gravity and surface tension [272]. There is no surface to attach, cells grow inside a bubble of growth media and spheroids hang in open bottomless wells which are often enclosed in the bottom of the plate in order to normalize the environmental humidity of the cells [264]. Phosphate buffer saline (PBS) is added to the reservoirs located on the peripheral rim of the plate and tray which are divided into sections to prevent the hanging drop dehydration during incubation [264]. Spheroid size is controlled by number of cells dispensed into each drop [220]. The droplet of media sufficient for cell aggregation and also small enough to hold droplet by surface tension, after 3D spheroid generation it can be dispense by adding extra drop of media in to the well and spheroid loaded to adjacent plate [222]. Micro-liquid adhesion with substrate surface is greater than cellular weight; cells aggregate, proliferate, and grow in to spheroids at liquid air interface. The well can typically accommodate up to 50 μ l of media while recommended drop volume is 10-20 μ l [269], and the spheroid size is determined by the cell density [220, 264]. There are

currently some commercially available hanging drop plates on the market, such as Perfecta3D® and Gravity PLUSTM [264]. Multicellular spheroids also can be create by co-suspending several cell types or else consecutive addition of different cell types to form separate cell layers. The merits are: able to produce uniform spheroid size, able to control size of spheroid by seeding density, homogenous spheroids and suitable for high throughput testing, higher replicability, low cost and comfortable to handling [268]. In the disadvantages side, plates are highly expensive, medium change and different drug treatment at different time points are impossible, not suitable for long term culture and also having small culture volume and osmolarity of the droplet will rise due to medium evaporation [222, 264, 265, 269]. In 2021, we have provided a thorough procedure for producing 3D glioma spheroids using hanging drop plate method [273].

1.10.1.3 Magnetic levitation

Magnetic levitation (Figure 9C) is a suspension culture technique; cells are preloaded with magnetic NPs or beads in dedicated plate and external magnetic fields to provide non-adhesion, plate like properties to facilitate cell aggregation and form uniform 3D spheroids / tumour spheres [220, 264]. It can be used on a variety of cell lines, particularly those that do not self-aggregate. The amount of cells that were able to internalize the particles determines spheroid development [264]. This method is highly efficient, simple, straightforward, possibility to replicate *in vivo* microenvironments, does not require specialized media, easier spheroid collection and changing of medium with minimal disruption. It also allows for the quick generation of 3D spheroids and is scalable for higher throughput [267]. In disadvantage side this method gives slight brownish colour to spheroids and which might be not suitable for some applications. Also some cells adhere to the bottom of plate without forming 3D spheroids and magnetic particles may

alter the cellular behaviours of these spheroids [222, 264, 269]. There haven't been many uses of magnetic levitation for the development of 3D glioma spheroids documented.

1.10.1.4 Spinner bioreactor

A spinner bioreactor (Figure 9D) has a container to hold cell suspension and impeller stirring continuously to minimize the cell adhesion to the surface. Bioreactors are closed systems used to strictly regulate factors such as dissolved oxygen, temperature, pH, and nutrients. Specific sensors inside the bioreactor linked to control software to monitor nutrition and metabolite input and outflow [248]. Continuous liquid flow prevents cell adhesion contamination, time-consuming manual operations and also uniformly distributes nutrition and oxygen to form 3D spheroids [248, 265]. This method is simple, able to mass production of spheroids and also suitable for long term culture [265]. While cells can be damaged by collision between cells and bioreactor wells (exposure to high shear force) and require specialized equipment's also difficult to obtain uniform spheroids [248, 265, 269].

1.10.2 Anchorage dependent (Scaffold Based)

The anchorage-dependent approach uses pre-designed porous membranes and polymeric fabric meshes called “scaffolds”, which can be constructed of natural or synthetic components to offer physical support (Figure 10A) [235, 274]. This physical support can provide structures from simple mechanical up to ECM-like structures. 3D spheres can be generated by seeding cells on three dimensional matrixes or by dispensing cells in liquid matrix followed by solidification and polymerization. Cells are embedded in extracellular components and able to initiate cell - cell and cell - matrix interactions, physical support for cell growth, adhesion and proliferation. In general, these features, as well as structural patterns, textures, and angulations, can be manipulated in an attempt to mimic ECM traits

particular to the tissue of interest [275]. There are several techniques use to create scaffold such as electrospinning (ES), stereolithography, 3D printing, solvent-casting particulate leaching (SCPL), freeze drying, shape deposition manufacturing, robotic micro assembly, phase inversion, selective laser sintering, fused deposition modelling [222, 269, 274].

1.10.2.1 Natural scaffolds

Biological / natural scaffolds provide physical support for cell growth as well as provide similar *in vivo* microenvironment with ECM components, growth factors, hormones and so forth. The biological scaffolds are made up of ECM components such as fibronectin, collagen, laminin, gelatin, chitosan, glycosaminoglycans (mainly hyaluronic acid), fibroin, agarose, alginate, starch (mainly additives), human decellularized ECM [226, 236, 269, 276]. Microscale mechanical features of biomaterials, such as stiffness, porosity, interconnectivity, and structural integrity, can influence cellular function [277]. Brain tumour specific ECM components such as proteoglycans, laminins, fibronectin, tenascins, collagens I, II, IV and glioma cells overexpress ECM components like hyaluronic acid, brevikan, tenascin-C, fibronectin, thrombospondin can be employed to engineer glioma-specific scaffolds to mimic similar *in vivo* glioma TME [221, 278].

The advantages of using biological scaffolds are highly similar to the *in vivo* conditions, can control similar composition / elasticity / porosity to get better ECM presentation and also possible to combine with ideal growth factors. Also it is able to improve biocompatibility, spatial distribution and lower toxicity [276]. Natural scaffolds also have higher biocompatibility and lower toxicity when compared to synthetic polymers. Disadvantages are it is expensive, time consuming, complex process and not suitable for large scale production, difficult to dissociate cells from scaffold for experiments such as flow cytometry, confocal imaging and risk of contaminations and disease transmission

[269]. We published and provided a thorough procedure for producing 3D glioma spheroids using a natural scaffolds based method [279].

1.10.2.2 Synthetic scaffolds

Polymeric scaffolds are a useful tool for investigating cell - ECM interactions due to the scaffold's capacity to duplicate the structure of the ECM. Polymeric hard scaffolds are also very valuable for investigating tissue regeneration and evaluating tumour cell therapies [222]. Single cell suspension can be grown in a pre-fabricated scaffold to generate 3D spheroids. These scaffold matrixes enable cellular growth, adhesion, and proliferation while also encouraging cells to create spatial dispersion and migration. These polymeric scaffolds have been designed to mimic the structure of *in vivo* tissues and easier to reproduce [276]. Matrix stiffness has been shown to have a major influence on tumour cell phenotypes and the usage of synthetic scaffolds has also been employed to investigate the effect of matrix stiffness on drug responsiveness [276]. The scaffolds can be create using polymers such as polyglycolic acid, polylactic acid, polyorthoesters and their co polymers or blends as well as aliphatic polyester polycaprolactone, polystyrene, polycaprolactone, polyethylene oxide, polyethylene glycol [236, 269]. The merits of using synthetic scaffold is that the capability of controlling stiffness, elasticity, porosity and permeability, higher versatility, augment workability, reproducibility, straightforward to use and mechanical qualities of synthetic materials can be adjusted according to the cell culture required, and their chemical composition is well characterized [269]. The demerits are lack of biodegradation in most of the polymers, which might affect the cellular activity [269]. However, some synthetic polymers can be tailored to degrade and also researchers are attempting to improve biodegradability [280].

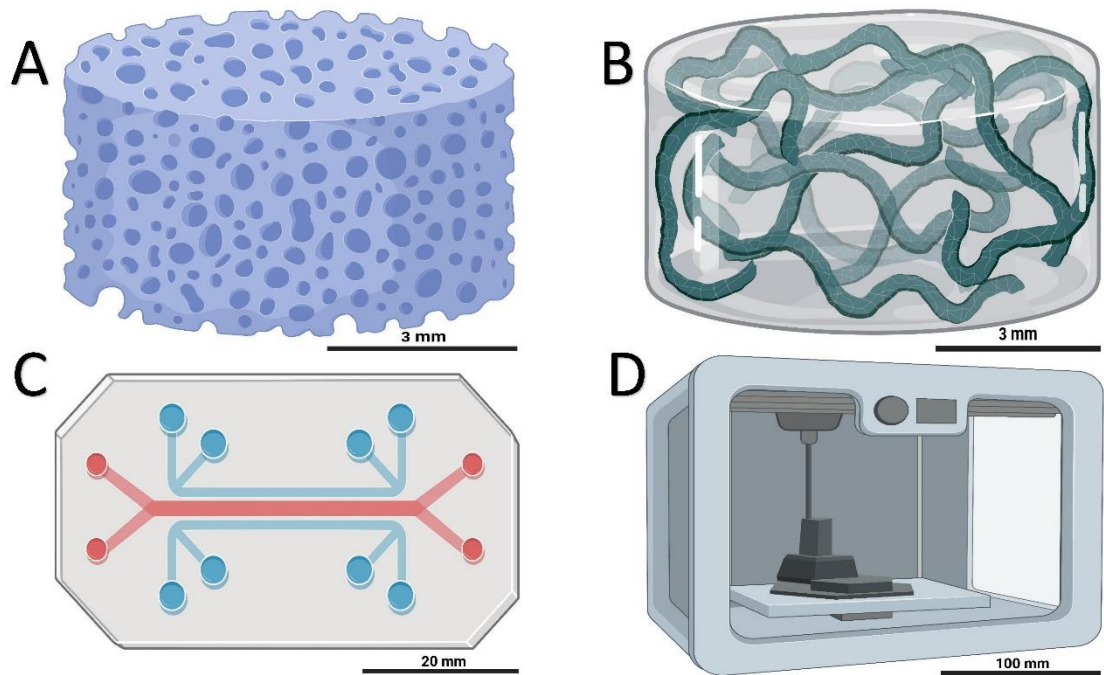


Figure 10: Anchorage dependent methods and specialized 3D culture platforms available for multicellular tumour spheroids formation. These methods include, A) Natural and synthetic scaffold based method; B) Hydrogels; C) Microfluidic devices; D) 3D Bio printer (Figure created with BioRender).

1.10.3 Anchorage dependent (Hydrogels)

Hydrogels (Figure 10B) provide multi-layer formats by cross-linked hydrophilic polymer chains and cells are embedded inside layers and able to grow to 3D spheroids providing cell - cell and cell - ECM interactions [248, 269], which has similar biochemical, structural and mechanical properties of an *in vivo* tissue. Hydrogels are in a liquid format at room temperature which become a gel at 37 °C incubation [229]. It helps cells to mix uniformly into the gel - liquid and proliferate non-destructively during the gelation process [269]. Mechanical strength, nutrition transport, topography, and degradation behaviours can all be adjusted by using polymers with varying compositions, crosslinking

density, and including bioactive compounds [274]. Hydrogels are 3D matrices or porous scaffolds can be divided into synthetics and natural hydrogels [248].

There are natural hydrogels made up using natural polymers – animal / plant - derived proteins such as aginate, hyaluronic acid, collagen, silk, fibrinogen, albumin, fibronectin, laminin, agarose, matrigel, gellan gum, gelatin, and chitosan [248]. Collagen is a major ECM component in connective tissues. Collagen type 1 animal based hydrogels are mostly used and successful since its ability to replicate the cellular microenvironment and tissue architecture. Collagen based hydrogels have good biocompatibility and cross linking pattern can be controlled by concentration and sonication time, which makes that suitable for range of tumours [269]. Alginate is another mostly using polymer derive from seaweed. The most commonly used natural hydrogel platform is reconstituted basement membrane matrix (Matrigel) derived from murine tumours [276]. Researchers used 3D matrigel to evaluate different anti-invasive compounds (NF-kB, GSK-3-B, COX-2, and tubulin inhibitors) toxicity and invasion inhibition in U-251 MG spheroids. The results indicated that the compound effectiveness is strongly linked to intra- and inter-tumour heterogeneity in patients [281].

Synthetic hydrogels are made up with synthetic polymers such as polylactic acid, poly (vinyl acetate), polyethylene glycol, polyacrylamide, polyacrylic acid, polyvinyl alcohol and polyvinylpyrrolidone are some of them [222, 248]. Natural hydrogels are progressively being replaced by synthetic hydrogels due to higher water absorption capacity, higher strength, longer stability, and extensive availability of raw chemical resources [282].

Advantages of using hydrogels for 3D cell culture includes controllable porosity, elasticity, variation in stiffness, high water content, able to provide similar microenvironment and reproducibly, able to provides rich network of ECM signals,

ability to construct combining both synthetic and natural materials and ability to couple with adhesion, proliferation, differentiation, and migration factors [248, 274, 276]. While demerits including physically weaker, lack of vasculature, natural gels composition can be inconstant and also lack of cross linked network for mechanical support 3D spheroid growth [269]. In future, researchers can try to develop hydrogels using similar ECM components and composition in a particular tissue / tumour site to get similar *in vivo* TME [269].

Hydrogels can also be designed to release therapeutics, while changing their retention period in the tissue. Scientists developed a ROS responsive hydrogel (zebularine - anti-PD1 antibody - NPs-gel) cross-linked by combining polyvinyl alcohol and N1-(4-boronobenzyl)-N3-(4-boronophenyl)-N1,N1,N3,N3-tetramethylpropane-1,3-diaminium (TSPBA) linker to utilize the acidic TME and ROS within tumours for the controlled release of zebularine, a demethylation agent, and a PD1 antibody. This combined treatment boosted cancer cell immunogenicity, reducing tumour growth and prolonging the survival time of B16F10-melanoma-bearing mice [283].

Researchers are mostly adopting low adhesion plate and hydrogel-based approaches to construct basic tumour models and multicellular tumour spheroids. Recently scientists investigated more advanced techniques and equipment to develop more complex brain tumour models to better mimic the biochemical interplay of the brain and brain cancers as technology evolved. To facilitate spheroid formation in 3D cell culture platforms, microfluidic devices may, for example, uniformly provide oxygen and nutrients while eliminating waste. For instance, advanced brain tumour models with intact BBB may be printed using 3D bio-printers to investigate the possibility of opening the BBB and enhancing chemotherapy delivery without adverse effects. It may also be used to investigate membrane-wrapped and co-culture models.

1.10.4 Microfluidic devices

Microfluidic devices (Figure 10C) process / manipulate micro liquids (usually less than 10 μ l) inside micro sized channels with dimension of 1-1000 μ m [284]. Microfluidic channels are connected to each other by porous membranes produce spheroids and able to formation, maintenance and testing inside single device with vasculature - mimicking microfluidic channel connections [220, 249, 265, 269]. Furthermore, this technology enables for the investigation of cell - cell interactions as well as interactions between different tissues [220].

Microfluidics are classified into two types: flow-based channel microfluidics (CMF) and electric-based digital microfluidics (DMF). Individual droplet manipulation, multistep processes, flexible electric-automatic control, and the ability for point-of-care are all benefits of DMF over CMF [285]. The physical barrier of microfluidic 3D cell culture system is composed of glass / silicon, polymers such as polydimethylsiloxane (PDMS), polymethylmethacrylate, polycarbonate and polystyrene. PDMS is the most often utilized substance due to biocompatibility, inexpensive, has good gas permeability and transparent capability, however, scaling-up process is more difficult [274]. Simple microfluidics devices are increasingly being fabricated and created by soft lithography techniques to develop patterned environments that are reasonably easy to fabricate and compatible with the majority of biological systems [222, 277].

Microfluidics technique capable of continuous perfusion for faster spheroid formation, to produce uniform size and shape spheroids for high-throughput screening, It allows patterning of cells and extracellular environment to create co culturing cells in spatially controlled manner, generation of and control signalling gradients, integration of perfusion, low reagent / sample consumption, which significantly reduces costs in bioanalysis, real-time imaging and to constructing tissue - level and organ level structures

in vitro [222, 229, 265, 272]. In the other hand disadvantage is it is highly expensive, hard to collect cells for analysis, hard to scale-up, need complicated equipment and complexity [256, 265, 269].

Microfluidic devices are complex dynamic micro scale environments that simulate 3D *in vivo* environments, such as a complex chemical gradient. Its micro scale dimensions are consistent with those of numerous *in vivo* microstructures and environments [286]. Capillaries in the brain, for example, ranging from 7-10 μm in diameter, with an average intercapillary distance of about 40 μm [287]. Microfluidic devices' versatility and simplicity of fabrication allow them to be used in a wide range of applications in glioma research. These include migration studies, biomarker assessment, cell sorting from tissue samples, and treatment effectiveness testing [288, 289]. The time course for culture is heavily influenced by cell type, cell density, and device type. Scientists might possibly obtain critical information on tumour status from specific patient samples using microfluidic devices and recommend personalized therapy within in two weeks [286].

Researchers demonstrated that organ-on-a-chip GBM model matched the clinical outcomes during the patient-specific sensitivity against TMZ. This technology has also been used to study the interaction within the perivascular niche, which suggests that glioma CSCs located around the vasculature and presenting with the lowest motility are most likely of the proneural subtype, while those with the highest invasiveness are most likely of the mesenchymal subtype; this further supports the role of the tumour niche on intratumoral heterogeneity and subsequent treatment response [290]. In another study, an oxygen and nutritional gradient is produced in the tumour cell embedded ECM containing core chamber by delivering a regular flow via one lateral channel while shutting the other [291]. This model replicates blood artery thrombosis in the brain, as seen in GBM growth, and allows for the observation of thrombosis - induced variables that impact invasion in

real time [291]. The promise of microfluidic devices as sophisticated artificial systems capable of mimicking *in vivo* nutrition and oxygen gradients during tumour progression [291].

The development of microfluidic technology has simplified, facilitated, and shortened the drug discovery process [292]. It also a valuable tools for the development of wide range of biological systems, from single-cell biophysical characterization to the miniaturization of a complete laboratory onto a single chip (lab-on-a-chip), and lately, the recapitulation of organ physiological parameters onto a chip (organ on chip / vasculature on a chip) [272, 293].

1.10.5 3D Bio printing

3D Bio printing (Figure 10D) is a novel bottom-up approach to fabricate complex biological constructs for 3D cell and tissue culture [235]. It is also able to control mechanical and biological properties of the construct with high resolution in the X, Y and Z planes [267]. 3D bio printing is layer-by-layer deposition of bio-inks [232] to build viable 3D constructions in a spatially specified way, guided by a computer-aided software [294, 295]. It's able to enhance additional factors (cell types, materials, growth factors, differentiation factors and print the 3D construct with extraordinary spatial control at high resolution through a layer by layer process [239, 294]. The main issue for bio printing is to print cells and bio-ink concurrently without impacting cell viability or substituting chemical solvents [248].

The bio-inks can be classifies as soft biomaterials (scaffold base bio-ink) and cells bio printed without an exogenous biomaterial (scaffold-free bio-ink) [295]. Layers of soft biomaterials are deposited to form an ECM, which contains live cells, arranged into a cell network that closely resembles the real tumour [296]. Single - step bio fabrication techniques including inkjet, micro extrusion, and laser - assisted bio printing uses with

soft biomaterials, which can fabricate 3D structures decreasing user input mistakes [277, 295]. While scaffold-free bio-ink, cells are grown up to small neo tissues that are three-dimensionally scattered and will eventually combine and develop to a more complicated structure. It is also possible to use 3D bio printing to create biosimilar a-cellular scaffolds and then include a cellular component using the top-down method (two-step fabrication), this approach has several limitations, including poor reproducibility, cell density control, and spatial distribution control [277, 295].

3D printing can applied to develop GBM models with vascular channels to get better understanding of six core and two emergent hallmarks underpin tumour development and metastasis [169]. Research team developed of an integrated platform that allows for the generation of an *in vitro* 3D GBM model with perfused vascular channels that allows for long-term culture and drug (TMZ) delivery [297]. GSCs have been revealed in recent research to have a role in tumour vascularization by secreting vascular endothelial growth factor (VEGF). Wang et al., 2018, used 3D printing to create a 3D glioma model to investigate the vascularization potential of patient-derived CSCs [298]. Heinrich et al. (2019) created a 3D - bioprinted mini-brain made up of GBM cells and macrophages to explore the interaction between glioma CSCs and other non-tumour cells. The authors discovered that glioma cells interact with macrophages and induce Tumour associated macrophages (TAM) polarization in patients' tissue [299].

Scientists used cellular and a-cellular components from the patient's adipose tissue to create a variety of customised bio-inks. After transplantation, these tailored patches will not elicit an immunological response, obviating the requirement for immunosuppression. This demonstrates the 3D printing approach's potential for organ replacement after failure or drug screening in a suitable anatomical framework [300]. 3D biological constructions are a novel and promising method of research not only in GBM but also in other diseases

[296]. Recently, researchers used this techniques and tailored hydrogel as a bio-ink to construct a thick, vascularized, perfusable cardiac patch and heart-like structure. These cardiac patches are a potential field for human tissue engineering since they perfectly match the patient's immunological, biological, biochemical, and anatomical features [300]. The similar technique can be applied by using the personalized brain patches, possible to replicate the architecture of tissues to get better understanding of the therapeutic efficiency.

Table 5: Different types of 3D cell culture techniques and their applications, outcomes in glioma research

3D cell culture technique	Cell line / type	Drug/ treatment combination	Outcomes	References
Ultra low attachment plates	CT-2A mouse glioma	Nano formulation of atorvastatin (ATV)	Growth inhibition was more significant for the micellar – ATV formulation compared to free ATV in 3D models.	[301]
	U-87 MG and C6 glioma cells (CCL-107)	Retinoid bexarotene (BXR) derivatives with dopamine (DA) and nitroethanolamine amide (NEA)	Tumourspheroids demonstrated higher resistance to the treatment. BXR-DA, BXR-NEA resulted in a synergetic cytotoxicity increase, induce apoptosis and inhibit cell spreading	[302]
	U-251 MG	CAP	CAP effectively induce 3D GBM cell death in a time-, dose-, treatment frequency, and ROS-dependent manner. CAP also reduce 3D GBM spheroid growth, cell proliferation and induce damage to the TME.	[106]
	U-87 MG	DOX loaded polymeric nanotubes	DOX loaded nanotubes significantly reduced the 3D cell viability in a dose dependent manner, whilst unloaded nanotubes showed no cytotoxicity.	[303]
Hanging drop plate	U87-MG	Poly(dimethylsiloxane) and resin-based drop array chip and a pillar array chip with alignment stoppers	Enhances the alignment between the chips for uniform placement of spheroids.	[304]
	LN-229	Silicon chips	Simple design elements enable high drug screening duplicates, direct on-chip real-time or high-resolution confocal imaging, and geometric control in 3D.	[305]
Spinner bioreactor	GBM 4, 8	-	Nonexistence of connexin43 reduces glioma invasion in 3D model	[306]
Ca-alginate scaffolds	U-251 MG	-	Gene expression profiling showed that cell cycle and DNA replication gene down-regulated, and genes involved in mitogen - activated protein kinase signaling, autophagy, drug metabolism through cytochrome P450, and ATP binding cassette transporter were up-regulated in 3D, compared to 2D cells.	[307]
Collagen Scaffold	U-87 MG	TMZ, Cisplatin (DDP), CCNU	With a substantially greater proportion of GSCs and upregulation of MGMT, 3D grown cells also displayed improved resistance to chemotherapeutic, alkylating drugs.	[308]
Polystyrene scaffolds coated with laminin	U-251 MG	-	The findings show that 3D context has an impact on integrin expression, particularly the upregulation of the laminin binding integrins alpha 6 and beta 4.	[309]

Hydrogels	U-87 MG	Novel bio-inspired brain matrix (BBM) composed of an agarose base and poly-L-lactic acid 6100 (PLA) fibers	BBM able to supports tumour growth, enables rapid tracking of neural stem cells migration and therapy.	[310]
	Patient-derived GBM cells	HMC3 microglia	Microglia co-culture significantly inhibited GBM invasion but enhanced proliferation	[311]
	D-270 MG, U-87 MG	Three patient-derived cell lines were compared including adult GBM cells, pediatric GBM cells, and diffuse pontine intrinsic glioma.	The findings imply that brain tumour behaviour is influenced by both patient age and tumour site. (tumour proliferation, invasion and morphology)	[312]
	U-251 MG	shRNAs targeting human LIMK1 and LIMK2	LIM kinase isoforms LIMK1 and LIMK2 strongly regulate GBM invasive motility and tumour progression and support.	[313]
Microfluidic device	Triple co- culture of U-87 MG, hCMEC / D3 cells and astrocytes.	Antibody-functionalized nutlin-3a loaded nanostructured lipid carriers (Ab-Nut-NLCs)	The approach successfully blocks dextran diffusion through the bioinspired BBB while enabling Ab-Nut-NLCs to pass through.	[314]
	U-251 MG, U-87 MG	TMZ and simvastatin	Cells were significantly less sensitive to drugs and induction of apoptosis in the 3D model as compared to 2D. Autophagy inhibition had no effect on TMZ and simvastatin - induced apoptosis.	[315]
3D bio printer	U-87 MG	N-cadherin (NCAD)	NCAD prevented spheroid formation and induced cell death in the 3D model	[316]
	GSCs	Compared the growth of GSCs alone or with astrocytes and neural precursor cells in a hyaluronic acid - rich hydrogel, with or without macrophage.	Whole - genome CRISPR screening using bio printed complex systems revealed distinct molecular dependencies in GSCs, relative to sphere culture.	[317]
	U-87 MG, SU3 glioma stem cell line	hydrogel scaffolds were printed (Gelatin / alginate / fibrinogen Hydrogel)	The 3D bio printed <i>in vitro</i> glioma model provided novel alternative tool for researching gliomagenesis, stem cell, , anticancer drug susceptibility and treatment resistance, while showed higher resistant to TMZ compared to the 2D glioma model.	[318]
	U-87 MG	3D model including alginates, MM6 monocyte / macrophages, ECM proteins (collagen-1, hyaluronic acid), and glioma associated stromal cells.	GBM stem cells demonstrated greater resistance to chemotherapeutic drugs in 3D printed tumour than in 2D monolayer cultures.	[319]

Table 6: Comparison of different 3D cell culture techniques and equipments, highlighting their respective merits and demerits for both 3D tumour model production and applications.

3D culture method	Benefits	Drawbacks	References
Low attachment plate	Relative simplicity	Relatively labour intensive	[233, 236, 248, 264, 266, 269]
	Reproducibility	No support or porosity	
	Relatively low cost	Only autocrine ECM existing	
	Faster spheroid production	Difficulty in mass production	
	Suitable for long-term culture	Lack of uniformity (size / shape)	
	Suitable for multicellular spheroids (MCS) and co-culture	Continuous passage culture is challenging	
	Possible to use a high-throughput screening	Not suitable for migration or invasion assays	
	Cells can easily be removed from the media and utilized in subsequent experiments.	Cell aggregates form as a result of cell motility in the media.	
	Uniform spheroid size control	Some cell lines need expensive plates coated with specific materials	
	Availability of pre-coated plates		
	Plates are optically transparent		
Useful for drug screening, as well as direct visualization and analysis.			
Hanging drop plate	Relative simplicity	Long term culture difficult	[233, 236, 264, 269]
	Uniform spheroid size control	Smaller culture volume	
	Co-culture feasibility	Impossible to medium exchange	
	Suitable for high-throughput testing	Not suitable for migration, invasion or cell viability assays	
	Relatively low cost	Smaller size of spheroids	
	Reproducibility	Labour intensive	
		Not suitable for drug testing	
Tedious spheroid handling and transfer			
Magnetic levitation	Relative simplicity	3D culture is coloured brown	[264, 269]
	Efficient	Limited applications	
	Not required specialized media	Cellular behaviour might affect	
	Easy to collect spheroids and change media	Numerous cells also attach to the plate's bottom	
	Capable of being employed on non-self-aggregating cells	Magnetic beads need pre-treatment and can be expensive	
	Suitable for mass production	Difficult to change media	

Spinner bioreactor	Relative simplicity	Larger medium volume needed	[236, 248, 264, 268, 269]
	Suitable for long-term culture	Special apparatus needed	
	Homogeneous media composition	Higher variability in size and shape	
	Customizable and controllable culture parameters	Exposed to high shear force	
	Possible to use a high-throughput screening	Not suitable for drug testing	
	Minimum labour	Higher costs	
	Stimulated metabolite transport		
	Higher similarity to the <i>in vivo</i> conditions		
Scaffold based	Mimic <i>in vivo</i> microenvironment	Difficulty of cell retrieval	[236, 238, 248, 264, 269, 274, 276]
	Relative ease handling	Low optical transparency	
	Suitable for long-term culture	Not suitable for drug testing	
	Suitable for co-culture	Variation in scaffold-to-scaffold	
	Compatibility with all types of cells and well plates	Limited high-throughput screening	
	Properties can be modified according to the study	Expensive for large scale production	
	It is simple to prepare for immunohistochemistry analysis.	Lack of uniformity (size/shape)	
	Higher similarity to the <i>in vivo</i> conditions	Scaffold materials may affect the cellular adhesion, growth and behaviour	
	Direct visualization	Restricted control over self-assembly	
	Availability of wide range of materials, including a decellularized matrix	Cells connected to the scaffolds flatten and proliferate in the same way as 2D cells	
Hydrogels	Cells can be easily recovered for further analysis	Low repeatability depending on cell line	[229, 233, 238, 248, 269, 276]
	Possible to use a high-throughput screening	Difficulty of cell recovery from hydrogel	
	Wide variety of polymers availability	Poor mechanical properties	
	The ability to customize properties	Low optical transparency	
	Higher similarity to the <i>in vivo</i> conditions	Natural hydrogel's components are variable and undefined	
	Cellular attachment, proliferation, and differentiation are all stimulated.	Bioactive ingredients in hydrogels may influence the structural formation	
	Suitable for study the aggressiveness of the cells and metastasis	Labour intensive and time consuming	
	Mimic <i>in vivo</i> microenvironment	Batch to batch variation	
Microfluidic device	Ability to control spheroids size and parameters	High cost for the microfabrication and devices	[229, 239, 248, 268, 269, 276, 292, 293]
	Continuous perfusion aids in the development of spheroids	Difficult to collect cells for further analysis	
	Real time imaging possible	Required expertise	
	Capable of incorporating vascular and circulation like components	Limited high-throughput screening options	

	Mimic <i>in vivo</i> microenvironment	Issues with contamination	
	High-throughput assays regarding toxicity, targeting, efficacy, and organ distribution	Design dependant outcomes	
	Commercially available		
	Higher gas permeability		
	Higher optical transparency		
	Large amounts of data may be obtained from small samples.		
	Able to construct <i>in vitro</i> organ specific device		
3D bio printing	Replicate the complex 3D tissue architecture	Higher Cost of bio printer and bio inks	[239, 292, 296]
	Possible to use a high-throughput screening	Low accuracy of cell positioning	
	Complex interactions between TME or ECM and cells	Printing resolution can yet be enhanced	
	Mimic <i>in vivo</i> microenvironment	Need photo crosslinking	
	Suitable for study the invasiveness of the cells and metastasis	Effective biomaterials are required.	
	Suitable for study the drug efficiency, cell signaling, immunologic interactions and cellular crosstalk		

1.11 Advance TME models and applications

1.11.1 Cancer stem cells (CSC)

CSC differ from typical stem cells in several ways, including hyper-efficient DNA repair processes, the expression of multidrug resistance-related ATP-binding cassette (ABC) membrane transporters, hypoxic niche tolerance, and the over-expression of anti-apoptotic proteins. Furthermore, in the case of cancer, the difference between CSCs and non-CSCs may be linked to epithelial-to-mesenchymal transition (EMT) [265, 277]. Scientists have recently focused on CSC due to their role in tumour growth, metastasis, recurrence and drug resistance, and 3D cell culture is a vital tool to studying that due to the abundance of CSC [244, 265, 269]. CSC from 3D cell culture have a distinct morphology signaling pathway profiles, cell – ECM and cell – cell interactions and gene expression pattern than CSCs from 2D culture [244, 265]. Multiple genes related with stress response, inflammation, redox signaling, hypoxia, and angiogenesis are up-regulated. In comparison to 2D cultures, CSC spheroid cultures demonstrated benefits such as increased paracrine cytokine production, stronger anti-apoptotic and anti-oxidative properties, and higher amounts of ECM proteins [222, 244]. GSC share features of GBM such as resistance to therapeutic treatments, high invasiveness, and similar epigenetic patterns. The DNA methylation pattern of GBM-derived cancer stem cells was analysed, and it was shown that these cells have the same methylation pattern as primary GBM derived xenograft tumours [320]. It implies that GSC culture conditions preserve the majority of their original epigenetic pattern, implying that GSC are legitimate and appropriate *in vitro* model for determining the functional effect of epigenetic alteration on cellular parameters [238, 320]. Researchers demonstrated that the growing GBM cells on 3D porous chitosan-alginate scaffolds greatly enhances proliferation and enrichment

of cells possessing the hallmarks of CSCs. The 3D model was discovered to be more tumourigenic and to promote the expression of genes involved in the EMT, which has been linked to the development of CSCs [321].

1.11.2 Blood–brain barrier (BBB)

BBB prevents several chemotherapeutic drugs from accumulating to effective concentrations in GBM and other brain tumours [169]. Researchers developed 3D-bioprinted GBM and BBB models, focusing on the TME compositions of GBM and BBB, appropriate biomaterials to imitate the *in-vivo* tissue architecture, and bio-printing methodologies for model fabrication. This model offer potential systems for more reliable mechanistic research and preclinical drug screens [322]. Hajal and colleagues (2022), also developed an *in vitro* model of the human BBB from stem cell-derived / primary brain endothelial cells, primary brain pericytes, and astrocytes that self-assembled within microfluidic devices. This BBB model showed important cellular structure and morphological traits, as well as molecular permeability values that are within the predicted *in vivo* range. These characteristics, together with a functional brain endothelial expression profile and the ability to test several repetitions rapidly and inexpensively, make these advance BBB models excellent for therapeutic discovery and development [323].

1.11.3 Immune cells

TME is entails of a diverse population of immune cells, including microglia, macrophages, CD4+ T cells, CD8+ T cells, regulatory T cells, myeloid-derived suppressor cells, natural killer (NK) cells, and dendritic cells, indicating that GBM has a strong immunological component [324]. Parenchymal microglia play critical roles in brain development, homeostasis maintenance, disorders and regulating several

mechanisms such as synaptic pruning, maturation, and angiogenesis [325]. Because of their ramified motile processes, parenchymal microglia are capable of monitoring and phagocytizing any hazardous chemicals [325]. Furthermore, microglia can enhance angiogenesis, emphasizing the importance of microglia-cerebral vasculature communication [325]. Macrophages are also engaged in brain homeostasis maintenance and reside in the non-parenchymal perivascular space, subdural meningeal spaces, and choroid plexus spaces [325, 326]. These Glioma associated microglia and macrophages have been demonstrated to adopt predominantly M2 phenotypes, leading to anti-inflammation / immunosuppression and hence aiding tumour development [324, 327]. Tumour cells appear to promote microglia mobility by upregulating genes involved in migration and invasion [324, 327]. IL- 10, MMPs, and arginase-1 are further immunosuppressive substances released by glioma-associated microglia and macrophages [324]. Furthermore, tumour cells and glioma associated microglia and macrophages secrete chemokines like monocyte chemoattractant protein-1, CCL2, capable of attracting myeloid derived suppressor cells such as immature macrophages, granulocytes, dendritic cells, and myeloid progenitors to the tumour [324, 326]. Ultimately they can promote tumour growth through the release of anti-inflammatory cytokines for instance transforming growth factor beta (TGF- β) and interleukin -10 (IL-10) [324, 326]. There is, however, a lack of advanced 3D GBM models to study parenchymal, peripheral immune cell crosstalk and immune cell infiltration.

1.11.4 Microbiome

Microbiome play an important role in the human immune system's induction, preparation, regulation, and function, while specific microbiota may also lead to immune suppression [328, 329]. Gut microbiota generates metabolites such as short chain fatty acids, which inhibit pro-inflammatory cytokine release, promote regulatory T cell growth and IL10

secretion [328, 329]. A portion of the circulating short chain fatty acids may potentially enter the CNS [329]. Furthermore, the integrity of the BBB is compromised during neuro-inflammation due to the actions of IL1, IL6, and TNF α [328, 329]. It has to be established if the microbiome - induced mediators or metabolites also affect the BBB disruption and elicit immune suppression in the brain [329]. The brain, glands, gut, immune cells, and gastrointestinal microbiota are all part of the microbiota–gut–brain axis. Gut microbiota also influences brain function and behaviour through neuronal, endocrine, and immunological pathways [329, 330]. Researchers revealed that the gut microbiome influences the anticancer immune response and reduces the effectiveness of chemotherapeutic cancer treatment [330]. The potential impact of the microbiome on brain tumour treatment techniques should be investigated with more advance 3D co-culture models with tumour - resident bacterial strains.

1.11.5 GBM / normal tissue interactions

Investigating GBM / normal tissue interactions are vital in brain cancer therapeutics hence, advanced 3D GBM co-culture models will be needed to develop, to explore the crosstalk and metabolic interactions between glioma cells and the normal glial cells such as astrocytes, oligodendrocytes, neurons and a range of normal resident brain cells. 3D cell culture also able to co culturing with different cell types, including mixed populations of tumour cells and cancer associated fibroblasts (CAF), to develop increasingly accurate *in vitro* models of disease and physiology [236]. The importance of GBM cellular interaction with endothelial cells can be studied with co culture techniques to get proper understanding of the endothelial interaction on tumour progression for identify novel therapeutic approaches [236, 256]. Also by adding cells such as blood vessels, can use to investigate interactions between blood vessels and cancer or how drug help to antiangiogenic effect in cancer. Researchers examined available *in vivo* data to calculate

the quantities and numerical ratios of GBM and normal brain cells necessary to establish a complete and incomplete GBM resection dual co-culture model. The results indicated that drug discovery utilizing this dual co-culture methodology is feasible and provides steady and reliable drug testing outcomes [331].

1.11.6 GBM organoids

GBM organoids are a novel experimental paradigm of modern reductionists' approach. The combination of embryonic stem cells or induced pluripotent stem cells or resident stem cells, contemporary 3D culture, controlled environment and differentiation techniques has allowed us to leverage pluripotent stem cells' self-organization capacity to form human brain-like tissues known as brain organoids or mini-brains [18, 296]. Brain organoids are a promising new technology that has opened up new avenues for cancer modeling, *ex vivo* investigation of molecular and cellular mechanisms [237, 296], while many properties of neural epithelial cells in these 3D tissues are cyto-architecturally analogous to the developing human brain [18, 220]. These organoids imitate the *in vivo* cell heterogeneity present in the TME by resembling the *in vivo* architecture of the tissue of origin and recapitulate cell proliferation, self-organization, and differentiation [220, 238]. A GBM model was created by genetically engineering brain organoids in a recent study. Researchers developed a GBM model organoid by inserting the HRasG12V oncogene into human brain organoids and using CRISPR / Cas9 to alter the fourth exon of the TP53 locus. This mutant cell, which has a characteristic similar to the aggressive mesenchymal subtype of GBM, proliferates quickly and invades the organoid. Furthermore, they revealed that primary human derived GBM cell lines can be transplanted into human cerebral organoids to induce tumours [220, 296, 332]. Recently, scientists also employed brain organoids to model CNS pathologies of COVID-19 and provide initial insights into the potential neurotoxic effect of SARS-CoV-2 [333]. Gunti

and colleagues (2021), reviewed several tumour organoid models, procedures for establish them, recent advances and applications of tumour organoids in detail [249]. Currently, basic organoid models are being used by researchers for therapeutic discovery and development. In future we need to develop multifactorial complex models incorporating CSC, BBB, GBM TME, including microbiomes, vasculature, extracellular matrix, infiltrating parenchymal and peripheral immune cells and molecules, exosomes and chemical gradients to develop personalized medicine and to achieve efficient therapeutic discovery and development.

1.12 Research question

Our research question is whether the CAP and US technologies (alone or in combination) will provide a novel cancer therapy solution. Our hypothesis is that CAP will be able to effectively induce cytotoxicity, while cavitation will allow retention and subsequent increase in the uptake of the active species, providing a significantly greater cytotoxicity effect in 3D GBM tumour spheroid models.

The research question were divided as follows:

- 1) GBM treatment has been ineffective so far, resulting in a five-year survival rate of less than 10%. Despite recent advancement in treatment options, the disease still remains largely incurable. Can we develop a novel and more effective GBM treatment methods?
- 2) Existing 2D cell culture models for therapeutic discovery and development against GBM have limitations. Can we optimize 3D cell culture systems that

promise more accurately simulating the natural *in vivo* environment, shape, tissue stiffness, stressors, gradients and cellular responses?

- 3) As our knowledge of CAP impact on cancer cells' biological and chemical functions continues to expand, there are still some gaps to be addressed. How does CAP affect cells that grow in a 3D matrix, and what are the cytotoxic and apoptotic outcome? Could the use of CAP, improve the effectiveness of GBM therapy and contribute to clinical utility in cancer treatment?
- 4) Can different US devices induce 3D tumour sphere cytotoxicity in a dose- and time- dependent manner?
- 5) Can US enhances drug diffusion, uptake, and cytotoxicity in 3D GBM spheroid models and what is the outcome when compared with 2D cell cultures?
- 6) Is it possible to combine US with CAP to improve GBM therapeutic effectiveness and to develop a novel cancer treatment method? In addition, can we investigate the apparent cell death mechanisms involved in GBM 3D tumour spheres?
- 7) What is the synergistic effect of US and plasma micro bubbles (PMB) and can effectively induce 3D GBM tumour sphere cell death in a time-, dose-, treatment frequency, and ROS-dependent manner?

1.13 Research aim and objectives

The aim of this project is to investigate the effectiveness of non-thermal therapies, such as CAP, US, and PMB (alone or in combination) for the treatment of GBM using 3D tumour spheroid models. Reporting for the first time the effects of such interaction and proving the basis to further development of this new approach for GBM therapy. Furthermore, it lays the foundation for the development of advanced 3D culture systems that can facilitate therapeutic discovery and development for brain cancer.

The aims and objectives were divided as follows:

- I. To construct and optimise different *in vitro* 3D GBM tumour spheroid models to closely mimic the natural *in vivo* environment, shape, and cellular response.
- II. To biologically characterise a novel CAP device, determining its optimum settings and effectively induce cytotoxicity in 3D GBM tumour spheres.
- III. To determine the optimum US probe device parameters for induction of cytotoxicity and US guided drug delivery to the 3D GBM models.
- IV. To evaluate the synergistic effect of CAP and US cavitation on 3D GBM models and to find out the apoptotic mechanism inducing cytotoxicity.
- V. To determine the optimum US water bath (WB) and PMB device parameters, establishing its cytotoxicity and sonoporation capacity.

CHAPTER 2 – MATERIALS AND METHODS

Part of this Chapter has been published.

- Lara J Carroll, Brijesh Tiwari, James F Curtin, **Janith Wanigasekara** 2021. U-251MG Spheroid generation using low attachment plate method protocol. protocols.io <https://dx.doi.org/10.17504/protocols.io.bszmnf46>
- Lara J Carroll, Brijesh Tiwari, James F Curtin, **Janith Wanigasekara** 2021. U-251MG Spheroid Generation Using Hanging Drop Method Protocol. protocols.io <https://dx.doi.org/10.17504/protocols.io.btstnnen>
- Lara J Carroll, Brijesh Tiwari, James F Curtin, **Janith Wanigasekara** 2021. U-251MG Spheroid generation using a scaffold based method protocol. protocols.io <https://dx.doi.org/10.17504/protocols.io.bszaqnf5w>
- Aisling Field, Brijesh Tiwari, James F Curtin, Julie Rose Mae Mondala, **Janith Wanigasekara** 2022. Ultrasound 96 Probe Device Protocol for cancer cell treatment. protocols.io <https://dx.doi.org/10.17504/protocols.io.b3udqns6>
- Aisling Field, James F Curtin, **Janith Wanigasekara**, Julie Rose Mae Mondala 2023. Liposome Encapsulation of Hydrophilic and Hydrophobic Drugs. protocols.io <https://dx.doi.org/10.17504/protocols.io.rm7vzymorlx1/v1>

See Appendix II – Non peer-reviewed

2 Materials and Methods

2.1 Chemicals

All chemicals used in this study were supplied by Sigma-Aldrich—Merck Group unless stated otherwise.

2.2 2D cell culture

The human GBM cell line (U-251 MG, formerly known as U-373 MG-CD14) was a gift from Michael Carty (Trinity College Dublin). U-87 MG, A-172 human GBMs and the human epidermoid carcinoma (A431) were purchased from an ATCC European distributor (LGC Standards). The absence of mycoplasma was checked by using a MycoAlert PLUS mycoplasma detection kit (Lonza). Cells were maintained in Dulbecco's modified Eagle medium (DMEM) - high glucose supplemented with 10% fetal bovine serum (FBS) and 1% penicillin/streptomycin. Cells were maintained in a humidified incubator containing 5% CO₂ atmosphere at 37°C in a TC flask T25, standard for adherent cells (Sarstedt). Cells were routinely sub-cultured when 80% confluence was reached using 0.25% w/v Trypsin-EDTA solution.

2.3 3D cell culture

Three different methods (low attachment plate, hanging drop plate, and natural scaffold) used to construct an *in vitro* 3D GBM and epidermoid tumour spheroid models to closely mimic the natural *in vivo* environment, shape, and cellular response.

2.3.1 Low attachment plate method

U-251 MG, U-87 MG, A-172 human GBM cells and A431 human epidermoid carcinoma cells were used to generate tumour spheroids. Separately, the single cell suspensions were centrifuged at 5000 rpm for 5 min, removed the supernatant, tapped the tube and re-

suspended the cell pellet in DMEM-high glucose supplemented with 10% FBS and 1% penicillin / streptomycin. The single cell suspensions (with desired seeding density) were transferred to a sterile reservoir and seeded 200 μ l / well into Nunclon™ Sphera™ 96-well low attachment plates (Thermo Fisher Scientific) using a multichannel pipette ensuring pipette tips do not touch the surface of the wells to protect the surface coating. The low attachment plates were centrifuged at 1250 rpm for 5 min for U-251 MG, U-87 MG, A-172 cells and 4000 rpm for 10 min for A431 cells followed by incubation (37 °C, 5% CO₂, 95% humidity) [106, 270, 271]. After 24 h of incubation, the media must be replenished. 100 μ l media was removed without disrupting the tumour spheres and 100 μ l of fresh media (DMEM + 10%FBS + 1% penicillin/streptomycin) was added into each well and incubate at 37 °C (5% CO₂, 95% humidity). Fresh media is added every second day by replenishing old media in each well. The sides of wells should be used to remove or add media, and pipetting should be carried out at average or below average speeds to avoid disruption to spheroids. Tumour spheroid formation was observed within 3 days for A431 and 4 days for U-251 MG, U-87 MG and A-172 [271]. Tumour spheroid formation was visually confirmed daily using an Optika XDS-2 trinocular inverse microscope equipped with a Camera ISH500, and their mean diameters were analyzed using “ImageJ version 1.53.e” software.

2.3.2 Hanging drop plate method

U-251 MG, U-87 MG, A-172 and A431 single cell suspensions (with desired seeding densities) were used to generate tumour spheroids using HDP1096 Perfecta3D® 96-Well hanging drop plate. PBS was added to the reservoirs located on the peripheral rims, which are divided into sections. 2 ml of PBS was added to each plate reservoir section, and 1 ml was added per tray reservoir section. This prevented the hanging drop from drying throughout the incubation period. In order to achieve 5000 cells per 20 μ l of hanging drop,

the single cell suspensions prepared in DMEM-high glucose supplemented with 10% FBS and 1% penicillin / streptomycin at a concentration of 2.5×10^5 cells/ml. Each hanging drop well was able to hold 20-50 μ l of cell suspension, and any volume above 50 μ l resulted in droplet instability. Hanging drops can be formed by carefully pipetting 20-50 μ l of cell suspension into the centre of each well from the top side of the plate. Hanging drops should be formed on and confined to the bottom of the plate. Placed the lid on the plate and inserted the assembly into a humidified cell culture incubator at 37 °C and 5% CO₂. Tumour spheroids formation was visually confirmed within 4 days for U-251 MG, U-87 MG, A-172 and A431 [271, 273]. 5 μ l of fresh media was added back into the hanging drops by placing the end of the pipette tips in the neck region of the access holes/wells and the fresh media was slowly dispensed into the access holes. Once formed, tumour spheres can be transferred from the hanging drop plate to low attachment plates / pre-coated wells in the dish by adding 50 μ l of fresh media into each hole.

2.3.3 Scaffold based method

U-251 MG, U-87 MG, A-172 and A431 single cell suspensions (with desired seeding densities) were used to generate tumour spheroids using cellusponge 3D scaffolds. A 9 mm cellusponge disk was slowly placed in the middle of each well in a 24-well plate and 100 μ L was seeded from a cell suspension with a cell density of 5000k cells/ml. Cellusponge disks with cells were incubated at 37 °C (5% CO₂, 95% humidity) for 3 h to remove any air bubbles within the cellusponge. After incubation, 500 μ L of DMEM-high glucose supplemented with 10% FBS and 1% penicillin/streptomycin was added slowly along the edge of each well in a 24-well plate. Plates with cellusponge scaffolds were incubated overnight at 37 °C, 5% CO₂, 95% humidity. After overnight incubation, the seeded scaffolds were transferred into a new well plate, the media was replenished and

the culture should be continued. Tumour spheroid formation was observed within 3 - 4 days [271, 279].

2.4 Image J analysis

Tumour spheroid formation was visually confirmed daily using an Optika XDS-2 trinocular inverse microscope equipped with a Camera ISH500, and their mean diameters were analysed using “ImageJ version 1.53.e” software (<http://imagej.nih.gov/ij/>). ImageJ is a free software that can be used for manually counting the cell numbers and calculating the cellular size (area / diameter) [334]. The ImageJ program was calibrated (set scale) using an image obtained from the same microscope with a known scale before it was used to calculate the cell size (in diameter). Following the calibration, the pictures of the tumour spheres were opened in the program, and a line was drawn across the diameter to measure the tumour sphere's size. The diameters of the spheroids were measured at least three times to obtain the mean and standard deviation.

2.5 Growth analysis at different incubations

The growth of U-251 MG, U-87 MG, A-172 and A431 tumour spheres were analysed during different incubation (ranging from 24 to 168 h). Cells (initial seeding density was 10000 cells/ml) were seeded in the above mentioned NunclonTMSpheraTM 96-well low attachment plates [271]. Fresh media were added every third day by replenishing old media in each well without disturbing the tumour spheroids. In the hanging drop plate method, 5000 cells / well were seeded in the HDP1096 Perfecta3D[®] 96-well Plate. While in scaffold based method, 5000k cells / ml were seeded in the hydroxipropylcellulose scaffold. The spheroid formation and growth were monitored daily by using an inverted phase-contrast microscope, and the sizes of the spheroids were measured as described above using at least nine spheroids within the three biological repetitions.

2.6 Growth analysis at different seeding densities

For growth analysis, varying numbers of U-251 MG, U-87 MG, A-172 and A431 cells (ranging from 2000 to 40 000 cells / ml) were seeded in the above mentioned Nunclon™ Sphera™ 96-well low attachment plates for 96 h. Fresh media were added every third day by replenishing old media in each well without disturbing the tumour spheroids. In the hanging drop plate method, cells (ranging from 1000 to 10000 cells / well) were seeded in the above mentioned HDP1096 Perfecta3D® 96-well Plate. While in scaffold based method, varying numbers of cells (ranging from 1×10^6 to 6×10^6 cells / ml) were seeded in the hydroxipropylcellulose scaffold. The spheroid formation was monitored after 96 h by using an inverted phase-contrast microscope, and the sizes of the spheroids were measured as explained in section 2.4, using at least nine spheroids within the three independent experiments.

2.7 Spheroid cells health analysis

Spheroid cell health was analysed using the alamarBlue cell viability reagent (Thermo Fisher Scientific). After the post treatment incubation, tumour spheres were washed with sterile PBS, trypsinized using a 0.25% w/v trypsin–EDTA solution and incubated for 3 h at 37°C with a 10% alamarBlue solution [106]. During the scaffold based method tumour spheres embedded in the cellusponge 3D scaffolds were incubated for 24 h instead of 3 h [335]. Fluorescence was measured using an excitation wavelength of 530 nm and an emission wavelength of 590 nm with a Varioskan Lux multiplate reader (Thermo Scientific). The fluorescence signals were normalized by spheroid size (in diameter); a higher ratio indicates healthier spheroids. The experiments consisted of three independent tests in which at least nine spheroids were measured throughout three biological repeats.

2.8 Pin to plate system

A pin to plate electrode design was employed to generate a large volume atmospheric discharge. The reactor consisted of 88 slightly convex pins attached stainless steel electrode (150 mm x 200 mm), paired with a flat stainless steel ground plate (200 mm x 250 mm) powered by an AC power supply (Leap100, PlasmaLeap Technologies, Dublin, Ireland). The schematic and image of the pin – to - plate device demonstrating the position of the microplates for cell treatment is shown in Figure 11. This Leap100 power supply has a discharge voltage up to 80 kV (p-p), resonance frequency from 30 kHz to 125 kHz, discharge frequency from 100 Hz to 3000 Hz and power from 50 W to 700 W. The air gap between the pin electrodes and the ground plate serves as the sample treatment area, with all samples in this study being placed in the centre. All the samples were treated at a resonant frequency of 55.51 kHz, with a discharge frequency of 1000 Hz and duty cycle of 73 μ s while, the discharge gap was kept at 40 mm. The pin to plate system configurations, electrical characterization and optical diagnostics were previously detailed by Scally in 2020 [336]. Cells were treated for a time range of 0 - 320 s (0, 20, 50, 100, 160, 320 s). The electrodes / sample treatment area was covered in a fitted container to minimize escape of CAP generated reactive species into the general environment.

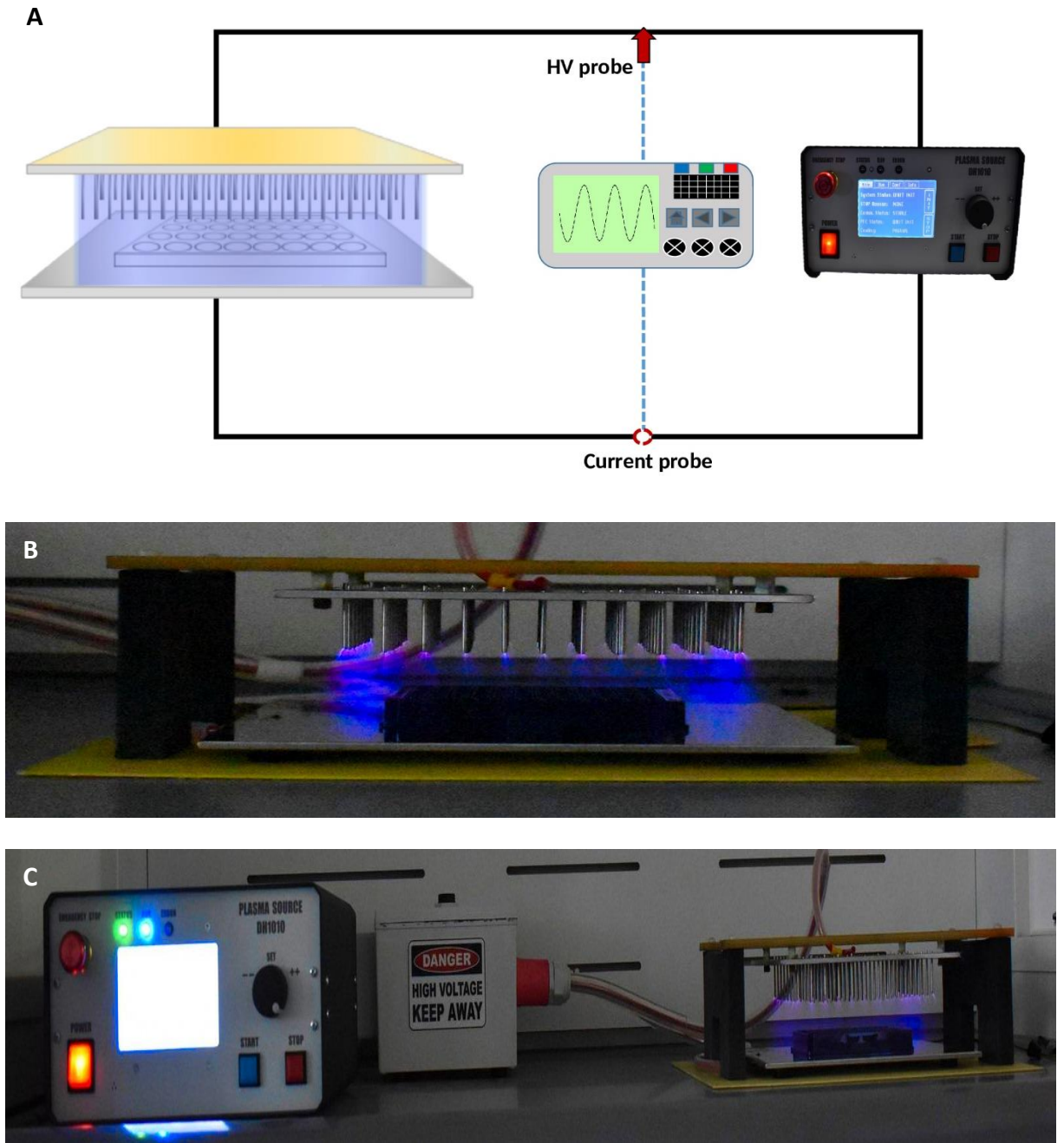


Figure 11: Dielectric barrier discharge (pin) system. A) Schematic of pin system B) Image of the pin – to - plate device demonstrating the position of the microplates for cell treatment C) a photograph of the pin system and atmospheric air discharge

2.9 Ultrasound probe device

The ultrasonic liquid processor (Figure 12A) used in this research was the VCX 750 [Dimensions H x W x D: (235 x 190 x 340 mm)]. It's robust and adaptable, processing a wide range of sample types and volumes for a variety of applications. The CVX 750 processor's maximum power output is 750 watt and its frequency is 20 kHz. This US device consists of a Ti6Al4V titanium alloy standard probe with a 13 mm tip diameter and a 139 mm replaceable tip length. We modified this by fixing a 96 well probe at the end of the replaceable tip. This 96 well probe is designed by using stainless steel, diameter of a tip is 2 mm and tip length is 20 mm. The 96-probe system is designed to fit perfectly into the 96 well plate (Figure 12B), which can be used to direct tumour sphere treatment. The retort stand is used to hold the US 96 probe unit vertically. A laboratory jack is used to hold the tumour sphere grown 96 well plate and to move it towards the 96 probes. A Sonics - Vibra cell power unit is needed to fix into this US 96 probe. Using the power unit, the US treatment time (0 to 99 min), temperature, pulser, and amplitude can be controlled. Experiments found that the best parameters to use are 20 % amplitude, pulses of 59 s on and 1 s off, with different time ranges (1, 3, 5, 10, and 20 min). During the treatment, place the sample (96 plate without lid) in the centre of the laboratory jack and slowly move it into the 96 probe. A 2 mm distance must be kept from the bottom of the well to the probe tip during the treatment. After setting up the unit, the device is turned on. The samples are treated with US using the parameters that were set.

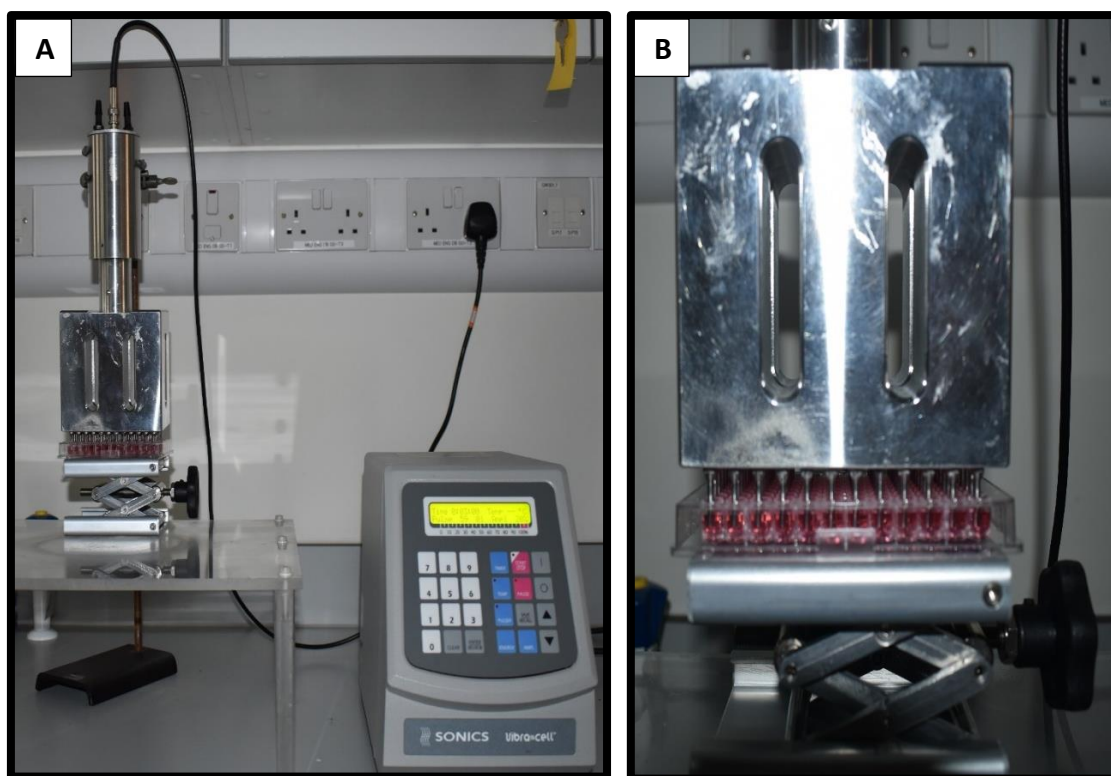


Figure 12: Ultrasound probe system. A) Image of US probe system B) Image of the probes demonstrating the position of the microplates for cell treatment.

2.10 Plasma microbubble (PMB) device

Plasma bubble reactors were fabricated using quartz tubes with an inner and outer diameter of 5.0 mm and 8.0 mm, respectively. Different numbers of laser drilled micro holes (1, 4 and 8 holes, 500 μm in diameter) were uniformly distributed around the base of the outer quartz tube. This allow compressed air to flow through the tube and diffuse into the aqueous solution. 1.0 L min^{-1} compress air flow speed used throughout the experiment and gas flow controlled by a gas flow controller (RS Components, Ireland) [128, 337]. A plasma-bubble discharge reactor was incorporated and powered by an AC power supply (Leap100, PlasmaLeap Technologies). The schematic and image of the PMB device demonstrating the position of the quartz tubes in a beaker for DMEM media treatment is shown in Figure 1. The Leap100 power supply has a discharge voltage up to 80 kV (p-p), resonance frequency from 30 to 125 kHz, discharge frequency from 100 to

3000 Hz, and power from 50 to 700 W. All the samples were treated at a resonant frequency of 55.51 kHz, with a discharge frequency of 1000 Hz and duty cycle of 73 μ s, while the input voltage was kept at 240 V. A discharge was created in bubbles exiting the reactor hole into the water / media (Figure 13), creating reactive species inside the bubbles that came into contact with the water through the large bubble / water interface surface area [338]. DMEM media was treated for a time range of 5–30 min to generate plasma activated MB.

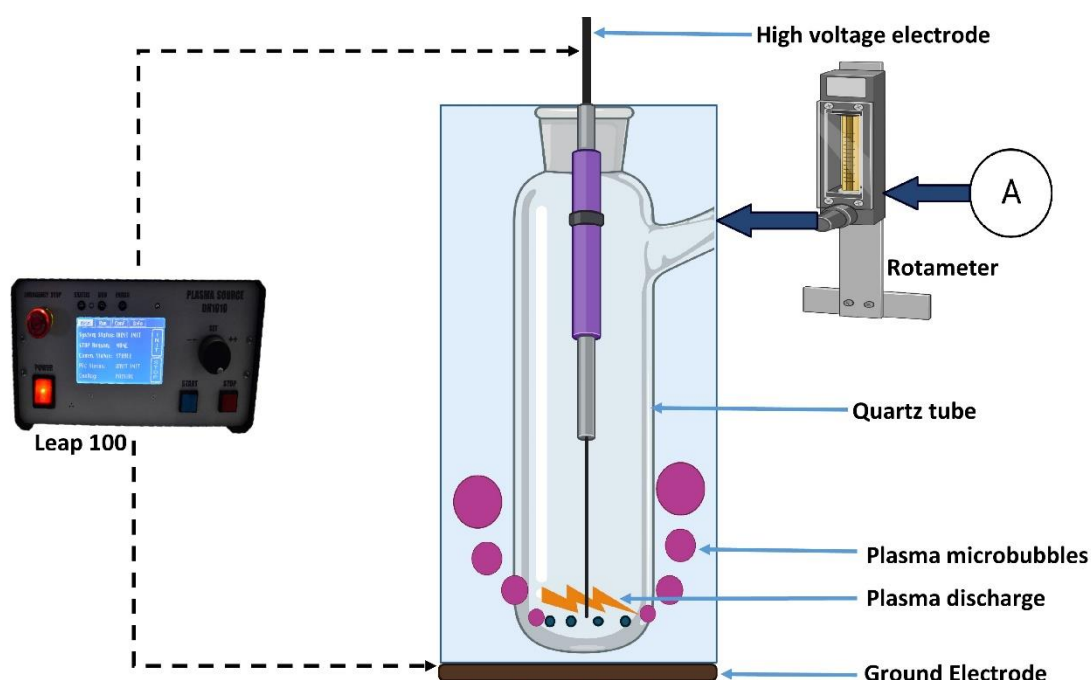


Figure 13: A schematic diagram of the plasma-bubble generator demonstrating the placement of the high voltage electrode, quartz tube, ground electrode, rotameter, leap 100 to generate PMB.

2.11 Ultrasound water bath (US-WB) device

An ultrasonic bath system (TI-H-5, Elma Hans Schmidbauer) was used for US generation and treatment. This is an US multi-frequency model with either 25 kHz or 45 kHz generated at the bottom of the water tank (Figure 14). The ultrasonic power was adjustable from 10% to 100%, and during this experiment we used 100% power (550 W). This device had several functions, including degas, normal, and sweep modes. However, during this experiment, we used the sweep mode for different doses of US since this mode was perfect for sound field distribution. No heating or cooling systems were used. A 96-well plate containing 100 μ l of media was placed in the water bath as shown in Figure 14.

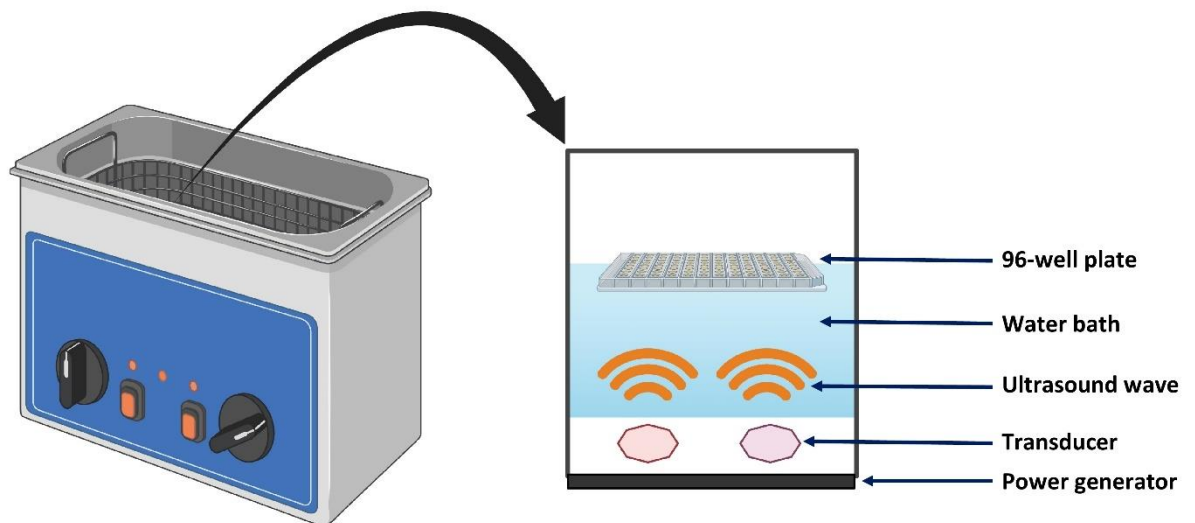


Figure 14: A schematic diagram of the US-WB used, illustrating the treatment position of the 96-well plate as well as the positioning of the transducers and power generator.

2.12 CAP and US treatments

U-251 MG and A431 cells were seeded at a density of 1×10^4 cells/well (100 μ l culture medium per well) into flat bottom 96-well plates (Sarstedt, Ltd) and were seeded at a density of 1×10^4 cells/well (200 μ l culture medium per well) into Nunclon™ Sphera™ 96-well -low attachment plates (Thermo Fisher Scientific) respectively, for 2D and 3D cell culture. Cells were incubated overnight at 37 °C in a humidified atmosphere. DMEM media without sodium pyruvate supplemented with 10% FBS and 1% penicillin / streptomycin, DMEM media supplemented with 0.11 g/L sodium pyruvate with 10% FBS and 1% penicillin / streptomycin and DMEM media supplemented with 0.11 g/L sodium pyruvate with 1% penicillin / streptomycin and without 10% FBS were used in this study as indicated. In the 2D cell culture, after 24 h incubation, 70–80% confluence was checked, 75 μ L of media were removed, leaving 25 μ L of media for treatment in each well. In the tumour spheres culture, after 3 days incubation for A431 and 4 days incubation for U-251 MG, 175 μ L of media were removed, leaving 25 μ L of media for treatment in each well, unless otherwise specified.

2.12.1 CAP treatment

Cells / tumour spheres were then treated with direct plasma exposure at six different time points (0, 20, 50, 100, 160 and 320 s) using a discharge voltage of 46 kV, frequency of 1000 Hz and using a duty cycle of 73 μ s. 75 μ L (for 2D) and 175 μ L (for 3D) of fresh culture media was added immediately following CAP treatment and incubated at 37 °C using 5% CO₂ for 24, 48, 72 and 96 h.

2.12.2 PMB treatment

DMEM media were treated with a PMB generator for different time points (5, 10, 15, 20, and 30 min) using a resonant frequency of 55.51 kHz, a discharge frequency of 1000 Hz, and a duty cycle of 73 μ s, while the input voltage was kept at 200 V. 100 μ L (for 2D) and 200 μ L (for 3D) of PMB containing media were added following the treatment and incubated at 37 °C using 5% CO₂ for 24, 48, 72, and 96 h.

2.12.3 US-WB treatment

Cells / tumour spheres were then treated with an US bath system at six different time points (0, 1, 3, 5, 10, and 20 min) using a TI-H-5 ultrasonic bath system. Using the power unit, the US treatment time (0 to 60 min), temperature, power, and frequency can be controlled. Experiments found that the best parameters to use are 100% power, and 45 kHz frequency with different time ranges (1, 3, 5, 10, and 20 min). 75 μ L (for 2D) and 175 μ L (for 3D) of fresh culture media were added immediately following the US treatment, and cells were incubated at 37 °C using 5% CO₂ for 24, 48, 72, and 96 h.

2.12.4 US probe treatment

In tumour sphere culture, after 3 days of incubation for A431 and 4 days of incubation for U-251 MG, 100 μ L of media were removed, leaving 100 μ L of media for treatment in each well, unless otherwise specified. Cells / tumour spheres were then treated with an US probe system at six different time points (0, 1, 3, 5, 10, and 20 min) using a Sonics - Vibra cell power unit, fixed into an US 96 probe. Using the power unit, the US treatment time (0 to 99 min), temperature, pulser, and amplitude can be controlled. Experiments found that the best parameters to use are 20 % amplitude, pulses of 59 s on and 1 s off, with different time ranges (1, 3, 5, 10, and 20 min). 50 μ L (for 2D) and 100 μ L (for 3D) of fresh culture media were added immediately following the US treatment, and cells were incubated at 37 °C using 5 % CO₂ for 24, 48, 72, and 96 h.

Dimethyl sulfoxide (DMSO) (20%) was used as a positive control. Single or multiple CAP / US / PMB treatments were carried out for the tumour spheres as where it is mentioned, where the multiple treatment is a combination of three individual treatments with a 24h incubation gap between each treatment.

2.12.5 CAP and US combination

The combinatory effect of US and direct CAP treatment was performed according to figure 15. Tumour spheres and cells were seeded and cultured as explained above. Next, tumour spheres containing 25 μ L of fresh DMEM medium were exposure to CAP with different time points (20, 50, 100, 160 and 320 s) using a discharge voltage of 46 kV, frequency of 1000 Hz and using a duty cycle of 73 μ s. Immediately after CAP treatment, Add 75 μ L of fresh DMEM medium in to each well and the 96-well plate containing the tumour spheres were placed in the US probe system for US treatment at six different time points (0, 1, 3, 5, 10, and 20 min) using a Sonics - vibra cell power unit. After treatment, 100 μ L of fresh medium was added and the tumour spheres were incubated for 96 h followed by cell viability analysis using alamarBlue assay.

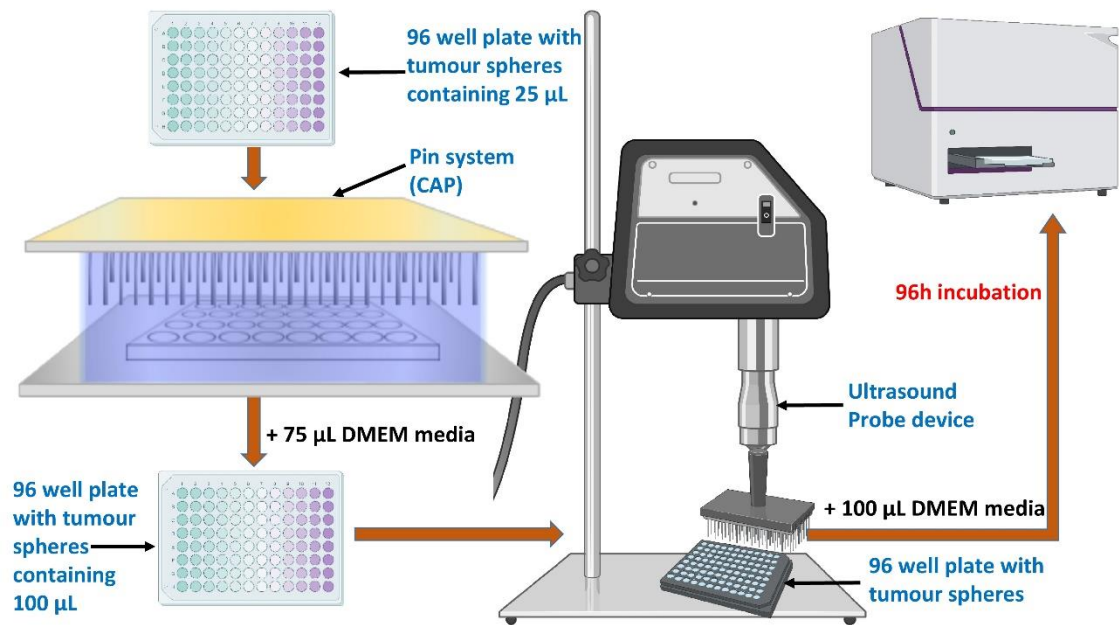


Figure 15: Scheme of the combination of cold atmospheric plasma with ultrasound. Tumour spheres were treated with direct plasma discharge followed by immediately ultrasound exposure.

2.13 alamarBlue cell viability assay

Cell viability was analysed using alamarBlue cell viability reagent (Thermo Fisher Scientific). After the post treatment incubation, the tumour spheres were washed with PBS, trypsinization using 0.25% w/v Trypsin-EDTA solution and incubated for 3 h at 37 °C with a 10% alamarBlue solution. Fluorescence was measured using an excitation wavelength of 530 nm and an emission wavelength of 590 nm with a Varioskan Lux multi-plate reader (Thermo Scientific). All experiments consisted of at least three independent tests with a minimum of 30 replicates per experiment and are presented as mean \pm S.E.M. The data (in fluorescence units from the microplate reader) for the test wells were normalised to the assay control, and cell growth was calculated as a change in viability over time.

2.14 CellTiter-Glo® 3D cell viability assay

3D cell viability was analysed using the CellTiter-Glo® 3D cell viability assay (Promega). After the post treatment incubation, homogeneous tumour spheres were removed from the 96-well low attachment culture plate and placed separately in single wells of a 96-well plate (Sarstedt). CellTiter-Glo® 3D reagent was added to each well and the luminescence signals were read after 25 min of incubation at room temperature using the Varioskan Lux multiplate reader (Thermo Scientific).

2.15 Live / Dead cell staining using Propidium Iodide (PI)

Tumour spheres were constructed using Nunclon™ Sphera™ 96-Well low attachment plates (Thermo Fisher Scientific). CAP was treated using pin system, US was treated using the US probe system and US-WB, and PMB was treated using a MB generator, as previously described. Following CAP or / and US treatment, wells were immediately replenished with media and incubated at 37 °C with 5% CO₂ for 24, 48, 72, and 96 h. To prepare for PI staining, the media was removed and the tumour spheres were washed with PBS and trypsinized into single cell suspension with a 0.25% w/v Trypsin-EDTA solution. After that, inactivate trypsin and collect cells from each treatment point into a single centrifuge tube for centrifugation at 250 x g for 5 min. The supernatant was then aspirated, and the pellet re-suspended in 1ml of 1X PBS. PI was then added to the cell suspension at 10 µg/mL and incubated for 1 min in the dark. PI fluorescence was then measured using a Beckman Coulter CytoFLEX flow cytometer with a 488 nm blue laser for excitation and a fluorescence channel I (FL1) standard filter for PI fluorescence, where PI binds to nuclear degradation from dead cells.

2.16 PI staining and confocal imaging

Tumour spheres were seeded in a Nunclon Sphera 60 mm dish (Thermo Fisher Scientific) at a density of 1×10^5 cells / ml and incubated at 37 °C using 5% CO₂ for 4 days. After tumour sphere formation, the media was removed, following 320 s of CAP treatment, and fresh media was added to the dish and incubated at 37 °C using 5% CO₂ for 24 h. After incubation, the tumour spheres were rinsed thrice with PBS and incubated with pre-warmed (37 °C) PI (10 µg/ml) containing media for 10 min at 37 °C. Cells were then washed once with PBS and loaded into fresh PBS. Tumour spheres were transferred to 35 mm glass-bottom dishes (Greiner Bio-One) and observed using a Zeiss LSM 510 confocal laser scanning microscope.

2.17 3D rendering

Representative confocal Z-scans of tumour spheres were processed for 3D reconstructions and visualization of the cell death penetration after treatment. Contrast dichroic stacks of images were rendered with 3D isosurfaces in computerized software (Surface tool, Imaris Bitplane) to limit the external border of the spheres. Then, PI positive nuclei were detected by positive fluorescence voxels as individual spots (Spots tool, Imaris Bitplane) considering the adequate threshold and resolution. Then, PI positive spots were labelled with a colour code according to the 3D distance to the border. 3D rotations of the tumour spheres and the addition of clipping planes were performed in rendering software to show the representative stack of images.

2.18 Chemical analysis of reactive species in cell culture medium

Nitrite and hydrogen peroxide concentrations were quantified using Griess reagent for nitrite and Amplex™ Red Hydrogen Peroxide/Peroxidase assay kit (ThermoFisher, USA), respectively. The assays were performed on a flat bottom 96-well plates (Sarstedt,

Ltd., Ireland). 25 µl of DMEM in the absence of sodium pyruvate and phenol red were exposure to pin – to - plate discharge at four different time points (20, 50, 100, 160 and 320 s) at 240 V, 1000 Hz with a 72 µs duty cycle. Plates were then incubating for 24 h before concentrations were quantified as described.

For nitrite quantification, 50 µL of Griess reagent for nitrite was added on 50 µL of medium (20 µL of treated medium + 30 µL of fresh medium) and incubated at room temperature for 30 min in the dark. Absorbance was then read at 548 nm. Hydrogen peroxide was quantified according to the kit protocol. 50 µl of a working solution of 100 µM Amplex™ red reagent and 0.2 U/mL Horse Radish Peroxidase (HRP) were added to 50 µL of medium (20 µL of treated medium + 30 µL of fresh medium). Following 30 min incubation at room temperature, in the dark, fluorescence was measured using an excitation of 530 nm and emission of 590 nm. A standard curve of sodium nitrite (0 – 100 µM) and hydrogen peroxide (0 – 20 µM) was used to determine nitrite and hydrogen peroxide concentrations.

2.19 Inhibitor studies

N-acetyl cysteine (NAC), sodium pyruvate and catalase were used as an antioxidant of reactive oxygen species. SP600125, z-VAD-fmk and E-64 were used as inhibitors of regulated cell death pathways.

2.19.1 ROS scavenger assays – NAC

The reactive oxygen species inhibitor N-acetyl cysteine (NAC) was used as a ROS scavenger. Tumour spheres were seeded and constructed as previously described. For the dose response curves, tumour spheres were incubated for 3 h at 37 °C with 4 mM NAC in DMEM in the presence and absence of pyruvate. 175 µL /100 µL of media was removed and the tumour spheres were exposed to CAP or / and US, depending on the

experiment. During PMB treatment, 200 μ L of media were removed, and tumour spheres were exposed to media with PMB. Post treatment, fresh media containing 4 mM of NAC was added and the cells incubated at 37 °C using 5% CO₂ for 24, 48, 72 and 96 h. The same procedure was carried out for the multiple CAP / US /PMB treated samples. Cell viability was measured using the alamarBlue assay as previously described. A NAC titration was performed, exposing the tumour spheres to a concentration range of 0 - 8 mM [106], cell viability was assessed after 96 h.

2.19.2 Sodium pyruvate

Sodium pyruvate titration was performed. Cells were exposed to a range of 0 to 10 mM. Cell viability was assessed after 96 h using alamarBlue assay.

2.19.3 Hydrogen peroxide scavenger assay - Catalase

Catalase (E.C. 1.11.1.6) is an antioxidant enzyme that is found in peroxisomes; it catalyses the decomposition of H₂O₂ to form water and molecular oxygen ($2 \text{H}_2\text{O}_2 \rightarrow 2 \text{H}_2\text{O} + \text{O}_2$) [60, 339, 340]. U-251 MG tumour spheres were seeded in Nunclon™ Sphera™ 96-Well low attachment plates (Thermo Fisher Scientific) at a density of 1×10^5 cells/ml and incubated at 37 °C using 5% CO₂ for 4 days. Catalase stock solution (1 mg/ml equivalent to 2,000-5,000 units/ml) was freshly prepared in sterile 1X PBS, and diluted to 0.1 mg/ml in fresh media for H₂O₂ inhibition. After the formation of the tumour spheres, replenished DMEM media, without sodium pyruvate and phenol red, containing 0.1 mg/ml catalase, were incubated for 1 h at 37 °C. CAP treatment was performed on the samples for 160 s and 320 s. MB was exposed to plasma for 5, 10, 20, and 30 min for the treatment. Then the fresh media with catalase was added to the dish and incubated 37 °C using 5% CO₂ for 24 h. After incubation, PI staining was carried out as explained in

section 2.15. PI fluorescence was then measured using a Beckman Coulter CytoFLEX flow cytometer with a blue laser (488 nm).

2.19.4 E-64

E-64 is an epoxide that inhibits irreversibly a wide variety of cysteine peptidases, including broad spectrum cathepsins. Cathepsins are cysteine proteases that activate in the lysosomal / autophagy pathway (late autophagy). E-64 was reconstituted in 100 % DMSO and stored at -20 °C with a stock concentration of 20 mM and a working concentration of 10 µM in DMEM. U-251 MG tumour spheres were pre-treated with E-64 for 1 h, then pipetted out and treated with CAP and US as explained before. After 24 or 96 h, cell viability was evaluated using the alamarBlue cell viability assay. Tumour spheres were also treated with 0.5% DMSO as a vehicle control.

2.19.5 SP600125

SP600125 is an inhibitor of the apoptosis associated JNK protein. SP600125 was reconstituted in DMSO and stored at -20 °C at a stock solution concentration of 25 mM, with a working solution concentration of 12.5 µM in DMEM. U-251 MG tumour spheres were pre-treated with SP600125 for 1 h. SP600125 was then pipetted out, 25 µL of fresh medium with SP600125 was added and tumour spheres were treated with CAP and US as previously described. Using an alamarBlue cell viability assay, the cell viability was measured after 24 or 96 h. Cells were also treated with 0.5% DMSO as a vehicle control.

2.19.6 zVAD-fmk

In order to evaluate if caspases play a role in cell death in U-251 MG cells with the synergistic effect of CAP and US, the commonly used general caspase inhibitor zVAD-fmk was used. zVAD-fmk was reconstituted in 100 % DMSO and frozen at -20 °C with a stock concentration of 10 mM and a working concentration of 25 µM in DMEM.

Following a 1 h pre-treatment with zVAD-fmk, media were removed from each well. Before treatment, 25 μ L of fresh medium was added and tumour spheres were exposure to CAP and US combination. After treatment, 175 μ L of fresh medium was added and tumour spheres were incubated for 24 or 96 h, analysed using the alamarBlue cell viability test. In addition, tumour spheres were treated with 0.5% DMSO as a vehicle control.

2.20 Detect ROS production using H2DCFDA Assay

A cell permeant non-fluorescent probe, 2, 7-dichlorodihydrofluorescein diacetate (H2DCFDA) dye (Thermo Fisher Scientific), was used to measure ROS generated by CAP and PMB treatments using flow cytometry. H2DCFDA is a chemically reduced form of fluorescein that is converted to the highly fluorescent 2', 7'-dichlorofluorescein (DCF) after the cleavage of the acetate groups by intracellular esterases and oxidation. U-251 MG tumour spheres were seeded in a Nunclon Sphera 60 mm dish (Thermo Fisher Scientific) at a density of 1×10^5 cells / ml with DMEM high glucose in the absence of sodium pyruvate and incubated at 37 °C using 5% CO₂ for 4 days. Subsequently the culture medium was removed and the tumour spheres were washed with 1X PBS. Tumour spheres were incubated with replenished DMEM media, without sodium pyruvate and phenol red, containing 25 μ M H2DCFDA, for 1h at 37 °C. Tumour spheres were washed with fresh medium once, then with 1X PBS, and then exposed to CAP at different time points (20 s, 160 s and 320 s) and PMB, (plasma exposed for different time points - 10, 20, and 30 min). Following CAP or PMB treatment, tumour spheres were incubated for 3 h at 37 °C using 5% CO₂. Tumour spheres were trypsinized into a single cell suspension, and all liquids, including media, washing PBS, and trypsinized cell suspension, were collected and centrifuged at 1200 rpm for 5 min. Cells were re-suspended in 1X PBS, and fluorescence was measured using a Beckman Coulter CytoFLEX flow cytometer with a 488 nm blue laser for excitation and FL1 standard filter for H2DCFDA measurement

(quantified using fluorescein isothiocyanate (FITC)-A channel; Ex 488 nm, Em 525-540 nm).

2.21 Tumour sphere sonoporation assay

PI was used to determine the sonoporation capability of the ultrasonic WB. 1×10^4 cells were seeded onto a Nunclon™ Sphera™ 96-well low attachment plates to tumour spheroid formation. PI (10 μ l / ml) was introduced shortly before treatment, and tumour spheres were then treated at 25 or 45 kHz frequencies, using 100% power in sweep mode at three different time points (1, 3, and 5 min). The tumour spheres were washed with PBS and trypsinized into single cell suspension with a 0.25% w/v Trypsin-EDTA solution. After that, inactivate trypsin and collect cells from each treatment point into a single centrifuge tube for centrifugation at 250 x g for 5 min. The supernatant was then aspirated, and the pellet was re-suspended in 1 ml of 1X PBS. PI fluorescence was detected using the FL2 A (PE - A) channel on a CytoFlex, Beckman Coulter flow cytometer. To measure the resealing of the membrane, the same conditions were applied to the tumour spheres as reported before. Tumour spheroids were treated with 25 kHz and 45 kHz frequencies for 1, 3, and 5 min. After 3 h of incubation, the tumour spheroids were trypsinised as explained above. PI was then added to the cell suspension at 10 μ g / mL and incubated for 3 min in the dark. PI fluorescence was then measured using a Beckman Coulter CytoFLEX flow cytometer using the FL2 A channel.

2.22 TMZ and DOX induced glioma cytotoxicity

Stock solutions of compounds were dissolved in DMSO and stored at -20 °C. These stocks were subsequently used to make the working solutions in media. The highest concentration of DMSO used was 0.5 %. For 2D cell culture, cells were seeded at a density of 1×10^4 cells (48 h) and 2.5×10^3 (144 h) exposure time period with 100 μ L media per well in 96-well plates (Sarstedt). For 3D cell culture, cells were seeded at a density of 1×10^4 cells / well (200 μ l of culture medium per well) into Nunclon™ Sphera™ 96-well low attachment plates (Thermo Fisher Scientific). Plates were incubated at 37 °C with 5% CO₂ to allow proper adherence (2D) and U-251 MG, U-87 MG, A-172, A431 tumour sphere formation (3D) as explained above. Existing media were removed from each well and cells / tumour spheres were treated with TMZ / DOX at varying concentrations (500 – 0.976 μ M; 100 μ L/well for 2D cells ; 200 μ L/well for 3D cells), 20 % (v/v) DMSO was used as a positive control, and 0.5 % (v/v) DMSO as a negative control, and incubated at the appropriate time point. No deleterious effects were observed from the negative control solvent. Another set of plates were treated with US using the same procedure as in section 2.12. After the post treatment incubation, the cytotoxicity of the cells / tumour spheres were measured using the CellTiter-Glo® 3D cell viability assay and / or alamarBlue cell viability reagents as mentioned above.

2.23 DOX sonoporation analysis

Doxorubicin hydrochloride (DOX.H) (Fisher Scientific) is a chemotherapeutic agent with intrinsic fluorescence, with excitation / emission of 470 / 585 nm. Stock solutions (1mg / 5ml) of compounds were dissolved in DMSO and stored at -20 °C. A431 and U-251 MG tumour spheres were seeded in a Nunclon Sphera 60 mm dish (Thermo Fisher Scientific)

at a density of 1×10^5 cells / ml using DMEM high glucose in the absence of sodium pyruvate and incubated at 37 °C using 5 % CO₂ for 3 to 4 days, respectively.

Subsequently, the culture medium was removed and the tumour spheres were washed with 1× PBS. Tumour spheres were replenished with DMEM media, without sodium pyruvate and phenol red, containing 10 µg / ml DOX.H. Subsequently dishes with tumour spheres were treated with US for 1 and 3 min, as described in the section 2.5. Then all the dishes (tumour spheres without US and DOX, with only US, with DOX and without US, DOX with 1 min of US, DOX with 3 min of US) were incubated for 24 h at 37 °C using 5 % CO₂. After the post treatment incubation, tumour spheres were trypsinized into a single cell suspension and centrifuged at 1200 rpm for 5 min. Cells were re-suspended in 1× PBS with fluorescence measured using a Beckman Coulter CytoFLEX flow cytometer with a 488 nm blue laser for excitation and FL1 standard filter for FITC measurement.

2.24 Mitochondrial membrane potential measurement

Dual-emission potential sensitive fluorescent dye JC-1, was used to measure mitochondrial membrane potential of tumour spheres following CAP / PMB and US treatment. Stock solutions of JC-1 dye (Biosciences, Ireland) were prepared at 1 mg/mL in DMSO, aliquoted out and stored in freezer (−20 °C) until required for use. U-251 MG tumour spheres were seeded in a Nunclon Sphera 60 mm dish (Thermo Fisher Scientific) at a density of 1×10^5 cells / ml using DMEM high glucose in the absence of sodium pyruvate and incubated at 37 °C using 5% CO₂ for 4 days.

After the tumour sphere growth; during PMB and US study, the growth medium was changed to a media containing PMB, and the tumour spheres were exposed to US for 1, 3, and 5 min. During CAP and US study, 25 µL of fresh DMEM without sodium pyruvate was added and tumour spheres were exposure to CAP, US combination. Following US

treatment, tumour spheres were incubated at 37 °C for appropriate time point. After the incubation, the tumour spheres were trypsinized into single cell suspension as explained before, then the media was removed, and stained with 2.5 µg / ml JC-1 dye. After an incubation period of 10 min at room temperature, in the absence of light, the cells were washed twice with PBS and collected by centrifugation at 1200 rpm for 5 min. The supernatant was discarded, and the cells were resuspended in 0.5 ml PBS for flow cytometric (Beckman Coulter CytoFLEX) analysis. Fluorescence intensity was measured with a blue laser (488 nm) using FITC and phycoerythrin (PE-A) emission filters with spectral overlap compensation (52% FITC/PE-A and 10% PE-A/FITC).

2.25 CFSE Cell Proliferation Assay

CellTrace™ Carboxyfluorescein succinimidyl ester (CFSE) cell proliferation assay kit, for flow cytometry (Thermo Fisher, Ireland) was used for this assay. The kit was kept at -20 °C and the CellTrace™ CFSE was reconstituted in 18 µl DMSO (stock solution), aliquoted and stored at -20 °C until use (one time use once thawed). As working solution, a 1:1000 dilution of the stock solution in PBS at 37 °C was utilised. U-251 MG tumour spheres (5×10^5) were harvested by trypsinisation and centrifuged at 300 x g for 5 min. The cells were resuspended in 1 ml of working solution, and incubated at 37 °C with 5% (v/v) CO₂, in dark. Every 5 min, cells were mixed gently. After adding 4 ml of DMEM to absorb unbound dye, the mixture was incubated at room temperature for 5 min. The cells were then centrifuged for 5 min at 300 x g. The supernatant was discarded, and the cells were resuspended in 20 mL in DMEM to seed cells at a density of 5×10^4 cells per well in 6-well plates. After tumour sphere formation, the growth media was discarded and the tumour spheres were treated with CAP and US, and further incubated for 96 h. Cells were collected by trypsinisation and centrifugation at 500 x g for 5 min, and resuspended in 0.1 ml PBS for flow analysis (Beckman Coulter CytoFLEX). The fluorescence

intensity was measured with a blue laser (488 nm) using FITC. To identify apoptotic cells, cells were also co-stained with 0.5 µg/ml PI for 3 minutes in the absence of light, to determine apoptotic cells. The Fluorescence intensity was measured with a blue laser (488 nm) using FITC and PE-A emission filters with spectral overlap compensation (42.80% FITC/PE-A). 1 mM of hydrogen peroxide was used as positive control.

2.26 Statistical analysis

All the experiments were replicated at least three independent times, unless otherwise stated. Prism versions 9.1.0, GraphPad Softwares, Inc. (USA) were used to carry out curve fitting and statistical analysis. Dose response curves were measured using non-linear regression after data been normalized with controls. Data are presented as a percentage and error bars of all figures were presented using the standard error of the mean (S.E.M), ordinary one-way and two-way analysis of variance (ANOVA) were performed accordingly (*P < 0.05, **P < 0.01, ***P < 0.001, ****p < 0.0001). Multiple comparison analysis were performed using Tukey's test or Šídák's test unless otherwise stated. CytExpert software was used for flow cytometry analysis and fluorescence mean of FITC-A or PE-A was use to plot the reading results in columns statistics.

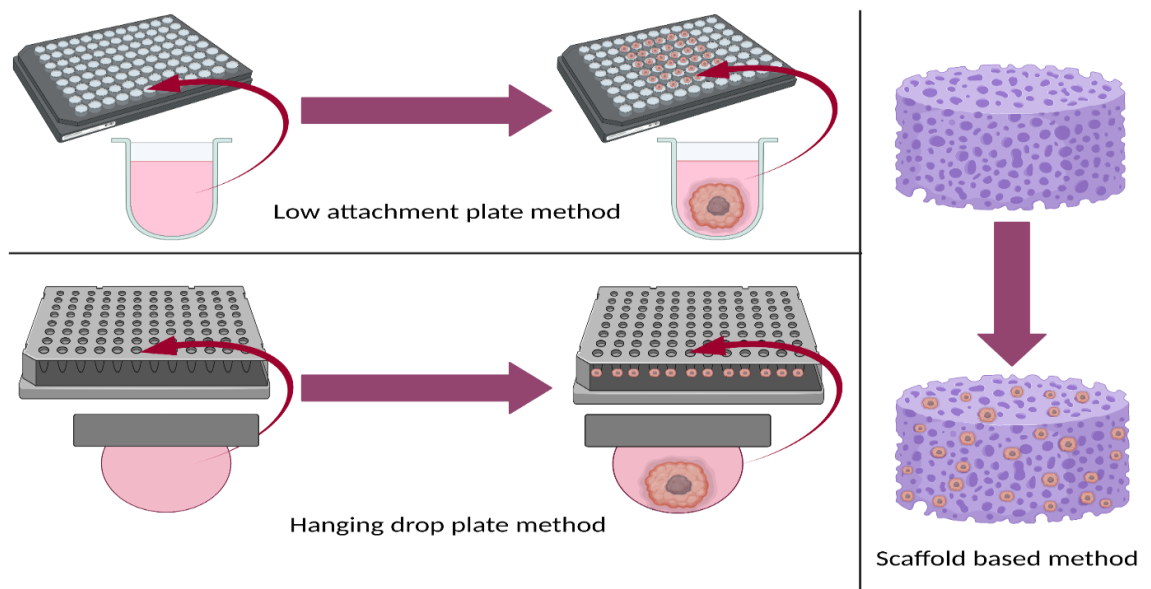
2.27 Data availability

Data was planned to be exploited based on advice from TU Dublin technology transfer office. Data was collected and saved in various file formats. All original data was stored with information on the experimental item, data, location, the experimenter, and the type of document, along with a general description of each group in the experiment. The original data will be accessible from on-site computers, my personal computer and a shared cloud drive. Original data was processed or saved as images, data sheets, or figures that could be accessed by Microsoft Office after analysis. Images were saved as .tif (at

least 300 dpi). The processed data was uploaded to the internal file server and shared with the main supervisor.

Curating and preserving of data: Original and processed data was preserved in a shared cloud-based server and made publicly available on TU Dublin Arrow open data system following preprint and peer-review publications. All relevant datasets that support the findings of this study will be uploaded into open science framework (OSF) and can be accessed using the following DOI link. All processed data in images, figures and original data sheets will be available in the published manuscripts and online supplementary materials to make data findable, accessible and referable. Usually data will be available as least internally before publication, but it may be unavailable if there's a failure with the corresponding software then assistance for accessing the data will be required or experiments will be repeated to acquire data.

CHAPTER 3 – OPTIMIZATION OF THREE-DIMENSIONAL (3D) *IN VITRO* CELL CULTURE MODELS TO ENHANCE GLIOBLASTOMA RESEARCH



A part of this chapter is published in the Journal PLOS One. (See Appendix II – Peer-reviewed)

- **Wanigasekara J**, Carroll LJ, Cullen PJ, Tiwari B, Curtin JF (2023) Three-Dimensional (3D) *in vitro* cell culture protocols to enhance glioblastoma research. PLOS ONE 18(2): e0276248. <https://doi.org/10.1371/journal.pone.0276248>

3 Optimization of three-dimensional (3D) *in vitro* cell culture models to enhance glioblastoma research

3.1 Rationale

3D cell culture models can help bridge the gap between *in vitro* cell cultures and *in vivo* responses by more accurately simulating the natural *in vivo* environment, shape, tissue stiffness, stressors, gradients and cellular response while avoiding the costs and ethical concerns associated with animal models [257, 271, 274, 341]. The inclusion of the third dimension in 3D cell culture influences the spatial organization of cell surface receptors that interact with other cells and imposes physical restrictions on cells in compared to 2D cell cultures [246, 257, 271]. Spheroids' distinctive cyto-architecture mimics *in vivo* cellular structure, gene expression, metabolism, proliferation, oxygenation, nutrition absorption, waste excretion, and drug uptake while preserving cell – ECM connections and communication, hence influencing molecular processes and cellular phenotypes [106, 267, 271, 274]. Ultimately, 3D models must have high-throughput application, easy and standardized culture protocols and analytic methodologies to get proper outcomes [274, 342]. In this chapter, we used three different anchorage-independent and anchorage-dependent methods such as; low attachment plate, hanging drop plate, and cellusponge natural scaffold based methods to construct three different *in vitro* 3D GBM tumour spheroid models (U-251 MG, U-87 MG and A-172) and one 3D epidermoid carcinoma (A431) to closely mimic the natural *in vivo* environment, shape, and cellular response [271]. The findings of this chapter have confirmed the ability of all these methods to create uniform tumour spheres, which we will utilize for further research.

3.2 Results and discussion

3.2.1 3D cell culture

GBM is distinguished by increased vascularization, significant cell heterogeneity, self-renewing CSCs and the interactions between tumour and microenvironment, all of which contribute to tumour progression [218, 257]. Tumour development, metastasis, angiogenesis, cytotoxicity resistance, and immune cell modulation are all influenced by the TME [106, 219]. There is a gap in mostly accessible GBM pre-clinical models and 3D cell culture is able to fill this gap by providing more reliable models to study the correlation between TME, tumour reoccurrence and therapy resistance.

Three distinct approaches, such as low attachment plate (Figure 16-II), hanging drop plate (Figure 16-III), and scaffold based methods (Figure 16-IV) were used to create U-251 MG, U-87 MG, A-172 3D human GBM and A431 epidermoid carcinoma cell culture models. This facilitated 3D cell–cell and cell–ECM interactions and mirrored the diffusion-limited distribution of oxygen, nutrients, metabolites, and signaling molecules seen in the microenvironment of *in vivo* tumours [106]. Most research to date has used 2D cell culture (Figure 16-I), which has limitations as experimental models to predict biological responses, as explained previously.

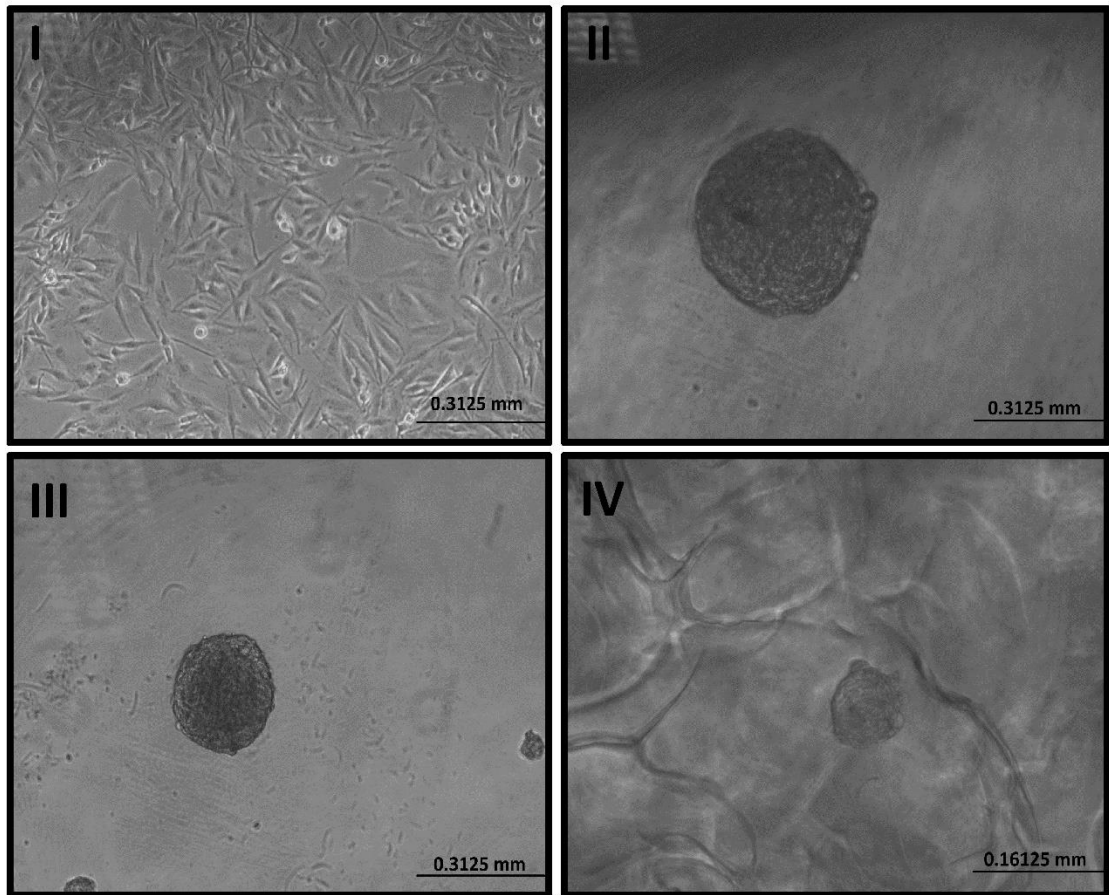


Figure 16: Development of U-251 MG human GBM 3D in vitro cell culture model. I). Image of U-251 MG 2D cells in T75 flask II) 3D tumour sphere constructed in low adhesion plate. III). 3D tumour sphere constructed in hanging drop plate. IV) 3D tumour sphere constructed in hydroxipropylcellulose scaffold. Tumour spheroid formation was visually confirmed using an Optika XDS-2 trinocular inverse microscope equipped with a Camera ISH500.

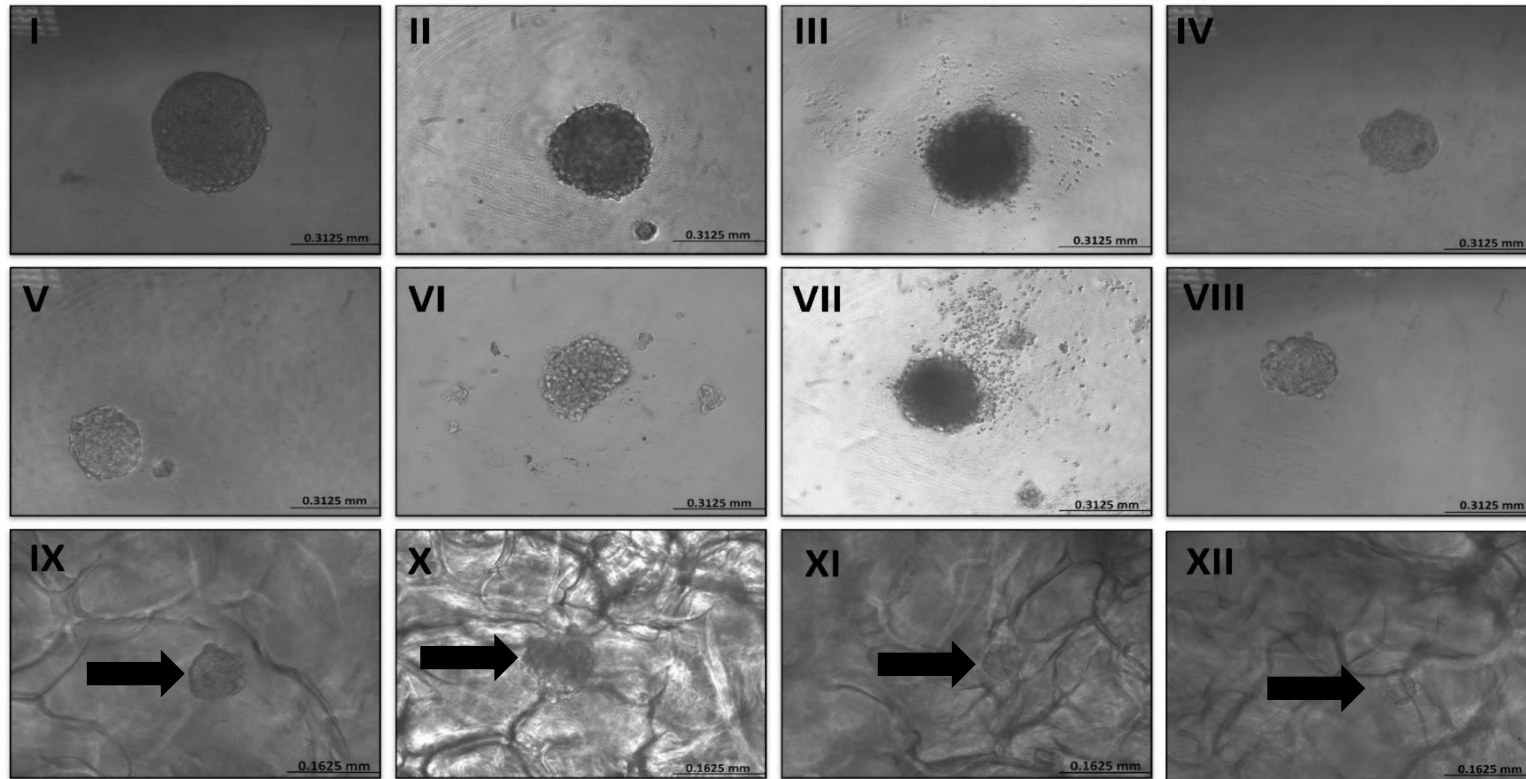


Figure 17: Development of U-251 MG, U-87, A-172 and A431 3D *in vitro* cell culture models using low attachment plate, hanging drop plate and scaffold based method. I) U-251 MG, II) U-87 MG, III) A-172, IV) A431 tumour spheroids formation after 96 h of incubation using low attachment plate method, V) U-251 MG, VI) U-87 MG, VII) A-172, VIII) A431 tumour spheroids formation after 96 h of incubation using hanging drop plate method, IX) U-251 MG, X) U-87 MG, XI) A-172, XII) A431 tumour spheroids formation after 96 h of incubation using scaffold based method

Cell seeding and tumour spheroid construction were carried out as previously explained. U-251 MG, U-87 MG, and A-172 human GBM spheroids formation and growth were monitored daily by using an inverted phase-contrast microscope, and their mean diameters were analysed using “ImageJ version1.53.e” software for at least three independent experiments. U-251 MG tumour sphere growth during the low attachment plate method was found to be significantly increased with the incubation time, the size ranging from 135 μm , 229 μm , 323 μm and 461 μm (Figure 17-I) for 24 to 96 h incubation respectively. U-87 MG tumour spheres were significantly increased with the incubation time, the size range from 129 μm , 234 μm , 303 μm and 357 μm (Figure 17-II) for 24 to 96 h incubation respectively. While, A-172 tumour spheres also showed same behaviour with the increasing incubation time and the sizes range from 71 μm , 191 μm , 240 μm and 367 μm (Figure 17-III) for 24 to 96 h incubation respectively.

U-251 MG tumour sphere growth during the hanging drop plate method was shown to be considerably enhanced with the incubation time, the size ranging from 105 μm , 139 μm , 208 μm and 269 μm (Figure 17-V) for 24 to 96 h incubation respectively. U-87 MG tumour spheres were significantly increased with the incubation time, the size range from 92 μm , 143 μm , 224 μm and 252 μm (Figure 17-VI) for 24 to 96 h incubation respectively. While, A-172 tumour spheres also showed same behaviour with the increasing incubation time and the sizes range from 63 μm , 131 μm , 207 μm and 265 μm (Figure 17-VII) for 24 to 96 h incubation, respectively. The hanging drop plate method produced smaller size spheroids compared to low attachment plate method.

U-251 MG tumour sphere growth in hydroxipropylcellulose 3D scaffold was shown to be considerably enhanced with incubation time, with sizes ranging from 22 μm , 49 μm , 70 μm , and 110 μm for 24 to 96 h incubation, respectively (Figure 17-IX). U-87 MG tumour spheres were significantly increased with the incubation time, the size range from

28 μm , 55 μm , 90 μm and 143 μm (Figure 17-X) for 24 to 96 h incubation respectively. While, A-172 tumour spheres size also significantly enhanced with the increasing incubation time and the sizes range from 17 μm , 51 μm , 69 μm and 97 μm (Figure 17-XI) for 24 to 96 h incubation respectively.

The growth of A431 epidermoid tumour spheres using the low attachment plate method was observed to significantly increase with longer incubation times, with sizes ranging from 96 μm , 139 μm , 194 μm and 257 μm (Figure 17-IV) for 24 to 96 h of incubation respectively. Similarly, the hanging drop plate method also demonstrated a substantial enhancement in A431 tumour sphere growth with increasing incubation time, with sizes ranging from 57 μm , 103 μm , 153 μm and 194 μm (Figure 17-VII) respectively, for 24 to 96 h of incubation. Furthermore, A431 tumour sphere growth in the hydroxypropylcellulose 3D scaffold was also notably increased with longer incubation periods, with sizes ranging from 23 μm , 45 μm , 54 μm , and 79 μm (Figure 17-XII) for 24 to 96 h incubation.

These results proved that these protocols have the ability to develop 3D tumour spheres and the presence of heterogeneous cellular subpopulations such as actively proliferating, quiescent, hypoxic, and necrotic cells [220, 225, 236].

3.2.2 Effects of different growth media

Larger tumour sphere growth was observed when grown in DMEM high glucose media with 10% FBS compared to media without FBS. According to the initial seeding density, growth medium composition and incubation time, the tumour sphere diameters varied from 100 to 650 μm . The largest tumour spheres were observed with 10 000, 15 000 and 20 000 cells/ml initial seeding densities. It was also observed that exponential growth (Log) was achieved within the initial 4 days of growth, after which the growth curve became stationary, followed by a second growth phase after 7 days of incubation due to

an increased number of dead cells inside the tumour sphere core (Figure 18A and 18B). Two-way ANOVA demonstrated that there is a significant difference in tumour sphere (grown in serum medium) diameter between the each initial seeding densities as shown in Figure 18A. However there was no significant difference between diameters at day 4, 5 and 6 in 10 000, 15 000 and 20 000 cells / ml seeding densities. In Figure 18B, there was no significant difference in tumour sphere (grown in without serum medium) diameter between the 10 000 and 20 000 cells / ml initial seeding densities. A full description of tukey's multiple comparisons test is provided in the Appendix I.

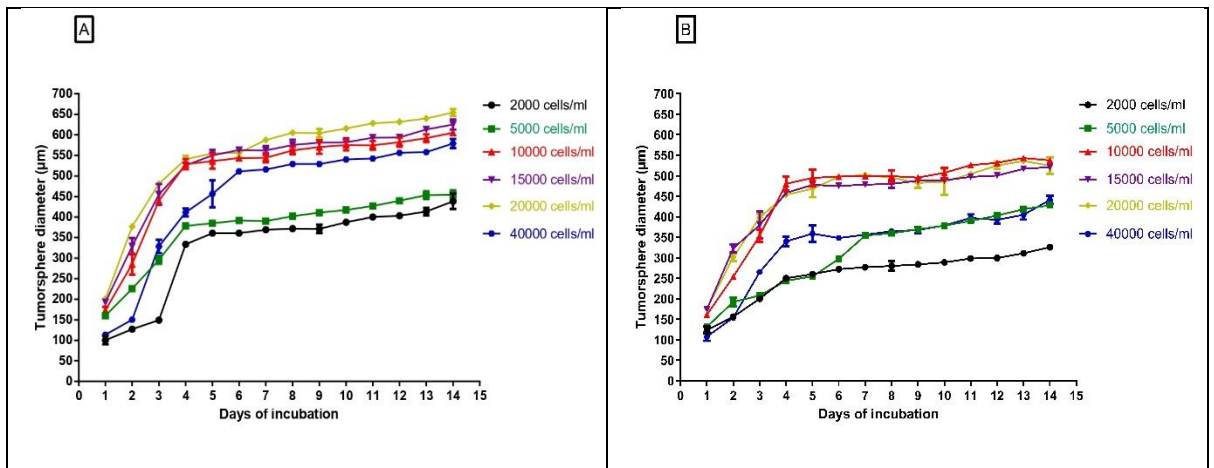


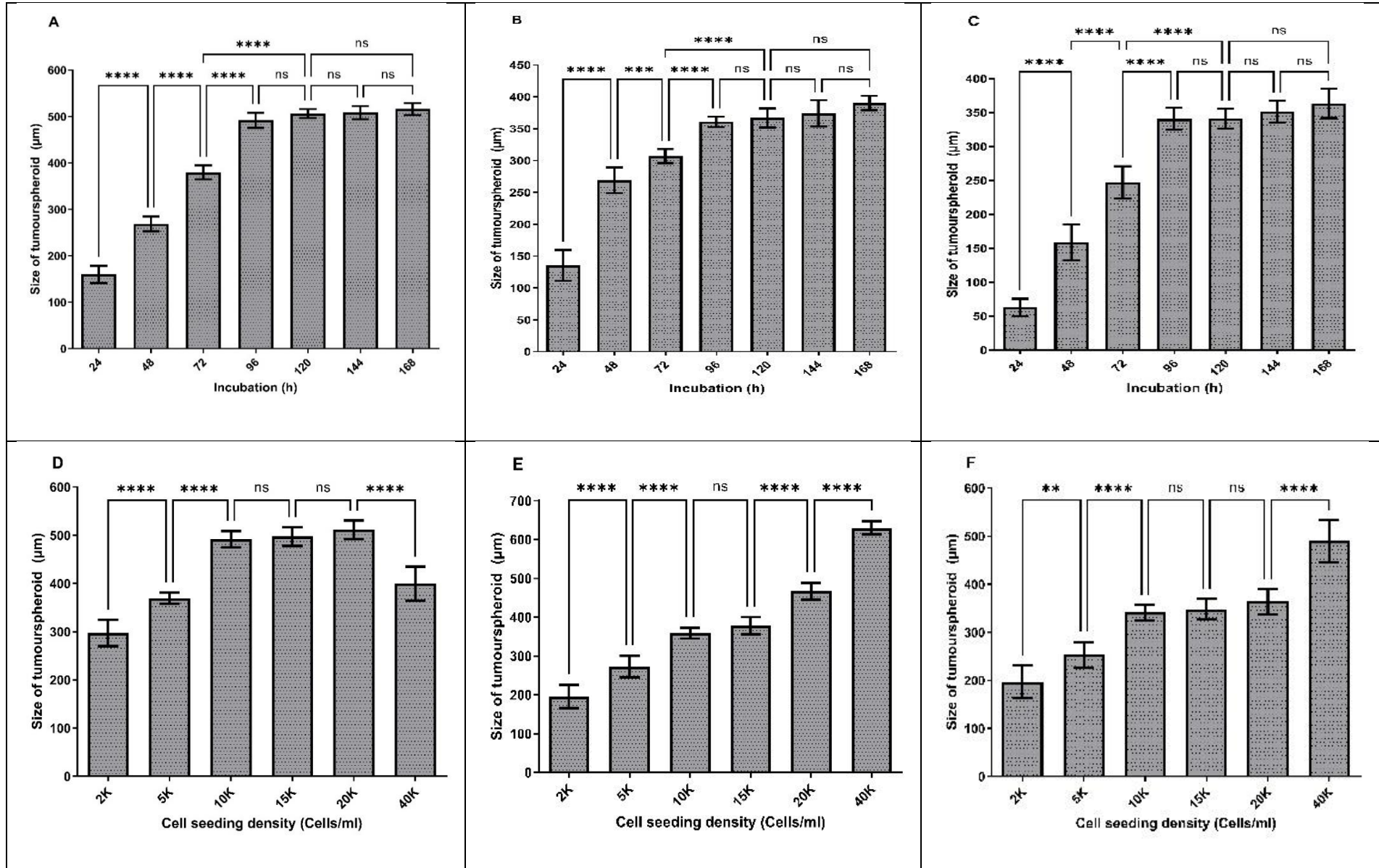
Figure 18: Development of U-251 MG human GBM 3D in vitro cell culture model in different media compositions. Growth kinetics analysis of U-251 MG spheroids at increasing seeding density in low attachment plate method A) with serum medium. B) without serum medium.

3.2.3 Optimization of low attachment plate method

The optimum U-251 MG (Figure 19A), U-87 MG (Figure 19B) and A-172 (Figure 19C) tumour spheroids formations were observed within 96 h of incubation for the 10000 cells / ml initial seeding density. One-way ANOVA demonstrated that there were significant differences in tumour spheres diameter during 24 - 96 h incubation, while there was no significant difference during 96 - 168 h incubation. It was also observed that exponential growth (Log) was achieved within the initial 4 days of growth, after which the growth curve became stationary in all these three GBM cell lines.

For growth analysis, varying numbers of U-251 MG, U-87 MG and A-172 cells (ranging from 2000 to 40 000 cells / ml) were seeded in the Nunclon™ Sphera™ 96-well low attachment plates as explained above. The largest U-251 MG tumour spheres were observed with 10 000, 15 000, and 20 000 cells / ml initial seeding densities after 96 h of incubation. One-way ANOVA demonstrated that there was a significant difference in tumour sphere diameter between each initial seeding densities as shown in Figure 19D. However, there was no significant difference between diameters in 10 000, 15 000, and 20 000 cells / ml seeding densities. The largest U-87 MG tumour spheres were observed with 40 000 cells/ml initial seeding densities after 96 h incubation. One-way ANOVA demonstrated that there was a significant difference in tumour sphere diameter between each of the initial seeding densities as shown in Figure 19E. However, there was no significant difference between diameters at 10 000 and 15 000 cells / ml seeding densities. While, the largest A-172 tumour spheres were observed with 40 000 cells / ml initial seeding densities after 96 h incubation. One-way ANOVA demonstrated that there was a significant difference in tumour sphere diameter between each of the initial seeding densities as shown in Figure 19F. Though, there was no significant difference between diameters in 10 000, 15 000, and 20 000 cells / ml seeding densities.

U-251 MG, U-87 MG and A-172 cells health analysed after 96 h incubation using alamarBlue cell viability reagent as explained above and the fluorescence signals were normalized by spheroid size (diameter in μm). A higher ratio suggests that the spheroids are healthier. During U-251 MG growth confirmed that 5000 and 10 000 cells / ml initial seeding densities were having highest spheroids cell health. One-way ANOVA confirmed that there was no significant difference in tumour sphere health during 5000 and 10 000 cells / ml (Figure 19G). During U-87 MG growth, it was confirmed that 10 000 and 15 000 cells / ml initial seeding densities were having highest spheroids cell health. One-way ANOVA confirmed that there was no significant difference in tumour sphere health during 10 000 and 15 000 cells / ml (Figure 19H). During A-172 growth confirmed that 10 000, 15 000 and 20 000 cells / ml initial seeding densities were the ones having the highest spheroids cell health. One-way ANOVA confirmed that there was no significant difference in tumour sphere health during 10 000, 15 000 and 20 000 cells / ml (Figure 19I). A full description of tukey's multiple comparisons test is provided in the Appendix I.



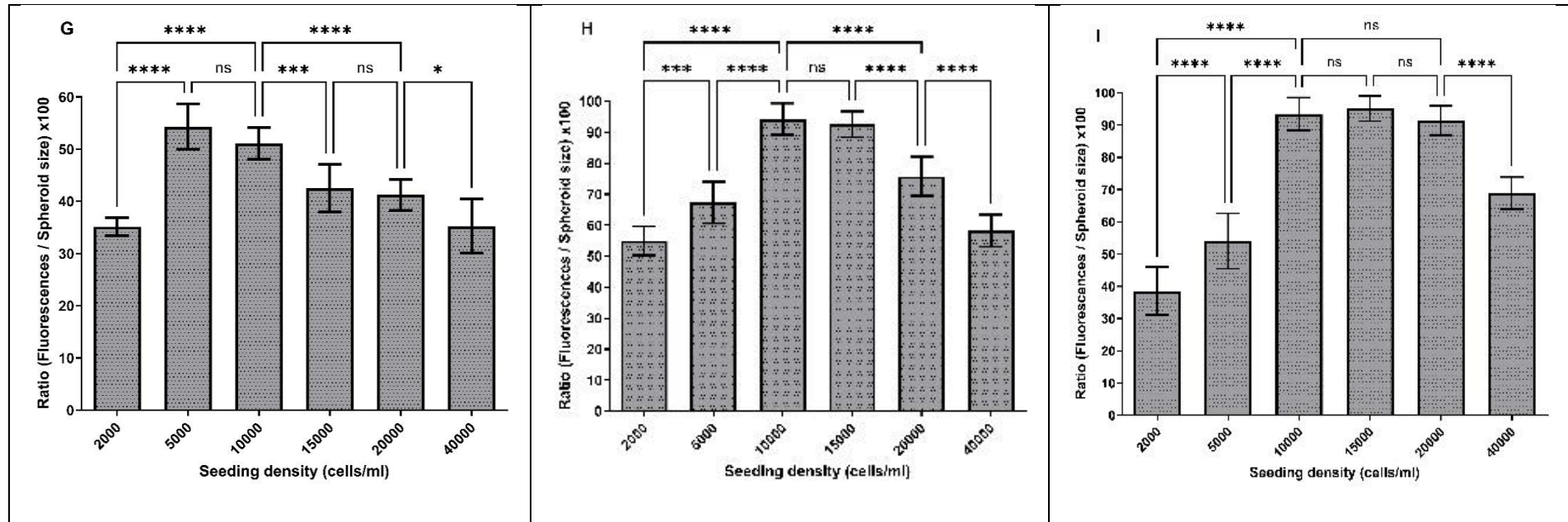


Figure 19: Development of human GBM 3D in vitro cell culture models using low attachment plate method. A) U-251 MG, B) U-87 MG, C) A-172 tumour spheres growth (diameter in μm) analysis during different incubations. D) U-251 MG E) U-87 MG, F) A-172 growth analysis after 96 h incubation (diameter in μm) at increasing seeding density. The mean of the diameter was used to plot the values on columns and analysed using one-way ANOVA with tukey's post-test (ns, not significant ($p > 0.05$); $*p < 0.05$; $**p < 0.01$, $***p < 0.001$; $****p < 0.0001$). G) U-251 MG H) U-87 MG, I) A-172 spheroid cell health analysed and a higher ratio indicates healthier spheroids. The mean of the [(fluorescence / spheroid size) x 100] was used to plot the values on columns and analysed using one-way ANOVA with tukey's post-test (ns, not significant ($p > 0.05$); $*p < 0.05$; $**p < 0.01$, $***p < 0.001$; $****p < 0.0001$).

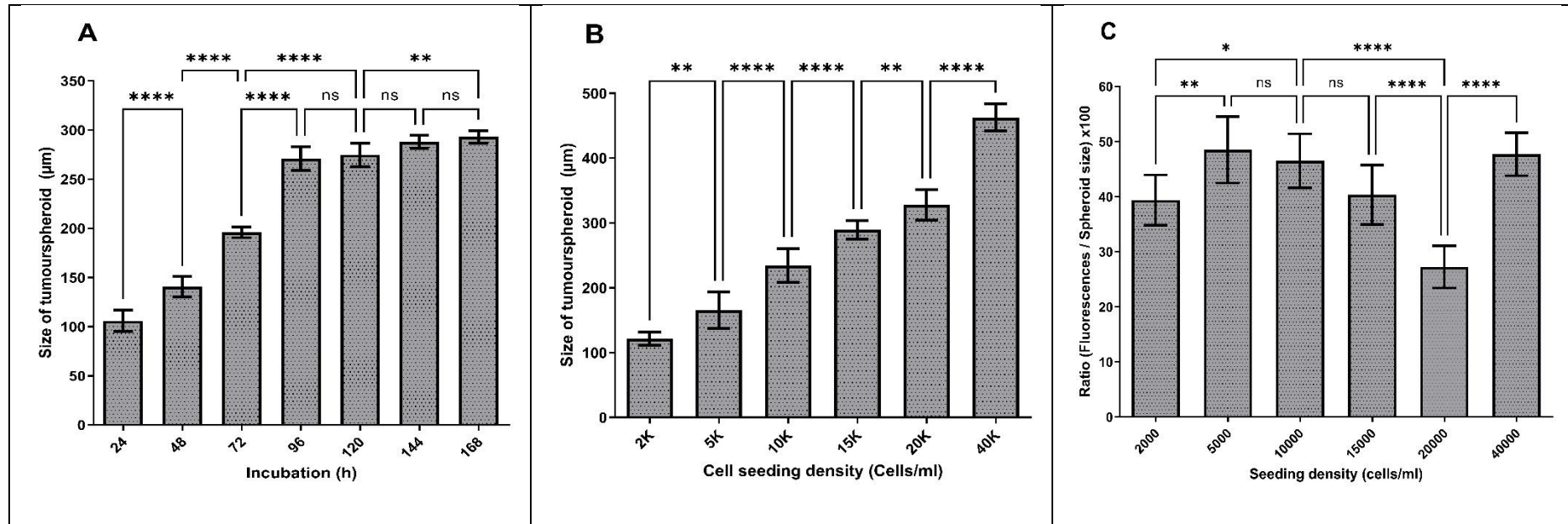


Figure 20: Development of A431 human epidermoid carcinoma 3D in vitro cell culture models using low attachment plate method. A) A431 tumour spheres growth (diameter in µm) analysis during different incubations. B) A431 growth analysis after 96 h incubation (diameter in µm) at increasing seeding density. The mean of the diameter was used to plot the values on columns and analysed using one-way ANOVA with tukey's post-test (ns, not significant ($p > 0.05$); * $p < 0.05$; ** $p < 0.01$, *** $p < 0.001$; **** $p < 0.0001$). C) A431 spheroid cell health analysed and a higher ratio indicates healthier spheroids. The mean of the [(fluorescence / spheroid size) x 100] was used to plot the values on columns and analysed using one-way ANOVA with tukey's post-test (ns, not significant ($p > 0.05$); * $p < 0.05$; ** $p < 0.01$, *** $p < 0.001$; **** $p < 0.0001$).

The optimum A431 (Figure 20A) tumour spheroids formations were observed within 96 h of incubation for the 10000 cells / ml initial seeding density. One-way ANOVA demonstrated that there were significant differences in tumour spheres diameter during 24 - 96 h incubation, while there was no significant difference during 96 - 168 h incubation. It was also observed that exponential growth (Log) was achieved within the initial 4 days of growth, after which the growth curve became stationary in the epidermoid carcinoma cell line. During the growth analysis, the largest A431 tumour spheres were observed during the 40000 cells / ml initial seeding densities after 96 h of incubation. One-way ANOVA demonstrated that there was a significant difference in tumour sphere diameter between each initial seeding densities as shown in Figure 20B. A431 cells health analysed after 96 h incubation as explained above and the fluorescence signals were normalized by spheroid size (diameter in μm). During A431 growth confirmed that 5000, 10 000 and 40 000 cells / ml initial seeding densities were having highest spheroids cell health. One-way ANOVA confirmed that there was no significant difference in tumour sphere health during 5000 and 10 000 cells / ml (Figure 20C). A full description of tukey's multiple comparisons test is provided in the Appendix I.

We studied tumour sphere growth in low attachment plates with various seeding densities and observed tumour sphere growth ranging in diameter from 150 to 650 μm . Our findings are correlate with the tumour sphere diameters determined by Singh et al [343]. According to the results, 10000 cells / ml initial seeding density was the most suitable seeding density for low attachment plate method and all the above GBM cell lines were able to produce healthy tumour spheres after 96 h incubation. Throughout this thesis, we used the same protocols to generate U-251 MG and A431 tumour spheres and successfully studied plasma or / and US-induced cytotoxicity in 3D tumour spheroids [106].

This results also proved low attachment plate's ability to promote aggregation of cells by cell-cell and cell-ECM interactions while blocking the ECM interaction to the plastic surface. Which can be used as a pre-clinical model due to its simplicity, efficiency, higher reproducibility and also possible to generate a wide range of tumour cell types using the same protocol in any laboratory conditions [222, 235, 265, 269].

3.2.4 Optimization of hanging drop plate method

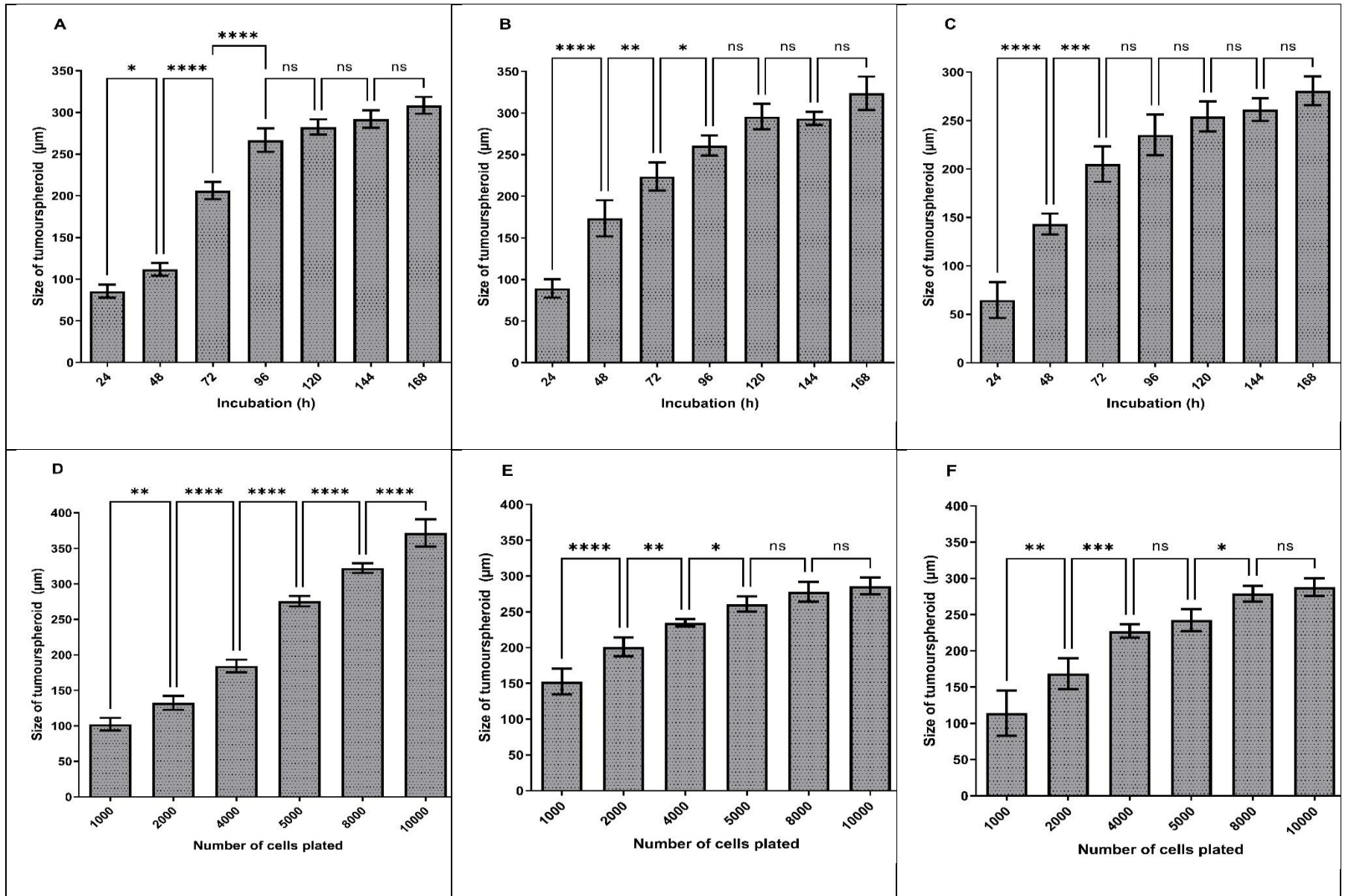
The optimum U-251 MG (Figure 21A), U-87 MG (Figure 21B) and A-172 (Figure 21C) tumour spheroids formations were attained after 96 h of incubation for the 5000 cells / well initial seeding density by achieving a size range of 251 - 285 μm , 252 - 279 μm and 217 - 265 μm respectively. One-way ANOVA indicated that there were significant differences in tumour spheres diameter during 24 - 96 h incubation, while, there were no significant difference during 96 - 168 h incubation. It was also observed that exponential growth (Log) was achieved within the initial 4 days of growth, after which the growth curve became stationary in all these three GBM cell lines.

For growth analysis, varying numbers of U-251 MG, U-87 MG and A-172 cells (ranging from 1000 to 10 000 cells / well) were seeded in the HDP1096 Perfecta3D® hanging drop plates and the mean sizes were computed after 96 h of incubation. The largest U-251 MG tumour spheres were observed with 10 000 cells / well initial seeding densities after 96 h incubation. As illustrated in Figure 21D, one-way ANOVA revealed a significant difference in tumour sphere diameter between each initial seeding density. The largest U-87 MG tumour spheres were observed with 8 000 to 10 000 cells / well initial seeding densities after 96 h of incubation. One-way ANOVA demonstrated that there is a significant difference in tumour sphere diameter between each of the initial seeding densities as shown in Figure 21E. However, there was no significant difference between diameters in 5 000, 8 000 and 10 000 cells / well seeding densities. While the largest A-

172 tumour spheres were observed with 8 000 to 10 000 cells / well initial seeding densities after 96 h of incubation. One-way ANOVA demonstrated that there is a significant difference in tumour sphere diameter between each of the initial seeding densities as shown in Figure 21F. Though, there was no significant difference between diameters in 4 000 to 5 000, and 8 000 to 10 000 cells / well seeding densities.

During the U-251 MG spheroids cell health investigation, it was established that the initial seeding density of 5000 cells / well had the best spheroids cell health. The substantial difference in 4000 to 5000 cells / well and 5000 to 8000 cells / well was verified by one-way ANOVA, however there was no significant difference in tumour sphere health at the other seeding densities (Figure 21G).

U-87 MG growth confirmed that 5 000 cells / well initial seeding density was having highest spheroids cell health. One-way ANOVA confirmed that there was no significant difference in tumour sphere health during 4 000, 5 000, 8 000 and 10 000 cells / well (Figure 21H). During A-172 growth confirmed that 5 000, 8 000 and 10 000 cells/well initial seeding densities were having highest spheroids cell health. One-way ANOVA confirmed that there was no significant difference in tumour sphere health during 5 000, 8 000 and 10 000 cells / well (Figure 21I). A full description of tukey's multiple comparisons test is provided in the Appendix I.



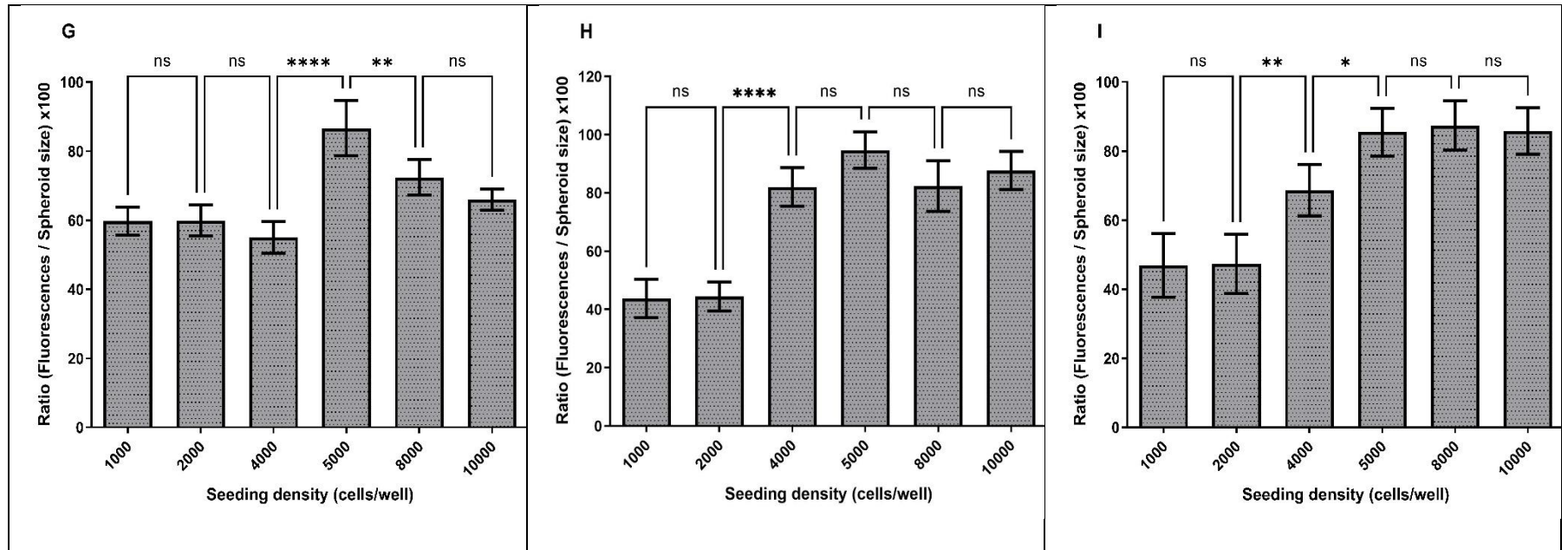


Figure 21: Development of human GBM 3D in vitro cell culture model using hanging drop plate method. A) U-251 MG, B) U-87 MG, C) A-172 tumour spheres growth (diameter in μm) analysis during different incubations. D) U-251 MG E) U-87 MG, F) A-172 growth analysis after 96 h incubation (diameter in μm) at increasing seeding density. The mean of the diameter was used to plot the values on columns and analysed using one-way ANOVA with tukey's post-test (ns, not significant ($p > 0.05$); * $p < 0.05$; ** $p < 0.01$, *** $p < 0.001$; **** $p < 0.0001$). G) U-251 MG H) U-87 MG, I) A-172 spheroid cell health analysed and a higher ratio indicates healthier spheroids. The mean of the [(fluorescence / spheroid size) x 100] was used to plot the values on columns and analysed using one-way ANOVA with tukey's post-test (ns, not significant ($p > 0.05$); * $p < 0.05$; ** $p < 0.01$, *** $p < 0.001$; **** $p < 0.0001$).

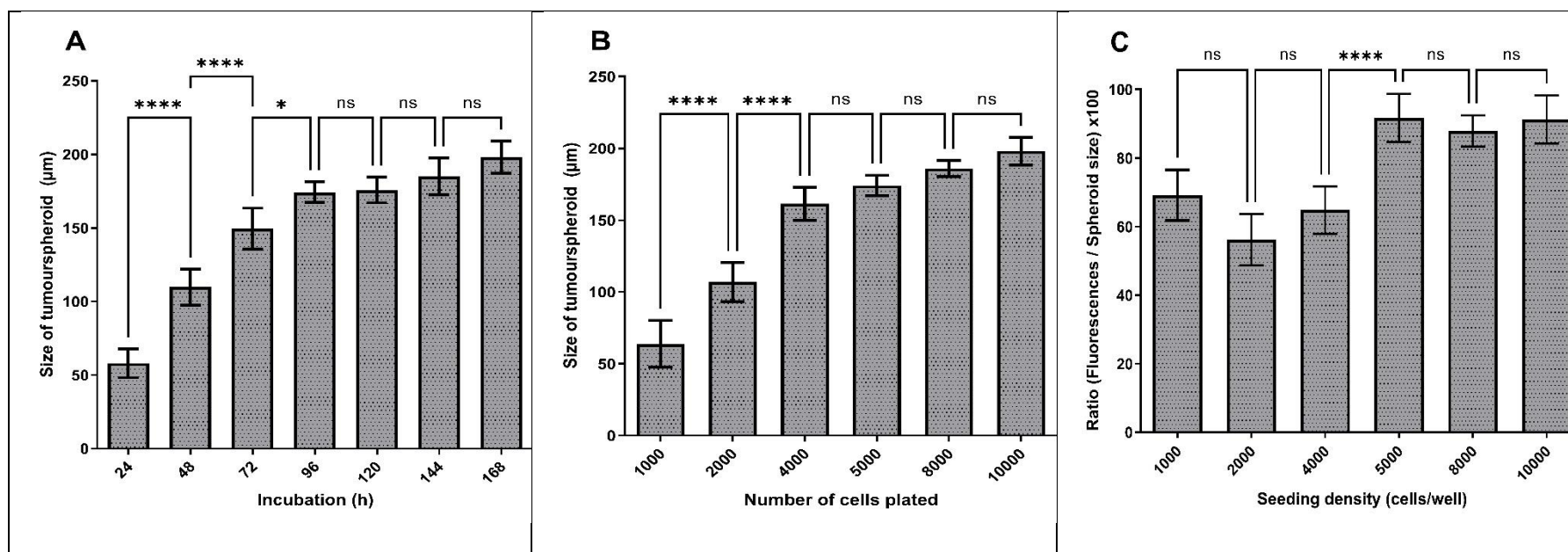


Figure 22: Development of human epidermoid carcinoma 3D in vitro cell culture model using hanging drop plate method. A) A431 tumour spheres growth (diameter in μm) analysis during different incubations. B) A431 growth analysis after 96 h incubation (diameter in μm) at increasing seeding density. The mean of the diameter was used to plot the values on columns and analysed using one-way ANOVA with tukey's post-test (ns, not significant ($p > 0.05$); $*p < 0.05$; $**p < 0.01$, $***p < 0.001$; $****p < 0.0001$). C) A431 spheroid cell health analysed and a higher ratio indicates healthier spheroids. The mean of the [(fluorescence / spheroid size) x 100] was used to plot the values on columns and analysed using one-way ANOVA with tukey's post-test (ns, not significant ($p > 0.05$); $*p < 0.05$; $**p < 0.01$, $***p < 0.001$; $****p < 0.0001$).

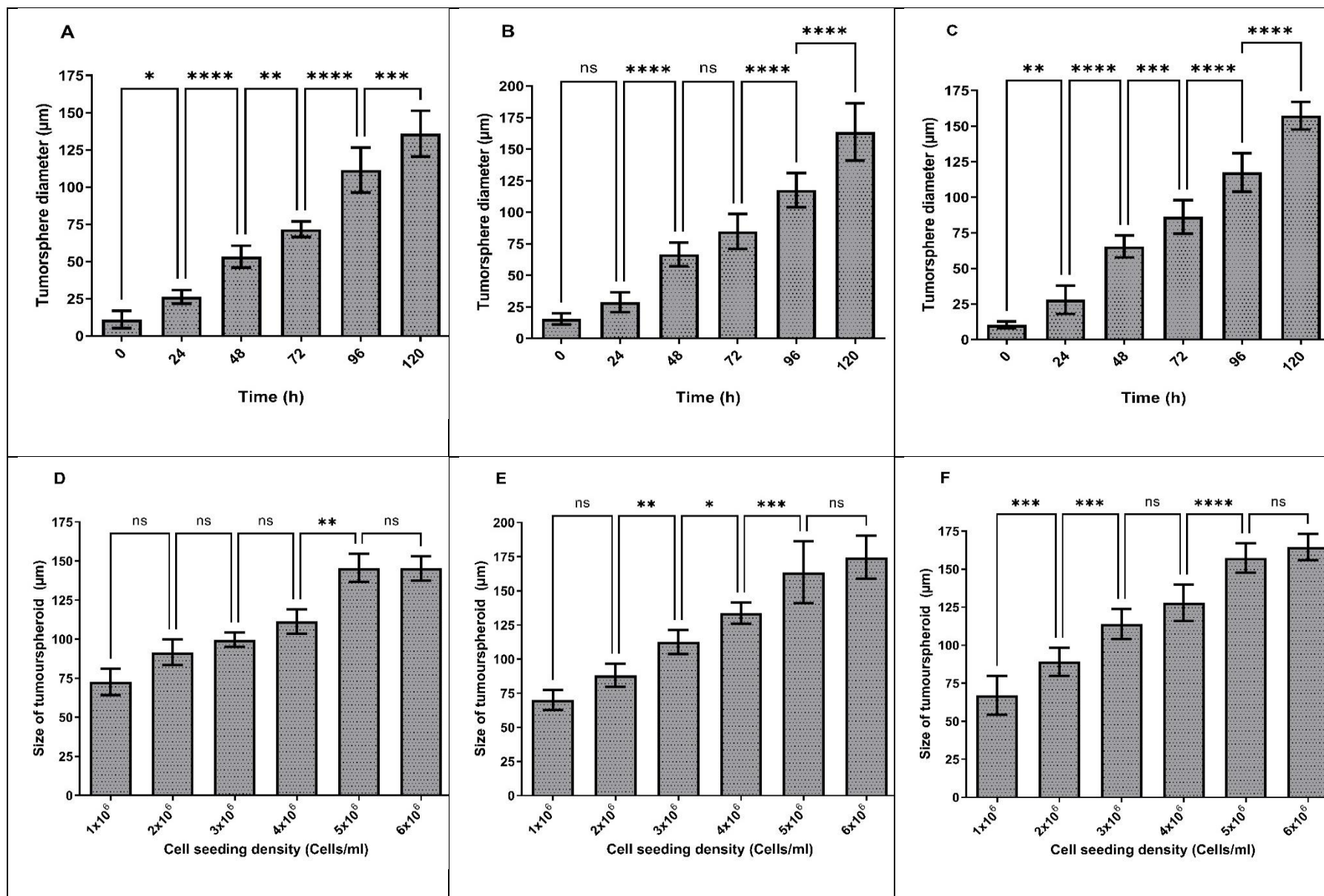
The optimum A431 (Figure 22A) tumour spheroids formations were observed within 96 h of incubation for the 10000 cells / ml initial seeding density. One-way ANOVA demonstrated that there were significant differences in tumour spheres diameter during 24 - 96 h incubation, while there was no significant difference during 96 - 168 h incubation. It was also observed that exponential growth (Log) was achieved within the initial 4 days of growth, after which the growth curve became stationary in the epidermoid carcinoma cell line. During the growth analysis, the largest A431 tumour spheres were observed during the 10 000 cells / ml initial seeding densities after 96 h of incubation. One-way ANOVA demonstrated that there was a significant difference in tumour sphere diameter between 1000 to 4000 cells / ml initial seeding densities, while there was no significant difference during 4000 - 10000 cells/ml as shown in Figure 22B. A431 cells health analysed after 96 h incubation as explained above and the fluorescence signals were normalized by spheroid size (diameter in μm). During A431 growth confirmed that 5000, 8 000 and 10 000 cells / ml initial seeding densities were having highest spheroids cell health. One-way ANOVA confirmed that there was no significant difference in tumour sphere health during 5000 to 10 000 cells / ml (Figure 22C). A full description of tukey's multiple comparisons test is provided in the Appendix I.

We studied tumour sphere growth in hanging drop plates with various seeding densities and observed tumour sphere growth ranging in diameter from 100 to 400 μm . According to the results, 5000 cells / well initial seeding density was the most suitable seeding density for the hanging drop plate method, and all the above GBM cell lines were able to produce healthy tumour spheres after 96 h incubation. This result also proved the hanging drop plate's ability to produce uniform sized spheroids, ability to control the size of spheroid by seeding density, higher replicability, lower cost, and ability of tumour sphere mass production within a shorter time period [222, 264, 265, 269].

3.2.5 Optimization of 3D scaffolds based method

The largest U-251 MG and A-172 tumour spheroids formation were attained after 120 h incubation by achieving a size range 110 - 156 μm (Figure 23A) and 146 – 174 μm (Figure 23C) for the 5000k cells/ml initial seeding density respectively. One-way ANOVA indicated that there were significant difference in tumour sphere diameter throughout the incubation. The optimum U-87 MG tumour spheroid formation was observed within 120 h of incubation (size range from 133 – 191 μm) for the 5000 k cells / ml initial seeding density. One-way ANOVA indicated that there were significant differences in tumour spheres diameter during 24 - 120 h incubation, while, there was no significant difference during 48 – 72 h incubation (Figure 23B).

For growth analysis, varying numbers of U-251 MG, U-87 MG and A-172 (ranging from 1×10^6 to 6×10^6 cells / ml) were seeded in the hydroxipropylcellulose 3D scaffolds. Fresh media were added every third day by replenishing old media in each well without disturbing the scaffolds, and the mean sizes were calculated after 120 h of incubation. The largest U-251 MG tumour spheres were detected with 5×10^6 and 6×10^6 cells/ml initial seeding densities after 120 h of incubation. One-way ANOVA verified that there is a significant difference in tumour sphere diameter between 4×10^6 and 5×10^6 seeding densities, while there was no significant difference in diameters between 5×10^6 and 6×10^6 cells/ml initial seeding densities as shown in Figure 23D. The largest U-87 MG and A-172 tumour spheres were observed with 5×10^6 and 6×10^6 cells/ml initial seeding densities after 120 h of incubation. One-way ANOVA demonstrated that there were significant difference in tumour sphere diameter between each initial seeding densities as shown in Figure 23E and Figure 23F respectively. However, there was no significant difference between diameters in 5×10^6 and 6×10^6 cells/ml seeding densities.



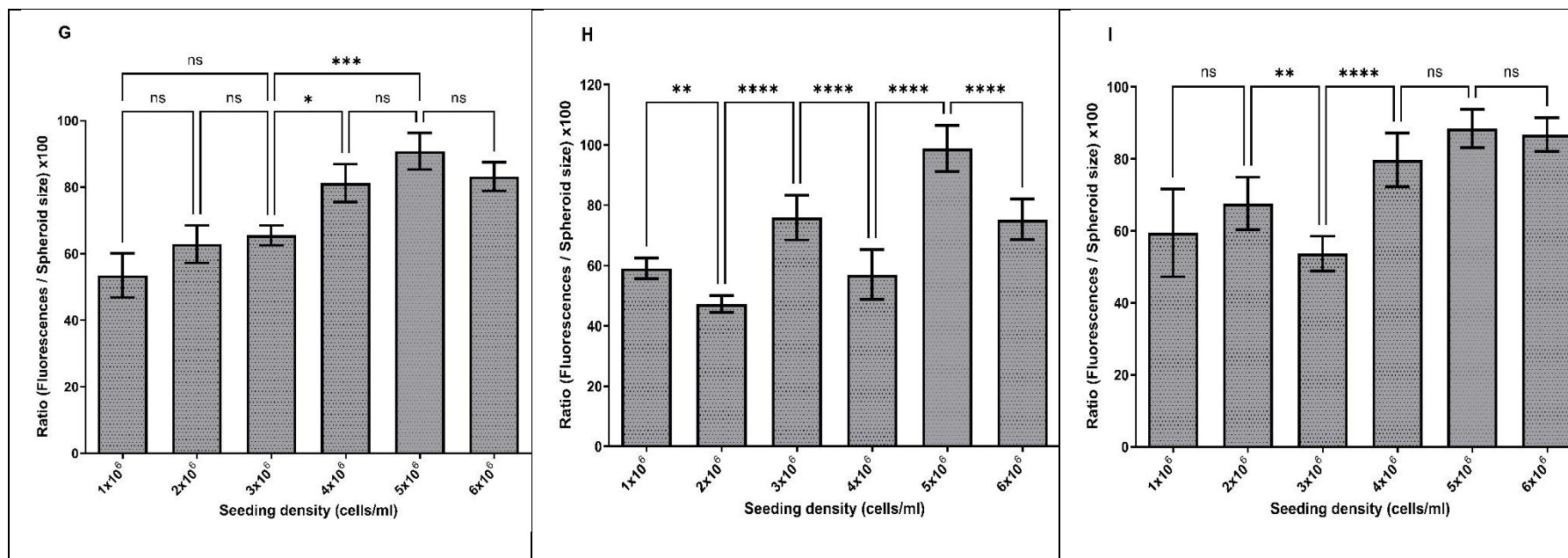


Figure 23: Development of human GBM 3D in vitro cell culture model using cellusponge 3D scaffolds. A) U-251 MG, B) U-87 MG, C) A-172 tumour spheres growth (diameter in μm) analysis during different incubations. D) U-251 MG E) U-87 MG, F) A-172 growth analysis after 120 h incubation (diameter in μm) at increasing seeding density. The mean of the diameter was used to plot the values on columns and analysed using one-way ANOVA with tukey's post-test (ns, not significant ($p > 0.05$); $*p < 0.05$; $**p < 0.01$, $***p < 0.001$; $****p < 0.0001$). G) U-251 MG H) U-87 MG, I) A-172 spheroid cell health analysed and a higher ratio indicates healthier spheroids. The mean of the [(fluorescence / spheroid size) x 100] was used to plot the values on columns and analysed using one-way ANOVA with tukey's post-test (ns, not significant ($p > 0.05$); $*p < 0.05$; $**p < 0.01$, $***p < 0.001$; $****p < 0.0001$).

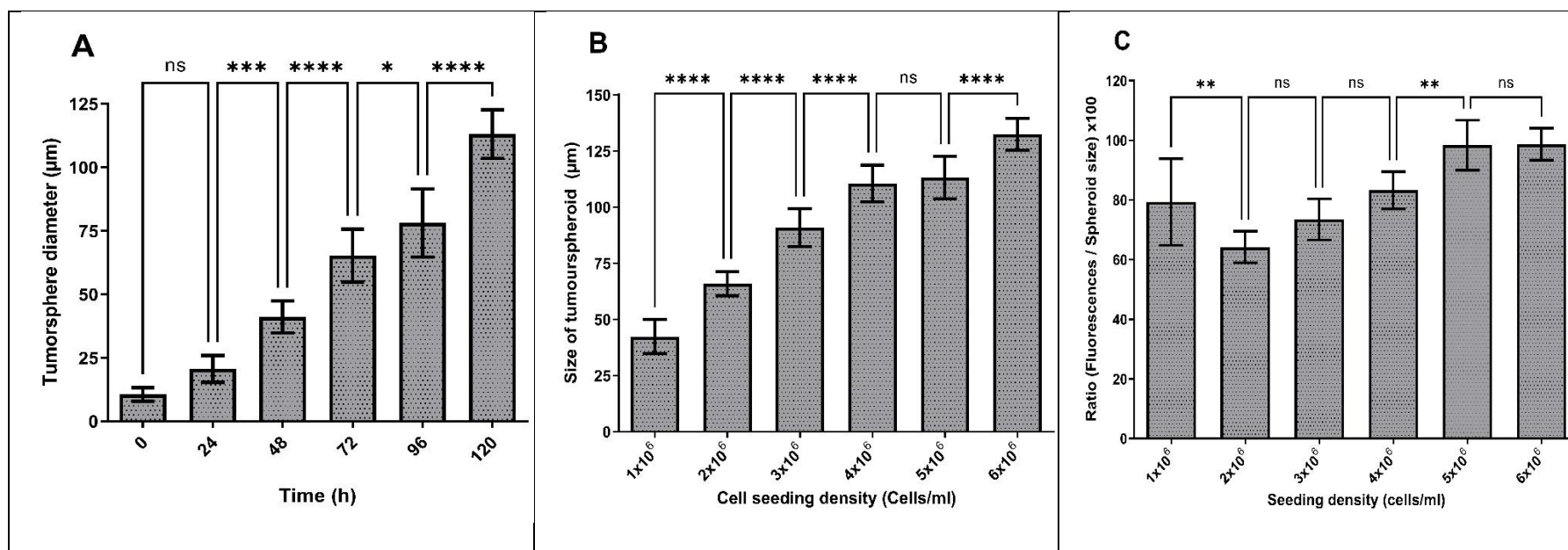


Figure 24: Development of human epidermoid carcinoma 3D in vitro cell culture model using cellusponge 3D scaffolds. A) A431 tumour spheres growth (diameter in μm) analysis during different incubations. B) A431 growth analysis after 120 h incubation (diameter in μm) at increasing seeding density. The mean of the diameter was used to plot the values on columns and analysed using one-way ANOVA with tukey's post-test (ns, not significant ($p > 0.05$); $*p < 0.05$; $**p < 0.01$, $***p < 0.001$; $****p < 0.0001$). C) A431 spheroid cell health analysed and a higher ratio indicates healthier spheroids. The mean of the [(fluorescence / spheroid size) x 100] was used to plot the values on columns and analysed using one-way ANOVA with tukey's post-test (ns, not significant ($p > 0.05$); $*p < 0.05$; $**p < 0.01$, $***p < 0.001$; $****p < 0.0001$).

U-251 MG, U-87 MG and A-172 spheroids cell health were analysed after 120 h of incubation as explained above, U-251 MG growth confirmed that 5×10^6 cells / ml initial seeding density was having highest spheroids cell health. One-way ANOVA confirmed that there were significant difference in tumour sphere health during 4×10^6 , 5×10^6 and 6×10^6 cells / ml. While there was a significant difference between 3×10^6 and 4×10^6 densities as shown in Figure 23G.

During U-87 MG growth, it was confirmed that 5×10^6 cells / ml initial seeding densities were having the highest spheroids cell health. One-way ANOVA confirmed that there were significant differences in tumour spheres health from 1×10^6 to 6×10^6 cells / ml (Figure 23H). During A-172 growth, it was confirmed that 5×10^6 and 6×10^6 cells / ml initial seeding densities had the highest spheroids cell health. One-way ANOVA confirmed that there was no significant difference in tumour sphere health during 4×10^6 , 5×10^6 and 6×10^6 cells / ml (Figure 23I). A full description of tukey's multiple comparisons test is provided in the Appendix I.

The optimum A431 (Figure 24A) tumour spheroids formations were observed within 120 h of incubation for the 10000 cells / ml initial seeding density. One-way ANOVA demonstrated that there were significant differences in tumour spheres diameter during 24 - 120 h incubations. It was also observed the exponential growth throughout the incubations time (from 24 – 120 h) in the epidermoid carcinoma cell line. During the growth analysis, the largest A431 tumour spheres were observed during the 6×10^6 cells / ml initial seeding densities after 96 h of incubation. One-way ANOVA demonstrated that there was a significant difference in tumour sphere diameter between 5×10^6 to 6×10^6 cells/ml initial seeding densities as shown in Figure 24B. A431 cells health analysed after 96 h incubation as explained above and the fluorescence signals were normalized by spheroid size (diameter in μm). During A431 growth confirmed that 5×10^6 and 6×10^6

cells / ml initial seeding densities were having highest spheroids cell health. One-way ANOVA confirmed that there was no significant difference in tumour sphere health during 5×10^6 to 6×10^6 cells/ml (Figure 24C). A full description of tukey's multiple comparisons test is provided in the Appendix I.

We studied tumour sphere growth in hydroxipropylcellulose 3D scaffolds with various seeding densities and observed tumour sphere growth ranging in diameter from 50 to 200 μm . According to the results, 5×10^6 cells / well initial seeding density was the most suitable seeding density for the scaffold based method and all the above GBM and epidermoid carcinoma cell lines were able to produce healthy tumour spheres after 120 h of incubation. These results also proved the biological scaffold's higher biocompatibility and its possibility to control scaffold's composition, porosity, and elasticity to get better GBM ECM representation [269, 276]. This protocol can be applied to hydroxipropylcellulose scaffolds or any other natural scaffold [308] and possible to generate wide range of tumour sphere types in any laboratory. It is also possible to improve scaffold chemistry and composition to mimic the physiological architecture of any GBM tumours.

3.2.6 Analysis of 3D cell viability

The effects of TMZ cytotoxicity on the different GBM cell lines were studied using U-251 MG, U-87 MG and A-172 tumour spheres. TMZ induced cytotoxicity was studied using two different cell viability assays as shown in Figure 25. The CellTiter-Glo® 3D cell viability assay quantifies the amount of ATP present, which is a marker for the presence of metabolically active cells, to determine the number of viable cells in a 3D cell culture [344]. While alamarBlue cell viability, resazurin is used as an oxidation-reduction (REDOX) indicator that undergoes colorimetric change in response to cellular metabolic reduction [345]. TMZ treated tumour spheres (concentration gradient from 500

μM to $0.97 \mu\text{M}$), were post incubated for 6 days at 37°C . An IC_{50} of $143.6 \mu\text{M}$ ($135.2 \pm 152.6 \mu\text{M}$), $71.25 \mu\text{M}$ ($66.41 \pm 76.44 \mu\text{M}$), and $111.0 \mu\text{M}$ ($103.1 \pm 119.4 \mu\text{M}$) were found for U-251 MG, U-87 MG and A-172 tumour spheres respectively, when analysed by using the alamarBlue cell viability assay (Figure 25A). An IC_{50} of $174.4 \mu\text{M}$ ($160.5 \pm 189.5 \mu\text{M}$), $76.06 \mu\text{M}$ ($70.81 \pm 81.70 \mu\text{M}$), and $134.0 \mu\text{M}$ ($115.5 \pm 155.3 \mu\text{M}$) were found for U-251 MG, U-87 MG and A-172 tumour spheres respectively, when analysed by using the CellTiter-Glo® 3D cell viability assay (Figure 25B). Two-way ANOVA demonstrated that there were significant differences in viability between the different TMZ concentrations and different cell lines ($p < 0.0001$). A full description of tukey's multiple comparisons test is provided in the Appendix I. According to these results, it was postulated that as U-87 MG has the highest TMZ sensitivity, while U-251 MG tumour spheres showed highest cell viability with TMZ treatment. TMZ induced cytotoxicity in all three cell lines showed similar values, when comparing both cell viability assays. However, comparatively higher IC_{50} values were observed from the CellTiter-Glo® 3D cell viability assay, and this may be due to the difference in assay chemistries and metabolic targets in viability assays [271].

The effects of diffusion of the active dyes through the matrices and their subsequent bioavailability to the cells can lead to misinterpretation of the results obtained. The concern is addressed in the present study by converting tumour spheres into single cells before cell viability analysis using the alamarBlue cell viability assay. This method can be successfully applied to tumour spheres constructed using low attachment plate and hanging drop plate methods since it is possible to collect cells after the growth / treatment. Bonnier and colleagues (2015), reported the way to use the alamarBlue cell viability assay for tumour spheres constructed using hydrogels or scaffold based methods. During this method tumour sphere embedded in gels were incubated with alamarBlue for 24 h instead

of 3 h to get high diffusion of the active dyes through the matrices to cells, similar to our study [335]. On the other hand, the CellTiter-Glo® 3D cell viability assay is quicker, easier to use and directly applies to the tumour spheres constructed using low attachment plate, hanging drop plate and scaffold based method.

Ultimately, these basic 3D cell culture models can be further improved to study the role of the BBB and chemotherapeutic resistance in GBM [169], exploring GBM / normal tissue interactions. The potential impact of the microbiome, TME, vasculature, infiltrating parenchymal and peripheral immune cells on GBM treatment techniques can also be further investigated with more advanced 3D co-culture models [346]. In the future, advances in 3D cell culture will make it possible to generate whole 3D *in vitro* GB organoids, leading to personalized treatments for GBM [244, 276, 347].

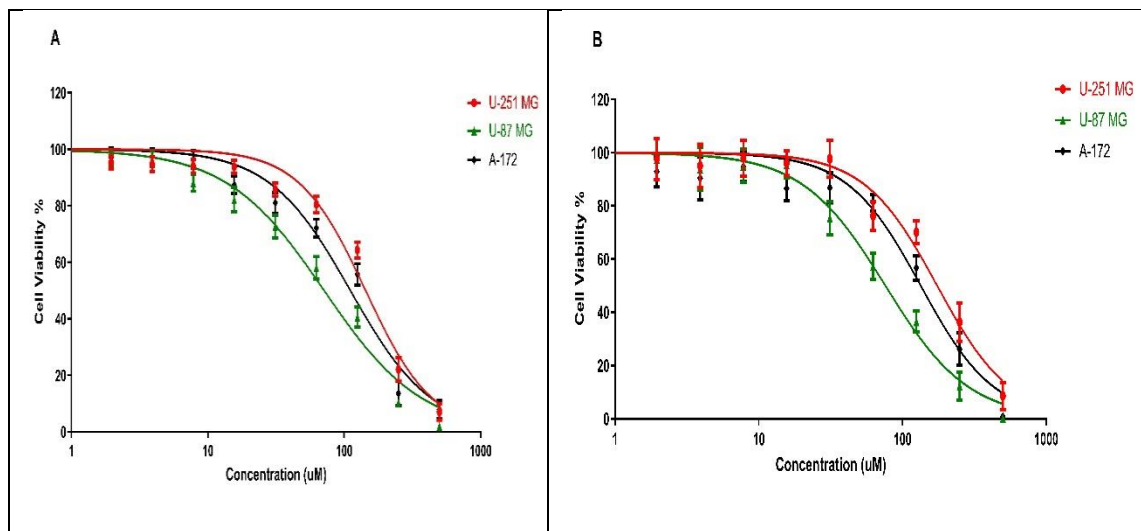


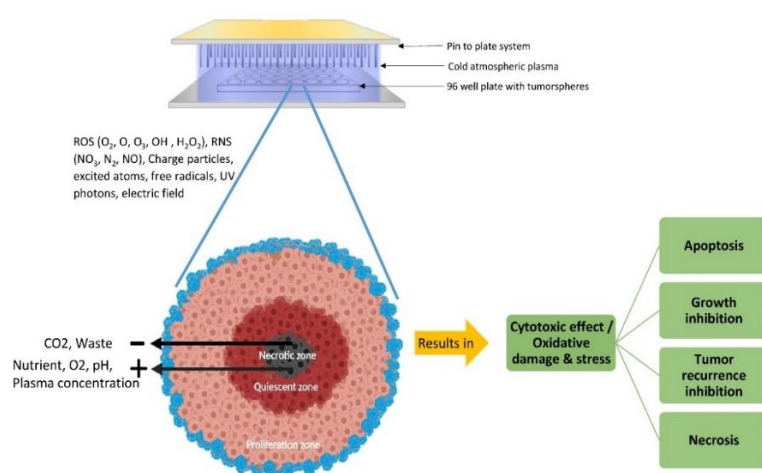
Figure 25: TMZ induced cytotoxicity in U-251 MG, U-87 MG and A-172 tumour spheres with 6 days post treatment incubation. A) Cytotoxicity analysis by using alamarBlue cell viability assay B) CellTiter-Glo® 3D cell viability assay.

3.3 Conclusion

These findings demonstrated that the protocols were capable of developing 3D tumour spheres. Larger and healthier tumour spheres were grown in DMEM high glucose media with 10% FBS when compared to media without FBS when using the low attachment plate method. The optimum formation of GBM tumour spheroids (U-251 MG, U-87 MG, and A-172) and the highest spheroid cell health occurred within 96 h of incubation with an initial seeding density of 10,000 cells / ml. The optimum formation of epidermoid tumour spheroids (A431) and highest spheroid cell health occurred within 96 h of incubation with an initial seeding density of 10,000 cells / ml.

Using the hanging drop plate method, the optimum, largest, and healthiest GBM (U-251 MG, U-87 MG, and A-172) tumour spheroids were achieved after 96 h of incubation with an initial seeding density of 5,000 cells / well. The optimum, largest, and healthiest A431 tumour spheroids were observed within 96 h of incubation with an initial seeding density of 10,000 cells / ml. When using the scaffold-based method, the optimal, largest, and healthiest U-251 MG, U-87 MG, A-172, and A431 tumour spheroids were formed after 120 h of incubation with an initial seeding density of 5×10^6 cells / ml. Furthermore, our findings suggested that U-87 MG has the highest sensitivity to TMZ, whereas U-251 MG tumour spheres demonstrated the highest cell viability when treated with TMZ. The alamarBlue cell viability assay can effectively assess cell viability in tumour spheres generated using the anchorage independent methods, while the CellTiter-Glo® 3D cell viability assay can be used for both anchorage dependent and independent methods.

CHAPTER 4 – PLASMA INDUCED ROS DEPENDENT CYTOTOXICITY IN GLIOBLASTOMA 3D TUMOUR SPHERES



Part of this chapter has been published in Plasma Process and Polymer journal. (See Appendix II – Peer-reviewed)

- **Wanigasekara, J., Barcia, C., Cullen, P. J., Tiwari, B., Curtin, J. F.** Plasma induced reactive oxygen species-dependent cytotoxicity in glioblastoma 3D tumour spheres. *Plasma Processes Polym.* 2022; 19:e2100157. <https://doi.org/10.1002/ppap.202100157>
- **Wanigasekara, J., Barcia, C., Cullen, P. J., Tiwari, B. and Curtin, J. F.** Outside Front Cover: Plasma Process. Polym. 4/2022. *Plasma Process Polym.* 2022; 19: 2270010. <https://doi.org/10.1002/ppap.202270010>

4 Plasma induced ROS dependent cytotoxicity in glioblastoma 3d tumour spheres

4.1 Rationale

GBM is the most common and aggressive adult malignant primary brain tumour and has low survival rate as extensively explained in the first chapter [348-350]. Better outcomes with the existing standard therapy hampered by poor prognosis, high invasiveness, high resistant to chemotherapy and the inability to traverse the BBB [350, 351]. Therefore we explore the suitability of novel CAP for efficacious *in vivo* GBM diagnosis, prognosis, and treatment [60]. The CAP device used throughout this research is a promising novel therapeutic method for cancer treatment; due to the fact that it operates at atmospheric pressure and near room temperature, while having low power requirements [352]. While our understanding of the biological and chemical effects of CAP on cancer cells is expanding, several gaps remain, for example, the effects of CAP on cells growing in a 3D lattice [97, 98, 257]. In the present study, for the first time we used *in vitro* 3D tumour spheroid models to better understand the effects of CAP using pin device on GBM (U-251 MG) and epidermoid carcinoma (A431) cells [353].

This chapter focuses on determining the optimal configuration for a novel pin device and assessing its potential for inducing cytotoxicity in 3D tumour spheroids, as well as comparing its effect to 2D monolayer cells [225, 242]. Additionally, we investigate the impact of RONS on the cytotoxicity triggered by the device on tumour spheres. This study provides valuable insights into the cytotoxic effects of the pin-to-plate system, highlighting its potential for treating GBM and its feasibility for future combination strategies.

4.2 Results and discussion

4.2.1 Pin-to-plate discharge presents cytotoxicity towards GBM cells in a time / dose-dependent manner

The TME plays a key role in tumour progression, metastasis, angiogenesis, cytotoxicity resistance, and immune cell modulation [354, 355]. We employed a U-251 MG 3D cell culture model which enabled cell-cell and cell-ECM interactions in all three dimensions and mimicked diffusion-limited distribution of oxygen, nutrients, metabolites, and signalling molecules common in the microenvironment of *in vivo* tumours. Most of the research on the effects of CAP on cancer cells have been investigated by using 2D monolayer cell cultures [105, 356] and a growing number on animal models [118, 120]. There are also a few studies carried out using the pin to plate design [105, 336] however this is the first time that we are reporting the approach for induced cytotoxicity in 3D tumour spheroids.

We have tested tumour spheres growth with different seeding densities and observed tumour sphere growth ranging from 100 to 650 μm in diameter. Our findings correlates with the tumour spheres sizes obtained by Singh et al., 2020 [343]. We used this diffusion limited 3D cell culture model to explore the diffusion of cytotoxic reactive species throughout the tumour sphere, rate of cell death, and effects of single and multiple CAP treatment on the cell-cell and cell-ECM interactions.

The tumour sphere size and resistance to CAP treatment was enhanced when the tumour spheres were cultured in media containing serum, which is in agreement with others [357]. Previous studies from our research group demonstrated that the optimal discharge frequency using the pin to plate reactor was 1000 Hz, producing the highest overall RONS within the plasma. Correspondingly, the highest cytotoxic responses were also observed

for 1000 Hz [336]. We therefore used a resonant frequency of 55.51 kHz with discharge frequency 1000 Hz and duty cycle 73 μ s for exploring the technology's potential for 3D cell cultures.

Firstly, the effects of plasma discharge on the GBM tumour spheres were studied under two different media compositions (DMEM high glucose with and without the presence of 10% FBS). Plasma treated tumour spheres were post incubated at 24, 48 and 96 h at 37 °C. An IC₅₀ of 386.3 s (375.9 \pm 397.1 s), 460.7 s (449.4 \pm 472.4 s), 769.3 s (742.5 \pm 797.0 s) were found for tumour spheres grown in a media with serum, CAP treated and post incubated at 24, 48 and 96 h respectively. An IC₅₀ of 82 s (80.68 \pm 83.33 s), 172.4 s (170.3 \pm 174.6 s), 237.4 s (230.5 \pm 244.5 s) were found for tumour spheres grown in media without serum, CAP treated and post incubated at 24, 48 and 96 h respectively (Figure 26A). Two-way ANOVA demonstrated that there is a significant difference in viability between the doses of CAP, different post treatment incubations and media used for tumour spheres growth (P<0.0001). A full description of tukey's multiple comparisons test is provided in the Appendix I. According to these results, tumour spheres grown in high glucose DMEM with 10% FBS showed higher CAP resistance (Figure 26A) and growth rate (Figure 18A), likely more similarly reflecting the *in vivo* conditions. Hence, we use media supplemented with 10% serum for all further tumour spheres to get better representation of the *in vivo* effects.

Next, we compare the effects of the plasma discharge on U-251 MG human GBM and A431 human epidermoid carcinoma (2D and 3D cells) in DMEM high glucose with 10% FBS medium after 24 h incubation time. An IC₅₀ of 386.3 s (375.9 \pm 397.1 s) and 160.4 s (157.0 \pm 163.9 s) were found for U-251 MG 3D and 2D cells, respectively and an IC₅₀ of 125.5 s (123.2 \pm 127.9 s) and 50.77 s (49.67 \pm 51.90 s) were found for A431 3D and 2D cells, respectively (Figure 26 B). Two-way ANOVA shows that there is a significant

difference in U-251 MG and A431 (2D and 3D) cell viability between the doses of CAP and different cell lines ($P < 0.0001$). A full description of tukey's multiple comparisons test can be seen in the Appendix I. When using a single CAP treatment, U-251 MG 3D tumour spheres displayed greater resistance to CAP compared with the 2D cell cultures with U-251 MG cells also showing a higher treatment resistance compared to the A431 cell lines.

Subsequently, we determine the cytotoxic effects of a single CAP treatment on GBM tumour spheres (in DMEM media with and without sodium pyruvate). An IC_{50} of 355.1 s (342.3 ± 368.5 s), 429.8 s (422.7 ± 437.1 s), 490.4 s (475.2 ± 506.1 s) were found for U-251 MG tumour spheres single CAP treated and post incubated in media without pyruvate medium for 24, 48 and 96 h respectively (Figure 27A). An IC_{50} of 74.82 s (74.10 ± 75.54 s), 88.05 s (87.45 ± 88.65 s) and 76.74 s (75.42 ± 78.09) were found for multiple CAP treated and post incubated U-251 MG tumour spheres in media without pyruvate medium for 24, 48 and 96 h respectively (Figure 27A).

An IC_{50} of 386.3 s (375.9 ± 397.1 s), 460.7 s (449.4 ± 472.4 s), 769.3 s (742.5 ± 797.0 s) were found for tumour spheres single CAP treated and post incubated in media with pyruvate for 24, 48 and 96 h respectively (Figure 27B). An IC_{50} of 75.01 s (74.05 ± 75.98 s), 100.1 s (97.85 ± 102.5 s) and 76.24 s (74.25 ± 78.28 s) were found for multiple CAP treated and post incubated U-251 MG tumour spheres in media with pyruvate for at 24, 48 and 96 h respectively (Figure 27B). These data confirmed that the pyruvate free media resulted in greater effects. Depending on the cytotoxicity results (Figure 27), the single plasma discharge did not induce full cytotoxicity in the tumour spheres, even at the highest dose at 24 h incubation (320 s, cell viability = 49.16 – 58.94% in figure 27B).

Since the single CAP treatment was not enough to induce higher cytotoxicity and halt tumour regrowth, we hypothesised that the use of multiple (3 consecutive daily) CAP

treatments would result in more favourable outcomes. The two-way ANOVA demonstrated that there is a significant difference in viability between each dose of multiple CAP, different post treatment incubations and media used for tumour spheres growth ($P < 0.0001$). A full description of the tukey's multiple comparisons test can be seen in the Appendix I. The differences in IC_{50} values and significant difference between different media used (DMEM high glucose with and without pyruvate) shows a protective effect of sodium pyruvate. These experiments identified multiple CAP treatment as a most successful way to induce effective cytotoxicity in the target tumour spheres.

To compare plasma effectivity towards different cell lines, single and multiple CAP treatments of both U-251 MG and A431 tumour spheres were carried out. For single CAP treatment, cell viability after 24 h was 54.33% (IC_{50} - 390.6 s) and 18.22% (IC_{50} -125.5 s) for U-251 MG and A431 tumour spheres respectively with the highest dose (320 s) (Figure 26C). CAP treated tumour spheres incubated for a longer time period (96 h), led to cell viability increases in both cell lines. Cell viability with the highest dose was found to be 75.83% (IC_{50} - 777.3 s) and 35.46% (IC_{50} - 225.0 s) for U-251 MG and A 431 tumour spheres respectively (Figure 26C).

The kinetic response to CAP treatment over time was markedly different. For 2D cultures, significantly more cell death was evident 96 h after treatment compared with 24 h, with cytotoxicity found to be ROS-dependent [105]. Conversely, for both U-251 MG and A431 3D tumour spheres, the induced cytotoxicity after 24 h was proportional to the plasma dosage but were found to partially recover their RONS damage and regrow, similar to previous reports [121] and in contrast to cells grown in the 2D monolayer [105]. Our data also shows that the U-251 MG cell line is highly resistant to single dose plasma treatments and able to regrow quicker when compared to A431. These results have

important implications for future animal model and human trials where single CAP treatments may be insufficient to yield significant benefits.

For the multiple CAP treatments and incubation at 24 h, cell viability with the highest dose was 8.22% ($IC_{50} - 70.59$) and 0.76% ($IC_{50} - 46.65$) for U-251 MG and A431 tumour spheres respectively (Figure 26D). With a post treatment incubation of 96 h, cell viability was 12.82% ($IC_{50} - 77.38$) and 0.59% ($IC_{50} - 51.44$) for U-251 MG and A431 tumour spheres respectively (Figure 26D). According to the results it confirmed that U-251 MG human GBM tumour spheres were more resistant to plasma treatment when compared to the A431 human epidermoid carcinoma. However, multiple CAP treatment significantly induced cytotoxicity in tumour spheres and it was able to fully / partially inverse tumour spheres regrowth ability in A431 / U-251 MG respectively. Multiple CAP doses successfully reduced U-251 MG tumour spheres regrowth rates. Two-way ANOVA demonstrated that there is a significant difference in the viability between single and multiple CAP doses, post treatment incubation period and cell line used for tumour spheres growth ($P < 0.0001$). A full description of the tukey's multiple comparisons test is available in the Appendix I. Based on the analysis it is demonstrated that the pin to plate device could induce tumour sphere cytotoxicity in dose and time dependent manner.

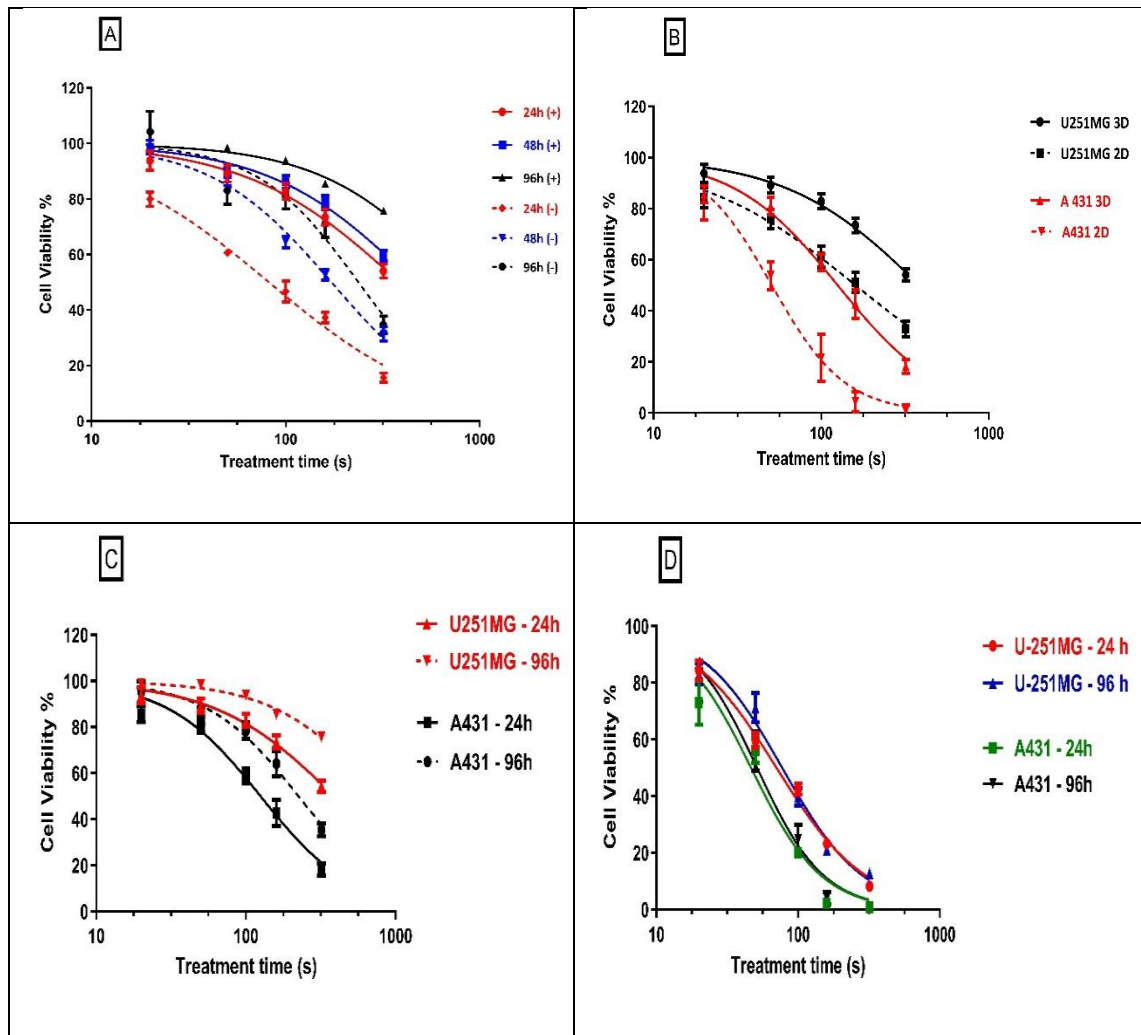


Figure 26: U-251 MG CAP treatment. A) U-251 MG tumour spheres single CAP treatment and post treatment incubation at 24, 48 and 96 h [with serum media represented as a (+) and without serum media represented as (-)] B) U-251 MG and A431 3D, 2D cell cytotoxicity comparison after CAP treatment and 24 h post treatment incubation C) Comparison of U-251 MG and A431 single CAP treatments with 24 h and 96 h incubations. D) Comparison of U-251 MG and A431 multiple CAP treatment with 24 h and 96 h incubation

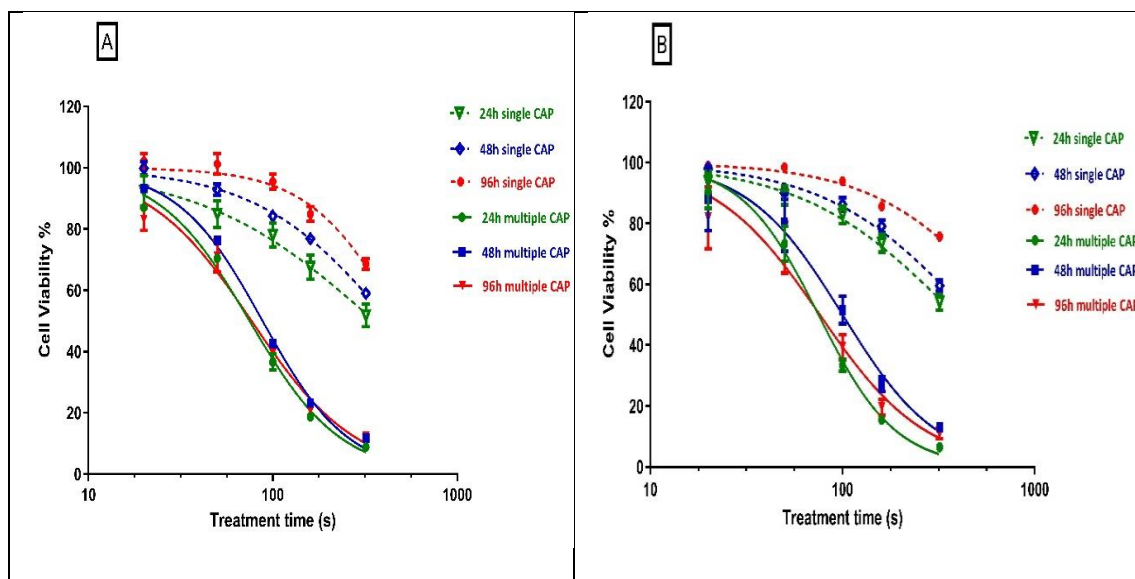


Figure 27: *U-251 MG CAP treatment with and without sodium pyruvate medium. A) U-251 MG single and multiple (3 consecutive daily) CAP treatment (without pyruvate medium) and post treatment incubation at 24, 48 and 96 h. B) U-251 MG single and multiple CAP treatment (with pyruvate medium).*

4.2.2 Effect of CAP treatment on tumour sphere cell membrane damage

PI was used to validate the pin-to-plate induced cell death and cytotoxicity in U-251 MG tumour spheres. PI is a membrane impermeable, fluorescent, nucleic acid intercalating agent, allowing identification of dead cells with compromised plasma membranes in a population in tumour spheres. PI uptake was measured 24 h post single (Figure 28A) and multiple (Figure 28B) CAP treatments. The PI uptake increased to almost 45% and 90% respectively following single and multiple CAP treatments for 320 s as shown in figure 28C. This also proves that CAP treatment can damage the tumour sphere's cell membrane and induce cytotoxicity. This validates the alamarBlue assay data. Two-way ANOVA demonstrated that there was a significant difference in PI uptake between control and the

50 s, 100 s, 160 s and 320 s doses ($P < 0.0001$), while no significant difference was found between the control and 20 s for both single and multiple CAP treatment. A full description of tukey's multiple comparisons test can be seen in the Appendix I.

The outer layer of the spheroid is exposed to the surrounding medium and mainly composed of viable, proliferating cells [358]. It is tempting to hypothesise that when tumour spheres are exposed to CAP, gas-phase reactive species are first trapped by the surrounding medium and then initiate chemical reactions on the outer layer of cells, this then leads to cell death in the outer layer of cells, resulting in weakened cell-cell interactions and the disassembly of the tumour sphere. It was reported that despite the ability of RONS to penetrate throughout the entire depth of 3D tumour spheroids, apoptosis was observed only on the outermost layer or surface [116]. However, this is not what occurs in our case.

We used confocal microscopy alongside 3D reconstruction of stacked images to build 3 dimensional maps of the treated tumour spheres. The distance of each dead cell to the nearest surface of the tumour sphere was calculated and colour coded (Figure 29). With this analysis, we demonstrated that cytotoxicity, measured by PI uptake, increased significantly after multiple treatments. Even after a single CAP treatment, we observed a uniform distribution of dead cells throughout the tumour sphere. These data underscore the capacity of ROS generated by CAP to diffuse at least 150 μm from the surface of the tumour without limiting cytotoxicity, and that low doses of CAP (single treatments) cause a significant disruption of cell-cell and cell-ECM interactions throughout the tumour sphere.

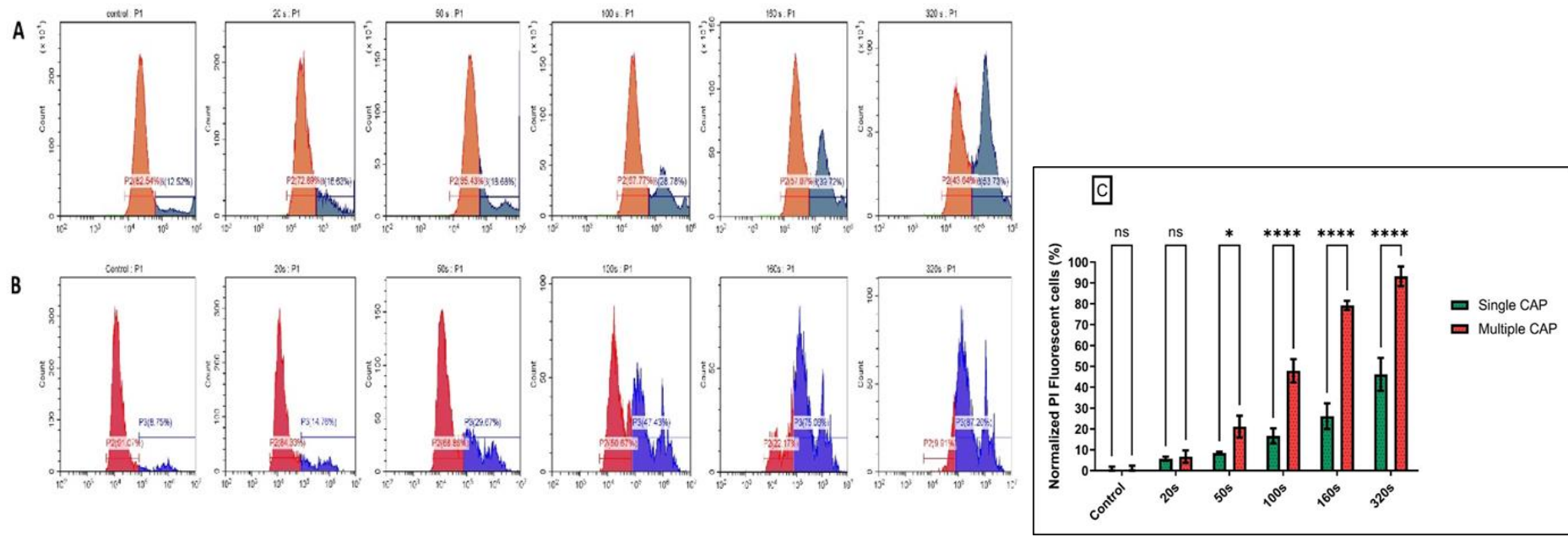


Figure 28: PI uptake in pin-to-plate treated U-251 MG tumour spheres. PI uptake was measured by flow cytometry and used as an indicator of cell death. Cells were treated at 240 V, 1000 Hz and 73 μ s for 0, 20, 50 100, 160 and 320 s. PI uptake was then measured in 24 h post treatment in (A) single CAP treatment (B) multiple CAP treatments (C) normalized PI uptake was then measured at 24 h post single and multiple treatments and represented as a bar chart. All the data points were statistically significant except Control and 20 s treatment times. (ns, not significant ($p > 0.05$); * $p < 0.05$; **** $p < 0.0001$).

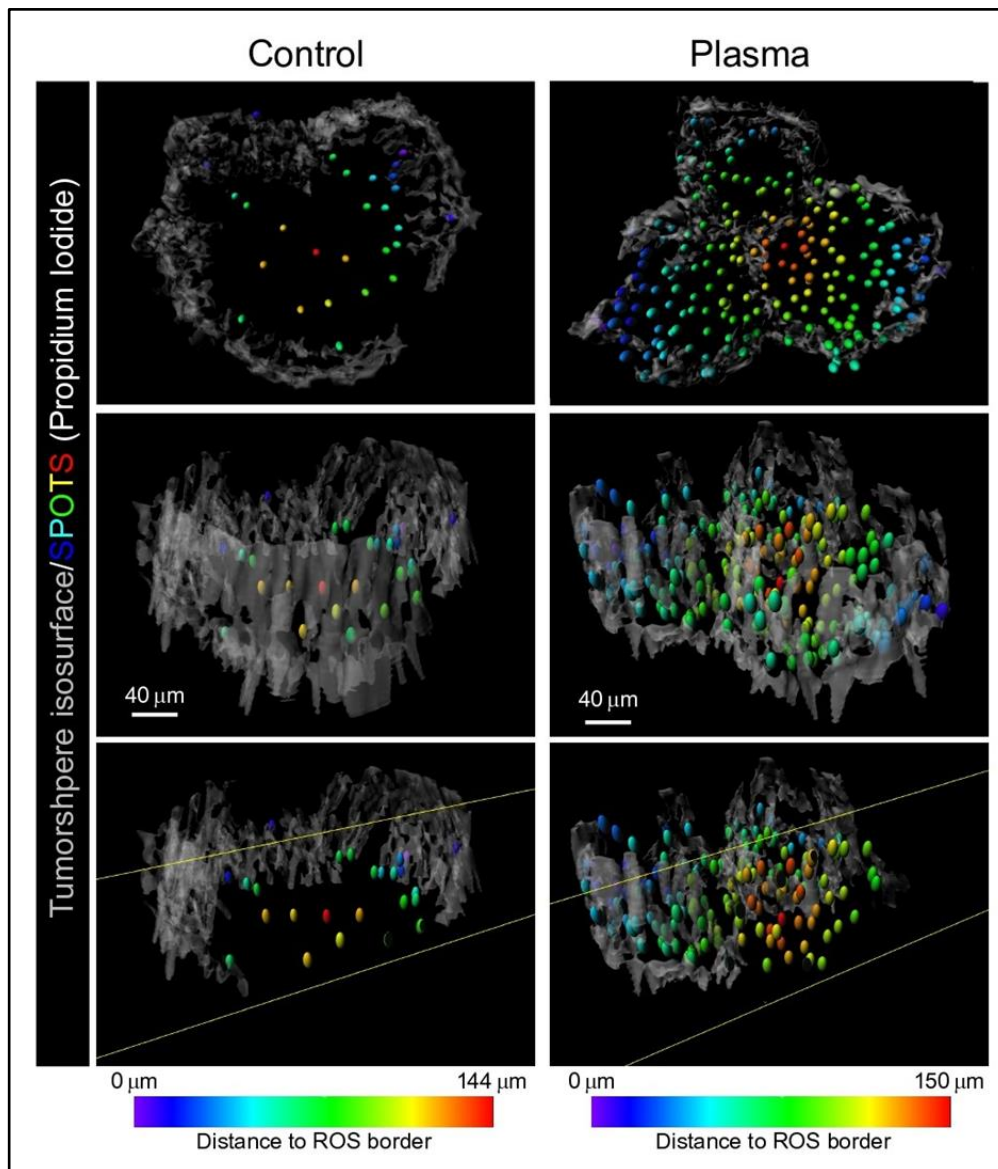


Figure 29: PI uptake in pin-to-plate treated U-251 MG tumour spheres. Fluorescence levels of control and 320 s CAP treated, PI stained U-251 MG tumour spheres observed by confocal microscopy detected by 3D software. Tumour sphere cell death identified in an each spot and distance to ROS border shown. Distance to the ROS border is colour coded according to the scale at the bottom

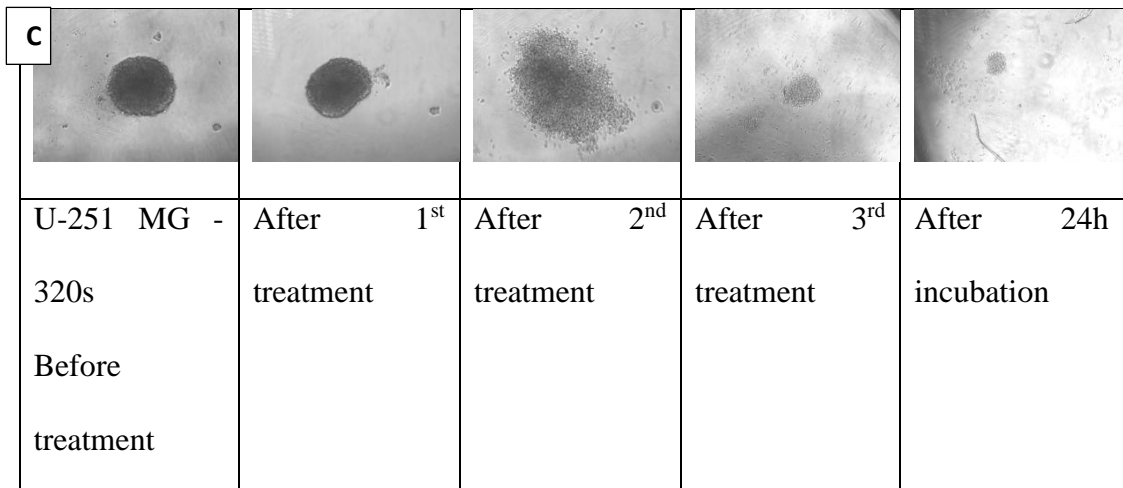
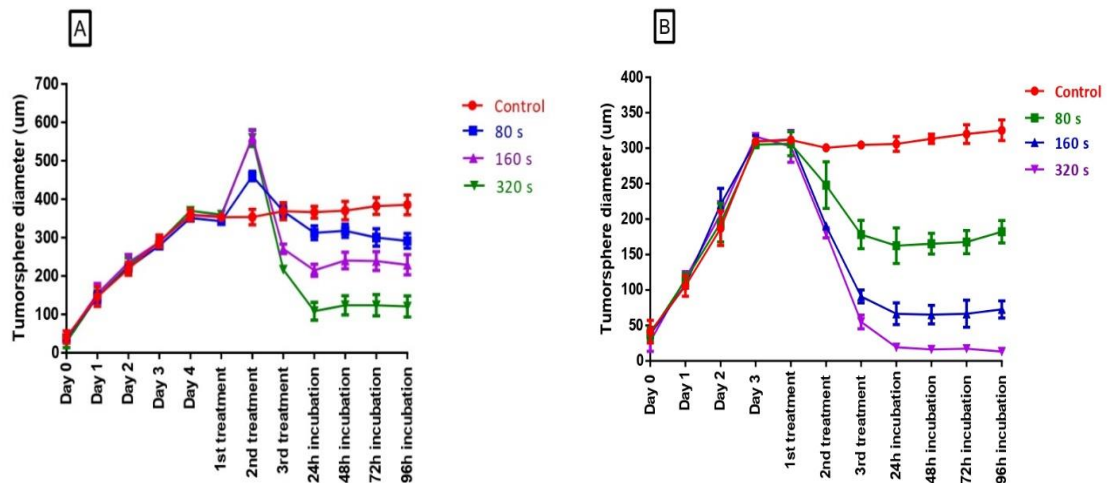
4.2.3 CAP induced morphological changes

Changes in the tumour sphere morphology induced by CAP treatment was studied to get better understanding about their mechanism of cell death. Tumour sphere diameter was found to be significantly reduced after the third CAP treatment (320 s) for both U-251 MG (Figure 30A) and A431 (Figure 30B) cell lines. Representative tumour sphere images showing the morphological changes induced by 320s CAP treatment for U-251 MG and A431 are shown in Figure 30C and 30D respectively.

Multiple CAP treatments induced significant, cumulative cytotoxicity. This was manifested by spheroid shrinkage and markedly reduced tumour regrowth ability which was achieved with lower overall doses of CAP. It is therefore likely that multiple CAP treatments over a relatively short period of time would be necessary for clinical applications, setting constraints on approaches to deliver CAP directly to the tumour site. Interestingly, the response of U-251 MG and A431 tumour spheres to multiple CAP treatments was visibly different. Whereas U-251 MG tumour spheres (Figure 30A) had no appreciable morphological change after the first treatment, swelled significantly at the second treatment and broke apart after the third treatment, A431 tumour spheres (Figure 30B) reduced in size after the first treatment and gradually broke apart on consecutive treatments. Overall, the outcome was essentially the same with enhanced cytotoxicity and inability to reform tumour spheres after multiple treatments, but the effects suggest that the cell-cell and cell-ECM interactions are different for each cell line.

Finally, to validate the above changes after multiple CAP treatment, we calculated the number of cells in the tumour sphere (cells/ml) accompanied by 0, 160 and 320 s CAP treatments. The number of cells in a tumour sphere rapid declined during each CAP treatment with the lowest cell number observed after a 24 h post treatment incubation period. Subsequently, the number of cells increased slightly for the 160 s treatment with

the overall cell amount slowly decreasing with the 320 s treatment (Figure 30E). Interestingly, U 251 MG tumour sphere diameter increased during the second CAP treatment (Figure 30A) while reducing cell number (Figure 30E). It is possible that multiple CAP treatments can weaken cell-cell and cell-ECM interactions, and due to this, the volume of the densely arranged tumour sphere started to increase, resulting in an increased tumour sphere diameter. On the other hand, a higher number of cells were dead and detached from the tumour sphere core, which was observed as a reduction in cell number. Two-way ANOVA demonstrated that there was a significant difference in the number of cells during the 24 h to 96 h incubation period ($P < 0.0001$). A full description of the tukey's multiple comparison test is available in the Appendix I.



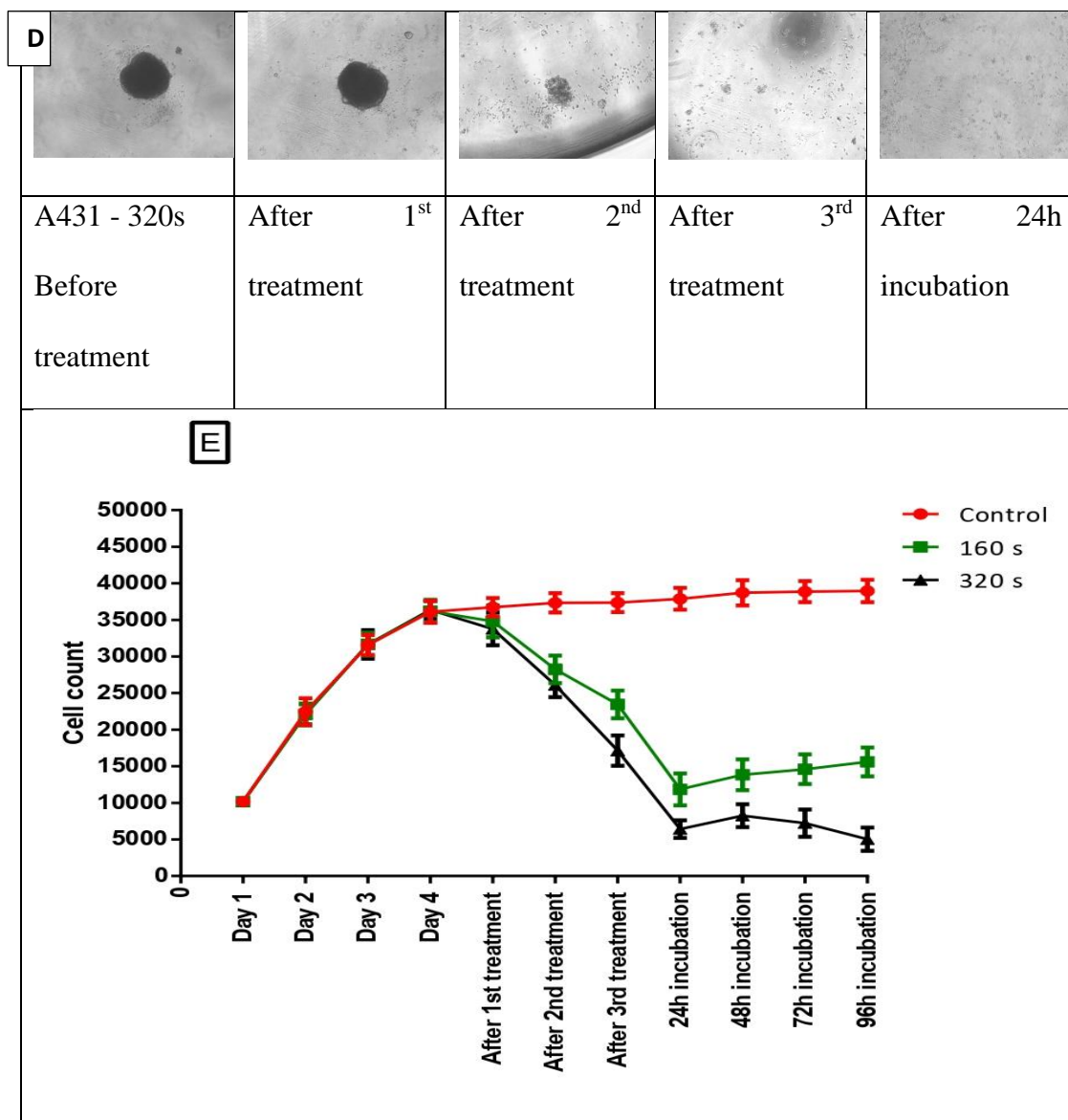


Figure 30: U-251 MG and A431 tumour spheres size (diameter) and cell count analysis followed by CAP treatment A) U-251 MG B) A431 C) U-251 MG tumour spheres morphological changes with CAP treatment D) A431 tumour spheres morphological changes with CAP treatment [Converted all of the images in 4C and 4D to greyscale and applied a simple linear brightness adjustment (+40%)]. E) U-251 MG tumour spheres cell count change with multiple CAP treatment.

4.2.4 Quantification of nitrite and hydrogen peroxide on medium

To gain a better understanding of the RONS present in the media following CAP treatments, the quantification of nitrite and hydrogen peroxide were performed. DMEM medium was exposure to multiple plasma discharges and incubated for 24 h post treatment. To quantify nitrite and hydrogen peroxide levels, Griess reagent and Amplex™ Red reagent were used, respectively. The results showed that the plasma discharge produced nitrite and hydrogen peroxide in a manner that depended on the dose of CAP tested. The highest concentration of nitrite observed was 338.1 μM , while the highest concentration of hydrogen peroxide was 454.6 μM during the 320 s CAP exposure, as shown in the Figure 31. When compared to previous results of CAP treatment using a DBD device, the culture medium in this study produced slightly lower amounts of nitrite and hydrogen peroxide by pin-to-plate device [359]. Two-way ANOVA demonstrated that there was a significant difference in nitrite and hydrogen peroxide levels between control and the 20 s, 50 s, 100 s, 160 s and 320 s doses ($P < 0.0001$). A full description of tukey's multiple comparisons test can be seen in the Appendix I.

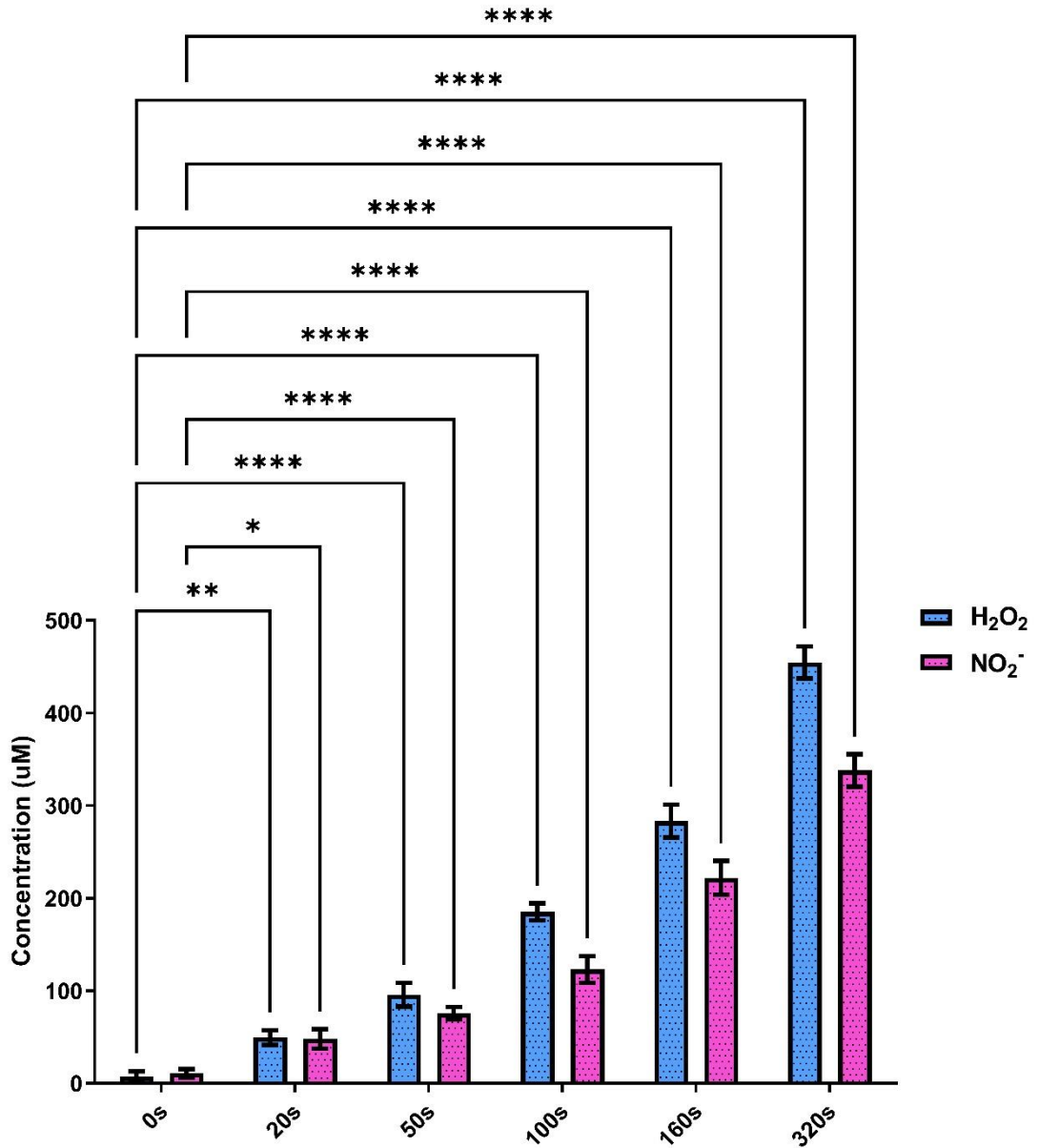


Figure 31: Measurement of H₂O₂ and NO₂⁻ concentrations after 20, 50, 100, 160, and 320 s CAP treatments using Amplex red hydrogen peroxide/peroxidase assay kit and Griess reagent kit. **p* < 0.05; ***p* < 0.01; *****p* < 0.0001

4.2.5 ROS production in U-251 MG tumour spheres

We evaluated intracellular reactive oxygen species by using H2DCFDA, a cell-permeable probe. Analysis of the histograms show significantly increasing levels of intracellular oxidised H2DCFDA and ROS as a function of treatment time (Figure 32A). The mean fluorescence levels of 80 s, 160 s and 320 s CAP treated tumour spheres were increased by a factor of 1, 1.6, and 3 times, respectively, compared to the negative control (Figure 32B).

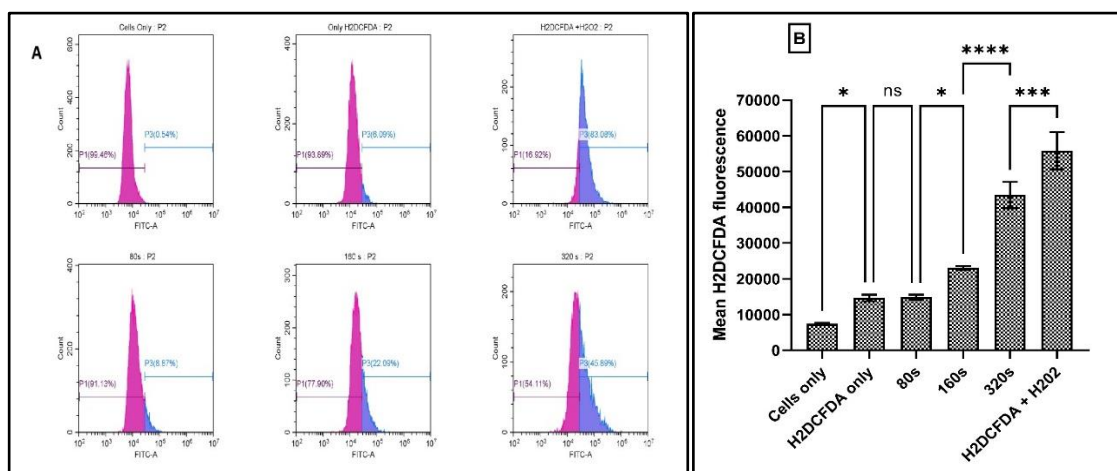


Figure 32: ROS production in U-251 MG tumour spheres. 3D cells were incubated with H2DCFDA and treated at three different doses of CAP (A) 3 h post treatment cells were collected and analysed using CytExpert software. (B) The mean of FITC channel was used to plot the values on columns and analysed using One Way ANOVA with tukey's post-test (Appendix I). All the data points were statistically significant except H2DCFDA only and 80s treatment times. (ns, not significant ($p > 0.05$); * $p < 0.05$; *** $p < 0.001$; **** $p < 0.0001$).

4.2.6 Pin-to-plate presents RONS dependent cytotoxicity

Tumour sphere response observed in the presence and absence of sodium pyruvate from single and multiple CAP treatments may indicate the presence of ROS dependent cytotoxic effects. The ROS-induced cytotoxic effect of the pin to plate system was evaluated by using different treatment time points (0, 20, 50, 100, 160 and 320 s) with NAC employed as a ROS scavenger.

The highest CAP treatment resistance was evident in the tumour spheres treated in the high glucose DMEM with pyruvate and NAC. The second highest cytotoxicity resistance was observed in the high glucose DMEM without pyruvate and with NAC. The highest cytotoxicity was shown in tumour spheres treated in high glucose DMEM without pyruvate or NAC and high glucose DMEM with pyruvate and without NAC respectively (Figure 33). This confirms that the cytotoxicity induced by the pin system is mainly dependent on RONS. NAC significantly protected the target tumour spheres from CAP induced cytotoxicity at each applied dose, post treatment incubation period, media compositions and single / multiple treatments ($P < 0.0001$), whereas sodium pyruvate did not significantly protect against cytotoxicity. A full description of Tukey's multiple comparisons test and all the IC_{50} values and ranges are shown in the Table 7.

Titration of NAC was performed to confirm the optimum working concentrations. Two-way ANOVA demonstrated that there was no significant difference between 2 mM, 4 mM and 8 mM of NAC, showing that increases or decreases in NAC concentration of around 2-8 mM does not change the protective effects (Figure 34).

Table 7: IC₅₀ Values and ranges of, U-251 MG single and multiple CAP treatment with, without NAC in with and without pyruvate media. (S.CAP=Single CAP, M.CAP=Multiple CAP, +=with, - =without)

CAP treatment - Incubation	Media composition	IC ₅₀	IC ₅₀ Range	Hillslope	Figure
S. CAP – 24 h	+ NAC, + pyruvate	1053 s	841.2 - 1317	0.1047	32A
	+ NAC, - pyruvate	522.6 s	505.7 – 540.1	0.02177	32A
	- NAC, + pyruvate	386.3 s	375.9 – 397.1	0.01614	32A
	- NAC, - pyruvate	355.1 s	342.3 – 368.5	0.01674	32A
S. CAP – 48 h	+ NAC, + pyruvate	1594 s	1275 – 1993	0.05906	32B
	+ NAC, - pyruvate	596.9 s	581.5 – 612.7	0.01666	32B
	- NAC, + pyruvate	460.7 s	449.4 – 472.4	0.01501	32B
	- NAC, - pyruvate	429.8 s	422.7 – 437.1	0.01121	32B
S. CAP – 96 h	+ NAC, + pyruvate	3788 s	1839 - 7804	0.1194	32C
	+ NAC, - pyruvate	877.9 s	842.5 - 914.7	0.02204	32C
	- NAC, + pyruvate	769.3 s	742.5 -797.0	0.01805	32C
	- NAC, - pyruvate	490.4 s	475.2 - 506.1	0.03920	32C
M. CAP – 24 h	+ NAC, + pyruvate	584.2 s	537.2 – 635.4	0.06834	32D
	+ NAC, - pyruvate	473.2 s	447.2- 500.6	0.03074	32D
	- NAC, + pyruvate	75.01 s	74.05 – 75.98	0.02804	32D
	- NAC, - pyruvate	74.82 s	74.10 – 75.54	0.01480	32D
M. CAP – 48 h	+ NAC, + pyruvate	723.0 s	661.4 – 790.3	0.06742	32E
	+ NAC, - pyruvate	630.8 s	580.5- 685.5	0.05223	32E
	- NAC, + pyruvate	100.1 s	97.85 – 102.5	0.03752	32E
	- NAC, - pyruvate	88.05 s	87.45 – 88.65	0.01206	32E
M. CAP - 96 h	+ NAC, + pyruvate	695.6 s	627.1 – 771.7	0.05648	32F
	+ NAC, - pyruvate	423.0 s	401.2 – 446.0	0.04369	32F
	- NAC, + pyruvate	76.24 s	74.25 – 78.28	0.03364	32F
	- NAC, - pyruvate	76.74 s	75.42 – 78.09	0.02120	32F

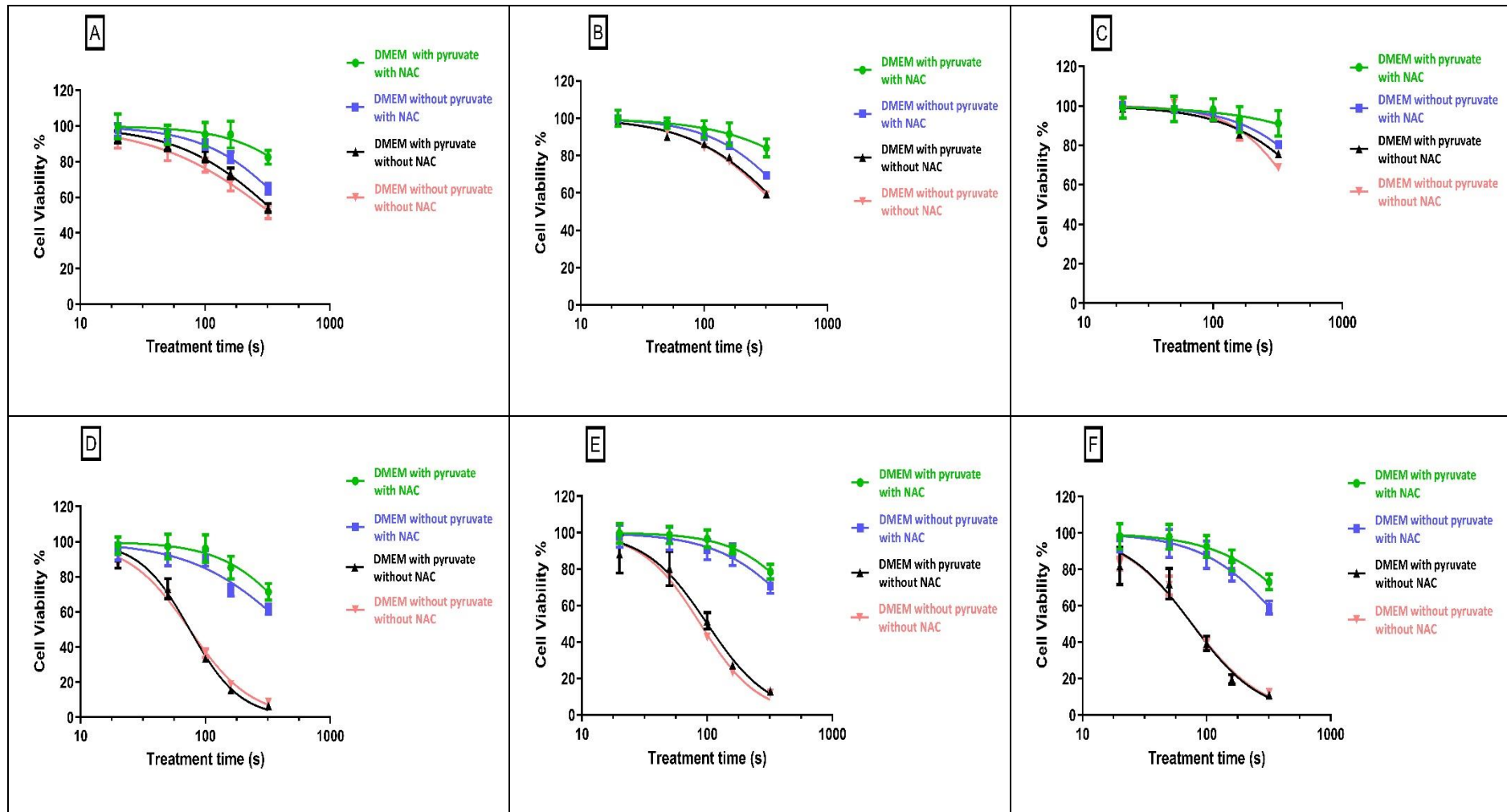


Figure 33: U-251 MG single and multiple CAP treatment with and without NAC in with and without pyruvate media. A) single CAP 24 h B) single CAP 48 h C) single CAP 96 h D) multiple CAP 24 h E) multiple CAP 48 h F) multiple CAP 96 h incubation.

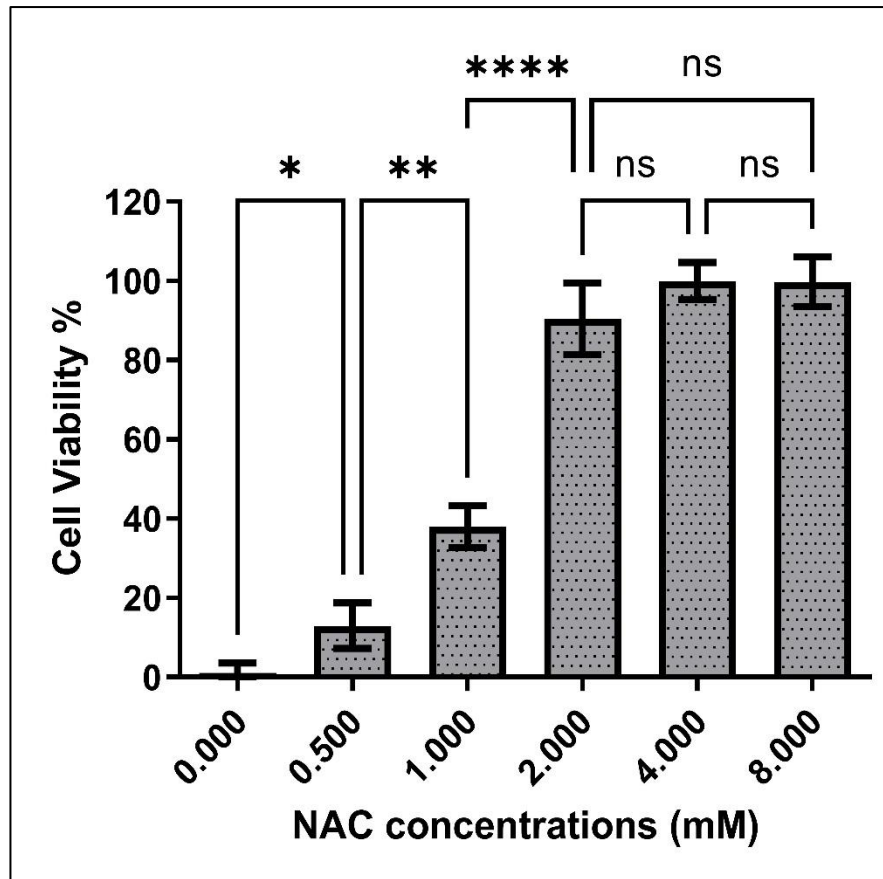


Figure 34: Titration of NAC using 0.5 mM, to 8 mM of NAC. (ns, not significant ($p > 0.05$); * $p < 0.05$; ** $p < 0.01$, **** $p < 0.0001$).

4.2.7 Catalase as a hydrogen peroxide scavenger

PI uptake was measured 24 h after a single CAP treatment (160 s, 320 s) and compared to PI uptake with and without catalase (Figure 35A). Catalase reduced the PI uptake slightly from 31% to 23% after 160 s CAP treatment, while it significantly reduced cytotoxicity from 51% to 34% after 320 s CAP treatment (Figure 35B). There was no significant difference between 160 s with and without catalase, while there was a significant difference between 320 s with and without catalase. According to this experiment catalase is able to slightly reverse the CAP induced cytotoxicity, proving that

hydrogen peroxide generated in pin to plate device contributes to the observed tumour sphere cytotoxicity.

Plasma induced apoptosis in tumour sphere was previously shown to depend on H_2O_2 , NO_2^- , and NO_3^- and it is demonstrated that these diffuse longer distances than short-lived species such as O_2^- , OH^\bullet , and ONOOH/ONOO^- [219, 356]. In our case, cell-permeable NAC is protective, yet catalase was unable to fully protect cells from CAP, indicating that reactive species other than hydrogen peroxide also play a role in the 3D tumour sphere model. Therefore, the response of U-251 MG tumour spheres to CAP is different to previous reports, and indeed to U-251 MG cells grown in 2D cultures where we found, using the same plasma system where CAP treatment induced predominantly H_2O_2 -dependent cytotoxicity [105]. Together, our data indicates a relative resistance of U-251 MG tumour spheres to hydrogen peroxide during CAP-induced cell death. Cell death may instead be mediated by other ROS species we have previously measured in the plasma plume or media, including OH, N_2 second positive system, N_2^+ first negative system, nitrate and ozone [336]. Alternatively, direct generation of intracellular ROS may account for some of the cytotoxicity observed.

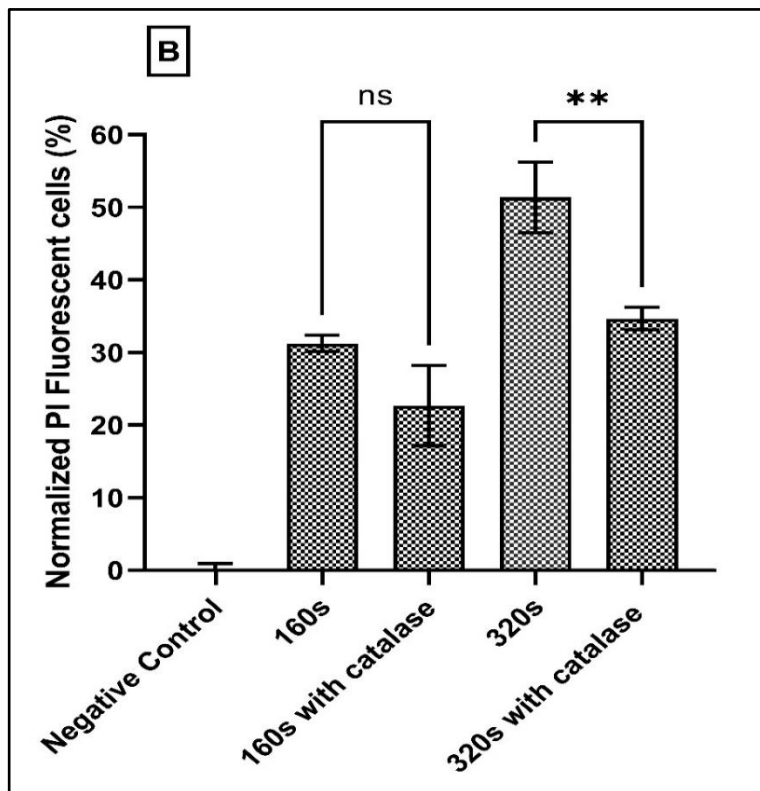
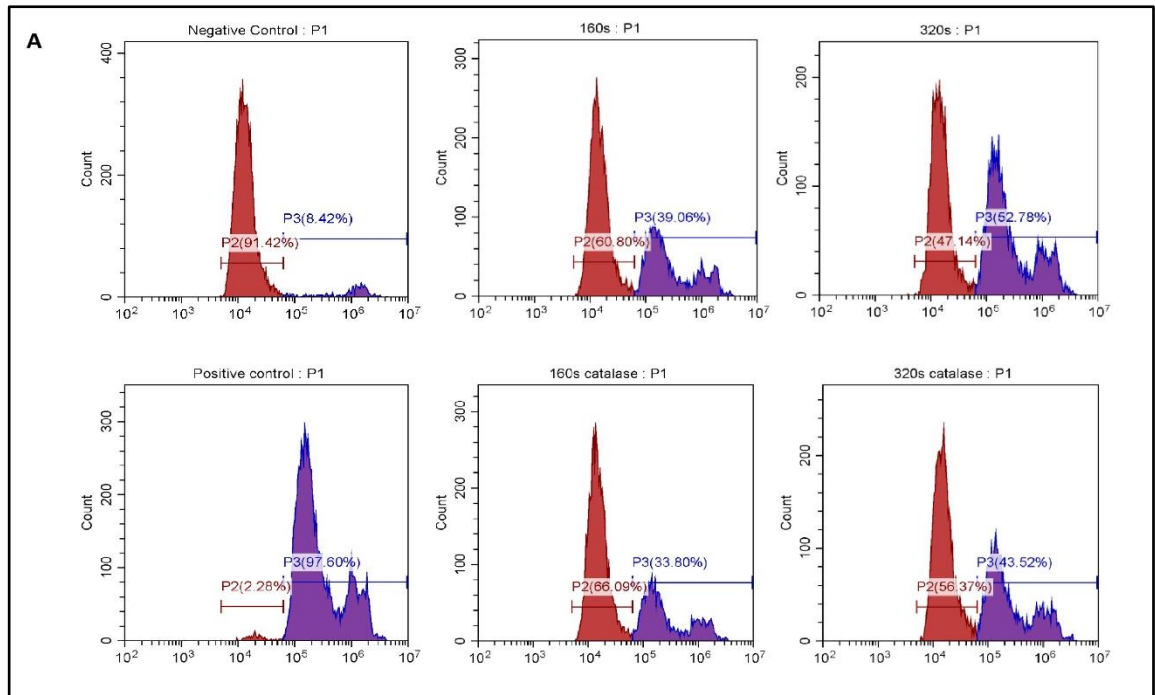


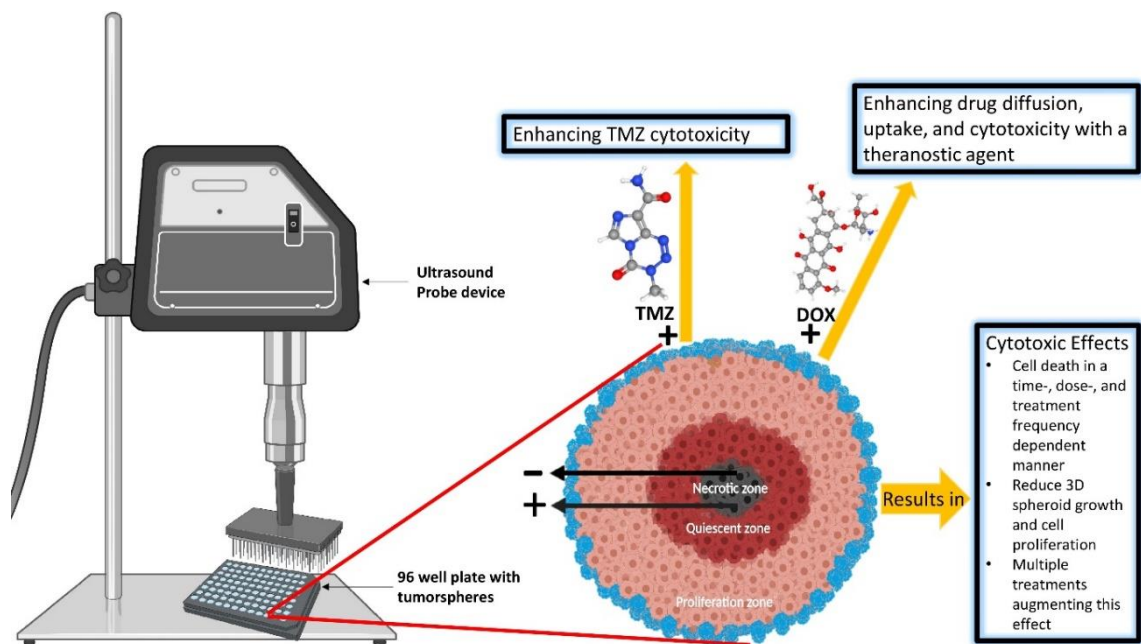
Figure 35: PI uptake in CAP treated U-251 MG tumour spheres in the presence and absence of catalase. PI uptake was measured by flow cytometry and used as an indicator of cell death. PI uptake was measured 24 h post treatment.

A) Histograms of negative control, 160 s CAP treated with and without catalase, 320 s CAP treated with and without catalase and positive control. B) Normalized PI uptake was then measured at 24 h post treatment, represented as a bar chart and analysed using One Way ANOVA with tukey's post-test (Appendix I). (ns, not significant ($p > 0.05$); ** $p < 0.01$).

4.3 Conclusion

CAP treatment can effectively induce 3D GBM tumour sphere cell death in a time, dose, treatment frequency and ROS dependent manner. CAP is also able to reduce 3D GBM spheroid growth, cell proliferation and induce damage to the TME. CAP generated from the pin to plate device induces cytotoxicity throughout the tumour sphere, likely via long-lived RONS (H_2O_2 , NO_2^- , and NO_3^-) and also other reactive species, with multiple treatments augmenting this cytotoxic effect. Our results indicate the importance of CAP-generated long and short-lived species for the growth inhibition and cell cytotoxicity of solid GBM tumours, as they are necessary to achieve a sustained reduction of 3D GBM spheroids *in vitro*. Furthermore, our results set important limitations on the likely approach needed when translating CAP into a clinical setting, with an approach that allows multiple treatments favourable over a single treatment.

CHAPTER 5 – ULTRASOUND MEDIATED DRUG DIFFUSION, UPTAKE, AND CYTOTOXICITY IN GLIOBLASTOMA 3D TUMOUR SPHERE MODEL



A part of this chapter is submitted for publication in the Biomaterials journal. (See Appendix II – Non peer-reviewed)

- **Wanigasekara J**, Mondala J, Cullen PJ, Tiwari B, Curtin JF. Ultrasound-mediated drug diffusion, uptake, and cytotoxicity in glioblastoma 3D tumour sphere model.

5 Ultrasound mediated drug diffusion, uptake, and cytotoxicity in GBM 3D tumour sphere model and synergistic effects of US and CAP

5.1 Rationale

GBM is the most prevalent, aggressive, fatal, highly vascularized, and malignant primary brain tumour in adults and despite multimodal treatments, glioma recurrence and death rates are significant as discussed before in chapter I [40, 257, 360, 361]. Conventional chemotherapeutic drugs such as DOX and TMZ may be used to overcome the challenge of eradicating metastasized cancer [361, 362]. Researchers are interested in potential non-invasive adjuvant treatments, including drug delivery technologies using as US, that might improve therapeutic efficacy [363], since these chemotherapeutics alone were insufficient to meet the end objective [40, 361, 362, 364]. In this study we aim to enhance the efficiency of GBM treatment by decreasing TMZ cytotoxicity resistance using US [361], and to use DOX as a reporter, to study further the sonoporation effects with a theranostic agent.

US has promise as a cancer therapy since it is feasible to target specific anatomical locations with fewer side effects and higher efficacy [362, 365]. US capable of creating a transient pores in plasma membrane and through these pores, molecules may access the cytosol [87, 363]. Under optimal circumstances, cells survive this process, retaining a significant number of intracellular molecules and seeming to regain normal function within hours [363, 366]. In some situations, cellular damage is too severe, and cells die via necrosis or programmed death [366]. Researchers used the sonoporation capability of US in conjunction with several chemotherapeutics [180, 367], short hairpin RNA [180, 368], antibodies [180, 369], genes [180], and viruses [180, 370] delivery. Due to

beneficial biological interactions (explained in chapter I), US has developed a rising interest in the subject of drug delivery in recent decades [28, 192, 362, 363, 366, 371-373].

3D tumour spheroids provides more accurate models to explore the association between TME, tumour reoccurrence, and drug resistance [257]. Hence, in the present study, we used 3D tumour spheroid models to better model and study the effects of US on human GBM and human epidermoid carcinoma. Typically, drug combination assessments using US for the treatment of GBM are performed in 2D cell cultures. In this work, for the first time, the therapeutic impact of the US 96-probe device and the synergistic potential of a specific drug combination on diffusion through a tumour, uptake by cells in a tumour sphere, and ultimately cytotoxicity comparisons in 3D GBM spheroids with 2D cultures were examined.

5.2 Results and discussion

5.2.1 US probe presents cytotoxicity towards GBM and epidermoid carcinoma cells in a time / dose-dependent manner.

Tumour development, metastasis, angiogenesis, cytotoxicity resistance, and immune cell modulation are all influenced by the TME [106, 219, 257]. Cells in 3D cell culture have physiological cell-cell and cell-ECM component interactions that allow cells to grow *in vitro* in a TME resembling *in vivo* GBM conditions [106, 220, 257]. The low attachment plate method was used in this study for the *in vitro* generation of U-251 MG and A431 tumour spheroids and we were able to create uniform tumour spheres that closely mimic the natural *in vivo* environment, shape, and cellular response [220, 268]. We used this diffusion-limited 3D cell culture model to explore the diffusion of cytotoxic reactive

species and chemotherapeutics throughout the tumour sphere, rate of cell death, and effects of single and multiple US treatments on the cell – cell and cell – ECM interactions [106]. Most of the research on the effects of US on cancer cells have been investigated by using 2D monolayer cell cultures [87, 363] and a growing number of animal models [367, 369]. We believe that this is the first time that the US 96 probe approach has been reported for drug diffusion through a tumour sphere, uptake by cells in a tumour sphere, and ultimately induced cytotoxicity in 3D tumour spheroids compared to 2D monolayer cells.

Firstly, in this research, we compared the effects of the US probe on U-251 MG human GBM and A431 human epidermoid carcinoma (2D and 3D cells) in DMEM high glucose with 10% FBS medium after 24 h of incubation. An IC_{50} of 162.9 min (129.5 ± 205.0 min), 115.2 min (90.19 ± 147.3 min) and 22.78 min (22.19 ± 23.39 min) were found for U-251 MG 2D cells, while an IC_{50} of 26.48 min (25.35 ± 27.66 min), 21.80 min (20.95 ± 22.69 min) and 12.04 min (11.82 ± 12.27 min) were found for U-251 MG 3D tumour spheres during single, double and triple US treatments respectively (Figure 36A).

During studies of A431 human epidermoid carcinoma, an IC_{50} of 46.0 min (42.46 ± 49.83 min), 38.05 min (35.07 ± 41.29 min), and 17.05 min (16.77 ± 17.33 min) were found for A431 2D cells while an IC_{50} of 17.14 min (16.87 ± 17.43 min), 11.40 min (11.20 ± 11.60 min), and 9.239 min (9.018 ± 9.466 min) were found for A431 3D tumour spheres during single, double, and triple US treatments, respectively (Figure 36B). Two-way ANOVA shows that there is a significant difference in U-251 MG and A431 (2D and 3D) cell viability between the doses of US and different cell culture models ($p < 0.0001$). A full description of tukey's multiple comparisons test can be seen in the Appendix I.

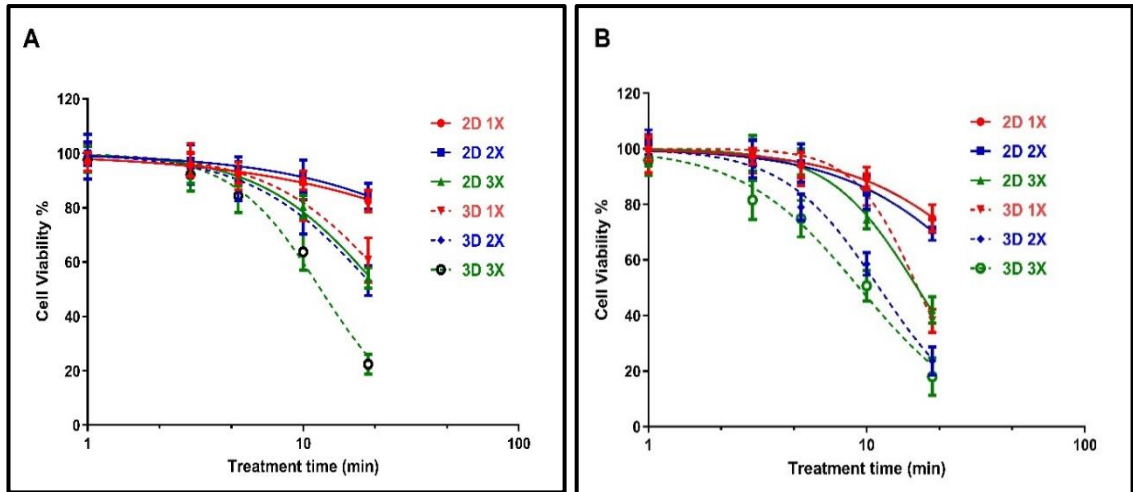


Figure 36: GBM cell line U-251 MG and epidermoid carcinoma cell line A431 US probe treatment. A) Comparison of 2D and 3D U-251 MG US treatments (single, double and triple) and post treatment incubation at 24 h B) Comparison of 2D and 3D A431 cell cytotoxicity induced by US (single, double and triple) and post treatment incubation at 24 h.

U-251 MG and A431 3D tumour spheres displayed lesser resistance to US therapies than 2D cell cultures throughout single, double and triple treatments. This US treatment sensitivity in 3D tumour spheres might be influenced by the differences in cellular organization, additional dimension, polarity, and geometry of 3D spheroids [222, 257]. US treatments were also able to effectively induce 2D cell and 3D tumour sphere cell death in a dose and treatment frequency dependent manner in both U-251 MG and A431. However, U-251 MG cells showed a higher treatment resistance compared to the A431 cell lines.

Subsequently, we determine the cytotoxic effects of a single and multiple US treatments on GBM tumour spheres with different incubation times. An IC_{50} of 75.22 min (58.16 ± 97.29 min), and 26.41 min (25.55 ± 27.31 min) were found for U-251 MG tumour spheres during single and fivefold US treatments, respectively, with 8 h post treatment incubation

(Figure 37A). An IC_{50} of 24.87 min (24.35 ± 25.39 min), 9.18 min (9.08 ± 9.29 min), (Figure 37B) and 30.95 min (29.55 ± 32.42 min), 7.91 min (7.78 ± 8.04 min), (Figure 37C) and 57.91 min (44.60 ± 75.20 min), 8.46 min (8.33 ± 8.60 min) (Figure 37D) were found for U-251 MG tumour spheres during single and fivefold US treatments with 24 h, 48 h and 72 h post treatment incubations, respectively. Finally, an IC_{50} of 42.73 min (38.81 ± 47.05 min), 7.96 min (7.85 ± 8.08 min), (Figure 37E) and 15.48 min (15.10 ± 15.87 min), 6.00 min (5.88 ± 6.12 min) (Figure 37F) were found for U-251 MG tumour spheres during single and five-fold US treatments with 96 h and 120 h post treatment incubations, respectively. A full description of the IC_{50} values and ranges during 1X, 2X, 3X, 4X, and 5X US treatments are shown as a Table 8. A two-way ANOVA demonstrated that there is a significant difference in viability between the doses of single and multiple US, and different post treatment incubations ($p < 0.0001$). A full description of tukey's multiple comparison test is provided in the Appendix I.

Depending on the cytotoxicity results (Figure 37), the single US exposure did not induce full cytotoxicity in the tumour spheres, even at the highest US dose (20 min) at the longest incubation (120 h), and the cell viability was 42.56 % according to Figure 37F. Since the single US treatment was not enough to induce higher cytotoxicity and halt tumour regrowth, we hypothesised that the use of multiple (up to five consecutive daily) US treatments would result in more favourable outcomes. The hypothesis proved according to the data, the lowest cytotoxicity observed during single US treatment with 8 h post treatment incubations, while highest cytotoxicity observed during five consecutive daily US treatments with 120 h post treatment incubations.

This results confirmed that multiple US treatments significantly induced cytotoxicity in tumour spheres and it was able to fully / partially inverse tumour sphere regrowth ability in U-251 MG, respectively. These results have important implications for future animal

model and human trials where single US treatments may be insufficient to yield significant benefits. According to Paškevičiūtė et al., 2020, US has no impact on the viability of MDA-MB-231 triple-negative breast cancer cells or A549 non-small cell lung cancer cells [363]. Consistent with these findings, we did not observe any significant cytotoxicity effect at the single US treatment up to 2 min of US exposure. Our results demonstrate that US alone is capable of inducing cytotoxicity when cells / tumour spheres are exposed to prolonged durations of US, and that multiple treatments augment these effects. US-treated tumour spheres incubated for a longer time period (120 h) led to cell viability decrease and significantly more cell death compared with 8 h. When US exposure length and treatment frequency are increased, persistent pore formation in membranes, lysis, and ultimately cell death and tumour sphere damage result [87, 363].

The kinetic response to the US treatment over time was markedly different when compared to the CAP treatment [106]. In our previous study, we used U-251 MG tumour spheres and CAP treated to evaluate the cytotoxicity response, where significantly more cell death was evident in short-term post treatment incubations compared with long-term incubations [106]. Ultimately, based on the analysis, it is demonstrated that the US 96-probe device could induce tumour sphere cytotoxicity in a dose- and time-dependent manner.

Table 8: *IC₅₀ Values and ranges of, U-251 MG single and multiple US treatment with different incubations.*

US post treatment incubation	Treatment frequency	IC ₅₀ (min)	IC ₅₀ Range (min)	Hillslope	Figure
8 h	1X	75.22	58.16 to 97.29	0.1079	3A
	2X	47.25	40.76 to 54.78	0.1173	3A
	3X	33.55	30.93 to 36.39	0.05671	3A
	4X	27.91	26.98 to 28.86	0.03511	3A
	5X	26.41	25.55 to 27.31	0.07038	3A
24 h	1X	24.87	24.35 to 25.39	0.02533	3B
	2X	20.35	19.66 to 21.06	0.03761	3B
	3X	11.91	11.77 to 12.05	0.01649	3B
	4X	10.39	10.23 to 10.56	0.02537	3B
	5X	9.186	9.080 to 9.294	0.01730	3B
48 h	1X	30.95	29.55 to 32.42	0.02445	3C
	2X	28.93	27.28 to 30.68	0.02901	3C
	3X	16.36	15.98 to 16.74	0.01490	3C
	4X	12.11	11.88 to 12.34	0.01912	3C
	5X	7.907	7.776 to 8.041	0.02260	3C
72 h	1X	57.91	44.60 to 75.20	0.09236	3D
	2X	39.33	36.27 to 42.65	0.02985	3D
	3X	26.21	24.95 to 27.53	0.02611	3D
	4X	17.15	16.70 to 17.62	0.02527	3D
	5X	8.468	8.333 to 8.605	0.02142	3D
96 h	1X	42.73	38.81 to 47.05	0.05389	3E
	2X	39.30	35.70 to 43.27	0.04173	3E
	3X	17.54	17.03 to 18.07	0.01626	3E
	4X	12.52	12.27 to 12.77	0.02337	3E
	5X	7.969	7.853 to 8.086	0.02794	3E
120 h	1X	15.48	15.10 to 15.87	0.02266	3F
	2X	16.90	16.46 to 17.34	0.03330	3F
	3X	10.12	9.873 to 10.37	0.03132	3F
	4X	9.154	8.969 to 9.342	0.02958	3F
	5X	6.002	5.883 to 6.124	0.03623	3F

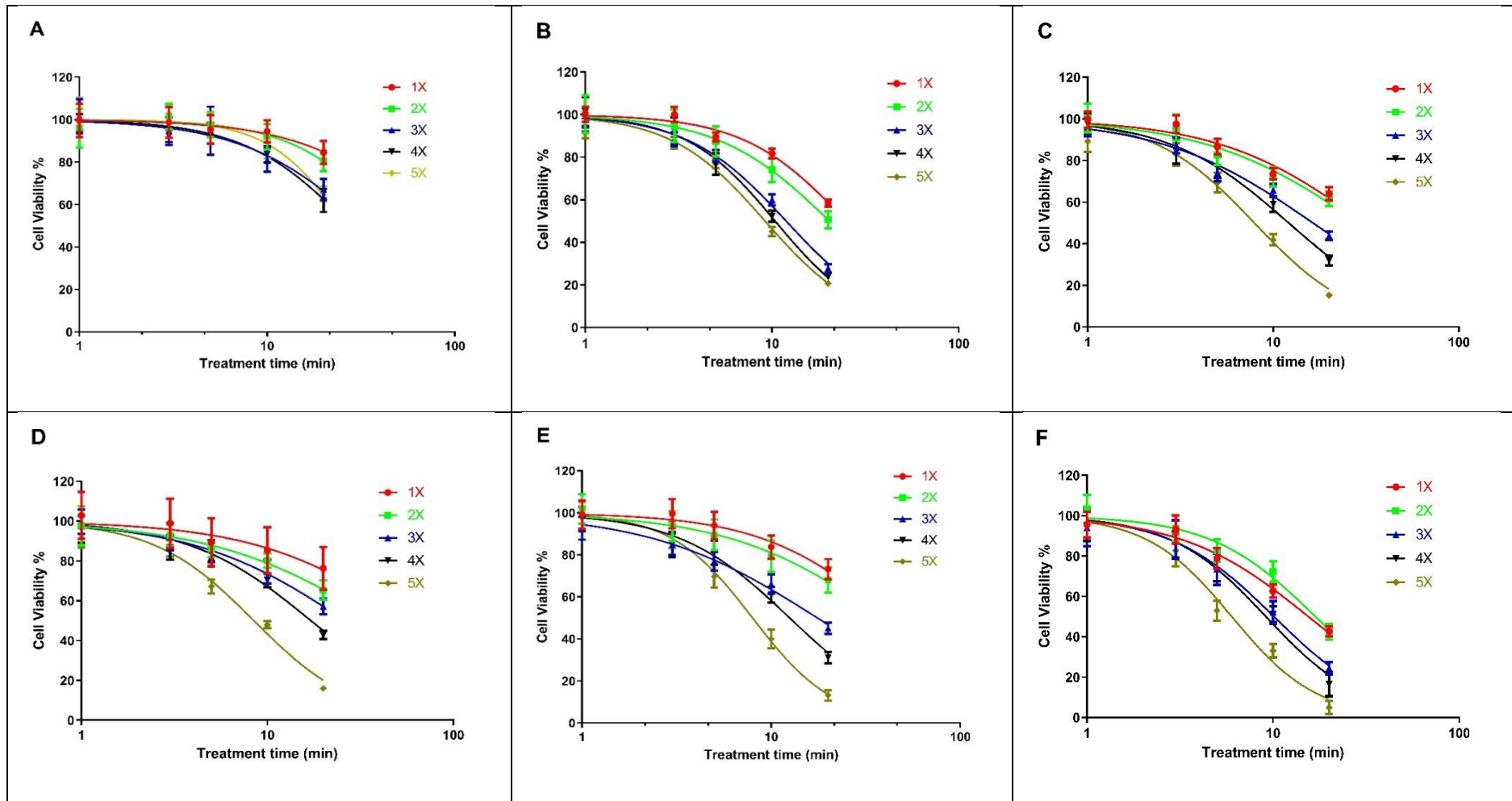
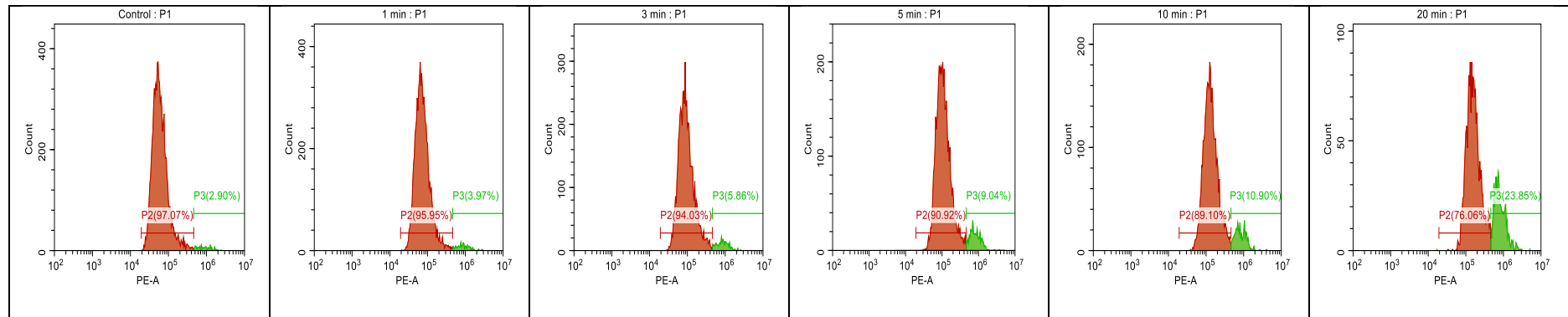
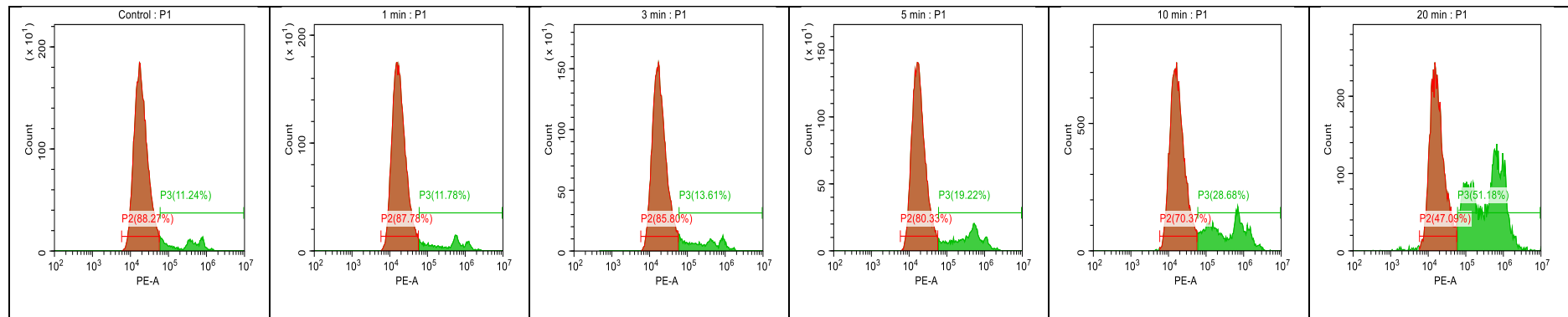
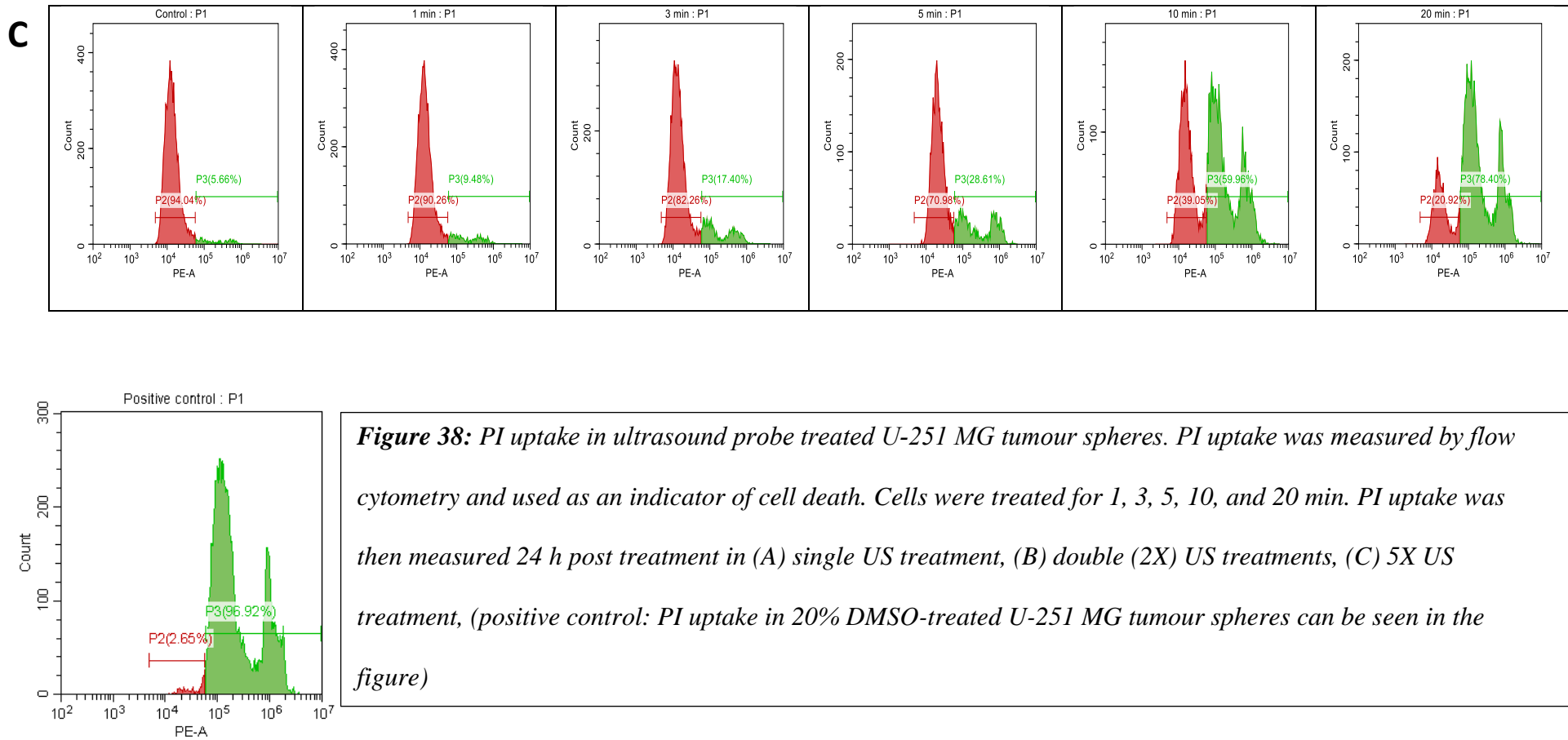


Figure 37: U-251 MG tumour sphere single and multiple US treatments with different incubations. (A) 8 h, (B) 24 h, (C) 48 h, (D) 72 h, (E) 96 h and (F) 120 h post treatment incubations.

A**B**



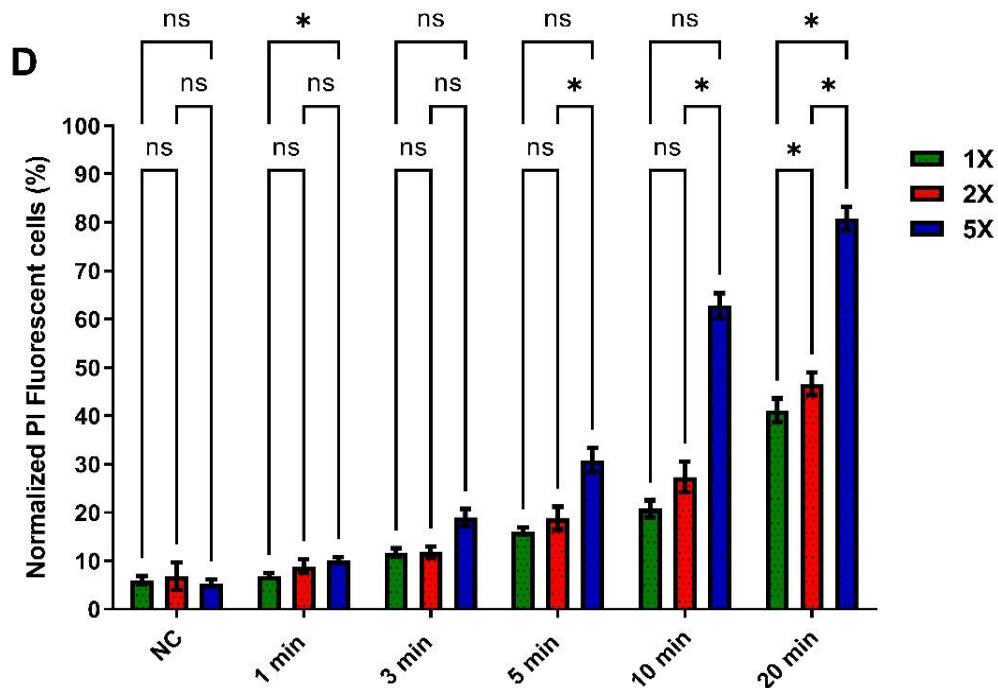


Figure 38: PI uptake in ultrasound probe treated U-251 MG tumour spheres. PI uptake was measured by flow cytometry and used as an indicator of cell death. Cells were treated for 1, 3, 5, 10, and 20 min. (D) normalized PI uptake was then measured at 24 h post single and multiple treatments and represented as a bar chart. The panel A-C are representative of 3 replicates. All the data points were statistically significant except control and 1 min treatment times. ns, not significant, $*p \leq 0.05$; $****p \leq 0.0001$

5.2.2 Effect of US treatment on tumour sphere cell membrane damage

PI was used to validate the US 96-probe induced cell death and cytotoxicity in U-251 MG tumour spheres. PI is a membrane-impermeable, fluorescent, nucleic acid intercalating agent that allows identification of dead cells with compromised plasma membranes in a population of tumour spheres. PI uptake was measured 24 h post single (Figure 38A), double (Figure 38B), and five consecutive daily (Figure 38C) US treatments. The

percentage of cells permeable to PI increased to almost 40%, 45% and 80%, respectively, following single, double, and five multiple US treatments for 20 min, as shown in Figure 38D. This also proves that US treatment can damage the tumour sphere's cell membrane and induce cytotoxicity. This validates the alamarBlue cell viability assay data. Two-way ANOVA demonstrated that there was a significant difference in PI uptake between 5 and 10 min US doses for double and five multiple US treatments ($p < 0.0001$), also a significant difference was found in the 20 min for both single and multiple US treatments (Figure 38D). A full description of tukey's multiple comparisons test can be seen in the Appendix I. Validating our findings, researchers discovered that US inhibited spheroid growth, metabolic activity, disrupted spheroid integrity, and increased DNA double strand breaks, leading to damage in human prostate cancer (PC-3) and GBM (U-87 MG) cell lines [374].

5.2.3 Tumour spheres morphological changes induced by US probe

Changes in the tumour sphere morphology induced by US treatments were studied to get a better understanding of their mechanism of cell death. U-251 MG tumour sphere diameter was found to be significantly reduced after the first US treatment for both 10, and 20 min treatment times (Figure 39B). Representative tumour sphere images showing the morphological changes induced by 20 min of US treatment for U-251 MG as shown in Figure 39A. Multiple US treatments induced significant, cumulative cytotoxicity. This was manifested by spheroid rupture, shrinkage, and markedly reduced tumour regrowth ability, which was achieved with a longer overall US treatment time. It is therefore likely that multiple US treatments over a relatively longer period of time would be necessary for clinical applications. Interestingly, tumour spheres reduced in size after the second US treatment and gradually broke apart on consecutive treatments. The U-251 MG

tumour spheres had no significant morphological change after the first US treatment and 24 h of incubation (Figure 39A-II), when compared to tumour sphere before treatment (Figure 39A-I). Then tumour spheres swelled, ruptured significantly after the second (Figure 39A-III) and third (Figure 39A-IV) treatments, and disintegrated after the fourth (Figure 39A-V) and fifth (Figure 39A-VI) treatments.

Overall, the outcome was identical, with enhanced cytotoxicity and an inability to reform tumour spheres after multiple US treatments. It is possible that multiple US treatments can weaken cell–cell and cell–ECM interactions, and due to this, the volume of the densely arranged tumour sphere started to decrease, resulting in a decreased tumour sphere diameter. A two way ANOVA demonstrated that there was a significant difference in the tumour sphere diameter during each US treatment time ($p < 0.0001$). A full description of tukey's multiple comparison test is available in the Appendix I.

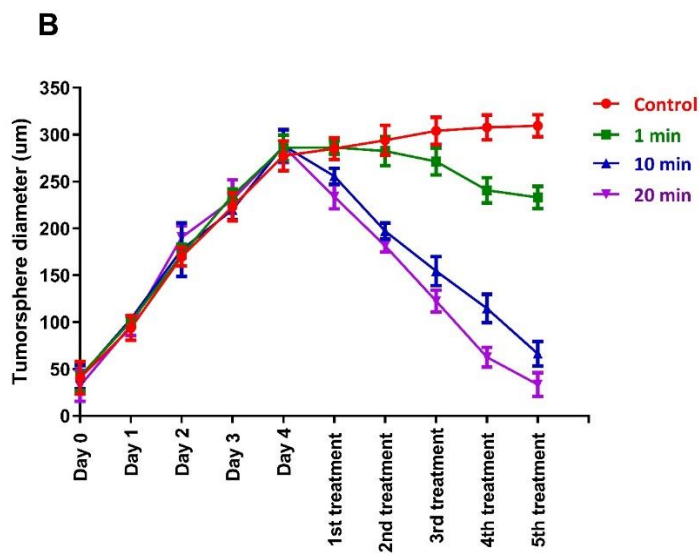
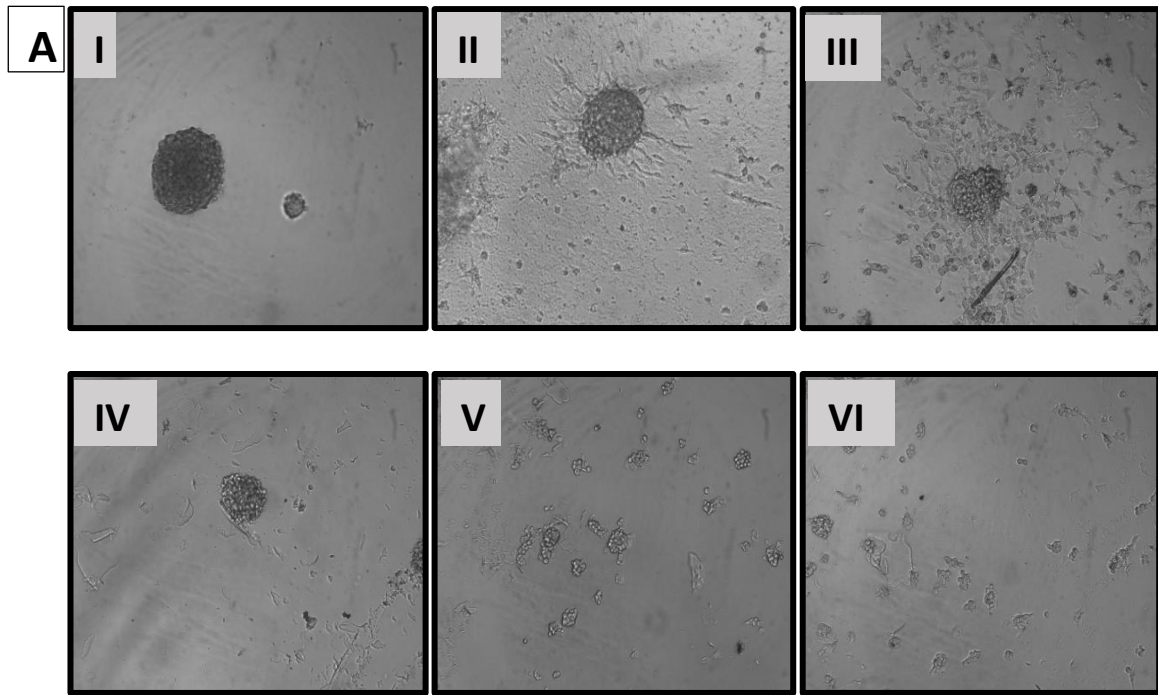
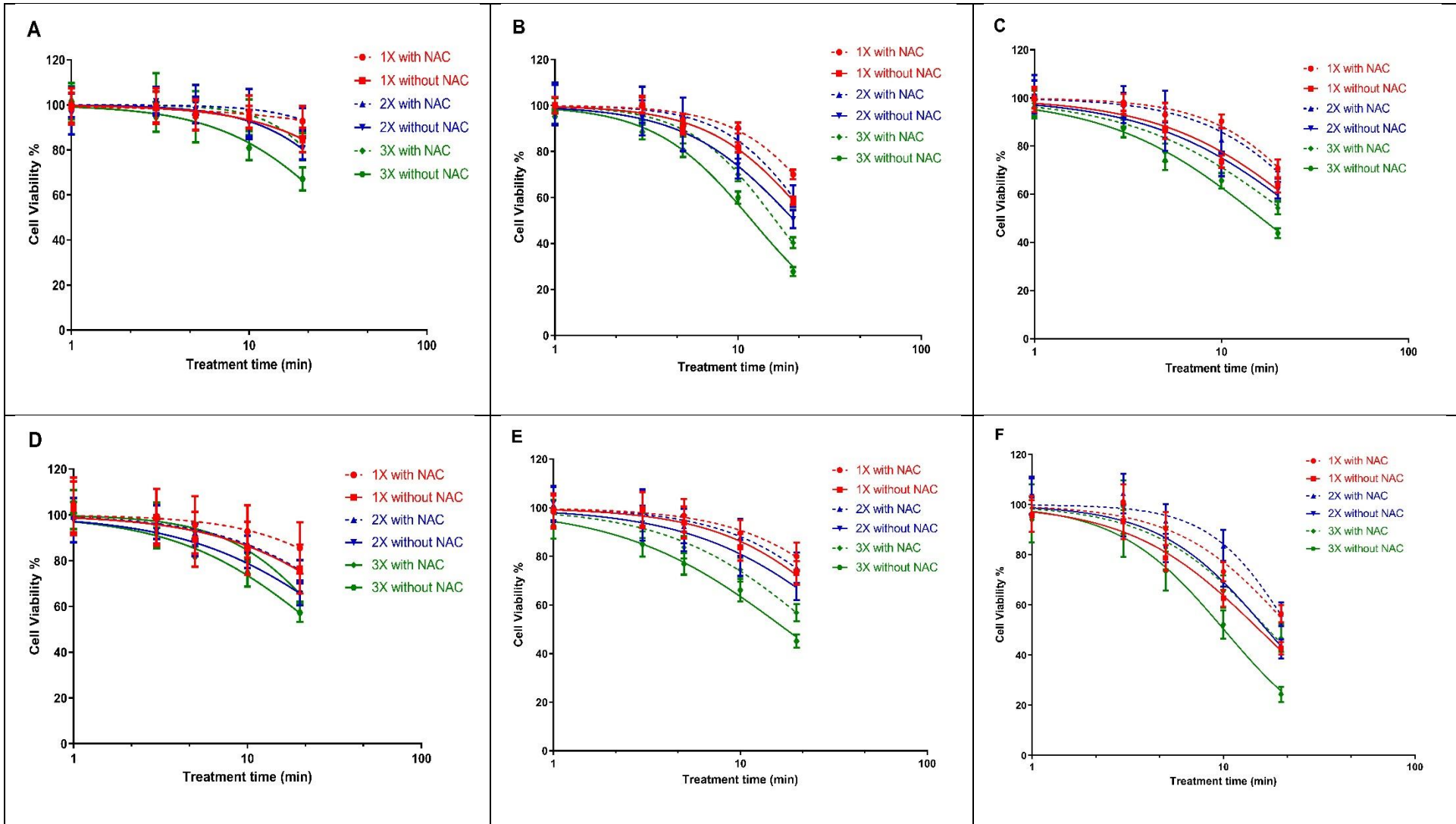


Figure 39: U-251 MG tumour sphere morphology and size (diameter) variation analysis followed by US treatment. A) U-251 MG tumour sphere morphological changes with 20 min US treatment (I-before US treatment, II – 24 h after 1st treatment, III – 24 h after 2nd treatment, IV – 24 h after 3rd treatment, V – 24 h after 4th treatment, VI – 24 h after 5th treatment) B) U-251 MG tumour sphere size (diameter) followed by different US treatments.

5.2.4 Ultrasound presents RONS-dependent cytotoxicity

The ROS-induced cytotoxic effect of the US 96-probe system was evaluated by using different treatment time points (0, 1, 3, 5, 10, and 20 min) with NAC employed as a ROS scavenger. The highest US treatment resistance was evident in the tumour spheres treated in the high glucose DMEM with NAC. While, the highest cytotoxicity was shown in tumour spheres treated in high glucose DMEM without NAC (Figure 40 A-F). This confirms that the cytotoxicity induced by the US 96 probe system is also dependent on RONS. NAC significantly protected the target tumour spheres from US-induced cytotoxicity at each applied dose, post treatment incubation period, and single / multiple treatments ($p < 0.0001$). All the IC_{50} values and ranges are shown in the table 9. A full description of tukey's multiple comparisons test shown in the Appendix I. Titration of NAC was performed to confirm the optimum working concentrations. Two-way ANOVA demonstrated that there was no significant difference between 2, 4, and 8 mM of NAC, showing that increases or decreases in NAC concentration of around 4–8 mM do not change the protective effects (Figure 40G).



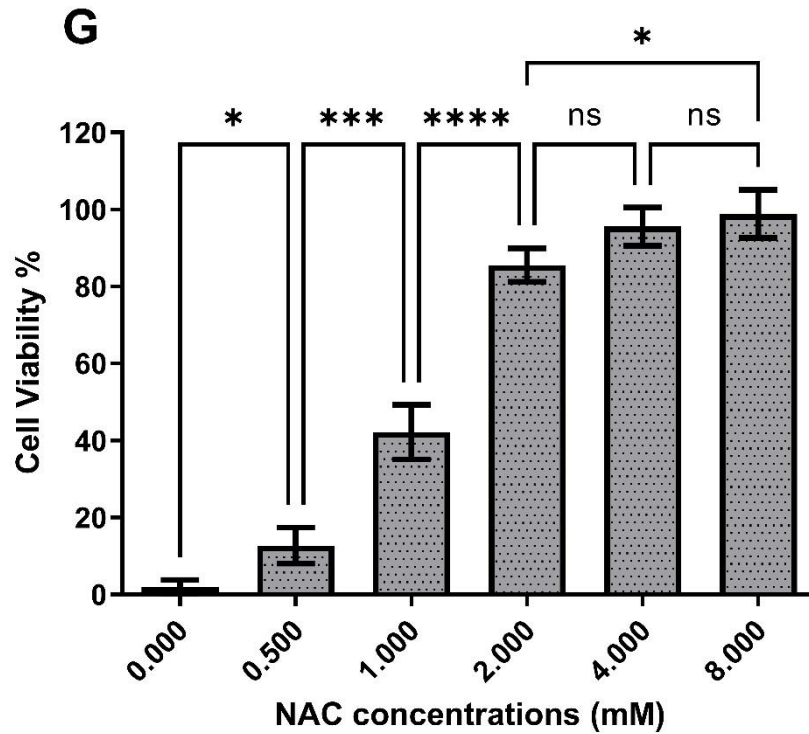


Figure 40: U-251MG single, double and triple US treatment with and without NAC. A) 8 h B) 24 h C) 48 h D) 72 h E) 96 h F) 120 h post-treatment incubation G) titration of NAC. (ns, not significant ($p > 0.05$); * $p < 0.05$; *** $p < 0.001$; **** $p < 0.0001$).

Table 9: IC₅₀ values and ranges of, U-251 MG single and multiple US treatment with different incubations with and without NAC:

US post treatment incubation	US treatment frequency and media composition	IC ₅₀ (min)	IC ₅₀ Range (min)	Hillslope	Figure
8 h	1X with NAC	639.8	153.2 to 2672	0.1396	5A
	1X without NAC	75.22	58.16 to 97.29	0.1079	5A
	2X with NAC	78.75	37.05 to 167.4	0.5073	5A
	2X without NAC	47.25	40.76 to 54.78	0.1173	5A
	3X with NAC	37.84	32.77 to 43.69	0.2353	5A
	3X without NAC	33.55	30.93 to 36.39	0.05671	5A
24 h	1X with NAC	32.33	31.29 to 33.40	0.04158	5B
	1X without NAC	24.87	24.35 to 25.39	0.02533	5B

	2X with NAC	24.89	23.90 to 25.93	0.07036	5B
	2X without NAC	20.35	19.66 to 21.06	0.03761	5B
	3X with NAC	16.04	15.89 to 16.20	0.01765	5B
	3X without NAC	11.91	11.77 to 12.05	0.01649	5B
48 h	1X with NAC	35.40	33.64 to 37.24	0.04826	5C
	1X without NAC	30.95	29.55 to 32.42	0.02445	5C
	2X with NAC	35.56	33.03 to 38.28	0.05722	5C
	2X without NAC	28.93	27.28 to 30.68	0.02901	5C
	3X with NAC	24.30	23.33 to 25.30	0.02074	5C
	3X without NAC	16.36	15.98 to 16.74	0.01490	5C
72 h	1X with NAC	79.86	48.52 to 131.4	0.1952	5D
	1X without NAC	57.91	44.60 to 75.20	0.09236	5D
	2X with NAC	56.79	50.09 to 64.39	0.04775	5D
	2X without NAC	39.33	36.27 to 42.65	0.02985	5D
	3X with NAC	30.46	29.03 to 31.95	0.04703	5D
	3X without NAC	26.21	24.95 to 27.53	0.02611	5D
96 h	1X with NAC	56.89	48.52 to 66.72	0.07956	5E
	1X without NAC	42.73	38.81 to 47.05	0.05389	5E
	2X with NAC	46.66	41.02 to 53.08	0.07191	5E
	2X without NAC	39.30	35.70 to 43.27	0.04173	5E
	3X with NAC	25.61	24.67 to 26.59	0.02192	5E
	3X without NAC	17.54	17.03 to 18.07	0.01626	5E
120 h	1X with NAC	22.87	22.01 to 23.76	0.04092	5F
	1X without NAC	15.48	15.10 to 15.87	0.02266	5F
	2X with NAC	22.47	21.75 to 23.20	0.07362	5F
	2X without NAC	16.90	16.46 to 17.34	0.03330	5F
	3X with NAC	17.24	16.58 to 17.94	0.04320	5F
	3X without NAC	10.12	9.873 to 10.37	0.03132	5F

5.2.5 Effect of US on TMZ delivery in human GBM and epidermoid carcinoma cell models

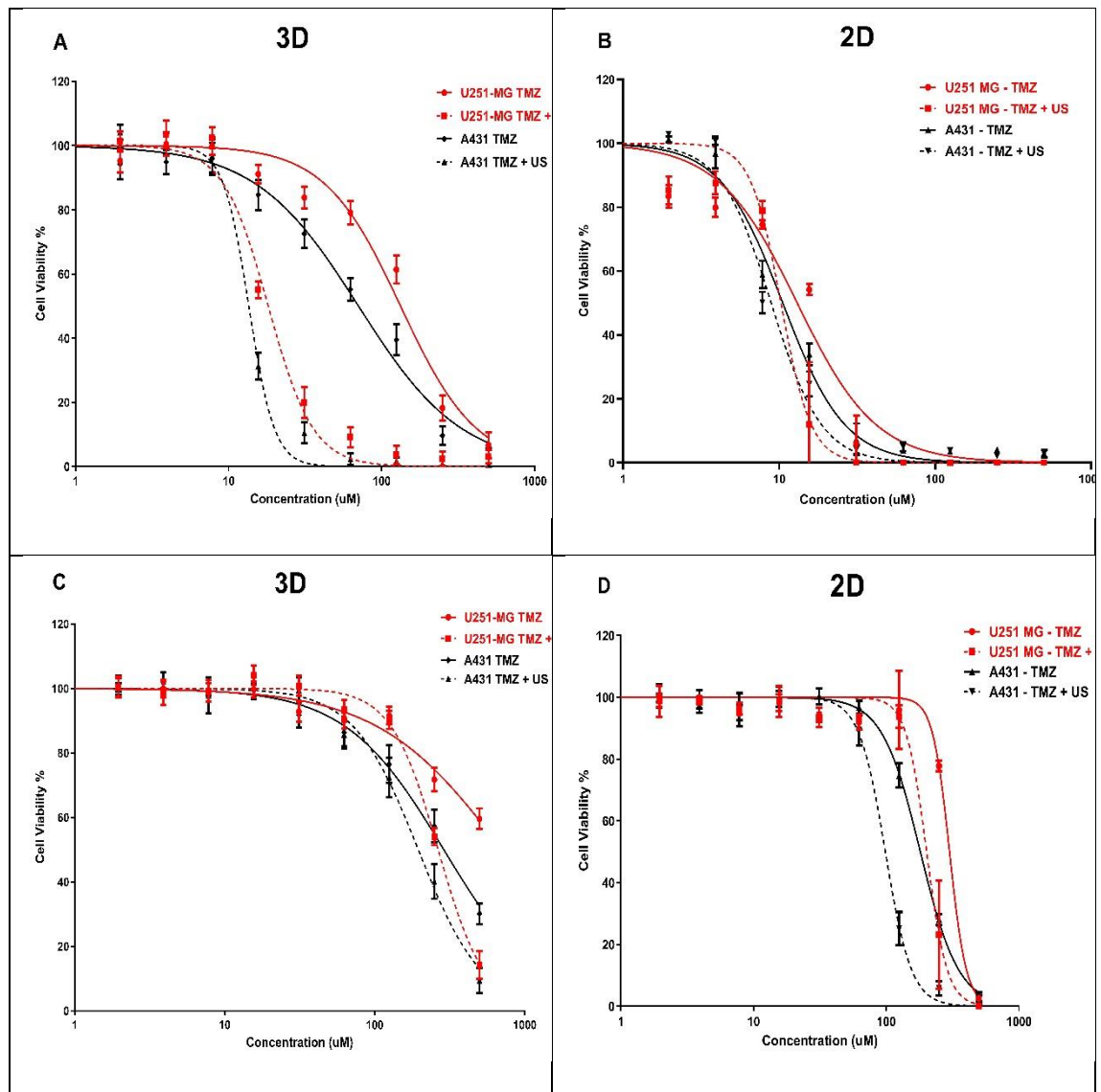


Figure 41: TMZ cytotoxicity analysis with and without US (3 min) combination using U-251 MG and A431 2D cells and 3D tumour spheroids. A) TMZ cytotoxicity in 3D cell cultures after 144 h incubation B) TMZ cytotoxicity in 2D cell cultures after 144 h incubation C) TMZ cytotoxicity in 3D cell cultures after 48 h incubation D) TMZ cytotoxicity in 2D cell cultures after 48 h incubation.

Initially, we explored the effects of the 3 min US exposure on TMZ delivery into U-251 MG human GBM and A431 human epidermoid carcinoma after 144 h of post-treatment incubation time. An IC_{50} of 133.0 μ M ($124.8 \pm 141.8 \mu$ M) and 18.16 μ M ($17.34 \pm 19.01 \mu$ M) were found for U-251 MG 3D spheroids during TMZ treatment without and with US, respectively (Figure 41A), while an IC_{50} of 70.63 μ M ($65.98 \pm 75.60 \mu$ M) and 13.55 μ M ($13.14 \pm 13.98 \mu$ M) were found for A431 3D spheroids during TMZ treatment without and with 3 min US exposure respectively, after 144 h post treatment incubation (Figure 41A).

After investigating the synergistic effect of US and TMZ on 3D tumour spheres, we then looked at its effect in U-251 MG and A431 on 2D cells with 144 h post treatment incubations. An IC_{50} of 13.06 μ M ($10.85 \pm 15.52 \mu$ M) and 10.27 μ M ($9.086 \pm 11.66 \mu$ M) were found for U-251 MG 2D cells during TMZ treatment without and with US, respectively (Figure 41B), while an IC_{50} of 10.55 μ M ($9.728 \pm 11.45 \mu$ M) and 8.898 μ M ($8.121 \pm 9.780 \mu$ M) were found for A431 2D cells during TMZ treatment without and with 3 min US exposure respectively (Figure 41B).

Then we reduced the post treatment incubation time to 48 h to investigate the cytotoxic effects at shorter incubations (Figure 41C and 41D). An IC_{50} of 300.1 μ M ($272.1 \pm 331.1 \mu$ M) and 201.8 μ M ($185.4 \pm 219.7 \mu$ M) were found for U-251 MG 2D cells during TMZ treatment without and with US, respectively (Figure 41D), while an IC_{50} of 180.9 μ M ($172.8 \pm 189.3 \mu$ M) and 98.53 μ M ($93.59 \pm 103.7 \mu$ M) were found for A431 2D cells during TMZ treatment without and with US, respectively (Figure 41D). Interestingly, an IC_{50} of 707.6 μ M ($629.5 \pm 795.3 \mu$ M) and 264.9 μ M ($256.7 \pm 273.4 \mu$ M) were found for U-251 MG 3D spheroids during TMZ treatment without and with US, respectively (Figure 41C), while an IC_{50} of 288.7 μ M ($274.4 \pm 303.7 \mu$ M) and 195.2 μ M ($186.3 \pm$

204.5 μM) were found for A431 3D spheroids during TMZ treatment without and with 3 min US exposure, respectively after 48 h post treatment incubation (Figure 41C).

It is noteworthy that the sensitivity of TMZ was significantly enhanced after the US treatment in the U-251 MG and A431 on 3D tumour spheroids relative to 2D cells. When tumour spheroids were incubated with TMZ at the highest concentration (500 μM) for 48 h after US treatment, cell viability decreased approximately from 59.58% to 14.31% in U-251 MG; and from 30.15% to 9.37% in A431 tumour spheres (Figure 41C). This pattern of TMZ cytotoxicity intensified after 144 h of incubation. At doses of TMZ greater than 15 μM , where a four-fold increase in cytotoxicity can be observed in tumour spheres, while only around one-fold increase in cytotoxicity can be observed in 2D cells. When tumour spheroids are incubated with TMZ 62 μM for 144 h after US treatment, cell viability decreases approximately from 79.11% to 9.21% in U-251 MG and from 55.25% to 2.35% in A431 tumour spheres (Figure 41A).

It was also found that there was an increase in TMZ cytotoxicity in longer post-treatment incubations compared to shorter incubations. This evidence demonstrates the ability of US to increase cytotoxicity with TMZ. The intracellular redox status and the decrease and activation of antioxidant related signalling molecules determine TMZ resistance. Combining TMZ with US seems to minimise this TMZ resistance and may provide a solution to TMZ cytotoxicity and resistance [40, 375]. This results also demonstrates the important of adopting 3D cell culture models in pre-clinical research to get accurate outcome from toxicological assessments. Overall, our findings suggest that the combination of US and TMZ is a promising approach to enhance the efficacy of GBM and epidermoid carcinoma chemotherapy.

5.2.6 Effect of US on DOX delivery in human GBM and epidermoid carcinoma cell models

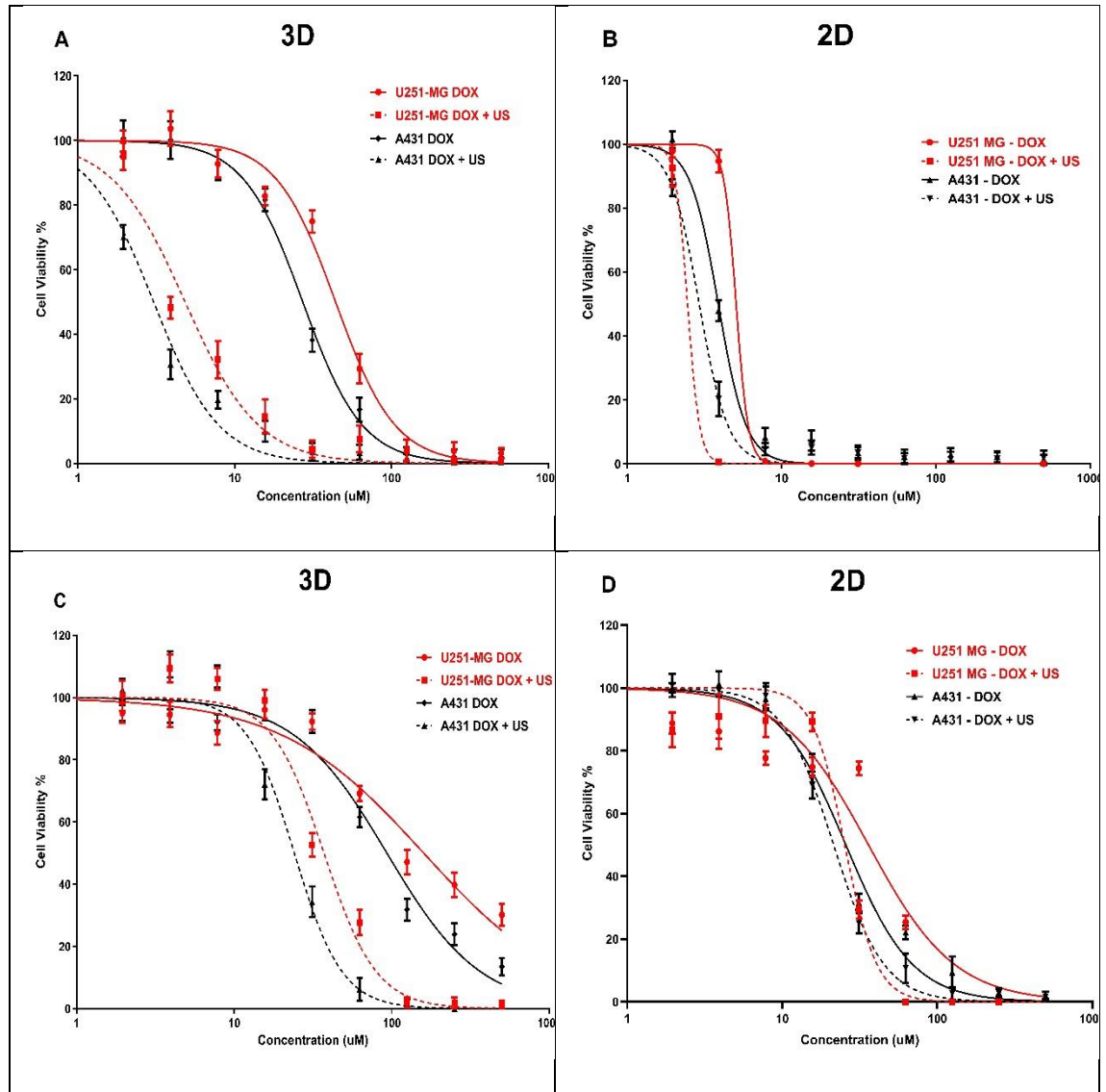


Figure 42: DOX cytotoxicity analysis with and without US (3 min) combination using U-251 MG and A431 2D cells and 3D tumour spheres. A) DOX cytotoxicity in U-251 MG and A431 3D cells with 144 h incubation B) DOX cytotoxicity in 2D cells with 144 h incubation C) DOX cytotoxicity in U-251 MG and A431 3D cells with 48 h incubation D) DOX cytotoxicity in 2D cells with 48 h incubation.

To elucidate the mechanism further, the theranostic chemotherapeutic agent DOX is used to correlate cytotoxicity with uptake into tumour cells and distribution throughout the tumour sphere. We explore the effects of the 3 min US exposure on DOX delivery into U-251 MG human GBM and A431 human epidermoid tumour spheres after 144 h of post-treatment incubation time. An IC_{50} of 44.00 μ M ($41.80 \pm 46.31 \mu$ M) and 4.835 μ M ($4.503 \pm 5.190 \mu$ M) were found for U-251 MG 3D spheroids during DOX treatment without and with US, respectively (Figure 42A), while an IC_{50} of 27.18 μ M ($26.10 \pm 28.31 \mu$ M) and 3.045 μ M ($2.874 \pm 3.227 \mu$ M) were found for A431 3D spheroids during DOX treatment without and with 3 min US exposure, respectively, after 144 h post treatment incubation (Figure 42A).

After investigating the synergistic effect of US and DOX on 3D tumour spheres, we then extended our study to compare the activity of U-251 MG and A431 in 2D cells with 144 h post treatment incubations. An IC_{50} of 5.072 μ M ($4.701 \pm 5.472 \mu$ M) and 2.454 μ M ($1.965 \pm 3.065 \mu$ M) were found for U-251 MG 2D cells during DOX treatment without and with US, respectively (Figure 42B), while an IC_{50} of 3.884 μ M ($3.721 \pm 4.055 \mu$ M) and 2.922 μ M ($2.786 \pm 3.065 \mu$ M) were found for A431 2D cells during DOX treatment without and with 3 min US exposure, respectively (Figure 42B).

Then we reduced the post treatment incubation time to 48 h to investigate the cytotoxic effects at shorter incubations (Figure 42C and 42D). An IC_{50} of 36.02 μ M ($27.89 \pm 45.30 \mu$ M) and 25.33 μ M ($22.83 \pm 27.96 \mu$ M) were found for U-251 MG 2D cells during DOX treatment without US and with US, respectively (Figure 42D), while an IC_{50} of 25.73 μ M ($23.45 \pm 28.31 \mu$ M) and 21.45 μ M ($20.06 \pm 22.94 \mu$ M) were found for A431 2D cells during TMZ treatment without US and with US, respectively (Figure 42D). An IC_{50} of 159.4 μ M ($145.0 \pm 175.2 \mu$ M) and 37.13 μ M ($35.03 \pm 39.35 \mu$ M) were found for U-251 MG 3D spheroids during DOX treatment without and with US, respectively (Figure 42C),

while an IC_{50} of $93.10 \mu\text{M}$ ($86.89 \pm 99.76 \mu\text{M}$) and $24.08 \mu\text{M}$ ($22.79 \pm 25.45 \mu\text{M}$) were found for A431 3D spheroids during DOX treatment without and with 3 min US exposure, respectively, after 48 h post treatment incubation (Figure 42C).

Increasing the incubation time is the most crucial way to differentiate between the effectiveness of DOX with and without US. In some studies, it was determined that US did not improve DOX (concentration $10 \mu\text{M}$) cytotoxicity in monolayer cultured cancer cells and 3D tumour spheroid models with up to a 2 min US exposure and shorter post-treatment incubations, such as 1 h and 2 h [363]. Similarly, in our work, we observed no significant cytotoxicity up to $10 \mu\text{M}$ DOX with or without US for U-251 MG and A431 cells / tumour spheroids after 48 h of post-treatment incubation (Figures 42C and 42D).

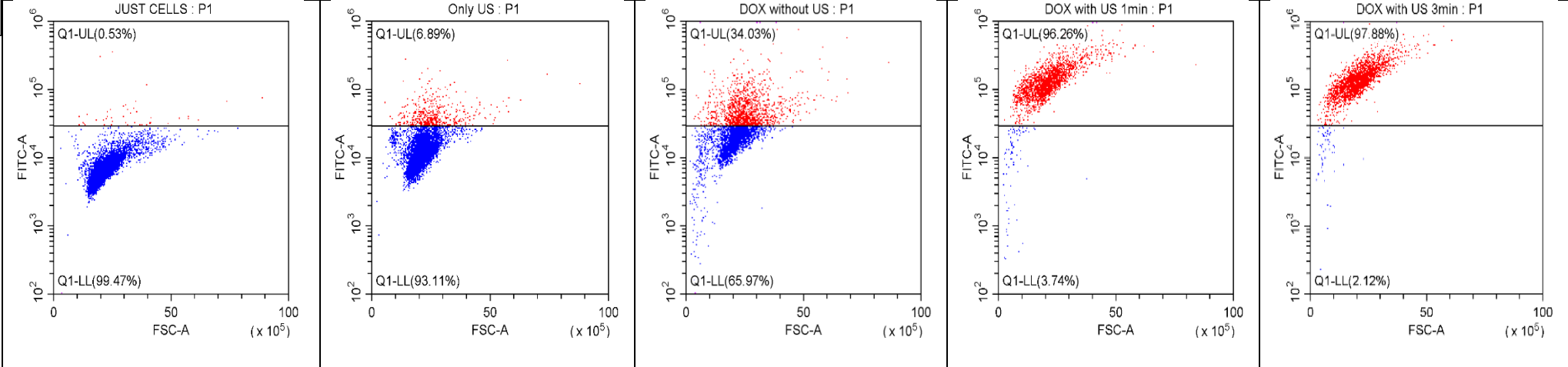
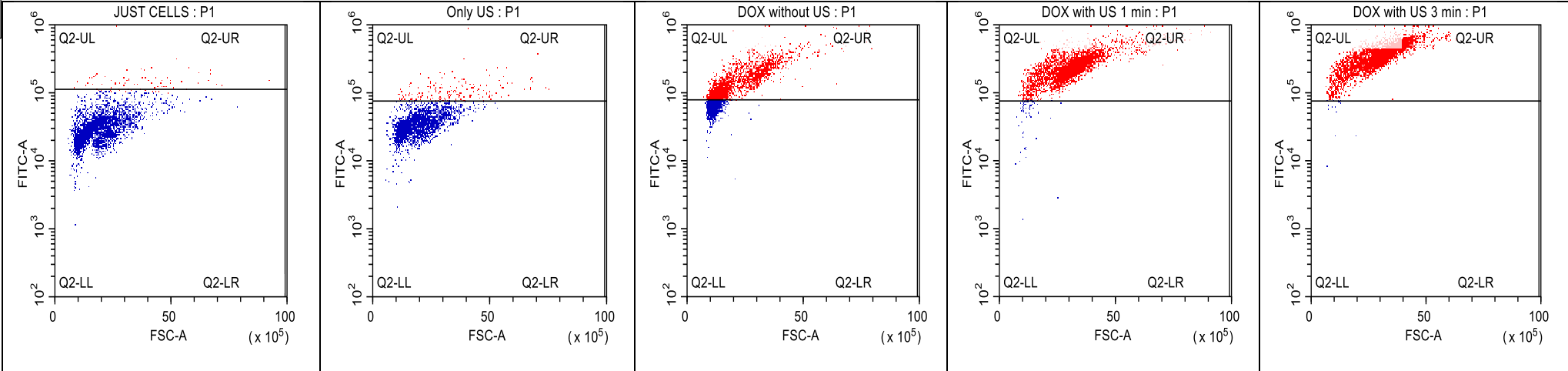
However, when the DOX concentration was increased above $10 \mu\text{M}$, cytotoxicity was enhanced, and the US was able to augment DOX toxicity. We were able to induce cytotoxicity even at a lower DOX concentration, once we incubated cells / tumour spheroids for a longer period of time (144 h). When tumour spheroids are incubated with DOX $10 \mu\text{M}$ for 144 h after US treatment, cell viability approximately decreased from 90 % to 20 % in U-251 MG and from 90% to 10% in A431 tumour spheres.

According to our study, DOX cytotoxicity rises marginally when combined with US treatment in U-251 MG GBM and A431 epidermoid cancer in 2D cells, while showing considerably increased DOX sensitivity in 3D tumour spheroids. When combined with US, the IC_{50} in 3D GBM spheroids was reduced by more than four-fold; however, the reduction in 2D cells was a little bit above one-fold during 48 h of post-treatment incubation. This same pattern of DOX cytotoxicity was intensified over a 144 h of incubation. When combined with US, the IC_{50} in 3D GBM spheroids was reduced by more than nine-fold; however, the reduction in 2D cells was only two-fold.

This study also suggests that US may enhance the cytotoxicity of DOX. In U-251 MG and A431 3D tumour spheroids, the sensitivity of DOX was considerably increased after US therapy. When tumour spheroids are incubated with DOX at higher concentration (500 μ M) for 48 h after US treatment, cell viability decreased approximately from 30.15% to 1.25% in U-251 MG, and from 13.51% to 2.39% in A431 tumour spheres. This same pattern of DOX cytotoxicity was observed over a 6 day incubation period. At doses of DOX greater than 125 μ M, U-251 MG cytotoxicity increased by more than twentyfold; while A431 cytotoxicity increased by more than ten-fold, when exposed to US. When tumour spheroids are incubated with DOX 500 μ M for 6 days after US treatment, cell viability approximately decreased from 30.15% to 1.25% in U-251 MG and from 13.51% to 1.13% in A431 tumour spheres.

DOX is one of the most widely used chemotherapeutic drugs used to treat a wide variety of neoplasms in humans [376]. It is a sequence selective DNA intercalating agent that targets topoisomerase II, resulting in DNA damage and the production of ROS, which are principally responsible for its cytotoxic effects [377]. DOX as a drug is cell cycle non-specific; however, a maximal impact has been recorded during the G₀/G₁ phase of the cell cycle, resulting in damage repair, cell cycle arrest, or apoptosis depending on the level of DNA damage [377, 378]. DOX has lower response rates, lower selectivity, and higher complication rates. Consequently, it is essential to optimise drug delivery to a specific cancer site while reducing the dosage for normal cells and tissues [377].

Overall, our results indicate that the combination of US and DOX is a potential combination therapy for enhancing the efficacy, cytotoxicity of DOX in the treatment of GBM and epidermoid cancer spheroids and also demonstrate the significance of 3D cell culture models over 2D cells in drug delivery and discovery research.

A**B**

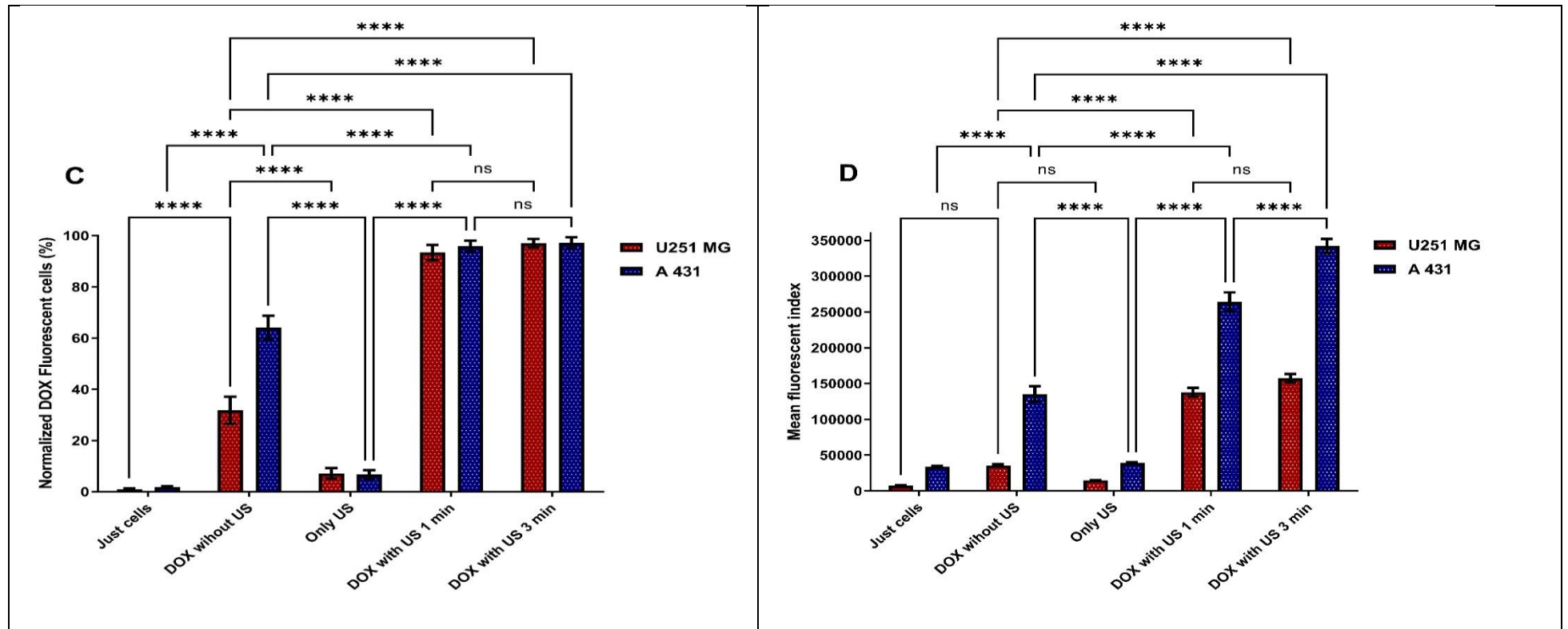


Figure 43: Ultrasound enhanced penetration of DOX.H fluorescence analysis using flow cytometry of U-251 MG and A431 tumour spheres. A) U-251 MG B) A431 C) The normalized % of DOX positive cells was then measured at 48 h post treatment incubation and represented as a bar chart. All the data points were statistically significant except DOX with US 1 min and 3 min treatment times. D) The mean fluorescence index was measured at 48 h post treatment incubation, used to plot the values on columns to identify the amount of DOX getting into tumour sphere. All the data points were statistically significant except U-251 MG DOX with US 1 min and 3 min treatment times. ns, not significant, **** $p \leq 0.0001$

DOX.H is a naturally fluorescent anthracycline antibiotic that has been isolated from *Streptomyces peucetius var. caesioides*. It is a hydroxylated derivative of daunorubicin, a water-soluble anticancer agent. To verify the US-induced sonoporation in U-251 MG tumour spheres, the intracellular fluorescence intensity of DOX.H was evaluated by flow cytometry. DOX uptake was measured with and without US after 48 h of incubation by using U-251 MG (Figure 43A) and A431 (Figure 43B) tumour spheres. Sonoporation is the development of pores in cell membranes produced by US [363]. According to estimates, the pore size may range from 1 nm to several micrometres [363]. Pore resealing occurs very fast and the duration ranges from a few to 180 s [363]. During this period, penetration of DOX into tumour spheres was observed. As seen in Figure 43A, the DOX uptake in U-251 MG tumour spheres rose to almost 96.26% and 97.88% following 1 min and 3 min US treatments, respectively, compared to DOX without US (34.03%). While in Figure 43B, it can be seen that, DOX uptake in A431 tumour spheres increased to almost 98.37% and 99.69% following 1 min and 3 min US treatments, respectively, compared to DOX without US (68.60%). The percentage of tumour sphere cells, that encounter DOX is shown in Figure 43C and we observed DOX increase with US due to the drug's migration through the tumour sphere. Drug diffusion in 3D model is enhanced by US (as indicated by % uptake).

Figure 43D depicts the average quantity of DOX entering the cells in a tumour sphere. The higher mean fluorescence index values with US treatments indicate that sonoporation has occurred in the cells. Ultimately, it demonstrates that the US is increasing both the percentage of cells encountering DOX and the amount of DOX going into each cell. This leads to improved cytotoxicity in the 3D culture model with US exposure, as we proved in the previous section (Figure 42). According to our findings, transient DOX

sonoporation augmented by ultrasonic therapy in 3D tumour spheres is a promising strategy for enhancing therapeutic efficacy and selective cytotoxicity in the future.

5.2.7 Cold atmospheric plasma and ultrasound presents synergistic cytotoxicity towards GBM and epidermoid carcinoma

In the initial stage of our research, we examined how combining CAP with various durations of US treatment (1, 3, 10, and 20 min) affected the U-251MG GBM 3D tumour spheres with 96 h of post treatment incubation period (Figure 44). We found that the highest cytotoxic effect occurred when 20 min of US treatment was combined with a 20 s CAP treatment (Figure 44A). This resulted in a reduction of cell viability to 62.75% and 19.14% during single and multiple treatments, respectively. We then increased the CAP treatment time to 100 s, while keeping the US treatment dose constant. This led to an increase in cytotoxicity, resulting in a decrease in cell viability to 54.86% and 11.57% when combined with 20 min of US treatment (Figure 44B). Further increasing the CAP treatment time to 160 s resulted in a reduction in cell viability to 42.28% and 4.56% during single and multiple treatments, respectively (Figure 44C). Finally, we studied the effects of combining 320 s of CAP treatment with different durations of US treatment and found that the highest reduction in cell viability was 21.6% and 2.9% during single and multiple treatments, respectively, when combined with 20 min of US treatment (Figure 44D).

Ultimately, the effectiveness of combining CAP and US appears to improve as the duration of US / CAP treatment increases, with the most optimal and highest cytotoxic results observed with a 20 min of US combined with 320 s of CAP. Two-way ANOVA shows that there was a significant difference in U-251 MG cell viabilities between the

different combinations of US and CAP, and different treatments (single and multiple) ($p < 0.0001$). A full description of tukey's multiple comparisons test can be seen in the Appendix I.

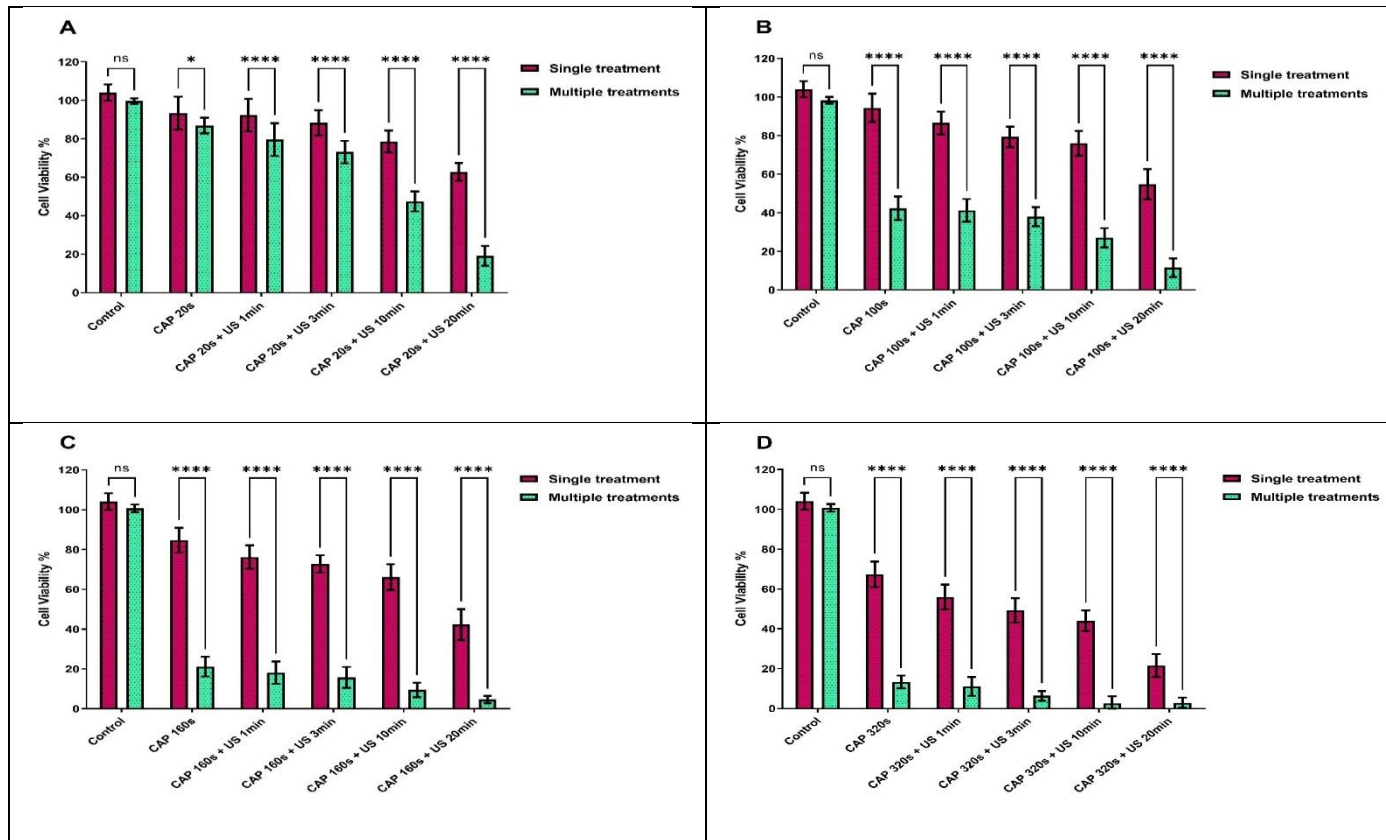


Figure 44: Synergistic effect of CAP and US (1, 3, 10 and 20 min) treatments on U-251MG GBM 3D tumour spheres with 96 h of post treatment incubation. A) Combination of 20 s of CAP treatment with different US treatments, B) combination of 100 s of CAP treatment with different US treatments, C) Combination of 160 s of CAP treatment with different US treatments, D) combination of 320 s of CAP treatment with different US treatments. (ns, not significant, $*p \leq 0.05$; $****p \leq 0.0001$).

Once the synergistic effect of combining CAP and US on U-251 MG GBM tumour spheres was established, the objective was to investigate whether this effect would also be present in other cell lines. Therefore, A431 epidermoid carcinoma tumour spheres were exposed to varying durations of CAP treatment (20, 100, 160, and 320 s) and different durations of US treatment (1, 3, 10, and 20 min), followed by a 96 h incubation period (Figure 45). Similar to the U-251 MG GBM tumour spheres, the combination of 20 min of US treatment with a 20 s CAP treatment showed the highest cytotoxic effect. This resulted in a reduction of cell viability to 57.56% and 13.64% during single and multiple treatments, respectively (Figure 45A). When the CAP treatment duration was increased to 100 s without changing the US doses, the cytotoxicity increased, leading to a decrease in cell viability to 44.53% and 5.54% when combined with 20 minutes of US treatment (Figure 45B). Further increasing the CAP treatment duration to 160 s resulted in a reduction in cell viability to 31.97% and 0.55% during single and multiple treatments, respectively (Figure 45C). Finally, when the combination of 320 s of CAP treatment with different durations of US treatment was examined, the highest reduction in cell viability was 14.51% and 1.75% during single and multiple treatments, respectively, when combined with 20 min of US treatment (Figure 45D).

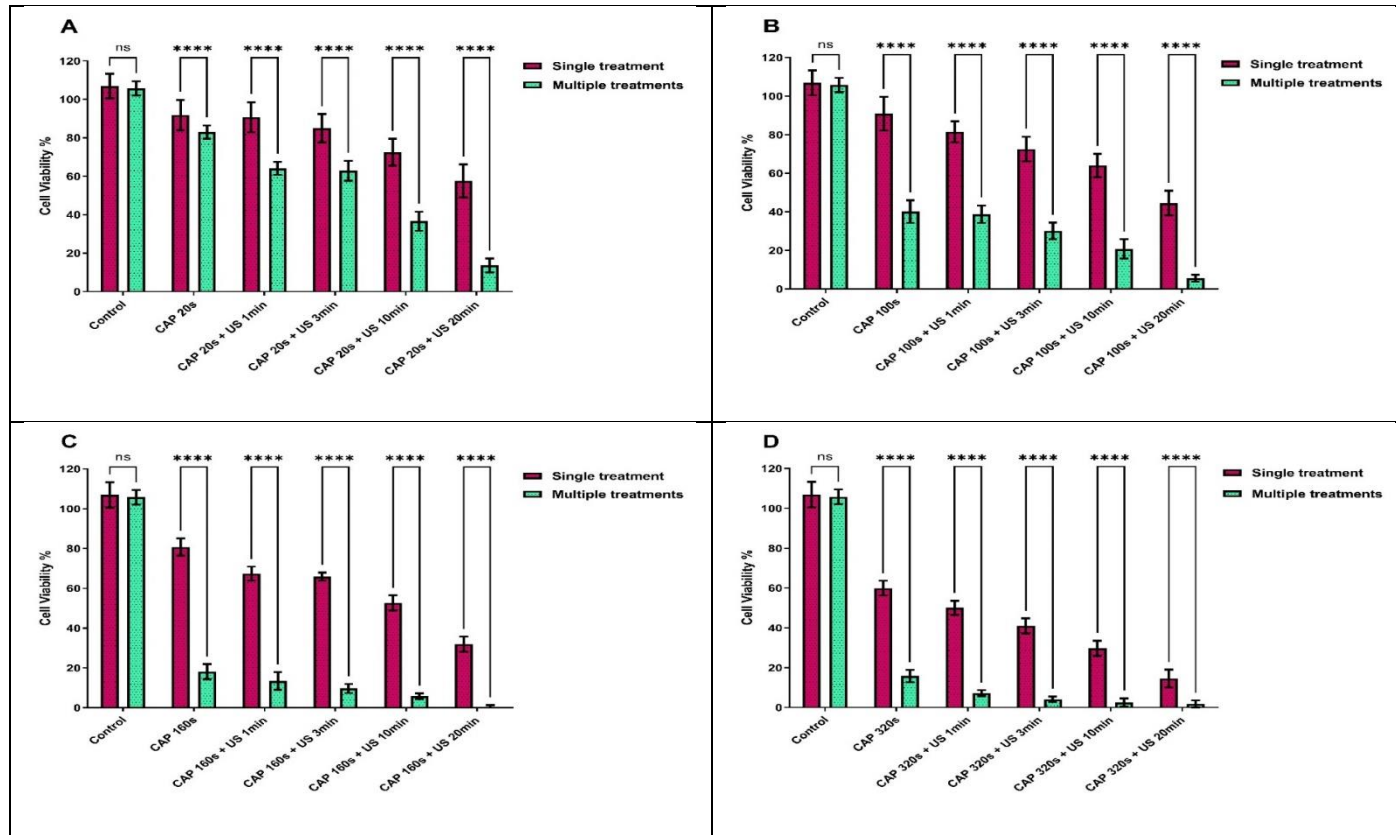


Figure 45: Synergistic effect of CAP and US (1, 3, 10 and 20 min) treatments on A431 epidermoid tumour spheres with 96 h of post treatment incubation. A) Combination of 20 s of CAP treatment with different US treatments, B) combination of 100 s of CAP treatment with different US treatments, C) combination of 160 s of CAP treatment with different US treatments, D) combination of 320 s of CAP treatment with different US treatments. (ns, not significant; **** $p \leq 0.0001$)

Two-way ANOVA shows that there was a significant difference in U-251 MG cell viabilities between the different combinations of US and CAP, and different treatments (single and multiple) ($p < 0.0001$) (Figure 45). A full description of tukey's multiple comparisons test can be seen in the Appendix I.

The results presented in this study demonstrate the potential of combining CAP and US as a viable strategy for GBM therapy, with reproducible synergistic effects observed in the U251-MG GBM cell line. Moreover, the findings from the A431 studies indicate that the CAP / US treatment approach promotes higher cytotoxicity compared to either CAP (chapter 4) [60] or US (chapter 5)[28, 87] alone, regardless of the cell line used. We already established that the CAP induced cytotoxicity throughout the tumour sphere, potentially through the presence of long-lived RONS (H_2O_2 , NO_2^- , and NO_3^-) and also other reactive species [60, 379]. This study is the first to report on the potential of combining US with CAP for cancer therapy using 3D cell culture models, and opens the door for future research to validate this synergistic effect in advance models and further explore this interactions.

5.2.8 US and CAP promotes synergistic effect dependent of apoptosis, JNK, caspases and cysteines

Given our existing understanding of how CAP and US work together and the contribution of RONS to their combined effect, the focus shifted to investigating mitochondrial health and the activation of specific pathways involved in programmed cell death. Initially, to understand the molecular mechanism underlying the death of GBM tumour spheres in response to the combined treatments of US and CAP, an experiment was conducted. U-251 MG tumour spheres were subjected to various inhibitors, such as zVAD-fmk, which

inhibits caspases, SP600125, which inhibits JNK, and E-64, which inhibits cysteine proteases.

ZVAD-fmk is a type of apoptosis inhibitor that can impede caspase-dependent cell death. This pan-caspase inhibitor has a wide range of effects and can permeate cells to bind to the catalytic site of caspases irreversibly [380, 381]. Furthermore, it can also induce necroptosis by inhibiting the activity of caspases 3, 7, and 8 [382]. SP600125 is a potent cell-permeable and reversible inhibitor, prevent the activation of JNK, which plays a role in both cancer cellular apoptosis and survival [383, 384]. Phosphorylation of JNK is inhibited in a dose-dependent manner, which typically leads to the down regulation of Beclin-1 and reduced autophagy [385]. E-64 is a type of cysteine protease inhibitor that is highly selective and potent, and it irreversibly binds to the active thiol group in many cysteine proteases such as papain, cathepsins B, H, D, and L, forming a thioether linkage [386, 387]. E-64 is preferred for *in vivo* studies because of its ability to specifically inhibit these enzymes, as well as its permeability in cells and tissues with low toxicity [388, 389]. The appropriate, non-toxic concentration of each inhibitor was obtained from most recent studies that had investigated the inhibitory effects of cell death in the U-251 MG cell line [85, 390-392]. The concentrations used in this study were 25 μM of zVAD-fmk, 12.5 μM of SP600125, and 15 μM of E-64.

Initially, we investigated the impact of using inhibitors with single treatments of 320 s CAP and different durations of single US treatments (1, 3, 10, 20 min) on U-251 MG GBM tumour spheres with 96 h of post treatment incubation (Figure 46). We found that there was no significant difference in synergistic cytotoxicity between tumour spheres incubated with the E-64 / zVAD-fmk inhibitor and tumour spheres without an inhibitor (Figure 46A). Nevertheless, we observed significant differences in cytotoxicity between the tumour spheres that were incubated with SP600125 and the tumour spheres without

an inhibitor, but only when the CAP was combined with US treatment durations of 3 min or greater (Figure 46A). Finally, we were able to observe significant cytotoxicity protection when tumour spheres were incubated with NAC, during all the different combinational treatments.

We subsequently expanded our investigation to determine the protective effect of these inhibitors in combination with multiple treatments of CAP and US. Remarkably, we observed significant cell viability increase during all the different CAP and US combinations, with all the various inhibitors (zVAD-fmk, SP600125, E-64, and NAC) when compared to negative control (Figure 46B). This results confirms that the cytotoxicity induced by the synergistic US and CAP is also dependent on RONS. Furthermore, the outcomes indicated that at single treatments of CAP and US, it had the potential to activate the JNK signalling pathway. However, during multiple treatments, it appeared to trigger multiple pathways of cell demise, including caspase-dependent, JNK-dependent, and calpain-mediated cell death. The findings imply that the activation of caspase-dependent and JNK-dependent signalling pathways could have initiated apoptosis or programmed cell death [393, 394]. Additionally, calpain-mediated cell death or cytotoxicity may also contribute to this process by causing lysosome-associated membrane permeability, which leads to the release of cathepsin B and cathepsin D from lysosomes into the cytoplasm [395-397].

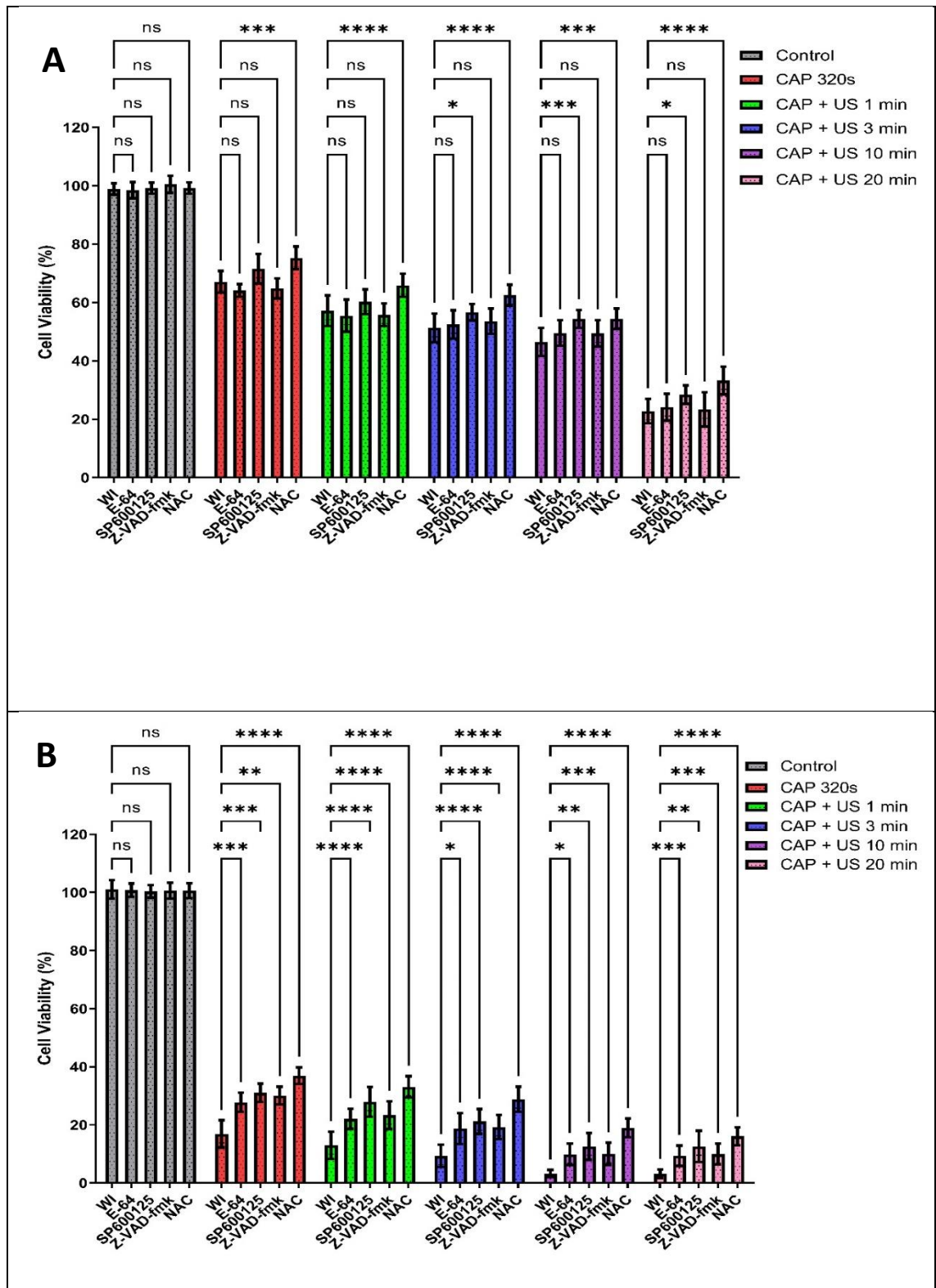
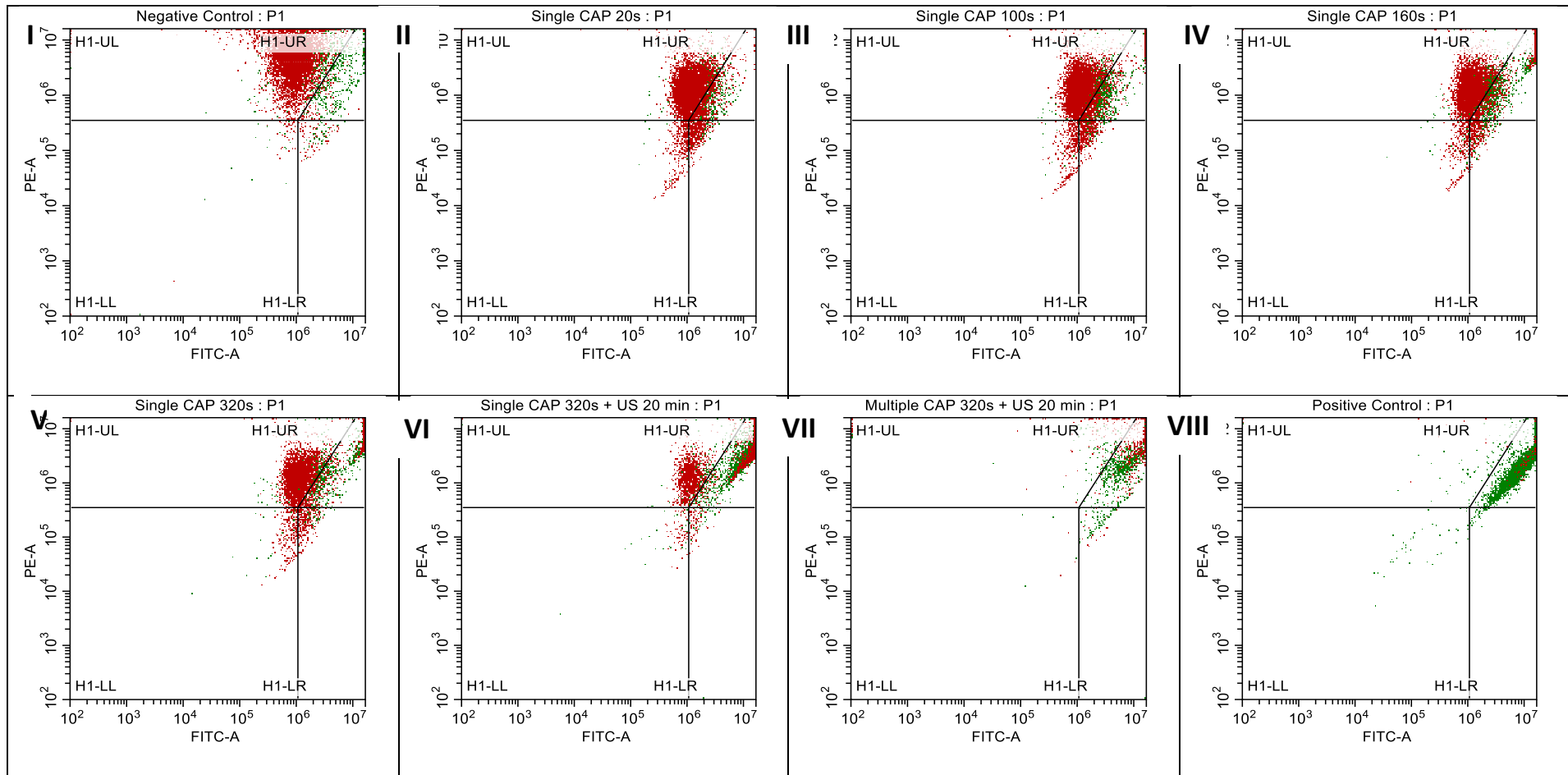


Figure 46: Inhibitor studies of 320 s CAP and different US treated U-251 MG tumour spheres with 96 h of post treatment incubation. A) Single CAP and single US treatment B) multiple CAP and multiple US treatment. (ns, not significant ($p > 0.05$); * $p < 0.05$; ** $p < 0.01$, *** $p < 0.001$; **** $p < 0.0001$).

5.2.9 Mitochondrial membrane depolarisation and cell proliferation assay

U-251 MG tumour spheres were subjected to staining with JC-1 dye. The purpose was to determine the changes in the mean fluorescence ratio of JC-1 monomers and dimers in these tumour spheres, following treatment with different doses of CAP alone and in combination with US treatment. Figure 47 shows that a reduction in $\Delta\Psi_m$ was seen after a post-treatment incubation of 96 h with 10.34%, 15.62%, 27.45%, and 36.05% loss observed during single 20 s (Figure 47A-II), 100 s (Figure 47A-III), 160 s (Figure 47A-IV), and 320 s CAP treatments (Figure 47A-V), respectively. The highest loss in $\Delta\Psi_m$ was observed with 320 s single CAP treatment, where it was 36.05%. Next, the effect of combining 320 s CAP treatment with 20 min of US exposure was investigated. During this treatment, a loss of 77.11% in $\Delta\Psi_m$ was observed (Figure 47A-VI), and this effect slightly increased to 77.47% with multiple treatments (Figure 47A-VII). Additionally, 1 mM H₂O₂ exposure was used as a positive control (Figure 47A-VIII).

The results of the One-way ANOVA analysis demonstrated that there was a significant difference in viability among the various doses of single CAP treatments (except negative control and 20 s CAP treatment), US combinations, and treatment frequencies (single and multiple) ($p < 0.0001$) (Figure 47B). A full description of the tukey's multiple comparison test can be found in the Appendix I. These findings support the previous alamarBlue and PI results and suggest that the depolarization of mitochondria is one of the characteristics of cell death induced by the synergistic effect of CAP and US.



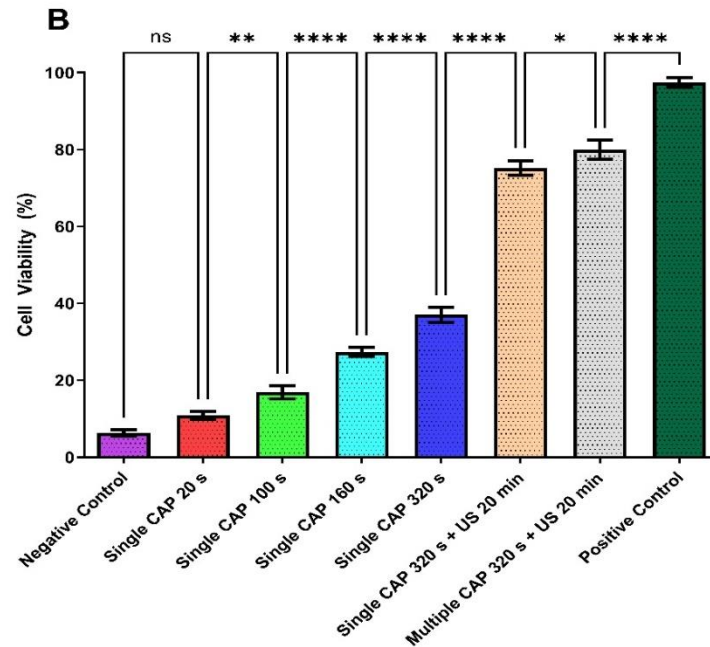


Figure 47: Mitochondrial membrane depolarisation in U-251 MG tumour spheres analysis by JC-1 dye and flow cytometry. A) JC-1 uptake was then measured 96 h post treatment in (I) negative control, (II) single 20 s CAP, (III) single 100 s CAP, (IV) single 160 s CAP, (V) single 320 s CAP, (VI) single CAP 320 s and 20 min US, (VII) multiple CAP 320 s and 20 min US (VIII) positive control (1 mM H₂O₂ used as positive control). B) Percentage of cell viability was then measured at 96 h post treatment, represented as a bar chart and analyzed using one-way ANOVA with tukey's post-test. (ns, not significant ($p > 0.05$); * $p < 0.05$; ** $p < 0.01$; **** $p < 0.0001$).

The role of mitochondrial membrane potential ($\Delta\Psi_m$) is crucial in mitochondrial function and it serves as an early indicator of intrinsic apoptosis [398, 399]. Our findings demonstrate that the combined effect of CAP and US generates ROS, which can accumulate in cells and cause oxidative stress. This oxidative stress can lead to mitochondrial dysfunction.

In order to verify the results of cell proliferation obtained using a haemocytometer, CFSE cell proliferation kit was utilized to track distinct generations of proliferating cells via flow cytometry. The CFSE dye was used to label live cells and monitor proliferation as the signal weakened due to cell division, resulting in different peaks on a flow cytometry histogram. To determine whether apoptosis was responsible for the cessation of cell proliferation, PI cell impermeable dye was also used to co-stain the cells. U-251 MG cells were stained with the CFSE staining solution and used to develop 3D tumour spheres. These tumour spheres were then treated with various single CAP and US combination doses, as well as a positive control (20% DMSO), and incubated for 96 h. Finally, the tumour spheres were co-stained with PI and analyzed using flow cytometry.

According to the histograms, it was observed that an increase in the dosages of CAP and US led to a reduction in cell proliferation and an induction of apoptosis. The combination of 320 s of CAP and 3 min of US resulted in the highest amount of apoptotic cells and the highest inhibition of cell proliferation (Figure 48). Results obtained from this study show that the synergistic effect of US and CAP is capable of inhibiting the cell proliferation of U-251MG GBM tumour spheres.

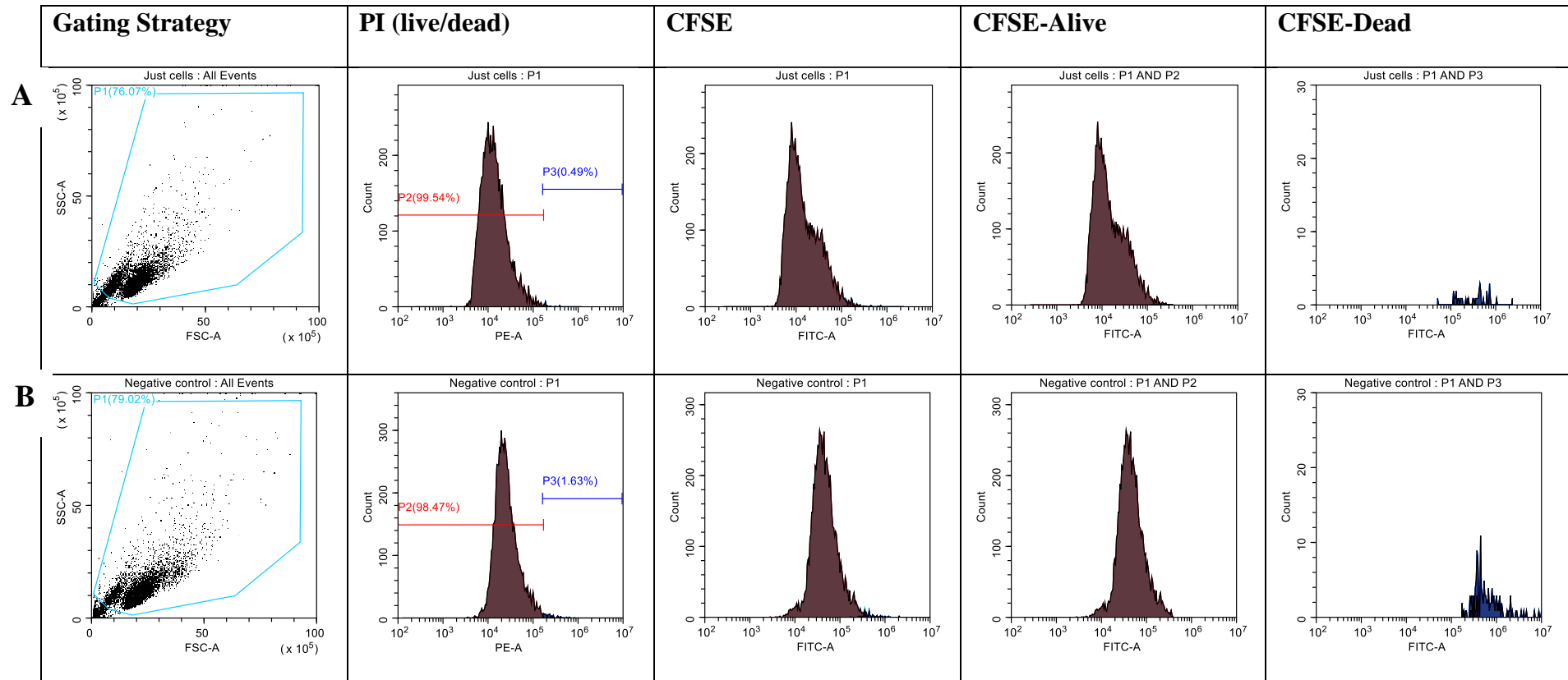


Figure 48: Histograms of CFSE proliferation of U-251 MG tumour spheres with CAP and US treatments. A) Cells without CFSE staining, B) negative control (cells with CFSE staining and without treatment).

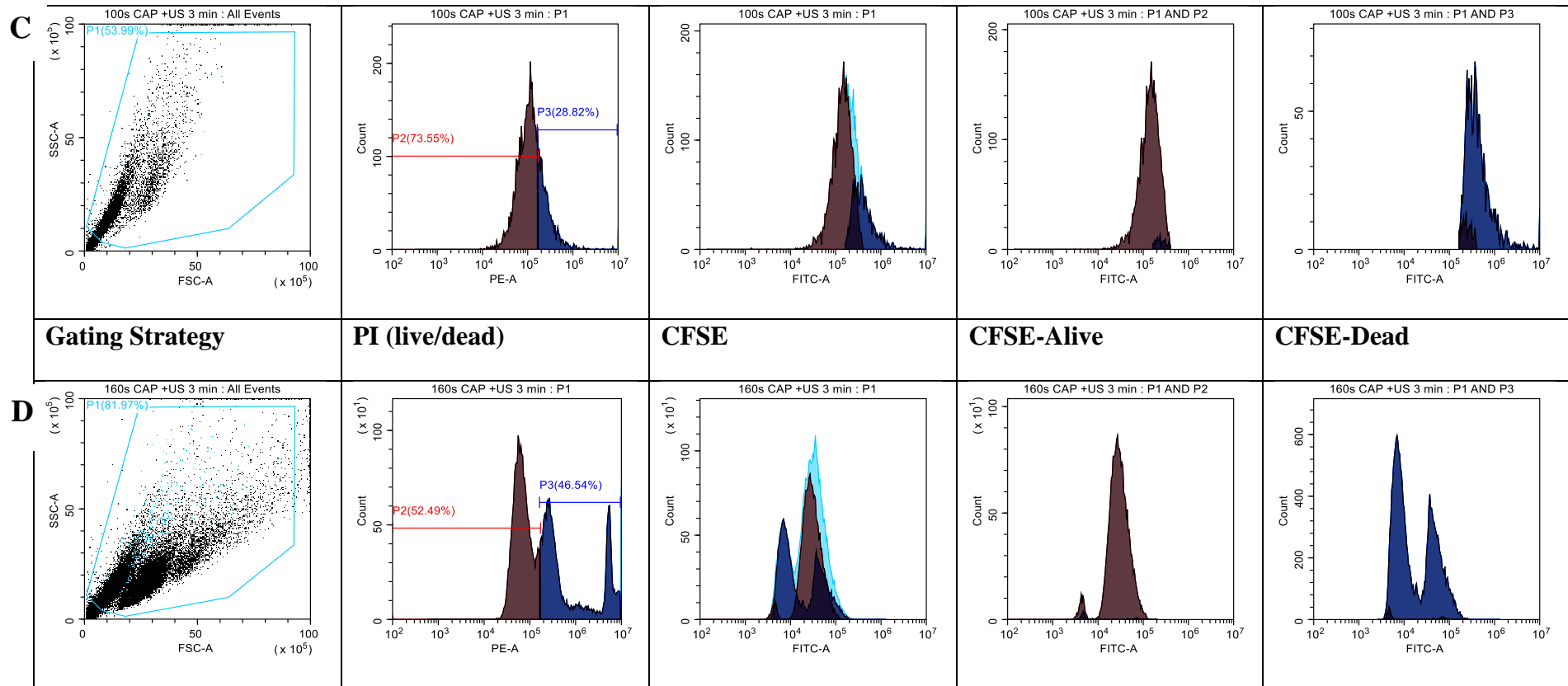


Figure 48: Histograms of CFSE proliferation of U-251 MG tumour spheres with CAP and US treatments. C) 100 s CAP treatment, followed by 3 min US treatment D) 160 s CAP treatment, followed by 3 min US treatment

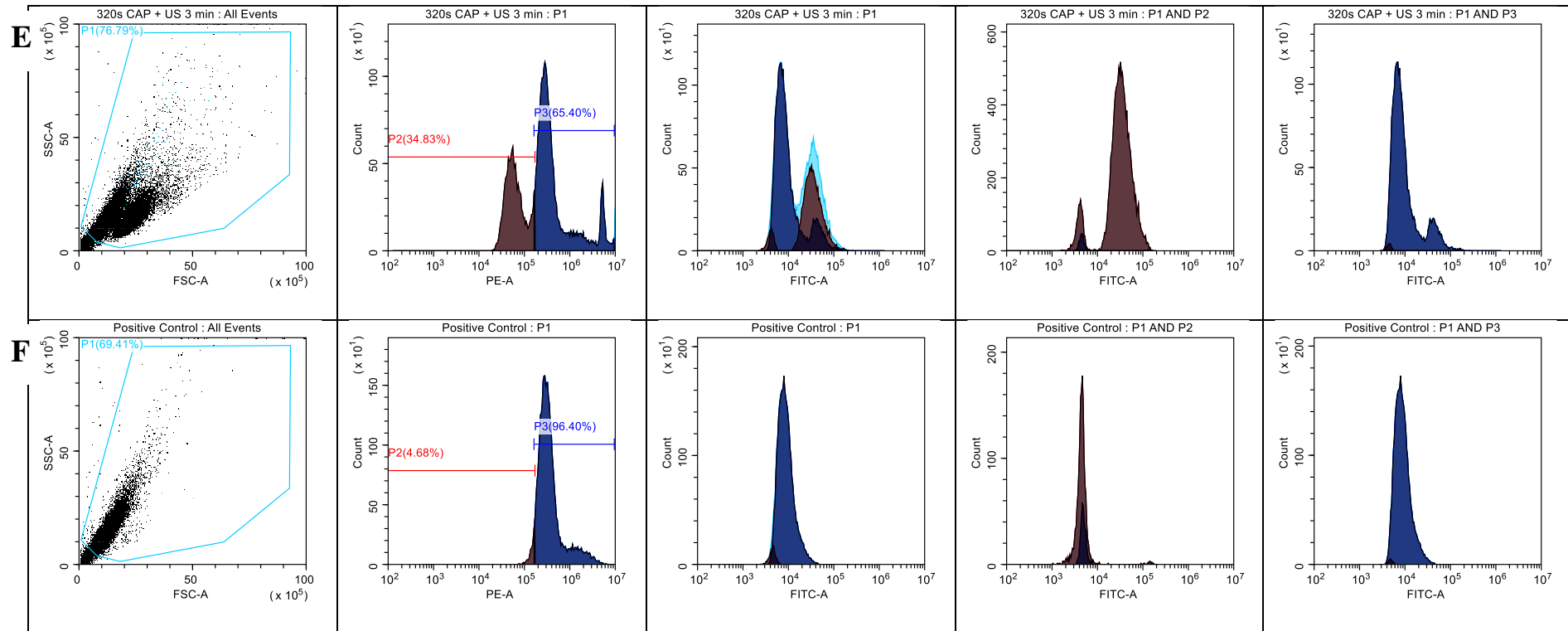


Figure 48: Histograms of CFSE proliferation of U-251 MG tumour spheres with CAP and US treatments. E) 320 s CAP treatment, followed by 3 min US treatment F) positive control (PC; 20% DMSO). Shown are the gating strategy conducted; determination of live and dead cells using PI – P2 (live cells), P3 (dead cells); cell proliferation; cell proliferation population of live cells; cell proliferation of dead cells.

5.3 Conclusion

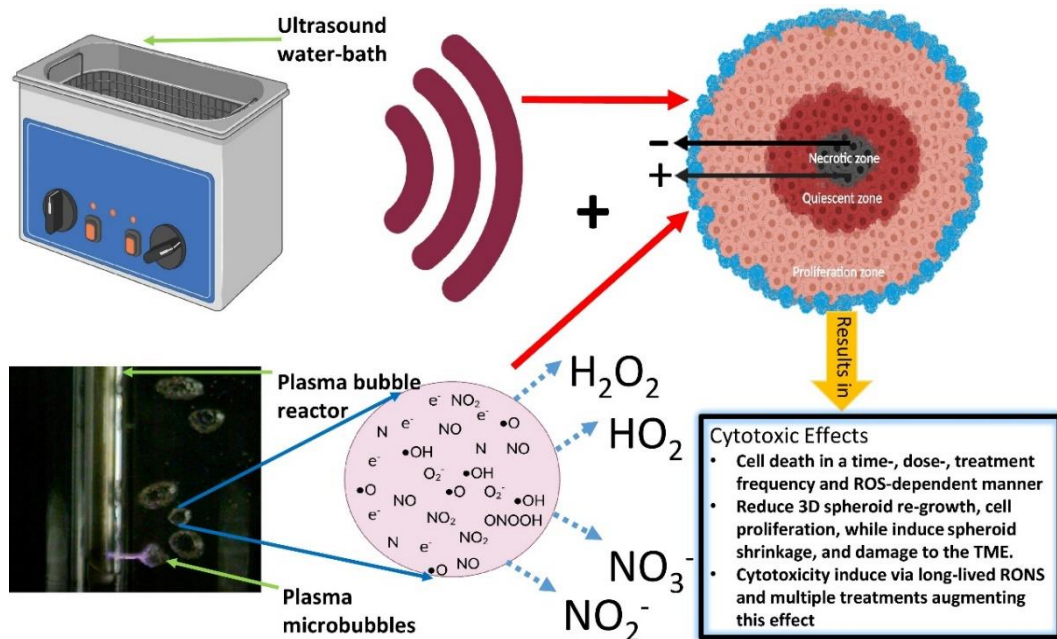
US treatment can effectively induce 3D GBM and epidermoid carcinoma tumour sphere cell death in a time-, dose-, and treatment frequency dependent manner. US is also able to reduce 3D GBM spheroid growth and cell proliferation and induce damage to the TME. Furthermore, our results set important limitations on the likely approach needed, when translating US into a clinical setting, with an approach that allows multiple treatments favourable over a single treatment. Our findings illustrate the significance of US exposure time adjustment in order to achieve cytotoxicity and / or effective drug delivery. Less than three min of US exposure duration is optimal for transient sonoporation without damaging tumour spheres. When US exposure duration exceeds 3 min and / or treatment frequency is increased, enhanced cytotoxicity, persistent pore formation in membranes, lysis, subsequent leakage of cellular content, cell inactivation, or cell death occur in the tumour sphere.

The combination of US and TMZ enhanced the efficiency of GBM and epidermoid carcinoma treatment by enhancing TMZ induced cytotoxicity in 3D tumour spheres compared to 2D cells.

DOX, as a reporter, indicated that drug diffusion in 3D models and drug uptake into cells in tumour spheres are significantly enhanced by US. This leads to improved cytotoxicity in the 3D culture models with US, which is not evident in the 2D culture model, in which the cells are bathed in drug and the effects of sonoporation are muted. Ultimately, our study demonstrates the significance of employing 3D cell culture models for pre-clinical research, since 2D cell culture, followed by animal testing and clinical trials, has resulted in 95% of clinical trial failures due to inadequate prediction of human efficacy and toxicity.

The synergistic effect US and CAP promotes higher cytotoxicity dependent on RONS compared to either CAP or US alone in 3D cell culture models. This combination approach has the potential to be an effective strategy for treating GBM. Our results indicate that the single treatments of CAP and US activate the JNK signalling pathway, while multiple treatments can trigger multiple cell demise pathways, including caspase-dependent, JNK - dependent, and calpain - mediated cell death. Additionally, our findings demonstrate that the synergistic effect of CAP and US generates ROS, which can cause oxidative stress and lead to mitochondrial dysfunction. Furthermore, this synergy is capable of inhibiting the cell proliferation of 3D tumour spheres.

CHAPTER 6 – SYNERGISTIC CYTOTOXICITY EFFECT OF ULTRASOUND AND PLASMA MICROBUBBLE IN GLIOBLASTOMA 3D TUMOUR SPHERE MODEL



A part of this chapter is submitted for publication in the Plasma Processes and Polymers journal. (See Appendix II – Non peer-reviewed)

- **Wanigasekara J**, Cullen PJ, Tiwari B, Curtin JF. Synergistic cytotoxicity effect of ultrasound and plasma microbubble in glioblastoma 3D tumour sphere.

6 Synergistic cytotoxicity effect of ultrasound and plasma microbubble in glioblastoma 3D tumour sphere model

6.1 Rationale

GBM is the most prevalent, malignant, primary brain tumour in adults as explained in chapter 1, [400, 401] and despite recent advancements in multimodal treatment, and supportive care, the prognosis remains poor, and long-term survival is uncommon [400, 401]. There is a definite need for improved treatment options, and substantial efforts have been made to investigate US and MB approach [28]. Combinational therapy of MB [372] and US is capable of achieving efficient chemotherapy [402, 403], gene therapy [404], anti-vascular therapy [405], sonodynamic therapy [406], BBB disruption [360, 407], contrast imaging [406] and also enhance immune response [408]. However, in our research we used PMBs to study the cytotoxicity effect with the combination of US. During CAP production, several chemically diverse long- and short- lived RONS are generated as explained before [128, 338]. Gas phase plasma discharges through bubbles, also known as cold plasma activated MBs / PMB, are especially intriguing given the potential for bubbles to improve RONS delivery into liquid phase [128]. Utilizing PMB to transport RONS is seen as a viable strategy for enhancing the efficacy of GBM therapy. Researchers investigated the effectiveness of PMB in different applications such as degrading organic pollutants [409], biofilms [410], in-situ decontamination of pathogens [338] and algal cell inactivation [128]. In our study, we used 3D tumour spheroids with cell – cell and cell – ECM component interactions, which enables cells to develop *in vitro* in a TME that closely reflects GBM *in vivo* conditions [257, 411]. Hence, in the present study, we employed *in vitro* 3D tumour spheroid models to investigate the combinational effects of US and PMB on U-251 MG human GBM and A431 human epidermoid

carcinoma under different conditions. We believe that this is the first time that we are reporting the US combined PMB approach for induced cytotoxicity in 3D models.

6.2 Results and discussion

6.2.1 US-WB presents cytotoxicity towards GBM and epidermoid carcinoma

Although extensive pre-clinical research has been conducted in the fields of plasma medicine [60, 113, 149] and US [87, 374] for GBM research, there are still unknowns regarding the efficacy of these combination therapies in 3D cell culture models. The majority of research published in the field of US uses models that do not address the TME [87]. This comes at the expense of developing treatments for a 2D model that may not be able to inhibit tumour cell proliferation due to its physiological and structural variations. To resolve this issue, US and PMB combinational treatments in 3D GBM tumour spheroids were investigated for the first time.

A 3D culture model imitates the TME, cellular organisation, additional dimension, polarity, and geometry, which influence cellular functions such as proliferation, aggregation, differentiation, survival, morphology, gene / protein expression, communication, and responses to external stimuli [222, 257]. Due to this, 3D spheroids will provide a better understanding of complex biological / physiological behaviour, cell - cell interactions, tumour characteristics, drug discovery, metabolic profiling, and representation for toxicological testing, as well as improve the accuracy and safety of drug screening, thereby increasing the likelihood of discovering effective therapeutic methods [222, 257].

Initially, in this research, we compared the effects of the US-WB alone on U-251 MG human GBM and A431 human epidermoid carcinoma tumour spheres in DMEM high glucose with 10% FBS medium after 24 h and 96 h of incubations (Figure 49). In the study of the US-WB effect on U-251 MG and A431, with 24 h post treatment incubation, 45 kHz US with 10 min of treatment showed the highest cytotoxic effect. The cell viability reductions of 82.5%, 69.9%, and 60.9% were found for U-251 MG 3D tumour spheres during single, double, and triple 45 kHz 10 min US treatments, respectively (Figure 49A). Then we increased the post treatment incubation time to 96 h, and the cell viability reduction was 74.7%, 63.2%, and 52.2% found for U-251 MG 3D tumour spheres during single, double, and triple 45 kHz 10 min US treatments, respectively (Figure 49B).

During studies of A431 human epidermoid carcinoma, a cell viability reduction of 73.6%, 71.6%, and 54.3% were found during single, double, and triple 45 kHz 10 min US treatments, respectively, with 24 h post treatment incubation (Figure 49C). While single, double, and triple 45 kHz US treatments of 10 min resulted in cell viability reductions of 74.2%, 60.5%, and 48.5%, respectively, with 96 h post-treatment incubation (Figure 49D). A full description of the U-251 MG and A431 cell viability levels during 24 h and 96 h post US treatment incubations are shown in the Table 10. Two-way ANOVA shows that there was a significant difference in U-251 MG and A431 cell viabilities between the different doses of US, different frequencies, and different post treatment incubations ($p < 0.0001$). A full description of tukey's multiple comparisons test can be seen in the Appendix I.

To begin, we investigated the effect of a single US exposure on tumour spheres and discovered that the single US exposure (1X) did not induce cytotoxicity in the tumour spheres (Figure 49A). Since the single US treatment was not enough to induce significant

cytotoxicity, we hypothesised that the use of double (two consecutive daily) and triple (three consecutive daily) US treatments would result in more favourable outcomes. The hypothesis was proved according to the data, the lowest cytotoxicity was observed during a single 25 kHz US treatment for 3 min with 24 h post treatment incubations in both cell lines, while the highest cytotoxicity was observed during three consecutive daily 45 kHz US treatments for 10 min with 96 h post treatment incubations in both cell lines. This finding confirmed that multiple US treatments significantly induced cytotoxicity in tumour spheres and were able to fully / partially inhibit tumour sphere regrowth ability in U-251 MG, and A431, respectively. It was also proven that higher frequencies of US, longer exposure times, and longer post treatment incubations are favourable conditions in cancer treatment. When the duration and frequency of US exposure are increased, persistent pore formation in membranes, lysis, and ultimately cell death and tumour sphere damage occur [87, 363]. These results have important implications for future animal model and human trials where single US treatments may be insufficient to yield significant benefits.

The direct effect caused by US is considered to be tissue ablation. This is intensively studied through the use of high intensity focus US, through its thermal effects, which promotes coagulative necrosis and protein denaturation [412]. Mechanical mechanisms that result in subcellular fragmentation are also capable of causing tumour ablation. As necrosis and potential apoptosis are caused by ablation, it may be sufficient to overcome the resistance of cancer cells. Moreover, cavitation may lead to transient membrane damage. When the repair is effective, the cells may survive, undergo apoptosis and autophagy, or undergo necrosis; when the repair fails or permanent membrane damage occurs, the cells may undergo necrosis and lysis [173, 365, 412].

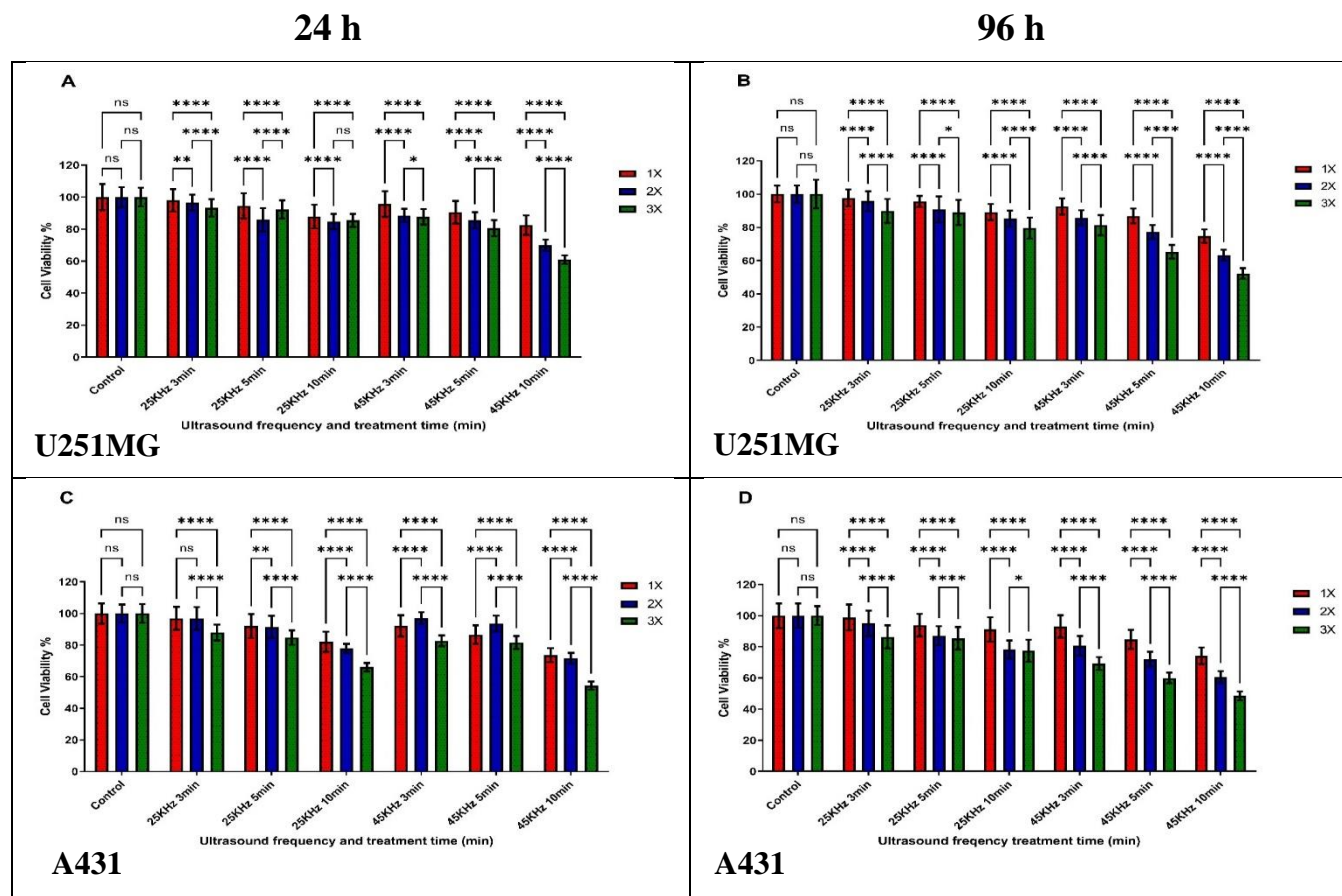


Figure 49: U-251 MG and A431 tumour sphere single and multiple US-WB treatments (US treatment time from 3 to 10 min and US frequency of 25 kHz and 45 KHz) with different incubations. A) U-251 MG single and multiple US treatments with a 24 h post treatment incubation. B) U-251 MG single and multiple US treatments with a 96 h post treatment incubation C) A431 single and multiple US treatments with a 24 h post treatment incubation D) A431 single and multiple US treatments with a 96 h post treatment incubation. (ns, not significant ($p > 0.05$); $*p < 0.05$; $**p < 0.01$, $***p < 0.001$; $****p < 0.0001$)

6.2.2 PMB presents cytotoxicity towards GBM and epidermoid carcinoma

Next, we compare the cytotoxic effects of the single PMB on U-251 MG human GBM and A431 human epidermoid carcinoma tumour spheres in DMEM high glucose with 10% FBS medium after 24 h and 96 h of post treatment incubation times. DMEM media was treated for a time range of 5–30 min to generate plasma activated MB. An IC_{50} of 64.92 min (54.28 ± 77.66 min) and 57.44 min (51.32 ± 64.29 min) were found for U-251 MG tumour spheres during 24 h and 96 h post treatment incubations, respectively (Figure 50A). An IC_{50} of 37.71 min (35.62 ± 39.94 min) and 27.33 min (26.30 ± 28.39 min) were found for A431 tumour spheres during 24 h and 96 h post treatment incubations, respectively (Figure 50A).

Given the positive results obtained in previous study using multiple treatments (three individual treatments with a 24 h incubation gap between each treatment), we further investigated the cytotoxic effect of multiple PMB exposure on U-251 MG and A431 tumour spheres in DMEM high glucose with 10% FBS medium after 24 h and 96 h post treatment incubation times. An IC_{50} of 62.98 min (59.63 ± 66.52 min) and 45.27 min (43.09 ± 47.55 min) were found for U-251 MG tumour spheres during 24 h and 96 h post treatment incubations, respectively (Figure 50B). An IC_{50} of 31.63 min (30.39 ± 32.91 min) and 26.56 min (25.23 ± 27.96 min) were found for A431 tumour spheres during 24 h and 96 h post treatment incubations, respectively (Figure 50B). A two-way ANOVA reveals a significant difference in U-251 MG and A431 cell viability between post-treatment incubations and different single and multiple PMB doses ($p < 0.0001$). A full description of tukey's multiple comparisons test can be seen in the Appendix I. Overall, U-251 MG tumour spheroids showed higher treatment resistance compared to the A431 tumour spheres. In both cell lines, PMB treated tumour spheres incubated for a longer time period (96 h) resulted in a decrease in cell viability. These experiments identified

multiple PMB treatments as the most successful way to induce effective cytotoxicity in the target tumour spheres. In our prior study using CAP, we found that 3D tumour spheres showing significantly more cell death were evident 24 h after treatment compared with 96 h [60]. However, the kinetic response to PMB treatment over time was markedly different.

Plasma - liquid interaction creates a unique physiochemical environment with highly reactive plasma generated species, allowing for several direct chemical reactions at the plasma - liquid interface as well as indirect cascade events in the solution [337]. According to the latest research, the solution's most stable and abundant ROS and RNS are H_2O_2 , NO_2^- , and NO_3^- . Plasma phase interactions and cross reactions between RONS and liquid components are able to generate short-lived molecules such as ozone (O_3), superoxide anion ($\text{O}_2^{\bullet-}$), nitric oxide ($\bullet\text{NO}$), and peroxyxynitrite anion (ONOO^-) [413]. High speed image of a discharge forming PMB and plasma chemistry in the bubble can be seen in the Figure 51.

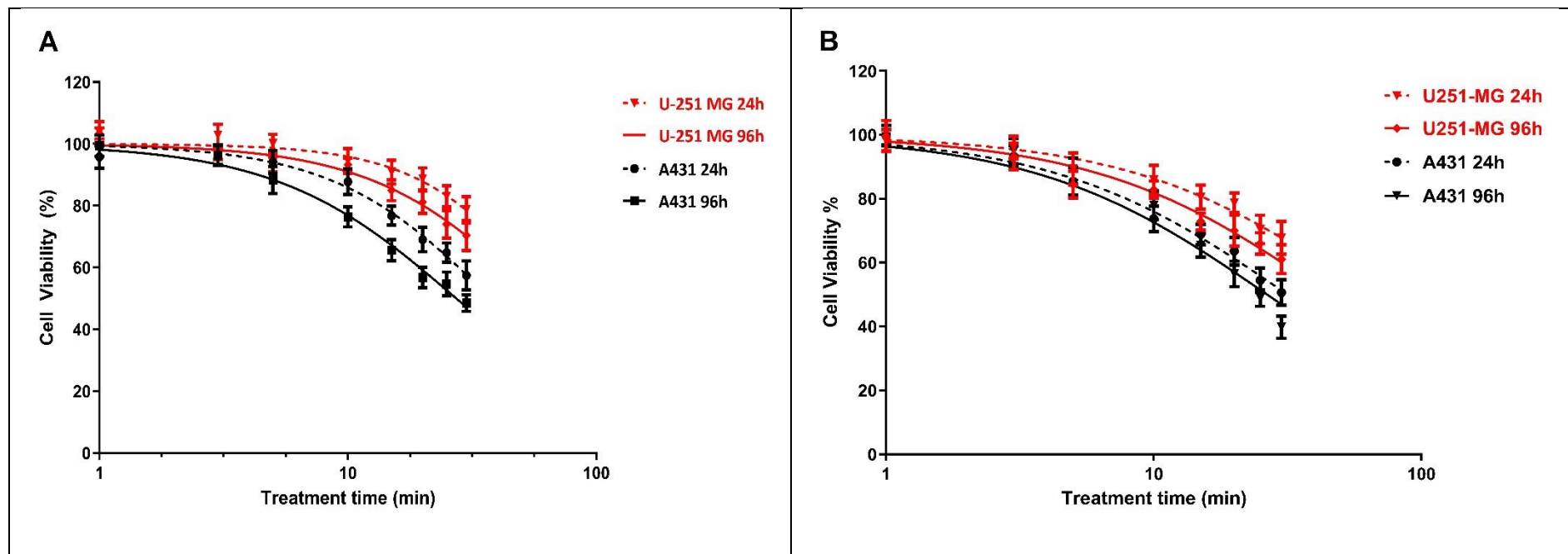


Figure 50: U-251 MG and A431 tumour sphere single and multiple PMB treatments with different incubations. A) U-251 MG and A431 tumour sphere cytotoxicity with single PMB treatment, with 24 h and 96 h post treatment incubations. B) U-251 MG and A431 tumour sphere cytotoxicity with multiple PMB treatment with 24 h and 96 h post treatment incubations.

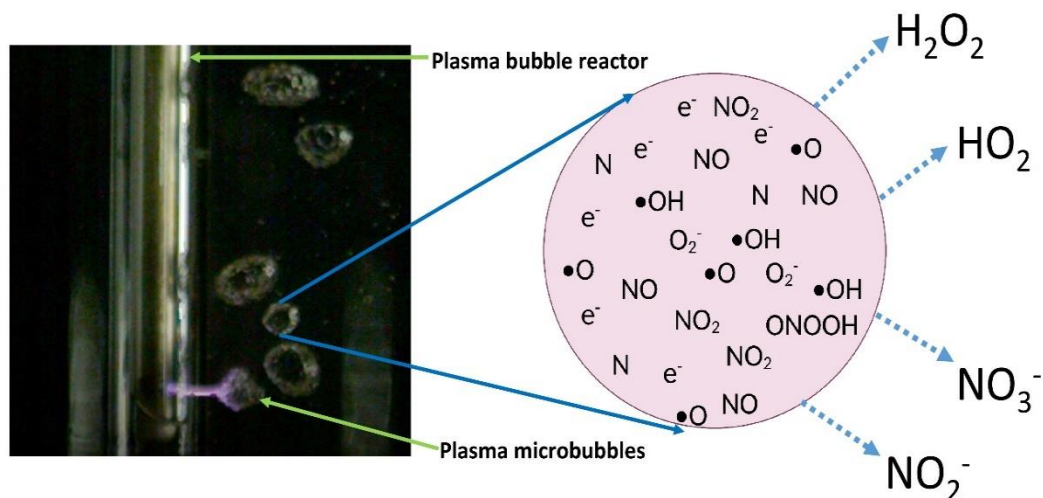


Figure 51: High speed image of a discharge forming PMB and plasma chemistry in the bubble

6.2.3 PMB and US presents synergistic cytotoxicity towards GBM and epidermoid carcinoma

Further investigate the synergistic cytotoxic effects of US and PMB on U-251 MG human GBM tumour spheres with 24 h and 96 h post treatment incubations. During the study of the single US and single PMB effects, the combination of PMB 30 min with 45 kHz US for 10 min of treatment showed the highest cytotoxic effect. The cell viability reductions of 49.4% (Figure 52A) and 40.3% (Figure 52B) were observed for 3D tumour spheres during the 24 h and 48 h post treatment incubations, respectively. Similarly, during the study of the multiple US and multiple PMB effects, the combination of PMB 30 min with 45 kHz US for 10 min treatment showed the highest cytotoxic effect. The cell viability reductions of 7.2% (Figure 52C) and 2% (Figure 52D) were observed for 3D tumour spheres during 24 h and 48 h post treatment incubations, respectively. The two-way

ANOVA demonstrated that there was a significant difference in viability between each dose of single / multiple US and PMB combinations, different post treatment incubations ($p < 0.0001$). A full description of tukey's multiple comparisons test can be seen in the Appendix I. Based on the analysis, it is demonstrated that the synergistic effect of US and PMB could induce tumour sphere cytotoxicity in a dose- and time- dependent manner. These results have important implications for future animal and human trials where the combinations of single US and PMB treatments may be insufficient to yield significant benefits and need to focus more on multiple consecutive treatments.

Using a GBM 3D cell culture model, researchers revealed that low intensity pulsed focused US decreased spheroid growth metabolic activity and enhanced DNA double-strand breaks [374]. We were unable to elicit substantial cytotoxic effects, growth metabolic decreases, or DNA double strand breakage with the use of low intensity US alone, but we were able to do so using a multiple treatments and combination of PMB.

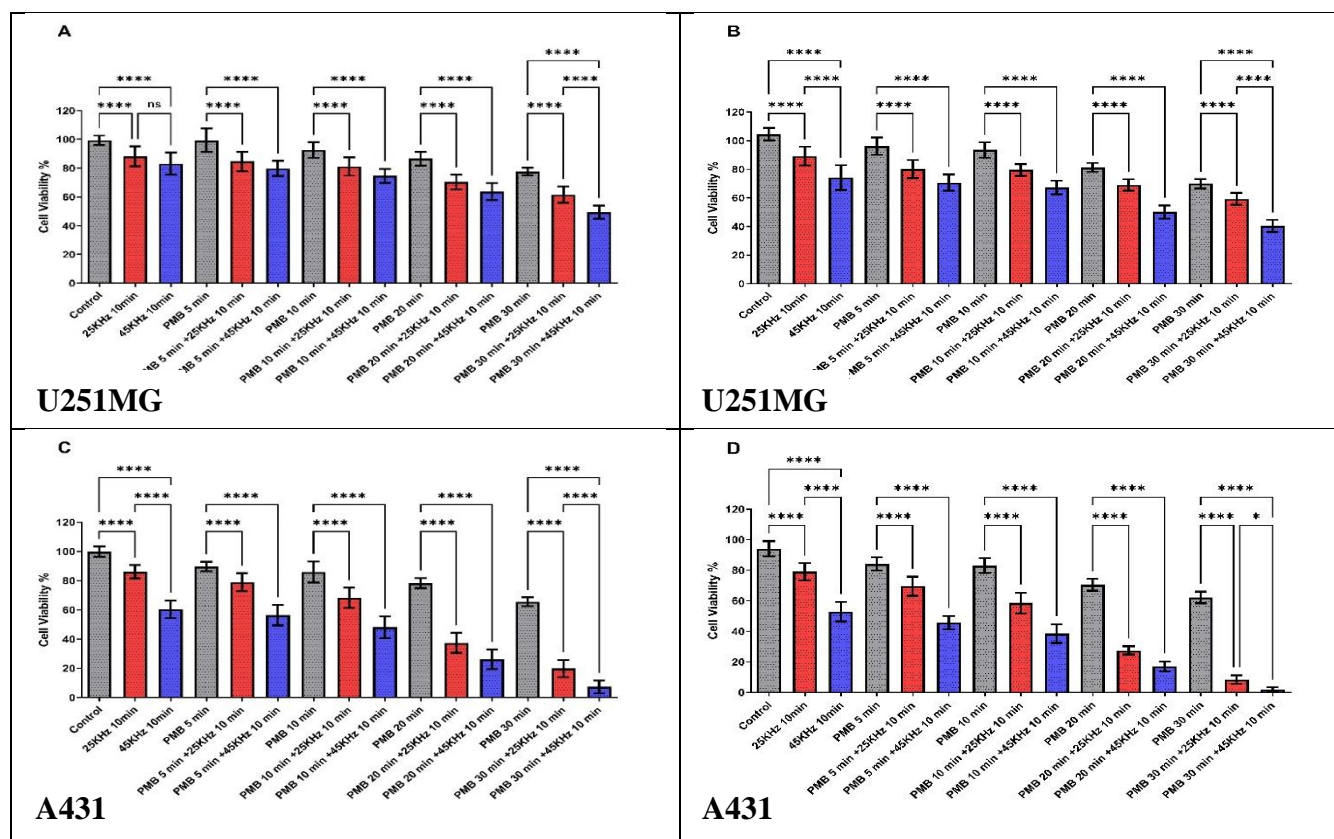


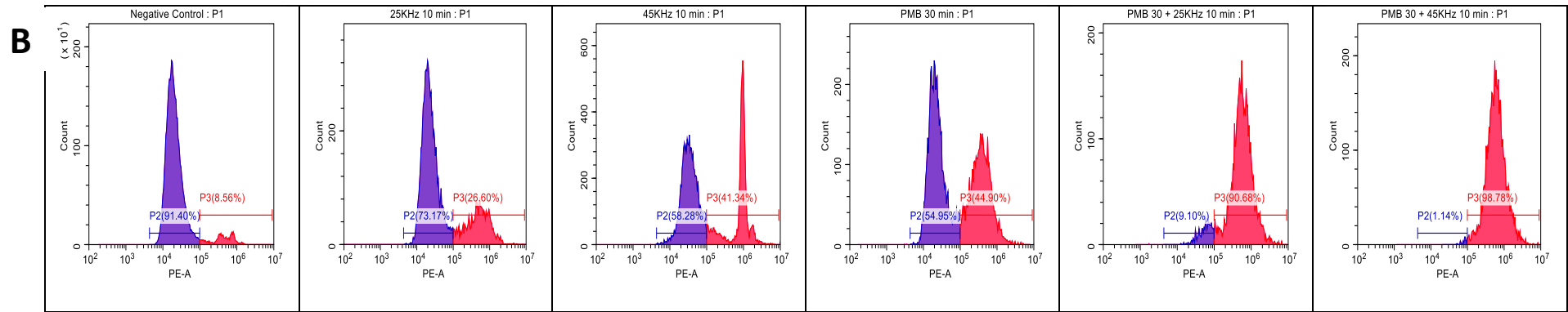
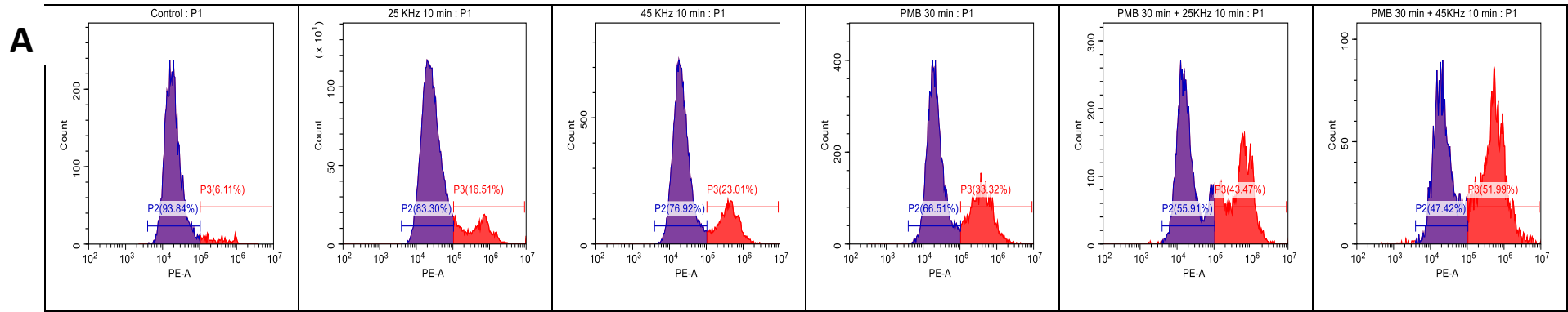
Figure 52: Synergistic effect of US and PMB treatment on U-251 MG tumour sphere with different incubations. A) U-251 MG single US and PMB treatments with 24 h incubation B) U-251 MG single US and PMB treatment with 96 h incubation C) U-251 MG multiple US and PMB treatment with 24 h incubation D) U-251 MG multiple US and PMB treatment with 96 h incubation. (ns, not significant ($p > 0.05$); * $p < 0.05$; ** $p < 0.01$, *** $p < 0.001$; **** $p < 0.0001$).

6.2.4 Effect of US and PMB treatment on tumour sphere cell membrane damage

PI was used to validate the US and PMB induced cell death and cytotoxicity in U-251 MG tumour spheres. PI is a membrane impermeable, fluorescent, nucleic acid intercalating agent that allows identification of dead cells with compromised plasma membranes in a population of tumour spheres. PI uptake was measured 96 h post single (Figure 53A) and multiple (Figure 53B) US or / and PMB treatments.

The PI uptake increased to almost 17% and 42%, respectively, following a single US 25 kHz 10 min treatment combined with 30 min single plasma treated MB (Figure 53A). When a single US 45 kHz 10 min treatment was combined with a 30 min single plasma treated MB, PI uptake increased from 28% to 54% (Figure 53A). During multiple US and PMB treatments, the PI uptake increased to almost 24% and 87%, respectively, following multiple US 25 kHz 10 min treatments combined with a 30 min plasma treated MB (Figure 53B). While, PI uptake increased from 47% to 95%, when US 45 kHz 10 min treatment combined with 30 min plasma treated MB (Figure 53B). This also proves that a combination of US and PMB treatments can damage the tumour sphere's cell membrane and induce cytotoxicity. This validates the alamarBlue assay data.

A two-way ANOVA demonstrated that there was a significant difference in PI uptake between single and multiple US or / and PMB treatments ($p < 0.0001$), while no significant difference was found between the controls for both single and multiple treatments (Figure 53C). A full description of tukey's multiple comparisons test can be seen in the Appendix I.



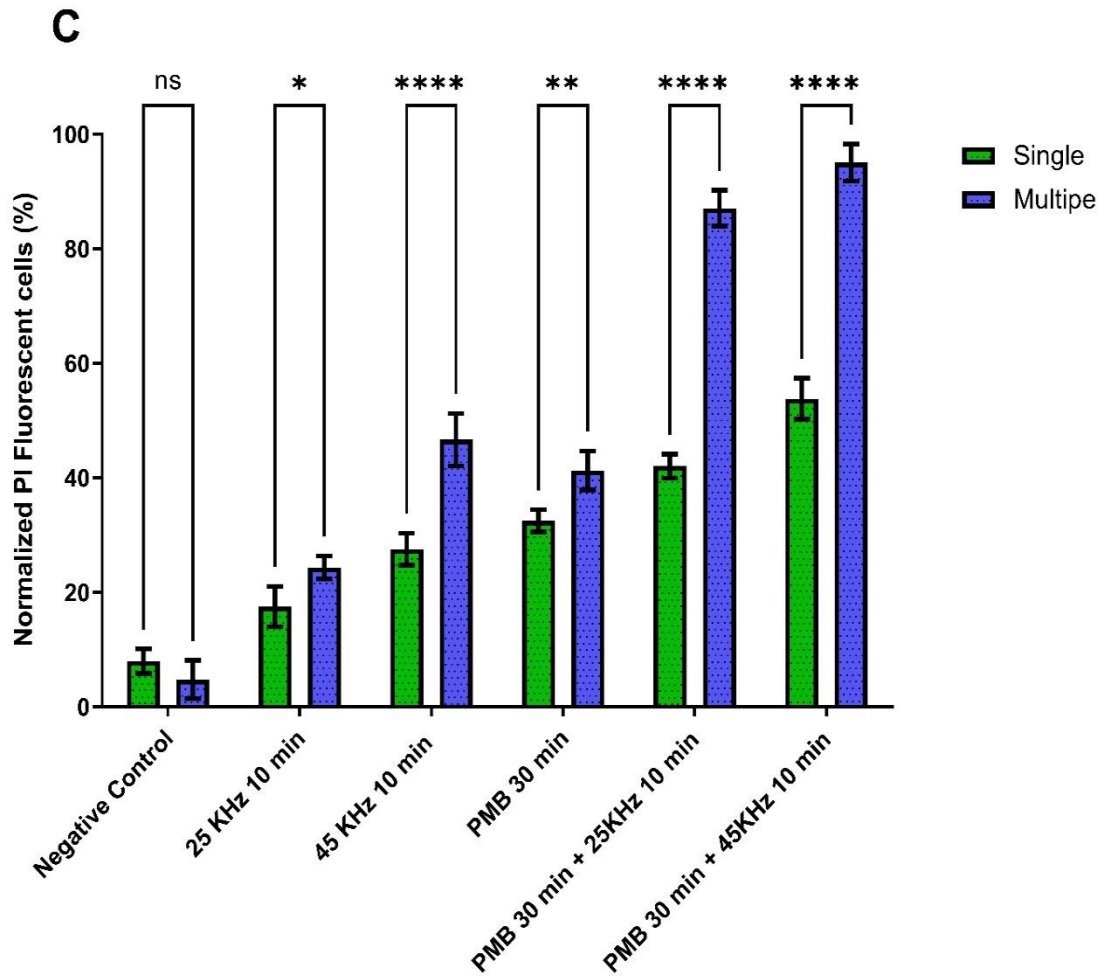


Figure 53: PI uptake in US and PMB treated U-251 MG tumour spheres. PI uptake was measured by flow cytometry and used as an indicator of cell death. Tumour spheres were treated for 10 min with 25 kHz and 45 kHz US with and without PMB as shown above. PI uptake was then measured 96 h post treatment in (a) single US and PMB treatment, (b) multiple US and PMB treatments, (c) normalized PI uptake was then measured at 96 h post single and multiple treatments and represented as a bar chart. All the data points were statistically significant except control. (ns, not significant, $*p \leq 0.05$; $**p < 0.01$, $****p \leq 0.0001$)

6.2.5 US and PMB induced morphological changes

Changes in the tumour sphere morphology induced by US or / and PMB treatments were studied to get a better understanding of their mechanisms of cell death. Representative tumour sphere images showing the morphological changes induced by different US and / or PMB treatments for U-251 MG as shown in Figure 54A.

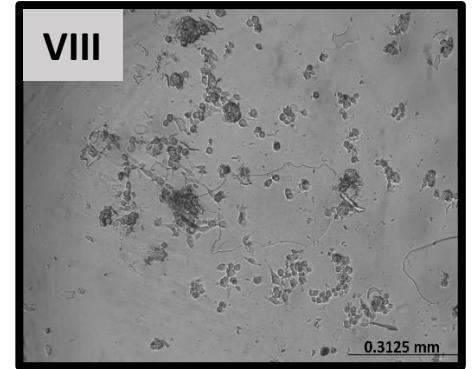
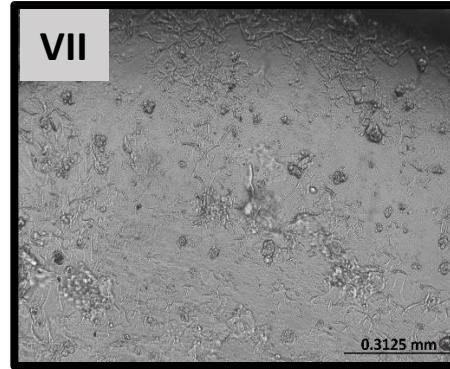
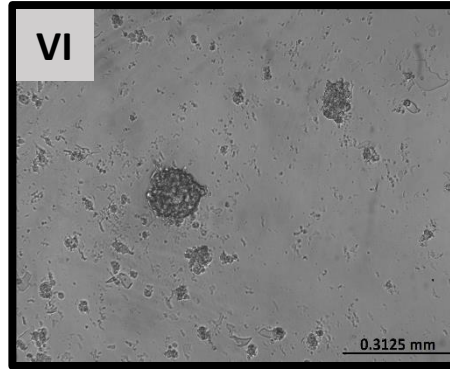
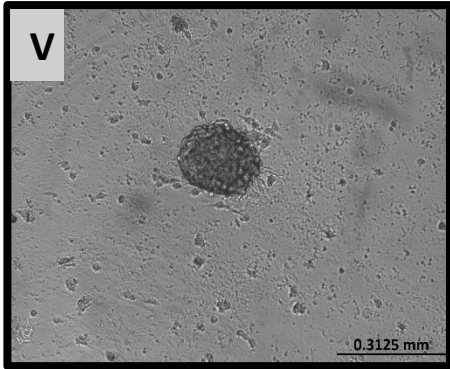
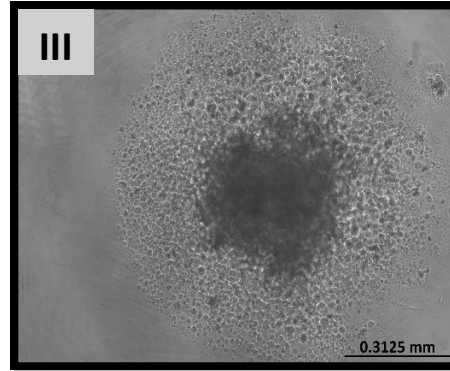
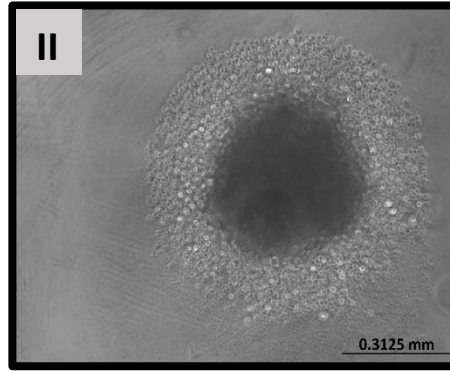
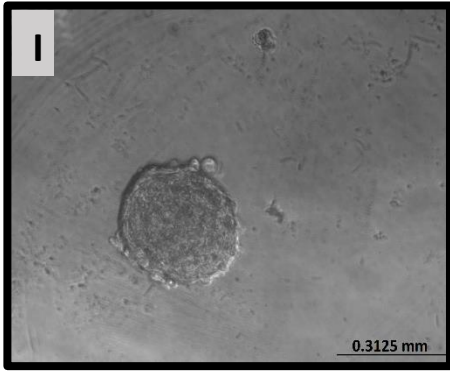
U-251 MG tumour sphere diameter was found to be significantly increased after 10 min of both 25 kHz (Figure 54A-II) and 45 kHz (Figure 54A-III) US treatments. It is possible that US treatments can weaken cell – cell and cell – ECM interactions, and due to this, the volume of the densely arranged tumour sphere started to increase, resulting in an increased tumour sphere diameter. On the other hand, tumour sphere diameter was found to be significantly reduced after the PMB treatment (Figure 54A-IV) compared to the control (Figure 54A-I) and a higher number of cells detaching from the tumour sphere core can be observed during PMB treatment.

The combination of US and PMB induced significant, cumulative cytotoxicity. This was manifested by spheroid rupture, shrinkage, and markedly reduced tumour regrowth ability, which was achieved with a 25 kHz single US and single PMB treatment (Figure 54A-V), This outcome was enhanced with a 45 kHz single US and single PMB treatment (Figure 54A-VI). Tumour spheres broke apart during the combination of 25 kHz multiple US and multiple PMB, causing damage to TME (Figure 54A-VII), and this effect was amplified when multiple PMB were combined with 45 kHz multiple US (Figure 54A-VIII). It is therefore likely that the combinational effect of multiple US and PMB treatments would be necessary to significantly induce cytotoxicity, induce spheroid shrinkage, reduce 3D GBM spheroid regrowth, reduce cell proliferation, and induce damage to the TME. Finally, to validate the above changes with each US and / or PMB treatment, we monitored tumour spheres after treatments by using an inverted phase-

contrast microscope, and the sizes of the spheroids (diameters) were measured as explained above for at least three independent experiments. The tumour sphere diameter rapidly declined during combination treatment of single PMB and US compared to PMB or US treatments alone, while this difference increased with multiple treatments (Figure 54B). Two-way ANOVA demonstrated that there was a significant difference in the tumour spheres sizes during the single and multiple treatments of 25 kHz US and PMB; 45 kHz US and PMB; and 30 min of PMB ($p < 0.0001$) (Figure 54B). A full description of Tukey's multiple comparison test is available in the Appendix I.

Exposed to the surrounding media, the outer layer of the tumour spheroid is mostly composed of viable, proliferating cells [257]. With the assistance of PMB, a plasma-liquid interaction produced reactive species [337]. As we hypothesize previously, these species dissolve in the medium, initiate chemical reactions on the outer layer of the tumour sphere, which ultimately led to cell death in the outer layer of cells, which in turn resulted in a reduction of the tumour sphere's diameter [60]. It is possible that longer US treatments can permanently open the membrane and also weaken cell – cell and cell – ECM interactions [87]. As a consequence of this, the volume of the densely arranged tumour sphere started to increase, which resulted in an increase of the tumour sphere's diameter. The synergistic effect of US and PMB, which proves previous findings [60], shows its ability to reduce cell – cell and cell – ECM interactions, damage cell membranes, and enhance the ability of RONS to penetrate throughout the entire depth of 3D tumour spheroids with the aid of aquaporins [149], which in turn increases cytotoxicity and apoptosis.

A



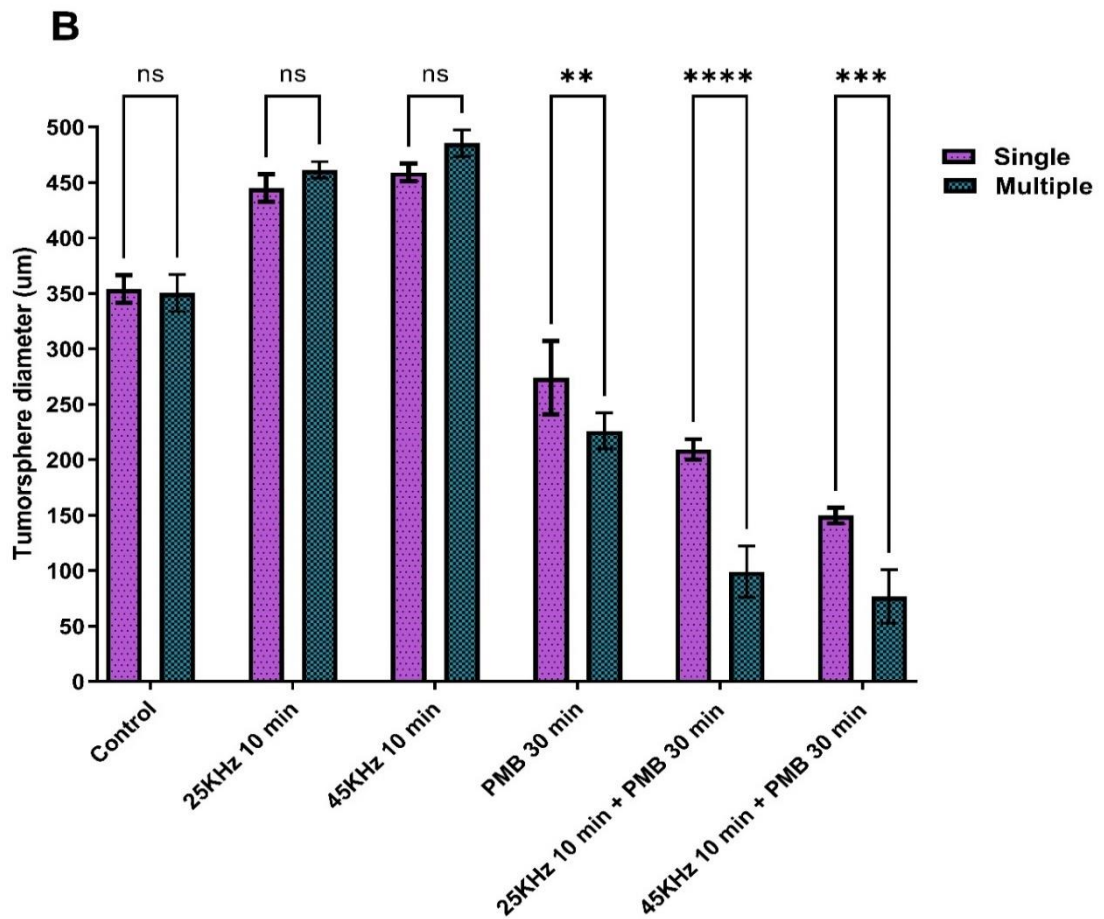
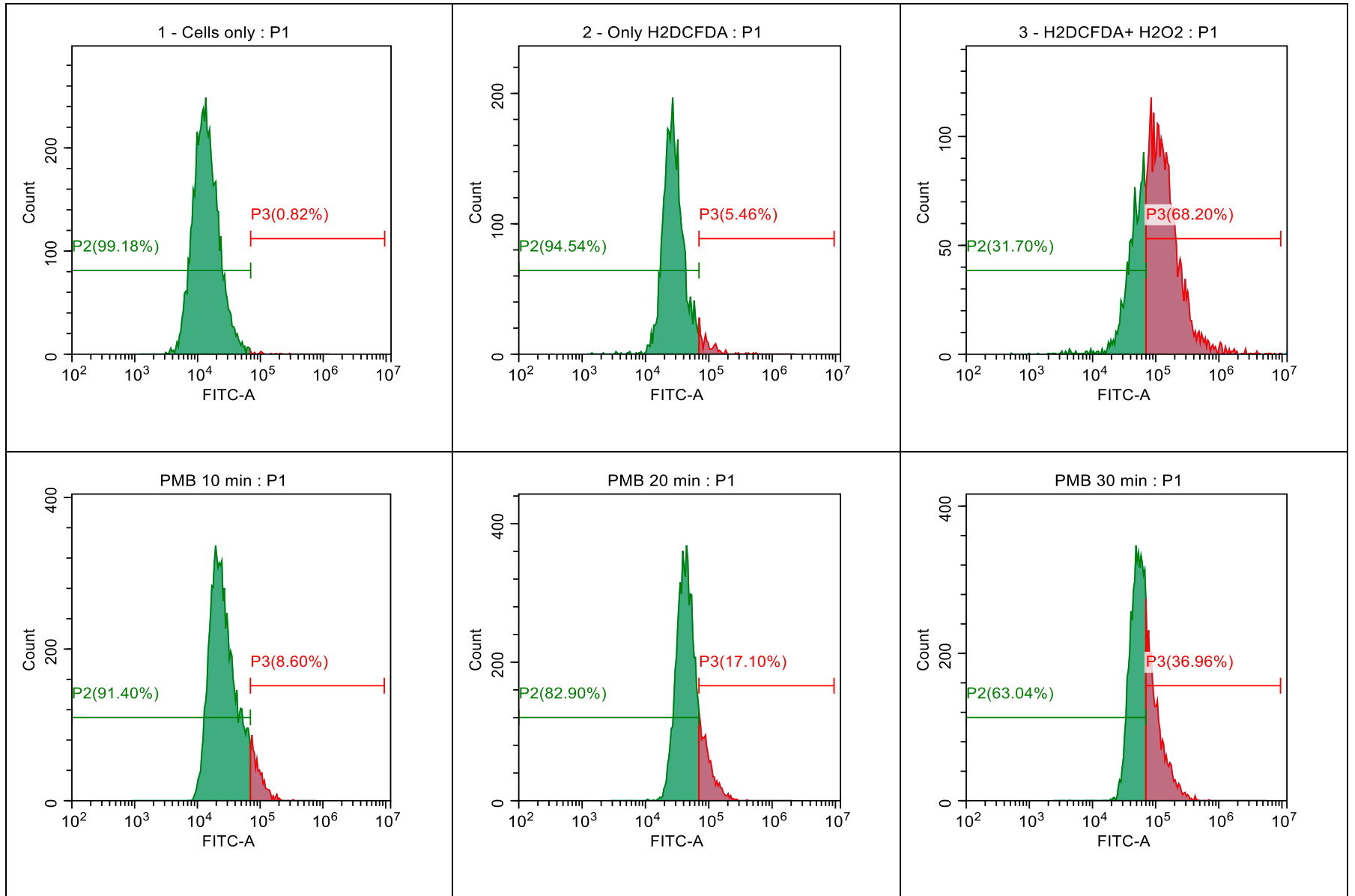


Figure 54: U-251 MG tumour sphere morphology and size (diameter) variation analysis followed by US and PMB treatments. A) U-251 MG tumour sphere morphological changes with different US (10 min) / PMB (30 min of plasma exposure) treatments and 24 h post treatment incubation (I- Control; II – 25 kHz single US treatment; III – 45 kHz single US treatment; IV – Single PMB treatment; V – 25 kHz single US and single PMB treatment; VI – 45 kHz single US and single PMB treatments; VII – 25 kHz multiple US and multiple PMB treatment; VIII – 45 kHz multiple US and multiple PMB treatments) (converted all of the panels [a] to grayscale and applied a simple linear brightness adjustment [+40%]). B) U-251 MG tumour sphere size (diameter) followed by different US and PMB treatments. (ns ($p > 0.05$); ** $p < 0.01$, *** $p < 0.001$; **** $p < 0.0001$).

6.2.6 ROS production in U-251 MG tumour spheres

We evaluated intracellular reactive oxygen species by using H₂DCFDA, a cell-permeable probe. Analysis of the histograms shows significantly increasing levels of intracellular-oxidized H₂DCFDA and ROS as a function of plasma treatment time in the MB (Figure 55A). The mean fluorescence levels of 10, 20, and 30 min PMB treated tumour spheres were increased by a factor of 1.6, 3.1, and 6.8 times, respectively, compared to the negative control (Figure 55B). One-way ANOVA demonstrated that there was a significant difference in the mean fluorescence levels during all the different PMB treatments ($p < 0.0001$); while there was no significant difference between the control and the PMB 10 min treatment (Figure 55B). A full description of Tukey's multiple comparison test is available in the Appendix I.

A



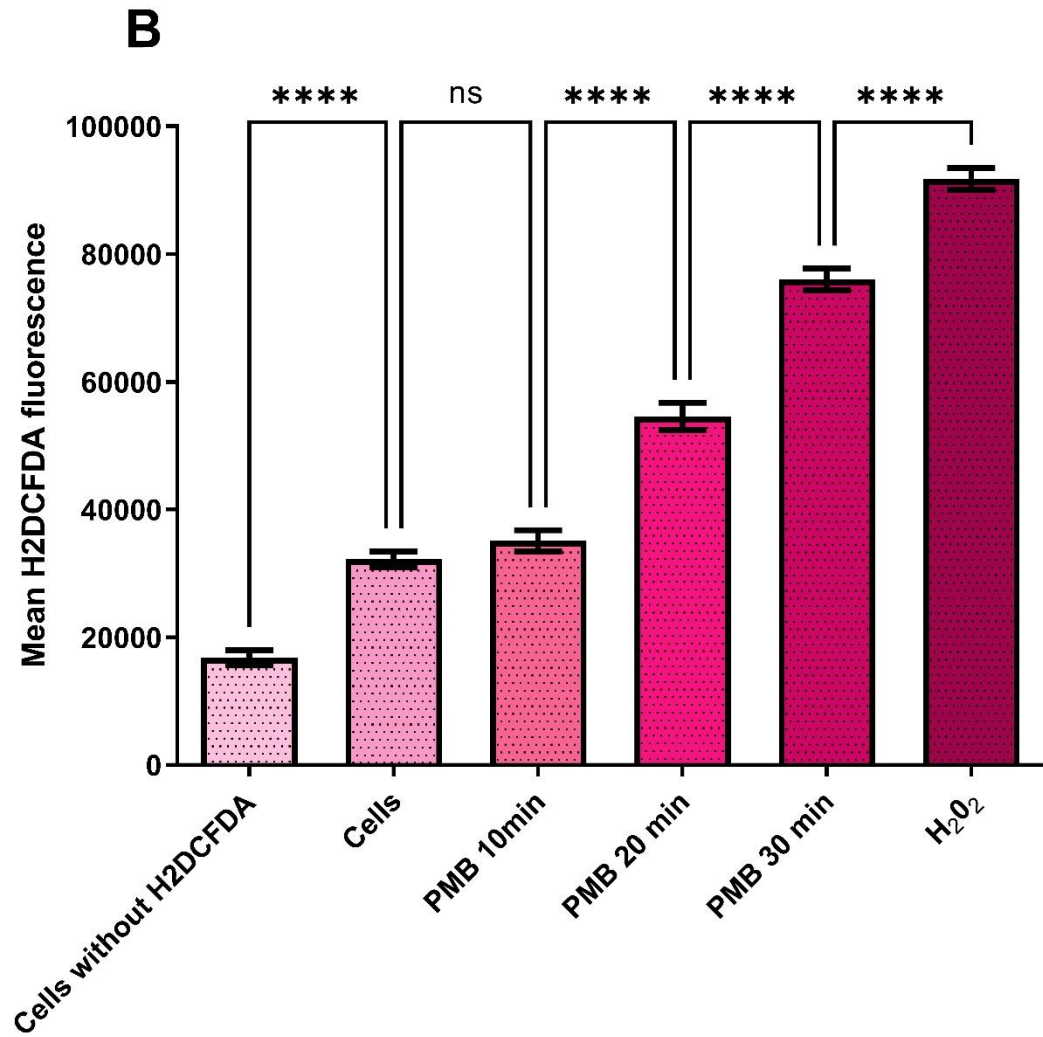


*Figure 55: ROS production in U-251 MG tumour spheres. A) 3D cells were incubated with H2DCFDA and treated at three different doses of PMB, 3 h post treatment cells were collected and analyzed using CytExpert software. B) The mean of the FITC channel was used to plot the values on columns and analysed using one-way ANOVA with tukey's post-test. All the data points were statistically significant except cells and PMB 10 min treatment times. ns, not significant ($p > 0.05$); **** $p < 0.0001$*

6.2.7 PMB presents RONS - dependent cytotoxicity

Tumour spheres grow in a DMEM medium in the presence and absence of sodium pyruvate, which used to study the cytotoxic responses to multiple PMB treatments. The ROS induced cytotoxic effect of PMB was investigated using different treatment time points (1, 3, 5, 10, 15, 20, 25, and 30 min) with NAC employed as a ROS scavenger. An IC_{50} of 63.69 min (53.9 ± 75.25 min), 89.46 min (71.53 ± 111.9 min), 131.0 min (91.03 ± 188.4 min), and 170.8 min (111.0 ± 262.9 min) were found for multiple PMB treated tumour spheres in a media without pyruvate without NAC, with pyruvate without NAC, without pyruvate with NAC, and with pyruvate with NAC, respectively, at 24 h post treatment incubation (Figure 56A). While, an IC_{50} of 44.45 min (40.21 ± 49.98 min), 54.23 min (47.71 ± 63.12 min), 127.5 min (99.6 ± 172.4 min), and 206.0 min (137.7 ± 350.4 min) were found for multiple PMB treated tumour spheres in a media without pyruvate without NAC, with pyruvate without NAC, without pyruvate with NAC, and with pyruvate with NAC, respectively, at 96 h post treatment incubation (Figure 56B). According to the data, the highest PMB treatment resistance was evident in tumour spheres treated in the high glucose DMEM with pyruvate and NAC. The second highest cytotoxicity resistance was observed in the high glucose DMEM without pyruvate and with NAC. The highest cytotoxicity was shown in tumour spheres treated in high glucose DMEM without pyruvate or NAC and high glucose DMEM with pyruvate and without NAC, respectively (Figures 56A and 56B).

Then, using different US and PMB combinations in DMEM with / without pyruvate and with/without NAC, we assessed the ROS induced synergistic cytotoxic effect of the PMB and US. We were able to observe a significant reduction in cytotoxicity in the U-251 MG tumour spheres treated with NAC in all the different combination treatments during the 24 h (Figure 56C) and 96 h (Figure 56D) post treatment incubations. A two-way ANOVA

demonstrated that there is a significant difference in viability between the different combinations, doses, and post treatment incubations ($p < 0.0001$). A full description of tukey's multiple comparison test is provided in the Appendix I.

This confirms that the cytotoxicity induced by PMB is mainly dependent on RONS. NAC significantly protected the target tumour spheres from PMB induced cytotoxicity at each applied doses, post-treatment incubation periods, media compositions, and different combinations of multiple treatments ($p < 0.0001$), whereas sodium pyruvate did not significantly protect against cytotoxicity. A full description of tukey's multiple comparison test and all the IC_{50} values and ranges are shown in the Appendix I. Titration of NAC was performed to confirm the optimum working concentrations. Two-way ANOVA demonstrated that there was no significant difference between 2, 4, and 8 mM of NAC, showing that increases or decreases in NAC concentrations of around 2 – 8 mM do not change the protective effects (Figure in the Appendix I).

In our case, cell-permeable NAC is protective, and PMB induced cytotoxicity is ROS dependent. Our findings correlate with the previous studies [60, 113, 414], which also characterised plasma induced RONS in both the gas and liquid phases of the system [113, 414].

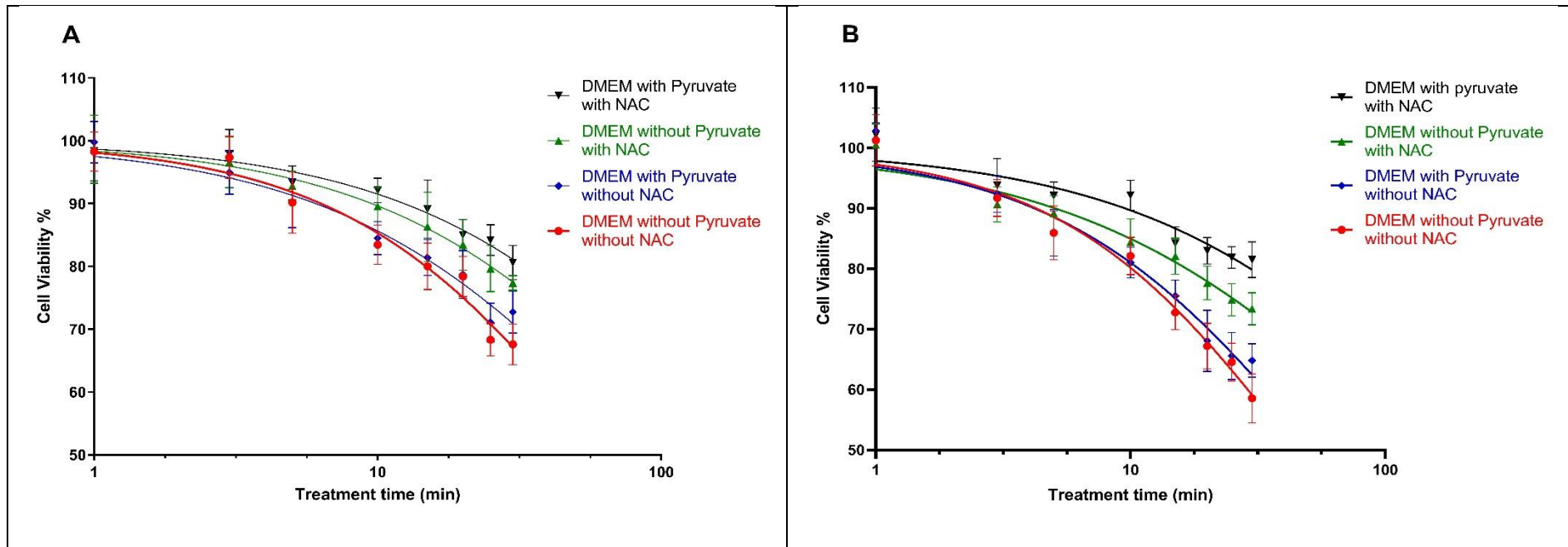


Figure 56: U-251 MG tumour sphere multiple US and PMB treatment with and without NAC and sodium pyruvate. A) Multiple PMB treatment with 24 h incubation B) multiple PMB treatment with 96 h incubation.

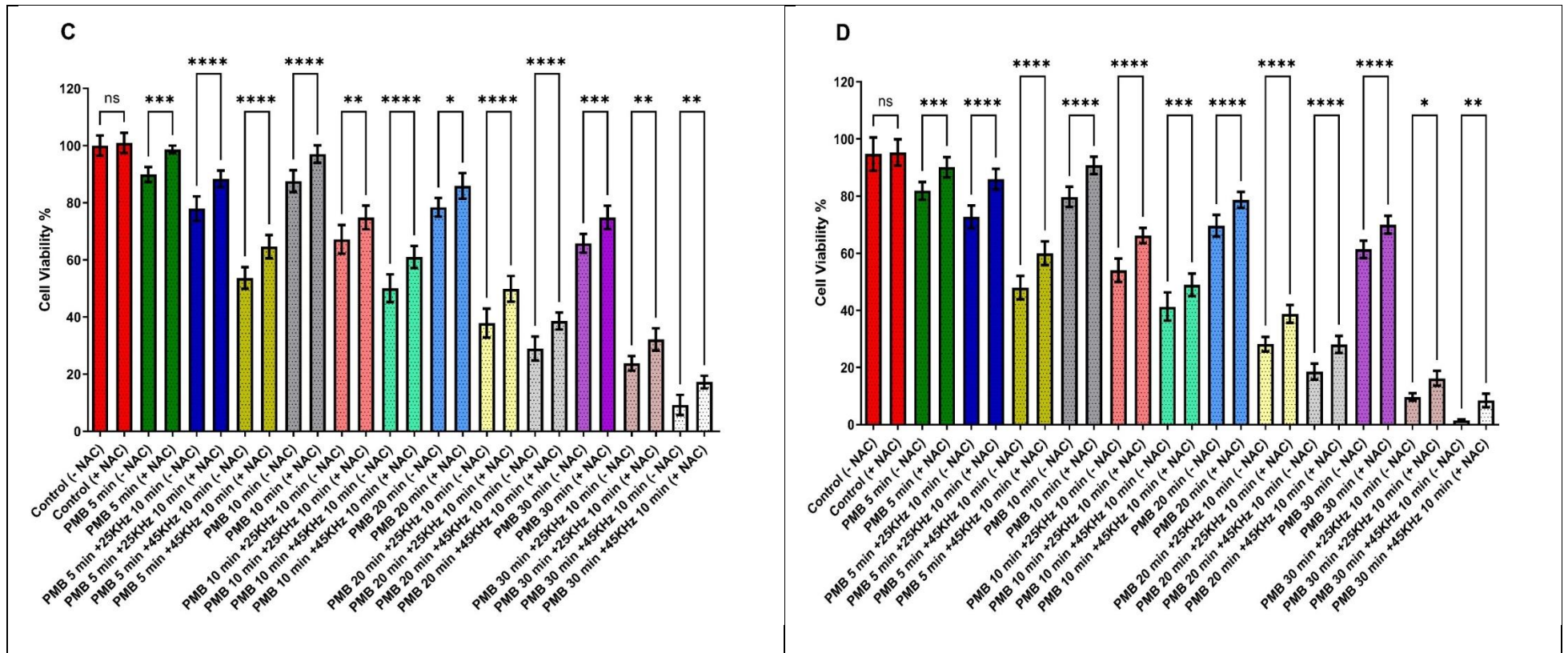


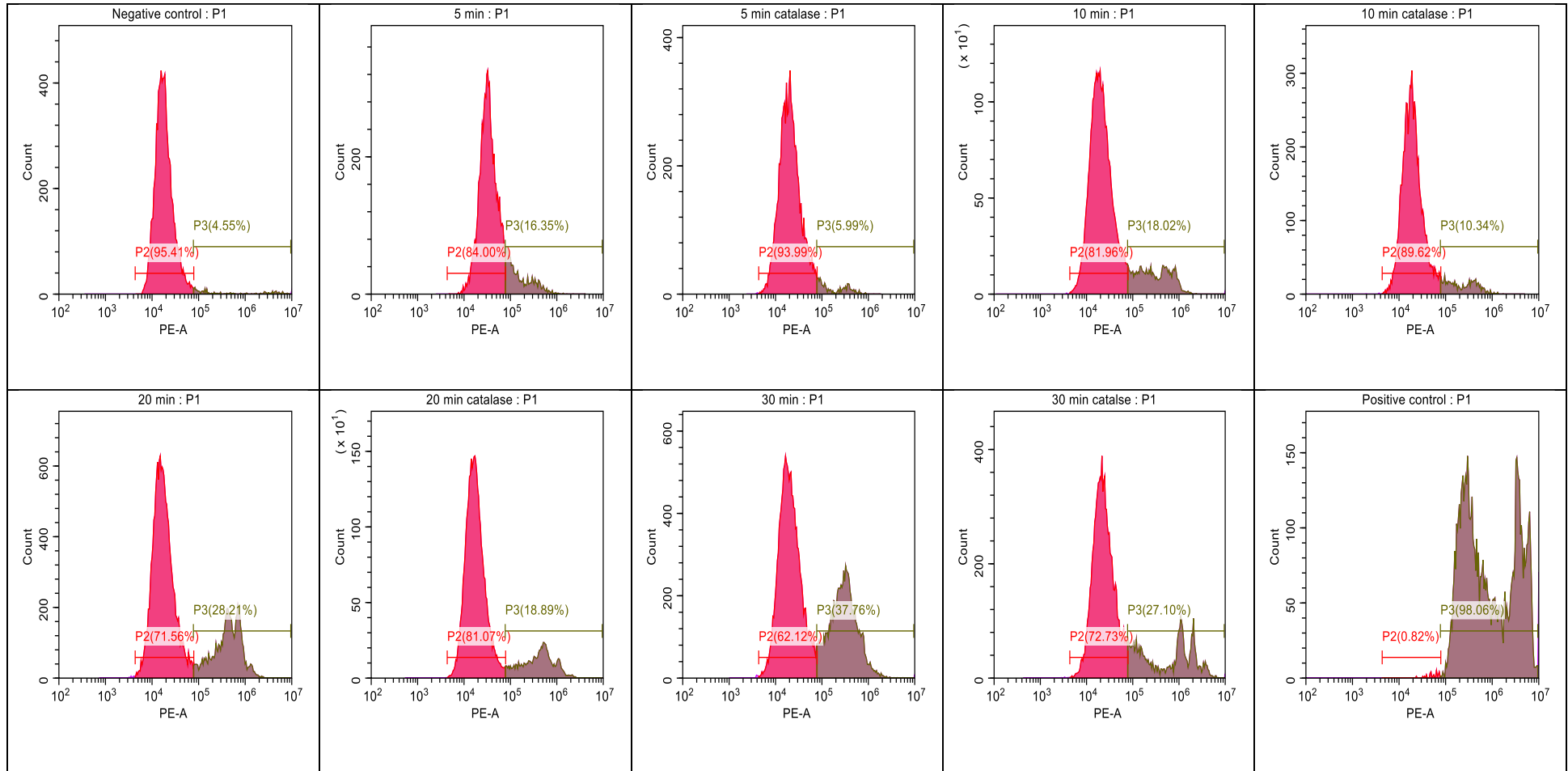
Figure 56: U-251 MG tumour sphere multiple US and PMB treatment with and without NAC and sodium pyruvate. C) synergistic cytotoxicity with different multiple US and PMB treatment with 24 h incubation D) synergistic cytotoxicity with different multiple US and PMB treatment with 96 h incubation. (ns, not significant ($p > 0.05$); $*p < 0.05$; $**p < 0.01$, $***p < 0.001$; $****p < 0.0001$).

6.2.8 Catalase as hydrogen peroxide scavenger

PI uptake was measured 24 h after a single PMB treatment (5, 10, 20, and 30 min plasma treated) and compared to PI uptake with and without catalase (Figure 57A). Catalase reduced the PI uptake to 5.9% from 16.3% with 5 min treated PMBs and to 10.3% from 18% with 10 min treated PMBs. While it significantly reduced PI uptake to 18.8% from 28.2% and to 27.1% from 37.7% with 20 min and 30 min treated PMBs, respectively (Figure 57A). There was no significant difference between 5 min treated PMBs with and without catalase, while there was a significant difference between all the other treatments with and without catalase. According to this experiment, catalase is able to slightly reverse the PMB- induced cytotoxicity, proving that hydrogen peroxide generated in the PMB generator contributes to the observed tumour sphere cytotoxicity.

Hydroxyl radicals, which emerge from the interactions of liquid with energetic electrons or excited species, are crucial components of the plasma - liquid interface process and play crucial roles in the formation of secondary reactive species [337, 415]. It has been discovered that the combination of OH radicals is responsible for the majority of the formation of H₂O₂ in plasma-liquid interactions. This occurs primarily as a result of three different pathways: the transfer of gaseous H₂O₂ (g) from the combination of gaseous OH radicals, the recombination of dissolved OH radicals, and plasma - induced UV photolysis of water [337, 415]. Consistent with our findings, researchers also reported that H₂O₂ plays an important partial role in GBM cytotoxicity induction by using 2D [113] and 3D [60, 149] cell culture models. Similar to what we discovered in our earlier research [60], we discovered that catalase was unable to provide complete protection to cells against PMB. This finding suggests that reactive species other than hydrogen peroxide also play a role in the tumour sphere's cytotoxicity.

Similar to our results, it has been proven that, plasma induced cytotoxicity in tumour sphere is depend on long lived RONS such as H_2O_2 , NO_2^- , and NO_3^- , and that these species diffuse more widely throughout the tumour sphere than short lived species, such as O_2^- , OH^\bullet , and $\text{ONOOH}/\text{ONOO}^-$ [60, 113, 149].

A

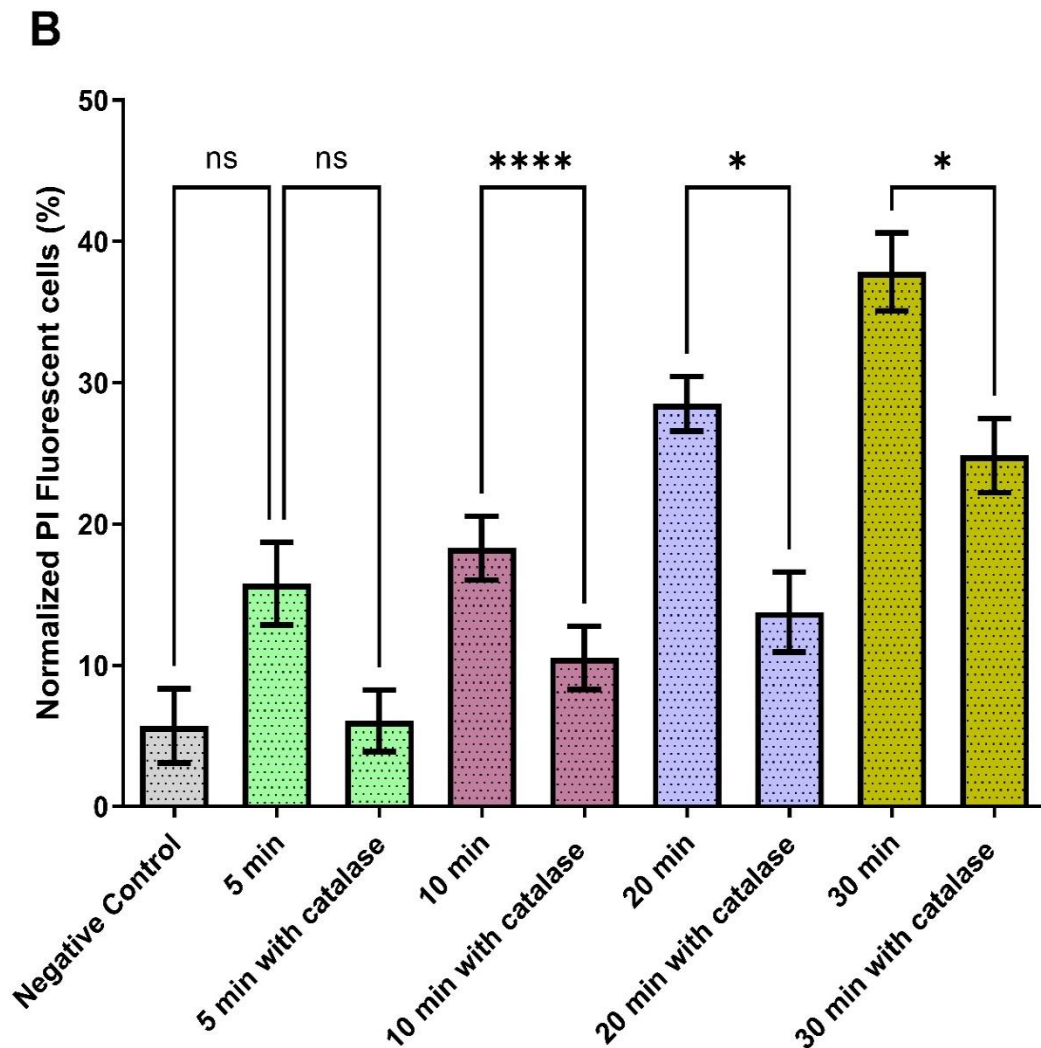
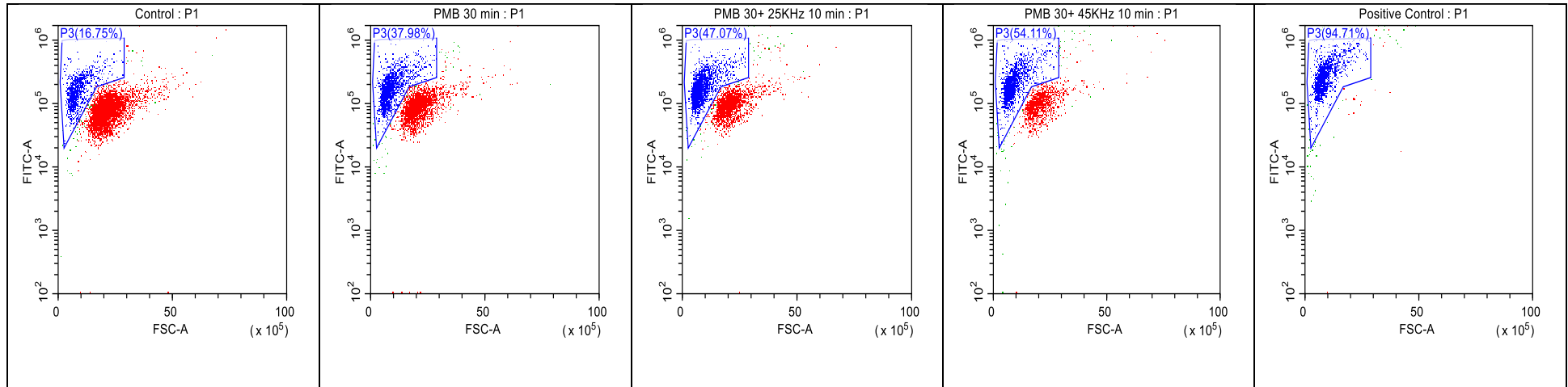
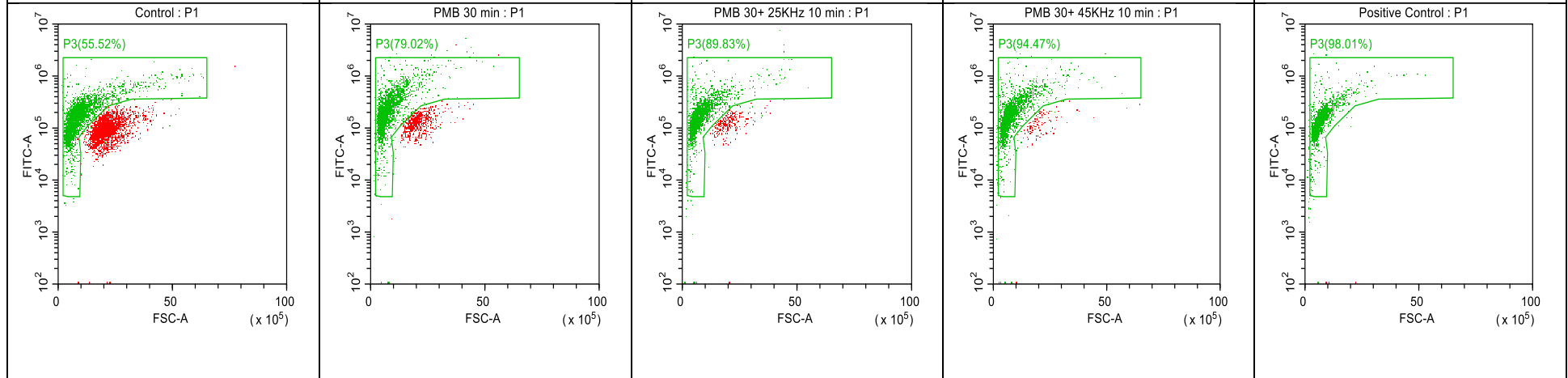


Figure 57: PI uptake in PMB treated U-251 MG tumour spheres in the presence and absence of catalase. PI uptake was measured by flow cytometry and used as an indicator of cell death. PI uptake was measured 24 h post treatment. (a) Histograms of negative control, 5, 10, 20, and 30 min plasma treated MB with and without catalase, and positive control. (b) normalized PI uptake was then measured at 24 h post treatment, represented as a bar chart and analyzed using one-way ANOVA with tukey's post-test (Appendix I). ns, not significant ($p > 0.05$); * $p \leq 0.05$; **** $p \leq 0.0001$.

6.2.9 Mitochondrial membrane potential analysis

Mitochondrial membrane potential ($\Delta\Psi_m$) is an important factor of mitochondrial function and can be an indicator of early intrinsic apoptosis. Mitochondria play an important role in ROS mediated cell death by both producing and augmenting cellular responses to reactive species [416]. The accumulation of ROS in cells can result in oxidative stress, which leads to mitochondrial dysfunction, and plasma is known to cause the loss of the mitochondrial membrane potential ($\Delta\Psi_m$). We therefore investigated whether PMB and US affected mitochondrial membrane depolarization. U-251 MG tumour spheres were stained with JC-1. To determine the changes in the JC-1 monomer / dimer mean fluorescence ratio in U-251 MG tumour spheres, 30 min of PMB treated media alone and in combination with US treatment were evaluated.

As shown in Figure 58, loss in $\Delta\Psi_m$ was observed after 96 h of post treatment incubation with only 47% and 54% cell viability, during single PMB with 25 kHz of 10 min US and single PMB with 45 kHz of 10 min US respectively (Figure 58A). During multiple treatments, 89.8% and 94.5% loss in $\Delta\Psi_m$ were observed, during multiple PMB with 25 kHz of 10 min US and multiple PMB with 45 kHz of 10 min US respectively (Figure 58B). The extent of membrane depolarization by multiple PMB with multiple 45 kHz of 10 min US was almost similar to that observed when tumour spheres are exposed to 1 mM H_2O_2 treatment as a positive control. Two-way ANOVA demonstrated that there is a significant difference in viability between the different combinations, and treatment frequencies (single and multiple) ($p < 0.0001$). A full description of tukey's multiple comparison test is provided in the Appendix I. The findings corroborate the alamarBlue and PI findings, indicating that depolarization of the mitochondria is one of the features of cell death caused by the synergistic effect of PMB and US.

A**B**

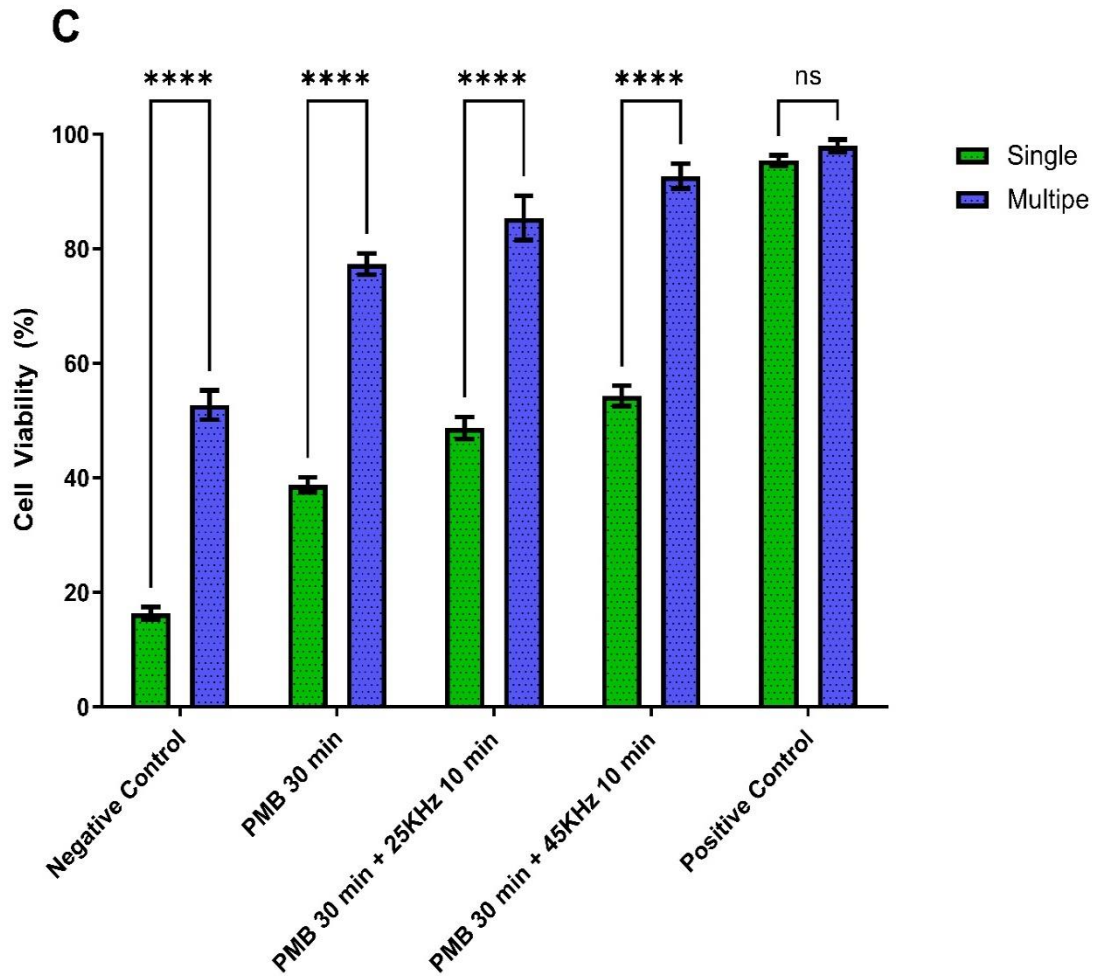


Figure 58: Mitochondrial membrane depolarisation in U-251 MG tumour spheres analysis by JC-1 dye and flow cytometry. JC-1 uptake was then measured 96 h post treatment in (A) single US and PMB treatment, (B) multiple US and PMB treatments and 1 mM H₂O₂ used as positive control. C) percentage of cell viability was then measured at 96 h post treatment, represented as a bar chart and analyzed using two-way ANOVA with tukey's post-test. ns, not significant ($p > 0.05$); **** $p \leq 0.0001$.

6.3 Conclusion

The present work highlighted the potential of PMB and US application for the treatment of GBM and epidermoid carcinoma spheroids. The combinational treatment of US and PMB can effectively induce 3D GBM and epidermoid tumour sphere cell death in a time-, dose-, treatment frequency, and ROS- dependent manner. It was also demonstrated that the synergistic treatment elicited substantial cytotoxic effects, growth metabolic decreases, damage to the tumour sphere's cell membrane, and DNA double strand breakage. Synergistic effect of PMB and US were able to significantly reduce 3D GBM spheroid regrowth and cell proliferation, while induce cytotoxicity, spheroid shrinkage, and damage to the TME. PMB induces cytotoxicity throughout the tumour sphere, likely via long lived RONS (H_2O_2 , NO_2^- , and NO_3^-) and also other reactive species, with multiple treatments augmenting this cytotoxic effect. Mitochondrial depolarization is one of the hallmarks of cell death caused by the synergistic treatment. In addition, our findings impose significant limits on the probable method required to translate US and PMB into a clinical context, with multiple treatments being favoured over a single treatment.

CHAPTER 7 - GENERAL DISCUSSION

7 General Discussion

GBM, an adult-type diffuse grade 4 glioma (IDH wild type), is the most prevalent, aggressive, fatal, highly vascularized, malignant primary brain tumour in adults with a poor prognosis [417-419]. Despite existing therapies such as surgical resection, radiation therapy and chemotherapy like TMZ, patient survival remains largely unchanged over the last three decades [52, 420, 421]. The high failure rate of clinical trials, due to inefficient treatment methods and imperfect pre-clinical models that limit our ability to predict efficacy and toxicity in humans [257, 422]. GBM remains the most difficult to treat due to various factors such as its location in the brain tissue, the existence of the BBB, GBM stem cells, multidrug resistance, complex heterogeneity, and aggressive infiltrative growth [257, 423, 424]. Novel and effective therapeutic strategies are urgently needed that can overcome GBM resistance, cross the BBB and minimize off-target side effects on patient's quality of life [257, 425]. In order to tackle the problem of inefficient treatment methods, we are exploring the potential of non - thermal techniques such as CAP and US for the treatment of GBM in this study [28, 60]. Additionally, to address the challenge posed by imperfect pre-clinical models, we have developed and employed 3D tumour spheroid models in our research [271].

In our study, we are exploring the potential of CAP as a novel therapeutic method for treating GBM [60]. CAP's ability to selectively target cancer cells compared to normal cells makes it a promising candidate for treating GBM [426]. One reason for this selectivity is that cancer cells are more sensitive to oxidative stress than normal cells [427]. Another factor is that cancer cells have a higher number of aquaporins in their membranes, which can transport higher amounts of charged particles, RONS (including hydroxyl, hydrogen peroxide, superoxide, hydroxyl radical, singlet oxygen, ozone, nitric

oxide, nitrogen dioxide, dinitrogen tetroxide, nitrogen trioxide, nitrous oxide, and peroxyxynitrite), excited atoms, electrons, free radicals, and other species produced by CAP into cancer cells compared to normal cells [60, 84, 428]. This increased concentration of RONS and oxidative stress ultimately leads to apoptosis, or programmed cell death [429, 430]. US possesses the capability of penetrating deep into the body and delivering energy to a specific location [28, 431]. Additionally, it induces inertial cavitation, resulting in sonoporation, which disrupts the bilayer of the cell membrane and forms transient pores [28, 432, 433]. This cavitation effect has been investigated for its potential to temporarily open the BBB and to enhance the anti - tumour effects [193, 434]. This approach targets several hallmarks of cancer, overcoming resistance to cell death by inducing coagulative necrosis, apoptosis, and reducing tumour growth, proliferation, invasion, and metastasis [28, 435, 436]. Moreover, it inhibits tumour neovascularization, promotes thrombosis, and prevents metastasis while also enhancing immune responses [437, 438]. Initially, we investigated the cytotoxicity induced by CAP alone, and then examined the potential of US to enhance drug diffusion, uptake, and cytotoxicity. Based on the characteristics of these two therapeutic modalities, we hypothesized that combining CAP and US would offer a promising treatment approach for GBM. We then delved further into exploring the synergistic effects of CAP and US on inducing cytotoxicity and apoptosis. Subsequently, we utilized MB devices to create PMB in a liquid medium, which we reasoned would be more effective in penetrating tissue than direct CAP treatment, and studied the synergistic effects of PMB and US. In order to tackle the second challenge, of inaccurate pre-clinical therapeutic outcomes resulting from imperfect pre-clinical models, we have optimized and implemented the use of 3D tumour spheroid models in our research [271]. A major concern is the widespread usage of models that do not consider the TME, such as the widely used 2D cell culture model [222, 439]. These 2D model that are not be able to

control tumour cell growth in natural conditions due to physiological and structural differences [440, 441]. Therefore, 3D culture systems have been developed to provide a more accurate representation of treatment outcomes under 3D conditions, resembling the nutrient and oxygen gradients and architecture of solid tumours [257, 271]. These 3D culture systems promise more accurate therapeutic models of GBM - TME, which includes unique anatomical, cellular, and molecular features of human GBM [257, 442, 443]. Ultimately, 3D cell culture can overcome the limitations of conventional 2D cell culture, and compared to animal testing, using 3D cell culture models for *in vitro* GBM treatment offers a broader selection of techniques, better measurements of outcomes, better control of variables, scalable testing, comparatively lower cost, avoidance of ethical issues, and a reductionist approach to accurately model a particular aspect of a disease [241, 444, 445].

In the third chapter of my PhD, I optimized three distinct methods for constructing *in vitro* 3D GBM tumour spheroid models and 3D epidermoid carcinoma model using both anchorage - independent and anchorage - dependent approaches [271]. These methods included low attachment plates [270], hanging drop plates [273], and cellusponge natural scaffold - based methods [279]. The objective was to closely mimic the natural *in vivo* environment, shape, and cellular response [446]. The results of the study demonstrated that these protocols were capable of developing uniform 3D tumour spheres and could facilitate the presence of heterogeneous cellular subpopulations, such as actively proliferating, quiescent, hypoxic, and necrotic cells [257, 271]. Additionally, these methods were found to be suitable for use in any laboratory conditions without the need for expensive laboratory equipment [271]. Recently, several 3D bio-mimicking human GBM cell culture models have been established employing technologies distinct from

those we investigated, including synthetic scaffolds [447, 448], hydrogels [449, 450], microfluidic devices [451, 452], 3D bio printers [453, 454]. To date, no studies have compared the appropriateness of available viability methods such as alamarBlue and CellTiter-Glo® 3D, for evaluating 3D GBM cell culture models. Additionally, many researchers have utilized image analysis techniques to evaluate cytotoxicity instead of using cell viability assays [149, 455]. Previous studies have shown that alamarBlue cell viability assays require longer incubation times when used with 3D spheroids [456]. This is due to the limited diffusion of active dyes through the matrices and reduced bioavailability, which can lead to inaccurate representation of overall cytotoxicity [271, 456, 457]. To address this issue, we converted tumour spheres into single cells prior to cell viability analysis, a technique similar to that used in flow cytometric analysis [222, 458]. Ultimately, our study found that the alamarBlue cell viability assay, using the protocols we optimized, is effective for evaluating cell viability in tumour spheres generated through anchorage - independent methods [271]. Additionally, the CellTiter-Glo® 3D cell viability assay can be used for both anchorage - dependent and -independent methods [459].

The fourth chapter aimed to address the gaps and unknowns in the efficacy of CAP treatments for 3D GBM spheroids [60]. While significant pre-clinical work has been conducted on 2D monolayer cell cultures [105, 336, 356] and an increasing number of animal models [118, 120, 460], the effectiveness of these treatments in 3D GBM spheroids remains uncertain [97, 98, 257]. Therefore, this study investigated the cytotoxicity induced by a pin-to-plate CAP device in 3D GBM tumour spheroids, representing the first attempt to fill this knowledge gap. Our decision to utilize the pin-to-plate device in this study was based on its promising therapeutic outcomes in previous

2D GBM research [87, 113, 414] and its ability to operate at atmospheric pressure and near room temperature, with low power requirements [352, 414, 461, 462]. On the other hand, the array of pins and plate electrode in this device provide a stable and diffuse discharge over the surface, making it a suitable option [414, 461, 462]. Additionally, the discharge is known to diffuse to a larger area than just the pin tip [414, 461]. This results in a focusing effect, generating a more energetic and dense plasma with a higher number of streamer channels [414, 462]. The increased gas collision and excitation rates from these channels produce higher levels of reactive species [414]. As a result, there are more opportunities for interactions between the reactive species and the treated samples, leading to faster treatment processes and enhanced cytotoxic and apoptotic outcomes [60, 113]. Our research group's prior studies indicated that the pin-to-plate reactor produced the greatest overall RONS and cytotoxicity in the plasma at a discharge frequency of 1000 Hz [113, 336]. Therefore, to assess the CAP technology's potential for 3D cell cultures, we utilized a resonant frequency of 55.51 kHz, with a discharge frequency of 1000 Hz, voltage 240 V and a duty cycle of 73 μ s [60]. To begin the CAP induce cytotoxicity studies, we compare the impact of the plasma discharge on 2D and 3D cell culture models of human GBM and epidermoid carcinoma. Our results showed that the 3D tumour spheres were more resistance to CAP compared to the 2D cell cultures [60]. 3D tumour spheres have a more complex and heterogeneous microenvironment that better mimics the *in vivo* TME [463, 464]. This complexity can result in regions of low oxygen and nutrient availability (hypoxic core), as well as enhanced intercellular interactions [257, 445, 465], which can affect the effectiveness of CAP treatment. Also, due to the architecture and cell - cell, cell - ECM interactions in spheroids can affect the uptake, penetration, and distribution of the reactive species into the core of the spheroid, making it more resistant to the CAP treatments compared to 2D cells [60, 465, 466]. Furthermore,

the 3D TME can promote the formation and maintenance of CSCs through hypoxia, nutrient deprivation, and increased intercellular interactions [467-469]. Due to this, 3D tumour spheroids have a higher numbers of CSCs compared to 2D cells [444, 470]. These self-renewing and differentiating CSCs play a crucial role in tumour initiation, progression, and therapeutic resistance [444, 471, 472]. Moreover, the GBM cell line exhibited greater treatment resistance in comparison to the epidermoid carcinoma cell lines. These findings suggest that treatment of GBM is a greater challenge compared to epidermoid carcinomas [30, 60]. The impact of a single CAP treatment on GBM tumour spheres was assessed using alamarBlue cell viability assay, and the use of sodium pyruvate, a H₂O₂ scavenger revealed differences in cytotoxic effects, suggesting the involvement of reactive species and it's activating of the Akt signalling pathway [473-475]. The study established evidence for the role of RONS in the observed cytotoxicity and concluded that pin to plate was a suitable approach for further exploration [105]. The single plasma discharge did not result in significant cytotoxicity in the tumour spheres, necessitating the use of multiple CAP treatments to achieve significantly induced cytotoxicity throughout the tumour spheres [60]. Another study involving the use of CAP also showed that multiple treatments are more effective compared to single treatments [149]. The results showed that the pin-to-plate device could induce cytotoxicity in tumour spheres and damage the tumour sphere's cell membrane in a dose- and time-dependent manner [60, 113]. There was a marked difference in the kinetic response to CAP treatment over time. Previous studies have shown that for 2D cultures, longer incubation times result in significantly more cell death compared to shorter incubation times [105]. In contrast, for 3D tumour spheres, the induced cytotoxicity after a shorter incubation time was higher and proportional to the plasma dosage but showed partial recovery from RONS damage and regrowth, similar to previous reports [121] and in contrast to cells

grown in the 2D monolayer [105]. We hypothesise that the ability of tumours to regrow during longer incubation might be due to the presence of a higher population of CSCs in tumour spheres [472, 476, 477]. However, after multiple treatments, we observed a weakening of both cell-cell and cell-ECM interactions, resulting in a higher number of dead cells detaching from the tumour sphere core [60]. This ultimately led to an inability to reform tumour spheres after multiple treatments. Our study highlights the significance of reactive species delivered by the CAP in reducing 3D GBM spheroids size similar to Maldonado et al., (2018) [149]. The results of our study shed light on the findings of Chen et al., (2017) [120] in nude mice, where CAP treatment was shown to reduce the size of GBM tumours in immuno-compromised mice [120]. It is possible that this reduction was achieved through a combination of the effects described in our work, such as damage to the TME, induction of cell death, and reduction of cell proliferation [60]. The spheroid's outer layer, which primarily consists of viable and proliferating cells, is in direct contact with the surrounding medium, gas - phase / liquid - phase reactive species from the CAP [149, 358, 478]. This exposure may increase the likelihood of initiating cell death only in the outer layer of spheroid [116, 149]. To determine whether the cytotoxic effects of the CAP are limited to the outer layer or extend throughout the spheroid, used confocal image analysis. Our findings demonstrate that the CAP is capable of diffusing RONS throughout the tumour sphere, rather than being limited solely to the surface [60, 479]. Additionally, we observed a uniform distribution of dead cells throughout the tumour sphere contradict Zhang et al., (2019)'s previous findings [116]. We measured intracellular levels of ROS and observed a significant increase as a function of treatment time. However, short-term exposure to CAP did not enhance intracellular levels of ROS [60]. Higher exposure time, on the other hand, indicated higher levels of ROS. Our extracellular analysis revealed that the CAP device produced RONS even during the shorter plasma exposures. The absence

of intracellular ROS levels for shorter exposure times suggests that intracellular antioxidants effectively reduce RONS levels when exposed to CAP [480, 481]. Therefore, short-lived reactive species that are not reduced by intracellular antioxidants may play a crucial role in the observed cytotoxic effects in GBM cells [482]. The researchers discovered that exposing cancer cells to direct CAP for a shorter duration is adequate to trigger their sensitivity to ROS and RNS in 2D cell culture [82, 84, 113]. However, in our study using 3D cell culture models, this was not observed. The analysis of ROS scavenger (NAC) and H₂O₂ scavenger (catalase) during the pin system's cytotoxicity assessment indicates that the cytotoxicity induced by the system primarily depends on RONS and its diffusion to the intracellular compartment aided by aquaporins [143, 483]. The results show that NAC effectively protected the target tumour spheres from CAP induced cytotoxicity, while catalase only slightly reverses the CAP induced cytotoxicity [60]. Ultimately, indicated that ROS plays a major role, while H₂O₂ plays a partial role in CAP induced cytotoxicity in tumour spheres [60]. This suggests that in the 3D tumour sphere model, reactive species apart from hydrogen peroxide also have a part to play, which differs from the 2D cultures [60]. In the 2D cultures, CAP treatment resulted mainly in cytotoxicity that depended on H₂O₂ [105]. It has been established that plasma induced apoptosis in tumour spheres is dependent on H₂O₂, NO₂⁻, and NO₃⁻ and that these species diffuse longer distances than short-lived species such as O₂⁻, OH^{*}, and ONOOH/ONOO⁻ [60, 219, 356]. Clinical trial carried out for treating head and neck cancer and they found that CAP treatment not only reduced contamination of ulcerations caused by the cancer but also inhibited tumour growth and resulted in visible local destruction after two weeks of treatment [163]. The CAP treatments showed low side effects and brought benefits to patients in various aspects, such as providing an easy-to-handle treatment, alleviating cancer-related pain, promoting weight gain, and potentially prolonging survival [163]. In

another study, researchers have reported successful clinical applications of CAP to treat squamous cell carcinoma patients. Tumour reductions were reported by CAP treatment, along with increased tumour decontamination and reductions in tumour mass [164]. These applications demonstrates the potential future utility of CAP in clinical trials [123].

In the fifth chapter, our study was then shifted to the investigating the impact of the US probe device's capabilities on enhancing cytotoxicity and improving GBM treatment efficiency by reducing TMZ cytotoxicity [361, 484]. Additionally, we sought to investigate the effects of sonoporation in conjunction with a theranostic agent. The research compared the effects of the US probe on human GBM and epidermoid carcinoma in both 2D and 3D cells. The US treatments were effective in inducing cell death in both 2D and 3D cells in a dose and treatment frequency dependent manner. On the contrary to the observed response during CAP treatment, the study revealed that 3D tumour spheres were more susceptible to US therapies compared to 2D cell cultures [60]. This sensitivity in 3D tumour spheres may be due to differences in cellular organization, additional dimension, polarity, and geometry [222, 257, 485]. Based on the cytotoxicity outcomes, a single exposure to US did not result in increased cytotoxicity or halt tumour regrowth in tumour spheres, similar to the previous findings with CAP [60]. However, with multiple US treatments, we were able to achieve these outcomes. Our findings indicate that US alone can induce cytotoxicity and damage the tumour sphere's cell membrane, when cells or tumour spheres are exposed to prolonged durations of US, and multiple treatments can enhance these effects. US has the ability to create transient pores in the plasma membrane, enabling the entry of molecules into the cytosol, while cells can typically withstand this process [486, 487]. However, with prolong exposure, this could be attributed to the persistent formation of pores in the membranes, weaken cell – cell

and cell – ECM interactions, resulting in lysis and eventual death of cells and damage to the tumour sphere and cells die via necrosis or programmed death [87, 363]. Additionally, in confirmation of our results, researchers found that US hindered spheroid growth, metabolic activity, disrupted spheroid integrity, and increased DNA double - strand breaks, leading to apoptosis [374, 488]. The drug delivery studies performed using diffusion-limited 3D cell culture model to investigate the induction of cytotoxicity and diffusion throughout the tumour sphere [271]. To the best of our knowledge, this is the first report on the use of the US 96 probe approach to examine drug diffusion through a tumour sphere, cellular uptake by cells within a tumour sphere, and a subsequent comparison of cytotoxicity between 3D spheroids and 2D monolayer cells.

US was able to increase the cytotoxicity with TMZ / DOX and the sensitivity was significantly enhanced after the US treatment in the 3D tumour spheroids relative to 2D cells. This results also evident the advantage of using 3D cell culture models in pre-clinical research to get accurate outcomes [257]. It was also found that there was an increase drug induce cytotoxicity in longer post-treatment incubations compared to shorter incubations. Combining TMZ / DOX with US seems to minimise this chemo-resistance and may provide a promising approach by increasing cytotoxicity [40, 375]. This enhanced effectiveness and cytotoxicity may be the result of US enhancing TMZ / DOX delivery to tumour cells by increasing cell permeability, which in turn increases drug uptake [28, 489]. On the other hand, US can induce mechanical effects, alter the cellular structure of the tumour sphere, and induce thermal effects; this could increase the ability of DOX / TMZ to cause DNA damage and initiate cell death. Additional research was conducted to investigate the US assisted sonoporation of drugs via pores in cell membranes, the uptake into tumour cells, and the dispersion throughout the tumour sphere [363]. The results indicate that US increases both the percentage of cells encountering

DOX and the quantity of DOX entering each cell. As a result, exposure to US leads to enhanced cytotoxicity in the 3D tumour spheroid models.

Following an exploration of CAP and US independently, further investigation was required to assess the synergistic cytotoxicity and apoptotic effects on 3D tumour spheroids. The objective was to determine whether the sonoporation that occurs when cells are exposed to an US field can augment the effects induced by CAP [60]. The outcome demonstrate the potential of combining CAP and US as a viable strategy for GBM therapy, with reproducible synergistic effects and also promotes higher cytotoxicity via RONS compared to CAP [60] or US [28, 87] alone, regardless of the cell line used. This study is the first to report on the potential of combining US with CAP for cancer therapy using 3D cell culture models, and opens the door for future research to validate this synergistic effect in advance models and further explore this interactions. The research focus has shifted towards mitochondrial health and the activation of specific pathways involved in programmed cell death, given our current understanding of how CAP and US work together and the contribution of RONS to their synergistic effect [399, 490]. The preliminary inhibitor studies performed using caspase, calpain - cathepsin and JNK inhibitors to determine cell death mechanism(s) involved has revealed that the single treatments of CAP and US activate the JNK signalling pathway. However, with multiple treatments, multiple pathways for cell demise are triggered, including caspase - dependent, JNK - dependent, and calpain - mediated cell death. These findings suggest that a combination treatment may induce cell death, where the involvement of caspases, calpain-cathepsins, and stress kinase is dependent on the frequency of US and CAP exposure [393-397]. The results of our study indicate that inhibition of cell proliferation and mitochondrial dysfunction in 3D tumour spheres after combined treatments. This effect may be attributed due to the accumulation of ROS produced by CAP, which induces

oxidative stress in cells. Such oxidative stress can then cause mitochondrial dysfunction [398, 399]. ROS - mediated oxidative damage has been identified as a primary mechanism of apoptosis in cancer cells [491, 492]. The promotion of apoptosis in U-251 MG cells via ROS was also investigated and reported [493]. US appears to enhance the cellular interaction of CAP by promoting sonoporation, enabling cells to uptake higher levels of RONS. Moreover, US deliver local energy to facilitate chemical reactions [28, 494], which can amplify the impact of even small quantities of RONS produced by the pin-to-plate device. Lastly, this synergistic effect can be particularly beneficial for treating GBM. Using direct pin to plate CAP device, we have demonstrated the capability to effectively inducing apoptosis in cancer cells, and have the advantage of being able to be used *in vivo* [123, 125]. Researchers are investigating the capabilities of PAM devices that generate plasma within a liquid medium, that can be administered to cancer cells [126, 127, 495, 496]. PAM device have been proven to be efficacious in stimulating apoptosis in cancer cells [126-128, 495, 496]. PAM devices have a limitation in terms of their ability to dissolve RONS in the liquid medium, which can potentially reduce their effectiveness in inducing apoptosis [495, 496].

In the sixth chapter, to address this issue, we have decided to investigate the use of a PMBs as a means to enhance the solubility of RONS in liquid phase [128, 337] and to get the added benefit of better tissue penetration capabilities [497, 498]. The interaction between plasma and liquid generates a distinctive physiochemical environment characterized by reactive species generated by the plasma [99, 499]. This, in turn, enables various chemical reactions to take place directly at the interface between the plasma and liquid, as well as indirect cascade events within the solution [337, 497]. PMB - treated

liquids can penetrate targets that cannot be directly treated with direct plasma, and they are also a safer alternative as they do not require direct exposure to high voltages [500]. In this study, US device known as the US-WB system was employed to explore the effects of various US modes and frequencies on both cytotoxicity and sonoporation [87, 432, 501]. Since the frequency of the US field can influence its impact, two different frequencies (25 kHz and 45 kHz) were tested to determine the optimal frequency [501]. Lower frequencies also increase the likelihood of cavitation [501, 502]. Additionally, a US sweep mode was employed to improve the uniformity of the US field by eliminating low performance zones, standing waves, and dead spots [503]. Similar to our previous findings with the US probe, the US-WB was also able to induce significant cytotoxicity and partially inhibit the regrowth ability of tumour spheres following multiple US treatments. We have demonstrated that higher frequencies of US, longer exposure times, and longer post - treatment incubations are favourable conditions for the cytotoxicity due to persistent pore formation in membranes, lysis, TME damage, and ultimately cell death and necrosis [87, 173, 363, 365, 412]. Subsequently, we researched the synergistic cytotoxic effects of US and PMB and we believe that we are reporting the first time of utilizing a combined US and PMB approach to induce cytotoxicity in 3D models. It has been discovered that the combined treatments of US and PMB can induce cytotoxicity and apoptosis in tumour spheres in a dose-, time-, and ROS- dependent manner. By utilizing a 3D cell culture model of GBM, scientists demonstrated that US decreased metabolic activity in spheroid growth while also increasing DNA double - strand breaks [374, 504]. The application of US alone failed to induce significant cytotoxic effects, cause damage to the cell membrane of the tumour sphere, or enhance DNA double strand breakage. However, through the utilization of multiple treatments and combining it with PMB, we were able to achieve these results. The combinational treatments, resulting in a

significant reduction in 3D GBM spheroid regrowth and cell proliferation, along with inducing cytotoxicity, spheroid shrinkage, and damage to the TME. Synergistic effect induce cytotoxicity across the entire tumour sphere, most likely by means of long - lasting RONS such as H_2O_2 , NO_2^- , and NO_3^- , as well as short-lasting species, such as O_2^- , OH^\bullet , and $\text{ONOOH}/\text{ONOO}^-$ [60, 113, 149]. Recent studies indicate that the most abundant and stable RONS are in the solution are H_2O_2 , NO_2^- , and NO_3^- [60, 379, 505]. When plasma and liquid components interact, they create cross reactions that produce short - lived molecules like ozone, superoxide anion, nitric oxide, and peroxyxynitrite anion [413, 506]. One of the key markers of cell death caused by this combined treatment is mitochondrial depolarization. Our hypothesis is that by combining PMB with US, we can enhance the effectiveness of RONS generated by the plasma - liquid interaction [337]. The RONS can dissolve through PMB and initiate chemical reactions on the outer layer of the tumour sphere, leading to cell death [60]. In addition, the US-WB can facilitate the uptake of ROS by promoting membrane opening, a process called sonoporation [433, 507]. By combining PMB with US, we can sonoporate the RONS into the core of the tumour sphere, which can induce cytotoxicity throughout the tumour sphere. This approach may be more effective than using direct plasma treatment alone, as PMB - treated liquids can penetrate targets with the assistance of US, which cannot be directly treated with direct plasma [60].

CHAPTER 8 – CONCLUSION AND FUTURE WORK

8 Conclusion and future work

8.1 Conclusion

To address the research question of inaccurate pre-clinical therapeutic outcomes resulting from imperfect pre-clinical models, my first objective was to construct and optimise different *in vitro* 3D GBM tumour spheroid models. I was able to complete this objective and integrated the usage of 3D tumour spheroid models throughout the research. Our research revealed that the optimized procedures enabled the growth of 3D tumour spheres. The optimum formation of GBM / epidermoid tumour spheroids and the highest spheroid cell health was observed after 96 h of incubation with an initial seeding density of 10,000 cells / ml using the low attachment plate method. When compared to media without serum, larger and healthier tumour spheres were grown in serum containing media. The hanging drop plate method produced the most optimal, largest, and healthiest GBM tumour spheroids after 96 h of incubation at an initial seeding density of 5,000 cells per well. For epidermoid carcinoma, the optimum, largest, and healthiest tumour spheroids were achieved after 96 h of incubation with an initial seeding density of 10,000 cells per well. On the other hand, utilizing the scaffold-based method resulted in the formation of the optimal, largest, and healthiest GBM / epidermoid tumour spheroids after 120 h of incubation at an initial seeding density of 5×10^6 cells / ml. Additionally, our research results indicated that U-87 MG displayed the greatest susceptibility to TMZ, while U-251 MG tumour spheres exhibited the highest cell viability after exposure to TMZ. Also, we discovered that alamarBlue cell viability assay is a suitable method for evaluating cell viability in tumour spheres generated through anchorage - independent techniques. Alternatively, the CellTiter-Glo® 3D cell viability assay can be used for both anchorage-dependent and independent techniques.

Then I concentrated on the research question of developing novel and more effective GBM treatment methods. My second and third objectives were to biologically characterize a novel CAP, US and PMB devices, determining its optimum settings and effectively induce cytotoxicity in 3D GBM tumour spheres. We find out that the use of CAP (alone), US (alone), and the combination of US and CAP / PMB treatments can effectively induce 3D GBM and epidermoid tumour spheroid cell death, and this effect is dependent on factors such as time, dosage, treatment frequency, and the presence of ROS. Additionally, these single or synergistic treatments were also able to significantly reduce 3D GBM spheroid regrowth cell proliferation, growth metabolic and while induce, cytotoxic effects, DNA double strand breaks, damage to the tumour sphere's cell membrane, spheroid shrinkage, and damage to the TME.

We also find out that CAP (alone), PMB (alone) and in combination of US treatments were able to induce cytotoxicity throughout the tumour sphere, likely via long - lived RONS (H_2O_2 , NO_2^- , and NO_3^-) and also other reactive species. Our findings suggest that these reactive species are crucial for inhibiting growth and inducing cytotoxicity in solid GBM tumours and are necessary to achieve sustained reduction of 3D GBM spheroids *in vitro*. In addition, our findings impose substantial limits on the anticipated methods required to translate CAP / PMB / US into a clinical context, with a strategy that favours multiple treatments over a single treatment.

My fourth objective was to evaluate the synergistic effect of CAP and US cavitation on 3D GBM models and to find out the apoptotic mechanism inducing cytotoxicity. The combination of US and CAP has a synergistic effect that leads to higher cytotoxicity in 3D tumour sphere models compared to either CAP or US alone, and this effect is dependent RONS. Our findings suggest that this combined approach has the potential to be an effective strategy for treating GBM. Single treatments of CAP and US activate the

JNK signaling pathway, while multiple treatments can trigger multiple cell demise pathways, including caspase-dependent, JNK-dependent, and calpain-mediated cell death. Moreover, our results demonstrate that the synergistic effect of CAP and US generates ROS, leading to oxidative stress and mitochondrial dysfunction. Additionally, this synergy can effectively inhibit the proliferation of 3D tumour spheres.

One of my objectives was to determine the optimum US probe device parameters for induction of cytotoxicity and US guided drug delivery to the 3D GBM models. Our study on drug delivery highlights the importance of adjusting the duration of US exposure to achieve effective drug delivery and cytotoxicity. We found that an exposure duration of less than three minutes is optimal for inducing transient sonoporation without causing damage to tumour spheres. However, when the duration of US exposure exceeds three minutes and / or the treatment frequency is increased, it results in enhanced cytotoxicity, persistent pore formation in cell membranes, lysis, leakage of cellular contents, cell inactivation, or cell death in the tumour sphere. Our study also demonstrated that combining US and TMZ enhances the cytotoxicity of GBM and epidermoid carcinoma in 3D tumour spheres compared to 2D cells. We used DOX as a reporter to show that US improves drug diffusion in 3D models and drug uptake into cells in tumour spheres, leading to enhanced cytotoxicity that is not observed in 2D culture models, where the cells are exposed to drug directly and the effects of sonoporation are minimal. These results emphasize the importance of using 3D cell culture models in preclinical research, as relying solely on 2D cell culture models followed by animal testing and clinical trials has resulted in a 95% failure rate due to inadequate prediction of human efficacy and toxicity.

8.2 Future work / new research questions

This study has identified exciting potentials of using basic 3D cell models to successfully enhance the therapeutic effectivity during pre-clinical studies involving CAP, US and PMB. It also raises several new research questions. Based on my findings during PhD research, the future focus can be shifted towards developing advanced 3D cell models that can facilitate the discovery and development of treatments for brain cancer.

8.2.1 First new research question

Microbiome play an important role in the human immune system's induction, preparation, regulation, and function, while specific microbiota may also lead to immune suppression [328, 329, 508]. Gut microbiota generates metabolites such as short chain fatty acids, which inhibit pro-inflammatory cytokine release, promote regulatory T cell growth and IL10 secretion [328, 329, 509]. A portion of the circulating short chain fatty acids may potentially enter the CNS [329]. Furthermore, the integrity of the BBB is compromised during neuro-inflammation due to the actions of IL1, IL6, and TNF α [328, 329]. It has to be established if the microbiome - induced mediators or metabolites also affect the BBB disruption and elicit immune suppression in the brain [329, 510]. The brain, glands, gut, immune cells, and gastrointestinal microbiota are all part of the microbiota – gut – brain axis. Gut microbiota also influences brain function and behaviour through neuronal, endocrine, and immunological pathways [329, 330, 510]. Researchers revealed that the gut microbiome influences the anticancer immune response and reduces the effectiveness of chemotherapeutic cancer treatment [330, 511].

The potential impact of the microbiome on brain tumour treatment techniques should be investigated with more advance 3D co-culture models with tumour-resident bacterial

strains and the first new research question will be to explore this research gap. This can be addressed by establishing standardize 3D microbiome model using 3D tumour spheres, semi permeable membranes, 3D bio printing, and CSCs. In this thesis, we have demonstrated the capability of developing *in vitro* 3D tumour spheroids and cancer stem cells using the low attachment plate, hanging drop plate, and cellusponge natural scaffold based methods and also confirmed the ability of all these methods to create uniform tumour spheres. A schematic of this 3D microbiome model, which can be developed in the future, has been indicated in Figure 59. Using my findings as a solid preliminary study, a semipermeable membrane will be able to develop to encapsulate a microbiome, allowing only metabolites to flow through the barrier into 3D cells. Further, these models will be able to be used to identify the potential impact of the microbiome on brain tumour treatment.

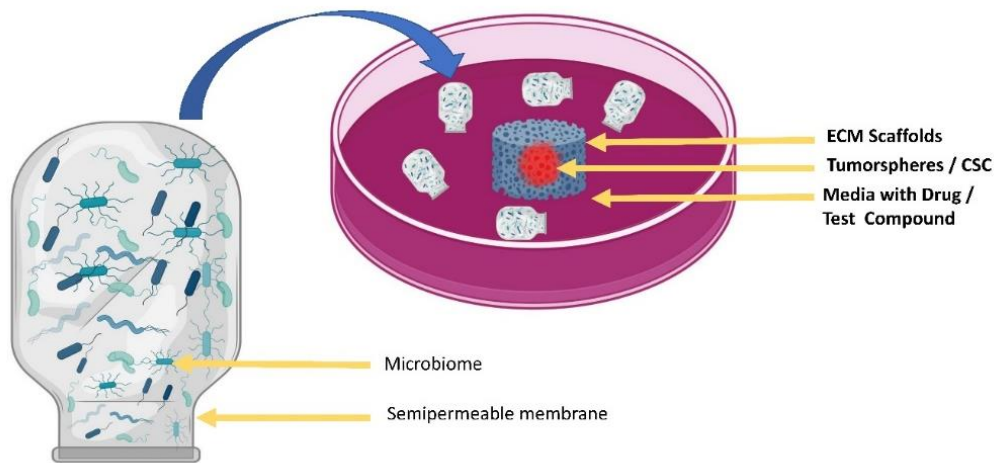


Figure 59: A schematic of the proposed 3D microbiome model.

8.2.2 Second new research question

BBB prevents several chemotherapeutic drugs from accumulating to effective concentrations in GBM and other brain tumours [512-514]. In this new research question, we will be able to develop 3D bio printed GBM and BBB models, focusing on the TME compositions of GBM and BBB, appropriate biomaterials to imitate the *in-vivo* tissue architecture, and bio - printing methodologies for model fabrication. This model will offer potential systems for more reliable mechanistic research, preclinical drug screens, excellent for therapeutic discovery and development [257]. This will be able to develop standardize vascular monolayer model (BBB model) using 3D tumour spheres, human hepatoma, 3D bio printing, 3D printers and cancer stem cells as show in Figure 60. These models will be able to use to, measure BBB permeability, study effect of BBB on drug diffusion in to GBM site and further will be able to study the application of US to enhance drug delivery through BBB using these models.

8.2.3 Third new research question

Cells in a 3D spheroids have varying microenvironment conditions due to the non-homogeneous vascular supply as extensively explained in chapter 1 [233-235, 257]. The third new research question will be to develop a standard chemical gradient 3D multicellular spheroid model to further investigate proliferation rate, drug delivery rate, interstitial pressure, perfusion, access to O₂, nutrients and acidity in different zones [220, 225, 236, 257].

8.2.4 Fourth new research question

This research has discovered the promising potentials of CAP, US, and PMB for developing novel treatments for GBM [28, 60]. As mentioned earlier, GBM is known for its resistance to treatment, which is partly attributed to the presence of CSCs [515, 516]. Exploring CSCs in GBM can yield important insights on the underlying resistance mechanisms as well as potential strategies for overcoming them [515-517]. Therefore, studying CSCs in GBM is a crucial novel field of research that has the potential to enhance our comprehension of resistance mechanisms, improve the efficacy of novel treatments, and facilitate the selection of targeted combined therapies, such as CAP and US. However, additional investigation into the combined effects of CAP and US using more advanced 3D stem cell culture models is required to fully explore their potential synergy.

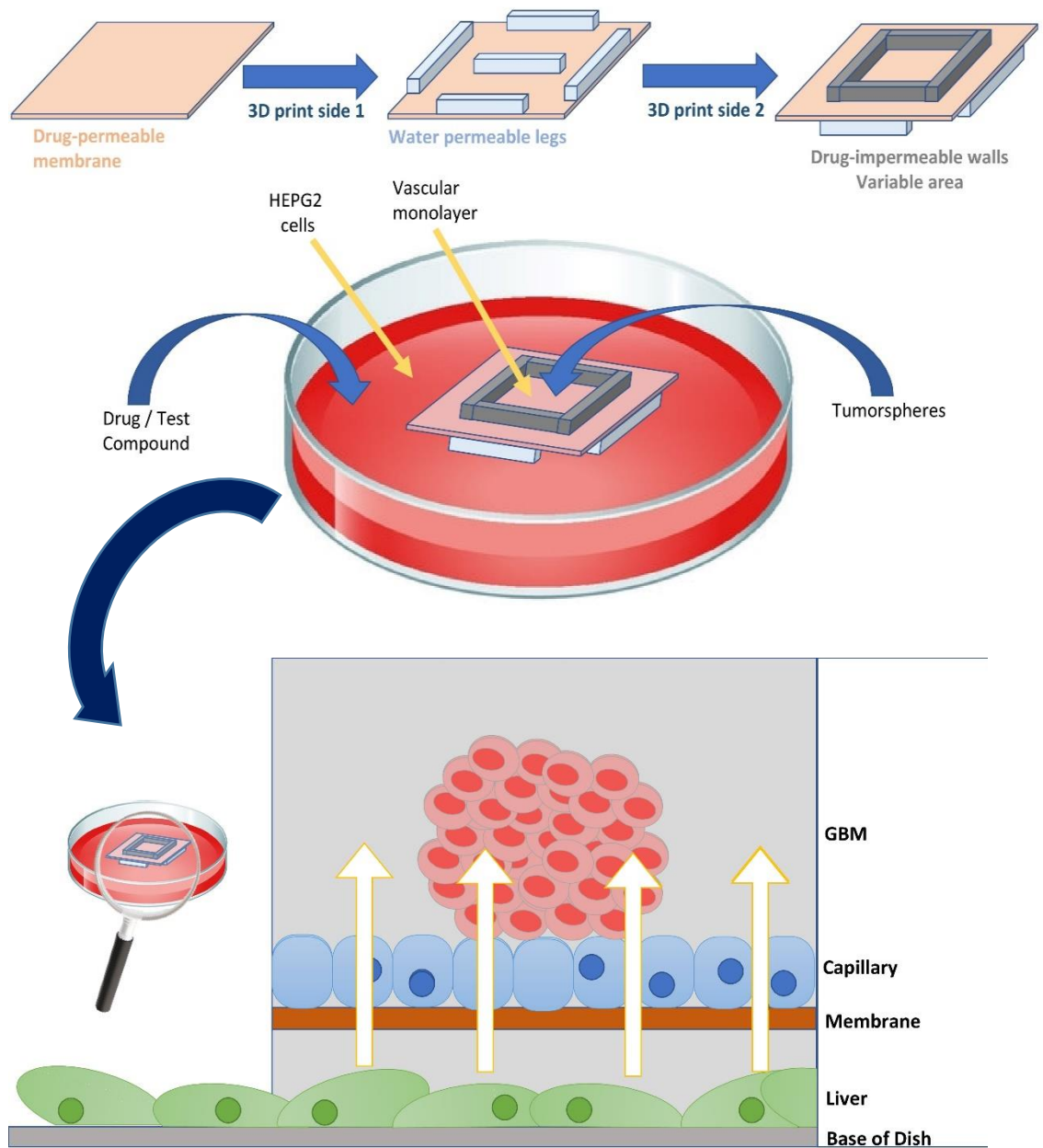


Figure 60: A schematic of the proposed standardize vascular monolayer model

References

1. WHO. Cancer. Online Available at: <<https://www.who.int/news-room/fact-sheets/detail/cancer>> (Accessed 2 February 2023). 2022.
2. Ene CI, Ferguson SD. Surgical Management of Brain Metastasis: Challenges and Nuances. *Frontiers in Oncology*. 2022;12. doi: 10.3389/fonc.2022.847110.
3. Ferlay J, Colombet M, Soerjomataram I, Parkin DM, Piñeros M, Znaor A, et al. Cancer statistics for the year 2020: An overview. *International Journal of Cancer*. 2021;149(4):778-89. doi: <https://doi.org/10.1002/ijc.33588>.
4. Hassanpour SH, Dehghani M. Review of cancer from perspective of molecular. *Journal of Cancer Research and Practice*. 2017;4(4):127-9. doi: <https://doi.org/10.1016/j.jcrpr.2017.07.001>.
5. Hanahan D. Hallmarks of Cancer: New Dimensions. *Cancer Discov*. 2022;12(1):31-46. Epub 2022/01/14. doi: 10.1158/2159-8290.Cd-21-1059. PubMed PMID: 35022204.
6. Hanahan D, Weinberg RA. The Hallmarks of Cancer. *Cell*. 2000;100(1):57-70. doi: [https://doi.org/10.1016/S0092-8674\(00\)81683-9](https://doi.org/10.1016/S0092-8674(00)81683-9).
7. Hanahan D, Weinberg RA. Hallmarks of cancer: The next generation. *Cell*. 2011;144(5):646-74. doi: 10.1016/j.cell.2011.02.013.
8. Lah TT, Novak M, Breznik B. Brain malignancies: Glioblastoma and brain metastases. *Seminars in Cancer Biology*. 2020;60:262-73. doi: <https://doi.org/10.1016/j.semcan.2019.10.010>.
9. Aldape K, Brindle KM, Chesler L, Chopra R, Gajjar A, Gilbert MR, et al. Challenges to curing primary brain tumours. *Nature Reviews Clinical Oncology*. 2019;16(8):509-20. doi: 10.1038/s41571-019-0177-5.

10. Lapointe S, Perry A, Butowski NA. Primary brain tumours in adults. *Lancet*. 2018;392(10145):432-46. Epub 2018/08/01. doi: 10.1016/s0140-6736(18)30990-5. PubMed PMID: 30060998.
11. Roda E, Bottone MG. Editorial: Brain Cancers: New Perspectives and Therapies. *Frontiers in Neuroscience*. 2022;16. doi: 10.3389/fnins.2022.857408.
12. Bi J, Chowdhry S, Wu S, Zhang W, Masui K, Mischel PS. Altered cellular metabolism in gliomas — an emerging landscape of actionable co-dependency targets. *Nature Reviews Cancer*. 2020;20(1):57-70. doi: 10.1038/s41568-019-0226-5.
13. Louis DN, Perry A, Wesseling P, Brat DJ, Cree IA, Figarella-Branger D, et al. The 2021 WHO Classification of Tumors of the Central Nervous System: a summary. *Neuro Oncol*. 2021;23(8):1231-51. Epub 2021/06/30. doi: 10.1093/neuonc/noab106. PubMed PMID: 34185076; PubMed Central PMCID: PMC8328013.
14. G ST, Biswas M, O GK, Tiwari A, H SS, Turk M, et al. A Review on a Deep Learning Perspective in Brain Cancer Classification. *Cancers (Basel)*. 2019;11(1). Epub 2019/01/24. doi: 10.3390/cancers11010111. PubMed PMID: 30669406; PubMed Central PMCID: PMC6356431.
15. Komori T. Grading of adult diffuse gliomas according to the 2021 WHO Classification of Tumors of the Central Nervous System. *Lab Invest*. 2022;102(2):126-33. Epub 2021/09/11. doi: 10.1038/s41374-021-00667-6. PubMed PMID: 34504304.
16. Ostrom QT, Cioffi G, Waite K, Kruchko C, Barnholtz-Sloan JS. CBTRUS Statistical Report: Primary Brain and Other Central Nervous System Tumors Diagnosed in the United States in 2014-2018. *Neuro Oncol*. 2021;23(12 Suppl 2):iii1-iii105. Epub 2021/10/06. doi: 10.1093/neuonc/noab200. PubMed PMID: 34608945; PubMed Central PMCID: PMC8491279.

17. Kiskova T, Kubatka P, Büsselberg D, Kassayova M. The Plant-Derived Compound Resveratrol in Brain Cancer: A Review. *Biomolecules*. 2020;10(1):161. PubMed PMID: doi:10.3390/biom10010161.
18. Mariappan A, Goranci-Buzhala G, Ricci-Vitiani L, Pallini R, Gopalakrishnan J. Trends and challenges in modeling glioma using 3D human brain organoids. *Cell Death & Differentiation*. 2021;28(1):15-23. doi: 10.1038/s41418-020-00679-7.
19. Wen PY, Weller M, Lee EQ, Alexander BM, Barnholtz-Sloan JS, Barthel FP, et al. Glioblastoma in adults: a Society for Neuro-Oncology (SNO) and European Society of Neuro-Oncology (EANO) consensus review on current management and future directions. *Neuro Oncol*. 2020;22(8):1073-113. Epub 2020/04/25. doi: 10.1093/neuonc/noaa106. PubMed PMID: 32328653; PubMed Central PMCID: PMC7594557.
20. Hanif F, Muzaffar K, Perveen K, Malhi SM, Simjee Sh U. Glioblastoma Multiforme: A Review of its Epidemiology and Pathogenesis through Clinical Presentation and Treatment. *Asian Pac J Cancer Prev*. 2017;18(1):3-9. Epub 2017/02/28. doi: 10.22034/apjcp.2017.18.1.3. PubMed PMID: 28239999; PubMed Central PMCID: PMC5563115.
21. Tamimi AF, Juweid M. Epidemiology and Outcome of Glioblastoma. In: De Vleeschouwer S, editor. *Glioblastoma*. Brisbane (AU): Codon Publications
Copyright: The Authors.; 2017.
22. Schwartzbaum JA, Fisher JL, Aldape KD, Wrensch M. Epidemiology and molecular pathology of glioma. *Nature Clinical Practice Neurology*. 2006;2(9):494-503. doi: 10.1038/ncpneuro0289.

23. Luo J, Junaid M, Hamid N, Duan J-J, Yang X, Pei D-S. Current understanding of gliomagenesis: from model to mechanism. *International Journal of Medical Sciences*. 2022;19(14):2071-9. doi: 10.7150/ijms.77287.
24. Comprehensive genomic characterization defines human glioblastoma genes and core pathways. *Nature*. 2008;455(7216):1061-8. Epub 2008/09/06. doi: 10.1038/nature07385. PubMed PMID: 18772890; PubMed Central PMCID: PMC2671642.
25. Taylor OG, Brzozowski JS, Skelding KA. Glioblastoma Multiforme: An Overview of Emerging Therapeutic Targets. *Frontiers in Oncology*. 2019;9. doi: 10.3389/fonc.2019.00963.
26. Pearson JRD, Regad T. Targeting cellular pathways in glioblastoma multiforme. *Signal Transduction and Targeted Therapy*. 2017;2(1):17040. doi: 10.1038/sigtrans.2017.40.
27. Fisher JP, Adamson DC. Current FDA-Approved Therapies for High-Grade Malignant Gliomas. *Biomedicines*. 2021;9(3). Epub 2021/04/04. doi: 10.3390/biomedicines9030324. PubMed PMID: 33810154; PubMed Central PMCID: PMC8004675.
28. Wanigasekara J, de Carvalho AMA, Cullen PJ, Tiwari B, Curtin JF. Converging technologies: targeting the hallmarks of cancer using ultrasound and microbubbles. *Trends in Cancer*. 2021. doi: <https://doi.org/10.1016/j.trecan.2021.07.004>.
29. Pardridge WM. Drug Targeting to the Brain. *Pharmaceutical Research*. 2007;24(9):1733-44. doi: 10.1007/s11095-007-9324-2.
30. Stupp R, Mason WP, van den Bent MJ, Weller M, Fisher B, Taphoorn MJB, et al. Radiotherapy plus Concomitant and Adjuvant Temozolomide for Glioblastoma. *New*

England Journal of Medicine. 2005;352(10):987-96. doi: 10.1056/NEJMoa043330.
PubMed PMID: 15758009.

31. Aparicio-Blanco J, Sanz-Arriazu L, Lorenzoni R, Blanco-Prieto MJ. Glioblastoma chemotherapeutic agents used in the clinical setting and in clinical trials: Nanomedicine approaches to improve their efficacy. *Int J Pharm.* 2020;581:119283. Epub 2020/04/03. doi: 10.1016/j.ijpharm.2020.119283. PubMed PMID: 32240807.

32. Paolillo M, Boselli C, Schinelli S. Glioblastoma under Siege: An Overview of Current Therapeutic Strategies. *Brain Sci.* 2018;8(1). Epub 2018/01/18. doi: 10.3390/brainsci8010015. PubMed PMID: 29337870; PubMed Central PMCID: PMC5789346.

33. Ohka F, Natsume A, Wakabayashi T. Current trends in targeted therapies for glioblastoma multiforme. *Neurol Res Int.* 2012;2012:878425. Epub 2012/04/25. doi: 10.1155/2012/878425. PubMed PMID: 22530127; PubMed Central PMCID: PMC3317017.

34. Davis ME. Glioblastoma: Overview of Disease and Treatment. *Clin J Oncol Nurs.* 2016;20(5 Suppl):S2-8. Epub 2016/09/27. doi: 10.1188/16.Cjon.S1.2-8. PubMed PMID: 27668386; PubMed Central PMCID: PMC5123811.

35. Sacko O, Benouaich-Amiel A, Brandicourt P, Niaré M, Charni S, Cavandoli C, et al. The Impact of Surgery on the Survival of Patients with Recurrent Glioblastoma. *Asian J Neurosurg.* 2021;16(1):1-7. Epub 2021/07/03. doi: 10.4103/ajns.AJNS_180_20. PubMed PMID: 34211860; PubMed Central PMCID: PMC8202372.

36. Anjum K, Shagufta BI, Abbas SQ, Patel S, Khan I, Shah SAA, et al. Current status and future therapeutic perspectives of glioblastoma multiforme (GBM) therapy: A review. *Biomed Pharmacother.* 2017;92:681-9. Epub 2017/06/06. doi: 10.1016/j.biopha.2017.05.125. PubMed PMID: 28582760.

37. Larson EW, Peterson HE, Lamoreaux WT, MacKay AR, Fairbanks RK, Call JA, et al. Clinical outcomes following salvage Gamma Knife radiosurgery for recurrent glioblastoma. *World J Clin Oncol.* 2014;5(2):142-8. Epub 2014/05/16. doi: 10.5306/wjco.v5.i2.142. PubMed PMID: 24829861; PubMed Central PMCID: PMC4014786.
38. Wang D, Wang C, Wang L, Chen Y. A comprehensive review in improving delivery of small-molecule chemotherapeutic agents overcoming the blood-brain/brain tumor barriers for glioblastoma treatment. *Drug Deliv.* 2019;26(1):551-65. Epub 2020/01/14. doi: 10.1080/10717544.2019.1616235. PubMed PMID: 31928355; PubMed Central PMCID: PMC6534214.
39. Lee SY. Temozolomide resistance in glioblastoma multiforme. *Genes Dis.* 2016;3(3):198-210. Epub 2016/05/11. doi: 10.1016/j.gendis.2016.04.007. PubMed PMID: 30258889; PubMed Central PMCID: PMC6150109.
40. Shaw P, Kumar N, Privat-Maldonado A, Smits E, Bogaerts A. Cold Atmospheric Plasma Increases Temozolomide Sensitivity of Three-Dimensional Glioblastoma Spheroids via Oxidative Stress-Mediated DNA Damage. *Cancers (Basel).* 2021;13(8). Epub 2021/05/01. doi: 10.3390/cancers13081780. PubMed PMID: 33917880; PubMed Central PMCID: PMC8068248.
41. Alifieris C, Trafalis DT. Glioblastoma multiforme: Pathogenesis and treatment. *Pharmacol Ther.* 2015;152:63-82. Epub 2015/05/07. doi: 10.1016/j.pharmthera.2015.05.005. PubMed PMID: 25944528.
42. Byrne KF, Pal A, Curtin JF, Stephens JC, Kinsella GK. G-protein-coupled receptors as therapeutic targets for glioblastoma. *Drug Discov Today.* 2021;26(12):2858-70. Epub 2021/07/17. doi: 10.1016/j.drudis.2021.07.008. PubMed PMID: 34271165.

43. Ghosh D, Nandi S, Bhattacharjee S. Combination therapy to checkmate Glioblastoma: clinical challenges and advances. *Clin Transl Med.* 2018;7(1):33. Epub 2018/10/18. doi: 10.1186/s40169-018-0211-8. PubMed PMID: 30327965; PubMed Central PMCID: PMC6191404.
44. Yu W, Zhang L, Wei Q, Shao A. O6-Methylguanine-DNA Methyltransferase (MGMT): Challenges and New Opportunities in Glioma Chemotherapy. *Frontiers in Oncology.* 2020;9. doi: 10.3389/fonc.2019.01547.
45. Ganipineni LP, Danhier F, Pr eat V. Drug delivery challenges and future of chemotherapeutic nanomedicine for glioblastoma treatment. *J Control Release.* 2018;281:42-57. Epub 2018/05/14. doi: 10.1016/j.jconrel.2018.05.008. PubMed PMID: 29753958.
46. Lakomy R, Kazda T, Selingerova I, Poprach A, Pospisil P, Belanova R, et al. Real-World Evidence in Glioblastoma: Stupp's Regimen After a Decade. *Frontiers in Oncology.* 2020;10. doi: 10.3389/fonc.2020.00840.
47. Kiskova T, Kubatka P, B usselberg D, Kassayova M. The Plant-Derived Compound Resveratrol in Brain Cancer: A Review. *Biomolecules.* 2020;10(1). Epub 2020/01/23. doi: 10.3390/biom10010161. PubMed PMID: 31963897; PubMed Central PMCID: PMC67023272.
48. Kesari S. Understanding glioblastoma tumor biology: the potential to improve current diagnosis and treatments. *Semin Oncol.* 2011;38 Suppl 4:S2-10. Epub 2011/12/07. doi: 10.1053/j.seminoncol.2011.09.005. PubMed PMID: 22078644.
49. Zhao M, van Straten D, Broekman MLD, Pr eat V, Schiffelers RM. Nanocarrier-based drug combination therapy for glioblastoma. *Theranostics.* 2020;10(3):1355-72. Epub 2020/01/16. doi: 10.7150/thno.38147. PubMed PMID: 31938069; PubMed Central PMCID: PMC6956816.

50. Jena L, McErlean E, McCarthy H. Delivery across the blood-brain barrier: nanomedicine for glioblastoma multiforme. *Drug Deliv Transl Res.* 2020;10(2):304-18. Epub 2019/11/16. doi: 10.1007/s13346-019-00679-2. PubMed PMID: 31728942; PubMed Central PMCID: PMC7066289.
51. Paolillo M, Schinelli S. Integrins and Exosomes, a Dangerous Liaison in Cancer Progression. *Cancers (Basel).* 2017;9(8). Epub 2017/09/22. doi: 10.3390/cancers9080095. PubMed PMID: 28933725; PubMed Central PMCID: PMC5575598.
52. Bausart M, Pr at V, Malfanti A. Immunotherapy for glioblastoma: the promise of combination strategies. *Journal of Experimental & Clinical Cancer Research.* 2022;41(1):35. doi: 10.1186/s13046-022-02251-2.
53. Alphant ry E. Nano-Therapies for Glioblastoma Treatment. *Cancers (Basel).* 2020;12(1). Epub 2020/01/23. doi: 10.3390/cancers12010242. PubMed PMID: 31963825; PubMed Central PMCID: PMC7017259.
54. Hashemi M, abbasiazam A, Oraee-Yazdani S, Lenzer J. Response of human glioblastoma cells to hyperthermia: Cellular apoptosis and molecular events. *Tissue and Cell.* 2022;75:101751. doi: <https://doi.org/10.1016/j.tice.2022.101751>.
55. Le Rhun E, Preusser M, Roth P, Reardon DA, van den Bent M, Wen P, et al. Molecular targeted therapy of glioblastoma. *Cancer Treat Rev.* 2019;80:101896. Epub 2019/09/22. doi: 10.1016/j.ctrv.2019.101896. PubMed PMID: 31541850.
56. Kessler AF, Fr mbling GE, Gross F, Hahn M, Dzokou W, Ernestus RI, et al. Effects of tumor treating fields (TTFields) on glioblastoma cells are augmented by mitotic checkpoint inhibition. *Cell Death Discov.* 2018;4:12. Epub 2018/09/14. doi: 10.1038/s41420-018-0079-9. PubMed PMID: 30210815; PubMed Central PMCID: PMC6125382.

57. Zhang H, Wang R, Yu Y, Liu J, Luo T, Fan F. Glioblastoma Treatment Modalities besides Surgery. *J Cancer*. 2019;10(20):4793-806. Epub 2019/10/11. doi: 10.7150/jca.32475. PubMed PMID: 31598150; PubMed Central PMCID: PMC6775524.
58. Hua L, Wang Z, Zhao L, Mao H, Wang G, Zhang K, et al. Hypoxia-responsive lipid-poly-(hypoxic radiosensitized polyprodrug) nanoparticles for glioma chemo- and radiotherapy. *Theranostics*. 2018;8(18):5088-105. Epub 2018/11/16. doi: 10.7150/thno.26225. PubMed PMID: 30429888; PubMed Central PMCID: PMC6217062.
59. He Z, Charleton C, Devine RW, Kelada M, Walsh JMD, Conway GE, et al. Enhanced pyrazolopyrimidinones cytotoxicity against glioblastoma cells activated by ROS-Generating cold atmospheric plasma. *Eur J Med Chem*. 2021;224:113736. Epub 2021/08/14. doi: 10.1016/j.ejmech.2021.113736. PubMed PMID: 34384944.
60. Wanigasekara J, Barcia C, Cullen PJ, Tiwari B, Curtin JF. Plasma induced reactive oxygen species-dependent cytotoxicity in glioblastoma 3D tumourspheres. *Plasma Processes and Polymers*. 2022;19(4):2100157. doi: <https://doi.org/10.1002/ppap.202100157>.
61. Sener U, Ruff MW, Campian JL. Immunotherapy in Glioblastoma: Current Approaches and Future Perspectives. *Int J Mol Sci*. 2022;23(13). Epub 2022/07/10. doi: 10.3390/ijms23137046. PubMed PMID: 35806051; PubMed Central PMCID: PMC9266573.
62. Reardon DA, Brandes AA, Omuro A, Mulholland P, Lim M, Wick A, et al. Effect of Nivolumab vs Bevacizumab in Patients With Recurrent Glioblastoma: The CheckMate 143 Phase 3 Randomized Clinical Trial. *JAMA Oncology*. 2020;6(7):1003-10. doi: 10.1001/jamaoncol.2020.1024.

63. Weller M, Butowski N, Tran DD, Recht LD, Lim M, Hirte H, et al. Rindopepimut with temozolomide for patients with newly diagnosed, EGFRvIII-expressing glioblastoma (ACT IV): a randomised, double-blind, international phase 3 trial. *The Lancet Oncology*. 2017;18(10):1373-85. doi: [https://doi.org/10.1016/S1470-2045\(17\)30517-X](https://doi.org/10.1016/S1470-2045(17)30517-X).
64. Cloughesy T, Petrecca K, Walbert T, Butowski N, Salacz M, Perry J, et al. LTBK-08. TOCA 511 & TOCA FC VERSUS STANDARD OF CARE IN PATIENTS WITH RECURRENT HIGH GRADE GLIOMA. *Neuro-Oncology*. 2019;21(Supplement_6):vi284-vi. doi: 10.1093/neuonc/noz219.1199.
65. Agrahari V. The exciting potential of nanotherapy in brain-tumor targeted drug delivery approaches. *Neural Regen Res*. 2017;12(2):197-200. Epub 2017/04/13. doi: 10.4103/1673-5374.200796. PubMed PMID: 28400793; PubMed Central PMCID: PMC5361495.
66. Chakroun RW, Zhang P, Lin R, Schiapparelli P, Quinones-Hinojosa A, Cui H. Nanotherapeutic systems for local treatment of brain tumors. *Wiley Interdiscip Rev Nanomed Nanobiotechnol*. 2018;10(1). Epub 2017/05/26. doi: 10.1002/wnan.1479. PubMed PMID: 28544801; PubMed Central PMCID: PMC5701865.
67. Glaser T, Han I, Wu L, Zeng X. Targeted Nanotechnology in Glioblastoma Multiforme. *Front Pharmacol*. 2017;8:166. Epub 2017/04/15. doi: 10.3389/fphar.2017.00166. PubMed PMID: 28408882; PubMed Central PMCID: PMC5374154.
68. Wanigasekara J, Witharana C, editors. *Applications of Nanotechnology in Drug Delivery and Design-An Insight*2016.

69. Chamindri Witharana JW. Drug Delivery Systems: A New Frontier in Nanotechnology. *International Journal of Medical Research & Health Sciences*. 2017; 6((9)):11 - 4.
70. He Z, Liu K, Byrne HJ, Cullen PJ, Tian F, Curtin JF. Chapter 8 - Combination Strategies for Targeted Delivery of Nanoparticles for Cancer Therapy. In: Mohapatra SS, Ranjan S, Dasgupta N, Mishra RK, Thomas S, editors. *Applications of Targeted Nano Drugs and Delivery Systems*: Elsevier; 2019. p. 191-219.
71. Játiva P, Ceña V. Use of nanoparticles for glioblastoma treatment: a new approach. *Nanomedicine (Lond)*. 2017;12(20):2533-54. Epub 2017/09/28. doi: 10.2217/nnm-2017-0223. PubMed PMID: 28952878.
72. He Z, Liu K, Manaloto E, Casey A, Cribaro GP, Byrne HJ, et al. Cold Atmospheric Plasma Induces ATP-Dependent Endocytosis of Nanoparticles and Synergistic U373MG Cancer Cell Death. *Scientific Reports*. 2018;8(1):5298. doi: 10.1038/s41598-018-23262-0.
73. Manaloto E, Gowen AA, Lesniak A, He Z, Casey A, Cullen PJ, et al. Cold atmospheric plasma induces silver nanoparticle uptake, oxidative dissolution and enhanced cytotoxicity in glioblastoma multiforme cells. *Archives of Biochemistry and Biophysics*. 2020;689:108462. doi: <https://doi.org/10.1016/j.abb.2020.108462>.
74. Gidwani M, Singh AV. Nanoparticle enabled drug delivery across the blood brain barrier: in vivo and in vitro models, opportunities and challenges. *Curr Pharm Biotechnol*. 2014;14(14):1201-12. Epub 2014/05/09. doi: 10.2174/1389201015666140508122558. PubMed PMID: 24809717.
75. Shin SA, Moon SY, Kim WY, Paek SM, Park HH, Lee CS. Structure-Based Classification and Anti-Cancer Effects of Plant Metabolites. *Int J Mol Sci*. 2018;19(9).

Epub 2018/09/12. doi: 10.3390/ijms19092651. PubMed PMID: 30200668; PubMed Central PMCID: PMC6163735.

76. Schmidt BM, Ribnicky DM, Lipsky PE, Raskin I. Revisiting the ancient concept of botanical therapeutics. *Nat Chem Biol.* 2007;3(7):360-6. Epub 2007/06/20. doi: 10.1038/nchembio0707-360. PubMed PMID: 17576417.

77. Gordaliza M. Natural products as leads to anticancer drugs. *Clin Transl Oncol.* 2007;9(12):767-76. Epub 2007/12/27. doi: 10.1007/s12094-007-0138-9. PubMed PMID: 18158980.

78. Fridlender M, Kapulnik Y, Koltai H. Plant derived substances with anti-cancer activity: from folklore to practice. *Front Plant Sci.* 2015;6:799. Epub 2015/10/21. doi: 10.3389/fpls.2015.00799. PubMed PMID: 26483815; PubMed Central PMCID: PMC4589652.

79. Muniraj N, Siddharth S, Sharma D. Bioactive Compounds: Multi-Targeting Silver Bullets for Preventing and Treating Breast Cancer. *Cancers (Basel).* 2019;11(10). Epub 2019/10/18. doi: 10.3390/cancers11101563. PubMed PMID: 31618928; PubMed Central PMCID: PMC6826729.

80. Luo H, Vong CT, Chen H, Gao Y, Lyu P, Qiu L, et al. Naturally occurring anti-cancer compounds: shining from Chinese herbal medicine. *Chinese Medicine.* 2019;14(1):48. doi: 10.1186/s13020-019-0270-9.

81. George BP, Abrahamse H. Increased Oxidative Stress Induced by Rubus Bioactive Compounds Induce Apoptotic Cell Death in Human Breast Cancer Cells. *Oxid Med Cell Longev.* 2019;2019:6797921. Epub 2019/07/10. doi: 10.1155/2019/6797921. PubMed PMID: 31281587; PubMed Central PMCID: PMC6589211.

82. Yan D, Cui H, Zhu W, Nourmohammadi N, Milberg J, Zhang LG, et al. The Specific Vulnerabilities of Cancer Cells to the Cold Atmospheric Plasma-Stimulated Solutions. *Scientific Reports*. 2017;7(1):4479. doi: 10.1038/s41598-017-04770-x.
83. Semmler ML, Bekeschus S, Schäfer M, Bernhardt T, Fischer T, Witzke K, et al. Molecular Mechanisms of the Efficacy of Cold Atmospheric Pressure Plasma (CAP) in Cancer Treatment. *Cancers (Basel)*. 2020;12(2). Epub 2020/01/26. doi: 10.3390/cancers12020269. PubMed PMID: 31979114; PubMed Central PMCID: PMC7072164.
84. Yan D, Sherman JH, Keidar M. Cold atmospheric plasma, a novel promising anti-cancer treatment modality. *Oncotarget*. 2017;8(9):15977-95. Epub 2016/11/16. doi: 10.18632/oncotarget.13304. PubMed PMID: 27845910; PubMed Central PMCID: PMC5362540.
85. Conway GE, Casey A, Milosavljevic V, Liu Y, Howe O, Cullen PJ, et al. Non-thermal atmospheric plasma induces ROS-independent cell death in U373MG glioma cells and augments the cytotoxicity of temozolomide. *British Journal of Cancer*. 2016;114(4):435-43. doi: 10.1038/bjc.2016.12.
86. Fridman G, Friedman G, Gutsol A, Shekhter AB, Vasilets VN, Fridman A. Applied Plasma Medicine. *Plasma Processes and Polymers*. 2008;5(6):503-33. doi: <https://doi.org/10.1002/ppap.200700154>.
87. Aguiar de Carvalho AM, Scally L, Tiwari B, Cullen PJ, Curtin JF. Synergistic cytotoxicity from cold atmospheric plasma and ultrasound in glioma cells. *Plasma Processes and Polymers*. 2022;19(8):2200042. doi: <https://doi.org/10.1002/ppap.202200042>.
88. He Z, Liu K, Scally L, Manaloto E, Gunes S, Ng SW, et al. Cold Atmospheric Plasma Stimulates Clathrin-Dependent Endocytosis to Repair Oxidised Membrane and

Enhance Uptake of Nanomaterial in Glioblastoma Multiforme Cells. *Scientific Reports*. 2020;10(1):6985. doi: 10.1038/s41598-020-63732-y.

89. Heinlin J, Morfill G, Landthaler M, Stolz W, Isbary G, Zimmermann JL, et al. Plasma medicine: possible applications in dermatology. *J Dtsch Dermatol Ges*. 2010;8(12):968-76. Epub 2010/08/20. doi: 10.1111/j.1610-0387.2010.07495.x. PubMed PMID: 20718902.

90. Bernhardt T, Semmler ML, Schäfer M, Bekeschus S, Emmert S, Boeckmann L. Plasma Medicine: Applications of Cold Atmospheric Pressure Plasma in Dermatology. *Oxid Med Cell Longev*. 2019;2019:3873928. Epub 2019/10/01. doi: 10.1155/2019/3873928. PubMed PMID: 31565150; PubMed Central PMCID: PMC6745145 publication of this paper.

91. Roman H, Auber M, Bourdel N, Martin C, Marpeau L, Puscasiu L. Postoperative recurrence and fertility after endometrioma ablation using plasma energy: retrospective assessment of a 3-year experience. *J Minim Invasive Gynecol*. 2013;20(5):573-82. Epub 2013/06/14. doi: 10.1016/j.jmig.2013.02.016. PubMed PMID: 23759693.

92. Deb S, Deen S, Ashford KS, Harwood A, Newman C, Powell MC. Histological quantification of the tissue damage caused by PlasmaJet™ coagulator. *Gynecological Surgery*. 2010;7(4):441-6. doi: 10.1007/s10397-010-0582-3.

93. Nezhat C, Kho KA, Morozov V. Use of neutral argon plasma in the laparoscopic treatment of endometriosis. *Jsls*. 2009;13(4):479-83. Epub 2010/03/06. doi: 10.4293/108680809x12589998403967. PubMed PMID: 20202387; PubMed Central PMCID: PMC3030779.

94. Sagawa T, Takayama T, Oku T, Hayashi T, Ota H, Okamoto T, et al. Argon plasma coagulation for successful treatment of early gastric cancer with intramucosal

invasion. *Gut*. 2003;52(3):334-9. Epub 2003/02/14. doi: 10.1136/gut.52.3.334. PubMed PMID: 12584212; PubMed Central PMCID: PMCPMC1773547.

95. Kang W-S, Hong Y-C, Hong Y-B, Kim J-H, Uhm HS. Atmospheric-pressure cold plasma jet for medical applications. *Surface and Coatings Technology*. 2010;205:S418-S21. doi: <https://doi.org/10.1016/j.surfcoat.2010.08.138>.

96. Keidar M, Yan D, Sherman JH. *Cold Plasma Cancer Therapy*: Morgan & Claypool Publishers; 2019. Available from: <https://dx.doi.org/10.1088/2053-2571/aafb9c>.

97. Brany D, Dvorska D, Halasova E, Skovierova H. Cold Atmospheric Plasma: A Powerful Tool for Modern Medicine. *International Journal of Molecular Sciences*. 2020;21(8). doi: 10.3390/ijms21082932. PubMed PMID: WOS:000535565300274.

98. Dai XF, Bazaka K, Thompson EW, Ostrikov K. Cold Atmospheric Plasma: A Promising Controller of Cancer Cell States. *Cancers*. 2020;12(11). doi: 10.3390/cancers12113360. PubMed PMID: WOS:000592769600001.

99. Rezaei F, Vanraes P, Nikiforov A, Morent R, De Geyter N. Applications of Plasma-Liquid Systems: A Review. *Materials (Basel)*. 2019;12(17). Epub 2019/08/30. doi: 10.3390/ma12172751. PubMed PMID: 31461960; PubMed Central PMCID: PMCPMC6747786.

100. Keidar M, Walk R, Shashurin A, Srinivasan P, Sandler A, Dasgupta S, et al. Cold plasma selectivity and the possibility of a paradigm shift in cancer therapy. *British Journal of Cancer*. 2011;105(9):1295-301. doi: 10.1038/bjc.2011.386.

101. Zelzer M, Albutt D, Alexander MR, Russell NA. The Role of Albumin and Fibronectin in the Adhesion of Fibroblasts to Plasma Polymer Surfaces. *Plasma Processes and Polymers*. 2012;9(2):149-56. doi: <https://doi.org/10.1002/ppap.201100054>.

102. Isbary G, Heinlin J, Shimizu T, Zimmermann JL, Morfill G, Schmidt H-U, et al. Successful and safe use of 2 min cold atmospheric argon plasma in chronic wounds: results of a randomized controlled trial. *British Journal of Dermatology*. 2012;167(2):404-10. doi: <https://doi.org/10.1111/j.1365-2133.2012.10923.x>.
103. Kalghatgi S, Friedman G, Fridman A, Clyne AM. Endothelial Cell Proliferation is Enhanced by Low Dose Non-Thermal Plasma Through Fibroblast Growth Factor-2 Release. *Annals of Biomedical Engineering*. 2010;38(3):748-57. doi: 10.1007/s10439-009-9868-x.
104. Shi L, Ito F, Wang Y, Okazaki Y, Tanaka H, Mizuno M, et al. Non-thermal plasma induces a stress response in mesothelioma cells resulting in increased endocytosis, lysosome biogenesis and autophagy. *Free Radic Biol Med*. 2017;108:904-17. Epub 2017/05/04. doi: 10.1016/j.freeradbiomed.2017.04.368. PubMed PMID: 28465262.
105. de Carvalho AMA, Behan S, Scally L, Sarangapani C, Malone R, Cullen P, et al. Pin Electrode Reactor: A novel cold atmospheric plasma device and its potential in glioblastoma treatment. *bioRxiv*; 2021.
106. Wanigasekara J, Barcia C, Cullen PJ, Tiwari B, Curtin JF. Plasma induced reactive oxygen species-dependent cytotoxicity in glioblastoma 3D tumourspheres. *Plasma Processes and Polymers*. doi: 10.1002/ppap.202100157. PubMed PMID: WOS:000739177800001.
107. Kong MG, Keidar M, Ostrikov K. Plasmas meet nanoparticles—where synergies can advance the frontier of medicine. *Journal of Physics D: Applied Physics*. 2011;44(17):174018. doi: 10.1088/0022-3727/44/17/174018.
108. Babington P, Rajjoub K, Canady J, Siu A, Keidar M, Sherman JH. Use of cold atmospheric plasma in the treatment of cancer. *Biointerphases*. 2015;10(2):029403. doi: 10.1116/1.4915264.

109. Recek N, Cheng X, Keidar M, Cvelbar U, Vesel A, Mozetic M, et al. Effect of Cold Plasma on Glial Cell Morphology Studied by Atomic Force Microscopy. *PLOS ONE*. 2015;10(3):e0119111. doi: 10.1371/journal.pone.0119111.
110. Stoffels E, Sakiyama Y, Graves DB. Cold Atmospheric Plasma: Charged Species and Their Interactions With Cells and Tissues. *IEEE Transactions on Plasma Science*. 2008;36(4):1441-57. doi: 10.1109/TPS.2008.2001084.
111. Park SR, Lee HW, Hong JW, Lee HJ, Kim JY, Choi Bb-r, et al. Enhancement of the killing effect of low-temperature plasma on *Streptococcus mutans* by combined treatment with gold nanoparticles. *Journal of Nanobiotechnology*. 2014;12(1):29. doi: 10.1186/s12951-014-0029-5.
112. Ulfig A, Leichert LI. The effects of neutrophil-generated hypochlorous acid and other hypohalous acids on host and pathogens. *Cell Mol Life Sci*. 2021;78(2):385-414. Epub 2020/07/15. doi: 10.1007/s00018-020-03591-y. PubMed PMID: 32661559; PubMed Central PMCID: PMC7873122.
113. de Carvalho AMA, Behan S, Scally L, Sarangapani C, Malone R, Cullen PJ, et al. Pin Electrode Reactor: A novel cold atmospheric plasma device and its potential in glioblastoma treatment. *bioRxiv*. 2021:2021.01.08.425903. doi: 10.1101/2021.01.08.425903.
114. Malyavko A, Yan D, Wang Q, Klein AL, Patel KC, Sherman JH, et al. Cold atmospheric plasma cancer treatment, direct versus indirect approaches. *Materials Advances*. 2020;1(6):1494-505. doi: 10.1039/D0MA00329H.
115. Liedtke KR, Diedrich S, Pati O, Freund E, Flieger R, Heidecke CD, et al. Cold Physical Plasma Selectively Elicits Apoptosis in Murine Pancreatic Cancer Cells In Vitro and In Ovo. *Anticancer Res*. 2018;38(10):5655-63. Epub 2018/10/03. doi: 10.21873/anticancerres.12901. PubMed PMID: 30275184.

116. Zhang H, Zhang J, Liu Z, Xu D, Guo L, Liu D, et al. Evaluation of the anticancer effects induced by cold atmospheric plasma in 2D and 3D cell-culture models. *Plasma Processes and Polymers*. 2019;16(12). doi: 10.1002/ppap.201900072.
117. Zhang J, Liu D, Zhang H, Xia W, Liu Y, Sun B, et al. Influence of liquid coverage on the anticancer effects of a helium plasma jet on 3D tumor spheroids. *Plasma Processes and Polymers*. 2020;17(7). doi: 10.1002/ppap.201900213.
118. Pasqual-Melo G, Nascimento T, Sanches LJ, Blegniski FP, Bianchi JK, Sagwal SK, et al. Plasma Treatment Limits Cutaneous Squamous Cell Carcinoma Development In Vitro and In Vivo. *Cancers*. 2020;12(7). doi: 10.3390/cancers12071993.
119. Szili EJ, Oh J-S, Fukuhara H, Bhatia R, Gaur N, Nguyen CK, et al. Modelling the helium plasma jet delivery of reactive species into a 3D cancer tumour. *Plasma Sources Science and Technology*. 2017;27(1). doi: 10.1088/1361-6595/aa9b3b.
120. Chen Z, Simonyan H, Cheng X, Gjika E, Lin L, Canady J, et al. A Novel Micro Cold Atmospheric Plasma Device for Glioblastoma Both In Vitro and In Vivo. *Cancers (Basel)*. 2017;9(6). Epub 2017/05/31. doi: 10.3390/cancers9060061. PubMed PMID: 28555065; PubMed Central PMCID: PMC5483880.
121. Karki SB, Gupta TT, Yildirim-Ayan E, Eisenmann KM, Ayan H. Investigation of non-thermal plasma effects on lung cancer cells within 3D collagen matrices. *Journal of Physics D: Applied Physics*. 2017;50(31). doi: 10.1088/1361-6463/aa7b10.
122. Emelyanov OA, Feklistov EG, Smirnova NV, Kolbe KA, Zinoviev EV, Asadulaev MS, et al. Corona discharge plasma application for in vitro modulation of fibroblast proliferation and wound healing. *AIP Conference Proceedings*. 2019;2179(1):020006. doi: 10.1063/1.5135479.
123. Faramarzi F, Zafari P, Alimohammadi M, Moonesi M, Rafiei A, Bekeschus S. Cold Physical Plasma in Cancer Therapy: Mechanisms, Signaling, and Immunity. *Oxid*

Med Cell Longev. 2021;2021:9916796. Epub 2022/03/15. doi: 10.1155/2021/9916796.

PubMed PMID: 35284036; PubMed Central PMCID: PMCPMC8906949 this article.

124. Bekeschus S, Schmidt A, Weltmann K-D, von Woedtke T. The plasma jet kINPen – A powerful tool for wound healing. *Clinical Plasma Medicine*. 2016;4(1):19-28. doi: <https://doi.org/10.1016/j.cpme.2016.01.001>.

125. Xu D, Ning N, Xu Y, Xia W, Liu D, Chen H, et al. Effect of He Plasma Jet Versus Surface Plasma on the Metabolites of Acute Myeloid Leukemia Cells. *Front Oncol*. 2021;11:552480. Epub 2021/04/06. doi: 10.3389/fonc.2021.552480. PubMed PMID: 33816218; PubMed Central PMCID: PMCPMC8010173.

126. Azzariti A, Iacobazzi RM, Di Fonte R, Porcelli L, Gristina R, Favia P, et al. Plasma-activated medium triggers cell death and the presentation of immune activating danger signals in melanoma and pancreatic cancer cells. *Scientific Reports*. 2019;9(1):4099. doi: 10.1038/s41598-019-40637-z.

127. Utsumi F, Kajiyama H, Nakamura K, Tanaka H, Mizuno M, Ishikawa K, et al. Effect of Indirect Nonequilibrium Atmospheric Pressure Plasma on Anti-Proliferative Activity against Chronic Chemo-Resistant Ovarian Cancer Cells In Vitro and In Vivo. *PLOS ONE*. 2013;8(12):e81576. doi: 10.1371/journal.pone.0081576.

128. Rao NRH, Chu X, Hadinoto K, Angelina, Zhou R, Zhang T, et al. Algal cell inactivation and damage via cold plasma-activated bubbles: Mechanistic insights and process benefits. *Chemical Engineering Journal*. 2023;454:140304. doi: <https://doi.org/10.1016/j.cej.2022.140304>.

129. Keidar M, Yan D, Beilis, II, Trink B, Sherman JH. Plasmas for Treating Cancer: Opportunities for Adaptive and Self-Adaptive Approaches. *Trends Biotechnol*. 2018;36(6):586-93. Epub 2017/08/02. doi: 10.1016/j.tibtech.2017.06.013. PubMed PMID: 28755977.

130. Kim GJ, Kim W, Kim KT, Lee JK. DNA damage and mitochondria dysfunction in cell apoptosis induced by nonthermal air plasma. *Applied Physics Letters*. 2010;96(2):021502. doi: 10.1063/1.3292206.
131. Biscop E, Lin A, Boxem WV, Loenhout JV, Backer J, Deben C, et al. Influence of Cell Type and Culture Medium on Determining Cancer Selectivity of Cold Atmospheric Plasma Treatment. *Cancers (Basel)*. 2019;11(9). Epub 2019/09/05. doi: 10.3390/cancers11091287. PubMed PMID: 31480642; PubMed Central PMCID: PMC6770138.
132. Köritzer J, Boxhammer V, Schäfer A, Shimizu T, Klämpfl TG, Li YF, et al. Restoration of sensitivity in chemo-resistant glioma cells by cold atmospheric plasma. *PLoS One*. 2013;8(5):e64498. Epub 2013/05/25. doi: 10.1371/journal.pone.0064498. PubMed PMID: 23704990; PubMed Central PMCID: PMC3660344.
133. Siu A, Volotskova O, Cheng X, Khalsa SS, Bian K, Murad F, et al. Differential Effects of Cold Atmospheric Plasma in the Treatment of Malignant Glioma. *PLOS ONE*. 2015;10(6):e0126313. doi: 10.1371/journal.pone.0126313.
134. Yoshikawa N, Liu W, Nakamura K, Yoshida K, Ikeda Y, Tanaka H, et al. Plasma-activated medium promotes autophagic cell death along with alteration of the mTOR pathway. *Scientific Reports*. 2020;10(1):1614. doi: 10.1038/s41598-020-58667-3.
135. Akter M, Jangra A, Choi SA, Choi EH, Han I. Non-Thermal Atmospheric Pressure Bio-Compatible Plasma Stimulates Apoptosis via p38/MAPK Mechanism in U87 Malignant Glioblastoma. *Cancers (Basel)*. 2020;12(1). Epub 2020/01/23. doi: 10.3390/cancers12010245. PubMed PMID: 31963881; PubMed Central PMCID: PMC7016658.
136. Li W, Yu KN, Bao L, Shen J, Cheng C, Han W. Non-thermal plasma inhibits human cervical cancer HeLa cells invasiveness by suppressing the MAPK pathway and

decreasing matrix metalloproteinase-9 expression. *Scientific Reports*. 2016;6(1):19720. doi: 10.1038/srep19720.

137. Min T, Xie X, Ren K, Sun T, Wang H, Dang C, et al. Therapeutic Effects of Cold Atmospheric Plasma on Solid Tumor. *Frontiers in Medicine*. 2022;9. doi: 10.3389/fmed.2022.884887.

138. Tanaka H, Mizuno M, Ishikawa K, Toyokuni S, Kajiyama H, Kikkawa F, et al. Molecular mechanisms of non-thermal plasma-induced effects in cancer cells. *Biol Chem*. 2018;400(1):87-91. Epub 2018/10/07. doi: 10.1515/hsz-2018-0199. PubMed PMID: 30291778.

139. Ayoub NM, Jaradat SK, Al-Shami KM, Alkhalifa AE. Targeting Angiogenesis in Breast Cancer: Current Evidence and Future Perspectives of Novel Anti-Angiogenic Approaches. *Front Pharmacol*. 2022;13:838133. Epub 2022/03/15. doi: 10.3389/fphar.2022.838133. PubMed PMID: 35281942; PubMed Central PMCID: PMC8913593.

140. Haralambiev L, Neuffer O, Nitsch A, Kross NC, Bekeschus S, Hinz P, et al. Inhibition of Angiogenesis by Treatment with Cold Atmospheric Plasma as a Promising Therapeutic Approach in Oncology. *Int J Mol Sci*. 2020;21(19). Epub 2020/10/01. doi: 10.3390/ijms21197098. PubMed PMID: 32993057; PubMed Central PMCID: PMC7582386.

141. Liu H, Qiu W, Sun T, Wang L, Du C, Hu Y, et al. Therapeutic strategies of glioblastoma (GBM): The current advances in the molecular targets and bioactive small molecule compounds. *Acta Pharmaceutica Sinica B*. 2022;12(4):1781-804. doi: <https://doi.org/10.1016/j.apsb.2021.12.019>.

142. Yan D, Talbot A, Nourmohammadi N, Sherman JH, Cheng X, Keidar M. Toward understanding the selective anticancer capacity of cold atmospheric plasma—A model

based on aquaporins (Review). *Biointerphases*. 2015;10(4):040801. doi: 10.1116/1.4938020.

143. Yan D, Xiao H, Zhu W, Nourmohammadi N, Zhang LG, Bian K, et al. The role of aquaporins in the anti-glioblastoma capacity of the cold plasma-stimulated medium. *Journal of Physics D: Applied Physics*. 2017;50(5):055401. doi: 10.1088/1361-6463/aa53d6.

144. Agre P, King LS, Yasui M, Guggino WB, Ottersen OP, Fujiyoshi Y, et al. Aquaporin water channels – from atomic structure to clinical medicine. *The Journal of Physiology*. 2002;542(1):3-16. doi: <https://doi.org/10.1113/jphysiol.2002.020818>.

145. Wu B, Beitz E. Aquaporins with selectivity for unconventional permeants. *Cellular and Molecular Life Sciences*. 2007;64(18):2413-21. doi: 10.1007/s00018-007-7163-2.

146. Almasalmeh A, Krenc D, Wu B, Beitz E. Structural determinants of the hydrogen peroxide permeability of aquaporins. *The FEBS Journal*. 2014;281(3):647-56. doi: <https://doi.org/10.1111/febs.12653>.

147. de Meyer F, Smit B. Effect of cholesterol on the structure of a phospholipid bilayer. *Proceedings of the National Academy of Sciences*. 2009;106(10):3654-8. doi: doi:10.1073/pnas.0809959106.

148. Chiu SW, Jakobsson E, Mashl RJ, Scott HL. Cholesterol-Induced Modifications in Lipid Bilayers: A Simulation Study. *Biophysical Journal*. 2002;83(4):1842-53. doi: 10.1016/S0006-3495(02)73949-0.

149. Privat-Maldonado A, Gorbanev Y, Dewilde S, Smits E, Bogaerts A. Reduction of Human Glioblastoma Spheroids Using Cold Atmospheric Plasma: The Combined Effect of Short- and Long-Lived Reactive Species. *Cancers (Basel)*. 2018;10(11). Epub

2018/10/27. doi: 10.3390/cancers10110394. PubMed PMID: 30360539; PubMed Central PMCID: PMC6266784.

150. Zandsalimi F, Aghamiri S, Roshanzamiri S, Shahmohamadnejad S, Ghanbarian H. The emerging role of cold atmospheric plasma in glioblastoma therapy. *Plasma Processes and Polymers*. 2020;17(10):1900189. doi: <https://doi.org/10.1002/ppap.201900189>.

151. Ribassin-Majed L, Marguet S, Lee AWM, Ng WT, Ma J, Chan ATC, et al. What Is the Best Treatment of Locally Advanced Nasopharyngeal Carcinoma? An Individual Patient Data Network Meta-Analysis. *J Clin Oncol*. 2017;35(5):498-505. Epub 2016/12/06. doi: 10.1200/jco.2016.67.4119. PubMed PMID: 27918720; PubMed Central PMCID: PMC5791836.

152. Vandamme M, Robert E, Dozias S, Sobilo J, Lerondel S, Le Pape A, et al. Response of Human Glioma U87 Xenografted on Mice to Non Thermal Plasma Treatment. 2011;1(1):27-43. doi: 10.1615/PlasmaMed.v1.i1.30.

153. Kaushik NK, Kaushik N, Min B, Choi KH, Hong YJ, Miller V, et al. Cytotoxic macrophage-released tumour necrosis factor-alpha (TNF- α) as a killing mechanism for cancer cell death after cold plasma activation. *Journal of Physics D: Applied Physics*. 2016;49(8):084001. doi: 10.1088/0022-3727/49/8/084001.

154. Azzariti A, Iacobazzi RM, Di Fonte R, Porcelli L, Gristina R, Favia P, et al. Plasma-activated medium triggers cell death and the presentation of immune activating danger signals in melanoma and pancreatic cancer cells. *Sci Rep*. 2019;9(1):4099. Epub 2019/03/13. doi: 10.1038/s41598-019-40637-z. PubMed PMID: 30858524; PubMed Central PMCID: PMC6411873.

155. Almeida ND, Klein AL, Hogan EA, Terhaar SJ, Kedda J, Uppal P, et al. Cold Atmospheric Plasma as an Adjunct to Immunotherapy for Glioblastoma Multiforme. *World Neurosurgery*. 2019;130:369-76. doi: <https://doi.org/10.1016/j.wneu.2019.06.209>.
156. Simonyan H, Chen Z, Sherman J, Cheng X, Keidar M, Young CN. INTRACRANIAL TARGETING OF GLIOBLASTOMA MULTIFORME WITH COLD ATMOSPHERIC PLASMA. *The FASEB Journal*. 2018;32(S1):599.3-.3. doi: https://doi.org/10.1096/fasebj.2018.32.1_supplement.599.3.
157. Daeschlein G, Hillmann A, Gumbel D, Sicher C, Podewils Sv, Stope MB, et al. Enhanced Anticancer Efficacy by Drug Chemotherapy and Cold Atmospheric Plasma Against Melanoma and Glioblastoma Cell Lines In Vitro. *IEEE Transactions on Radiation and Plasma Medical Sciences*. 2018;2(2):153-9. doi: 10.1109/TRPMS.2018.2789659.
158. Chen G, Chen Z, Wen D, Wang Z, Li H, Zeng Y, et al. Transdermal cold atmospheric plasma-mediated immune checkpoint blockade therapy. *Proceedings of the National Academy of Sciences*. 2020;117(7):3687-92. doi: [doi:10.1073/pnas.1917891117](https://doi.org/10.1073/pnas.1917891117).
159. Gunes S, He Z, van Acken D, Malone R, Cullen PJ, Curtin JF. Platinum nanoparticles inhibit intracellular ROS generation and protect against cold atmospheric plasma-induced cytotoxicity. *Nanomedicine: Nanotechnology, Biology and Medicine*. 2021;36:102436. doi: <https://doi.org/10.1016/j.nano.2021.102436>.
160. Kaushik NK, Kaushik N, Wahab R, Bhartiya P, Linh NN, Khan F, et al. Cold Atmospheric Plasma and Gold Quantum Dots Exert Dual Cytotoxicity Mediated by the Cell Receptor-Activated Apoptotic Pathway in Glioblastoma Cells. *Cancers (Basel)*. 2020;12(2). Epub 2020/02/23. doi: 10.3390/cancers12020457. PubMed PMID: 32079108; PubMed Central PMCID: PMC7072464.

161. Sagwal SK, Pasqual-Melo G, Bodnar Y, Gandhirajan RK, Bekeschus S. Combination of chemotherapy and physical plasma elicits melanoma cell death via upregulation of SLC22A16. *Cell Death Dis.* 2018;9(12):1179. Epub 2018/12/07. doi: 10.1038/s41419-018-1221-6. PubMed PMID: 30518936; PubMed Central PMCID: PMC6281583.
162. Mateu-Sanz M, Tornín J, Ginebra M-P, Canal C. Cold Atmospheric Plasma: A New Strategy Based Primarily on Oxidative Stress for Osteosarcoma Therapy. *Journal of Clinical Medicine.* 2021;10(4):893. PubMed PMID: doi:10.3390/jcm10040893.
163. Metelmann H-R, Nedrelow DS, Seebauer C, Schuster M, von Woedtke T, Weltmann K-D, et al. Head and neck cancer treatment and physical plasma. *Clinical Plasma Medicine.* 2015;3(1):17-23. doi: <https://doi.org/10.1016/j.cpme.2015.02.001>.
164. Metelmann H-R, Seebauer C, Miller V, Fridman A, Bauer G, Graves DB, et al. Clinical experience with cold plasma in the treatment of locally advanced head and neck cancer. *Clinical Plasma Medicine.* 2018;9:6-13. doi: <https://doi.org/10.1016/j.cpme.2017.09.001>.
165. Hoffmann M, Bruch HP, Kujath P, Limmer S. Cold-plasma coagulation in the treatment of malignant pleural mesothelioma: results of a combined approach. *Interact Cardiovasc Thorac Surg.* 2010;10(4):502-5. Epub 2010/01/16. doi: 10.1510/icvts.2009.223768. PubMed PMID: 20075037.
166. Friedman PC, Miller V, Fridman G, Lin A, Fridman A. Successful treatment of actinic keratoses using nonthermal atmospheric pressure plasma: A case series. *J Am Acad Dermatol.* 2017;76(2):349-50. Epub 2017/01/17. doi: 10.1016/j.jaad.2016.09.004. PubMed PMID: 28088998.
167. Marches A, Clement E, Albérola G, Rols MP, Cousty S, Simon M, et al. Cold Atmospheric Plasma Jet Treatment Improves Human Keratinocyte Migration and Wound

Closure Capacity without Causing Cellular Oxidative Stress. *Int J Mol Sci.* 2022;23(18). Epub 2022/09/24. doi: 10.3390/ijms231810650. PubMed PMID: 36142561; PubMed Central PMCID: PMC9504313.

168. Canavese G, Ancona A, Racca L, Canta M, Dumontel B, Barbaresco F, et al. Nanoparticle-assisted ultrasound: A special focus on sonodynamic therapy against cancer. *Chem Eng J.* 2018;340:155-72. Epub 2019/03/19. doi: 10.1016/j.cej.2018.01.060. PubMed PMID: 30881202; PubMed Central PMCID: PMC6420022.

169. Wanigasekara J, de Carvalho AMA, Cullen PJ, Tiwari B, Curtin JF. Converging technologies: targeting the hallmarks of cancer using ultrasound and microbubbles. *Trends in Cancer.* 2021;7(10):886-90. doi: 10.1016/j.trecan.2021.07.004.

170. Izadifar Z, Babyn P, Chapman D. Mechanical and Biological Effects of Ultrasound: A Review of Present Knowledge. *Ultrasound in Medicine & Biology.* 2017;43(6):1085-104. doi: <https://doi.org/10.1016/j.ultrasmedbio.2017.01.023>.

171. Haar Gt. Ultrasound bioeffects and safety. *Proceedings of the Institution of Mechanical Engineers, Part H: Journal of Engineering in Medicine.* 2010;224(2):363-73. doi: 10.1243/09544119jeim613. PubMed PMID: 20349824.

172. Johansson L, Singh T, Leong T, Mawson R, McArthur S, Manasseh R, et al. Cavitation and non-cavitation regime for large-scale ultrasonic standing wave particle separation systems – In situ gentle cavitation threshold determination and free radical related oxidation. *Ultrasonics Sonochemistry.* 2016;28:346-56. doi: <https://doi.org/10.1016/j.ultsonch.2015.08.003>.

173. Mauri G, Nicosia L, Xu Z, Di Pietro S, Monfardini L, Bonomo G, et al. Focused ultrasound: tumour ablation and its potential to enhance immunological therapy to cancer. *Br J Radiol.* 2018;91(1083):20170641. Epub 2017/11/24. doi: 10.1259/bjr.20170641. PubMed PMID: 29168922; PubMed Central PMCID: PMC5965486.

174. Tu J, Zhang H, Yu J, Liufu C, Chen Z. Ultrasound-mediated microbubble destruction: a new method in cancer immunotherapy. *Onco Targets Ther.* 2018;11:5763-75. Epub 2018/09/27. doi: 10.2147/ott.S171019. PubMed PMID: 30254469; PubMed Central PMCID: PMC6140758.
175. Sanwal R, Joshi K, Ditmans M, Tsai SSH, Lee WL. Ultrasound and Microbubbles for Targeted Drug Delivery to the Lung Endothelium in ARDS: Cellular Mechanisms and Therapeutic Opportunities. *Biomedicines.* 2021;9(7). Epub 2021/08/07. doi: 10.3390/biomedicines9070803. PubMed PMID: 34356867; PubMed Central PMCID: PMC8301318.
176. Hanahan D, Weinberg RA. Hallmarks of cancer: the next generation. *Cell.* 2011;144(5):646-74. Epub 2011/03/08. doi: 10.1016/j.cell.2011.02.013. PubMed PMID: 21376230.
177. Garg AD, Maes H, van Vliet AR, Agostinis P. Targeting the hallmarks of cancer with therapy-induced endoplasmic reticulum (ER) stress. *Mol Cell Oncol.* 2015;2(1):e975089. Epub 2015/01/01. doi: 10.4161/23723556.2014.975089. PubMed PMID: 27308392; PubMed Central PMCID: PMC4905250.
178. O'Brien WD, Jr. Ultrasound-biophysics mechanisms. *Prog Biophys Mol Biol.* 2007;93(1-3):212-55. Epub 2006/08/29. doi: 10.1016/j.pbiomolbio.2006.07.010. PubMed PMID: 16934858; PubMed Central PMCID: PMC1995002.
179. Levenback BJ, Sehgal CM, Wood AK. Modeling of thermal effects in antivasular ultrasound therapy. *J Acoust Soc Am.* 2012;131(1):540-9. Epub 2012/01/28. doi: 10.1121/1.3662048. PubMed PMID: 22280615; PubMed Central PMCID: PMC3283906.

180. Wood AKW, Sehgal CM. A review of low-intensity ultrasound for cancer therapy. *Ultrasound in Medicine and Biology*. 2015;41(4):905-28. doi: 10.1016/j.ultrasmedbio.2014.11.019.
181. van den Bijgaart RJ, Eikelenboom DC, Hoogenboom M, Fütterer JJ, den Brok MH, Adema GJ. Thermal and mechanical high-intensity focused ultrasound: perspectives on tumor ablation, immune effects and combination strategies. *Cancer Immunol Immunother*. 2017;66(2):247-58. Epub 2016/09/03. doi: 10.1007/s00262-016-1891-9. PubMed PMID: 27585790; PubMed Central PMCID: PMC5281669.
182. Mazzawi N, Kimmel E, Tsarfaty I. The effect of low-intensity ultrasound and met signaling on cellular motility and morphology. *Applied Acoustics*. 2019;143:1-6. doi: <https://doi.org/10.1016/j.apacoust.2018.07.035>.
183. Wood AK, Sehgal CM. A review of low-intensity ultrasound for cancer therapy. *Ultrasound Med Biol*. 2015;41(4):905-28. Epub 2015/03/03. doi: 10.1016/j.ultrasmedbio.2014.11.019. PubMed PMID: 25728459; PubMed Central PMCID: PMC4362523.
184. Hernandez C, Huebener P, Schwabe RF. Damage-associated molecular patterns in cancer: a double-edged sword. *Oncogene*. 2016;35(46):5931-41. Epub 2016/04/19. doi: 10.1038/onc.2016.104. PubMed PMID: 27086930; PubMed Central PMCID: PMC5119456.
185. Peruzzi G, Sinibaldi G, Silvani G, Ruocco G, Casciola CM. Perspectives on cavitation enhanced endothelial layer permeability. *Colloids Surf B Biointerfaces*. 2018;168:83-93. doi: 10.1016/j.colsurfb.2018.02.027. PubMed PMID: 29486912.
186. Ogawa R, Morii A, Watanabe A, Cui Z-G, Kondo T. Bioeffects of Ultrasound and Its Therapeutic Application. In: Ashokkumar M, editor. *Handbook of Ultrasonics and Sonochemistry*. Singapore: Springer Singapore; 2015. p. 1-26.

187. Carneiro BA, El-Deiry WS. Targeting apoptosis in cancer therapy. *Nat Rev Clin Oncol.* 2020;17(7):395-417. Epub 2020/03/24. doi: 10.1038/s41571-020-0341-y. PubMed PMID: 32203277; PubMed Central PMCID: PMC8211386.
188. van den Bijgaart RJE, Eikelenboom DC, Hoogenboom M, Fütterer JJ, den Brok MH, Adema GJ. Thermal and mechanical high-intensity focused ultrasound: perspectives on tumor ablation, immune effects and combination strategies. *Cancer Immunology, Immunotherapy.* 2017;66(2):247-58. doi: 10.1007/s00262-016-1891-9.
189. Bunevicius A, McDannold NJ, Golby AJ. Focused Ultrasound Strategies for Brain Tumor Therapy. *Oper Neurosurg (Hagerstown).* 2020;19(1):9-18. Epub 2019/12/20. doi: 10.1093/ons/opz374. PubMed PMID: 31853548; PubMed Central PMCID: PMC7293897.
190. Sultan D, Ye D, Heo GS, Zhang X, Luehmann H, Yue Y, et al. Focused Ultrasound Enabled Trans-Blood Brain Barrier Delivery of Gold Nanoclusters: Effect of Surface Charges and Quantification Using Positron Emission Tomography. *Small.* 2018;14(30):e1703115. Epub 2018/07/03. doi: 10.1002/sml.201703115. PubMed PMID: 29966035.
191. Idbaih A, Canney M, Belin L, Desseaux C, Vignot A, Bouchoux G, et al. Safety and Feasibility of Repeated and Transient Blood-Brain Barrier Disruption by Pulsed Ultrasound in Patients with Recurrent Glioblastoma. *Clin Cancer Res.* 2019;25(13):3793-801. Epub 2019/03/21. doi: 10.1158/1078-0432.Ccr-18-3643. PubMed PMID: 30890548.
192. Mainprize T, Lipsman N, Huang Y, Meng Y, Bethune A, Ironside S, et al. Blood-Brain Barrier Opening in Primary Brain Tumors with Non-invasive MR-Guided Focused Ultrasound: A Clinical Safety and Feasibility Study. *Sci Rep.* 2019;9(1):321. Epub 2019/01/25. doi: 10.1038/s41598-018-36340-0. PubMed PMID: 30674905; PubMed Central PMCID: PMC6344541.

193. Barzegar-Fallah A, Gandhi K, Rizwan SB, Slatter TL, Reynolds JNJ. Harnessing Ultrasound for Targeting Drug Delivery to the Brain and Breaching the Blood-Brain Tumour Barrier. *Pharmaceutics*. 2022;14(10). Epub 2022/10/28. doi: 10.3390/pharmaceutics14102231. PubMed PMID: 36297666; PubMed Central PMCID: PMC9607160.
194. Qu F, Wang P, Zhang K, Shi Y, Li Y, Li C, et al. Manipulation of Mitophagy by "All-in-One" nanosensitizer augments sonodynamic glioma therapy. *Autophagy*. 2020;16(8):1413-35. Epub 2019/11/02. doi: 10.1080/15548627.2019.1687210. PubMed PMID: 31674265; PubMed Central PMCID: PMC7480814.
195. Yang Q, Zhou Y, Chen J, Huang N, Wang Z, Cheng Y. Gene Therapy for Drug-Resistant Glioblastoma via Lipid-Polymer Hybrid Nanoparticles Combined with Focused Ultrasound. *Int J Nanomedicine*. 2021;16:185-99. Epub 2021/01/16. doi: 10.2147/IJN.S286221. PubMed PMID: 33447034; PubMed Central PMCID: PMC7802796.
196. Hou R, Liang X, Li X, Zhang X, Ma X, Wang F. In situ conversion of rose bengal microbubbles into nanoparticles for ultrasound imaging guided sonodynamic therapy with enhanced antitumor efficacy. *Biomater Sci*. 2020;8(9):2526-36. Epub 2020/03/28. doi: 10.1039/c9bm02046b. PubMed PMID: 32215400.
197. Costley D, Mc Ewan C, Fowley C, McHale AP, Atchison J, Nomikou N, et al. Treating cancer with sonodynamic therapy: A review. *International Journal of Hyperthermia*. 2015;31(2):107-17. doi: 10.3109/02656736.2014.992484.
198. Mills CC, Kolb EA, Sampson VB. Development of Chemotherapy with Cell-Cycle Inhibitors for Adult and Pediatric Cancer Therapy. *Cancer Res*. 2018;78(2):320-5. Epub 2018/01/10. doi: 10.1158/0008-5472.Can-17-2782. PubMed PMID: 29311160; PubMed Central PMCID: PMC5771851.

199. Otmani K, Lewalle P. Tumor Suppressor miRNA in Cancer Cells and the Tumor Microenvironment: Mechanism of Deregulation and Clinical Implications. *Front Oncol.* 2021;11:708765. Epub 2021/11/02. doi: 10.3389/fonc.2021.708765. PubMed PMID: 34722255; PubMed Central PMCID: PMC6982438.
200. Si W, Shen J, Zheng H, Fan W. The role and mechanisms of action of microRNAs in cancer drug resistance. *Clinical Epigenetics.* 2019;11(1):25. doi: 10.1186/s13148-018-0587-8.
201. Tian Y, Liu Z, Tan H, Hou J, Wen X, Yang F, et al. New Aspects of Ultrasound-Mediated Targeted Delivery and Therapy for Cancer. *Int J Nanomedicine.* 2020;15:401-18. Epub 2020/02/06. doi: 10.2147/ijn.S201208. PubMed PMID: 32021187; PubMed Central PMCID: PMC6982438.
202. Lin L, Fan Y, Gao F, Jin L, Li D, Sun W, et al. UTMD-Promoted Co-Delivery of Gemcitabine and miR-21 Inhibitor by Dendrimer-Entrapped Gold Nanoparticles for Pancreatic Cancer Therapy. *Theranostics.* 2018;8(7):1923-39. Epub 2018/03/21. doi: 10.7150/thno.22834. PubMed PMID: 29556365; PubMed Central PMCID: PMC5858509.
203. Mullick Chowdhury S, Wang TY, Bachawal S, Devulapally R, Choe JW, Abou Elkacem L, et al. Ultrasound-guided therapeutic modulation of hepatocellular carcinoma using complementary microRNAs. *J Control Release.* 2016;238:272-80. Epub 2016/08/10. doi: 10.1016/j.jconrel.2016.08.005. PubMed PMID: 27503707; PubMed Central PMCID: PMC5185600.
204. Dimceviski G, Kotopoulis S, Bjanec T, Hoem D, Schjott J, Gjertsen BT, et al. A human clinical trial using ultrasound and microbubbles to enhance gemcitabine treatment of inoperable pancreatic cancer. *J Control Release.* 2016;243:172-81. Epub 2016/11/05. doi: 10.1016/j.jconrel.2016.10.007. PubMed PMID: 27744037.

205. Tran VL, Novell A, Tournier N, Gerstenmayer M, Schweitzer-Chaput A, Mateos C, et al. Impact of blood-brain barrier permeabilization induced by ultrasound associated to microbubbles on the brain delivery and kinetics of cetuximab: An immunoPET study using ⁸⁹Zr-cetuximab. *J Control Release*. 2020;328:304-12. Epub 2020/08/30. doi: 10.1016/j.jconrel.2020.08.047. PubMed PMID: 32860928.
206. Zhong H, Li R, Hao YX, Guo YL, Hua X, Zhang XH, et al. Inhibition effects of high mechanical index ultrasound contrast on hepatic metastasis of cancer in a rat model. *Acad Radiol*. 2010;17(11):1345-9. Epub 2010/08/20. doi: 10.1016/j.acra.2010.06.013. PubMed PMID: 20719546.
207. Xing Y, Lu X, Pua EC, Zhong P. The effect of high intensity focused ultrasound treatment on metastases in a murine melanoma model. *Biochem Biophys Res Commun*. 2008;375(4):645-50. Epub 2008/08/30. doi: 10.1016/j.bbrc.2008.08.072. PubMed PMID: 18727919; PubMed Central PMCID: PMCPMC2638084.
208. Jolly MK, Ware KE, Gilja S, Somarelli JA, Levine H. EMT and MET: necessary or permissive for metastasis? *Mol Oncol*. 2017;11(7):755-69. Epub 2017/05/27. doi: 10.1002/1878-0261.12083. PubMed PMID: 28548345; PubMed Central PMCID: PMCPMC5496498.
209. Gonzalez H, Hagerling C, Werb Z. Roles of the immune system in cancer: from tumor initiation to metastatic progression. *Genes Dev*. 2018;32(19-20):1267-84. Epub 2018/10/03. doi: 10.1101/gad.314617.118. PubMed PMID: 30275043; PubMed Central PMCID: PMCPMC6169832.
210. Cohen-Inbar O, Xu Z, Sheehan JP. Focused ultrasound-aided immunomodulation in glioblastoma multiforme: a therapeutic concept. *J Ther Ultrasound*. 2016;4:2. Epub 2016/01/26. doi: 10.1186/s40349-016-0046-y. PubMed PMID: 26807257; PubMed Central PMCID: PMCPMC4722768.

211. Dewitte H, Van Lint S, Heirman C, Thielemans K, De Smedt SC, Breckpot K, et al. The potential of antigen and TriMix sonoporation using mRNA-loaded microbubbles for ultrasound-triggered cancer immunotherapy. *J Control Release*. 2014;194:28-36. Epub 2014/08/26. doi: 10.1016/j.jconrel.2014.08.011. PubMed PMID: 25151979.
212. Schiliro C, Firestein BL. Mechanisms of Metabolic Reprogramming in Cancer Cells Supporting Enhanced Growth and Proliferation. *Cells*. 2021;10(5). Epub 2021/05/06. doi: 10.3390/cells10051056. PubMed PMID: 33946927; PubMed Central PMCID: PMC8146072.
213. Peruzzi G, Sinibaldi G, Silvani G, Ruocco G, Casciola CM. Perspectives on cavitation enhanced endothelial layer permeability. *Colloids and Surfaces B: Biointerfaces*. 2018;168:83-93. doi: 10.1016/j.colsurfb.2018.02.027.
214. Su C, Ren X, Nie F, Li T, Lv W, Li H, et al. Current advances in ultrasound-combined nanobubbles for cancer-targeted therapy: a review of the current status and future perspectives. *RSC Adv*. 2021;11(21):12915-28. Epub 2022/04/16. doi: 10.1039/d0ra08727k. PubMed PMID: 35423829; PubMed Central PMCID: PMC8697319.
215. Gray MD, Lyon PC, Mannaris C, Folkes LK, Stratford M, Campo L, et al. Focused Ultrasound Hyperthermia for Targeted Drug Release from Thermosensitive Liposomes: Results from a Phase I Trial. *Radiology*. 2019;291(1):232-8. Epub 2019/01/16. doi: 10.1148/radiol.2018181445. PubMed PMID: 30644817.
216. Dimcevski G, Kotopoulos S, Bjånes T, Hoem D, Schjøtt J, Gjertsen BT, et al. A human clinical trial using ultrasound and microbubbles to enhance gemcitabine treatment of inoperable pancreatic cancer. *Journal of controlled release*. 2016;243:172-81. doi: 10.1016/j.jconrel.2016.10.007.

217. Carpentier A, Canney M, Vignot A, Reina V, Beccaria K, Horodyckid C, et al. Clinical trial of blood-brain barrier disruption by pulsed ultrasound. *Sci Transl Med*. 2016;8(343):343re2. Epub 2016/06/17. doi: 10.1126/scitranslmed.aaf6086. PubMed PMID: 27306666.
218. Tatla AS, Justin AW, Watts C, Markaki AE. A vascularized tumoroid model for human glioblastoma angiogenesis. *Scientific Reports*. 2021;11(1):19550. doi: 10.1038/s41598-021-98911-y.
219. Chhetri A, Rispoli JV, Lelièvre SA. 3D Cell Culture for the Study of Microenvironment-Mediated Mechanostimuli to the Cell Nucleus: An Important Step for Cancer Research. *Frontiers in Molecular Biosciences*. 2021;8. doi: 10.3389/fmolb.2021.628386.
220. Foglietta F, Canaparo R, Muccioli G, Terreno E, Serpe L. Methodological aspects and pharmacological applications of three-dimensional cancer cell cultures and organoids. *Life Sciences*. 2020;254. doi: 10.1016/j.lfs.2020.117784. PubMed PMID: WOS:000541489200011.
221. Mohiuddin E, Wakimoto H. Extracellular matrix in glioblastoma: opportunities for emerging therapeutic approaches. *Am J Cancer Res*. 2021;11(8):3742-54. PubMed PMID: WOS:000692198900001.
222. Jensen C, Teng Y. Is It Time to Start Transitioning From 2D to 3D Cell Culture? *Frontiers in Molecular Biosciences*. 2020;7. doi: 10.3389/fmolb.2020.00033. PubMed PMID: WOS:000525139400001.
223. Rodrigues J, Heinrich MA, Teixeira LM, Prakash J. 3D In Vitro Model (R)evolution: Unveiling Tumor-Stroma Interactions. *Trends in Cancer*. 2021;7(3):249-64. doi: 10.1016/j.trecan.2020.10.009. PubMed PMID: WOS:000629199500011.

224. Li SL, Zhang Z, Han L. 3D Spheroids Propel Tumor Characterization. *Trends in Cancer*. 2020;6(8):622-4. doi: 10.1016/j.trecan.2020.05.002. PubMed PMID: WOS:000562896800002.
225. Colombo E, Cattaneo MG. Multicellular 3D Models to Study Tumour-Stroma Interactions. *Int J Mol Sci*. 2021;22(4). Epub 2021/02/11. doi: 10.3390/ijms22041633. PubMed PMID: 33562840; PubMed Central PMCID: PMC7915117.
226. Tomas-Bort E, Kieler M, Sharma S, Candido JB, Loessner D. 3D approaches to model the tumor microenvironment of pancreatic cancer. *Theranostics*. 2020;10(11):5074-89. doi: 10.7150/thno.42441. PubMed PMID: WOS:000534489700012.
227. Koh I, Kim P. In Vitro Reconstruction of Brain Tumor Microenvironment. *BioChip J*. 2019;13(1):1-7. doi: 10.1007/s13206-018-3102-6. PubMed PMID: WOS:000462447100001.
228. Hatlen RR, Rajagopalan P. Environmental interplay: Stromal cells and biomaterial composition influence in the glioblastoma microenvironment. *Acta Biomater*. 2021;132:421-36. doi: 10.1016/j.actbio.2020.11.044. PubMed PMID: WOS:000696645300004.
229. Carter EP, Roozitalab R, Gibson SV, Grose RP. Tumour microenvironment 3D-modelling: simplicity to complexity and back again. *Trends in Cancer*. 2021;7(11):1033-46. doi: 10.1016/j.trecan.2021.06.009. PubMed PMID: WOS:000709306500008.
230. Caragher S, Chalmers AJ, Gomez-Roman N. Glioblastoma's Next Top Model: Novel Culture Systems for Brain Cancer Radiotherapy Research. *Cancers*. 2019;11(1). doi: 10.3390/cancers11010044. PubMed PMID: WOS:000457233300074.

231. Yuki K, Cheng N, Nakano M, Kuo CJ. Organoid Models of Tumor Immunology. *Trends Immunol.* 2020;41(8):652-64. doi: 10.1016/j.it.2020.06.010. PubMed PMID: WOS:000554494500004.
232. Ferreira LP, Gaspar VM, Mano JF. Decellularized Extracellular Matrix for Bioengineering Physiometric 3D in Vitro Tumor Models. *Trends Biotechnol.* 2020;38(12):1397-414. doi: 10.1016/j.tibtech.2020.04.006. PubMed PMID: WOS:000590396200010.
233. Fontana F, Raimondi M, Marzagalli M, Sommariva M, Gagliano N, Limonta P. Three-Dimensional Cell Cultures as an In Vitro Tool for Prostate Cancer Modeling and Drug Discovery. *International Journal of Molecular Sciences.* 2020;21(18). doi: 10.3390/ijms21186806. PubMed PMID: WOS:000580285800001.
234. Darrigues E, Nima ZA, Griffin RJ, Anderson JM, Biris AS, Rodriguez A. 3D cultures for modeling nanomaterial-based photothermal therapy. *Nanoscale Horiz.* 2020;5(3):400-30. doi: 10.1039/c9nh00628a. PubMed PMID: WOS:000518686600002.
235. Stankovic T, Randelovic T, Dragoj M, Buric SS, Fernandez L, Ochoa I, et al. In vitro biomimetic models for glioblastoma-a promising tool for drug response studies. *Drug Resistance Updates.* 2021;55. doi: 10.1016/j.drug.2021.100753. PubMed PMID: WOS:000636429200003.
236. Alzeeb G, Metges JP, Corcos L, Le Jossic-Corcos C. Three-Dimensional Culture Systems in Gastric Cancer Research. *Cancers.* 2020;12(10). doi: 10.3390/cancers12102800. PubMed PMID: WOS:000584595400001.
237. Klein E, Hau AC, Oudin A, Golebiewska A, Niclou SP. Glioblastoma Organoids: Pre-Clinical Applications and Challenges in the Context of Immunotherapy. *Front Oncol.* 2020;10:18. doi: 10.3389/fonc.2020.604121. PubMed PMID: WOS:000600646600001.

238. Paolillo M, Comincini S, Schinelli S. In Vitro Glioblastoma Models: A Journey into the Third Dimension. *Cancers*. 2021;13(10):25. doi: 10.3390/cancers13102449. PubMed PMID: WOS:000654678600001.
239. Kitaeva KV, Rutland CS, Rizvanov AA, Solovyeva VV. Cell Culture Based in vitro Test Systems for Anticancer Drug Screening. *Front Bioeng Biotechnol*. 2020;8:9. doi: 10.3389/fbioe.2020.00322. PubMed PMID: WOS:000529260900001.
240. Poornima K, Francis AP, Hoda M, Eladl MA, Subramanian S, Veeraraghavan VP, et al. Implications of Three-Dimensional Cell Culture in Cancer Therapeutic Research. *Front Oncol*. 2022;12. doi: 10.3389/fonc.2022.891673.
241. Habanjar O, Diab-Assaf M, Caldefie-Chezet F, Delort L. 3D Cell Culture Systems: Tumor Application, Advantages, and Disadvantages. *International Journal of Molecular Sciences*. 2021;22(22):12200. PubMed PMID: doi:10.3390/ijms222212200.
242. Farhat J, Pandey I, AlWahsh M. Transcending toward Advanced 3D-Cell Culture Modalities: A Review about an Emerging Paradigm in Translational Oncology. *Cells*. 2021;10(7). doi: 10.3390/cells10071657.
243. Sayde T, El Hamoui O, Alies B, Gaudin K, Lespes G, Battu S. Biomaterials for Three-Dimensional Cell Culture: From Applications in Oncology to Nanotechnology. *Nanomaterials*. 2021;11(2). doi: 10.3390/nano11020481. PubMed PMID: WOS:000622960300001.
244. Xu XD, Li LF, Luo LT, Shu LL, Si XL, Chen ZZ, et al. Opportunities and challenges of glioma organoids. *Cell Commun Signal*. 2021;19(1):13. doi: 10.1186/s12964-021-00777-0. PubMed PMID: WOS:000706237100002.
245. Pampaloni F, Reynaud EG, Stelzer EHK. The third dimension bridges the gap between cell culture and live tissue. *Nature Reviews Molecular Cell Biology*. 2007;8(10):839-45. doi: 10.1038/nrm2236. PubMed PMID: WOS:000249642900016.

246. Edmondson R, Broglie JJ, Adcock AF, Yang L. Three-dimensional cell culture systems and their applications in drug discovery and cell-based biosensors. *Assay Drug Dev Technol.* 2014;12(4):207-18. Epub 2014/05/17. doi: 10.1089/adt.2014.573. PubMed PMID: 24831787; PubMed Central PMCID: PMC4026212.
247. Nii T, Makino K, Tabata Y. Three-Dimensional Culture System of Cancer Cells Combined with Biomaterials for Drug Screening. *Cancers.* 2020;12(10):24. doi: 10.3390/cancers12102754. PubMed PMID: WOS:000584236500001.
248. Brancato V, Oliveira JM, Correlo VM, Reis RL, Kundu SC. Could 3D models of cancer enhance drug screening? *Biomaterials.* 2020;232. doi: 10.1016/j.biomaterials.2019.119744. PubMed PMID: WOS:000514748200006.
249. Gunti S, Hoke ATK, Vu KP, London NR. Organoid and Spheroid Tumor Models: Techniques and Applications. *Cancers.* 2021;13(4):17. doi: 10.3390/cancers13040874. PubMed PMID: WOS:000623392400001.
250. Han K, Pierce SE, Li A, Spees K, Anderson GR, Seoane JA, et al. CRISPR screens in cancer spheroids identify 3D growth-specific vulnerabilities. *Nature.* 2020;580(7801):136-+. doi: 10.1038/s41586-020-2099-x. PubMed PMID: WOS:000519162500002.
251. Nguyen R, Won S, Zhou G, Read SA, Ahlenstiel G, George J, et al. Application of organoids in translational research of human diseases with a particular focus on gastrointestinal cancers. *Biochim Biophys Acta-Rev Cancer.* 2020;1873(2):12. doi: 10.1016/j.bbcan.2020.188350. PubMed PMID: WOS:000532683000002.
252. de Dios-Figueroa GT, Aguilera-Marquez JDR, Camacho-Villegas TA, Lugo-Fabres PH. 3D Cell Culture Models in COVID-19 Times: A Review of 3D Technologies to Understand and Accelerate Therapeutic Drug Discovery. *Biomedicines.* 2021;9(6).

Epub 2021/06/03. doi: 10.3390/biomedicines9060602. PubMed PMID: 34073231; PubMed Central PMCID: PMC8226796.

253. Law AMK, Rodriguez de la Fuente L, Grundy TJ, Fang G, Valdes-Mora F, Gallego-Ortega D. Advancements in 3D Cell Culture Systems for Personalizing Anti-Cancer Therapies. *Front Oncol.* 2021;11:782766. Epub 2021/12/18. doi: 10.3389/fonc.2021.782766. PubMed PMID: 34917509; PubMed Central PMCID: PMC8669727.

254. Heydari Z, Moeinvaziri F, Agarwal T, Pooyan P, Shpichka A, Maiti TK, et al. Organoids: a novel modality in disease modeling. *Bio-Design and Manufacturing.* 2021;4(4):689-716. doi: 10.1007/s42242-021-00150-7.

255. HICKS WH, BIRD CE, PERNIK MN, HAIDER AS, DOBARIYA A, ABDULLAH KG, et al. Large Animal Models of Glioma: Current Status and Future Prospects. *Anticancer Research.* 2021;41(11):5343-53. doi: 10.21873/anticancer.15347.

256. Wang C, Li JF, Sinha S, Peterson A, Grant GA, Yang F. Mimicking brain tumor-vasculature microanatomical architecture via co-culture of brain tumor and endothelial cells in 3D hydrogels. *Biomaterials.* 2019;202:35-44. doi: 10.1016/j.biomaterials.2019.02.024. PubMed PMID: WOS:000463304400004.

257. Wanigasekara J, Cullen PJ, Bourke P, Tiwari B, Curtin JF. Advances in 3D culture systems for therapeutic discovery and development in brain cancer. *Drug Discovery Today.* 2022:103426. doi: <https://doi.org/10.1016/j.drudis.2022.103426>.

258. Akter F, Simon B, de Boer NL, Redjal N, Wakimoto H, Shah K. Pre-clinical tumor models of primary brain tumors: Challenges and opportunities. *Biochim Biophys Acta Rev Cancer.* 2021;1875(1):188458. Epub 2020/11/06. doi: 10.1016/j.bbcan.2020.188458. PubMed PMID: 33148506; PubMed Central PMCID: PMC8669727.

259. Balasubramanian B, Venkatraman S, Myint KZ, Janvilisri T, Wongprasert K, Kumkate S, et al. Co-Clinical Trials: An Innovative Drug Development Platform for Cholangiocarcinoma. *Pharmaceuticals (Basel)*. 2021;14(1). Epub 2021/01/15. doi: 10.3390/ph14010051. PubMed PMID: 33440754; PubMed Central PMCID: PMC7826774.
260. Mak IW, Evaniew N, Ghert M. Lost in translation: animal models and clinical trials in cancer treatment. *Am J Transl Res*. 2014;6(2):114-8. Epub 2014/02/04. PubMed PMID: 24489990; PubMed Central PMCID: PMC3902221.
261. Bédard P, Gauvin S, Ferland K, Caneparo C, Pellerin È, Chabaud S, et al. Innovative Human Three-Dimensional Tissue-Engineered Models as an Alternative to Animal Testing. *Bioengineering (Basel)*. 2020;7(3):115. doi: 10.3390/bioengineering7030115. PubMed PMID: 32957528.
262. Yuan X, Curtin J, Xiong Y, Liu G, Waschmann-Hogiu S, Farkas DL, et al. Isolation of cancer stem cells from adult glioblastoma multiforme. *Oncogene*. 2004;23(58):9392-400. Epub 2004/11/24. doi: 10.1038/sj.onc.1208311. PubMed PMID: 15558011.
263. Johnson S, Chen H, Lo PK. In vitro Tumorsphere Formation Assays. *Bio Protoc*. 2013;3(3). Epub 2013/02/05. doi: 10.21769/bioprotoc.325. PubMed PMID: 27500184; PubMed Central PMCID: PMC4972326.
264. Mapanao AK, Voliani V. Three-dimensional tumor models: Promoting breakthroughs in nanotheranostics translational research. *Applied Materials Today*. 2020;19. doi: 10.1016/j.apmt.2019.100552. PubMed PMID: WOS:000545903500002.
265. Zhang CY, Yang ZT, Dong DL, Jang TS, Knowles JC, Kim HW, et al. 3D culture technologies of cancer stem cells: promising ex vivo tumor models. *J Tissue Eng*.

2020;11:17. doi: 10.1177/2041731420933407. PubMed PMID:
WOS:000545647100001.

266. Park Y, Huh KM, Kang SW. Applications of Biomaterials in 3D Cell Culture and Contributions of 3D Cell Culture to Drug Development and Basic Biomedical Research. *International Journal of Molecular Sciences*. 2021;22(5). doi: 10.3390/ijms22052491. PubMed PMID: WOS:000628286300001.

267. Belfiore L, Aghaei B, Law AMK, Dobrowolski JC, Raftery LJ, Tjandra AD, et al. Generation and analysis of 3D cell culture models for drug discovery. *European Journal of Pharmaceutical Sciences*. 2021;163. doi: 10.1016/j.ejps.2021.105876. PubMed PMID: WOS:000660292700006.

268. Reidy E, Leonard NA, Treacy O, Ryan AE. A 3D View of Colorectal Cancer Models in Predicting Therapeutic Responses and Resistance. *Cancers*. 2021;13(2). doi: 10.3390/cancers13020227. PubMed PMID: WOS:000611865700001.

269. Lv DL, Hu ZT, Lu L, Lu HS, Xu XL. Three-dimensional cell culture: A powerful tool in tumor research and drug discovery. *Oncology Letters*. 2017;14(6):6999-7010. doi: 10.3892/ol.2017.7134. PubMed PMID: WOS:000417293400092.

270. J Carroll L, Tiwari B, F Curtin J, Wanigasekara J. U-251MG Spheroid generation using low attachment plate method protocol. *protocols.io*. 2021. doi: 10.17504/protocols.io.bszmnf46.

271. Wanigasekara J, Carroll LJ, Cullen PJ, Tiwari B, Curtin JF. Three-Dimensional (3D) in vitro cell culture protocols to enhance glioblastoma research. *PLoS One*. 2023;18(2):e0276248. Epub 2023/02/09. doi: 10.1371/journal.pone.0276248. PubMed PMID: 36753513; PubMed Central PMCID: PMC9907841.

272. Dundar B, Markwell SM, Sharma NV, Olson CL, Mukherjee S, Brat DJ. Methods for in vitro modeling of glioma invasion: Choosing tools to meet the need. *Glia*.

- 2020;68(11):2173-91. doi: 10.1002/glia.23813. PubMed PMID: WOS:000561634300001.
273. J Carroll L, Tiwari B, F Curtin J, Wanigasekara J. U-251MG Spheroid Generation Using Hanging Drop Method Protocol. *protocolsio*. 2021. doi: 10.17504/protocols.io.btstnnen.
274. Paradiso F, Serpelloni S, Francis LW, Taraballi F. Mechanical Studies of the Third Dimension in Cancer: From 2D to 3D Model. *International Journal of Molecular Sciences*. 2021;22(18). doi: 10.3390/ijms221810098. PubMed PMID: WOS:000700292300001.
275. Dijkstra KK, Cattaneo CM, Weeber F, Chalabi M, van de Haar J, Fanchi LF, et al. Generation of Tumor-Reactive T Cells by Co-culture of Peripheral Blood Lymphocytes and Tumor Organoids. *Cell*. 2018;174(6):1586-+. doi: 10.1016/j.cell.2018.07.009. PubMed PMID: WOS:000443841000024.
276. Fisher MF, Rao SS. Three-dimensional culture models to study drug resistance in breast cancer. *Biotechnology and Bioengineering*. 2020;117(7):2262-78. doi: 10.1002/bit.27356. PubMed PMID: WOS:000528726700001.
277. Ruiz-Garcia H, Alvarado-Estrada K, Schiapparelli P, Quinones-Hinojosa A, Trifiletti DM. Engineering Three-Dimensional Tumor Models to Study Glioma Cancer Stem Cells and Tumor Microenvironment. *Front Cell Neurosci*. 2020;14:21. doi: 10.3389/fncel.2020.558381. PubMed PMID: WOS:000584708800001.
278. Cornelison RC, Yuan JX, Tate KM, Petrosky A, Beeghly GF, Bloomfield M, et al. A patient-designed tissue-engineered model of the infiltrative glioblastoma microenvironment. *npj Precis Oncol*. 2022;6(1):54. doi: 10.1038/s41698-022-00290-8.

279. J Carroll L, Tiwari B, F Curtin J, Wanigasekara J. U-251MG Spheroid generation using a scaffold based method protocol. *protocols.io*. 2021. doi: 10.17504/protocols.io.bszqnf5w.
280. Dirauf M, Muljajew I, Weber C, Schubert US. Recent advances in degradable synthetic polymers for biomedical applications - Beyond polyesters. *Progress in Polymer Science*. 2022;129:101547. doi: <https://doi.org/10.1016/j.progpolymsci.2022.101547>.
281. Darrigues E, Zhao EH, De Loose A, Lee MP, Borrelli MJ, Eoff RL, et al. Biobanked Glioblastoma Patient-Derived Organoids as a Precision Medicine Model to Study Inhibition of Invasion. *International Journal of Molecular Sciences*. 2021;22(19):16. doi: 10.3390/ijms221910720. PubMed PMID: WOS:000708006400001.
282. Ahmed EM. Hydrogel: Preparation, characterization, and applications: A review. *Journal of Advanced Research*. 2015;6(2):105-21. doi: <https://doi.org/10.1016/j.jare.2013.07.006>.
283. Ruan H, Hu Q, Wen D, Chen Q, Chen G, Lu Y, et al. A Dual-Bioresponsive Drug-Delivery Depot for Combination of Epigenetic Modulation and Immune Checkpoint Blockade. *Adv Mater*. 2019;31(17):e1806957. Epub 2019/03/12. doi: 10.1002/adma.201806957. PubMed PMID: 30856290.
284. Nielsen JB, Hanson RL, Almughamsi HM, Pang C, Fish TR, Woolley AT. Microfluidics: Innovations in Materials and Their Fabrication and Functionalization. *Anal Chem*. 2020;92(1):150-68. Epub 2019/11/14. doi: 10.1021/acs.analchem.9b04986. PubMed PMID: 31721565; PubMed Central PMCID: PMC7034066.
285. Zhai J, Li HR, Wong AHH, Dong C, Yi SH, Jia YW, et al. A digital microfluidic system with 3D microstructures for single-cell culture. *Microsyst Nanoeng*. 2020;6(1):10. doi: 10.1038/s41378-019-0109-7. PubMed PMID: WOS:000512731300002.

286. Li XJ, Valadez AV, Zuo P, Nie Z. Microfluidic 3D cell culture: potential application for tissue-based bioassays. *Bioanalysis*. 2012;4(12):1509-25. Epub 2012/07/17. doi: 10.4155/bio.12.133. PubMed PMID: 22793034; PubMed Central PMCID: PMC3909686.
287. Wong AD, Ye M, Levy AF, Rothstein JD, Bergles DE, Searson PC. The blood-brain barrier: an engineering perspective. *Front Neuroeng*. 2013;6:7. Epub 2013/09/07. doi: 10.3389/fneng.2013.00007. PubMed PMID: 24009582; PubMed Central PMCID: PMC3757302.
288. Kim D, Wu X, Young AT, Haynes CL. Microfluidics-Based in Vivo Mimetic Systems for the Study of Cellular Biology. *Accounts of Chemical Research*. 2014;47(4):1165-73. doi: 10.1021/ar4002608.
289. Cai X, Briggs RG, Homburg HB, Young IM, Davis EJ, Lin YH, et al. Application of microfluidic devices for glioblastoma study: current status and future directions. *Biomed Microdevices*. 2020;22(3):60. Epub 2020/09/02. doi: 10.1007/s10544-020-00516-1. PubMed PMID: 32870410.
290. Yi HG, Jeong YH, Kim Y, Choi YJ, Moon HE, Park SH, et al. A bioprinted human-glioblastoma-on-a-chip for the identification of patient-specific responses to chemoradiotherapy. *Nat Biomed Eng*. 2019;3(7):509-19. doi: 10.1038/s41551-019-0363-x. PubMed PMID: WOS:000474416500008.
291. Ayuso JM, Monge R, Martinez-Gonzalez A, Virumbrales-Munoz M, Llamazares GA, Berganzo J, et al. Glioblastoma on a microfluidic chip: Generating pseudopalisades and enhancing aggressiveness through blood vessel obstruction events. *Neuro-Oncology*. 2017;19(4):503-13. doi: 10.1093/neuonc/now230. PubMed PMID: WOS:000400894900008.

292. Radhakrishnan J, Varadaraj S, Dash SK, Sharma A, Verma RS. Organotypic cancer tissue models for drug screening: 3D constructs, bioprinting and microfluidic chips. *Drug Discov Today*. 2020;25(5):879-90. doi: 10.1016/j.drudis.2020.03.002. PubMed PMID: WOS:000541749200009.
293. Rodrigues RO, Sousa PC, Gaspar J, Banobre-Lopez M, Lima R, Minas G. Organ-on-a-Chip: A Preclinical Microfluidic Platform for the Progress of Nanomedicine. *Small*. 2020;16(51):19. doi: 10.1002/sml.202003517. PubMed PMID: WOS:000592105400001.
294. Datta P, Dey M, Ataie Z, Unutmaz D, Ozbolat IT. 3D bioprinting for reconstituting the cancer microenvironment. *npj Precis Oncol*. 2020;4(1):13. doi: 10.1038/s41698-020-0121-2. PubMed PMID: WOS:000552695000001.
295. Matai I, Kaur G, Seyedsalehi A, McClinton A, Laurencin CT. Progress in 3D bioprinting technology for tissue/organ regenerative engineering. *Biomaterials*. 2020;226:32. doi: 10.1016/j.biomaterials.2019.119536. PubMed PMID: WOS:000498330900001.
296. Gomez-Oliva R, Dominguez-Garcia S, Carrascal L, Abalos-Martinez J, Pardillo-Diaz R, Verastegui C, et al. Evolution of Experimental Models in the Study of Glioblastoma: Toward Finding Efficient Treatments. *Front Oncol*. 2021;10:16. doi: 10.3389/fonc.2020.614295. PubMed PMID: WOS:000617048300001.
297. Ozturk MS, Lee VK, Zou HY, Friedel RH, Intes X, Dai GH. High-resolution tomographic analysis of in vitro 3D glioblastoma tumor model under long-term drug treatment. *Sci Adv*. 2020;6(10):11. doi: 10.1126/sciadv.aay7513. PubMed PMID: WOS:000519001400023.
298. Wang XZ, Li XD, Dai XL, Zhang XZ, Zhang J, Xu T, et al. Bioprinting of glioma stem cells improves their endotheliogenic potential. *Colloids and Surfaces B-*

Biointerfaces. 2018;171:629-37. doi: 10.1016/j.colsurfb.2018.08.006. PubMed PMID: WOS:000447575400076.

299. Heinrich MA, Bansal R, Lammers T, Zhang YS, Schiffelers RM, Prakash J. 3D-Bioprinted Mini-Brain: A Glioblastoma Model to Study Cellular Interactions and Therapeutics. *Adv Mater.* 2019;31(14):9. doi: 10.1002/adma.201806590. PubMed PMID: WOS:000467974100005.

300. Noor N, Shapira A, Edri R, Gal I, Wertheim L, Dvir T. 3D Printing of Personalized Thick and Perfusable Cardiac Patches and Hearts. *Adv Sci.* 2019;6(11):10. doi: 10.1002/advs.201900344. PubMed PMID: WOS:000470189500013.

301. Lübtow MM, Oerter S, Quader S, Jeanclos E, Cubukova A, Krafft M, et al. In Vitro Blood-Brain Barrier Permeability and Cytotoxicity of an Atorvastatin-Loaded Nanoformulation Against Glioblastoma in 2D and 3D Models. *Mol Pharm.* 2020;17(6):1835-47. Epub 2020/04/22. doi: 10.1021/acs.molpharmaceut.9b01117. PubMed PMID: 32315193.

302. Gretskeya NM, Gamisonia AM, Dudina PV, Zakharov SS, Sherstyanykh G, Akasov R, et al. Novel bexarotene derivatives: Synthesis and cytotoxicity evaluation for glioma cells in 2D and 3D in vitro models. *Eur J Pharmacol.* 2020;883:11. doi: 10.1016/j.ejphar.2020.173346. PubMed PMID: WOS:000569146600001.

303. Alghamdi M, Chierchini F, Eigel D, Taplan C, Miles T, Pette D, et al. Poly(ethylene glycol) based nanotubes for tuneable drug delivery to glioblastoma multiforme. *Nanoscale Advances.* 2020;2(10):4498-509. doi: 10.1039/d0na00471e. PubMed PMID: WOS:000586010700016.

304. Roh H, Kim H, Park JK. Construction of a Fibroblast-Associated Tumor Spheroid Model Based on a Collagen Drop Array Chip. *Biosensors-Basel.* 2021;11(12):14. doi: 10.3390/bios11120506. PubMed PMID: WOS:000735613500001.

305. Ganguli A, Mostafa A, Saavedra C, Kim Y, Le P, Faramarzi V, et al. Three-dimensional microscale hanging drop arrays with geometric control for drug screening and live tissue imaging. *Sci Adv.* 2021;7(17):15. doi: 10.1126/sciadv.abc1323. PubMed PMID: WOS:000656713700002.
306. Khosla K, Naus CC, Sin WC. Cx43 in Neural Progenitors Promotes Glioma Invasion in a 3D Culture System. *International Journal of Molecular Sciences.* 2020;21(15):9. doi: 10.3390/ijms21155216. PubMed PMID: WOS:000559058300001.
307. Chaicharoenaudomrung N, Kunhorm P, Promjantuek W, Rujanapun N, Heebkaew N, Soraksa N, et al. Transcriptomic Profiling of 3D Glioblastoma Tumoroids for the Identification of Mechanisms Involved in Anticancer Drug Resistance. *In Vivo.* 2020;34(1):199-211. doi: 10.21873/invivo.11762. PubMed PMID: WOS:000504753200024.
308. Lv DL, Yu SC, Ping YF, Wu HB, Zhao XL, Zhang HR, et al. A three-dimensional collagen scaffold cell culture system for screening anti-glioma therapeutics. *Oncotarget.* 2016;7(35):56904-14. doi: 10.18632/oncotarget.10885. PubMed PMID: WOS:000386911600077.
309. Ma NKL, Lim JK, Leong MF, Sandanaraj E, Ang BT, Tang C, et al. Collaboration of 3D context and extracellular matrix in the development of glioma stemness in a 3D model. *Biomaterials.* 2016;78:62-73. doi: 10.1016/j.biomaterials.2015.11.031. PubMed PMID: WOS:000368955200007.
310. Carey-Ewend AG, Hagler SB, Bomba HN, Goetz MJ, Bago JR, Hingtgen SD. Developing Bioinspired Three-Dimensional Models of Brain Cancer to Evaluate Tumor-Homing Neural Stem Cell Therapy. *Tissue Eng Part A.* 2020. Epub 2020/10/22. doi: 10.1089/ten.tea.2020.0113. PubMed PMID: 33085922.

311. Chen JWE, Jan LMB, Leary S, Sarkaria JN, Steelman AJ, Gaskins HR, et al. Crosstalk between microglia and patient-derived glioblastoma cells inhibit invasion in a three-dimensional gelatin hydrogel model. *J Neuroinflamm.* 2020;17(1):15. doi: 10.1186/s12974-020-02026-6. PubMed PMID: WOS:000594808900002.
312. Wang C, Sinha S, Jiang XY, Fitch S, Wilson C, Caretti V, et al. A comparative study of brain tumor cells from different age and anatomical locations using 3D biomimetic hydrogels. *Acta Biomater.* 2020;116:201-8. doi: 10.1016/j.actbio.2020.09.007. PubMed PMID: WOS:000577516000012.
313. Chen J, Ananthanarayanan B, Springer KS, Wolf KJ, Sheyman SM, Tran VD, et al. Suppression of LIM Kinase 1 and LIM Kinase 2 Limits Glioblastoma Invasion. *Cancer Res.* 2020;80(1):69-78. doi: 10.1158/0008-5472.Can-19-1237. PubMed PMID: WOS:000505668200010.
314. Tricinci O, De Pasquale D, Marino A, Battaglini M, Pucci C, Ciofani G. A 3D Biohybrid Real-Scale Model of the Brain Cancer Microenvironment for Advanced In Vitro Testing. *Adv Mater Technol.* 2020;5(10):10. doi: 10.1002/admt.202000540. PubMed PMID: WOS:000561753800001.
315. Samiei E, Seyfoori A, Toyota B, Ghavami S, Akbari M. Investigating Programmed Cell Death and Tumor Invasion in a Three-Dimensional (3D) Microfluidic Model of Glioblastoma. *International Journal of Molecular Sciences.* 2020;21(9):24. doi: 10.3390/ijms21093162. PubMed PMID: WOS:000535581700133.
316. Smits IPM, Blaschuk OW, Willerth SM. Novel N-cadherin antagonist causes glioblastoma cell death in a 3D bioprinted co-culture model. *Biochem Biophys Res Commun.* 2020;529(2):162-8. doi: 10.1016/j.bbrc.2020.06.001. PubMed PMID: WOS:000551875700006.

317. Tang M, Xie Q, Gimple RC, Zhong Z, Tam T, Tian J, et al. Three-dimensional bioprinted glioblastoma microenvironments model cellular dependencies and immune interactions. *Cell Res.* 2020;30(10):833-53. doi: 10.1038/s41422-020-0338-1. PubMed PMID: WOS:000538006500001.
318. Dai XL, Ma C, Lan Q, Xu T. 3D bioprinted glioma stem cells for brain tumor model and applications of drug susceptibility. *Biofabrication.* 2016;8(4):11. doi: 10.1088/1758-5090/8/4/045005. PubMed PMID: WOS:000386140500001.
319. Hermida MA, Kumar JD, Schwarz D, Lavery KG, Di Bartolo A, Ardron M, et al. Three dimensional in vitro models of cancer: Bioprinting multilineage glioblastoma models. *Adv Biol Regul.* 2020;75:100658. Epub 2019/11/16. doi: 10.1016/j.jbior.2019.100658. PubMed PMID: 31727590.
320. Lee EJ, Rath P, Liu J, Ryu D, Pei L, Noonepalle SK, et al. Identification of Global DNA Methylation Signatures in Glioblastoma-Derived Cancer Stem Cells. *J Genet Genomics.* 2015;42(7):355-71. Epub 2015/08/04. doi: 10.1016/j.jgg.2015.06.003. PubMed PMID: 26233891; PubMed Central PMCID: PMC4648292.
321. Kievit FM, Florczyk SJ, Leung MC, Wang K, Wu JD, Silber JR, et al. Proliferation and enrichment of CD133+ glioblastoma cancer stem cells on 3D chitosan-alginate scaffolds. *Biomaterials.* 2014;35(33):9137-43. doi: <https://doi.org/10.1016/j.biomaterials.2014.07.037>.
322. Tang M, Rich JN, Chen S. Biomaterials and 3D Bioprinting Strategies to Model Glioblastoma and the Blood–Brain Barrier. *Adv Mater.* 2021;33(5):2004776. doi: <https://doi.org/10.1002/adma.202004776>.
323. Hajal C, Offeddu GS, Shin Y, Zhang S, Morozova O, Hickman D, et al. Engineered human blood–brain barrier microfluidic model for vascular permeability analyses. *Nature Protocols.* 2022;17(1):95-128. doi: 10.1038/s41596-021-00635-w.

324. Passaro AP, Lebos AL, Yao Y, Stice SL. Immune Response in Neurological Pathology: Emerging Role of Central and Peripheral Immune Crosstalk. *Frontiers in Immunology*. 2021;12:676621-. doi: 10.3389/fimmu.2021.676621. PubMed PMID: 34177918.
325. Koizumi T, Kerkhofs D, Mizuno T, Steinbusch HWM, Foulquier S. Vessel-Associated Immune Cells in Cerebrovascular Diseases: From Perivascular Macrophages to Vessel-Associated Microglia. *Frontiers in Neuroscience*. 2019;13. doi: 10.3389/fnins.2019.01291.
326. You H, Baluszek S, Kaminska B. Supportive roles of brain macrophages in CNS metastases and assessment of new approaches targeting their functions. *Theranostics*. 2020;10(7):2949-64. doi: 10.7150/thno.40783. PubMed PMID: 32194848.
327. Wei J, Chen P, Gupta P, Ott M, Zamler D, Kassab C, et al. Immune biology of glioma-associated macrophages and microglia: functional and therapeutic implications. *Neuro Oncol*. 2020;22(2):180-94. Epub 2019/11/05. doi: 10.1093/neuonc/noz212. PubMed PMID: 31679017; PubMed Central PMCID: PMC7442334.
328. Ge Y, Wang X, Guo Y, Yan J, Abuduwaili A, Aximujiang K, et al. Gut microbiota influence tumor development and Alter interactions with the human immune system. *Journal of Experimental & Clinical Cancer Research*. 2021;40(1):42. doi: 10.1186/s13046-021-01845-6.
329. Mehrian-Shai R, Reichardt JKV, Harris CC, Toren A. The Gut–Brain Axis, Paving the Way to Brain Cancer. *Trends in Cancer*. 2019;5(4):200-7. doi: <https://doi.org/10.1016/j.trecan.2019.02.008>.
330. Viaud S, Saccheri F, Mignot G, Yamazaki T, Daillère R, Hannani D, et al. The Intestinal Microbiota Modulates the Anticancer Immune Effects of Cyclophosphamide. *Science*. 2013;342(6161):971-6. doi: doi:10.1126/science.1240537.

331. Schmitt C, Adamski V, Rasch F, Adelung R, Lucius R, Synowitz M, et al. Establishment of a glioblastoma in vitro (in)complete resection dual co-culture model suitable for drug testing. *Annals of Anatomy - Anatomischer Anzeiger*. 2020;228:151440. doi: <https://doi.org/10.1016/j.aanat.2019.151440>.
332. Ogawa J, Pao GM, Shokhirev MN, Verma IM. Glioblastoma Model Using Human Cerebral Organoids. *Cell Reports*. 2018;23(4):1220-9. doi: 10.1016/j.celrep.2018.03.105.
333. Ramani A, Müller L, Ostermann PN, Gabriel E, Abida-Islam P, Müller-Schiffmann A, et al. SARS-CoV-2 targets neurons of 3D human brain organoids. *EMBO J*. 2020;39(20):e106230-e. Epub 2020/09/23. doi: 10.15252/embj.2020106230. PubMed PMID: 32876341.
334. Perera D, Senanayake H, Thoradeniya T, editors. Determination of adipocyte cell size by H & E stained adipose tissue and collagenase digested isolated adipocytes 2018.
335. Bonnier F, Keating ME, Wróbel TP, Majzner K, Baranska M, Garcia-Munoz A, et al. Cell viability assessment using the Alamar blue assay: A comparison of 2D and 3D cell culture models. *Toxicology in Vitro*. 2015;29(1):124-31. doi: <https://doi.org/10.1016/j.tiv.2014.09.014>.
336. Scally L, Behan S, de Carvalho AMA, Sarangapani C, Tiwari B, Malone R, et al. Diagnostics of a large volume pin-to-plate atmospheric plasma source for the study of plasma species interactions with cancer cell cultures. *Plasma Processes and Polymers*. doi: 10.1002/ppap.202000250. PubMed PMID: WOS:000621067300001.
337. Zhou R, Zhang T, Zhou R, Wang S, Mei D, Mai-Prochnow A, et al. Sustainable plasma-catalytic bubbles for hydrogen peroxide synthesis. *Green Chemistry*. 2021;23(8):2977-85. doi: 10.1039/D1GC00198A.

338. Mai-Prochnow A, Alam D, Zhou R, Zhang T, Ostrikov K, Cullen PJ. Microbial decontamination of chicken using atmospheric plasma bubbles. *Plasma Processes and Polymers*. 2021;18(1):2000052. doi: <https://doi.org/10.1002/ppap.202000052>.
339. Glorieux C, Calderon PB. Catalase, a remarkable enzyme: targeting the oldest antioxidant enzyme to find a new cancer treatment approach. *Biol Chem*. 2017;398(10):1095-108. Epub 2017/04/07. doi: 10.1515/hsz-2017-0131. PubMed PMID: 28384098.
340. Nandi A, Yan LJ, Jana CK, Das N. Role of Catalase in Oxidative Stress- and Age-Associated Degenerative Diseases. *Oxid Med Cell Longev*. 2019;2019:9613090. Epub 2019/12/13. doi: 10.1155/2019/9613090. PubMed PMID: 31827713; PubMed Central PMCID: PMC6885225.
341. Langhans SA. Three-Dimensional in Vitro Cell Culture Models in Drug Discovery and Drug Repositioning. *Frontiers in Pharmacology*. 2018;9. doi: 10.3389/fphar.2018.00006.
342. Fang Y, Eglén RM. Three-Dimensional Cell Cultures in Drug Discovery and Development. *SLAS Discov*. 2017;22(5):456-72. Epub 2017/05/19. doi: 10.1177/1087057117696795. PubMed PMID: 28520521; PubMed Central PMCID: PMC6448717.
343. Singh SK, Abbas S, Saxena AK, Tiwari S, Sharma LK, Tiwari M. Critical role of three-dimensional tumorsphere size on experimental outcome. *BioTechniques*. 2020;69(5):333-8. doi: 10.2144/btn-2020-0081.
344. Eilenberger C, Rothbauer M, Ehmoser EK, Ertl P, Küpcü S. Effect of Spheroidal Age on Sorafenib Diffusivity and Toxicity in a 3D HepG2 Spheroid Model. *Sci Rep*. 2019;9(1):4863. Epub 2019/03/21. doi: 10.1038/s41598-019-41273-3. PubMed PMID: 30890741; PubMed Central PMCID: PMC6425026.

345. Rampersad SN. Multiple applications of Alamar Blue as an indicator of metabolic function and cellular health in cell viability bioassays. *Sensors (Basel)*. 2012;12(9):12347-60. Epub 2012/11/01. doi: 10.3390/s120912347. PubMed PMID: 23112716; PubMed Central PMCID: PMC3478843.
346. Gupta N, Liu JR, Patel B, Solomon DE, Vaidya B, Gupta V. Microfluidics-based 3D cell culture models: Utility in novel drug discovery and delivery research. *Bioeng Transl Med*. 2016;1(1):63-81. doi: 10.1002/btm2.10013. PubMed PMID: 29313007.
347. Andreatta F, Beccaceci G, Fortuna N, Celotti M, De Felice D, Lorenzoni M, et al. The Organoid Era Permits the Development of New Applications to Study Glioblastoma. *Cancers*. 2020;12(11):16. doi: 10.3390/cancers12113303. PubMed PMID: WOS:000592830300001.
348. Lapointe S, Perry A, Butowski NA. Primary brain tumours in adults. *Lancet*. 2018;392(10145):432-46. doi: 10.1016/s0140-6736(18)30990-5. PubMed PMID: 30060998.
349. Bi JF, Chowdhry S, Wu SH, Zhang WJ, Masui K, Mischel PS. Altered cellular metabolism in gliomas - an emerging landscape of actionable co-dependency targets. *Nature Reviews Cancer*. 2020;20(1):57-70. doi: 10.1038/s41568-019-0226-5. PubMed PMID: WOS:000504714500008.
350. Mariappan A, Goranci-Buzhala G, Ricci-Vitiani L, Pallini R, Gopalakrishnan J. Trends and challenges in modeling glioma using 3D human brain organoids. *Cell Death and Differentiation*. 2021;28(1):15-23. doi: 10.1038/s41418-020-00679-7. PubMed PMID: WOS:000595351800001.
351. Mahmoud BS, AlAmri AH, McConville C. Polymeric Nanoparticles for the Treatment of Malignant Gliomas. *Cancers*. 2020;12(1). doi: 10.3390/cancers12010175. PubMed PMID: WOS:000516826700175.

352. Lin L, Keidar M. A map of control for cold atmospheric plasma jets: From physical mechanisms to optimizations. *Applied Physics Reviews*. 2021;8(1). doi: 10.1063/5.0022534. PubMed PMID: WOS:000629734500001.
353. Weiswald L-B, Bellet D, Dangles-Marie V. Spherical Cancer Models in Tumor Biology. *Neoplasia*. 2015;17(1):1-15. doi: <https://doi.org/10.1016/j.neo.2014.12.004>.
354. Joshi RS, Kanugula SS, Sudhir S, Pereira MP, Jain S, Aghi MK. The Role of Cancer-Associated Fibroblasts in Tumor Progression. *Cancers*. 2021;13(6):1399. PubMed PMID: doi:10.3390/cancers13061399.
355. Chhetri A, Rispoli JV, Lelièvre SA. 3D Cell Culture for the Study of Microenvironment-Mediated Mechanostimuli to the Cell Nucleus: An Important Step for Cancer Research. *Frontiers in Molecular Biosciences*. 2021;8(22). doi: 10.3389/fmolb.2021.628386.
356. Gjika E, Pal-Ghosh S, Kirschner ME, Lin L, Sherman JH, Stepp MA, et al. Combination therapy of cold atmospheric plasma (CAP) with temozolomide in the treatment of U87MG glioblastoma cells. *Scientific Reports*. 2020;10(1):16495. doi: 10.1038/s41598-020-73457-7.
357. Piletz JE, Drivon J, Eisenga J, Buck W, Yen S, McLin M, et al. Human Cells Grown With or Without Substitutes for Fetal Bovine Serum. *Cell Med*. 2018;10:2155179018755140. Epub 2018/06/06. doi: 10.1177/2155179018755140. PubMed PMID: 32634183; PubMed Central PMCID: PMC6172986.
358. Białkowska K, Komorowski P, Bryszewska M, Miłowska K. Spheroids as a Type of Three-Dimensional Cell Cultures-Examples of Methods of Preparation and the Most Important Application. *International journal of molecular sciences*. 2020;21(17):6225. doi: 10.3390/ijms21176225. PubMed PMID: 32872135.

359. Tsoukou E, Bourke P, Boehm D. Understanding the Differences Between Antimicrobial and Cytotoxic Properties of Plasma Activated Liquids. 2018;8(3):299-320. doi: 10.1615/PlasmaMed.2018028261.
360. Sun Y, Wang H, Wang P, Zhang K, Geng X, Liu Q, et al. Tumor targeting DVDMS-nanoliposomes for an enhanced sonodynamic therapy of gliomas. *Biomaterials science*. 2019;7 3:985-94.
361. Xu Y, Shen M, Li Y, Sun Y, Teng Y, Wang Y, et al. The synergic antitumor effects of paclitaxel and temozolomide co-loaded in mPEG-PLGA nanoparticles on glioblastoma cells. *Oncotarget*. 2016;7(15):20890-901. Epub 2016/03/10. doi: 10.18632/oncotarget.7896. PubMed PMID: 26956046; PubMed Central PMCID: PMC4991499.
362. Lee S, Jeon H, Shim S, Im M, Kim J, Kim JH, et al. Preclinical study to improve microbubble-mediated drug delivery in cancer using an ultrasonic probe with an interchangeable acoustic lens. *Scientific Reports*. 2021;11(1):12654. doi: 10.1038/s41598-021-92097-z.
363. Paškevičiūtė M, Januškevičienė I, Sakalauskienė K, Raišutis R, Petrikaitė V. Evaluation of low-intensity pulsed ultrasound on doxorubicin delivery in 2D and 3D cancer cell cultures. *Scientific Reports*. 2020;10(1):16161. doi: 10.1038/s41598-020-73204-y.
364. Ortiz R, Perazzoli G, Cabeza L, Jiménez-Luna C, Luque R, Prados J, et al. Temozolomide: An Updated Overview of Resistance Mechanisms, Nanotechnology Advances and Clinical Applications. *Curr Neuropharmacol*. 2021;19(4):513-37. Epub 2020/06/27. doi: 10.2174/1570159x18666200626204005. PubMed PMID: 32589560; PubMed Central PMCID: PMC8206461.

365. Jagannathan J, Sanghvi NT, Crum LA, Yen CP, Medel R, Dumont AS, et al. High-intensity focused ultrasound surgery of the brain: part 1--A historical perspective with modern applications. *Neurosurgery*. 2009;64(2):201-10; discussion 10-1. Epub 2009/02/05. doi: 10.1227/01.Neu.0000336766.18197.8e. PubMed PMID: 19190451; PubMed Central PMCID: PMCPMC4068031.
366. Zarnitsyn VG, Kamaev PP, Prausnitz MR. Ultrasound-enhanced chemotherapy and gene delivery for glioma cells. *Technol Cancer Res Treat*. 2007;6(5):433-42. Epub 2007/09/20. doi: 10.1177/153303460700600509. PubMed PMID: 17877433.
367. Baghbani F, Chegeni M, Moztarzadeh F, Mohandesi JA, Mokhtari-Dizaji M. Ultrasonic nanotherapy of breast cancer using novel ultrasound-responsive alginate-shelled perfluorohexane nanodroplets: In vitro and in vivo evaluation. *Materials Science and Engineering: C*. 2017;77:698-707. doi: <https://doi.org/10.1016/j.msec.2017.02.017>.
368. Li H, Wang Z, Zhang J, Yuan C, Zhang H, Hou X, et al. Enhanced shRNA delivery by the combination of polyethylenimine, ultrasound, and nanobubbles in liver cancer. *Technol Health Care*. 2019;27(S1):263-72. Epub 2019/05/03. doi: 10.3233/thc-199025. PubMed PMID: 31045545; PubMed Central PMCID: PMCPMC6597992.
369. Kinoshita M, McDannold N, Jolesz FA, Hynynen K. Noninvasive localized delivery of Herceptin to the mouse brain by MRI-guided focused ultrasound-induced blood-brain barrier disruption. *Proceedings of the National Academy of Sciences*. 2006;103(31):11719-23. doi: doi:10.1073/pnas.0604318103.
370. Greco A, Di Benedetto A, Howard CM, Kelly S, Nande R, Dementieva Y, et al. Eradication of therapy-resistant human prostate tumors using an ultrasound-guided site-specific cancer terminator virus delivery approach. *Mol Ther*. 2010;18(2):295-306. Epub 2009/11/06. doi: 10.1038/mt.2009.252. PubMed PMID: 19888195; PubMed Central PMCID: PMCPMC2839288.

371. Idbaih A, Canney M, Belin L, Desseaux C, Vignot A, Bouchoux G, et al. Safety and Feasibility of Repeated and Transient Blood–Brain Barrier Disruption by Pulsed Ultrasound in Patients with Recurrent Glioblastoma. *Clinical Cancer Research*. 2019;25(13):3793-801. doi: 10.1158/1078-0432.Ccr-18-3643.
372. Lee S, Al-Kaabi L, Mawart A, Khandoker A, Alsafar H, Jelinek HF, et al. Ultrasound-mediated drug delivery by gas bubbles generated from a chemical reaction. *Journal of Drug Targeting*. 2018;26(2):172-81. doi: 10.1080/1061186X.2017.1354001.
373. Pi Z, Huang Y, Shen Y, Zeng X, Hu Y, Chen T, et al. Sonodynamic Therapy on Intracranial Glioblastoma Xenografts Using Sinoporphyrin Sodium Delivered by Ultrasound with Microbubbles. *Ann Biomed Eng*. 2019;47(2):549-62. Epub 2018/10/21. doi: 10.1007/s10439-018-02141-9. PubMed PMID: 30341739.
374. Landgraf L, Kozlowski A, Zhang X, Fournelle M, Becker FJ, Tretbar S, et al. Focused Ultrasound Treatment of a Spheroid In Vitro Tumour Model. *Cells*. 2022;11(9). Epub 2022/05/15. doi: 10.3390/cells11091518. PubMed PMID: 35563823; PubMed Central PMCID: PMC9099905.
375. Rwei P, Alex Gong CS, Luo LJ, Lin MB, Lai JY, Liu HL. In vitro investigation of ultrasound-induced oxidative stress on human lens epithelial cells. *Biochem Biophys Res Commun*. 2017;482(4):954-60. Epub 2016/11/30. doi: 10.1016/j.bbrc.2016.11.139. PubMed PMID: 27894841.
376. Pefani-Antimisiari K, Athanasopoulos DK, Marazioti A, Sklias K, Rodi M, de Lastic A-L, et al. Synergistic effect of cold atmospheric pressure plasma and free or liposomal doxorubicin on melanoma cells. *Scientific Reports*. 2021;11(1):14788. doi: 10.1038/s41598-021-94130-7.

377. Nitiss JL. Targeting DNA topoisomerase II in cancer chemotherapy. *Nat Rev Cancer*. 2009;9(5):338-50. Epub 2009/04/21. doi: 10.1038/nrc2607. PubMed PMID: 19377506; PubMed Central PMCID: PMCPMC2748742.
378. Kim HS, Lee YS, Kim DK. Doxorubicin exerts cytotoxic effects through cell cycle arrest and Fas-mediated cell death. *Pharmacology*. 2009;84(5):300-9. Epub 2009/10/16. doi: 10.1159/000245937. PubMed PMID: 19829019.
379. Girard PM, Arbabian A, Fleury M, Bauville G, Puech V, Dutreix M, et al. Synergistic Effect of H₂O₂ and NO₂ in Cell Death Induced by Cold Atmospheric He Plasma. *Sci Rep*. 2016;6:29098. Epub 2016/07/02. doi: 10.1038/srep29098. PubMed PMID: 27364563; PubMed Central PMCID: PMCPMC4929573.
380. Fransolet M, Noël L, Henry L, Labied S, Blacher S, Nisolle M, et al. Evaluation of Z-VAD-FMK as an anti-apoptotic drug to prevent granulosa cell apoptosis and follicular death after human ovarian tissue transplantation. *J Assist Reprod Genet*. 2019;36(2):349-59. Epub 2018/11/06. doi: 10.1007/s10815-018-1353-8. PubMed PMID: 30390176; PubMed Central PMCID: PMCPMC6420548.
381. Kim SO, Han J. Pan-caspase inhibitor zVAD enhances cell death in RAW246.7 macrophages. *J Endotoxin Res*. 2001;7(4):292-6. Epub 2001/11/22. doi: 10.1179/096805101101532873. PubMed PMID: 11717584.
382. Li X, Yao X, Zhu Y, Zhang H, Wang H, Ma Q, et al. The Caspase Inhibitor Z-VAD-FMK Alleviates Endotoxic Shock via Inducing Macrophages Necroptosis and Promoting MDSCs-Mediated Inhibition of Macrophages Activation. *Frontiers in Immunology*. 2019;10. doi: 10.3389/fimmu.2019.01824.
383. Wu Q, Wu W, Jacevic V, Franca TCC, Wang X, Kuca K. Selective inhibitors for JNK signalling: a potential targeted therapy in cancer. *Journal of Enzyme Inhibition and Medicinal Chemistry*. 2020;35(1):574-83. doi: 10.1080/14756366.2020.1720013.

384. Bennett BL, Sasaki DT, Murray BW, O'Leary EC, Sakata ST, Xu W, et al. SP600125, an anthrapyrazolone inhibitor of Jun N-terminal kinase. *Proceedings of the National Academy of Sciences*. 2001;98(24):13681-6. doi: doi:10.1073/pnas.251194298.
385. Lou L, Hu D, Chen S, Wang S, Xu Y, Huang Y, et al. Protective role of JNK inhibitor SP600125 in sepsis-induced acute lung injury. *Int J Clin Exp Pathol*. 2019;12(2):528-38. Epub 2020/01/15. PubMed PMID: 31933857; PubMed Central PMCID: PMC6945091.
386. Matsumoto K, Mizoue K, Kitamura K, Tse WC, Huber CP, Ishida T. Structural basis of inhibition of cysteine proteases by E-64 and its derivatives. *Biopolymers*. 1999;51(1):99-107. Epub 1999/06/25. doi: 10.1002/(sici)1097-0282(1999)51:1<99::Aid-bip11>3.0.Co;2-r. PubMed PMID: 10380357.
387. Shockey WA, Kieslich CA, Wilder CL, Watson V, Platt MO. Dynamic Model of Protease State and Inhibitor Trafficking to Predict Protease Activity in Breast Cancer Cells. *Cell Mol Bioeng*. 2019;12(4):275-88. Epub 2019/11/14. doi: 10.1007/s12195-019-00580-5. PubMed PMID: 31719914; PubMed Central PMCID: PMC6816728.
388. Zhang Z, Huang Z, Dai H, Wei L, Sun S, Gao F. Therapeutic Efficacy of E-64-d, a Selective Calpain Inhibitor, in Experimental Acute Spinal Cord Injury. *Biomed Res Int*. 2015;2015:134242. Epub 2015/08/05. doi: 10.1155/2015/134242. PubMed PMID: 26240815; PubMed Central PMCID: PMC4512559.
389. Wadhawan M, Singh N, Rathaur S. Inhibition of Cathepsin B by E-64 Induces Oxidative Stress and Apoptosis in Filarial Parasite. *PLOS ONE*. 2014;9(3):e93161. doi: 10.1371/journal.pone.0093161.
390. Haas B, Klinger V, Keksel C, Bonigut V, Kiefer D, Caspers J, et al. Inhibition of the PI3K but not the MEK/ERK pathway sensitizes human glioma cells to alkylating drugs. *Cancer Cell International*. 2018;18(1):69. doi: 10.1186/s12935-018-0565-4.

391. Tuomela J, Sandholm J, Kauppila JH, Lehenkari P, Harris KW, Selander KS. Chloroquine has tumor-inhibitory and tumor-promoting effects in triple-negative breast cancer. *Oncol Lett.* 2013;6(6):1665-72. doi: 10.3892/ol.2013.1602.
392. Hwang SY, Yoo BC, Jung JW, Oh ES, Hwang JS, Shin JA, et al. Induction of glioma apoptosis by microglia-secreted molecules: The role of nitric oxide and cathepsin B. *Biochim Biophys Acta.* 2009;1793(11):1656-68. Epub 2009/09/15. doi: 10.1016/j.bbamcr.2009.08.011. PubMed PMID: 19748528.
393. Wen X, Lin ZQ, Liu B, Wei YQ. Caspase-mediated programmed cell death pathways as potential therapeutic targets in cancer. *Cell Prolif.* 2012;45(3):217-24. Epub 2012/03/21. doi: 10.1111/j.1365-2184.2012.00814.x. PubMed PMID: 22429822; PubMed Central PMCID: PMC3063296.
394. Dhanasekaran DN, Reddy EP. JNK signaling in apoptosis. *Oncogene.* 2008;27(48):6245-51. Epub 2008/10/22. doi: 10.1038/onc.2008.301. PubMed PMID: 18931691; PubMed Central PMCID: PMC3063296.
395. Cheng SY, Wang SC, Lei M, Wang Z, Xiong K. Regulatory role of calpain in neuronal death. *Neural Regen Res.* 2018;13(3):556-62. Epub 2018/04/07. doi: 10.4103/1673-5374.228762. PubMed PMID: 29623944; PubMed Central PMCID: PMC5900522.
396. Alu A, Han X, Ma X, Wu M, Wei Y, Wei X. The role of lysosome in regulated necrosis. *Acta Pharm Sin B.* 2020;10(10):1880-903. Epub 2020/11/10. doi: 10.1016/j.apsb.2020.07.003. PubMed PMID: 33163342; PubMed Central PMCID: PMC7606114.
397. Johansson AC, Appelqvist H, Nilsson C, Kågedal K, Roberg K, Ollinger K. Regulation of apoptosis-associated lysosomal membrane permeabilization. *Apoptosis.*

2010;15(5):527-40. Epub 2010/01/16. doi: 10.1007/s10495-009-0452-5. PubMed PMID: 20077016; PubMed Central PMCID: PMCPMC2850995.

398. Zhang S, Rao S, Yang M, Ma C, Hong F, Yang S. Role of Mitochondrial Pathways in Cell Apoptosis during He-Patic Ischemia/Reperfusion Injury. *Int J Mol Sci.* 2022;23(4). Epub 2022/02/27. doi: 10.3390/ijms23042357. PubMed PMID: 35216473; PubMed Central PMCID: PMCPMC8877300.

399. Wang C, Youle RJ. The role of mitochondria in apoptosis*. *Annu Rev Genet.* 2009;43:95-118. Epub 2009/08/08. doi: 10.1146/annurev-genet-102108-134850. PubMed PMID: 19659442; PubMed Central PMCID: PMCPMC4762029.

400. Biau J, Chautard E, De Schlichting E, Dupic G, Pereira B, Fogli A, et al. Radiotherapy plus temozolomide in elderly patients with glioblastoma: a “real-life” report. *Radiation Oncology.* 2017;12(1):197. doi: 10.1186/s13014-017-0929-2.

401. Tan AC, Ashley DM, López GY, Malinzak M, Friedman HS, Khasraw M. Management of glioblastoma: State of the art and future directions. *CA Cancer J Clin.* 2020;70(4):299-312. Epub 2020/06/02. doi: 10.3322/caac.21613. PubMed PMID: 32478924.

402. Canavese G, Ancona A, Racca L, Canta M, Dumontel B, Barbaresco F, et al. Nanoparticle-assisted ultrasound: A special focus on sonodynamic therapy against cancer. *Chemical Engineering Journal.* 2018;340:155-72. doi: <https://doi.org/10.1016/j.cej.2018.01.060>.

403. Escoffre JM, Mannaris C, Geers B, Novell A, Lentacker I, Averkiou M, et al. Doxorubicin liposome-loaded microbubbles for contrast imaging and ultrasound-triggered drug delivery. *IEEE Trans Ultrason Ferroelectr Freq Control.* 2013;60(1):78-87. Epub 2013/01/05. doi: 10.1109/tuffc.2013.2539. PubMed PMID: 23287915.

404. Carson AR, McTiernan CF, Lavery L, Grata M, Leng X, Wang J, et al. Ultrasound-targeted microbubble destruction to deliver siRNA cancer therapy. *Cancer Res.* 2012;72(23):6191-9. Epub 2012/09/27. doi: 10.1158/0008-5472.Can-11-4079. PubMed PMID: 23010078; PubMed Central PMCID: PMCPMC3654825.
405. Goertz DE, Todorova M, Mortazavi O, Agache V, Chen B, Karshafian R, et al. Antitumor effects of combining docetaxel (taxotere) with the antivasular action of ultrasound stimulated microbubbles. *PLoS One.* 2012;7(12):e52307. Epub 2013/01/04. doi: 10.1371/journal.pone.0052307. PubMed PMID: 23284980; PubMed Central PMCID: PMCPMC3527530.
406. Zheng Y, Zhang Y, Ao M, Zhang P, Zhang H, Li P, et al. Hematoporphyrin encapsulated PLGA microbubble for contrast enhanced ultrasound imaging and sonodynamic therapy. *J Microencapsul.* 2012;29(5):437-44. Epub 2012/02/04. doi: 10.3109/02652048.2012.655333. PubMed PMID: 22299595.
407. Wei KC, Tsai HC, Lu YJ, Yang HW, Hua MY, Wu MF, et al. Neuronavigation-guided focused ultrasound-induced blood-brain barrier opening: a preliminary study in swine. *AJNR Am J Neuroradiol.* 2013;34(1):115-20. Epub 2012/06/23. doi: 10.3174/ajnr.A3150. PubMed PMID: 22723060; PubMed Central PMCID: PMCPMC7966321.
408. Hu J, He J, Wang Y, Zhao Y, Fang K, Dong Y, et al. Ultrasound combined with nanobubbles promotes systemic anticancer immunity and augments anti-PD1 efficacy. *J Immunother Cancer.* 2022;10(3). Epub 2022/03/04. doi: 10.1136/jitc-2021-003408. PubMed PMID: 35236741; PubMed Central PMCID: PMCPMC8896049.
409. Liu Y, Zhang H, Sun J, Liu J, Shen X, Zhan J, et al. Degradation of aniline in aqueous solution using non-thermal plasma generated in microbubbles. *Chemical Engineering Journal.* 2018;345:679-87. doi: <https://doi.org/10.1016/j.cej.2018.01.057>.

410. Zhou R, Zhou R, Wang P, Luan B, Zhang X, Fang Z, et al. Microplasma Bubbles: Reactive Vehicles for Biofilm Dispersal. *ACS Applied Materials & Interfaces*. 2019;11(23):20660-9. doi: 10.1021/acsami.9b03961.
411. Rodrigues J, Heinrich MA, Teixeira LM, Prakash J. 3D *In Vitro* Model (R)evolution: Unveiling Tumor's Stroma Interactions. *Trends in Cancer*. 2021;7(3):249-64. doi: 10.1016/j.trecan.2020.10.009.
412. Hersh AM, Bhimreddy M, Weber-Levine C, Jiang K, Alomari S, Theodore N, et al. Applications of Focused Ultrasound for the Treatment of Glioblastoma: A New Frontier. *Cancers (Basel)*. 2022;14(19). Epub 2022/10/15. doi: 10.3390/cancers14194920. PubMed PMID: 36230843; PubMed Central PMCID: PMC9563027.
413. Sardella E, Veronico V, Gristina R, Grossi L, Cosmai S, Striccoli M, et al. Plasma Treated Water Solutions in Cancer Treatments: The Contrasting Role of RNS. *Antioxidants (Basel)*. 2021;10(4). Epub 2021/05/01. doi: 10.3390/antiox10040605. PubMed PMID: 33920049; PubMed Central PMCID: PMC8071004.
414. Scally L, Behan S, Aguiar de Carvalho AM, Sarangapani C, Tiwari B, Malone R, et al. Diagnostics of a large volume pin-to-plate atmospheric plasma source for the study of plasma species interactions with cancer cell cultures. *Plasma Processes and Polymers*. 2021;18(6):2000250. doi: <https://doi.org/10.1002/ppap.202000250>.
415. Zhang X, Zhou R, Bazaka K, Liu Y, Zhou R, Chen G, et al. Quantification of plasma produced OH radical density for water sterilization. *Plasma Processes and Polymers*. 2018;15(6):1700241. doi: <https://doi.org/10.1002/ppap.201700241>.
416. Ahn HJ, Kim KI, Kim G, Moon E, Yang SS, Lee J-S. Atmospheric-Pressure Plasma Jet Induces Apoptosis Involving Mitochondria via Generation of Free Radicals. *PLOS ONE*. 2011;6(11):e28154. doi: 10.1371/journal.pone.0028154.

417. Georgescu MM. Multi-Platform Classification of IDH-Wild-Type Glioblastoma Based on ERK/MAPK Pathway: Diagnostic, Prognostic and Therapeutic Implications. *Cancers (Basel)*. 2021;13(18). Epub 2021/09/29. doi: 10.3390/cancers13184532. PubMed PMID: 34572759; PubMed Central PMCID: PMC8470497.
418. Tom MC, Cahill DP, Buckner JC, Dietrich J, Parsons MW, Yu JS. Management for Different Glioma Subtypes: Are All Low-Grade Gliomas Created Equal? *American Society of Clinical Oncology Educational Book*. 2019;(39):133-45. doi: 10.1200/edbk_238353. PubMed PMID: 31099638.
419. Yang K, Wu Z, Zhang H, Zhang N, Wu W, Wang Z, et al. Glioma targeted therapy: insight into future of molecular approaches. *Molecular Cancer*. 2022;21(1):39. doi: 10.1186/s12943-022-01513-z.
420. Pretanvil JA, Salinas IQ, Piccioni DE. Glioblastoma in the elderly: treatment patterns and survival. *CNS Oncol*. 2017;6(1):19-28. Epub 2016/12/22. doi: 10.2217/cns-2016-0023. PubMed PMID: 28001088; PubMed Central PMCID: PMC6027939.
421. Beauchesne P, Bernier V, Carnin C, Taillandier L, Djabri M, Martin L, et al. Prolonged survival for patients with newly diagnosed, inoperable glioblastoma with 3-times daily ultrafractionated radiation therapy. *Neuro Oncol*. 2010;12(6):595-602. Epub 2010/06/01. doi: 10.1093/neuonc/noq008. PubMed PMID: 20511183; PubMed Central PMCID: PMC2940649.
422. Sun D, Gao W, Hu H, Zhou S. Why 90% of clinical drug development fails and how to improve it? *Acta Pharm Sin B*. 2022;12(7):3049-62. Epub 2022/07/23. doi: 10.1016/j.apsb.2022.02.002. PubMed PMID: 35865092; PubMed Central PMCID: PMC9293739.
423. Dymova MA, Kuligina EV, Richter VA. Molecular Mechanisms of Drug Resistance in Glioblastoma. *Int J Mol Sci*. 2021;22(12). Epub 2021/07/03. doi:

10.3390/ijms22126385. PubMed PMID: 34203727; PubMed Central PMCID: PMCPMC8232134.

424. Wu W, Klockow JL, Zhang M, Lafortune F, Chang E, Jin L, et al. Glioblastoma multiforme (GBM): An overview of current therapies and mechanisms of resistance. *Pharmacological Research*. 2021;171:105780. doi: <https://doi.org/10.1016/j.phrs.2021.105780>.

425. Tang L, Feng Y, Gao S, Mu Q, Liu C. Nanotherapeutics Overcoming the Blood-Brain Barrier for Glioblastoma Treatment. *Front Pharmacol*. 2021;12:786700. Epub 2021/12/14. doi: 10.3389/fphar.2021.786700. PubMed PMID: 34899350; PubMed Central PMCID: PMCPMC8655904.

426. Murillo D, Huergo C, Gallego B, Rodríguez R, Tornín J. Exploring the Use of Cold Atmospheric Plasma to Overcome Drug Resistance in Cancer. *Biomedicines*. 2023;11(1):208. PubMed PMID: doi:10.3390/biomedicines11010208.

427. Liou GY, Storz P. Reactive oxygen species in cancer. *Free Radic Res*. 2010;44(5):479-96. Epub 2010/04/08. doi: 10.3109/10715761003667554. PubMed PMID: 20370557; PubMed Central PMCID: PMCPMC3880197.

428. Chauvin J, Judée F, Yousfi M, Vicendo P, Merbahi N. Analysis of reactive oxygen and nitrogen species generated in three liquid media by low temperature helium plasma jet. *Sci Rep*. 2017;7(1):4562. Epub 2017/07/06. doi: 10.1038/s41598-017-04650-4. PubMed PMID: 28676723; PubMed Central PMCID: PMCPMC5496897.

429. Van Loenhout J, Freire Boullosa L, Quatannens D, De Waele J, Merlin C, Lambrechts H, et al. Auranofin and Cold Atmospheric Plasma Synergize to Trigger Distinct Cell Death Mechanisms and Immunogenic Responses in Glioblastoma. *Cells*. 2021;10(11):2936. PubMed PMID: doi:10.3390/cells10112936.

430. Mateu-Sanz M, Tornín J, Ginebra MP, Canal C. Cold Atmospheric Plasma: A New Strategy Based Primarily on Oxidative Stress for Osteosarcoma Therapy. *J Clin Med*. 2021;10(4). Epub 2021/03/07. doi: 10.3390/jcm10040893. PubMed PMID: 33672274; PubMed Central PMCID: PMCPMC7926371.
431. Izadifar Z, Izadifar Z, Chapman D, Babyn P. An Introduction to High Intensity Focused Ultrasound: Systematic Review on Principles, Devices, and Clinical Applications. *J Clin Med*. 2020;9(2). Epub 2020/02/13. doi: 10.3390/jcm9020460. PubMed PMID: 32046072; PubMed Central PMCID: PMCPMC7073974.
432. McKenzie TG, Karimi F, Ashokkumar M, Qiao GG. Ultrasound and Sonochemistry for Radical Polymerization: Sound Synthesis. *Chemistry – A European Journal*. 2019;25(21):5372-88. doi: <https://doi.org/10.1002/chem.201803771>.
433. Kudo N, Okada K, Yamamoto K. Sonoporation by single-shot pulsed ultrasound with microbubbles adjacent to cells. *Biophys J*. 2009;96(12):4866-76. Epub 2009/06/17. doi: 10.1016/j.bpj.2009.02.072. PubMed PMID: 19527645; PubMed Central PMCID: PMCPMC2712027.
434. Arsiwala TA, Sprowls SA, Blethen KE, Adkins CE, Saralkar PA, Fladeland RA, et al. Ultrasound-mediated disruption of the blood tumor barrier for improved therapeutic delivery. *Neoplasia*. 2021;23(7):676-91. Epub 2021/06/18. doi: 10.1016/j.neo.2021.04.005. PubMed PMID: 34139452; PubMed Central PMCID: PMCPMC8208897.
435. Ning Z, Zhu Z, Wang H, Zhang C, Xu L, Zhuang L, et al. High-intensity focused ultrasound enhances the effect of bufalin by inducing apoptosis in pancreatic cancer cells. *Onco Targets Ther*. 2019;12:1161-70. Epub 2019/03/14. doi: 10.2147/ott.S185953. PubMed PMID: 30863083; PubMed Central PMCID: PMCPMC6388946.

436. Wang LY, Zheng SS. Advances in low-frequency ultrasound combined with microbubbles in targeted tumor therapy. *J Zhejiang Univ Sci B*. 2019;20(4):291-9. Epub 2019/04/02. doi: 10.1631/jzus.B1800508. PubMed PMID: 30932374; PubMed Central PMCID: PMC6454312.
437. Yang Q, Zhang R, Tang P, Sun Y, Johnson C, Saredy J, et al. Ultrasound May Suppress Tumor Growth, Inhibit Inflammation, and Establish Tolerogenesis by Remodeling Innatome via Pathways of ROS, Immune Checkpoints, Cytokines, and Trained Immunity/Tolerance. *J Immunol Res*. 2021;2021:6664453. Epub 2021/02/26. doi: 10.1155/2021/6664453. PubMed PMID: 33628851; PubMed Central PMCID: PMC6454312.
438. Hu R, Zeng Q, Su X, Feng W, Xiang H. The Correlation between Targeted Contrast-Enhanced Ultrasound Imaging and Tumor Neovascularization of Ovarian Cancer Xenografts in Nude Mice. *J Healthc Eng*. 2021;2021:5553649. Epub 2021/04/06. doi: 10.1155/2021/5553649. PubMed PMID: 33815730; PubMed Central PMCID: PMC6454312. personal relationships that could have appeared to influence the work reported in this paper.
439. Duval K, Grover H, Han LH, Mou Y, Pegoraro AF, Fredberg J, et al. Modeling Physiological Events in 2D vs. 3D Cell Culture. *Physiology (Bethesda)*. 2017;32(4):266-77. Epub 2017/06/16. doi: 10.1152/physiol.00036.2016. PubMed PMID: 28615311; PubMed Central PMCID: PMC6454312.
440. Kapałczyńska M, Kolenda T, Przybyła W, Zajączkowska M, Teresiak A, Filas V, et al. 2D and 3D cell cultures - a comparison of different types of cancer cell cultures. *Arch Med Sci*. 2018;14(4):910-9. Epub 2018/07/14. doi: 10.5114/aoms.2016.63743. PubMed PMID: 30002710; PubMed Central PMCID: PMC6454312.

441. Boix-Montesinos P, Soriano-Teruel PM, Armiñán A, Orzáez M, Vicent MJ. The past, present, and future of breast cancer models for nanomedicine development. *Advanced Drug Delivery Reviews*. 2021;173:306-30. doi: <https://doi.org/10.1016/j.addr.2021.03.018>.
442. Sixto-Lopez Y, Marhuenda E, Garcia-Vazquez JB, Fragoso-Vazquez MJ, Rosales-Hernandez MC, Zacarias-Lara O, et al. Targeting Several Biologically Reported Targets of Glioblastoma Multiforme by Assaying 2D and 3D Cultured Cells. *Cellular and Molecular Neurobiology*. 2022;42(6):1909-20. doi: 10.1007/s10571-021-01072-9. PubMed PMID: WOS:000630625100001.
443. Riedel NC, de Faria FW, Alfert A, Bruder JM, Kerl K. Three-Dimensional Cell Culture Systems in Pediatric and Adult Brain Tumor Precision Medicine. *Cancers*. 2022;14(23):5972. PubMed PMID: doi:10.3390/cancers14235972.
444. Zhang CY, Yang ZT, Dong DL, Jang TS, Knowles JC, Kim HW, et al. 3D culture technologies of cancer stem cells: promising ex vivo tumor models. *Journal of Tissue Engineering*. 2020;11. doi: 10.1177/2041731420933407. PubMed PMID: WOS:000545647100001.
445. Barbosa MAG, Xavier CPR, Pereira RF, Petrikaitė V, Vasconcelos MH. 3D Cell Culture Models as Recapitulators of the Tumor Microenvironment for the Screening of Anti-Cancer Drugs. *Cancers (Basel)*. 2021;14(1). Epub 2022/01/12. doi: 10.3390/cancers14010190. PubMed PMID: 35008353; PubMed Central PMCID: PMC8749977.
446. Park Y, Huh KM, Kang SW. Applications of Biomaterials in 3D Cell Culture and Contributions of 3D Cell Culture to Drug Development and Basic Biomedical Research. *Int J Mol Sci*. 2021;22(5). Epub 2021/04/04. doi: 10.3390/ijms22052491. PubMed PMID: 33801273; PubMed Central PMCID: PMC87958286.

447. Barin N, Balcioglu HE, de Heer I, de Wit M, Lamfers MLM, van Royen ME, et al. 3D-Engineered Scaffolds to Study Microtubes and Localization of Epidermal Growth Factor Receptor in Patient-Derived Glioma Cells. *Small*. 2022;18(49). doi: 10.1002/sml.202204485. PubMed PMID: WOS:000864926300001.
448. Marchini A, Gelain F. Synthetic scaffolds for 3D cell cultures and organoids: applications in regenerative medicine. *Crit Rev Biotechnol*. 2022;42(3):468-86. Epub 2021/07/01. doi: 10.1080/07388551.2021.1932716. PubMed PMID: 34187261.
449. Dragoj M, Stojkovska J, Stanković T, Dinić J, Podolski-Renić A, Obradović B, et al. Development and Validation of a Long-Term 3D Glioblastoma Cell Culture in Alginate Microfibers as a Novel Bio-Mimicking Model System for Preclinical Drug Testing. *Brain Sciences*. 2021;11(8):1025. PubMed PMID: doi:10.3390/brainsci11081025.
450. Caliari SR, Burdick JA. A practical guide to hydrogels for cell culture. *Nature Methods*. 2016;13(5):405-14. doi: 10.1038/nmeth.3839.
451. Clancy A, Chen DY, Bruns J, Nadella J, Stealey S, Zhang YJ, et al. Hydrogel-based microfluidic device with multiplexed 3D in vitro cell culture. *Scientific Reports*. 2022;12(1). doi: 10.1038/s41598-022-22439-y. PubMed PMID: WOS:000873838100032.
452. Khot MI, Levenstein MA, de Boer GN, Armstrong G, Maisey T, Svavarsdottir HS, et al. Characterising a PDMS based 3D cell culturing microfluidic platform for screening chemotherapeutic drug cytotoxic activity. *Scientific Reports*. 2020;10(1):15915. doi: 10.1038/s41598-020-72952-1.
453. Matthiesen I, Jury M, Boroojeni FR, Ludwig SL, Holzreuter M, Buchmann S, et al. Astrocyte 3D culture and bioprinting using peptide functionalized hyaluronan

- hydrogels. *Science and Technology of Advanced Materials*. 2023;24(1). doi: 10.1080/14686996.2023.2165871. PubMed PMID: WOS:000919345500001.
454. Dey M, Ozbolat IT. 3D bioprinting of cells, tissues and organs. *Scientific Reports*. 2020;10(1):14023. doi: 10.1038/s41598-020-70086-y.
455. Murali VS, Chang B-J, Fiolka R, Danuser G, Cobanoglu MC, Welf ES. An image-based assay to quantify changes in proliferation and viability upon drug treatment in 3D microenvironments. *BMC Cancer*. 2019;19(1):502. doi: 10.1186/s12885-019-5694-1.
456. Eilenberger C, Kratz SRA, Rothbauer M, Ehmoser E-K, Ertl P, Küpcü S. Optimized alamarBlue assay protocol for drug dose-response determination of 3D tumor spheroids. *MethodsX*. 2018;5:781-7. doi: <https://doi.org/10.1016/j.mex.2018.07.011>.
457. Bonnier F, Keating ME, Wróbel TP, Majzner K, Baranska M, Garcia-Munoz A, et al. Cell viability assessment using the Alamar blue assay: a comparison of 2D and 3D cell culture models. *Toxicol In Vitro*. 2015;29(1):124-31. Epub 2014/10/11. doi: 10.1016/j.tiv.2014.09.014. PubMed PMID: 25300790.
458. Gong Y, Fan N, Yang X, Peng B, Jiang H. New advances in microfluidic flow cytometry. *ELECTROPHORESIS*. 2019;40(8):1212-29. doi: <https://doi.org/10.1002/elps.201800298>.
459. Kijanska M, Kelm J. In vitro 3D Spheroids and Microtissues: ATP-based Cell Viability and Toxicity Assays. In: Markossian S, Grossman A, Brimacombe K, Arkin M, Auld D, Austin C, et al., editors. *Assay Guidance Manual*. Bethesda (MD): Eli Lilly & Company and the National Center for Advancing Translational Sciences; 2004.
460. Moon IJ, Yun MR, Yoon HK, Lee KH, Choi SY, Lee WJ, et al. Treatment of atopic dermatitis using non-thermal atmospheric plasma in an animal model. *Scientific Reports*. 2021;11(1):16091. doi: 10.1038/s41598-021-95471-z.

461. Zhang L, Yang D-z, Wang W-c, Liu Z-j, Wang S, Jiang P-c, et al. Atmospheric air diffuse array-needles dielectric barrier discharge excited by positive, negative, and bipolar nanosecond pulses in large electrode gap. *Journal of Applied Physics*. 2014;116(11):113301. doi: 10.1063/1.4895982.
462. Liu ZJ, Wang WC, Yang DZ, Zhang S, Yang Y, Tang K. The effect of dielectric thickness on diffuse nanosecond dielectric barrier discharges using a needle array-plate electrode configuration in air at atmospheric pressure. *Journal of Applied Physics*. 2013;113(23). doi: 10.1063/1.4811293. PubMed PMID: WOS:000321011700010.
463. Zhu Y, Kang E, Wilson M, Basso T, Chen E, Yu Y, et al. 3D Tumor Spheroid and Organoid to Model Tumor Microenvironment for Cancer Immunotherapy. *Organoids*. 2022;1(2):149-67. PubMed PMID: doi:10.3390/organoids1020012.
464. Guan X, Huang S. Advances in the application of 3D tumor models in precision oncology and drug screening. *Front Bioeng Biotechnol*. 2022;10:1021966. Epub 2022/10/18. doi: 10.3389/fbioe.2022.1021966. PubMed PMID: 36246388; PubMed Central PMCID: PMC9555934.
465. Phukhum P, Phetcharaburanin J, Chaleekarn K, Kittirat Y, Kulthawatsiri T, Namwat N, et al. The impact of hypoxia and oxidative stress on proteo-metabolomic alterations of 3D cholangiocarcinoma models. *Scientific Reports*. 2023;13(1):3072. doi: 10.1038/s41598-023-30204-y.
466. Doctor A, Seifert V, Ullrich M, Hauser S, Pietzsch J. Three-Dimensional Cell Culture Systems in Radiopharmaceutical Cancer Research. *Cancers (Basel)*. 2020;12(10). Epub 2020/10/01. doi: 10.3390/cancers12102765. PubMed PMID: 32993034; PubMed Central PMCID: PMC7600608.
467. Vinci M, Gowan S, Boxall F, Patterson L, Zimmermann M, Court W, et al. Advances in establishment and analysis of three-dimensional tumor spheroid-based

functional assays for target validation and drug evaluation. *BMC Biology*. 2012;10(1):29. doi: 10.1186/1741-7007-10-29.

468. Aponte PM, Caicedo A. Stemness in Cancer: Stem Cells, Cancer Stem Cells, and Their Microenvironment. *Stem Cells Int*. 2017;2017:5619472. Epub 2017/05/06. doi: 10.1155/2017/5619472. PubMed PMID: 28473858; PubMed Central PMCID: PMC5394399.

469. He J, Xiong L, Li Q, Lin L, Miao X, Yan S, et al. 3D modeling of cancer stem cell niche. *Oncotarget*. 2018;9(1):1326-45. Epub 2018/02/09. doi: 10.18632/oncotarget.19847. PubMed PMID: 29416698; PubMed Central PMCID: PMC5787442.

470. Melissaridou S, Wiechec E, Magan M, Jain MV, Chung MK, Farnebo L, et al. The effect of 2D and 3D cell cultures on treatment response, EMT profile and stem cell features in head and neck cancer. *Cancer Cell Int*. 2019;19:16. Epub 2019/01/18. doi: 10.1186/s12935-019-0733-1. PubMed PMID: 30651721; PubMed Central PMCID: PMC6332598.

471. Huang T, Song X, Xu D, Tiek D, Goenka A, Wu B, et al. Stem cell programs in cancer initiation, progression, and therapy resistance. *Theranostics*. 2020;10(19):8721-43. Epub 2020/08/06. doi: 10.7150/thno.41648. PubMed PMID: 32754274; PubMed Central PMCID: PMC7392012.

472. Ayob AZ, Ramasamy TS. Cancer stem cells as key drivers of tumour progression. *Journal of Biomedical Science*. 2018;25(1):20. doi: 10.1186/s12929-018-0426-4.

473. Tornin J, Mateu-Sanz M, Rodríguez A, Labay C, Rodríguez R, Canal C. Pyruvate Plays a Main Role in the Antitumoral Selectivity of Cold Atmospheric Plasma in Osteosarcoma. *Scientific Reports*. 2019;9(1):10681. doi: 10.1038/s41598-019-47128-1.

474. Fernandez-Gomez FJ, Pastor MD, Garcia-Martinez EM, Melero-Fernandez de Mera R, Gou-Fabregas M, Gomez-Lazaro M, et al. Pyruvate protects cerebellar granular cells from 6-hydroxydopamine-induced cytotoxicity by activating the Akt signaling pathway and increasing glutathione peroxidase expression. *Neurobiol Dis.* 2006;24(2):296-307. Epub 2006/09/19. doi: 10.1016/j.nbd.2006.07.005. PubMed PMID: 16978869.
475. Kelts JL, Cali JJ, Duellman SJ, Shultz J. Altered cytotoxicity of ROS-inducing compounds by sodium pyruvate in cell culture medium depends on the location of ROS generation. *SpringerPlus.* 2015;4(1):269. doi: 10.1186/s40064-015-1063-y.
476. Zheng S, Xin L, Liang A, Fu Y. Cancer stem cell hypothesis: a brief summary and two proposals. *Cytotechnology.* 2013;65(4):505-12. Epub 2012/12/20. doi: 10.1007/s10616-012-9517-3. PubMed PMID: 23250634; PubMed Central PMCID: PMC3720968.
477. Bahmad HF, Cheaito K, Chalhoub RM, Hadadeh O, Monzer A, Ballout F, et al. Sphere-Formation Assay: Three-Dimensional in vitro Culturing of Prostate Cancer Stem/Progenitor Sphere-Forming Cells. *Front Oncol.* 2018;8:347. Epub 2018/09/14. doi: 10.3389/fonc.2018.00347. PubMed PMID: 30211124; PubMed Central PMCID: PMC6121836.
478. Zaroni M, Piccinini F, Arienti C, Zamagni A, Santi S, Polico R, et al. 3D tumor spheroid models for in vitro therapeutic screening: a systematic approach to enhance the biological relevance of data obtained. *Sci Rep.* 2016;6:19103. Epub 2016/01/12. doi: 10.1038/srep19103. PubMed PMID: 26752500; PubMed Central PMCID: PMC4707510.

479. Wanigasekara J, Barcia C, Cullen PJ, Tiwari B, Curtin JF. Outside Front Cover: Plasma Process. Polym. 4/2022. Plasma Processes and Polymers. 2022;19(4):2270010. doi: <https://doi.org/10.1002/ppap.202270010>.
480. Turrini E, Laurita R, Stancampiano A, Catanzaro E, Calcabrini C, Maffei F, et al. Cold Atmospheric Plasma Induces Apoptosis and Oxidative Stress Pathway Regulation in T-Lymphoblastoid Leukemia Cells. *Oxid Med Cell Longev*. 2017;2017:4271065. Epub 2017/09/28. doi: 10.1155/2017/4271065. PubMed PMID: 28947928; PubMed Central PMCID: PMC5602509.
481. Aranda-Rivera AK, Cruz-Gregorio A, Arancibia-Hernández YL, Hernández-Cruz EY, Pedraza-Chaverri J. RONS and Oxidative Stress: An Overview of Basic Concepts. *Oxygen*. 2022;2(4):437-78. PubMed PMID: doi:10.3390/oxygen2040030.
482. Qi X, Jha SK, Jha NK, Dewanjee S, Dey A, Deka R, et al. Antioxidants in brain tumors: current therapeutic significance and future prospects. *Molecular Cancer*. 2022;21(1):204. doi: 10.1186/s12943-022-01668-9.
483. Zubor P, Wang Y, Liskova A, Samec M, Koklesova L, Dankova Z, et al. Cold Atmospheric Pressure Plasma (CAP) as a New Tool for the Management of Vulva Cancer and Vulvar Premalignant Lesions in Gynaecological Oncology. *Int J Mol Sci*. 2020;21(21). Epub 2020/10/31. doi: 10.3390/ijms21217988. PubMed PMID: 33121141; PubMed Central PMCID: PMC7663780.
484. Jiapaer S, Furuta T, Tanaka S, Kitabayashi T, Nakada M. Potential Strategies Overcoming the Temozolomide Resistance for Glioblastoma. *Neurol Med Chir (Tokyo)*. 2018;58(10):405-21. Epub 2018/09/27. doi: 10.2176/nmc.ra.2018-0141. PubMed PMID: 30249919; PubMed Central PMCID: PMC6186761.
485. Nath S, Devi GR. Three-dimensional culture systems in cancer research: Focus on tumor spheroid model. *Pharmacol Ther*. 2016;163:94-108. Epub 2016/04/12. doi:

10.1016/j.pharmthera.2016.03.013. PubMed PMID: 27063403; PubMed Central PMCID: PMC4961208.

486. Zhou Y, Kumon RE, Cui J, Deng CX. The size of sonoporation pores on the cell membrane. *Ultrasound Med Biol.* 2009;35(10):1756-60. Epub 2009/08/04. doi: 10.1016/j.ultrasmedbio.2009.05.012. PubMed PMID: 19647924; PubMed Central PMCID: PMC2752487.

487. Przystupski D, Ussowicz M. Landscape of Cellular Bioeffects Triggered by Ultrasound-Induced Sonoporation. *International Journal of Molecular Sciences.* 2022;23(19):11222. PubMed PMID: doi:10.3390/ijms231911222.

488. Tharkar P, Varanasi R, Wong WSF, Jin CT, Chrzanowski W. Nano-Enhanced Drug Delivery and Therapeutic Ultrasound for Cancer Treatment and Beyond. *Frontiers in Bioengineering and Biotechnology.* 2019;7. doi: 10.3389/fbioe.2019.00324.

489. Nittayacharn P, Yuan HX, Hernandez C, Bielecki P, Zhou H, Exner AA. Enhancing Tumor Drug Distribution With Ultrasound-Triggered Nanobubbles. *J Pharm Sci.* 2019;108(9):3091-8. Epub 2019/05/17. doi: 10.1016/j.xphs.2019.05.004. PubMed PMID: 31095958; PubMed Central PMCID: PMC6708467.

490. Tait SW, Green DR. Mitochondrial regulation of cell death. *Cold Spring Harb Perspect Biol.* 2013;5(9). Epub 2013/09/05. doi: 10.1101/cshperspect.a008706. PubMed PMID: 24003207; PubMed Central PMCID: PMC3753705.

491. Redza-Dutordoir M, Averill-Bates DA. Activation of apoptosis signalling pathways by reactive oxygen species. *Biochimica et Biophysica Acta (BBA) - Molecular Cell Research.* 2016;1863(12):2977-92. doi: <https://doi.org/10.1016/j.bbamcr.2016.09.012>.

492. Yang H, Villani RM, Wang H, Simpson MJ, Roberts MS, Tang M, et al. The role of cellular reactive oxygen species in cancer chemotherapy. *Journal of Experimental & Clinical Cancer Research*. 2018;37(1):266. doi: 10.1186/s13046-018-0909-x.
493. Wu HL, Fu XY, Cao WQ, Xiang WZ, Hou YJ, Ma JK, et al. Induction of Apoptosis in Human Glioma Cells by Fucoxanthin via Triggering of ROS-Mediated Oxidative Damage and Regulation of MAPKs and PI3K-AKT Pathways. *J Agric Food Chem*. 2019;67(8):2212-9. Epub 2019/01/29. doi: 10.1021/acs.jafc.8b07126. PubMed PMID: 30688446.
494. Kiss AA, Geertman R, Wierschem M, Skiborowski M, Gielen B, Jordens J, et al. Ultrasound-assisted emerging technologies for chemical processes. *J Chem Technol Biotechnol*. 2018;93(5):1219-27. Epub 2018/05/22. doi: 10.1002/jctb.5555. PubMed PMID: 29780194; PubMed Central PMCID: PMC5947258.
495. Tanaka H, Mizuno M, Ishikawa K, Nakamura K, Kajiyama H, Kano H, et al. Plasma-Activated Medium Selectively Kills Glioblastoma Brain Tumor Cells by Down-Regulating a Survival Signaling Molecule, AKT Kinase. 2011;1(3-4):265-77. doi: 10.1615/PlasmaMed.2012006275.
496. Tanaka H, Bekeschus S, Yan D, Hori M, Keidar M, Laroussi M. Plasma-Treated Solutions (PTS) in Cancer Therapy. *Cancers (Basel)*. 2021;13(7). Epub 2021/05/01. doi: 10.3390/cancers13071737. PubMed PMID: 33917469; PubMed Central PMCID: PMC8038720.
497. Hong J, Zhang T, Zhou R, Zhou R, Ostikov K, Rezaeimotlagh A, et al. Plasma bubbles: a route to sustainable chemistry. *AAPPS Bulletin*. 2021;31(1):26. doi: 10.1007/s43673-021-00027-y.
498. Mai-Prochnow A, Zhou R, Zhang T, Ostikov K, Mugunthan S, Rice SA, et al. Interactions of plasma-activated water with biofilms: inactivation, dispersal effects and

mechanisms of action. *npj Biofilms and Microbiomes*. 2021;7(1):11. doi: 10.1038/s41522-020-00180-6.

499. Bolouki N, Kuan W-H, Huang Y-Y, Hsieh J-H. Characterizations of a Plasma-Water System Generated by Repetitive Microsecond Pulsed Discharge with Air, Nitrogen, Oxygen, and Argon Gases Species. *Applied Sciences*. 2021;11(13):6158. PubMed PMID: doi:10.3390/app11136158.

500. Sersenová D, Machala Z, Repiská V, Gbelcová H. Selective Apoptotic Effect of Plasma Activated Liquids on Human Cancer Cell Lines. *Molecules*. 2021;26(14). Epub 2021/07/25. doi: 10.3390/molecules26144254. PubMed PMID: 34299530; PubMed Central PMCID: PMC8304656.

501. Ojha KS, Burgess CM, Duffy G, Kerry JP, Tiwari BK. Integrated phenotypic-genotypic approach to understand the influence of ultrasound on metabolic response of *Lactobacillus sakei*. *PLOS ONE*. 2018;13(1):e0191053. doi: 10.1371/journal.pone.0191053.

502. Wu J, Nyborg WL. Ultrasound, cavitation bubbles and their interaction with cells. *Advanced Drug Delivery Reviews*. 2008;60(10):1103-16. doi: <https://doi.org/10.1016/j.addr.2008.03.009>.

503. Machado APDF, Sumere BR, Mekarú C, Martínez J, Bezerra RMN, Rostagno MA. Extraction of polyphenols and antioxidants from pomegranate peel using ultrasound: influence of temperature, frequency and operation mode. *International Journal of Food Science & Technology*. 2019;54(9):2792-801. doi: <https://doi.org/10.1111/ijfs.14194>.

504. Zhang X, Bobeica M, Unger M, Bednarz A, Gerold B, Patties I, et al. Focused ultrasound radiosensitizes human cancer cells by enhancement of DNA damage. *Strahlentherapie und Onkologie*. 2021;197(8):730-43. doi: 10.1007/s00066-021-01774-5.

505. Griseti E, Merbahi N, Golzio M. Anti-Cancer Potential of Two Plasma-Activated Liquids: Implication of Long-Lived Reactive Oxygen and Nitrogen Species. *Cancers (Basel)*. 2020;12(3). Epub 2020/03/25. doi: 10.3390/cancers12030721. PubMed PMID: 32204401; PubMed Central PMCID: PMCPMC7140060.
506. Arjunan KP, Sharma VK, Ptasinska S. Effects of atmospheric pressure plasmas on isolated and cellular DNA-a review. *Int J Mol Sci*. 2015;16(2):2971-3016. Epub 2015/02/03. doi: 10.3390/ijms16022971. PubMed PMID: 25642755; PubMed Central PMCID: PMCPMC4346876.
507. Tomizawa M, Shinozaki F, Motoyoshi Y, Sugiyama T, Yamamoto S, Sueishi M. Sonoporation: Gene transfer using ultrasound. *World J Methodol*. 2013;3(4):39-44. Epub 2014/09/23. doi: 10.5662/wjm.v3.i4.39. PubMed PMID: 25237622; PubMed Central PMCID: PMCPMC4145571.
508. Zheng D, Liwinski T, Elinav E. Interaction between microbiota and immunity in health and disease. *Cell Research*. 2020;30(6):492-506. doi: 10.1038/s41422-020-0332-7.
509. Kim CH, Park J, Kim M. Gut microbiota-derived short-chain Fatty acids, T cells, and inflammation. *Immune Netw*. 2014;14(6):277-88. Epub 2015/01/01. doi: 10.4110/in.2014.14.6.277. PubMed PMID: 25550694; PubMed Central PMCID: PMCPMC4275385.
510. Galland L. The gut microbiome and the brain. *J Med Food*. 2014;17(12):1261-72. Epub 2014/11/18. doi: 10.1089/jmf.2014.7000. PubMed PMID: 25402818; PubMed Central PMCID: PMCPMC4259177.
511. Cheng WY, Wu CY, Yu J. The role of gut microbiota in cancer treatment: friend or foe? *Gut*. 2020;69(10):1867-76. Epub 2020/08/08. doi: 10.1136/gutjnl-2020-321153. PubMed PMID: 32759302; PubMed Central PMCID: PMCPMC7497589.

512. Luo H, Shusta EV. Blood-Brain Barrier Modulation to Improve Glioma Drug Delivery. *Pharmaceutics*. 2020;12(11). Epub 2020/11/18. doi: 10.3390/pharmaceutics12111085. PubMed PMID: 33198244; PubMed Central PMCID: PMC7697580.
513. Haumann R, Videira JC, Kaspers GJL, van Vuurden DG, Hulleman E. Overview of Current Drug Delivery Methods Across the Blood-Brain Barrier for the Treatment of Primary Brain Tumors. *CNS Drugs*. 2020;34(11):1121-31. Epub 2020/09/24. doi: 10.1007/s40263-020-00766-w. PubMed PMID: 32965590; PubMed Central PMCID: PMC7658069 Vuurden, and Esther Hulleman declare that they have no conflicts of interest that might be relevant to the contents of this manuscript.
514. Mitusova K, Peltek OO, Karpov TE, Muslimov AR, Zyuzin MV, Timin AS. Overcoming the blood–brain barrier for the therapy of malignant brain tumor: current status and prospects of drug delivery approaches. *Journal of Nanobiotechnology*. 2022;20(1):412. doi: 10.1186/s12951-022-01610-7.
515. Mattei V, Santilli F, Martellucci S, Delle Monache S, Fabrizi J, Colapietro A, et al. The Importance of Tumor Stem Cells in Glioblastoma Resistance to Therapy. *Int J Mol Sci*. 2021;22(8). Epub 2021/05/01. doi: 10.3390/ijms22083863. PubMed PMID: 33917954; PubMed Central PMCID: PMC8068366.
516. Bryukhovetskiy I, Ponomarenko A, Lyakhova I, Zaitsev S, Zayats Y, Korneyko M, et al. Personalized regulation of glioblastoma cancer stem cells based on biomedical technologies: From theory to experiment (Review). *Int J Mol Med*. 2018;42(2):691-702. doi: 10.3892/ijmm.2018.3668.
517. Alves ALV, Gomes INF, Carloni AC, Rosa MN, da Silva LS, Evangelista AF, et al. Role of glioblastoma stem cells in cancer therapeutic resistance: a perspective on

antineoplastic agents from natural sources and chemical derivatives. *Stem Cell Research & Therapy*. 2021;12(1):206. doi: 10.1186/s13287-021-02231-x.

9. Appendices

9 Appendix

9.1 Appendix I All the Data and statistical outcomes

All relevant datasets and statistical outcomes that support the findings of this study are uploaded into OSF.io and can be accessed using the following DOI link:
<https://doi.org/10.17605/OSF.IO/28CHK> PhD thesis - Novel Therapeutic Approaches to Treat Brain Cancer Combining 3D Cell Culture Models, Cold Atmospheric Plasma and Airborne Acoustic Hosted on the Open Science Framework doi.org.


9.2 Appendix II First Pages of Peer-reviewed Publications

Only first pages of the Peer reviewed manuscripts are attached.



Forum

Converging technologies: targeting the hallmarks of cancer using ultrasound and microbubbles

Janith Wanigasekara,^{1,2,3,6}
 Andressa Maria Aguiar
 de Carvalho,^{1,2,3,6}
 Patrick J. Cullen,^{1,4}
 Brijesh Tiwari,² and
 James F. Curtin ^{1,3,5,*}



Various complex biological effects occur when ultrasonic compression waves travel through biological material. The myriad of biological outcomes instigated by ultrasound are evident when viewed through the lens of the hallmarks of cancer. Herein, we summarise the therapeutic potential of ultrasound, enhanced by microbubbles, for the treatment of cancer.

Biological effects of ultrasound

The hallmarks of cancer are a useful framework to distil and understand the underlying changes in this incredibly complex and diverse disease [1]. Six core and two emergent hallmarks underpin tumour development and metastasis. Two enabling hallmarks provide 'functional capabilities that allow cancer cells to survive, proliferate, and disseminate' (Figure 1). Drug development primarily focusses on singular receptors, whereas each hallmark is regulated by semi-redundant pathways allowing tumour adaptation and chemoresistance via mutation [1]. Therapies that broadly target hallmarks of cancer are therefore advantageous to prevent tumour adaptation. Ultrasound imparts focussed energy via ultrasonic compression waves

directly to cells and tissues. When used in combination with gas-filled microbubbles, the resultant microbubble oscillation, expansion and contraction, and bursting enhances the antitumour effects of ultrasound, broadly targeting several hallmarks of cancer. Here, we propose that ultrasound therapies can be codified within the hallmarks of cancer framework.

Resisting cell death

Many existing chemotherapies target receptors with the therapeutic intent to overcome or bypass inherent tumour resistance to cell death. Direct application of ultrasound can overcome resistance to cell death, inducing coagulative necrosis, apoptosis, and reduction of tumour growth [2]. However, in glioblastoma and other brain tumours, the blood–brain barrier (BBB) prevents many chemotherapeutic agents from accumulating to effective concentrations in tumours. Two clinical trials used minimally invasive ultrasound to temporarily and repeatedly open the BBB and enhance chemotherapeutic delivery without adverse effects [3,4]. A Phase I/II clinical trial (NCT02253212) enhanced carboplatin uptake without evident neurotoxicity using the implantable ultrasound device, sonocloud-1, combined with microbubbles [3], and a second Phase I trial (NCT02343991) effectively delivered doxorubicin- and temozolomide-loaded liposomes using low-intensity magnetic resonance (MR)-guided focussed ultrasound [4]. These approaches demonstrate the in-human feasibility of micro/nano bubbles and ultrasound to enhance drug delivery, improve penetration and bioavailability in the brain parenchyma, increase local intracerebral drug concentrations, while reducing systemic toxicology. Preclinical development of a sonodynamic therapy complex incorporating chlorin e6 and hydroxychloroquine into liposomes illustrates this point. The complex selectively accumulated in brain tumours during ultrasound-targeted microbubble destruction and hydroxychloroquine was released

to glioma cells, inducing reactive oxygen species (ROS) production, mitochondrial dysfunction, and MAPK/p38-PINK1-PRKN-dependent mitophagy [5].





Microbubbles and gene-loaded nanoparticles combined with ultrasound also provides a safe, effective, and targeted delivery system for genes. Microbubbles and a lipid-polymer hybrid nanoparticle complex were used as an ultrasound-mediated gene delivery carrier of clustered regularly interspaced short palindromic repeats (CRISPR)-Cas9 plasmids, targeting O6-methylguanine-DNA methyltransferase (MGMT), a DNA-repair gene protecting glioma cells from alkylating chemotherapeutics. Ultrasound induced BBB opening, allowing targeted delivery, gene protection from enzyme degradation, biocompatibility, prolonged survival, biosafety, and augmented transfection efficiency, while down-regulating MGMT expression and thereby sensitising cells to temozolomide [6].

Microbubbles loaded with the halogenated xanthene contrast agent rose bengal conjugated via stable amine linkages to dihexadecylamine combined with ultrasound has been used as a novel sonosensitiser delivery system in a preclinical *in vivo* study. Ultrasound converted loaded microbubbles into nanoparticles, resulting in enhanced drug accumulation in the tumour and ROS generation, leading to tumour growth inhibition with minimal side effects [7]. Ultimately, microbubbles combined with ultrasound can overcome cell death resistance. Future progress will be dependent on further development of materials that increase tumour cell death while minimising damage to surrounding cells. While not yet undergoing clinical trials, nanomaterials combined with ultrasound have potential to selectively ablate tumour tissue deep within the body.

Sustaining cell proliferation

Cancer cells deregulate the normal signals that control entry and progression through

Plasma induced reactive oxygen species-dependent cytotoxicity in glioblastoma 3D tumourspheres

Janith Wanigasekara^{1,2,3,4}  | Carlos Barcia⁵ | Patrick J. Cullen^{1,6}  |
Brijesh Tiwari²  | James F. Curtin^{1,3,4} 

¹BioPlasma Research Group, School of Food Science and Environmental Health, Technological University Dublin, Dublin, Ireland

²Department of Food Biosciences, Teagasc Food Research Centre, Ashtown, Dublin, Ireland

³Environmental Sustainability & Health Institute (ESHI), Technological University Dublin, Dublin, Ireland

⁴FOCAS Research Institute, Technological University Dublin, Dublin, Ireland

⁵Institut de Neurociències, Department of Biochemistry and Molecular Biology, School of Medicine, Universitat Autònoma de Barcelona, Bellaterra, Spain

⁶School of Chemical and Biomolecular Engineering, University of Sydney, Sydney, Australia

Correspondence

Janith Wanigasekara, BioPlasma Research Group, School of Food Science and Environmental Health, Technological University Dublin, Dublin, Ireland.
Email: janith.manoharawanigasekara@tudublin.ie

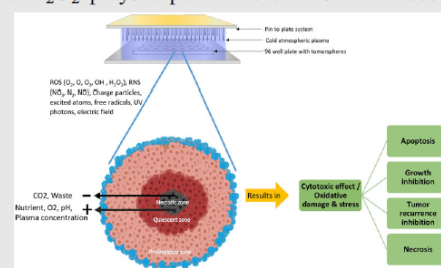
James F. Curtin, Dean of Engineering and Built Environment, Bioplasma Research Group, Technological University Dublin, Dublin, Ireland.
Email: james.curtin@tudublin.ie

Funding information

Science Foundation Ireland, Grant/Award Number: 17/CDA/4653; Teagasc Walsh Fellowships

Abstract

The aim of this study was to determine the effects of a pin-to-plate cold atmospheric plasma (CAP) on U-251 MG three-dimensional (3D) glioblastoma spheroids under different conditions. 3D tumourspheres showed higher resistance to the CAP treatment compared to 2D monolayer cells. A single CAP treatment was able to induce cytotoxicity, while multiple CAP treatments augmented this effect. CAP was also able to induce cytotoxicity throughout the tumoursphere, and we identified that reactive oxygen species (ROS) plays a major role, while H₂O₂ plays a partial role in CAP-induced cytotoxicity in tumourspheres. We conclude that ROS-dependent cytotoxicity is induced uniformly throughout glioblastoma and epidermoid tumourspheres by direct CAP treatment.



KEYWORDS

3D tumourspheres, cold atmospheric plasma, cytotoxicity, epidermoid, glioblastoma, reactive oxygen and nitrogen species, ROS dependent

[Correction added on 12 January 2022, after first online publication: IReL funding statement has been added.]

This is an open access article under the terms of the Creative Commons Attribution License, which permits use, distribution and reproduction in any medium, provided the original work is properly cited.

© 2022 The Authors. *Plasma Processes and Polymers* published by Wiley-VCH GmbH



Advances in 3D culture systems for therapeutic discovery and development in brain cancer

Reviews • KEYNOTE REVIEW

Janith Wanigasekara^{1,2,3,4,*}, Patrick J. Cullen^{1,5},
Paula Bourke⁶, Brijesh Tiwari³, James F. Curtin^{1,2,4,7,*}

¹BioPlasma Research Group, School of Food Science and Environmental Health, Technological University Dublin, Dublin, Ireland

²Environmental Sustainability and Health Institute (ESHI), Technological University Dublin, Dublin, Ireland

³Department of Food Biosciences, Teagasc Food Research Centre, Ashtown, Dublin, Ireland

⁴FOCAS Research Institute, Technological University Dublin, Dublin, Ireland

⁵School of Chemical and Biomolecular Engineering, University of Sydney, Sydney, Australia

⁶School of Biosystems and Food Engineering, University College Dublin, Dublin, Ireland

⁷Faculty of Engineering and Built Environment, Technological University Dublin, Dublin, Ireland

This review focuses on recent advances in 3D culture systems that promise more accurate therapeutic models of the glioblastoma multiforme (GBM) tumor microenvironment (TME), such as the unique anatomical, cellular, and molecular features evident in human GBM. The key components of a GBM TME are outlined, including microbiomes, vasculature, extracellular matrix (ECM), infiltrating parenchymal and peripheral immune cells and molecules, and chemical gradients. 3D culture systems are evaluated against 2D culture systems and *in vivo* animal models. The main 3D culture techniques available are compared, with an emphasis on identifying key gaps in knowledge for the development of suitable platforms to accurately model the intricate components of the GBM TME.

Keywords: 3D cell culture; glioma; tumor microenvironment; 3D bioprinter; scaffolds; hydrogels



Janith Wanigasekara has completed his BSc in Biochemistry (2014) and MSc in Biochemistry & Molecular Biology (2017) and is currently reading for his PhD in the School of Food Science and Environmental Health, Technological University Dublin, Ireland. His current research is focused on the application of novel therapeutic approaches such as cold atmospheric plasma, airborne acoustics, and microbubbles to treat brain cancer. He is also working on different 3D cell culture models and 3D bio printing. Janith is in receipt of a Teagasc Walsh funded scholarship.



Brijesh Tiwari is a Principal Research Officer at Teagasc and Professor (Adjunct) at University College Dublin (UCD), Ireland. He obtained his PhD from UCD School of Biosystems and Food Engineering. His research interest is in the area of novel technologies (ultrasonics and plasma) for chemical and biochemical applications. His current research investigates the application of these technologies on biological materials and role they play in modulating cellular activities. The impact of process control parameters and the physicochemical characteristics that these technologies have on biological materials are some examples of current research activities.



James Curtin is the Faculty Dean of Engineering & Built Environment at Technological University Dublin, Ireland. He obtained his PhD from University College Cork. His research interests focus on the development of therapies to treat glioblastoma and other malignant tumors. James' research explores the use of advanced technologies, including cold plasma and ultrasound, to improve delivery or activate cytotoxicity of novel therapeutic agents,

including nanomaterials, gene therapies, and prodrugs. His research group is also systematically developing cell culture models that more accurately represent the various microenvironments of glioblastoma and other solid tumors.

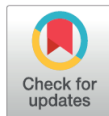
* Corresponding authors at: BioPlasma Research Group, School of Food Science and Environmental Health, Technological University Dublin, Dublin, Ireland. Wanigasekara, J. (janith.manoharawanigasekara@tudublin.ie), Curtin, J.F. (james.curtin@tudublin.ie).

<https://doi.org/10.1016/j.drudis.2022.103426> (Wangiasekara et al., 2022)

LAB PROTOCOL

Three-Dimensional (3D) *in vitro* cell culture protocols to enhance glioblastoma researchJanith Wanigasekara^{1,2,3,4*}, Lara J. Carroll¹, Patrick J. Cullen^{1,5}, Brijesh Tiwari³, James F. Curtin^{1,2,4*}

1 BioPlasma Research Group, School of Food Science and Environmental Health, Technological University Dublin, Dublin, Ireland, **2** Environmental Sustainability & Health Institute (ESHI), Technological University Dublin, Dublin, Ireland, **3** Department of Food Biosciences, Teagasc Food Research Centre, Ashtown, Dublin, Ireland, **4** FOCAS Research Institute, Technological University Dublin, Dublin, Ireland, **5** University of Sydney, School of Chemical and Biomolecular Engineering, Sydney, Australia

* james.curtin@tudublin.ie (JFC); janith.manoharawanigasekara@tudublin.ie (JW)

OPEN ACCESS

Citation: Wanigasekara J, Carroll LJ, Cullen PJ, Tiwari B, Curtin JF (2023) Three-Dimensional (3D) *in vitro* cell culture protocols to enhance glioblastoma research. PLOS ONE 18(2): e0276248. <https://doi.org/10.1371/journal.pone.0276248>

Editor: Nils Cordes, Technische Universitat Dresden, GERMANY

Received: May 5, 2022

Accepted: October 4, 2022

Published: February 8, 2023

Peer Review History: PLOS recognizes the benefits of transparency in the peer review process; therefore, we enable the publication of all of the content of peer review and author responses alongside final, published articles. The editorial history of this article is available here: <https://doi.org/10.1371/journal.pone.0276248>

Copyright: © 2023 Wanigasekara et al. This is an open access article distributed under the terms of the [Creative Commons Attribution License](https://creativecommons.org/licenses/by/4.0/), which permits unrestricted use, distribution, and reproduction in any medium, provided the original author and source are credited.

Data Availability Statement: All relevant datasets that support the findings of this study are uploaded into OSF.io and can be accessed using the following DOI link: <https://doi.org/10.17605/OSF>.

Abstract

Three-dimensional (3D) cell culture models can help bridge the gap between *in vitro* cell cultures and *in vivo* responses by more accurately simulating the natural *in vivo* environment, shape, tissue stiffness, stressors, gradients and cellular response while avoiding the costs and ethical concerns associated with animal models. The inclusion of the third dimension in 3D cell culture influences the spatial organization of cell surface receptors that interact with other cells and imposes physical restrictions on cells in compared to Two-dimensional (2D) cell cultures. Spheroids' distinctive cyto-architecture mimics *in vivo* cellular structure, gene expression, metabolism, proliferation, oxygenation, nutrition absorption, waste excretion, and drug uptake while preserving cell–extracellular matrix (ECM) connections and communication, hence influencing molecular processes and cellular phenotypes. This protocol describes the *in vitro* generation of tumourspheroids using the low attachment plate, hanging drop plate, and cellusponge natural scaffold based methods. The expected results from these protocols confirmed the ability of all these methods to create uniform tumourspheres.

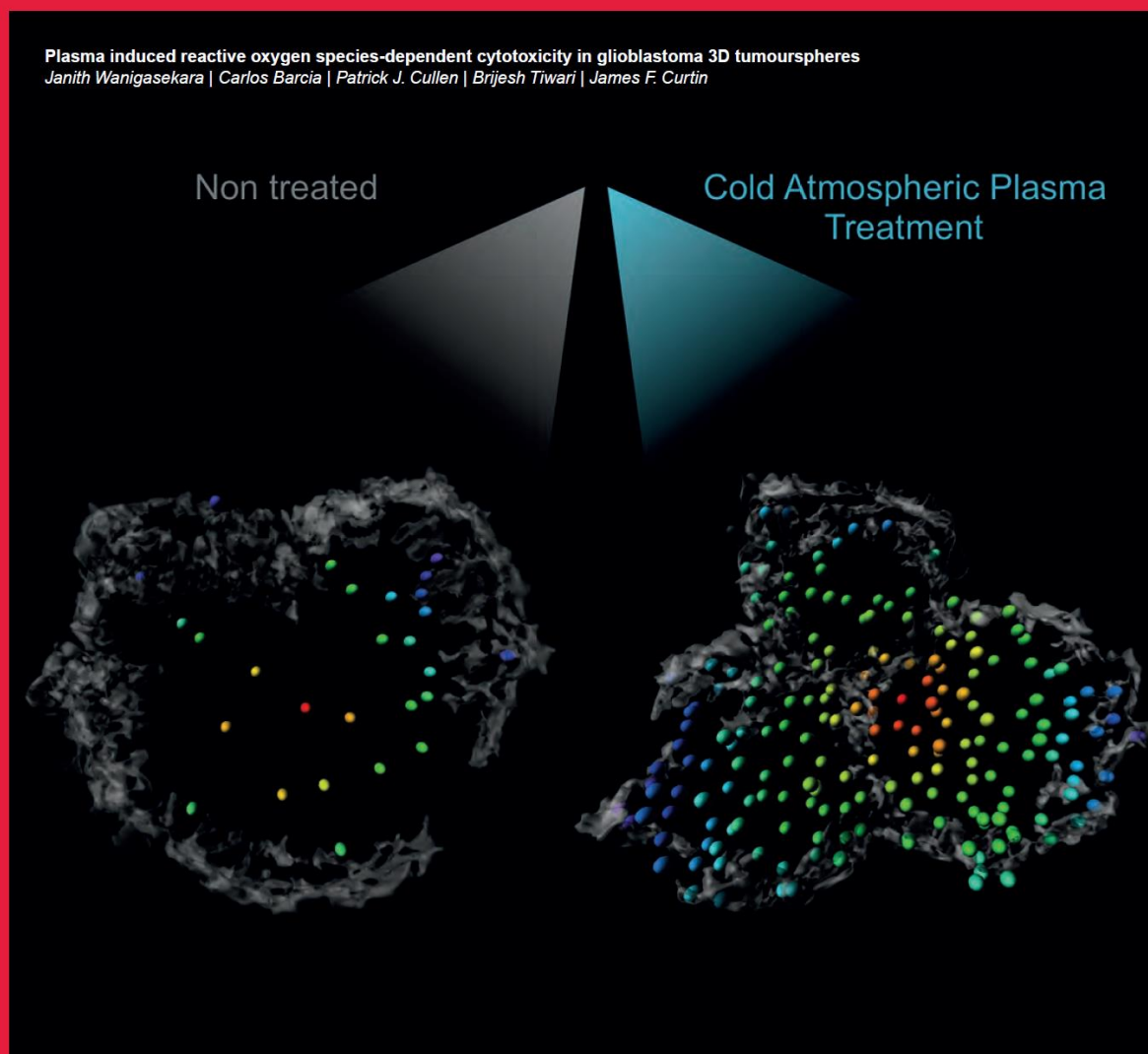
Introduction

Two-dimensional (2D) cell culture models have become a cornerstone of biological research due to its ease of use, cheap cost, and repeatability, however *in vivo* tissue complexity can only be reached utilizing Three-dimensional (3D) cell culture [1]. 3D cell cultures are an improved *in vitro* cell culture technology that uses an artificially produced microenvironment to grow cells in three dimensions. Cells in 3D cell culture contain natural cell-cell interactions as well as cell–extracellular matrix (ECM) component interactions, allowing them to proliferate *in vitro* in a microenvironment that closely reflects *in vivo* settings [2,3]. 3D cell culture is vital in drug testing, because it is capable of replacing both 2D cell culture and animal trials. The initial step of traditional drug development begins with 2D cell culture, followed by animal studies and clinical trials; around 95% of possible preclinical trials in all therapeutic areas fail to result in effective human treatments. The primary reason for this is that original data from 2D cell

<https://doi.org/10.1371/journal.pone.0276248> (Wanigasekara et al., 2023)

PLASMA PROCESSES AND POLYMERS

Plasma induced reactive oxygen species-dependent cytotoxicity in glioblastoma 3D tumourspheres
Janith Wanigasekara | Carlos Barcia | Patrick J. Cullen | Brijesh Tiwari | James F. Curtin



Editors-in-Chief: Dirk Hegemann, St. Gallen | Christian Oehr, Stuttgart |
Achim von Keudell, Bochum | Michael R. Wertheimer, Montreal

WILEY-VCH

<https://doi.org/10.1002/ppap.202270010> (Wangiasekara et al., 2022)

9.3 Appendix II Additional Publications and Outputs not Peer-reviewed

Only first pages of the manuscripts are attached.



FOOD

3D mammalian cell culture models in toxicology testing

3D cell culture can be successfully used as an alternative to laboratory animals, and as a cost-effective and time-saving tissue culture technique, which also reduces the trial period for drug testing.

Toxicology testing is performed to understand the adverse effects of drugs and chemical substances on humans and other living organisms. In the EU, the Registration, Evaluation, Authorisation and Restriction of Chemicals (REACH) regulation (EC 1907/2006) applies a “no data, no market” rule, and responsibility has been placed on industry to manage the risks from new chemicals and to provide safety information on them.

What is 3D cell culture?

3D cell culture (Figure 1) describes a number of techniques to grow cells in three dimensions, such as in a spheroid, using an artificially created microenvironment. Cells in 3D cell culture have physiological cell-cell interactions and cell-extracellular matrix component interactions, which allow cells to grow *in vitro* in an environment that closely resembles *in vivo* conditions. For example, spheres possess a hypoxic (oxygen-deprived) core resembling solid tumours with cells at the centre of the sphere having extremely low oxygen and nutrient concentrations. Spheres also show complex transport dynamics by creating diffusion gradients of drugs, oxygen, nutrients and waste, and also show resistance and drugs/chemical substances show low potency as an *in vivo* condition. The neighbour geometry and cellular support found in 3D cell cultures can improve gene expression, cellular communication, migration, differentiation, survival and growth similar to *in vivo* tissues, which provide better representation for toxicological testing. Mixed-cell populations can also be cultured in 3D to closely model human tissues. Hence, 3D cell culture plays a vital role in measuring biological responses to new chemicals.

Why should I use it?

Use of animals in toxicological research has been reduced due to the ethical concerns, expense, time consumption, and misleading results

due to differences between human and animal physiology. The REACH regulation’s stated aim is: “to ensure a high level of protection of human health and the environment from effects of hazardous chemicals. It strives for a balance: to increase our understanding of the possible hazards of chemicals, while at the same time avoiding unnecessary testing on animals” (European Chemicals Agency, 2020). 3D cell culture is a much better technique, which supports the ‘3Rs’ of animal research (replacement, reduction and refinement) and the REACH recommendation to perform humane animal toxicology research.

Conventional 2D cell cultures (Figure 1) are unable to detect organ-specific toxicity and have inadequate representation of cell migration, differentiation, signal transduction, survival and growth. A 2D cell culture does not reveal toxicological resistance (Figure 2), architecture as *in vivo* tissues, accurate depiction of cell polarisation or gene expression. It also provides unreliable predictions of *in vivo* drug efficiency and toxicity, which leads to low success rates in clinical trials. 3D cell culture can overcome the disadvantages of *in vivo* animal testing and conventional 2D cell culture by providing a more accurate platform for short- and long-term studies, demonstrating the long-term effects of the drugs.

Authors

Janith Wanigasekara
Doctoral researcher, Teagasc and School of Food Science and Environmental Health, Technological University Dublin

Brijesh Tiwari
Research Officer, Teagasc Food Research Centre, Ashtown, Dublin 15
Correspondence: brijesh.tiwari@teagasc.ie

James Curtin
Head of the School of Food Science and Environmental Health, Technological University Dublin



Ultrasound-mediated drug diffusion, uptake, and cytotoxicity in glioblastoma 3D tumour sphere model

Janith Wanigasekara^{1,2,3,4}, Julie Rose Mae Mondala^{1,2}, Patrick J. Cullen^{1,5}, Brijesh Tiwari³, James F. Curtin^{1,2,4,6*}

¹ BioPlasma Research Group, School of Food Science and Environmental Health, Technological University Dublin, Dublin, Ireland.

² Environmental Sustainability & Health Institute (ESHI), Technological University Dublin, Dublin, Ireland.

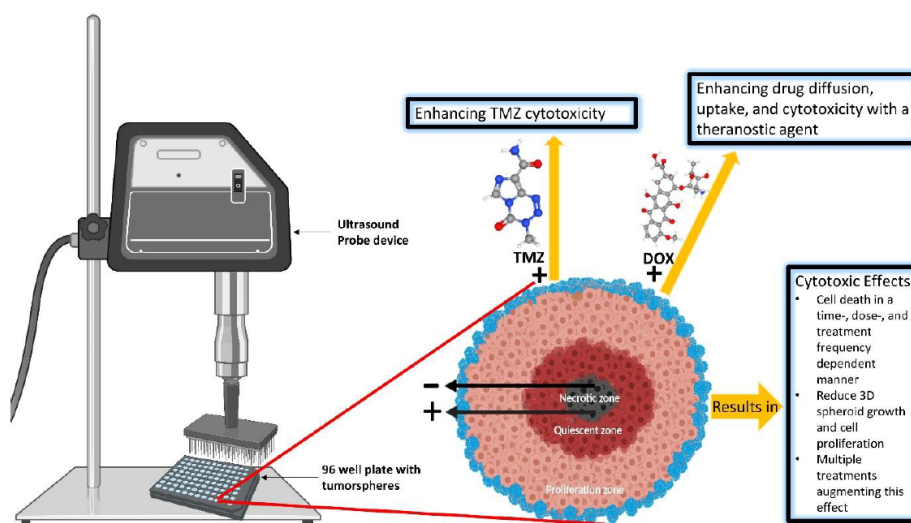
³ Department of Food Biosciences, Teagasc Food Research Centre, Ashtown, Dublin, Ireland.

⁴ FOCAS Research Institute, Technological University Dublin, Dublin, Ireland.

⁵ University of Sydney, School of Chemical and Biomolecular Engineering, Sydney, Australia.

⁶ Faculty of Engineering & Built Environment, Technological University Dublin, Dublin, Ireland.

* Corresponding author. *Email address:* janith.manoharawanigasekara@tudublin.ie; james.curtin@tudublin.ie



The manuscript has been submitted for publication in the Biomaterials Journal.

Synergistic cytotoxicity effect of ultrasound and plasma microbubble in glioblastoma 3D tumour spheres

Janith Wanigasekara^{1, 2, 3, 4*}, Patrick J. Cullen^{1, 5}, Brijesh Tiwari³, James F. Curtin^{1, 2, 4, 6*}

¹ BioPlasma Research Group, School of Food Science and Environmental Health, Technological University Dublin, Dublin, Ireland.

² Environmental Sustainability & Health Institute (ESHI), Technological University Dublin, Dublin, Ireland.

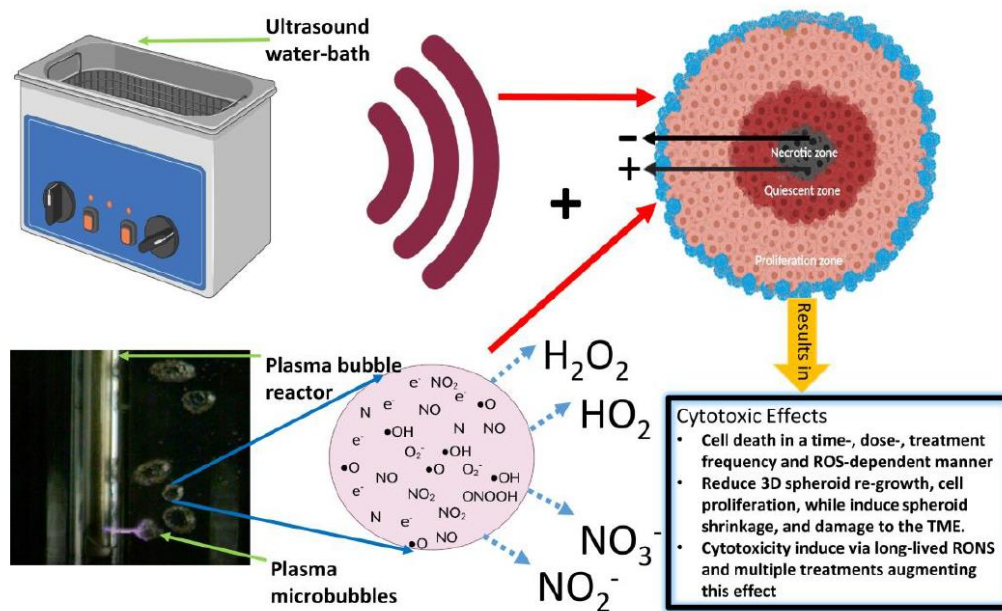
³ Department of Food Biosciences, Teagasc Food Research Centre, Ashtown, Dublin, Ireland.

⁴ FOCAS Research Institute, Technological University Dublin, Dublin, Ireland.

⁵ University of Sydney, School of Chemical and Biomolecular Engineering, Sydney, Australia.

⁶ Faculty of Engineering & Built Environment, Technological University Dublin, Dublin, Ireland.

* Corresponding authors. Email address: janith.manoharawanigasekara@tudublin.ie; james.curtin@tudublin.ie



The manuscript has been submitted for publication in the Plasma process and polymers Journal.

Extraction, purification and chemical characterization of phycobiliproteins from red microalgae (*Porphyridium purpureum*): A Novel approach

Shaba Noore^{1,2}, Ming Zhao², Janith Wanigasekara^{1,3,4}, Mohammad Gagaoua⁵, Eugene Dillon^{6,7}, Gerard Cagney^{6,7}, Claudio Fuentes-Grunewald^{8,9}, James. F. Curtin^{3,4}, Colm O'Donnell², *Brijesh K Tiwari^{1,2,7}

¹Department of Food Chemistry and Technology, Teagasc Food Research Centre, Ashtown, Dublin 15, Ireland

²School of Biosystems and Food Engineering, University College Dublin, Belfield, Dublin 4, Ireland

³School of Food Science & Environmental Health, College of Sciences & Health, Technological University Dublin, City Campus, Dublin, Ireland

⁴Environmental Sustainability & Health Institute (ESHI), Technological University Dublin, Dublin, Ireland.

⁵Food Quality and Sensory Science Department, Teagasc Food Research Centre, Dublin 15, Ashtown, Ireland

⁶Mass Spectrometry Resource, UCD Conway Institute of Biomolecular and Biomedical Research, University College Dublin, Belfield, Dublin, Ireland

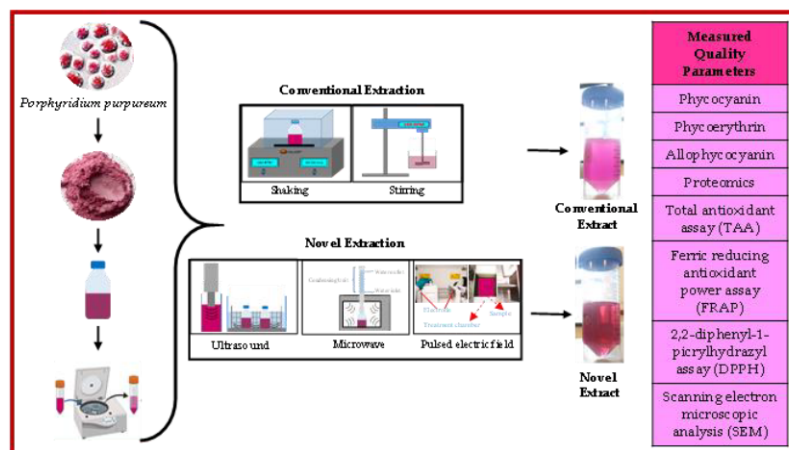
⁷BiOrbic, Bioeconomy SFI Research Centre, University College Dublin, Belfield, Dublin, Ireland

⁸College of Science, Bioscience Department, Swansea University, Singleton Park, SA2 8PP Swansea, United Kingdom.

⁹Beacon Development Department, King Abdullah University of Science and Technology (KAUST), Thuwal, Kingdom of Saudi Arabia

Contact information for corresponding author: Shaba Noore, University College Dublin, Belfield, Dublin, Ireland, shabanoore@ucdconnect.ie

Graphical Abstract



The manuscript has been submitted for publication in the Process Biochemistry Journal and is currently undergoing the peer-review process.

1 **Characterisation of laminarin extracted from brown seaweed *Laminaria digitata*, using optimized**
2 **ultrasound- and ultrafiltration-assisted extraction method**

3 Xianglu Zhu^{1,2}, Laura Healy^{2,3}, Janith Wanigasekara^{1,3,4}, Ming Zhao², Ramesh Babu Padamati⁵,
4 Shanmugapriya Karuppusamy^{1,2}, James F Curtin^{3,4}, Saravana Periaswamy Sivagnanam¹, Dilip K. Rai⁶,
5 Da-Wen Sun^{2*}, Brijesh K Tiwari¹

6
7 ¹*Department of Food Chemistry and Technology, Teagasc Food Research Centre, Ashtown, D15 DY05,*
8 *Dublin, Ireland*

9 ²*School of Biosystems and Food Engineering, University College Dublin, Belfield, D04 VIW8, Dublin,*
10 *Ireland*

11 ³*School of Food Science & Environmental Health, College of Sciences & Health, Technological*
12 *University Dublin, City Campus, Dublin, Ireland*

13 ⁴*Environmental Sustainability & Health Institute (ESHI), Technological University Dublin, Dublin,*
14 *Ireland.*

15 ⁵*School of Chemistry, AMBER Centre, Trinity College Dublin, Dublin 2, Ireland*

16 ⁶*Department of Food BioSciences, Teagasc Food Research Centre, Ashtown, Dublin 15, Ireland*

17

18 Abstract

19 The present study reported the extraction and characterisation of laminarin from *Laminaria digitata*.
20 Hydrochloric acid concentration and extraction time were investigated by central composite design for
21 optimizing extraction conditions. Regarding purification of the supernatant after the extraction process,
22 membrane ultrafiltration was selected over pH shifting, ethanol precipitation and freeze-drying. With
23 the assistance of ultrasound technology in the extraction process, the highest laminarin extraction yield
24 and purity were obtained up to $57.34 \pm 1.58\%$ and $81.10 \pm 0.37\%$, respectively. The molecular weight
25 of laminarin extracts is in the range of 5.61 to 5.95 kDa. The Fourier-transform infrared spectroscopy
26 (FT-IR) spectral features of the averaged spectra were depicted as absorbance peaks at the wavelengths
27 of 3340 cm^{-1} and 2922 cm^{-1} , which were related to O-H and C-H stretching of laminarin. US probe
28 extract showed the highest scavenging capacity of 52.96% while the HCl conventional extract exhibited
29 the lowest scavenging capacity of 30.82%. All the optimized laminarin extracts showed higher
30 cytotoxicity in A549, A431, and Caco-2 carcinomas, effectively inducing cancer cell death in a time-
31 and dose-dependent manner, and lower cytotoxicity in BEAS-2B normal human bronchial epithelial
32 cells when compared to commercial laminarin.

33 Keywords: Seaweed, laminarin, ultrasound, membrane ultrafiltration, cell-line, FT-IR

34

35 1. Introduction

36 Seaweeds have been commercially harvested for thousands of years in more than 50 countries, in waters
37 ranging from cold to tropical. The global market of seaweeds, with a current annual growth rate of

*Corresponding author. Email: dawen.sun@ucd.ie; URLs: <http://www.ucd.ie/refig>, <http://www.ucd.ie/sun>

The manuscript has been submitted for publication in the Nature Food Journal and is currently undergoing the peer-review process.

Extraction and biological activities of phycobiliproteins from *Porphyridium purpureum* using atmospheric cold plasma di-electric and jet systems

Shaba Noore^{1, 2}, Brijesh K. Tiwari^{1, 2}, Anet R. Jambrak³, Josipa Dukić³, Janith Wanigasekara^{1,4, 5}, James. F. Curtin^{4, 5}, Claudio Fuentes-Grunewald^{6, 7}, *Colm O'Donnell²

¹Department of Food Chemistry & Technology, Teagasc Food Research Centre, Ashtown, Dublin, Ireland

²School of Biosystems and Food Engineering, University College Dublin, Belfield, Dublin, Ireland

³Faculty of Food Technology and Biotechnology, University of Zagreb, Zagreb, Croatia

⁴School of Food Science & Environmental Health, College of Sciences & Health, Technological University Dublin, City Campus, Dublin, Ireland

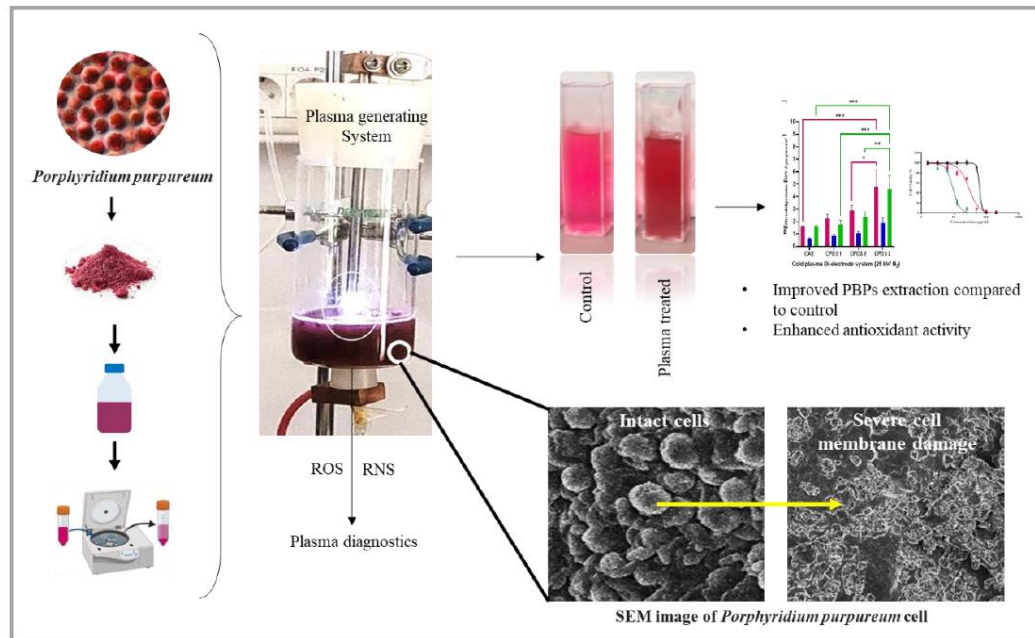
⁵Environmental Sustainability & Health Institute (ESHI), Technological University Dublin, Dublin, Ireland.

⁶College of Science, Bioscience Department, Swansea University, Singleton Park, SA2 8PP Swansea, United Kingdom.

⁷Beacon Development Department, King Abdullah University of Science and Technology (KAUST), Thuwal, Kingdom of Saudi Arabia

Contact information for corresponding author: Colm O'Donnell, University College Dublin, Belfield, Dublin, Ireland, colm.odonnell@ucd.ie

Graphical Abstract



The manuscript has been submitted for publication in the Antioxidants MDPI Journal and is currently undergoing the peer-review process.



MAY 05, 2021

U-251MG Spheroid generation using low attachment plate method protocol

Lara J Carroll¹, Brijesh Tiwari¹, James F Curtin¹, Janith Wanigasekara¹

¹Technological University Dublin



James F Curtin

Technological University Dublin

OPEN ACCESS

DOI:

dx.doi.org/10.17504/protocols.io.bs2mnf46

Protocol Citation: Lara J Carroll, Brijesh Tiwari, James F Curtin, Janith Wanigasekara 2021. U-251MG Spheroid generation using low attachment plate method protocol. [protocols.io](https://dx.doi.org/10.17504/protocols.io.bs2mnf46) <https://dx.doi.org/10.17504/protocols.io.bs2mnf46>

License: This is an open access protocol distributed under the terms of the [Creative Commons Attribution License](https://creativecommons.org/licenses/by/4.0/), which permits unrestricted use, distribution, and reproduction in any medium, provided the original author and source are credited

Protocol status: Working
We use this protocol and it's working

Created: Mar 04, 2021

Last Modified: May 05, 2021

PROTOCOL integer ID: 47885

ABSTRACT

3D cell culture is a process used to grow cells *in vitro* to mimic an *in vivo* environment. 3D cell models are very useful for understanding disease mechanisms and exploring drug therapeutics. 3D cultures can be grown from cells taken from cancer organoids in patients. Once grown, they can be used to screen for small molecule drugs or they can be genetically modified in order to analyse disease pathways or predict the toxicity or efficacy of a drug treatment. These cultures decrease the need to use animals in research and provides more reliable results as it uses human physiology.

This protocol describes the *in vitro* generation of spheroids using the low attachment plate method. This method uses low-adhesion plates that are coated with hydrophilic polymer to allow cells to cluster together, forming their own extracellular matrix, rather than sticking to the plate surface. The scaffold-free 3D cell culture models produced can more accurately reflect an *in vivo* microenvironment making them useful in the study of oncology, hepatotoxicity, neurology, nephrology and stem cell biology.

A



MAY 07, 2021

OPEN ACCESS

DOI:
dx.doi.org/10.17504/protocols.io.bszzqnf5w

Protocol Citation: Lara J Carroll, Brijesh Tiwari, James F Curtin, Janith Wanigasekara 2021. U-251MG Spheroid generation using a scaffold based method protocol.
protocols.io
<https://dx.doi.org/10.17504/protocols.io.bszzqnf5w>

License: This is an open access protocol distributed under the terms of the [Creative Commons Attribution License](#), which permits unrestricted use, distribution, and reproduction in any medium, provided the original author and source are credited

Protocol status: Working
 We use this protocol and it's working

Created: Mar 04, 2021

Last Modified: May 07, 2021

PROTOCOL integer ID:
 47888

U-251MG Spheroid generation using a scaffold based method protocol

Lara J Carroll¹, Brijesh Tiwari¹, James F Curtin¹, Janith Wanigasekara¹

¹Technological University Dublin

Technological University Dublin



James F Curtin
 Technological University Dublin

ABSTRACT

3D cell culture is a technique that is used to grow cells in vitro that will mimic an in vivo environment. 3D cell models are a helpful learning tool for researchers to better understand disease mechanisms and to explore different therapeutic properties of drugs. 3D cell cultures can be developed using patient derived cancer cells. Once they have been grown, these 3D cells can be used to screen for small molecule drugs or for genetic modification in for analysis of disease pathways or to predict drug treatments toxicity or efficacy. 3D cell cultures are a big step towards the more ethical testing of drug toxicity and efficacy as they decrease the need to use animals in research as well as providing more reliable results as the cells used are of human physiology.

Cellusponge are 3D porous hydroxypropylcellulose scaffolds that are designed for use with cells that do not require specific ligands. As well as the standard non-coated cellusponge, there are two more of the same type of scaffold available for use that are made with two different coatings to allow for improved adaptation of different cell types, these are called Cellusponge-Gal and Cellusponge-Col. Cellusponge is a no-coating approach that is intended for use in the development of general soft tissue 3D culture. It has been used as soft matrix for 3D cell culture and 3D tumour model.



MAY 05, 2021

OPEN ACCESS

DOI:
dx.doi.org/10.17504/protocols.io.btstnne

Protocol Citation: Lara J Carroll, Brijesh Tiwari, James F Curtin, Janith Wanigasekara 2021. U-251MG Spheroid Generation Using Hanging Drop Method Protocol.
protocols.io
<https://dx.doi.org/10.17504/protocols.io.btstnne>

License: This is an open access protocol distributed under the terms of the [Creative Commons Attribution License](#), which permits unrestricted use, distribution, and reproduction in any medium, provided the original author and source are credited

Protocol status: Working
 We use this protocol and it's working

Created: Mar 30, 2021

Last Modified: May 05, 2021

PROTOCOL integer ID:
 48691

U-251MG Spheroid Generation Using Hanging Drop Method Protocol

Lara J Carroll¹, Brijesh Tiwari¹, James F Curtin¹, Janith Wanigasekara¹

¹Technological University Dublin

Technological University Dublin

Low-cost, high-quality ...

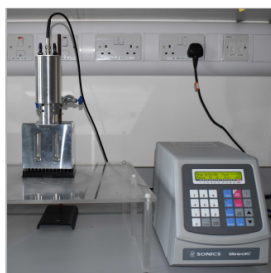


James F Curtin
 Technological University Dublin

ABSTRACT

The use of 3D cell culture has been a major step in developing cellular models that can mimic physiological tissues. Traditional 2D cell cultures are often unable to accurately represent the cellular functions and responses that are present in tissues, as a result, research findings based on 2D cultures tend to be skewed with limited predictive capability. 3D cell cultures can be grown from cells obtained from cancer organoids in patients. These models are useful for understanding disease mechanisms and exploring drug therapeutics in areas such as toxicity and efficacy.

In order to gather more physiologically relevant data, a variety of 3D cell culture techniques have been developed to mimic the *in vivo* characteristics of physiological tissues. This protocol describes *in vitro* generation of U-251MG spheroids using the hanging drop method. Advantages of using hanging drop plate method are, able to produce uniform size spheroids, low cost, comfortable to handling and suitable for short term culture. The main downside of this method is medium change, different drug treatment at different time points are impossible and labor intensive. This method uses the Perfecta3D hanging drop plate, a novel cell culture device that simplifies the process of spheroid formation, testing and analysis. Rather than having to invert the plates which often results in spillage or detachment, these plates are designed to create hanging drops using a plateau structure at the bottom of the plate.



FEB 12, 2023

🌐 Ultrasound 96 Probe Device Protocol for cancer cell treatment

Aisling Field¹, Brijeshtiwari², James F Curtin¹, Julie Rose Mae Mondala¹, Janith Wanigasekara¹

¹Technological University Dublin; ²Teagasc Food Research Centre Dublin

Technological University Dublin

TU Dublin



Aisling Field

OPEN ACCESS

DOI:

dx.doi.org/10.17504/protocols.io.e6nwkpdwvmk/v1

Protocol Citation: Aisling Field, Brijeshtiwari, James F Curtin, Julie Rose Mae Mondala, Janith Wanigasekara 2023. Ultrasound 96 Probe Device Protocol for cancer cell treatment. **protocols.io** <https://dx.doi.org/10.17504/protocols.io.e6nwkpdwvmk/v1>

MANUSCRIPT CITATION: Deprez, J., Lajoinie, G., Engelen, Y., De Smedt, S., & Lentacker, I. (2021). Opening doors with ultrasound and microbubbles: Beating biological barriers to promote drug delivery. *Advanced Drug Delivery Reviews*, 172, 9-36. doi: 10.1016/j.addr.2021.02.015. Pitt, W., Husseini, G., & Staples, B. (2004). Ultrasonic drug delivery - a general review. *Expert Opinion On Drug Delivery*, 1(1), 37-56. doi: 10.1517/17425247.1.1.37 Wanigasekara, J., de Carvalho, A., Cullen, P., Tiwari, B., & Curtin, J. (2021). Converging technologies: targeting the hallmarks of cancer using ultrasound and microbubbles. *Trends In Cancer*, 7(10), 886-890. doi: 10.1016/j.trecan.2021.07.004

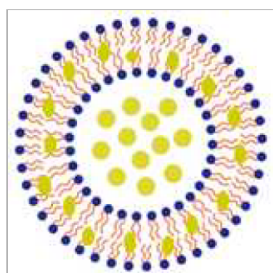
ABSTRACT

Ultrasound is a sound wave with frequencies ranging between 20 kHz and 20 MHz. Ultrasound is able to temporarily and repeatedly open the BBB safely and enhance chemotherapeutic delivery without adverse effects.(Deprez et al., 2021). This novel technique in drug delivery benefits from the powerful ability of ultrasound to produce cavitation activity. Cavitation is the generation and activity of gas-filled bubbles in a medium exposed to ultrasound. As the pressure wave passes through the media, gas bubbles expand at low pressure and contract at high pressure. This leads to oscillation which produces a circulating fluid flow known as microstreaming around the bubble with velocities and shear rates proportional to the amplitude of the oscillation. At high amplitudes the associated shear forces can cut open liposomes (Wanigasekara et al., 2021; Deprez et al., 2021).

Vesicles denser than the surrounding liquid are drawn into the shear field surrounding an oscillating bubble. If the shear stress is greater than the strength of the vesicle, it will burst and spill its contents. In a liposome, the vesicle will reform, often at a smaller size than before meeting the shear field. Hence, some interior liquid must be released during the break down. (Pitt et al., 2004)

This protocol describes the use of an ultrasound probe to trigger the release of liposomes in glioblastoma cells. This method uses an ultrasound device which is set to the following parameters: Time = 3 min, Pulse = 59 /01, Amplitude = 20%. The ultrasound technique is an easy and reliable technique making it useful in the study of a variety of areas such as oncology. When applied to an ultrasonic transducer, the Pulser part of the instrument generates short, large amplitude electric pulses of controlled energy, which are transformed into short ultrasonic pulses.

The VCX 750 is the ultrasonic liquid processor used for this experiment. It is powerful and versatile and can process a wide range of sample types and volumes for many different applications.



JAN 12, 2023

🌐 Liposome Encapsulation of Hydrophilic and Hydrophobic Drugs

Aisling Field¹, James F Curtin¹, Janith Wanigasekara¹, Julie Rose Mae Mondala¹

¹Technological University Dublin



Aisling Field

ABSTRACT

Dried reconstituted vesicles (DRV) are liposomes that are produced under mild conditions and can encapsulate very high amounts of hydrophilic solutes. These characteristics make this liposome type perfect for entrapment of drugs (Antimisariis, 2016). To produce DRV's, the lipid ingredients are firstly dissolved in an organic solvent (chloroform), dried on a rotary evaporator to obtain a thin film, followed by lipid hydration (in the aqueous medium at a temperature greater than the phase-transition temperature) and lastly to homogenize and reduce the vesicle size, where the extrusion technique is used. This process produces heterogeneous multilamellar vesicles. Cholesterol is added into the bilayer structure to aid liposome formation, and to stabilize against aggregation and drug leakage (Ahmad and Dwivedi, 2017).

The thin-film method is one of the most widely used liposome encapsulation methods. It is based on the generation of a thin film of lipids, formed on the inner wall of the rotary evaporator flask. The film is then hydrated with water. Before the hydration, it is integral that the lipid film is preheated above the lipids transitional temperature to enable a smoother creation of the bilayer, along with the vigorous shaking. This allows the film to peel off the flask and form liposomes. The liposomes generated are multilamellar vesicles of different sizes. The encapsulating substance can be added with the lipids before the formation of the thin film (hydrophobic compounds) or with the water (hydrophilic compounds). The advantage of this method is its high reproducibility even when working with small quantities of compounds (Šturm and PoklarUlrih, 2021).

This protocol describes the liposome encapsulation of hydrophobic and hydrophilic drugs using thin-film dispersed hydration method. Extrusion method with a polycarbonate membrane is used to make liposomes of suitable sizes that can be easily internalized by mammalian cells.

OPEN ACCESS

DOI:

dx.doi.org/10.17504/protocols.io.rm7vzymorlx1/v1

Protocol Citation: Aisling Field, James F Curtin, Janith Wanigasekara, Julie Rose Mae Mondala 2023. Liposome Encapsulation of Hydrophilic and Hydrophobic Drugs .

protocols.io

<https://dx.doi.org/10.17504/protocols.io.rm7vzymorlx1/v1>

MANUSCRIPT CITATION:

G. Antimisariis, S., 2016. Preparation of DRV Liposomes. [online] SpringerLink. Available at: [Accessed 25 October 2021].
 Ahmad, H. and K. Dwivedi, A., 2017. Novel lipid nanostructures for delivery of natural agents with antioxidant, antiinflammatory and antistroke potential: perspectives and outcomes. [online] Science Direct. Available at: [Accessed 25 October 2021].
 Šturm, L. and PoklarUlrih, N., 2021. Basic Methods for Preparation of Liposomes and Studying Their Interactions with Different Compounds, with the Emphasis on Polyphenols. [online] mdpi. Available at: [Accessed 23 November 2021].

Cold atmospheric plasma for Brain cancer treatment

W.M.J.M.B. Wanigasekara^{1,2}, J.F. Curtin¹, P.J. Cullen^{1,3}, B. Tiwari²

1. *BioPlasma Research Group, School of Food Science and Environmental Health, Technological University Dublin, Dublin, Ireland.*
2. *Teagasc Food Research Centre, Ashtown, Dublin, Ireland.*
3. *School of Chemical Engineering, University of New South Wales, Sydney, Australia.*

The Brain cancers are neoplasms that originate within the brain and spinal cord mainly from neurons or glial cells (astrocytes, oligodendrocytes and ependymal cells), pituitary gland, meninges, lymphatic tissue and cranial nerves. The existing brain tumour treatment methods are surgery, chemotherapy, Radio therapy and steroid therapy[1]. Cold atmospheric plasma (CAP) has been proposed as a novel therapeutic method for anticancer treatment, which can be applied to living tissues and cells. CAP is a partially ionized gas that contain charge particles, reactive oxygen and nitrogen species (ROS and RNS), excited atoms, free radicals, UV photons and electric field. ROS and RNS, combined or independently, able to initiate different signalling pathways in cells and to promote oxidative stress. It has been shown in-vitro that CAP in low concentration was able to stop tumour cells growing, to induce cell death in higher concentrations and that this was more effective than some standard treatment including radiation and chemotherapy[2,3,4].

Plasma induced biological effects include damage lipids, proteins, DNA, and induce apoptosis through plasma-generated ROS and RNS. Moreover, many studies have reported both in-vivo and in-vitro that plasma is a possible adjunct treatment in oncology as well as killing achieved for various types of cancers such as glioblastoma, breast cancer, bladder carcinoma, cervical carcinoma, skin carcinoma, pancreatic carcinoma, lung carcinoma, colon carcinoma, gastric carcinoma, melanoma and hepatocellular carcinoma. Usually jet plasma, dielectric barrier discharge (DBD) and corona discharge use for plasma medicine field and there are two types of cancer treatments available known as a direct and indirect treatment[2, 3, 5, 6].

Reference

- 1) S. Eimer et al., "Cyclopamine cooperates with EGFR inhibition to deplete stem-like cancer cells in glioblastoma-derived spheroid cultures", *Neuro-Oncology*, vol. 14, no. 12, pp. 1441-1451, 2012. Available: 10.1093/neuonc/nos266.
- 2) J. Schlegel, J. Köritzer and V. Boxhammer, "Plasma in cancer treatment", *Clinical Plasma Medicine*, vol. 1, no. 2, pp. 2-7, 2013. Available: 10.1016/j.cpme.2013.08.001.
- 3) Z. Chen et al., "Micro-Sized Cold Atmospheric Plasma Source for Brain and Breast Cancer Treatment", *Plasma Medicine*, vol. 8, no. 2, pp. 203-215, 2018. Available: 10.1615/plasmamed.2018026588.
- 4) Z. He et al., "Cold Atmospheric Plasma Induces ATP-Dependent Endocytosis of Nanoparticles and Synergistic U373MG Cancer Cell Death", *Scientific Reports*, vol. 8, no. 1, 2018. Available: 10.1038/s41598-018-23262-0.
- 5) M. Leduc, D. Guay, R. Leask and S. Coulombe, "Cell permeabilization using a non-thermal plasma", *New Journal of Physics*, vol. 11, no. 11, p. 115021, 2009. Available: 10.1088/1367-2630/11/11/115021.
- 6) H. Tanaka et al., "New Hopes for Plasma-Based Cancer Treatment", *Plasma*, vol. 1, no. 1, pp. 150-155, 2018. Available: 10.3390/plasma1010014.

Synergistic application of airborne acoustic and Plasma technologies for mitigation of Biofilms

Janith Wanigasekara^{1,3}, James F. Curtin¹, Patrick J. Cullen², Brijesh Tiwari³

1. BioPlasma Research Group, School of Food Science and Environmental Health, Technological University Dublin, Dublin, Ireland.
2. School of Chemical Engineering, University of New South Wales, Sydney, Australia.
3. Teagasc Food Research Centre, Ashtown, Dublin, Ireland.

The key objective of Ultrafilm is to deliver a novel solution for the eradication of 2D and 3D brain cancer cell cultures via the application of low temperature atmospheric pressure plasmas in combination with airborne acoustic technology. The Brain cancers are neoplasms that originate within the brain and spinal cord mainly from neurons or glial cells (astrocytes, oligodendrocytes and ependymal cells), pituitary gland, meninges, lymphatic tissue and cranial nerves. 3D cell culture allow the brain cancer cells to grow in all directions in invitro conditions and cells exist in 3D micro environments with intricate cell – cell and cell – matrix interaction for complex transport dynamics of nutrients and cells. 2D cell cultures are inadequate representation of their environment. The 3D spheroids more closely resemble in vivo tissue within their spheroid similar to the way cells would move in living tissue. Different 3D culture techniques such as cell aggregates (hanging drops, low adherence plates), hydrogels (natural & synthetic gels) and Scaffold support (Natural & synthetic scaffold) can be used for 3D cell culture.

Cold Atmospheric Plasma (CAP) can cause cell death in both prokaryotic and eukaryotic cells with cytotoxic effects resulting predominantly from oxidative damage to the cells' membrane and intra-cellular components, including DNA, through the action of reactive oxygen or nitrogen species (ROS/RNS). It has been shown invitro that CAP in low concentration was able to stop tumour cells growing, to induce cell death in higher concentrations and that this was more effective than some standard treatment including radiation and chemotherapy.

Mechanism of contact type ultrasound is largely attributed to various physical (acoustic streaming, cavitation, micromechanical shockwaves) and chemical mechanisms (e.g. free radicals, sonolysis of water). Whereas, limited knowledge is available for noncontact or airborne acoustic. High intensity ultrasound causes formation of cavitation bubbles, which can damage the DNA in cancer cells when they collapse due both to sudden changes in stress and release of free radicles (H^{\cdot} & OH^{\cdot}).

This project will design a prototype non-invasive acoustic based plasma prototype and to investigate the cellular, structural and biomolecular changes induced in the cell cultures. It will also characterise the degradation mechanism of cells extracellular matrices. It is expected that the Ultrafilm will develop novel non-thermal acoustic-plasma based intervention strategies for eradication of tumour cells in vitro and will lead to deeper insights into the cellular, chemical and structural behaviour in response to applied plasma and acoustic stresses.

TU Dublin Graduate Research Symposium 2019, Ireland

TU Dublin Graduate Research symposium 2019, Dublin, Ireland. Abstract, Oral Presentation - <http://dx.doi.org/10.13140/RG.2.2.25549.72165>

Treatment of Human Glioblastoma Spheroids using Cold Atmospheric Plasma



Janith Wanigasekara^{1,3}, James Curtin¹, Patrick Cullen², Brijesh Tiwari³
 School of Food Science and Environmental Health, Technological University Dublin, Ireland¹
 The School of Chemical and Biomedical Engineering, The University of Sydney, Australia²
 Teagasc Food Research Centre, Ashtown, Dublin, Ireland³



Introduction

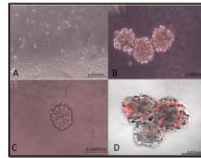
- Glioblastoma multiforme is the most common type of primary brain tumor and the most aggressive cancer (WHO grade IV), with 12–15-month median survival rate. The severity of the cancer promptly requires accurate diagnosis and curative therapeutic strategies that target the origin of gliomas cells.
- To increase the efficiency of glioblastoma treatment the objective of the research is to treat the U-251 MG human glioblastoma spheroids with cold atmospheric plasma (CAP) in treatment. CAP has been proposed as a novel therapeutic method for anticancer treatment. CAP is a partially ionized gas that contains charge particles, reactive oxygen and nitrogen species (ROS and RNS), excited atoms, free radicals, UV photons and electric field. CAP can cause cell death in both prokaryotic and eukaryotic cells with cytotoxic effects resulting predominantly from oxidative damage to the cells' membrane and intra-cellular components, including DNA, through the action of ROS and RNS.
- Three dimensional (3D) cell cultures is an advanced in-vitro cell culture technique use to grow cells in three dimensions using an artificially created microenvironment. Cells in 3D cell culture have physiological cell-cell interactions and cell–extra cellular matrix component interactions which allow cells to grow in-vitro in a microenvironment that closely resembles in-vivo conditions. 3D cell culture also able to co culturing with different cell types to develop increasingly accurate in vitro models of disease and physiology. The importance of glioblastoma multiforme cellular interaction with endothelial cells can be studied with co culture techniques to get proper understanding of the endothelial interaction on tumor progression for identify novel therapeutic approaches.

Methodology

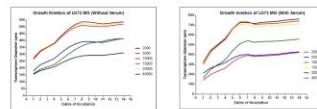
- U-251 MG human glioblastoma astrocytoma cells were used to construction of tumourspheres by using Nunclon™ Sphera™ U & flat bottom ultra low attachment plates
- Growth kinetics of U-251 MG spheroids grown with and without serum at increasing seeding densities were evaluated over a period of 2 weeks.
- U-251 MG tumoursphere CAP treatment was carried out by using novel dielectric barrier discharge (pin) system with Voltage - 240 V, Discharge Frequency - 1000Hz and Duty cycle 72 μs.
- Tumourspheres grown in flat bottom micro plate (with and without serum) were exposed to CAP for 20s, 50s, 100s, 160s and 320s and post treatment incubation carried out for 24h, 48h and 96h at 37 °C in a humidified incubator.
- Cell viability was analyzed using the Alamar blue assay and the fluorescence was measured (excitation, 560 nm; emission, 590 nm) by a Varioskan™ LUX multimode microplate reader.



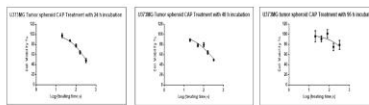
Results



(A) 2D cell culture of U-251MG cells in T75 flask (B) 3D cell culture of U-251MG in low-adhesion Nunclon™ Sphera™ flat bottom culture plate (C) 3D cell culture of U-251MG in low-adhesion Nunclon™ Sphera™ U bottom culture plate (D) 320s CAP treated, 24 hours incubated, propidium iodide stained tumourspheres



Tumourspheres showed larger spheroid growth (by diameter) with serum when compare to spheroid without serum and optimum seeding densities were 10x, 15x, 20x cells/ml.



IC-50 value; 24h incubation=275.2s, 48h incubation=347.4s, 96h incubation=1423s. According to the results tumourspheres show higher cytotoxicity with lower post incubation time. During 96h incubation tumourspheres recover the cell damage and regrows cells from the healthier cells in core of tumoursphere.



The IC50 value without serum in 24h incubation was 95.34 s and IC50 value with serum was 315.9s. Higher cell death in tumourspheres grown without serum compared to with serum.

Discussion

- The hypoxic (oxygen-deprived) cell population increase is proportional to the tumoursphere size and highly resistant to CAP treatment.
- 3D Spheroid growth characteristics vary based on cell origin, type, initial seeding density and 3D cell culture method.
- Higher cytotoxicity is observed with longer CAP treatment time and shorter post incubation time. This is due to short and long lived RNS (N₂, N₂⁺, ONOO and NO⁺) and ROS (*OH, O⁻, O₂⁻ and O₃) photons as well as heat, pressure gradient, charged particles, electrostatic and electromagnetic fields.
- Tumourspheres are able to regrow with post treatment incubation time and also show protective effect with the supplement of 10% serum.
- Tumourspheres grown without serum can reduce the re-growth ability and has higher cytotoxicity
- CAP treatment proven to be a promising treatment method for human glioblastoma astrocytoma.

Future experiments

Find the 3D glioblastoma spheroid cytotoxicity with multiple CAP treatments and efficiency of combinational therapy with ultrasound and nanoparticles.

Conclusion

CAP treatment can effectively reduce 3D glioblastoma spheroid growth and cell proliferation. CAP-generated short and long lived reactive nitrogen and oxygen species cause cell cytotoxicity and growth inhibition in 3D glioblastoma spheroids in vitro. These results demonstrate the potential of CAP therapies for cancer treatment.

References

- Scallly, L., Gulen, M., Weigang, L., Cullen, P., & Milosavljevic, V. (2018). Significance of a Non-Thermal Plasma Treatment on LDPE Biodegradation with *Pseudomonas Aeruginosa*. *Materials*, 11(10), 1925. <https://doi.org/10.3390/ma11101925>
- Wang, C., Li, J., Sinha, S., Peterson, A., Grant, G. A., & Yang, F. (2019). Mimicking brain tumor-vasculature microanatomical architecture via co-culture of brain tumor and endothelial cells in 3D hydrogels. *Biomaterials*, 202, 30–44. <https://doi.org/10.1016/j.biomaterials.2019.02.024>
- Zong, H., Verhaak, R. G., & Canali, P. (2012). The cellular origin for malignant glioma and prospects for clinical advancements. *Expert Review of Molecular Diagnostics*, 12(4), 383–394. <https://doi.org/10.1586/erm.12.30>

Acknowledgement



The project was been supported by Science Foundation Ireland (SFI) under Grant Number 17/CDA/4653

Science Foundation Ireland Science Summit 2020, Dublin, Ireland. Poster Presentation -

<http://dx.doi.org/10.13140/RG.2.2.11289.08809>

Introduction

- Glioblastoma multiforme (GBM) is the most common and aggressive malignant primary brain tumor. The existing treatments for GBMs are surgery, followed by radiation and chemotherapy. However, it is not completely effective as the median survival time is 15-16 months. The severity of the cancer promptly requires accurate diagnosis and curative therapeutic strategies that target the origin of gliomas cells^[1].
- Cold atmospheric plasma (CAP) has been proposed as a novel therapeutic method for anticancer treatment. CAP is a partially ionized gas that contains charge particles, reactive oxygen and nitrogen species (ROS and RNS), excited atoms, free radicals, UV photons and electric field. CAP can cause cell death with cytotoxic effects resulting predominantly from oxidative damage to the cells' membrane and intra-cellular components, including DNA, through the action of ROS and RNS^[2].
- Three dimensional (3D) cell culture is an advanced *in-vitro* cell culture technique used to grow cells in three dimensions using an artificially created microenvironment. 3D cells have physiological cell-cell interactions and cell-extra cellular matrix component interactions which allow cells to grow *in-vitro* in a microenvironment that closely resembles *in-vivo* conditions^[3].

Aims and Objectives

- Development of U-251 MG human glioblastoma astrocytoma into 3D *In-Vitro* cell culture Model to get reliable predictors of *In-vivo* drug efficacy and toxicity
- Application of novel CAP to increase the cytotoxicity and treatment efficiency of U-251 MG human glioblastoma tumourspheres

Methodology

- Development and optimization of U-251 MG human glioblastoma astrocytoma 3D *In-vitro* cell culture model
- In-vitro* studies and comparison of cancer cells in 2D vs. 3D culture
- Cytotoxic effect of CAP treatment using novel dielectric barrier discharge (pin) system

Results

1. U-251 MG human glioblastoma astrocytoma 3D *In-vitro* cell culture model was developed

Tumorspheres constructed and optimized by using Nunclon™ Sphera™ U & flat bottom plates (ultra-low attachment method).

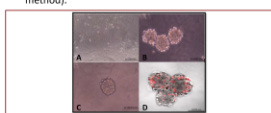


Figure 1: (A) 2D cell culture of U-251MG cells in T75 flask (B) 3D cell culture of U-251MG in low-adhesion Nunclon™ Sphera™ flat bottom culture plate (C) 3D cell culture of U-251MG in low-adhesion Nunclon™ Sphera™ U bottom culture plate (D) 320s CAP treated, 24h incubated, propidium iodide stained tumorspheres

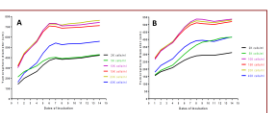


Figure 2: Growth kinetics of U-251 MG (A) With (B) Without Serum. Tumorspheres showed larger spheroid growth with serum (diameter 150-750µm) when compare to spheroid without serum (diameter 150-550µm) and optimum seeding densities were 10K, 15K, 20K cells/ml.

2. *In-vitro* studies and comparison of cancer cells in 2D vs. 3D culture

Different concentrations of dimethyl sulfoxide (DMSO) cytotoxicity towards 3D and 2D cell culture: U-251 MG 3D cells showed higher protectivity against DMSO (IC50=5.75% [v/v]) when compare to U-251 MG 2D cells (IC50 = 2.09% [v/v]).

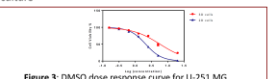


Figure 3: DMSO dose response curve for U-251 MG

3. Cytotoxic effect of CAP treatment using pin system

Tumorspheres were exposed to CAP (pin system at a Voltage - 240 V, Discharge Frequency - 1000Hz and Duty cycle - 72 µs) for 20s, 40s, 80s, 160s and 320s and post-treatment incubation carried out for 24h, 48h and 96h at 37 °C and cell viability was analyzed using Alamar blue assay.

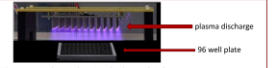


Figure 4: Dielectric barrier discharge (pin) system

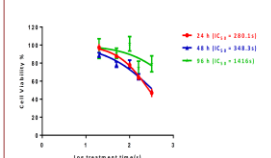


Figure 5: CAP treatment of U-251 MG tumorspheres
 IC-50 value; 24h incubation=280.1s, 48h incubation=348.3s, 96h incubation=1416s. According to the results, tumorspheres show higher cytotoxicity with lower post-incubation time. During 96h incubation, tumorspheres recover the cell damage and re-grows cells from the healthier cells in the core of tumorsphere.

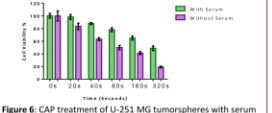


Figure 6: CAP treatment of U-251 MG tumorspheres with serum and without serum (24 h incubation)
 The IC50 values without serum was 95.34 s and with serum was 280.1s. Higher cell death was observed in tumorspheres grown without serum compared to with serum.

Discussion

- 3D spheroid growth characteristics vary based on seeding density, culture conditions and presence of growth factors.
- In comparison to 2D cell culture, 3D cell culture reveal toxicological resistance, architecture as *in-vivo* tissues, accurate depiction of cell polarization, gene expression, reliable predictions of *in-vivo* drug efficiency and toxicity.
- The hypoxic (oxygen-deprived) cell population increase is proportional to the tumorsphere size and highly resistant to CAP treatment.
- Higher cytotoxicity is observed with longer CAP treatment time and shorter post incubation time. This is due to short and long lived RNS (N₂, N₂⁺, ONCO- and NO⁺) and ROS (*OH, O, *O₂- and O₃) photons as well as heat, pressure gradient, charged particles, electrostatic and electromagnetic fields.
- Tumorspheres are able to regrow with post treatment incubation time and also show protective effect with the supplement of 10% serum.
- Tumorspheres grown without serum can reduce the re-growth ability and has higher cytotoxicity
- CAP treatment proven to be a promising treatment method for human glioblastoma astrocytoma.

Conclusions

CAP treatment can effectively reduce 3D glioblastoma spheroid growth and cell proliferation. CAP-generated short and long lived reactive nitrogen and oxygen species cause cell cytotoxicity and growth inhibition in 3D glioblastoma spheroids *in-vitro*. These results demonstrate the potential of CAP therapies for cancer treatment.



Contact Information

Janith Wanigasekara
 Email: Janith.ManoharaWanigasekara@tudublin.ie

References

- Bi, W. L., & Beroukhim, R. (2014). Beating the odds: Extreme long-term survival with glioblastoma. *Neuro-Oncology*, 16(9), 1159–1160. <https://doi.org/10.1093/neuonc/nou108>
- Semmler, M. L., Bekeschus, S., Schuler, M., Bernhardt, T., Fischer, T., Witzke, K., Seebauer, C., Rebl, H., Grambow, E., Vollmar, B., Nebe, J. B., Metzmann, H. R., Woelke, T., von Emmert, S., & Bockmann, L. (2020). Molecular Mechanisms of the Efficacy of Cold Atmospheric Pressure Plasma (CAP) in Cancer Treatment. *Cancers*, 12(2), 269. <https://doi.org/10.3390/cancers12020269>
- Edmondson, R., Brogle, J. J., Adcock, A. T., & Yang, L. (2014). Three-Dimensional Cell Culture Systems and Their Applications in Drug Discovery and Cell-Based Biosensors. *ASSAY and Drug Development Technologies*, 12(4), 207–218. <https://doi.org/10.1089/adbt.2014.573>

Acknowledgements

The project is been supported by Science Foundation Ireland (SFI) under Grant Number 17/CDA/4653



Comparison of 2D and 3D human glioblastoma multiforme cell culture models for cold atmospheric plasma induced cytotoxicity

Janith Wanigasekara a, b, c, Patrick J. Cullen a, e, f, Brijesh Tiwari b, James F. Curtin a, c, d*

a BioPlasma Research Group, School of Food Science and Environmental Health, Technological University Dublin, Dublin, Ireland.

b Department of Food Biosciences, Teagasc Food Research Centre, Ashtown, Dublin, Ireland.

c Environmental Sustainability & Health Institute (ESHI), Technological University Dublin, Dublin, Ireland.

d FOCAS Research Institute, Technological University Dublin, Dublin, Ireland.

e University of Sydney, School of Chemical and Biomolecular Engineering, Sydney, Australia.

f Plasmaleap Technologies, Merewether Building, City Road, Sydney, Australia

* Correspondence: james.curtin@tudublin.ie

3-dimensional (3D) cells are maintaining physiological cell-cell and cell-extracellular matrix interactions, more closely mimic the natural in-vivo environment. This provides accurate representation of plasma induced toxicological resistance, cellular responses and gene expression. This study compared novel pin-to-plate cold atmospheric plasma (CAP) device induced cytotoxicity of U-251MG human glioblastoma multiforme (GBM) in 3D and 2D cell cultures. U-251MG tumorsphere (low attachment plates - Nunclon™ Sphera™) and 2D cells were constructed, then dose response curves were established by exposing cells to six different doses of CAP (20 – 320s) at 240 V, 1000 Hz and 73 μs (duty cycle). After 24h incubation at 37°C the cell viability was measured using Alamar Blue™ assay. An IC50 of 160.4s (157.0s ± 163.9s) and 386.3s (375.9s ± 397.1s) was found for 2D cells and 3D cells, respectively. The viability of the U-251MG 3D cells were decreased, but they showed higher plasma induced cytotoxicity resistant compared to 2D-cultured cells. In conclusion, the pin-to-plate CAP device successfully induced GBM cell death in a dose dependent manner, and also 3D cell culture as better alternative to overcome the cons of in-vivo animal testing and conventional 2D cell culture by providing a more accurate platform for CAP application in GBM therapy.

Keywords: Cold atmospheric plasma, 3D cell culture, Glioblastoma multiforme, Cytotoxicity

Funding: The project has been supported by Science Foundation Ireland (SFI) under Grant Number 17/CDA/4653

Therapeutic ROS and Immunity in Cancer Conference 2021, Greifswald, Germany.

Abstract, Oral Presentation - <https://doi.org/10.3390/cancers13184549>

Novel Treatment Strategies for Glioblastoma 3D Tumoursphere Cytotoxicity Induction

Janith Wanigasekara ^{a, b, c}, Patrick J. Cullen ^{a, e, f}, Brijesh Tiwari ^b, James F. Curtin ^{a, c, d*}

^aBioPlasma Research Group, School of Food Science and Environmental Health, Technological University Dublin, Dublin, Ireland.

^bDepartment of Food Biosciences, Teagasc Food Research Centre, Ashtown, Dublin, Ireland.

^cEnvironmental Sustainability & Health Institute (ESHI), Technological University Dublin, Dublin, Ireland.

^dFOCAS Research Institute, Technological University Dublin, Dublin, Ireland.

^eUniversity of Sydney, School of Chemical and Biomolecular Engineering, Sydney, Australia.

^fPlasma-leap Technologies, Merewether Building, City Road, Sydney, Australia

Glioblastoma multiforme has become the most common and aggressive malignant primary brain tumor in adults. Thus, vital new technologies, such as cold atmospheric plasma (CAP) and ultrasound (US), are essential for in vivo glioblastoma diagnosis, prognosis, and treatment. The aim of this study is to determine the effects of a CAP and US on U-251 MG 3D glioblastoma spheroids under different conditions. All the 3D spheroids were CAP treated at a resonant frequency of 55.51 kHz, discharge frequency of 1000 Hz, duty cycle of 73 μ s and a time range of 0–320 seconds. The US treatment was carried out at a 20 kHz frequency, 20% amplitude, 59/1 pulses with time ranges of 1–20 minutes. During single plasma discharge, the highest cytotoxicity was induced at the highest dose (320 seconds) and an IC50 of 355.1 seconds (342.3 s \pm 368.5 s), 429.8 seconds (422.7 s \pm 437.1 s), and 490.4 seconds (475.2 s \pm 506.1) were found for tumourspheres post incubated at 24, 48, and 96 hours, respectively. The highest ultrasound induced cytotoxicity was observed with 20 minutes of treatment and an IC50 of 24.87 minutes (24.35 min \pm 25.39 minutes), 30.95 minutes (29.56 minutes \pm 32.42 minutes), and 42.73 minutes (38.82 minutes \pm 47.04 minutes) were found for tumourspheres post incubated at 24, 48 and 96 hours, respectively. CAP and US treatments (Individually) were able to effectively induce 3D glioblastoma tumoursphere cell death and damage to the tumour microenvironment in a time, dose, and treatment frequency dependent manner, while reducing 3D glioblastoma spheroid growth and cell proliferation.

Cold plasma treatment on recovery of phycobiliproteins from red microalgae (*Porphyridium purpureum*)

Shaba Noore^{1,2}, Janith Wanigasekara^{1,3,4}, Anet R. Jambrak⁵, Josipa Dukić⁵, Claudio Fuentes-Grunewald^{6,7}, James. F. Curtin^{3,4}, Brijesh K. Tiwari^{1,2}, *Colm O'Donnell²

¹*Department of Food Chemistry & Technology, Teagasc Food Research Centre, Ashtown, Dublin, Ireland*

²*School of Biosystems and Food Engineering, University College Dublin, Belfield, Dublin, Ireland*

³*School of Food Science & Environmental Health, College of Sciences & Health, Technological University Dublin, City Campus, Dublin, Ireland*

⁴*Environmental Sustainability & Health Institute (ESHI), Technological University Dublin, Dublin, Ireland.*

⁵*Faculty of Food Technology and Biotechnology, University of Zagreb, Zagreb, Croatia*

⁶*College of Science, Bioscience Department, Swansea University, Singleton Park, SA2 8PP Swansea, United Kingdom.*

⁷*Beacon Development Department, King Abdullah University of Science and Technology (KAUST), Thuwal, Kingdom of Saudi Arabia*

Over the recent years, there has been a strong interest in the downstream processing of microalgae for the extraction of phycobiliproteins (PBPs) as it is widely used in cosmetics, pharmaceutical and food formulations and due to its antiviral and anti-inflammatory properties. Additionally, it reflects cytotoxicity effect on cancer cells thereby demonstrating potentiate chemotherapeutic effect. The current study investigated on cold plasma using High Voltage Electrical Discharge (HVED) conducted by generator "IMP-SSPG-1200" (Impel group, Zagreb, Croatia) for PBPs extraction, as it's less expensive and has a potential for scale up. Fixed HVED parameters (i.e., 100 Hz of frequency, 400 nanoseconds of pulse width, 20 and 25 kV of electrical tension) were fixed for nitrogen gas supply for HVED treatments. The gap between electrodes was in a distance of 15 mm. For extraction, ratio of dry mass of microalgae (i.e., 2.5g of *Porphyridium purpureum* (P.p.)) to solvent (i.e., 50 mL distilled water) was 1:20. Six extraction protocols (i.e., 20 kV/3min, 20 kV/6min, 20 kV/9min, 25 kV/3min, 25 kV/6min, and 25 kV/9 min) and a control method were investigated for the extraction. The recovery rate of the extracts were calculated. UV-Vis spectroscopic method at spectral range of 300-700nm to estimate concentration of phycobiliproteins (phycoerythrin (PE); phycocyanin (PC) and allophycocyanin (APC)) in the extracted samples. Results indicates that the highest recovery rate of crude phycobiliproteins (50.32 ± 0.07 %) was estimated in samples treated with 25 kV/3min. UV-Vis spectroscopic method results demonstrate a similar trend of extraction yield with highest concentration of PEs, PCs and ACPs (0.38mg PEs, 0.14mg PCs, and 0.19mg ACPs per 100mg of P.p. extracts, respectively) in the samples treated with 25 kV/3min. Scanning electron microscope (SEM) analysis of P.p. biomass was also carried out to identify the structural damage post treatments.

American Society of Agricultural and Biological Engineers Symposium, 2022, Houston,
USA - Abstract, Oral presentation



Effects of novel extraction strategies on recovery of phycobiliproteins from *Porphyridium purpureum*

Shaba Noore^{1,2}, Ming Zhao², Janith Wanigasekara^{1,3,4}, Mohammad Gagaoua⁵, Eugene Dillon^{6,7}, Gerard Cagney^{6,7}, Claudio Fuentes-Grunewald^{8,9}, James. F. Curtin^{3,4}, Colm O'Donnell², *Brijesh K Tiwari^{1,2,7}

¹Department of Food Chemistry and Technology, Teagasc Food Research Centre, Ashtown, Dublin 15, Ireland

²School of Biosystems and Food Engineering, University College Dublin, Belfield, Dublin 4, Ireland

³School of Food Science & Environmental Health, College of Sciences & Health, Technological University Dublin, City Campus, Dublin, Ireland

⁴Environmental Sustainability & Health Institute (ESHI), Technological University Dublin, Dublin, Ireland.

⁵Food Quality and Sensory Science Department, Teagasc Food Research Centre, Dublin 15, Ashtown, Ireland

⁶Mass Spectrometry Resource, UCD Conway Institute of Biomolecular and Biomedical Research, University College Dublin, Belfield, Dublin, Ireland

⁷BiOrbic, Bioeconomy SFI Research Centre, University College Dublin, Belfield, Dublin, Ireland

⁸College of Science, Bioscience Department, Swansea University, Singleton Park, SA2 8PP Swansea, United Kingdom.

⁹Beacon Development Department, King Abdullah University of Science and Technology (KAUST), Thuwal, Kingdom of Saudi Arabia

Phycobiliproteins (PBPs) present in red microalgae (*Porphyridium purpureum*) are hydrophilic pigments made up of apoproteins, which are covalently bound with phycobilins. PBPs are primarily classified into three basic categories namely phycoerythins (PEs), phycocyanins (PCs) and allophycocyanins (APCs). PBPs are used in the formulation of nutrient-rich products due to their antiviral and anti-inflammatory properties. The two main objectives of this study were: 1) investigation on the effects of novel strategies using distilled water extraction combined with ultrasound-assisted extraction (UAE), microwave-assisted extraction (MAE), pulsed electric field -assisted extraction (PEFAE) and conventional assisted extraction (CAE) for the extraction of PBPs from microalgae (*Porphyridium purpureum*); and 2) characterisation of the PBPs extracted using SDS-PAGE and LC-MS. Fifteen extraction strategies (i.e., UAE (n=4), MAE (n=4), PEFAE (n=4), CAE (n=2) and a control method (n=x)) were investigated in this study. Based on the recovery rates of crude extracts calculated and the concentration of PBPs (PEs; PCs and APCs) analysed in the crude extracts using UV-spectrometric methods, selected samples were further analysed using SDS-PAGE and LC-MS. Cell culture studies on the antioxidant properties of the crude extracts were carried out. Scanning electron microscope (SEM) analysis was also carried out on the treated microalgae residues to analyse surface damage after extraction. The results indicated that the highest content of PBPs (0.56 ± 0.07 mg/ml) was observed in samples treated with UAE. Similarly, the highest antioxidant activities were also observed in the cell culture study of the UAE extracts.

21st International Union of Food Science and Technology World Congress, 2022,
Singapore - Abstract, Oral presentation

Ultrasound-assisted extraction and polymer-based encapsulation of phycoerythrin from *Phorphyridium purpureum*

Shaba Noore^{1,2}, Ming Zhao¹, Marta V. Vieira³, Pablo Fuciños³, Janith Wanigasekara^{2,4,5}, Colm O'Donnell¹, and Brijesh K. Tiwari^{1,2,*}

¹School of Biosystems and Food Engineering, University College Dublin, Belfield, D04 V1W8 Dublin, Ireland

²Department of Food Chemistry & Technology, Teagasc Food Research Centre, Ashtown, D15 DY05 Dublin, Ireland

³International Iberian Nanotechnology Laboratory, Food Processing, and Nutrition Research Group, Av. Mestre José Veiga s/n 4715-330 Braga, Portugal

⁴BioPlasma Research Group, School of Food Science and Environmental Health, Technological University Dublin, Dublin, Ireland

⁵Environmental Sustainability & Health Institute, Technological University Dublin, Dublin, Ireland

*Corresponding author email: brijesh.tiwari@teagasc.ie

Abstract

Aim: Phycoerythrin (PE), a red color phycobiliprotein, is employed to prepare biomarkers, food colorants, therapeutics, medicines, and health-promoting products. This study comprises two primary objectives, including 1) ultrasound-assisted extraction (UAE) of PE from freeze-dried biomass of *Phorphyridium purpureum* (*P.p*) in the aqueous phase; 2) encapsulation of a heat-sensitive compound (PE) with improved stability and functional properties.

Method: Initially, four UAE strategies and a control method were investigated for the extraction. Based on the recovery of crude extracts and their concentrations of phycoerythrin (PE), crude extracts were subjected to cytotoxicity analysis against A549 human lung carcinoma and Caco-2 human colorectal adenocarcinoma cells using Alamar blue assay. Further, these PE extracts were encapsulated using 5% inulin as the coating material (core-shell ratio of 1:3.3) using a nano-spray dryer (inlet temperature: 80 °C; gas flow 100 l/min; chamber pressure 31 hPa; spray rate 80%, pump 50%; vibration frequency 120 kHz). Physicochemical properties of the encapsulated extract were estimated, comprising the color, yield, and scanning electron microscopy (SEM) for size and morphology analyses.

Results: These results indicated that the PE concentration in the extracts was improved from 0.1 mg/100 g in the control sample compared with 0.55 mg/100 g of extract in the UAE-treated samples. Inulin with a 5% concentration level resulted in higher retention of red color (a^* + value), with 3.01 ± 1.08 µm particle size and $83.82 \pm 2.49\%$ yield. SEM micrographs of encapsulated freeze-dried PE extract confirmed its spherical shape. Additionally, cytotoxicity results indicated the effects of PE extract on A549 and Caco-2 cell lines studied under different concentration gradients (from 200 µg/ml to 1.5625 µg/ml) and cells post incubated for six days at 37 °C in 5% CO₂. An IC₅₀ of 157.6 µg/ml and 124.6 µg/ml for control and UAE samples in A549, while an IC₅₀ of 199.7 µg/ml and 149.0 µg/ml were found for control and UAE samples in Caco-2 cells. Two-way ANOVA demonstrated a significant difference in viability between the highest and lowest concentration ($P < 0.0001$).

Conclusion: Overall results demonstrated that UAE is more effective for the recovery of PE than the control extraction method. The obtained extract proved its potential as an anticancer agent. Moreover, inulin has shown to be a suitable carrier material for preparing encapsulates, focusing on the stability improvement of bioactive compounds.

36th European Federation of Food Science and Technology (EFFoST) International Conference, 2022 - Abstract, Poster presentation

Three-dimensional cell culture models to advance glioblastoma research and to improve therapeutic outcomes with novel devices

Janith Wanigasekara^{1,2,3}, P.J. Cullen⁴, Brijesh Tiwari³, James Curtin^{1,2,5}

¹BioPlasma Research Group, School of Food Science and Environmental Health, Technological University Dublin, Dublin, Ireland. ²Environmental Sustainability & Health Institute (ESHI), Technological University Dublin, Dublin, Ireland. ³Department of Food Biosciences, Teagasc Food Research Centre, Ashtown, Dublin, Ireland. ⁴School of Chemical and Biomolecular Engineering, University of Sydney, Sydney, Australia. ⁵Faculty of Engineering and Built Environment, Technological University Dublin, Dublin, Ireland.

Glioblastoma multiforme (GBM) is the most lethal primary brain tumor in adults, with an average survival time of about 12-15 months from initial diagnosis. This is particularly evident with GBM with no successful therapy that significantly improves survival since the introduction of temozolomide 20 years ago. The majority of therapies fail during clinical trials due to imperfect models that limit our ability to predict efficacy and toxicity in humans. Considerable efforts have been devoted to the implementation of reliable and affordable *in vitro* GBM models to get over/around most of these limitations. Three-dimensional (3D) cell culture models can help bridge the gap between *in vitro* cell cultures and *in vivo* responses by more accurately simulating the natural *in vivo* environment, shape, tissue stiffness, stressors, gradients and cellular response while avoiding the costs and ethical concerns associated with animal models.

3D GBM tumourspheroids generated using the low attachment, hanging drop, and cellusponge natural scaffold based methods. Then studied the effect of novel cold atmospheric plasma (CAP) and ultrasound using 3D glioblastoma spheroids under different conditions using light and confocal microscopic techniques. Reactive oxygen species-dependent cytotoxicity is induced uniformly throughout GBM tumourspheres by direct CAP treatment while ultrasound was able to induce cytotoxicity at longer-exposure and enhance drug delivery at shorter-exposure.









Microscopy Society of Ireland (MSI) Symposium, 2023, Cork, Ireland – Oral presentation

9.4 Appendix III Professional Development

As part of the PhD experience, it is essential to develop and refine both discipline specific and employability skills. Modules and extracurricular activities undertaken are listed below.

List of employability skills and discipline specific skills training

Modules completed as part of the structured PhD – 1. Discipline specific skills and 2. Employability skills. The required 40 credits for structured PhD has been fully completed.

	GRSO 1001: Research methods (5 ECTS)		GRSO 1012: Research integrity (5 ECTS)
	INTL 1005: Flow Cytometry (5 ECTS)		INTL 1000: Techniques & Strategies in Molecular Medicine (5 ECTS)
	INTL 1005: Fundamentals in Medical Device Design and Regulation (5 ECTS)		CH 510: Process Development & Scale-up in the Pharmaceutical Industry (5 ECTS)
	GradCAM: Philosophy of Technology (5 ECTS)		ENEH 1006: Applied Mathematical Modelling in Environment, Food and Health (5 ECTS)

Extracurricular activities

Extracurricular activity	Date
Laboratory demonstrator for Biochemistry and Pharmaceutical Microbiology	Jan 2019 – May 2022
Exam invigilator for exams office, TU Dublin	Jan 2022 – Sep 2022
Hourly Paid Assistant Lecturer (HPAL) for Organic, Inorganic and Physical Chemistry	Jan 2022 – Jun 2023
Senior demonstrator for Biochemistry and Pharmaceutical Microbiology	Sep 2022 – Jun 2023